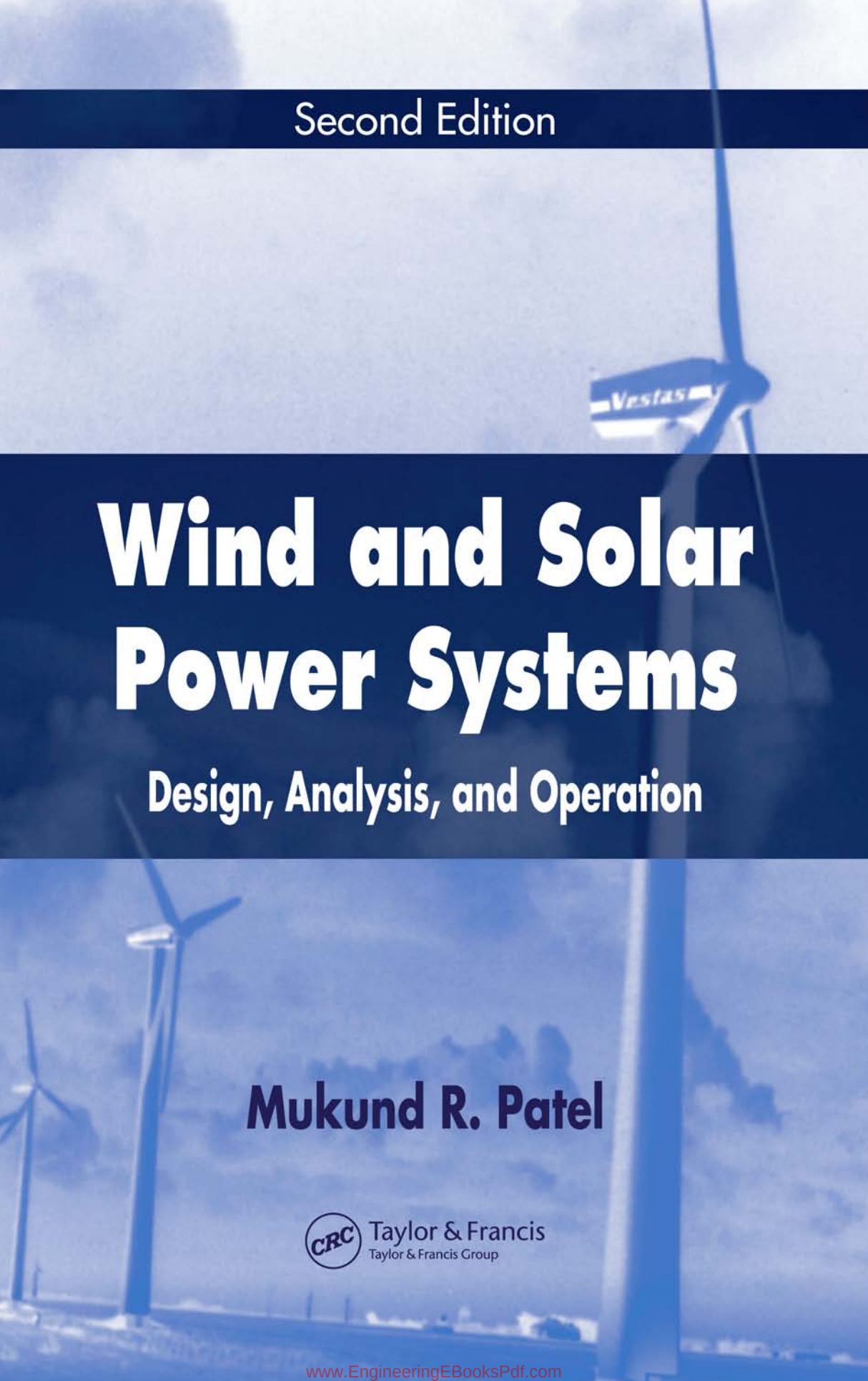

Second Edition

Wind and Solar Power Systems

Design, Analysis, and Operation

Mukund R. Patel

CRC Taylor & Francis
Taylor & Francis Group

Wind and Solar Power Systems

Design, Analysis, and Operation

Second Edition

Wind and Solar Power Systems

Design, Analysis, and Operation

Second Edition

Mukund R. Patel
U.S. Merchant Marine Academy
Kings Point, New York, U.S.A.

Taylor & Francis
Taylor & Francis Group

Boca Raton London New York Singapore

A CRC title, part of the Taylor & Francis imprint, a member of the
Taylor & Francis Group, the academic division of T&F Informa plc.

Cover photo: Original land use continues in a wind farm in Germany. (With permission from Vestas Wind Systems, Denmark.)

The wind and photovoltaic power technologies are rapidly evolving. Although reasonable care has been taken in preparing this book, neither the author nor the publisher assumes responsibility for any consequences of using the information. The diagrams disclosed herein are for illustration purposes only and may be covered by patents.

Published in 2006 by
CRC Press
Taylor & Francis Group
6000 Broken Sound Parkway NW, Suite 300
Boca Raton, FL 33487-2742

Printed in the United States of America on acid-free paper
10 9 8 7 6 5 4 3 2 1

International Standard Book Number-10: 0-8493-1570-0 (Hardcover)
International Standard Book Number-13: 978-0-8493-1570-1 (Hardcover)
Library of Congress Card Number 2005043904

Library of Congress Cataloging-in-Publication Data

Patel, Mukund R., 1942-
Wind and solar power systems : design, analysis, and operation / Mukund R. Patel.--2nd ed.
p. cm.
Includes bibliographical references and index.
ISBN 0-8493-1570-0 (alk. paper)
1. Wind power plants. 2. Solar power plants. 3. Photovoltaic power systems. I. Title.

TK1541.P38 2005
621.31'2136--dc22 2005043904

T&F informa
Taylor & Francis Group
is the Academic Division of T&F Informa plc.

Visit the Taylor & Francis Web site at
http://www.taylorandfrancis.com

and the CRC Press Web site at
http://www.crcpress.com

Dedication

Dedicated to my mother, Shakariba,
who practiced ingenuity, and to my children,
Ketan, Bina, and Vijal,
who flattered me by becoming engineers.

Preface

The phenomenal growth and new developments in wind and solar power technologies have made the second edition of this book necessary. It reflects the need for an expanded, revised, and updated version of the well-received first edition in just 5 years. During that time, the capital and energy costs of wind power have declined by 20%. Today, the cost of electricity from grid-connected wind farms is below 4 cents/kWh, and that from photovoltaic (PV) parks below 20 cents/kWh. The goal of ongoing research programs funded by the U.S. Department of Energy (DOE) and the National Renewable Energy Laboratory (NREL) is to bring wind energy cost below 3 cents/kWh and the PV energy cost below 15 cents/kWh by 2010. In capital and energy costs, wind now competes on its merits with the conventional power technologies, and has become the least expensive source of electrical power — traditional or new — in many parts of the world. It is also abundant and environmentally clean, bringing many indirect social benefits not fully reflected in the market economics. For these reasons, wind power now finds importance in the energy planning in all countries around the world. According to the DOE, prime wind locales of the world have the potential of supplying more than ten times the global energy needs. In the U.S., the DOE has established 21 partnerships with public and private bodies to develop turbines to generate economical power in low-wind-speed regions that would open up much larger areas of the country for rapid development of wind power. The Electric Power Research Institute (EPRI) estimates that wind energy will grow from less than 1% at present to as much as 10% of the U.S. electricity demand by 2020.

Around the world, the wind power generation capacity has seen an average annual growth rate of 30% during the period from 1993 to 2003. More than 8,000 MW of new wind capacity was added globally in 2003 with an investment value of $9 billion. This brought the total cumulative wind capacity to 40,000 MW. The most explosive growth occurred in Germany. Offshore wind farms are bringing a new dimension to the energy market. Many have been installed, and many more, each exceeding 300-MW capacity, are being installed or are in the planning stage. Most offshore farms are less than 10 km from the shore in less than 10 m depth of water. Denmark's plan to install 750 MW of new wind capacity by 2008, bringing its total to 4,000 MW for supplying 25% of the country's electricity, includes aggressive offshore plans. U.S. wind capacity is projected to reach 12,000 MW by 2015. Utilities and wind power developers have announced plans for more than 5,000 MW of new capacity in 15 states by 2006. Hydro-Quebec plans 1,000 MW of new capacity to be added between 2006 and 2012. In these new installations, 3-MW turbines are being routinely installed in many countries, with 5-MW machines available today for large offshore farms; 7-MW units are in prototype tests.

On the solar PV side, the cost of PV electricity is still high: between 15 and 25 cents/kWh. With the consumer cost of utility power ranging from 10 to 15 cents/kWh, PV cannot economically compete directly with utility power as yet, except in remote markets where utility power is not available and transmission line cost would be prohibitive. Many developing countries have large areas falling in this category, and that is where the most PV growth is taking place, such as in India and China. The worldwide solar PV is about $7 billion in annual business, mainly driven by Germany.

Worldwide, PV installations grew at an average annual rate of 25 to 30% during the period from 2000 to 2004. By the end of 2004, the cumulative PV capacity was 2,030 MW, with 1,000 MW in the U.S. The annual production of PV modules was 530 MW in 2004 and is projected to reach 1,600 MW by 2010. The present module prices are $6 to $7 per watt for 1-kW modules and $3 to $4 per watt for 1-MW plants. The emerging thin-film and concentrating PV cells are expected to reduce the module prices substantially in the near future.

After the restructuring of U.S. electrical utilities as mandated by the Energy Policy Act (EPAct) of 1992, industry leaders expected the power generation business, both conventional and renewable, to become more profitable in the long run. Their reasoning is that the generation business has been stripped of regulated prices and opened to competition among electricity producers and resellers. The transmission and distribution business, on the other hand, is still regulated. The American experience indicates that free business generates more profits than regulated business. Such is the experience in the U.K. and Chile, where the electrical power industry had long been structured similarly to the U.S. EPAct of 1992. Moreover, the renewable power price would be falling as the technology advances, whereas the price of the conventional power would rise with inflation, making the wind and PV even more profitable in the future.

North America's darkest blackout in 2003 with its estimated $10 billion in damage is bringing a new and sharp focus to distributed power generation. Because overloaded transmission lines caused the blackout, and it would take decades before new lines can be planned and built, the blackout has created a window of opportunity for distributed power generation from wind and PV. As most large-scale wind farms are connected to the grid lines, PV systems are expected to benefit more in distributed power generation growth.

The Author

Mukund R. Patel, Ph.D., P.E., is a research engineer, consultant, and educator with 40 years of hands-on involvement in designing and developing state-of-the-art electrical power equipment and systems. He has served as principal engineer at the General Electric Company in Valley Forge, Pennsylvania; fellow engineer at the Westinghouse Research & Development Center in Pittsburgh; senior staff engineer at Lockheed Martin Corporation in Princeton, New Jersey; development manager at Bharat Bijlee Limited, in Bombay, and as 3M Distinguished Visiting Professor at the University of Minnesota, Duluth. Presently, he is a professor of engineering at the U.S. Merchant Marine Academy at Kings Point, New York, and an associate editor of *Solar Energy Journal* published by the International Solar Energy Society.

Dr. Patel obtained his Ph.D. degree in electric power engineering from Rensselaer Polytechnic Institute, Troy, New York; M.S. in engineering management from the University of Pittsburgh; M.E. in electrical machine design from Gujarat University; and B.E. from Sardar Patel University, Vallabha Vidyanagar, Gujarat, India. He is a fellow of the Institution of Mechanical Engineers (U.K.), associate fellow of the American Institute of Aeronautics and Astronautics, a senior member of the IEEE, a registered professional engineer in Pennsylvania, and a member of Eta Kappa Nu, Tau Beta Pi, Sigma Xi, and Omega Rho.

Dr. Patel has presented and published about 50 papers at national and international conferences, holds several patents, and has earned recognition from the National Aeronautics and Space Administration for exceptional contribution to the photovoltaic power system design for the Upper Atmosphere Research Satellite. He is active in consulting and teaching short courses to professional engineers in the electrical power industry.

Dr. Patel lives in Yardley, Pennsylvania, with his wife, Sarla. They have three children, Ketan, Bina, and Vijal, and two grandchildren, Rayna and Dhruv. Dr. Patel can be reached at patelm@usmma.edu.

About This Book

The second edition of this book is an expanded, revised, and updated version, which was prepared when I was invited to teach a course as a visiting professor in emerging electrical power technologies at the University of Minnesota, Duluth. Teaching the full course to inquisitive students and short courses to professional engineers enhanced the contents in many ways. It is designed and tested to serve as textbook for a semester course for university seniors in electrical and mechanical engineering fields. For practicing engineers there is a detailed treatment of this rapidly growing segment of the power industry. Government policymakers will benefit by the overview of the material covered in the book, which is divided into 4 parts in 19 chapters.

Part A covers wind power technologies and ongoing programs in the U.S. and around the world. It includes engineering fundamentals, the probability distributions of wind speed, the annual energy potential of a site, the wind speed and energy maps of several countries, and wind power system operation and the control requirements. As most wind plants use induction generators for converting turbine power into electrical power, the theory of the induction machine performance and operation is reviewed. The electrical generator speed control for capturing maximum energy under wind fluctuations over the year is presented. The rapidly developing offshore wind farms with their engineering, operational, and legal aspects are covered in detail.

Part B covers solar photovoltaic (PV) technologies and current developments around the world. It starts with the energy conversion characteristics of the photovoltaic cell, and then the array design, effect of the environment variables, sun-tracking methods for maximum power generation, the controls, and emerging trends are discussed.

Part C starts with the large-scale energy storage technologies often required to augment nondispatchable energy sources, such as wind and PV, to improve the availability of power to users. It covers characteristics of various batteries, their design methods using the energy balance analysis, factors influencing their operation, and battery management methods. Energy density and the life and operating cost per kilowatthour delivered are presented for various batteries such as lead-acid, nickel-cadmium, nickel-metal-hydride, and lithium-ion. The energy storage by the flywheel, compressed air, and the superconducting coil, and their advantages over the batteries are reviewed. Basic theory and operation of the power electronic converters and inverters used in the wind and solar power systems are then presented. Over two billion people in the world not yet connected to the utility grid are the largest potential market of stand-alone power systems using wind and PV systems in hybrid with diesel generators or fuel cells, which are discussed in detail. The grid-connected renewable power systems are covered with voltage and frequency control methods needed for synchronizing the generator with the grid. The theory and

operating characteristics of the interconnecting transmission lines, voltage regulation, maximum power transfer capability, and static and dynamic stability are covered.

Part C continues with overall electrical system performance, the method of designing system components to operate at their maximum possible efficiency, static and dynamic bus performance, harmonics, and the increasingly important quality of power issues applicable to the renewable power systems. The total plant economy and the costing of energy delivered to the paying customers are presented. It also shows the importance of a sensitivity analysis to raise the confidence level of the investors. The profitability charts are presented for preliminary screening of potential sites. Also reviewed are past and present trends of wind and PV power, the declining-price model based on the learning curve, and the Fisher–Pry substitution model for predicting the future market growth of wind and PV power based on historical data on similar technologies. The effect of utility restructuring, mandated by the Energy Policy Act of 1992, and its benefits on the renewable power producers are discussed.

Part D covers the ancillary power system derived from the sun, the ultimate source of energy on the earth. It starts with the utility-scale solar thermal power plant using concentrating heliostats and molten salt steam turbine. It then covers solar-induced wind power, marine current power, ocean wave power, and hydropiezoelectric power generators. Finally, it examines in detail a novel contrarotating wind turbine that can improve the wind-to-electricity conversion efficiency by 25 to 40% from a given wind farm area. As the available wind farm areas, on land or offshore, are becoming constrained due to various environment reasons, this concept holds future potential. The last chapter includes detailed prototype construction and test methods to guide young researchers in this evolving field.

Lastly, Appendix 1 presents the National Electrical Code® as applicable to the renewable power sources. Appendix 2 gives sources of further information (names and addresses of government agencies, universities, and manufacturers active in renewable power around the world, references for further reading, list of acronyms, and conversion of units).

Acknowledgments

Any book of this nature on emerging technologies such as wind and photovoltaic power systems cannot possibly be written without help from many sources. I have been extremely fortunate to receive full support from many organizations and individuals in the field. They not only encouraged me to write on this timely subject but also provided valuable suggestions and comments during the development of the book.

For this second edition, I am grateful to Prof. Jose Femenia, head of the engineering department; Dr. Warren Mazek, Dean; and Vice Admiral Joseph Stewart, Superintendent, of the U.S. Merchant Marine Academy, Kings Point, New York, for supporting my research and publications, including a sabbatical leave for writing this book. I have benefited from the midshipmen at the academy who were taking this course and contributing to my learning as well.

A new chapter on emerging research on contrarotating wind turbines has been added with a special contribution from Dr. Kari Appa of Appa Technology Initiatives, Lake Forest, California.

For the first edition, Dr. Nazmi Shehadeh of the University of Minnesota, Duluth, gave me the start-up opportunity to develop and teach this subject to his students. Dr. Elliott Bayly of the World Power Technologies in Duluth shared with my students and me his long experience in the field. He helped me develop the course outline, which eventually led to the first edition of this book. Dr. Jean Posbic of Solarex Corporation in Frederick, Maryland, and Mr. Carl-Erik Olsen of Nordtank Energy Group/NEG Micon in Denmark kindly reviewed the draft and provided valuable suggestions for improvement. Bernard Chabot of ADEME, Valbonne, France, generously provided the profitability charts for screening the wind and photovoltaic power sites. Ian Baring-Gould of the National Renewable Energy Laboratory has been a source of useful information and the hybrid power plant simulation model.

Several institutions worldwide provided current data and reports on these rather rapidly developing technologies. They are the American Wind Energy Association, the American Solar Energy Association, the European Wind Energy Association, the National Renewable Energy Laboratory, the Riso National Laboratory in Denmark, the Tata Energy Research Institute in India, the California Energy Commission, and many corporations engaged in the wind and solar power technologies. Numerous individuals at these organizations gladly provided all the help I requested.

I wholeheartedly acknowledge the valuable support from you all.

Mukund R. Patel
Yardley, Pennsylvania

Contents

PART A Wind Power Systems

PART B Photovoltaic Power Systems

PART C System Integration

PART D Ancillary Power Technologies

Appendices

Index 433

Part A

Wind Power Systems

1 Introduction

1.1 INDUSTRY OVERVIEW

Globally, the total annual primary energy consumption in 2005 is estimated to be 500 quadrillion (10^{15}) Btu.[1] The U.S. consumes 105 quadrillion Btu, distributed in segments shown in Figure 1.1. About 40% of the total primary energy consumed is used in generating electricity. Nearly 70% of the energy used in our homes and offices is in the form of electricity. The worldwide demand of 15 trillion kWh in 2005 is projected to reach 19 trillion kWh in 2015. This constitutes a worldwide average annual growth of 2.6%. The growth rate in developing countries is projected to be approximately 5%, almost twice the world average.

Our world has been powered primarily by carbon fuels for more than two centuries, with some demand met by nuclear power plants over the last five decades. The increasing environmental concerns in recent years about global warming and the harmful effects of carbon emissions have created a new demand for clean and sustainable energy sources, such as wind, sea, sun, biomass, and geothermal power. Among these, wind and solar power have experienced remarkably rapid growth in the past 10 yr. Both are pollution-free sources of abundant power. Additionally, they generate power near load centers; hence, they eliminate the need of running high-voltage transmission lines through rural and urban landscapes. Deregulation, privatization, and consumer preferences for green power in many countries are expanding the wind and photovoltaic (PV) energy markets at an increasing pace.

The total electricity demand in the U.S. approached 4 trillion kWh in 2005, with a market value of $300 billion. To meet this demand, over 800 GW of electrical generating capacity is now installed in the U.S. For most of this century, the countrywide demand for electricity has increased with the gross national product (GNP). At that rate, the U.S. will need to install an additional 200-GW capacity by the year 2015.

China is now the world's second-largest consumer of electricity after the U.S. China's demand grew 15% in 2003, as against the 5% expected by economic planners. The country is managing the strained power grids with rolling blackouts. The total demand is now expected to exceed 460 GW by the end of 2005. India is another country whose energy demand is growing at more than 10% annually. This growth rate, in view of the large population base, makes these two countries rapidly growing electric power markets for all sources of electric energy, including the renewables.

The new capacity installation decisions today are becoming complicated in many parts of the world because of the difficulty in finding sites for new generation and transmission facilities of any kind. In the U.S., no nuclear power plants have been ordered or built since 1978[2] (Figure 1.2). Given the potential for cost overruns, safety-related design changes during the construction, and local opposition to new

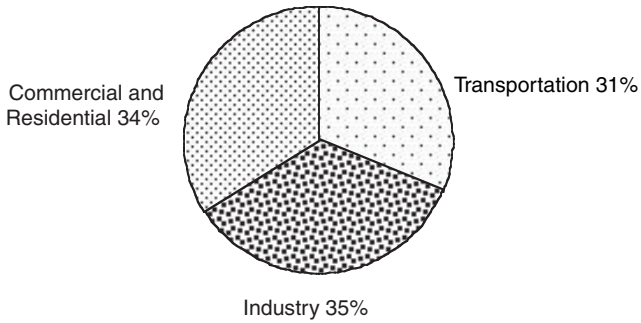

FIGURE 1.1 Primary energy consumption in the U.S. in three major sectors, with a total of 90 quadrillion Btu in 1997. (From U.S. Department of Energy, International Energy Outlook 2004 with Projections to 2020, DOE Office of the Integrated Analysis and Forecasting, April 2004.)

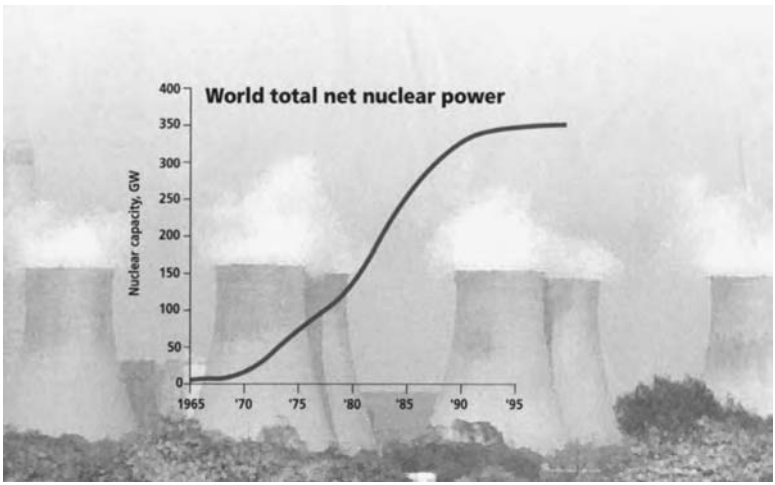

FIGURE 1.2 The stagnant nuclear power capacity worldwide. (From Felix, F., State of the Nuclear Economy, *IEEE Spectrum*, November 1997, pp. 29–32. With permission.)

plants, most utility executives have been reluctant to plan on new nuclear power plants during the last three decades. If no new nuclear plants are built and the existing plants are not relicensed at the expiration of their 40-yr terms, the nuclear power output is expected to decline sharply after 2010. This decline must be replaced by other means. With gas prices expected to rise in the long run, utilities are projected to turn increasingly to coal for base-load power generation. The U.S. has enormous reserves of coal, equivalent to more than 250 yr of use at the current level. However, this will need clean coal-burning technologies that are fully acceptable to the public.

Alternatives to nuclear and fossil fuel power are renewable energy technologies (hydroelectric, in addition to those previously mentioned). Large-scale hydroelectric projects have become increasingly difficult to carry through in recent years because

TABLE 1.1
Status of Conventional and Renewable Power Sources

Conventional	Renewable
Coal, nuclear, oil, and natural gas	Wind, solar, biomass, geothermal, and ocean
Fully matured technologies	Rapidly developing technologies
Numerous tax and investment subsidies embedded in national economies	Some tax credits and grants available from federal and some state governments
Accepted in society under a "grandfather clause" as a necessary evil	Being accepted on their own merit, even with limited valuation of their environmental and other social benefits

TABLE 1.2
Benefits of Using Renewable Electricity

Traditional Benefits	Nontraditional Benefits per Million kWh Consumed
Monetary value of kWh consumed	Reduction in emission
U.S. average 12 cents/kWh	750–100 t of CO_2
U.K. average 7.5 pence/kWh	7.5–10 t of SO_2
	3–5 t of NOx
	50,000 kWh reduction in energy loss in power lines and equipment
	Life extension of utility power distribution equipment
	Lower capital cost as lower-capacity equipment can be used (such as transformer capacity reduction of 50 kW per MW installed)

of the competing use of land and water. Relicensing requirements of existing hydroelectric plants may even lead to removal of some dams to protect or restore wildlife habitats. Among the other renewable power sources, wind and solar have recently experienced rapid growth around the world. Having wide geographical spread, they can be generated near the load centers, thus simultaneously eliminating the need for high-voltage transmission lines running through rural and urban landscapes.

The present status and benefits of renewable power sources are compared with conventional ones in Table 1.1 and Table 1.2, respectively. The renewables compare well with the conventionals in economy.

1.2 INCENTIVES FOR RENEWABLES

A great deal of renewable energy development in the U.S. occurred in the 1980s, and the prime stimulus was passage in 1978 of the Public Utility Regulatory Policies Act (PURPA). It created a class of nonutility power generators known as the *qualified facilities* (QFs). The QFs were defined to be small power generators utilizing renewable energy sources or cogeneration systems utilizing waste energy. For the first time, PURPA required electric utilities to interconnect with QFs and to purchase

QFs' power generation at "avoided cost," which the utility would have incurred by generating that power by itself. PURPA also exempted QFs from certain federal and state utility regulations. Furthermore, significant federal investment tax credit, research and development tax credit, and energy tax credit — liberally available up to the mid-1980s — created a wind energy rush in California, the state that also gave liberal state tax incentives. As of now, the financial incentives in the U.S. are reduced but are still available under the Energy Policy Act of 1992, such as the energy production tax credit of 1.5 cents/kWh delivered to a utility for the first 10 yr of the plant's operation. It was later raised to 1.8 cents/kWh to adjust for inflation. The potential impact of the 1992 act on renewable power producers is reviewed in Chapter 16.

Many energy scientists and economists believe that the renewables would get many more federal and state incentives if their social benefits were given full credit. For example, the value of not generating 1 t of CO_2, SO_2, and NOx, and the value of not building long high-voltage transmission lines through rural and urban areas are not adequately reflected in the present evaluation of the renewables. If the renewables get due credit for pollution elimination of 600 t of CO_2 per million kWh of electricity consumed, they would get a further boost with greater incentives than those presently offered by the U.S. government.

In the U.S., the conventional power plants are heavily subsidized — intangible drilling costs, depletion allowances, decommissioning tax credit, special tax treatments for coal royalties, and black and brown lung payments, etc. These add up to billions of dollars. At the 2.5-trillion-kWh/yr consumption rate, subsidies the conventional power plants receive amount to about 1 cent/kWh for every $25 billion, and the consumers eventually pay this in taxes. This does not take into account the direct military costs for protecting sea-lanes for petroleum shipments or nuclear storage and waste from terrorists, and the environmental cleanup and damages explicitly traceable to conventional energy sources.

For the U.S. wind and solar industries, there is additional competition in the international market. Other governments support green-power industries with well-funded research, low-cost loans, favorable tax-rate tariffs, and guaranteed prices not generally available to their U.S. counterparts. Under such incentives, the growth rate of wind power in Germany and India has been phenomenal over the last decade.

1.3 UTILITY PERSPECTIVE

Until the late 1980s, interest in the renewables was confined primarily to private investors. However, as the considerations of fuel diversity, the environment, and market uncertainties are becoming important factors in today's electric utility resource planning, renewable energy technologies are beginning to find their place in the utility resource portfolio. Wind and solar power, in particular, have the following advantages over power supplied by electric utilities:

- Both are highly modular, in that their capacity can be increased incrementally to match gradual load growth.

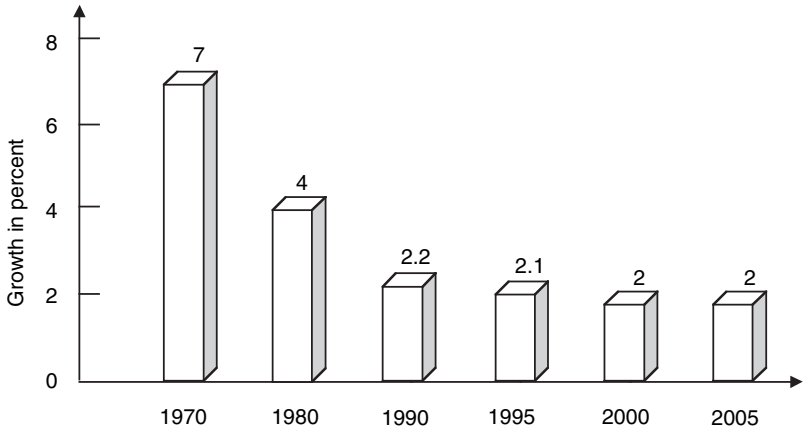

FIGURE 1.3 Growth of electricity demand in the U.S. (From U.S. Department of Energy and Electric Power Research Institute.)

- Their construction lead time is significantly shorter than that of conventional plants, thus reducing financial and regulatory risks.
- They use diverse fuel sources that are free of both cost and pollution.

Because of these benefits, many utilities and regulatory bodies have become increasingly interested in acquiring hands-on experience with renewable energy technologies in order to plan effectively for the future. These benefits are discussed in the following text in further detail.

1.3.1 Modularity for Growth

The electricity demand in the U.S. grew at 6 to 7% until the late 1970s, tapering to just 2% in the 1990s and beyond, as shown in Figure 1.3.

The 7% growth rate of the 1970s meant doubling the electric energy demand and the installed capacity every 10 yr. The decline in the growth rate since then has come partly from the improved efficiency in electricity utilization through programs funded by the U.S. Department of Energy. The small growth rate of the last decade is expected to continue well into the coming decades.

The most economical sizes of the conventional power plant had been 500-MW to 1000-MW capacities. These sizes could be justified until the 1970s, as they would be fully loaded in just a few years. At the present 2% growth rate, however, it would take decades before a 500-MW plant would be fully loaded after it is commissioned in service. Utilities are unwilling to take such long-term risks in making investment decisions. This has created a strong need for modularity in today's power generation industry.

Both wind and solar PV power are highly modular. They allow installations in stages as needed without losing economy of size in the first installation. PV power is even more modular than wind power. It can be sized to any capacity, as solar

arrays are priced directly by the peak generating capacity in watts and indirectly by square feet. Wind power is modular within the granularity of turbine size. Standard wind turbines come in different sizes ranging from a few kW to a few MW. For utility-scale installations, standard wind turbines in the recent past had been around 300 kW but are now 1 to 1.5 MW, and are moving into the 2 to 3 MW range. Prototypes of 5-MW wind turbines have been tested and are being made commercially available in Europe. A large plant may begin with the required number and size of wind turbines for the initial needs, adding more towers with no loss of economy when the plant needs to grow.

For small grids, modularity of PV and wind systems is even more important. Increasing demand may be more economically met by adding small increments of green-power capacity. Expanding or building a new conventional power plant in such cases may be neither economical nor free from market risks. Even when a small grid is linked by a transmission line to the main network, installing a wind or PV plant to serve growing demand may be preferable to laying another transmission line. Local renewable power plants can also benefit small power systems by moving generation near the load, thus reducing the voltage drop at the end of a long, overloaded line.

1.3.2 Emission Benefits

In 2005, the U.S. will produce almost 4 trillion kWh of electricity, 70% of it (2.8 trillion kWh) from fossil fuels and a majority of that from coal. The resulting emissions are estimated to exceed 2.5 billion tons of CO_2, 20 million tons of SO_2, and 8 million tons of NOx. The health effects of these emissions are of significant concern to the U.S. public. The electromagnetic field emission around high-voltage transmission lines is another concern that has also recently become an environmental issue.

Because of these issues, renewable energy sources are expected to be given importance in the energy planning of all countries around the world. Also, wind power has now become the least expensive source of new power — or of any power — as seen in Table 1.3. Consequently, wind power has seen the highest growth rate in installed generation capacity during the 1993 to 2003 period (Figure 1.4).

1.3.3 Consumer Choice

Green Pricing is a voluntary, renewable electricity program offered by about 350 retail distribution companies in the U.S. Since market deregulation, some 50,000, or 6%, of eligible users in Texas alone have switched to renewable energy sources. In the first green-certificate trading program in the U.S., Texas utilities are required to buy Renewable Energy Certificates on the open market to partially offset the amount of conventionally generated electricity they sell to customers. Each certificate represents 1 MWh produced from wind, solar, or other renewable energy sources. In these programs, consumers have an option of buying power from renewable sources at an extra price of about 1.5 cent/kWh or $5 per month extra for 300-kWh

TABLE 1.3
Generation, Investment, and External Costs for Various Power Generation Technologies on a Large Scale in the U.S.

Technology	Generation Cost (cents/kWh)	Investment Cost ($/W)	All External Costs[a] (cents/kWh)
Coal, thermal	3–5	1.0–1.5	2.0–15
Nuclear	3–8	1.2–2.0	0.2–0.6[b]
Gas combined cycle	3–5	0.5–0.7	1.0–4.0
Small hydro	5–10	0.8–1.2	—
Biomass, thermal	4–10	1.5–2.5	—
Wind	3–5	0.8–1.5	0.05–0.25
Solar, PV	20–35	6.0–8.0	0.05–0.25
Solar, thermal	15–30	4.0–6.0	—

[a] Estimated cost to society and environment.
[b] Not including nuclear waste and decommissioning cost.

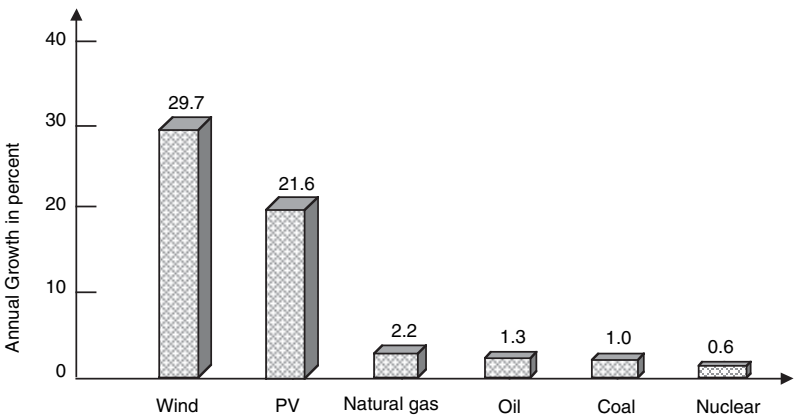

FIGURE 1.4 Average growth rate in installed capacity of various power plants during 1993 to 2003. (From *Renewable Energy World*, May–June 2004, p. 183.)

blocks. Nearly 350 MW of new renewable capacity have been installed as a result of such programs as of 2004, and more installations are being planned in the future. Out of this, more than 95% is through wind generation.

A 2003 survey of consumer willingness to pay premium for electric power from renewable sources is depicted in Figure 1.5.

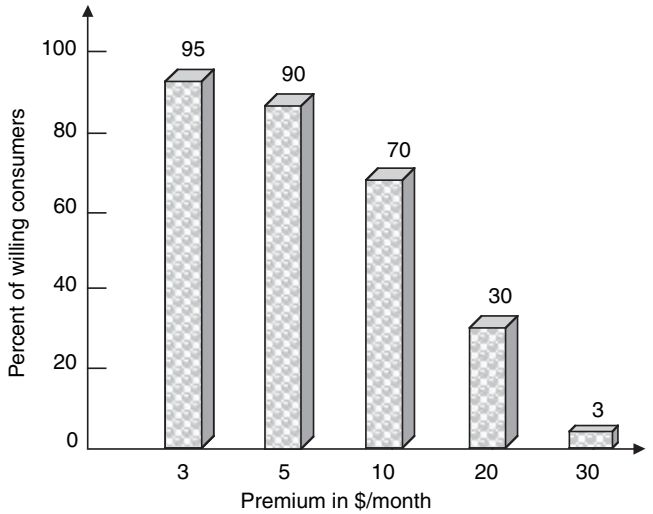

FIGURE 1.5 U.S. consumer willingness to pay premium for green power. (From Rahman, S., Green Power, *IEEE Power and Energy*, January–February 2003, p. 32.)

References

1. U.S. Department of Energy, International Energy Outlook 2004 with Projections to 2020, DOE Office of Integrated Analysis and Forecasting, April 2004.
2. Felix, F., State of the Nuclear Economy, *IEEE Spectrum*, November 1997, pp. 29–32.
3. Rahman, S., Green Power, *IEEE Power and Energy*, January–February 2003, pp. 30–37.

2 Wind Power

The first use of wind power was to sail ships in the Nile some 5000 yr ago. Many civilizations used wind power for transportation and other purposes: The Europeans used it to grind grains and pump water in the 1700s and 1800s. The first windmill to generate electricity in the rural U.S. was installed in 1890. An experimental grid-connected turbine with as large a capacity as 2 MW was installed in 1979 on Howard Knob Mountain near Boone, NC, and a 3-MW turbine was installed in 1988 on Berger Hill in Orkney, Scotland.

Today, even larger wind turbines are routinely installed, commercially competing with electric utilities in supplying economical, clean power in many parts of the world.

The average turbine size of wind installations was 300 kW until the early 1990s. New machines being installed are in the 1- to 3-MW capacity range. Wind turbines of 5-MW capacity have been fully developed and are under test operation in several countries, including the U.S. Figure 2.1 is a conceptual layout of a modern multi-megawatt wind tower suitable for utility-scale applications.[1]

Improved turbine designs and plant utilization have contributed to a decline in large-scale wind energy generation costs from 35 cents/kWh in 1980 to 3 to 4 cents/kWh in 2004 at favorable locations (Figure 2.2). At this price, wind energy has become the least expensive new source of electric power in the world, less expensive than coal, oil, nuclear, and most natural-gas-fired plants, competing with these traditional sources on its own economic merit. Hence, it has become economically attractive to utilities and electric cooperatives, with 30% growth from 1993 to 2003. Worldwide, over 40,000 MW of wind capacity has been installed, and more than 100,000-MW capacity by 2010 is predicted.

Major factors that have accelerated the development of wind power technology are as follows:

- High-strength fiber composites for constructing large, low-cost blades
- Falling prices of the power electronics associated with wind power systems
- Variable-speed operation of electrical generators to capture maximum energy
- Improved plant operation, pushing the availability up to 95%
- Economies of scale as the turbines and plants are getting larger in size
- Accumulated field experience (the learning-curve effect) improving the capacity factor up to 40%

2.1 WIND POWER IN THE WORLD

Because wind energy has become the least expensive source of new electric power that is also compatible with environment preservation programs, many countries promote wind power technology by means of national programs and market incentives.

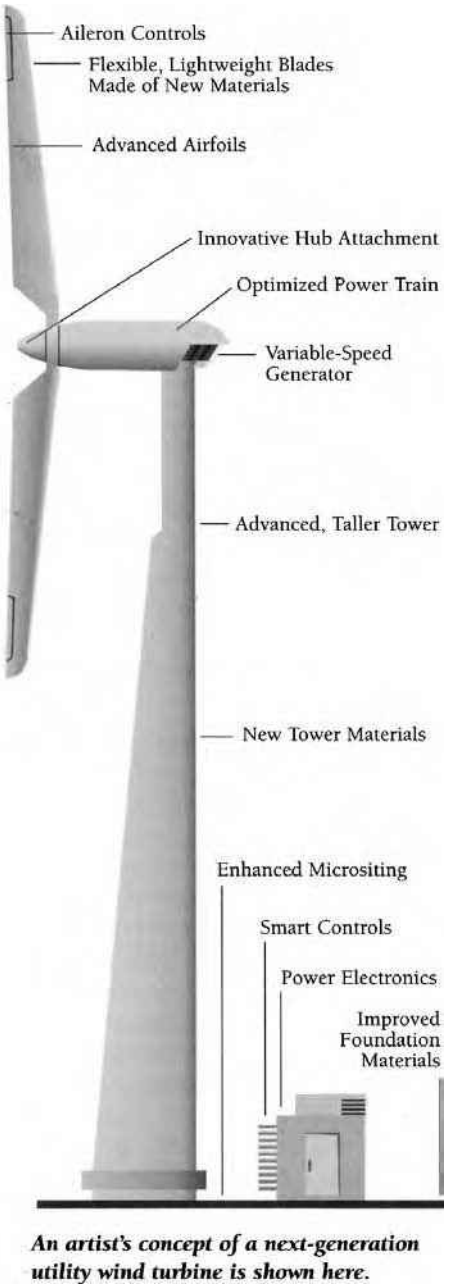

FIGURE 2.1 Modern wind turbine for utility-scale power generation.

The International Energy Agency (IEA), with funding from 14 countries, supports joint research projects and information exchange on wind power development.[2] The countries involved are Austria, Canada, Denmark, Finland, Germany, Italy, Japan,

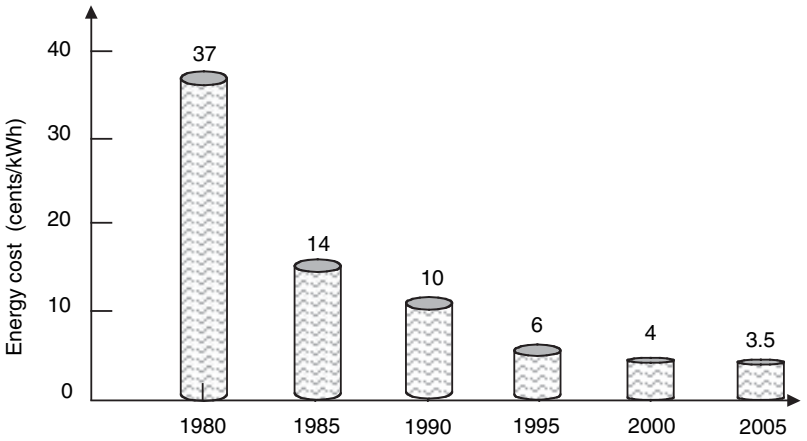

FIGURE 2.2 Declining cost of wind-generated electricity. (From AWEA; U.S. DOE; IEA.)

the Netherlands, New Zealand, Norway, Spain, Sweden, the U.K., and the U.S. By the beginning of 1995, more than 25,000 grid-connected wind turbines were operating in the IEA member countries, amounting to a rated power capacity of about 3,500 MW. Collectively, these turbines produced more than 6 million MWh of energy in 1995. In 2001, the worldwide wind power capacity was about 25,000 MW. Germany leads the way, followed by the U.S., Spain, Denmark, and India. In Germany, 8% of the electricity comes from renewable sources.

Table 2.1, with data compiled from various industry sources,[3] lists the added and accumulated capacity in various regions of the world during 2001 and 2002. The total accumulative wind capacity in 2002 worldwide was 32,037 MW. Of that, 7,227 MW was added in 2002, resulting in a 22.5% annual growth rate. A staggering 85% (6,163 MW) of the added capacity in 2002 was in Europe. The Global WindPower 2004 exposition in Chicago organized by the American Wind Energy Association (AWEA) and the European Wind Energy Association (EWEA) announced to its 3,500 delegates that 8,113-MW wind capacity was added globally in 2003 with the investment value of $9 billion. This represents a 26% growth rate and brings the cumulative total to 39,294 MW. The most explosive growth occurred in Germany.

The Canadian government announced the availability of C$260 million for the wind power industry to increase the current capacity of 200 MW in 2001 to 1000 MW by 2016. The 75-MW McBride Lake wind farm was completed in 2003 with 114 Vestas turbines at a cost of U.S. $64 million. It is located in Alberta, just east of the Rocky Mountains in the heart of Canada's fossil fuel production region.

Hydro-Quebec in 2003 announced 1000 MW of new wind energy to be added: 750 MW by Cartier Wind Energy, and 250 MW by Northland Power. Both of these prime contractors have selected 660 GE wind turbines of 1.5-MW capacity, to be commissioned between 2006 and 2012.

The outback of Western Australia, mostly off-grid, relies on diesel generators for electricity. A typical power plant provides 0.5 to 20 MW power at 240-V AC

TABLE 2.1
Installed Wind Capacity in Major Regions of the World

Region	Added MW in 2001	Accumulated MW in 2001	Added MW in 2002	Accumulated MW in 2002	Percentage Added in 2002
Americas	1745	4593	494	5087	6.8
Europe	4527	17,812	6163	23,832	85.3
South and East Asia	292	1870	291	2186	4.0
OECD Pacific	259	478	251	730	3.5
All other	1	175	27.3	202	0.4
Total World	6824	24,927	7227	32,037	100

Note: In the U.S., 1,687 MW was added in 2003 (36% increase over 2002); in Europe, the total cumulative capacity grew to 28,401 MW in 2003 (23% increase over 2002); globally in 2003, 8,113 MW of new wind capacity was added at $9 billion investment value to bring the cumulative total to 39,294 MW; the average growth rate of wind power from 1993–2003 was 30%.

Source: Gipe, P., The BTM Wind Report: World Market Update, *Renewable Energy World*, July–August 2003, pp. 66–83.

within the township boundaries. This electricity cost is significantly higher than that paid by dwellers in grid-connected cities. The region is flat and dry with bright sunlight and an average wind speed of 7 to 8 m/sec. The outback is favorable for renewables, especially wind power with government subsidies. About 20% of the total electricity in this region now comes from all renewable power sources of 18,000-MW total capacity.

Pacific Hydro Limited in Australia is installing a 180-MW wind farm in Portland, Victoria. The project will be the largest in the southern hemisphere. TXU Australia, a local utility, has agreed to purchase 50% of the wind farm output for a 10-yr period.

Wind power generation is the workhorse of renewable energy sources around the world. Even so, it is still a small percentage of the total energy sources. In the total global installed capacity of almost 3000 GW, wind power in 2004 represented only 45 GW (about 1.5%) of the total installed capacity. With the capacity factor around 35%, it generates a mere ½% of the energy. From the perspective of its vast potential, wind power has yet a long way to grow and mature. It has, however, started fast growth in that direction. The U.S. National Renewable Laboratory (NREL) and the United Nations Environment Program are jointly working on a new initiative to expand wind resource mapping and development throughout the world, especially in Africa, Asia, and Latin America.

Much of the new wind power development around the world can be attributed to government policies to promote renewable energy sources. The U.S.' renewable energy production and investment tax credits, the nonfossil fuel obligation of the U.K., Canada's wind power production incentive, and India's various tax rebates and exemptions are examples of such programs.

TABLE 2.2
U.S. States in Order of Wind Power Generating Potential

1. North Dakota	10. Iowa
2. Texas	11. Colorado
3. Kansas	12. New Mexico
4. South Dakota	13. Idaho
5. Montana	14. Michigan
6. Nebraska	15. New York
7. Wyoming	16. Illinois
8. Oklahoma	17. California
9. Minnesota	

Note: By way of comparison, Germany's potential is 100 GW; North Dakota's potential, 250 GW.

Source: Data from American Wind Energy Association.

2.2 U.S. WIND POWER DEVELOPMENT

About 90% of the usable wind resource in the U.S. lies in the Great Plains. The Energy Information Administration estimates that the U.S. wind capacity will reach 12,000 MW by 2015. Of this, utilities and wind power developers have announced plans for more than 5,000 MW of new capacity in 15 states by 2006. The 1992 Energy Policy Act initially specified 1.5 cents /kWh, which has now been adjusted to 1.8 cents/kWh for the first 10 yr of production to offset hidden subsidies for fossil fuel generation. AWEA estimates that wind energy in the U.S. could contribute to reduction of about 20% of the CO_2 emission that the U.S. has agreed to eliminate by 2010. Table 2.2 lists the U.S. states with the wind resources in the order of their potentials.

Large-scale wind power development in the U.S. has been going on since the late 1970s. In 1979, a 2-MW experimental machine was installed jointly by the Department of Energy and NASA on Howard Knob Mountain near Boone, NC. The system was designed and built by the General Electric Company using two 61-m-diameter rotor blades from the Boeing Aerospace Corporation. It was connected to the local utility grid and operated successfully.

Since 1984, the wind-generated electricity delivered to customers has been increasing rapidly, as seen in Figure 2.3, and the installed capacity in the U.S., along with that in Europe and the world, is shown in Figure 2.4. Until the late 1980s, most wind power plants in the U.S. were owned and operated by private investors or cooperatives in California, where more than 1,500 MW of wind-generating capacity was in operation by the end of 1991. That growth continues even today. The major benefit to the local utility company, Southern California Edison, is the elimination of the need to build new generating plants and transmission lines.

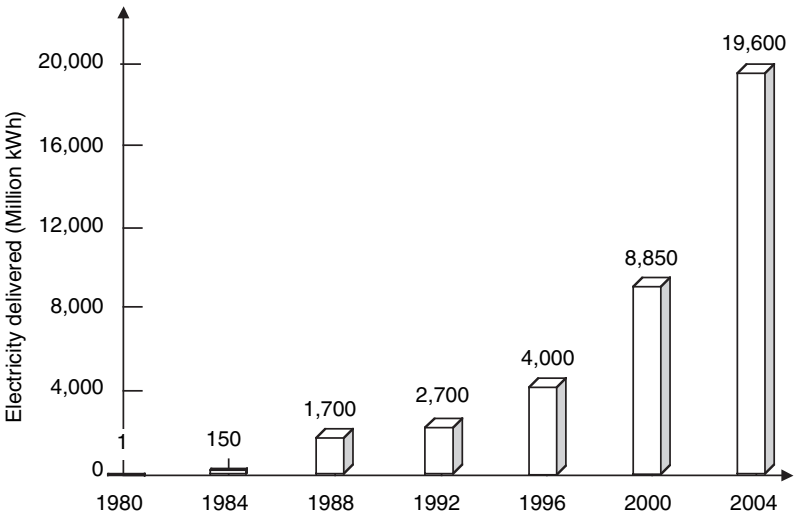

FIGURE 2.3 Electricity generated by U.S. wind power plants since 1984. (From AWEA and U.S. DOE.)

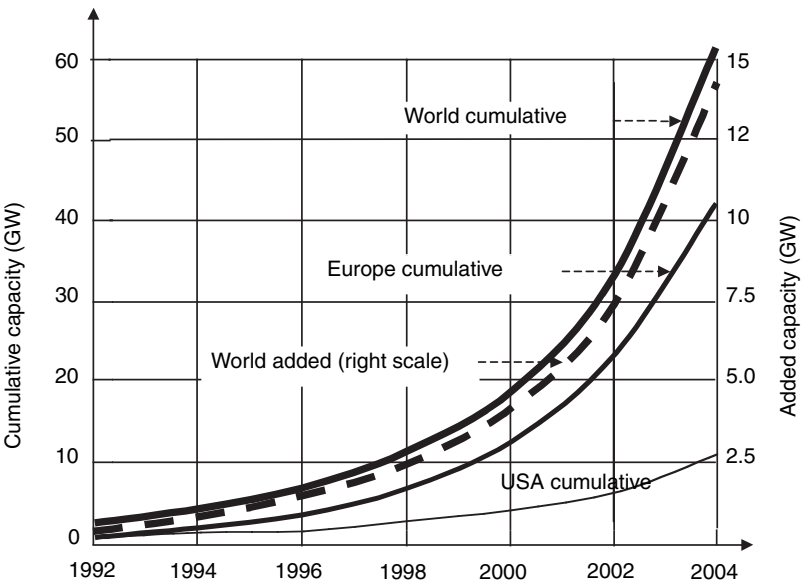

FIGURE 2.4 Added and cumulative wind power capacity in U.S., Europe, and the world. (From BTM Consultants, EWEA, AWEA, and IEA Wind Energy Annual Report, 2004.)

Technology development and the resulting price decline have caught the interest of a vast number of electric utilities outside California that are now actively developing wind energy as one element of the balanced resource mix.[4] Projects are being

built in Alaska, California, the Dakotas, Iowa, Minnesota, Texas, Vermont, Washington, and Wyoming. During 1994, several new wind energy projects were started, particularly in the Midwest. Iowa and Wyoming producers and utilities added a significant wind power capacity in the 1990s.[5] In 1995, a 35-MW utility-scale wind plant came online in Texas, which was expandable to a 250-MW capacity, enough to supply 100,000 homes. This plant has been under a 25-yr fixed-price contract to supply the City of Austin at 5 cents/kWh for generation and 1 cent/kWh for transmission. Nearly 700 MW of additional wind capacity was brought online in the U.S. by the end of 1996.

The Renewable Energy Portfolio Standard (RPS) and the renewable energy production tax credit (PTC) bill passed by the U.S. Senate in 2002 require utilities to produce 1% of their electricity from renewable sources by 2005, with this percentage rising steadily to 10% by 2020. The bill allows a credit trading system so that utilities can meet this requirement in the most cost-effective manner. The investments tax credit covers 30% of the investments cost for small systems below 75-kW capacity. The PTC provides 1.8 cents/kWh, indexed to inflation, during the first 10 yr of new wind plants.

The Net Metering Law, recently passed by 36 states, is proving advantageous to wind power economics. This law allows the owner of the plant to swap power with the grid over 1 yr. It allows power generation to be out of phase with the utilization. One can generate more power when the wind blows and use that from the grid when needed. The net use after the yearly swapping is billed at their regular retail rate, and the net excess fed back to the lines is given credit at their generation cost — typically 2 to 3 cents/kWh. School districts in the U.S. are also attracted to wind energy generation under this legislation. Because their load demand is highly skewed, mainly between 9 a.m. and 4 p.m. on weekdays for 9 months a year, a wind power plant with energy storage or a grid-connected power source would never be economical. However, the net energy metering law makes the wind plant economical. The Spirit Lake Community School District in Spirit Lake, IA, for example, installed wind turbines of capacity sufficient to meet its annual energy demand and save on the energy cost they paid to the utility company at a 9-cents/kWh rate. Their investment payback period was 6 to 7 yr. Although the turbines are located in the township areas and are in a geese migratory path, no bird kills or noise complaints have been reported.

The Wind-Powering America Initiative is a regionally based effort to increase the use of clean wind energy in the U.S. over the next two decades. The goals of the initiative are to:

- Meet 5% of the nation's energy needs with wind energy by 2020 (i.e., 80,000 MW installed)
- Double the number of states that have more than 20 MW of wind capacity by 2005 and triple it to 24 MW by 2010
- Increase wind power's contribution to federal electricity use to 5% by 2010

To achieve these goals, the initiative forms partnerships with federal agencies, state and local energy offices, Native American agencies, rural agencies and electrical

cooperatives, and utilities. The Department of Energy (DOE) has also established 21 partnerships with public and private bodies to develop turbines that can generate economical power in low-wind-speed regions that would open up much larger areas of the country for rapid development of wind power. Two counter-rotating turbines on each tower, a new concept presented in Chapter 19, has potential applications in low-wind regions.

At present, there are three large wind farms in the U.S.:

Northern Iowa: A 310-MW farm, with 180 to 200 turbines of 1.6-MW capacity each, under construction for a 2006 completion by MidAmerican Energy Company at a cost of $325 million.

Pacific Northwest: A 300-MW farm with 440 turbines, each rated 660 kW, installed over a 50-mi^2 area along the Oregon–Washington state line south of Walla Walla. The DOE's Bonneville Power Administration (BPA), which supplies about one half of the electricity used in the Pacific Northwest, has recently doubled the megawatthours of electricity it buys from wind projects. BPA has agreed to buy one third of the power from the state line wind project. BPA was in negotiation for up to 830-MW additional wind power, potentially making it the largest supplier of wind power in the U.S.

Texas: A 280-MW farm called King Mountain Wind Ranch in Upton County, West Texas.

The leading owners of wind farms in the U.S. are Florida Power & Light (FPL) Energy (2700 MW), Shell Wind (392 MW), American Electrical Power (310 MW), and PPM Energy (201 MW).

Two new 300-mi-long, 345-kV transmission lines were completed in Texas to help deliver wind power from the west to the load centers in the northern part of the state. New transmission lines are being planned to tap into the vast wind resource of the upper Great Plains states to take wind power to the load centers. Proposals for installing electrolyzers to obtain hydrogen and oxygen from wind power are also being examined. The hydrogen so obtained will be piped to the Chicago region for fuel cells, and the oxygen will be used to improve the combustion efficiency of the regional coal plants.

The state of Minnesota, in the early 1990s, mandated that Northern States Power acquire 425 MW of wind generation by 2002. The company developed about 100 MW of wind capacity over the next few years in the Buffalo Ridge–Lake Benton area in southwestern Minnesota near Holland and expanded to 425 MW by 2002. This area between the Mississippi and Missouri rivers has good steady winds and is accessible to transmission lines. To support this program, the state funded the windsmith education program at Minnesota West Community and Technical College to properly train the workforce with required skills to install, operate, and repair the wind power plants.

California, in late 2002, passed a bill that requires utilities to purchase 20% of their electricity from renewable energy producers by 2017, as against 12% at present, including hydroelectricity. Los Angeles Water and Power opened in 2004 a total of 80 turbines for 120-MW wind power in the Mojave Desert, 160 km north of Los Angeles. That boosted the city's power from the renewable sources from 2.2 to 3.7%.

New York State aims at 8% of its electricity coming from all renewable sources by 2012, excluding hydroelectricity. Its first 11.5-MW commercial wind farm was constructed in Madison County by Pacific Gas & Electric (PG&E). It consists of seven 1.65-MW Vestas turbines, each producing 24 million kWh of electric energy each year. The state also mandates that state agencies purchase 15% of their energy from renewable power generators.

The 541-m-tall Freedom Tower — the world's tallest building, proposed to replace the World Trade Center in New York City — will have wind turbines at the top. A cable suspension structure would create an open area above the building's 70 floors of office space and house the wind turbines that could provide 20% of the building's electric energy.

In Pennsylvania, potentials for utility-scale wind farms exist in the east–west belt around the Scranton–Wilkes Barre area and in a small area south of Pittsburgh. U.S. Wind Force of Wexford, PA, and Padoma Wind Power of LaJolla, CA, have formed a joint venture to finance, develop, construct, and sell wind farms up to 1500-MW total capacity in the mid-Atlantic region over the next 5 yr. It will comprise 10 or more sites in Maryland, West Virginia, and Pennsylvania. Even some educational institutions are getting involved in wind energy projects. In 2002, Drexel University in Philadelphia procured a 70-m-tall wind turbine that produced 4 million kWh a year, about 10% of its energy use.

During the 2000–2003 period, 900-MW new capacity was added in Texas, bringing the total to 1100 MW. A 204-MW wind farm is under construction in the eastern part of New Mexico. It will comprise 136 turbines, each of 1.5-MW capacity.

2.3 EUROPE AND THE U.K.

The wind power picture in Europe is rapidly changing. The 1995 projections on the expected wind capacity in 2000 were met in 1997, in approximately half of the time. Figure 2.5 depicts the wind capacity installed in European countries at the end of 2003. EWEA estimated that the EU's installed wind power capacity was 28,764 MW by the end of 2003, which was about 70% of the world's total. About 84% of the EU's capacity is installed in Germany, Spain, and Denmark. The new targets adopted by the EWEA are 40,000-MW capacity by 2010 and 100,000-MW by 2020. These targets form part of a series of policy objectives agreed upon by the association from time to time. Germany and Denmark lead Europe in wind power. Both have achieved phenomenal growth through guaranteed tariff based on the domestic electricity prices. Denmark's plan to install 750-MW new wind capacity by 2008 will bring the total to 4000 MW, supplying 25% of the total electricity by then.

Wind energy accounts for 4% of the total electricity used in Germany and 18% in Denmark. EWEA has increased its target for wind installation to 75 GW by 2010 and 180 GW by 2020. This means by 2010, EU will generate about 6% of European electricity, meeting the needs of some 90 million Europeans with all new electricity generation by wind, and meeting a third of the EU's total Kyoto commitment. The European wind industry has usually met or surpassed its targets in the past.

The EU manufactures about 80% of all wind turbines sold in the world. Riso National Laboratory of Denmark's 2002 edition of the annual status report on wind

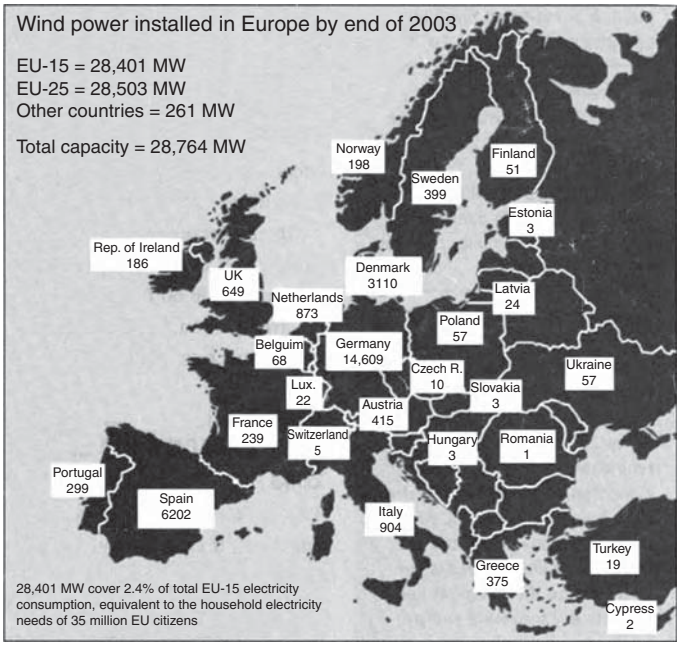

FIGURE 2.5 Installed wind capacity in European countries as of December 2003. (From *Renewable Energy World Magazine*, London, March–April 2004. With permission.)

industry, prepared by BTM Consult, gives the world's wind turbine market share breakdown as approximately 20% by Vestas, 18% by NEG Micon, 13% Enercon, 9% each by GE Wind, Gamesa, and Bonus, and 6% by Nordex.

In Denmark, wind energy cooperatives have dominated the development of wind power, with 80% of all Danish wind turbines privately owned by the cooperatives and local farmers. More than 100,000 families are members of the wind energy cooperatives. Recently, utilities have been increasing their role in establishing large offshore wind farms.

Spain, having no oil or natural gas reserves of its own and only a few coal mines, strongly relies on the external sources of energy. However, it has excellent wind resources, which are now under active development. In 1994, it had a mere 73 MW of wind capacity installed, which grew to 2,500 MW in 2000, producing over 6,000 GWh of electricity. The capacity has almost doubled each year from 1994 to 2000. In the Navarra region, wind supplies 22% of the electricity, and the Galicia region expects to generate 45% of electricity from wind by 2005. Spain plans to install 10,000 MW of new capacity in the 2001–2010 period.

France has perhaps the second-largest wind energy potential in Europe, after the U.K. Estimates on potential annual energy production in France are more than 70 TWh on land and 90 TWh from offshore sites located within 10 km of the shore where the sea depth is less than 10 m. The total 160 TWh represents a third of the present electricity generation in France.

France produced 15% of electricity from renewables in 2000, and the target is 21% by 2010. A mere 70 MW of its wind power capacity was operational in 2000. However, ADME[6] reports that a rather aggressive goal is set for a minimum of 5 to 10 GW to produce 29 TWh by 2010. This is to be achieved via a new rate system by providing a minimum profitability for projects on medium-quality sites. Following the first 5 yr at a minimum fixed guaranteed rate, the specific rate for each project in year 6 to 15 is from the average capacity factor measured during the first 5 yr.

The two best wind resources in France are: (1) northwest, along the English Channel and the Atlantic Ocean (Brittany, Normandy, Picardy, etc.) and (2) southeast, along the Mediterranean Sea (Languedoc, Rhone Valley, etc.). Despite such a large potential, the total installed capacity was a mere 60 MW in July 2001. However, France launched a national program in 1996, EOLE 2005, to install 250 to 500 MW of capacity by 2005 and to reach 5000 MW of wind capacity by 2010.[7] Several incentives have also been offered for renewable power generators.

Italy's commitment to wind power is very ambitious under the EU's Renewable Directive. In 1990, it had only 1.5 MW of wind capacity, which increased to 560 MW in 2001 and is forecast to grow to 2,500 MW by 2010 under the incentive scheme CIP6/92.[8]

The U.K.'s Renewable Obligation (RO), which became effective April 2002, requires that the U.K. utilities obtain a specified percentage of electricity from renewable sources, rising to 10% by 2010. They may produce or buy green electricity to meet the obligation or will have to pay a penalty. In 2004, there were 1000-MW wind plants in the pipeline, which will bring the total to 1650 MW by 2005. In a major boost to the U.K.'s wind power, the government has awarded planning consent for 19 offshore sites within a 12-mi shore limit to install 1500 turbines for a total capacity of 1500 MW, which will meet 1.5% of the U.K.'s energy need. The Scottish government has given permission for an additional 200-MW offshore wind farms with 60 turbines 9 km from the coast of Galloway.

2.4 INDIA

India has a 9 million km^2 land area with a population over one billion, of which 75% live in agrarian rural areas. The total power-generating capacity has grown from 1,300 MW in 1950 to about 100,000 MW in 1998 and 160,000 MW in 2004. The 2010 projections are 150,000 MW peak load, 200,000 MW peak capacity, and 900,000 GWh annual energy production. This amounts to an annual growth rate of about 9%. At this rate, India needs to add a 15,000-MW capacity every year. The electricity network reaches over 500,000 villages and powers 11 million agricultural water-pumping stations. Coal is the primary source of energy used to generate 70% of electricity. The remaining 25% comes from hydroelectricity, 4% from nuclear, and 1% from all other sources. However, coal mines are concentrated in certain areas, and transporting coal to other parts of the country is not easy. A third of the total electricity is used in the rural areas, where three fourths of the population lives. The transmission and distribution loss in the electrical network is relatively high at 25%. The environment in heavily populated areas is more of a concern in India than

TABLE 2.3
Installed Wind Power Generation Capacity in India by End of 2001

State	Installed Capacity (MW)
Tamil Nadu	828
Maharashtra	236
Gujarat	167
Andhra Pradesh	92
Karnataka	50
Madhya Pradesh	23
Rajasthan	14
All others	97
Total	1507

in other countries. For these reasons, the distributed power generation, such as wind plants near the load centers, is of great interest to the state-owned electricity boards.

India has initiated research and development to harness renewable energy sources since the 1970s. The country has adopted aggressive plans for developing these renewables. As a result, India today has a high growth rate in wind capacity and is one of the largest producers of wind energy in the world.[9–10] In 1998, it had over 1000-MW wind power capacity, 150 MW from small hydroelectric plants, 100 MW from biomass, and 30 MW from solar PV. In 2001, India's wind capacity was 1500 MW and India expects to install more than 1500 MW of wind power during the 2002 to 2007 5-yr plan. Suzlon Energy Limited has recently installed 1-MW turbines. Previously, only much lower-capacity machines were being installed. This indicates that wind energy is fast becoming a part of the national energy portfolio. Wind and PV power sources are not limited to lighting, pumping water, and telecommunication but also meet the entire electricity needs of isolated villages, hospitals, offshore oil exploration, and mining platforms. The Indian Renewable Energy Development Agency is set up specially for financing renewable energy projects at favorable terms.

It is estimated that India has about 45,000 MW of wind power potential in the most promising states from Rajasthan in the northeast to Tamil Nadu in the south. The government has identified 77 sites for economically feasible wind power generation, with a generating capacity of 4,000 MW of grid-quality power. Out of this, over 1,500 MW was installed by the end of 2001 as listed by states in Table 2.3. BTM Consultants projects that 2,800 MW will accumulate by 2005. With this, India now ranks among the first five countries in the world in wind power generation and provides attractive incentives to local and foreign investors. The Tata Energy Research Institute provides a link between the investors in India and in the U.S. Major incentives for renewable power plants in India are as follows:

- 100% depreciation of the total capital cost in the first year of operation
- 100% tax rebate on income from power generation for the first 10 yr
- Exemption form custom duty, excise duty, and sales taxes

India targets 10-GW rural capacity from renewable sources by 2012, sufficient for 18,000 remote villages. This represents 10% of the planned additional power capacity of the country. Over 80,000 villages still do not have electricity.

References

1. U.S. Department of Energy, Wind Energy Programs Overview, NREL Report No. DE-95000288, March 1995.
2. International Energy Agency, Wind Energy Annual Report, International Energy Agency Report by NREL, March 1995.
3. Gipe, P., The BTM Wind Report: World Market Update, *Renewable Energy World*, July–August 2003, pp. 66–83.
4. Utility Wind Interest Group, Utilities Move Wind Technology Across America, November 1995.
5. Anson, S., Sinclair, K., and Swezey, B., Profiles in Renewables Energy, Case Studies of Successful Utility-Sector Projects, DOE/NREL Report No. DE-930000081, National Renewable Energy Laboratory, Golden, Colorado, August 1994.
6. Chabot, B. and Saulnier, B., Fair and Efficient Rates for Large-Scale Development of Wind Power: the New French Solution, Canadian Wind Energy Association Conference, Ottawa, October 2001.
7. Belhomme, R., Wind Power Developments in France, *IEEE Power Engineering Review*, October 2002, pp. 21–24.
8. Pane, E. D., Wind Power Developments in France, *IEEE Power Engineering Review*, October 2002, pp. 25–28.
9. Gupta, A. K., Power Generation from Renewables in India, Ministry of Non-Conventional Energy Sources, New Delhi, India, 1997.
10. Hammons, T. J., Ramakumar, R., Fraser, M., Conners, S. R., Davies, M., Holt, E. A., Ellis, M., Boyers, J., and Markard, J., Renewable Energy Technology Alternatives for Developing Countries, *IEEE Power Engineering Review*, December 1997, pp. 10–21.

3 Wind Speed and Energy

The wind turbine captures the wind's kinetic energy in a rotor consisting of two or more blades mechanically coupled to an electrical generator. The turbine is mounted on a tall tower to enhance the energy capture. Numerous wind turbines are installed at one site to build a wind farm of the desired power generation capacity. Obviously, sites with steady high wind produce more energy over the year.

Two distinctly different configurations are available for turbine design, the horizontal-axis configuration (Figure 3.1) and the vertical-axis configuration (Figure 3.2). The horizontal-axis machine has been the standard in Denmark from the beginning of the wind power industry. Therefore, it is often called the *Danish wind turbine*. The vertical-axis machine has the shape of an egg beater and is often called the *Darrieus rotor* after its inventor. It has been used in the past because of its specific structural advantage. However, most modern wind turbines use a horizontal-axis design. Except for the rotor, most other components are the same in both designs, with some differences in their placements.

3.1 SPEED AND POWER RELATIONS

The kinetic energy in air of mass m moving with speed V is given by the following in joules:

$$\text{kinetic energy} = \frac{1}{2}mV^2 \tag{3.1}$$

The power in moving air is the flow rate of kinetic energy per second in watts:

$$\text{power} = \frac{1}{2}(\text{mass flow per second})V^2 \tag{3.2}$$

If
P = mechanical power in the moving air (watts),
ρ = air density (kg/m^3),
A = area swept by the rotor blades (m^2), and
V = velocity of the air (m/sec),

then the volumetric flow rate is AV, the mass flow rate of the air in kilograms per second is ρAV, and the mechanical power coming in the upstream wind is given by the following in watts:

$$P = \frac{1}{2}(\rho AV)V^2 = \frac{1}{2}\rho AV^3 \tag{3.3}$$

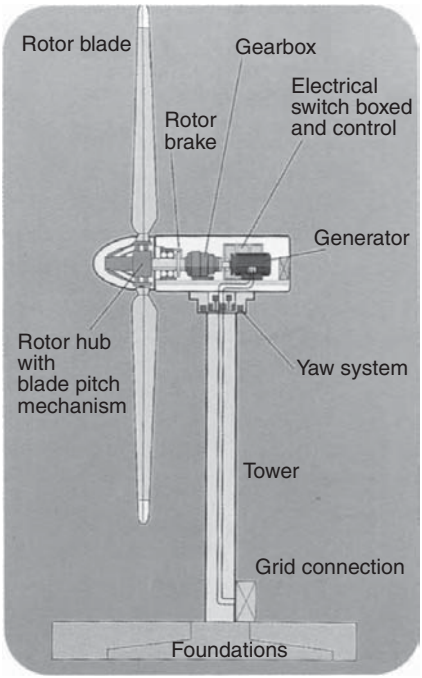

FIGURE 3.1 Horizontal-axis wind turbine showing major components. (Courtesy: Energy Technology Support Unit, DTI, U.K. With permission.)

FIGURE 3.2 Vertical-axis 33-m-diameter wind turbine built and tested by DOE/Sandia National Laboratory during 1994 in Bushland, TX.

Two potential wind sites are compared in terms of the specific wind power expressed in watts per square meter of area swept by the rotating blades. It is also referred to as the power density of the site, and is given by the following expression in watts per square meter of the rotor-swept area:

$$\text{specific power of the site} = \frac{1}{2}\rho V^3 \tag{3.4}$$

This is the power in the upstream wind. It varies linearly with the density of the air sweeping the blades and with the cube of the wind speed. The blades cannot extract all of the upstream wind power, as some power is left in the downstream air that continues to move with reduced speed.

3.2 POWER EXTRACTED FROM THE WIND

The actual power extracted by the rotor blades is the difference between the upstream and downstream wind powers. Using Equation 3.2, this is given by the following equation in units of watts:

$$P_o = \frac{1}{2}(\text{mass flow per second})\left\{V^2 - V_o^{\,2}\right\} \tag{3.5}$$

where
P_o = mechanical power extracted by the rotor, i.e., the turbine output power,
V = upstream wind velocity at the entrance of the rotor blades, and
V_o = downstream wind velocity at the exit of the rotor blades.

Let us leave the aerodynamics of the blades to the many excellent books available on the subject, and take a macroscopic view of the airflow around the blades. Macroscopically, the air velocity is discontinuous from V to V_o at the "plane" of the rotor blades, with an "average" of ½(V + V_o). Multiplying the air density by the average velocity, therefore, gives the mass flow rate of air through the rotating blades, which is as follows:

$$\text{mass flow rate} = \rho A \frac{V + V_o}{2} \tag{3.6}$$

The mechanical power extracted by the rotor, which drives the electrical generator, is therefore:

$$P_o = \frac{1}{2}\left[\rho A \frac{(V + V_o)}{2}\right](V^2 - V_o^2) \tag{3.7}$$

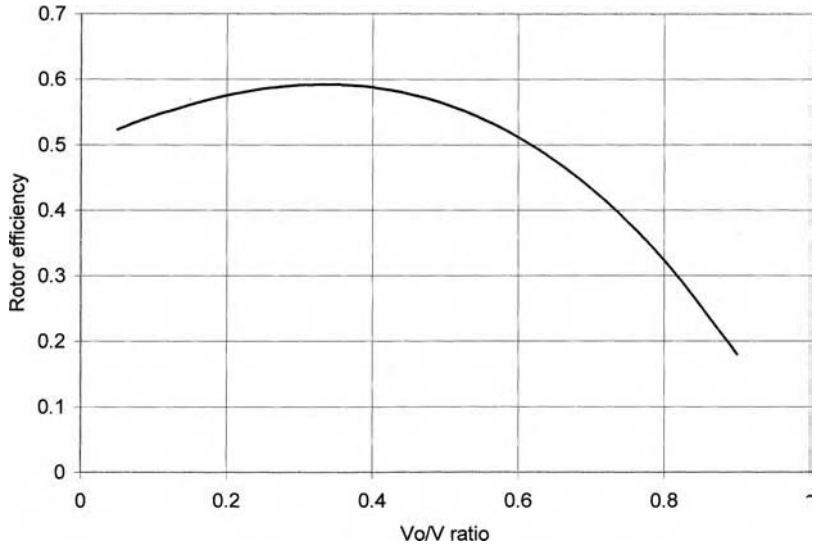

FIGURE 3.3 Rotor efficiency vs. V_o/V ratio has a single maximum. Rotor efficiency is the fraction of available wind power extracted by the rotor and fed to the electrical generator.

The preceding expression is algebraically rearranged in the following form:

$$P_o = \frac{1}{2}\rho A V^3 \frac{\left(1+\frac{V_o}{V}\right)\left[1-\left(\frac{V_o}{V}\right)^2\right]}{2} \tag{3.8}$$

The power extracted by the blades is customarily expressed as a fraction of the upstream wind power in watts as follows:

$$P_o = \frac{1}{2}\rho A V^3 C_p \tag{3.9}$$

where

$$C_p = \frac{\left(1+\frac{V_o}{V}\right)\left[1-\left(\frac{V_o}{V}\right)^2\right]}{2} \tag{3.10}$$

Comparing Equation 3.3 and Equation 3.9, we can say that C_p is the fraction of the upstream wind power that is extracted by the rotor blades and fed to the electrical

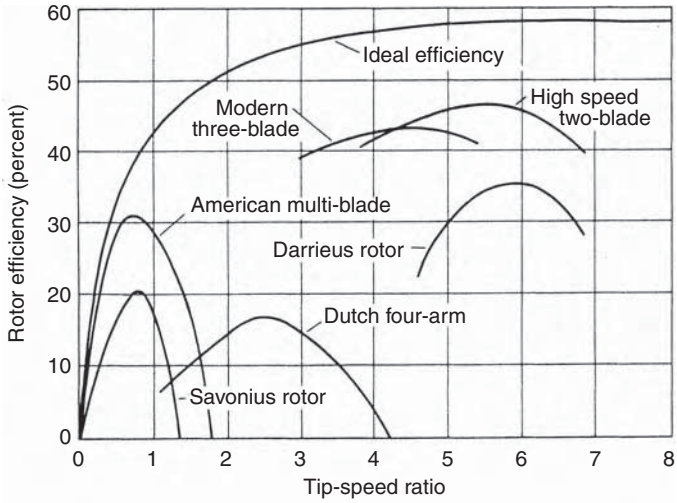

FIGURE 3.4 Rotor efficiency vs. V_o/V ratio for rotors with different numbers of blades. Two-blade rotors have the highest efficiency.

generator. The remaining power is dissipated in the downstream wind. The factor C_p is called the *power coefficient* of the rotor or the *rotor efficiency.*

For a given upstream wind speed, Equation 3.10 clearly shows that the value of C_p depends on the ratio of the downstream to the upstream wind speeds (V_o/V). A plot of power vs. (V_o/V) shows that C_p is a single-maximum-value function (Figure 3.3). It has the maximum value of 0.59 when the V_o/V ratio is one third. The maximum power is extracted from the wind at that speed ratio, i.e., when the downstream wind speed equals one third of the upstream speed. Under this condition (in watts):

$$P_{max} = \frac{1}{2}\rho A V^3 \times 0.59 \tag{3.11}$$

The theoretical maximum value of C_p is 0.59. C_p is often expressed as a function of the rotor tip-speed ratio (TSR) as shown in Figure 3.4. TSR is defined as the linear speed of the rotor's outermost tip to the upstream wind speed. The aerodynamic analysis of the wind flow around the moving blade with a given pitch angle establishes the relation between the rotor tip speed and the wind speed. In practical designs, the maximum achievable C_p ranges between 0.4 and 0.5 for modern high-speed two-blade turbines, and between 0.2 and 0.4 for slow-speed turbines with more blades. If we take 0.5 as the practical maximum rotor efficiency, the maximum power output of the wind turbine becomes a simple expression (in watts per square meter of swept area):

$$P_{max} = \frac{1}{4}\rho V^3 \tag{3.12}$$

3.3 ROTOR-SWEPT AREA

As seen in the preceding power equation, the output power of the wind turbine varies linearly with the rotor-swept area. For the horizontal-axis turbine, the rotor-swept area is:

$$A = \frac{\pi}{4} D^2 \tag{3.13}$$

where D is the rotor diameter.

For the Darrieus vertical-axis machine, determination of the swept area is complex as it involves elliptical integrals. However, approximating the blade shape as a parabola leads to the following simple expression for the swept area:

$$A = \frac{2}{3}(\text{maximum rotor width at the center})(\text{height of the rotor}) \tag{3.14}$$

The wind turbine efficiently intercepts the wind energy flowing through the entire swept area even though it has only two or three thin blades with solidity between 5 and 10%. The solidity is defined as the ratio of the solid area to the swept area of the blades. The modern two-blade turbine has a low solidity ratio. It is more cost-effective as it requires less blade material to sweep large areas.

3.4 AIR DENSITY

Wind power also varies linearly with the air density sweeping the blades. The air density ρ varies with pressure and temperature in accordance with the gas law:

$$\rho = \frac{p}{RT} \tag{3.15}$$

where
p = air pressure,
T = temperature on the absolute scale, and
R = gas constant.

The air density at sea level at 1 atm (14.7 psi) and 60°F is 1.225 kg/m^3. Using this as a reference, ρ is corrected for the site-specific temperature and pressure. The temperature and the pressure both vary with the altitude. Their combined effect on the air density is given by the following equation, which is valid up to 6,000 m (20,000 ft) of site elevation above sea level:

$$\rho = \rho_o e^{-\left\{\frac{0.297 H_m}{3048}\right\}} \tag{3.16}$$

where H_m is the site elevation in meters.

Equation 3.16 is often written in a simple form:

$$\rho = \rho_o - (1.194 \times 10^{-4} H_m) \tag{3.17}$$

The air density correction at high elevations can be significant. For example, the air density at 2000-m elevation would be 0.986 kg/m^3, 20% lower than the 1.225 kg/m^3 value at sea level.

For ready reference, the temperature varies with the elevation as follows in °C:

$$T = 15.5 - \frac{19.83 H_m}{3048} \tag{3.18}$$

3.5 GLOBAL WIND PATTERNS

Uneven heating and the rotation of the earth create the global wind patterns. The warm air rises near the equator, and the surface air moves toward the equator to replace the rising air. As a result, two major belts of global wind patterns are created. The wind between the equator and about 30° north and south latitudes moves east to west. These are called the trade winds because of their use in sailing ships on major trade routes in the past. There is little wind near the equator, as the air slowly rises upward rather than moving westward. The prevailing winds move from west to east in two belts between latitudes 30° and 60° north and south of the equator. This motion is caused by circulation of the trade winds in a closed loop. In many countries where the weather systems come from the west, the wind speed in the west is generally higher than in the east.

Two features of the wind — its speed and direction — are used in describing and forecasting weather. The wind direction is measured with a weather vane, a broad, flat blade attached to a spoke pivoted at one end. The wind impinging on the blade turns the spoke and lines up the blades in the wind direction. The wind direction is indicated by an arrow fastened to the spoke or by an electric meter remotely controlled by the weather vane. The wind direction is often indicated in terms of a 360° circular scale. On such a scale, 0° indicates the north, 90° indicates the east, 180° indicates the south, and 270° indicates the west.

The speed is measured with an instrument called an *anemometer*, which comes in several types. The most common type has three or four cups attached to spokes on a rotating shaft. The wind turns the cups and the shaft. The angular speed of the spinning shaft is calibrated in terms of the linear speed of the wind. In the U.S., the wind speed is reported in miles per hour or in nautical miles per hour (knots). In other countries, it is reported in kilometers per hour or sometimes in meters per second.

Ultrasonic anemometers available in the industry measure the wind speed and direction in one single unit. Figure 3.5 is one such meter from Gill Instruments in the U.K. It has optional output formats for wind speed and also detects the wind

FIGURE 3.5 Ultrasonic wind speed and direction meter. (From Gill Instruments Ltd., Lymington, U.K. With permission.)

direction. The two-axis design is suitable for fixed applications such as wind farms, meteorology, naval, aviation, and marine use. Designs with heaters are also available for use in extreme cold. The ultrasonic anemometer has no moving parts, and hence is more reliable and has a fast response. It requires no calibration at the installation site.

Industry-standard anemometers sample wind speed every 2 sec for 10 min and average these 300 data points every 10 min. A log is kept of these 10-min averages all day long. The raw speed data can be processed with suitable software if needed.

An optical sensor developed at the Georgia Institute of Technology in Atlanta may soon replace the conventional anemometer and improve measurement accuracy. The mechanical anemometer can register readings at a single location — where it is actually placed. A complex array of traditional anemometers is needed to monitor the wind speed over a large area such as in a wind farm. The new optical sensor is able to measure average crosswind speeds and directions over a long distance and is claimed to be more accurate than the mechanical anemometer. Figure 3.6 depicts the sensor's layout and the working principle. The sensor is mounted on a large telescope and a helium–neon laser of about 50-mm diameter. It projects a beam of light onto a target about 100 m away. The target is made of the type of reflective material used on road signs. The sensor uses a laser beam degradation phenomenon known as the *residual turbulent scintillation effect*. The telescope collects laser light reflected from the target and sends it through a unique optical path in the instrument.

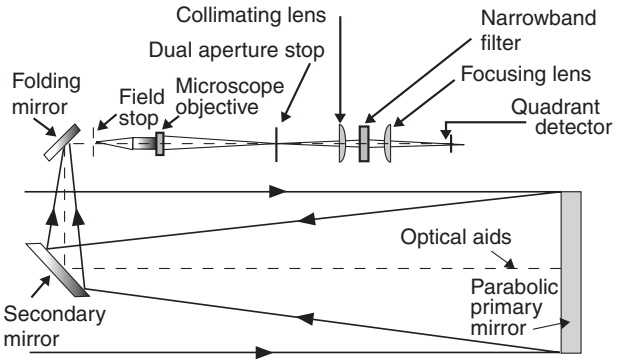

FIGURE 3.6 Optical wind speed sensor construction. (From Georgia Institute of Technology, Atlanta, GA. With permission.)

Each of the two tiny detectors monitors a spot on the target inside the laser beam and picks up shadowy waves or fringes moving across the laser beam. The waves are visible on the target itself. The fringes look much like the shadows of waves seen at the bottom of a swimming pool on a sunny day. Something similar to these shadows can be seen if a turbulent wind is viewed with a laser beam. Each detector registers the moment when a dark fringe passes its view. By digitizing the detected points, a computer can measure time and separation and, therefore, the average wind speed. The major advantage of the optical sensor is that it can measure the wind speed over a wide range from a faint wind to a gusty wind over a large area.

3.6 WIND SPEED DISTRIBUTION

Having a cubic relation with power, wind speed is the most critical data needed to appraise the power potential of a candidate site. The wind is never steady at any site. It is influenced by the weather system, the local land terrain, and its height above the ground surface. Wind speed varies by the minute, hour, day, season, and even by the year. Therefore, the annual mean speed needs to be averaged over 10 yr or more. Such a long-term average gives a greater confidence in assessing the energy-capture potential of a site. However, long-term measurements are expensive and most projects cannot wait that long. In such situations, the short-term data, for example, over 1 yr, is compared with long-term data from a nearby site to predict the long-term annual wind speed at the site under consideration. This is known as the *measure, correlate, and predict* (mcp) technique.

Because wind is driven by the sun and the seasons, the wind pattern generally repeats over a period of 1 yr. The wind site is usually described by the speed data averaged over calendar months. Sometimes, the monthly data is aggregated over the year for brevity in reporting the overall "windiness" of various sites. Wind speed variations over the period can be described by a probability distribution function.

3.6.1 Weibull Probability Distribution

The variation in wind speed is best described by the Weibull probability distribution function h with two parameters, the shape parameter k, and the scale parameter c. The probability of wind speed being v during any time interval is given by the following:

$$h(v) = \left(\frac{k}{c}\right)\left(\frac{v}{c}\right)^{(k-1)} e^{-\left(\frac{v}{c}\right)^k} \quad \text{for } 0 < v < \infty \tag{3.19}$$

In the probability distribution chart, h over a chosen time period is plotted against v, where h is defined as follows:

$$h = \frac{\text{fraction of time wind speed is between } v \text{ and } (v + \Delta v)}{\Delta v} \tag{3.20}$$

By definition of the probability function, the probability that the wind speed will be between zero and infinity during the entire chosen time period is unity, i.e.:

$$\int_0^\infty h\,dv = 1 \tag{3.21}$$

Because we often choose a time period of 1 yr, we express the probability function in terms of the number of hours in the year, such that:

$$h = \frac{\text{number of hours per year the wind is between } v \text{ and } (v + \Delta v)}{\Delta v} \tag{3.22}$$

The unit of h is hours per year per meter per second, and the integral (Equation 3.21) now becomes 8760 (the total number of hours in the year) instead of unity.

Figure 3.7 is the plot of h vs. v for three different values of k in Equation 3.19. The curve on the left with $k = 1$ has a heavy bias to the left, where most days are windless ($v = 0$). The curve on the right with $k = 3$ looks more like a normal bell-shaped distribution, where some days have high wind and an equal number of days have low wind. The curve in the middle with $k = 2$ is a typical wind speed distribution found at most sites. In this distribution, more days have speeds lower than the mean speed, whereas a few days have high wind. The value of k determines the shape of the curve and hence is called the *shape parameter.*

The Weibull distribution with $k = 1$ is called the *exponential distribution*, which is generally used in reliability studies. For $k > 3$, it approaches the normal distribution, often called the *Gaussian* or the *bell-shaped distribution.*

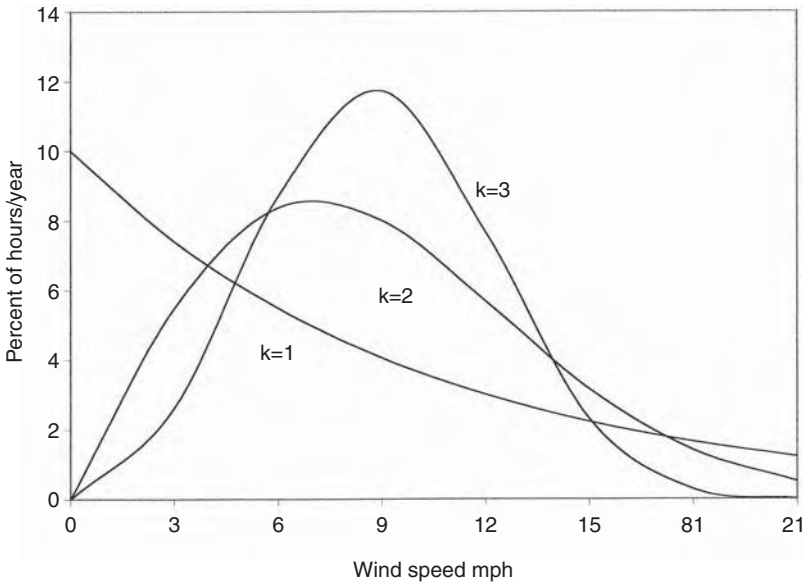

FIGURE 3.7 Weibull probability distribution function with scale parameter $c = 10$ and shape parameters $k = 1$, 2, and 3.

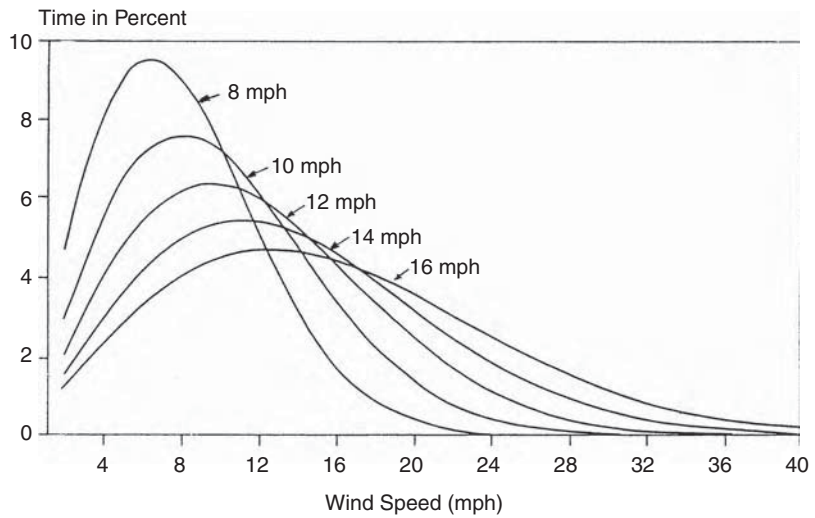

FIGURE 3.8 Weibull probability distribution with shape parameter $k = 2$ and scale parameters ranging from 8 to 16 mph.

Figure 3.8 shows the distribution curves corresponding to $k = 2$ with different values of c ranging from 8 to 16 mph (1 mph = 0.446 m/sec). For greater values of c, the curves shift right to the higher wind speeds. That is, the higher the c is, the

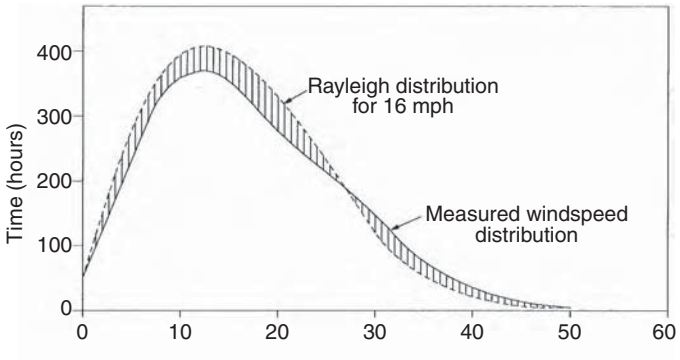

FIGURE 3.9 Rayleigh distribution of hours per year compared with measured wind speed distribution at St. Annes Head, Pembrokeshire, U.K.

greater the number of days that have high winds. Because this shifts the distribution of hours at a higher speed scale, c is called the *scale parameter.*

At most sites, wind speed has the Weibull distribution with $k = 2$, which is specifically known as the *Rayleigh distribution*. The actual measurement data taken at most sites compare well with the Rayleigh distribution, as seen in Figure 3.9. The Rayleigh distribution is then a simple and accurate enough representation of the wind speed with just one parameter, the scale parameter c.

Summarizing the characteristics of the Weibull probability distribution function:

$k = 1$ makes it the exponential distribution, $h = \lambda e^{-\lambda V}$ where $\lambda = 1/c$,

$k = 2$ makes it the Rayleigh distribution, $h = 2\lambda^2 v e^{-(\lambda v)^2}$, and

$k > 3$ makes it approach a normal bell-shaped distribution. (3.23)

Because most wind sites would have the scale parameter ranging from 10 to 20 mph (about 5 to 10 m/sec) and the shape parameter ranging from 1.5 to 2.5 (rarely 3.0), our discussion in the following subsections will center around those ranges of c and k.

Figure 3.10 displays the number of hours on the vertical axis vs. the wind speed on the horizontal axis. The three graphs (a), (b), and (c) are the distributions with different scale parameters $c = 10$, 15, and 20 mph, each with three values of the shape parameters $k = 1.5$, 2, and 3. The values of h in all three sets of curves are the number of hours in a year the wind is in the speed interval v and $(v + \Delta v)$. Figure 3.11 depicts the same plots in three-dimensional h–v–k space. It shows the effect of k in shifting the shape from the bell shape in the front right-hand side ($k = 3$) to the Rayleigh and to flatten shapes as the value of k decreases from 3.0 to 1.5. It is also observed from these plots that as c increases, the distribution shifts to higher speed values.

3.6.2 Mode and Mean Speeds

We now define the following terms applicable to wind speed:

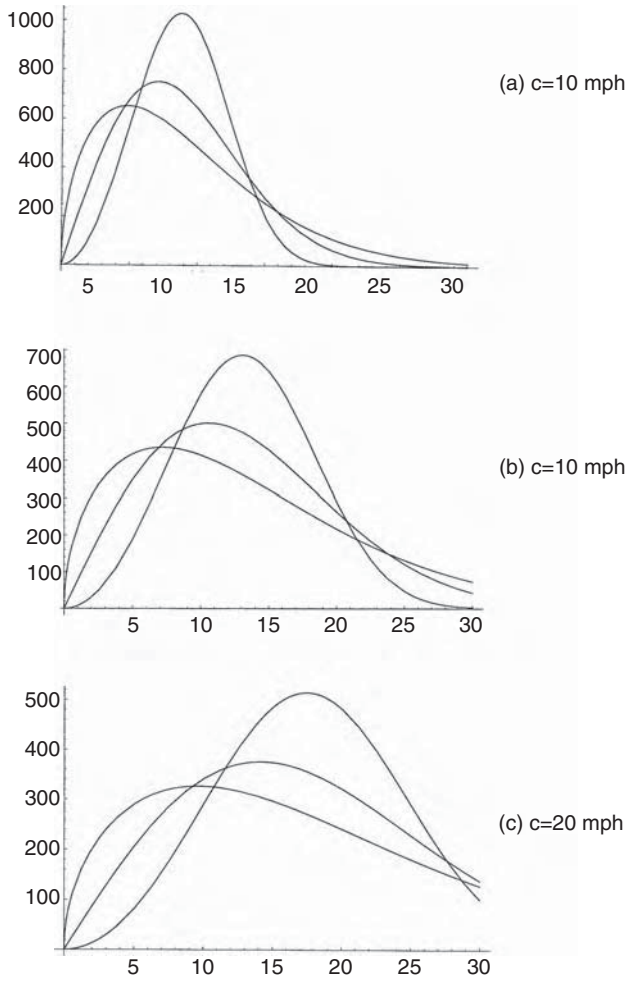

FIGURE 3.10 Weibull distributions of hours per year with three different shape parameters k = 1.5, 2, and 3, each with scale parameters c = 10, 15, and 20 mph.

Mode speed is defined as the speed corresponding to the hump in the distribution function. This is the speed of the wind most of the time.

Mean speed over the period is defined as the total area under the h–v curve integrated from $v = 0$ to ∞ and divided by the total number of hours in the period (8760 if the period is 1 yr). The annual mean speed is therefore the weighted average speed and is given by:

$$V_{\text{mean}} = \frac{1}{8760}\int_0^{\infty} hv\,\mathrm{d}v \tag{3.24}$$

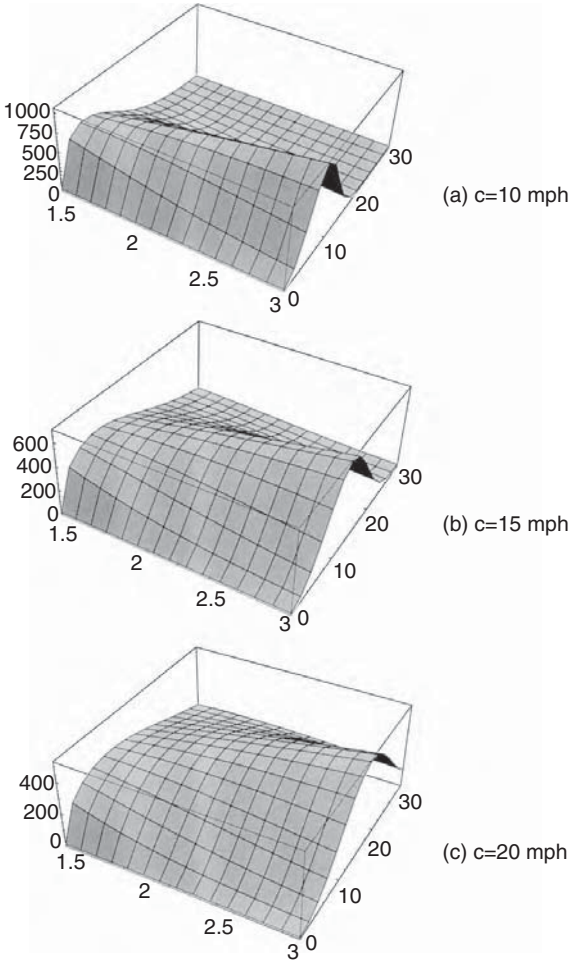

FIGURE 3.11 Three-dimensional *h*–*v*–*k* plots with *c* ranging from 10 to 20 mph and *k* ranging from 1.5 to 3.0.

For c and k values in the range found at most sites, the integral expression can be approximated to the Gamma function:

$$V_{\text{mean}} = c\sqrt{\left(1+\frac{1}{k}\right)} \tag{3.25}$$

For the Rayleigh distribution with $k = 2$, the Gamma function can be further approximated to the following:

$$V_{\text{mean}} = 0.90c \tag{3.26}$$

This is a very simple relation between the scale parameter c and V_{mean}, which can be used with reasonable accuracy. For example, most sites are reported in terms of their mean wind speeds. The c parameter in the corresponding Rayleigh distribution is then $c = V_{mean}/0.9$. The k parameter is, of course, 2.0 for the Rayleigh distribution. Thus, we have the Rayleigh distribution of the site using the generally reported mean speed as follows:

$$h(v) = \frac{2v}{c^2} e^{-\left(\frac{v}{c}\right)^2} = \frac{2v}{(V_{mean})^2} e^{-\left(\frac{v}{V_{mean}}\right)^2} \tag{3.27}$$

3.6.3 Root Mean Cube Speed

Wind power is proportional to the cube of the speed, and the energy collected over the year is the integral of $hv^3 \cdot dv$. We, therefore, define the root mean cube or the rmc speed in a manner similar to the root mean square (rms) value in alternating current (AC) electrical circuits:

$$V_{rmc} = \sqrt[3]{\frac{1}{8760}\int_0^\infty hv^3 dv} \tag{3.28}$$

The rmc speed is useful in quickly estimating the annual energy potential of the site. Using V_{rmc} in Equation 3.12 gives the annual average power generation in W/m^2:

$$P_{rmc} = \frac{1}{4}\rho V_{rmc}^3 \tag{3.29}$$

Then, we obtain the annual energy production potential of the site by simply multiplying the P_{rmc} value by the total number of hours in the year.

The importance of the rmc speed is highlighted in Table 3.1. It compares the wind power density at three sites with the same annual average wind speed of 6.3 m/sec. The San Gorgonio site in California has 66% greater power density than the Culebra site in Puerto Rico. The difference comes from having different shape factors k and, hence, different rmc speeds, although all have the same annual mean speed.

3.6.4 Mode, Mean, and RMC Speeds

The important difference between the mode, the mean, and the rmc speeds is illustrated in Table 3.2. The values of the three speeds are compiled for four shape parameters (k = 1.5, 2.0, 2.5, and 3.0) and three scale parameters (c = 10, 15, and 20 mph). The upstream wind power densities are calculated using the respective speeds in the wind power equation $P = \frac{1}{2}\rho V^3$ W/m^2 using the air mass density of 1.225 kg/m^3.

TABLE 3.1
Comparison of Three Wind Farm Sites with the Same Mean Wind Speed but Significantly Different Specific Power Densities

Site	Annual Mean Wind Speed (m/sec)	Annual Average Specific Power (W/m^2)
Culebra, PR	6.3	220
Tiana Beach, NY	6.3	285
San Gorgonio, CA	6.3	365

TABLE 3.2
Influence of Shape and Scale Parameters on the Mode, Mean, and RMC Speeds and the Energy Density

c	k	Mode Speed	Mean Speed	RMC Speed	Pmode (W/m^2)	Pmean (W/m^2)	Prmc (W/m^2)	Ermc (KWh/yr)
10	1.5	3.81	9.03	12.60	68	451	1225	5366
	2.0	7.07	8.86	11.00	216	426	814	3565
	2.5	8.15	8.87	10.33	331	428	675	2957
	3.0	8.74	8.93	10.00	409	436	613	2685
15	1.5	7.21	13.54	18.90	230	1521	4134	18107
	2.0	10.61	13.29	16.49	731	1439	2748	12036
	2.5	12.23	13.31	15.49	1120	1444	2278	9978
	3.0	13.10	13.39	15.00	1377	1472	2067	9053
20	1.5	9.61	18.05	25.19	544	3604	9790	42880
	2.0	13.14	17.72	22.00	1731	3410	6514	28531
	2.5	16.30	17.75	20.66	2652	3423	5399	23648
	3.0	17.47	17.86	20.00	3266	3489	4900	21462

Note: P = upstream wind power density in watts per square meter of the blade-swept area = $0.5\ \rho V^3$, where $\rho = 1.225\ kg/m^3$; the last column is the energy potential of the site in kWh per year per m^2 of the blade area, assuming a rotor efficiency C_p of 50% (i.e., the maximum power that can be converted into electric power is $0.25\ \rho\ V^3$).

We observe the following from the $c = 15$ rows:

For $k = 1.5$, the power density using the mode speed is 230 as against the correct value of 4134 W/m^2 using the rmc speed. The ratio of the incorrect to correct value of the power density is 1 to 18, a huge difference.

For $k = 2$, the power densities using the mode and rmc speeds are 731 and 2748 W/m^2, respectively, in the ratio of 1 to 3.76. The corresponding power

densities with the mean and the rmc speeds are 1439 and 2748 W/m^2 in the ratio of 1 to 1.91.

For $k = 3$, the power densities using the mode and rmc speeds are 1377 and 2067 W/m^2 respectively, in the ratio of 1 to 1.50. The corresponding power densities with the mean and the rmc speeds are 1472 and 2067 W/m^2, in the ratio of 1 to 1.40.

The last column in Table 3.2 gives the yearly energy potentials of the corresponding sites in kilowatthours per year per square meter of the blade area for the given k and c values. These values are calculated for a rotor efficiency C_p of 50%, which is the maximum that can be practically achieved.

Thus, regardless of the shape and the scale parameters, use of the mode or the mean speed in the power density equation would introduce a significant error in the annual energy estimate, sometimes off by several folds, making the estimates completely useless. Only the rmc speed in the power equation always gives the correct average power over a period.

The following example illustrates this point. A site has ¼ the number of hours in the year at 0, 10, 20, and 30 mph, with an annual average speed of 15 mph. The energy distribution at this site is shown in the following table:

Speed mph	0	10	20	30	(Avg. 15)
% h/yr	25	25	25	25	
% Energy/yr	0	3	22	75	

Annual wind energy using average speed = 3375 units

Annual wind energy using rmc speed = 9000 units

Energy potential estimated correctly using rmc speed = 2.67 × energy potential estimated incorrectly using average speed.

3.6.5 Energy Distribution

If we define the energy distribution function:

$$e = \frac{\text{kWh contribution in the year by the wind between } v \text{ and } (v + \Delta v)}{\Delta v} \tag{3.30}$$

then, for the Rayleigh speed distribution ($k = 2$), the energy distribution would look like the shaded curve in Figure 3.12. The wind speed curve has the mode at 5.5 m/sec and the mean at 6.35 m/sec. However, because of the cubic relation with speed, the maximum energy contribution comes from the wind speed at 9.45 m/sec. Above this speed, although V^3 continues to increase in a cubic manner, the number of hours at those speeds decreases faster than V^3. The result is an overall decrease in the yearly energy contribution. For this reason, it is advantageous to design the wind power system to operate at variable speeds in order to capture the maximum energy available during high-wind periods.

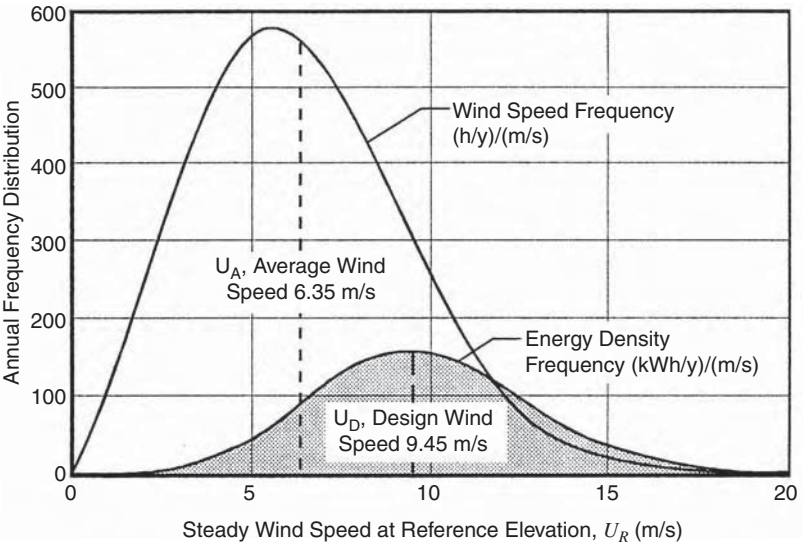

FIGURE 3.12 Annual frequency distributions of hours vs. wind speed and energy density per year with $c = 10$ and $k = 2$ (Rayleigh distribution).

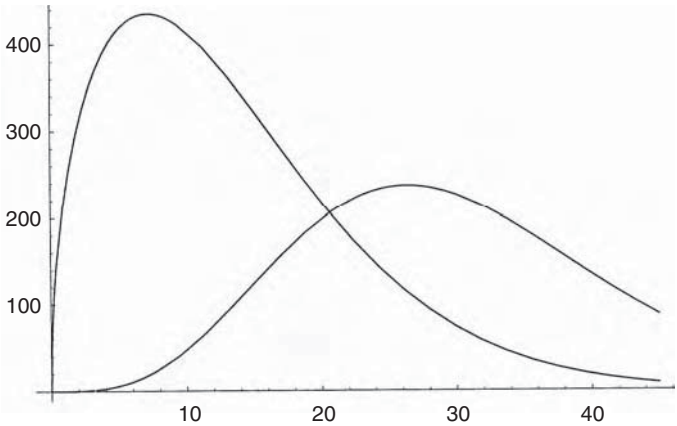

FIGURE 3.13 Rayleigh distributions of hours vs. wind speed and energy per year with $c = 15$ and $k = 1.5$.

Figure 3.13 is a similar chart showing the speed and energy distribution functions for a shape parameter of 1.5 and a scale parameter of 15 mph. The mode speed is 10.6 mph, the mean speed is 13.3 mph, and the rmc speed is 16.5 mph. The energy distribution function has the mode at 28.5 mph. That is, the most energy is captured at 28.5-mph wind speed, although the probability of wind blowing at that speed is low.

Comparing Figure 3.12 and Figure 3.13, we see that as the shape parameter value decreases from 2.0 to 1.5, the speed and the energy modes move farther apart.

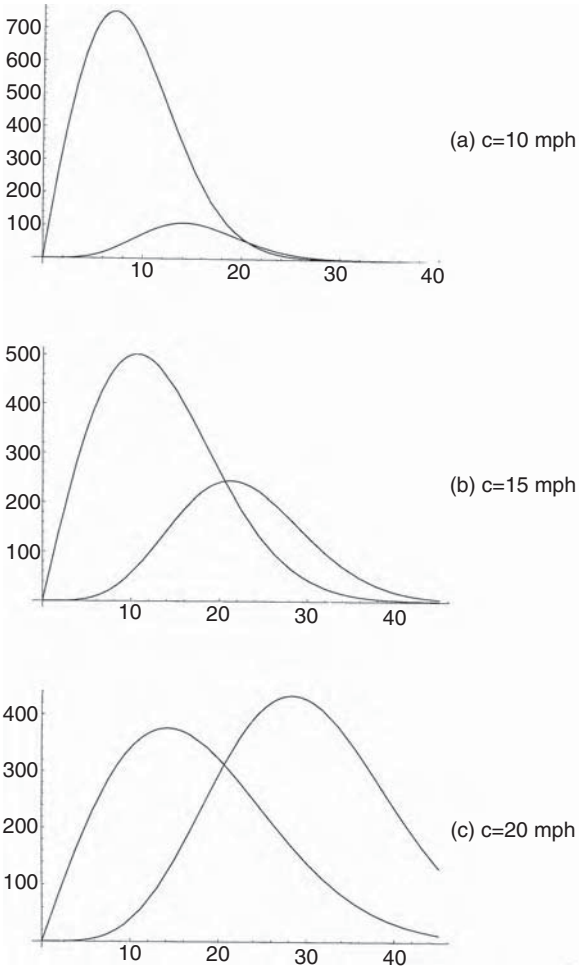

FIGURE 3.14 Rayleigh distributions of hours vs. wind speed and energy per year with k = 2 and c = 10, 15, and 20 mph.

On the other hand, as the speed distribution approaches the bell shape for $k > 3$, the speed and the energy modes get closer to each other.

Figure 3.14 compares the speed and the energy distributions with $k = 2$ (Rayleigh) and c = 10, 15, and 20 mph. As seen here, the relative spread between the speed mode and the energy mode remains about the same, although both shift to the right as c increases.

3.6.6 Digital Data Processing

The mean wind speed over a period of time is obtained by adding numerous readings taken over that period and dividing the sum by the number of readings. Many digital data loggers installed over the last few decades collected average wind speed data

primarily for meteorological purposes, as opposed to assessing wind power. They logged the speed every hour, and then averaged over the day, which, in turn, was averaged over the month and over the year. The averaging was done as follows:

$$V_{\text{avg}} = \frac{1}{n}\sum_{i=1}^{n} V_i \tag{3.31}$$

The month-to-month wind speed variation at a typical site over the year can be ± 30 to 35% over the annual average. As seen earlier, for assessing the wind power, the rmc speed is what matters. The rmc equivalent of the digital data logging is as follows:

$$V_{\text{rmc}} = \sqrt[3]{\frac{1}{n}\sum_{i=1}^{n} V_i^3} \tag{3.32}$$

The preceding equation does not take into account the variation in the air mass density, which is also a parameter (although of second order) in the wind power density. Therefore, a better method of processing wind speed data for power calculations is to digitize the yearly average power density as

$$P_{\text{rmc}} = \frac{1}{2n}\sum_{i=1}^{n} \rho_i V_i^3 \tag{3.33}$$

where
n = number of observations in the averaging period,
ρ_i = air density (kg/m^3), and
V_i = wind speed (m/sec) at the i^{th} observation time.

3.6.7 Effect of Hub Height

The wind shear at a ground-level surface causes the wind speed to increase with height in accordance with the following expression:

$$V_2 = V_1\left(\frac{h_2}{h_1}\right)^{\alpha} \tag{3.34}$$

where
V_1 = wind speed measured at the reference height h_1,
V_2 = wind speed estimated at height h_2, and
α = ground surface friction coefficient.

TABLE 3.3
Friction Coefficient α of Various Terrains

Terrain Type	Friction Coefficient α
Lake, ocean, and smooth, hard ground	0.10
Foot-high grass on level ground	0.15
Tall crops, hedges, and shrubs	0.20
Wooded country with many trees	0.25
Small town with some trees and shrubs	0.30
City area with tall buildings	0.40

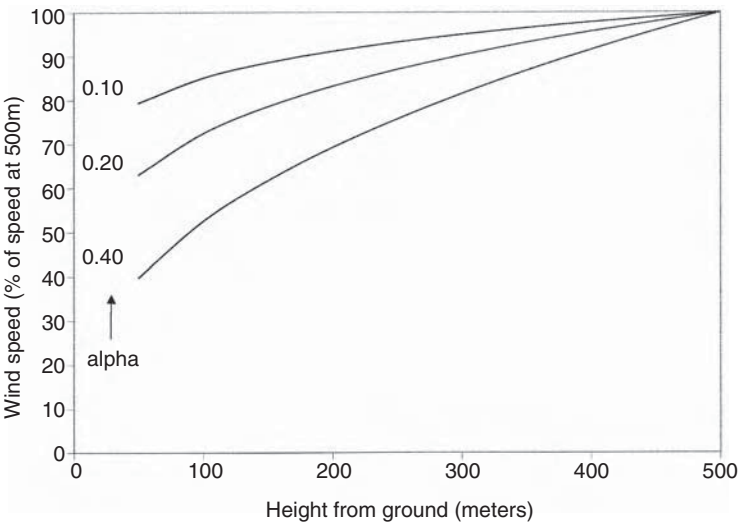

FIGURE 3.15 Wind speed variations with height over different terrain. Smooth, low-friction terrain with low α develops a thinner layer of slow wind near the surface and high wind at heights.

The friction coefficient α is low for smooth terrain and high for rough ones. The values of α for typical terrain classes are given in Table 3.3, and their effects on the wind speed at various heights are plotted in Figure 3.15. It is noteworthy that the offshore wind tower, being in low-α terrain, always sees a higher wind speed at a given height and is less sensitive to tower height.

Wind speed does not increase with height indefinitely, even at a slower rate. The data collected at Merida airport in Mexico show that typically wind speed increases with height up to about 450 m and then decreases (Figure 3.16)[1]. The wind speed at 450-m height can be 4 to 5 times greater than that near the ground surface.

Modern wind turbines operate on increasingly taller towers to take advantage of the increased wind speeds at higher altitudes. Very little is known about the turbulent wind patterns at these heights, which can damage the rotor. Of particular

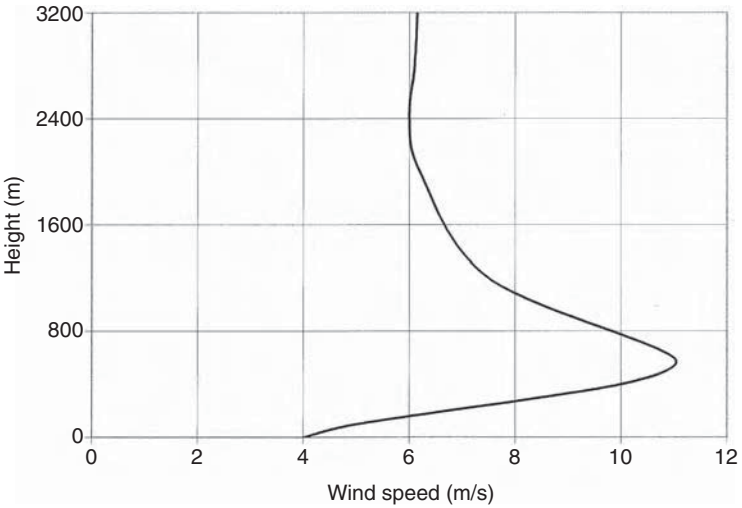

FIGURE 3.16 Wind speed variations with height measured at Merida airport, Yucatan, in Mexico. (From Schwartz, M.N. and Elliott, D.L., "Mexico Wind Resource Assessment Project," DOE/NREL Report No. DE95009202, National Renewable Energy Laboratory, Golden, Colorado, March 1995.)

interest on the Great Plains, where many wind farms will be located, are the high-level wind flows called *nocturnal jets* that dip close to the ground at night, creating violent turbulence. Engineers at the National Wind Technology Center (NWTC) have been measuring higher-altitude wind patterns and developing simulation models of the turbine's interaction with turbulent wind patterns to develop designs that can prevent potential damage to the rotor.

Due to the existence of Military Special Use Airspace (i.e., the military airspace less than 300 ft from ground level) for military testing and training across the U.S., the Air Force wind consultants advise contacting them prior to applying for permits on all federal and nonfederal lands. One can contact airforcewindconsult@pentagon.af.mil before selecting the tower height for a potential wind farm site.

3.6.8 Importance of Reliable Data

Some of the old wind speed data around the world may have been collected primarily for meteorological use with rough instruments and relatively poor exposure to the wind. This is highlighted by a recent wind resource study in Mexico.[1] Significant differences between the old and the new data have been found, as listed in Table 3.4. The 1983 Organización Latinoamericana de Energía (OLADE) Atlas of Mexico indicates very low energy potential, whereas the 1995 NREL data reports energy potentials several times greater. The values from the OLADE Atlas are from a few urban locations where anemometers could be poorly exposed to the prevailing winds. In contrast, the new NREL wind data come from a large number of stations, including open airport locations, and has incorporated the terrain effect in the final numbers. The message here is clear: it is important to have reliable data on the annual wind

TABLE 3.4
Comparison of Calculated Average Wind Power Density between 1983 OLADE Atlas and 1995 NREL Analysis for Several Locations in Mexico

		Wind Power Density (in W/m²)	
Region in Mexico	**Data Site**	**OLADE Atlas (1983)**	**NREL Data (1995)**
Yucatan Peninsula	Merida	22	165
	Campeche	23	120
	Chetumal	28	205
Northern Gulf Plain	Tampico	8	205
	Cuidad Victoria	32	170
	Matamoros	32	165
Central Highlands	Durango	8	140
	San Luis Potosi	35	155
	Zacatecas	94	270
Northwest	Chihuahua	27	120
	Hermosillo	3	80
	La Paz	10	85

Note: Data at 10-m height.

speed distribution over at least a few years before siting a wind farm with a high degree of confidence.

The most widely available wind speed data in the past came from weather stations at airports. Unfortunately, that is not very useful to wind farm planners, as airports are not necessarily located at favorable wind sites. Other widely used locations in towns and cities for wind measurements have been existing structures such as water towers. Such data can also be unreliable due to shear effect. Near the tower, the wind speed can be 10 to 15% higher or lower than the actual speed. This results in an energy estimate up to 52% on the high side or 60% on the low side, a difference of (1.52/0.60) 2.5 to 1. Such an enormous error could make a site look lucrative, whereas in fact it may not be even marginally economical.

Because airports were intentionally not built on high-wind sites, the good wind sites were left unmonitored for a long time. The new data from such sites are, therefore, limited to a few recent years. For this reason, one must verify the data in more than one way to ascertain high reliability and confidence in its use.

3.7 WIND SPEED PREDICTION

Because the available wind energy at any time depends on the wind speed at that time, which is a random variable, knowing the average annual energy potential of a site is one thing and the ability to accurately predict when the wind will blow is quite another thing. For the wind farm operator, this poses difficulties in system

scheduling and energy dispatching as the schedule of wind power availability is not known in advance. However, a reliable forecast of wind speed several hours in advance can give the following benefits:

- Generating schedule can efficiently accommodate wind generation in a timely manner
- Allows the grid-connected wind farm to commit to power purchase contracts in advance for a better price
- Allows investors to proceed with new wind farms and avoid the penalties they must pay if they do not meet their hourly generation targets

Therefore, development of short-term wind-speed-forecasting tools helps wind energy producers. NWTC researchers work in cooperation with the National Oceanic and Atmospheric Administration (NOAA) to validate the nation's wind resource maps and develop methods of short-term (1 to 4 h) wind forecasting. Alexiadis et al.[2] have also proposed a new technique for forecasting wind speed and power output up to several hours in advance. Their technique is based on cross-correlation at neighboring sites and artificial neural networks and is claimed to significantly improve forecasting accuracy compared to the persistence-forecasting model.

3.8 WIND ENERGY RESOURCE MAPS

The wind resource of a vast region or a country is mapped in terms of the wind speed, the wind power density in watts per square meter of the rotor-swept area, or the wind energy potential in kWh/m^2 per year. Often the wind resource is mapped in all three forms. The data is usually represented by contour curves, as it is the most useful and easily understood mapping technique. Along the contour line, the plotted parameter remains constant. For example, the isovent map plots the contour lines connecting sites having the same annual wind speed. The equipotential map shows the contour lines connecting sites having the same annual wind-energy-capture potential in units of kWh/m^2. The wind resource maps of many countries have been prepared in such contour form.

Estimates of wind resource are expressed in wind power classes ranging from class 1 to 7 (Table 3.5). Areas designated class 4 or greater are compatible with existing wind turbine technology. Power class-3 areas may become suitable with future technology. Class-2 areas would be marginal and class-1 areas unsuitable for wind energy development.

3.8.1 U.S. Wind Resource Map

U.S. wind resources are large enough to produce more than 3.4 trillion kWh of electricity each year. This is more than the entire nation will use in the year 2005. Figure 3.17 is the wind speed map, whereas Figure 3.18 is the wind power density map[3–5] of the U.S. The detailed wind maps of many U.S. states are being prepared and some of them are available on the Internet site www.truewind.com. The Department of Energy (DOE) estimates that almost 90% of the usable wind resource in

TABLE 3.5
Wind Energy Resource Classification with Wind Classes of Power Density

	10 m (33 ft) Hub		30 m (98 ft) Hub		50 m (164 ft) Hub	
Wind Class	Wind Power Density W/m^2	Speed[a] m/s (mph)	Wind Power Density W/m^2	Speed[a] m/sec (mph)	Wind Power Density W/m^2	Speed[a] m/sec (mph)
1	100	4.4 (9.8)	160	5.1 (11.4)	200	5.6 (12.5)
2	150	5.1 (11.5)	240	5.9 (13.2)	300	6.4 (14.3)
3	200	5.6 (12.5)	320	6.5 (14.6)	400	7.0 (15.7)
4	250	6.0 (13.4)	400	7.0 (15.7)	500	7.5 (16.8)
5	300	6.4 (14.3)	480	7.4 (16.6)	600	8.0 (17.9)
6	400	7.0 (15.7)	640	8.2 (18.3)	800	8.8 (19.7)
7	1000	9.4 (21.1)	1600	11.0 (24.7)	2000	11.9 (26.6)

Source: From Elliott, D.L. and Schwartz, M.N., Wind Energy Potential in the United States, Pacific Northwest Laboratory PNL-SA-23109, NTIS No. DE94001667, September 1993.

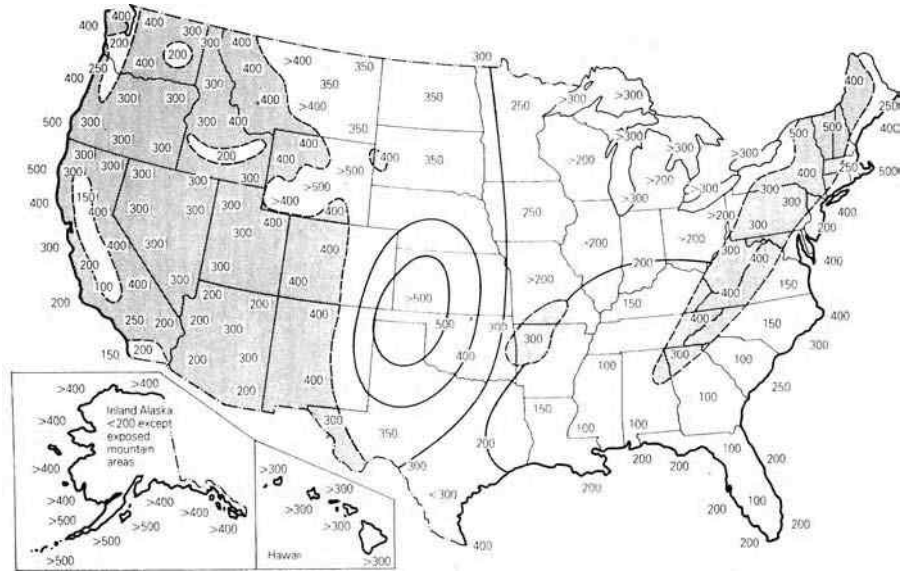

FIGURE 3.17 Annual average wind power density in W/m^2 in the U.S. at 50-m tower height. (From DOE/NREL.)

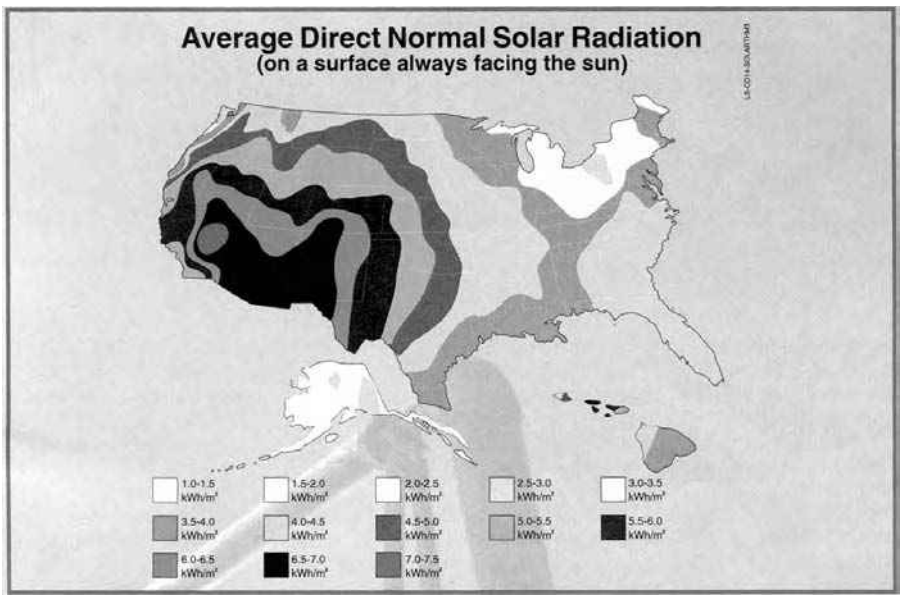

FIGURE 3.18 U.S. wind resource map. (From DOE/Battelle Pacific Northwest Laboratory.)

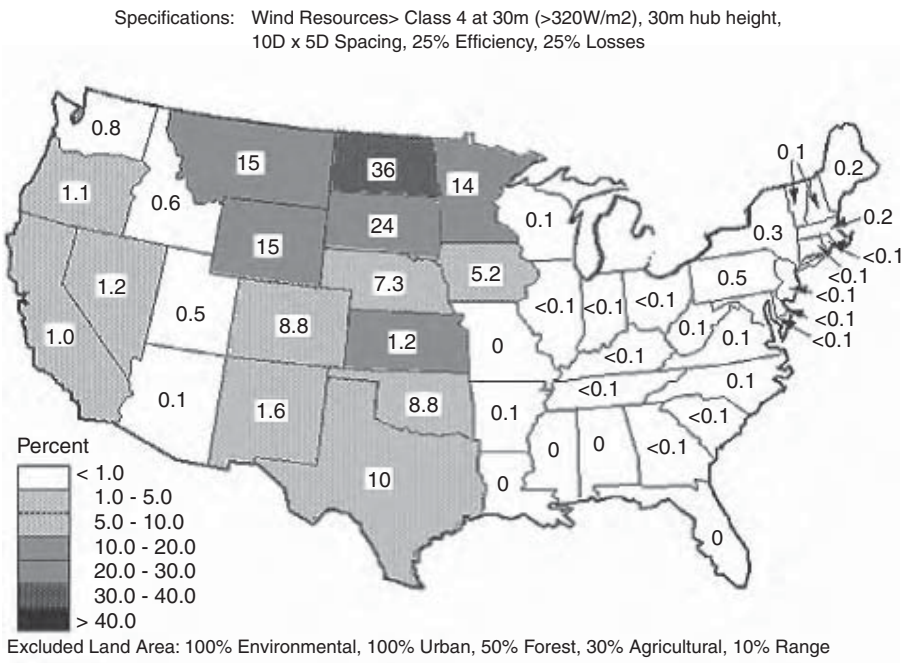

FIGURE 3.19 Wind electric potential as a percentage of total electric consumption in contiguous states of U.S. (From NREL/WETC, Golden, CO.)

the U.S. lies in the wind belt spanning the 11 Great Plains states. These states stretch from Montana, North Dakota, and Minnesota in the north to Texas in the south. The wind resources of this region have remained virtually untapped until recently. However, significant wind-power-generating capacity has been added in the wind belt states since the late 1990s.

Because the techniques of wind resource assessment have improved greatly in recent years, planning work began in 2000 to update the U.S. wind atlas. The work will produce regional-scale maps of the wind resource with resolution down to 1 km^2. The new atlas will take advantage of modern techniques for mapping, such as mesoscale models. It will also incorporate new meteorological, geographical, and terrain data. The program's advanced mapping of wind resources is another important element necessary for expanding wind-generating capacity in the U.S.

Estimates of the electricity that could potentially be generated by wind power are based on published wind resource data and exclude windy lands that are not suitable for development as a result of environmental and land-use considerations. Figure 3.19 shows the contribution that the wind energy of each state could make to meet the total electrical needs of the nation, assuming a moderate land exclusion scenario. The wind-generated electrical potential per grid cell was calculated from the available windy land area and the wind power classification assigned to each cell. The amount of electricity that can be generated depends on several factors, including the spacing between wind turbines, the hub height, the rotor efficiency,

TABLE 3.6
Electric Energy Production Potential at Wind Sites in Classes 4 or Higher

Power Class	Wind Power Density (W/m^2)	Average Power Intercepted (MW/km^2)	Average Power Output (MW/km^2)	Annual Energy Production (Million kWh/km^2)
4	450	7.07	1.33	11.65
5	550	8.64	1.62	14.19
6	700	11.00	2.06	18.04
7	900	14.14	2.65	23.21

Note: At 50-m hub height, 10 × 5 rotor diameter spacing, 25% efficiency, and 25% power losses. The 100% environmental, 100% urban, 50% forest, 30% agricultural, and 10% range areas have been excluded from these estimates.

Source: From Elliott, D.L. and Schwartz, M.N., "Wind Energy Potential in the United States," Pacific Northwest Laboratory PNL-SA-23109, NTIS No. DE94001667, September 1993.

and the estimated energy losses caused by wind turbine wakes, blade soiling, etc. The assumptions used for calculating the wind energy potential per unit of windy land area are given in Table 3.6. Estimates of wind turbine efficiency and power losses are based on data from existing turbines. For advanced turbines, efficiency is projected to be 30 to 35% and power losses, 10 to 15%. With these assumptions and exclusions, the wind electric potential is surprisingly large, more than 1.5 times the current electricity consumption of the U.S. North Dakota alone has enough potential energy from windy areas of class 4 and higher to supply 36% of the total electricity consumption of the 48 contiguous states.

Although the nation's wind potential is very large, only a part of it is being exploited by U.S. utilities (Figure 3.20). The economic viability of wind power will vary from utility to utility. Important factors not addressed in this study that influence land availability and wind electric potential include production–demand match (seasonal and daily), transmission and access constraints, public acceptance, and other technological and institutional constraints.

3.8.2 U.K. and Europe Wind Resources

The isovent map of the U.K. is shown in Figure 3.21 in terms of the annual average wind speed in knots at open sites excluding hilltops[6]. Scotland and the western shore of Ireland are the high-wind zones. The central portion of England has relatively low wind speeds.

The wind energy map in MWh/m^2 per year is shown in Figure 3.22.[6] The northwestern offshore sites show high energy potential of 5 MWh/m^2 per year.

The wind speed and energy maps of Europe have been combined into one map that is published by the Rios National Laboratory in Denmark. The map (Figure 3.23) has been prepared for a wind tower height of 50 m above the ground, with five different terrains. In the map, the darker areas have higher wind energy density.

FIGURE 3.20 U.S. utilities gaining experience in developing wind power generation projects. (From Wind energy program overview, DOE Report No. 10095-071, March 1995.)

FIGURE 3.21 Isovent map of the U.K. in knots at open sites, excluding hilltops. (From Freris, L.L., *Wind Energy Conversion Systems*, Prentice Hall, London, 1990.)

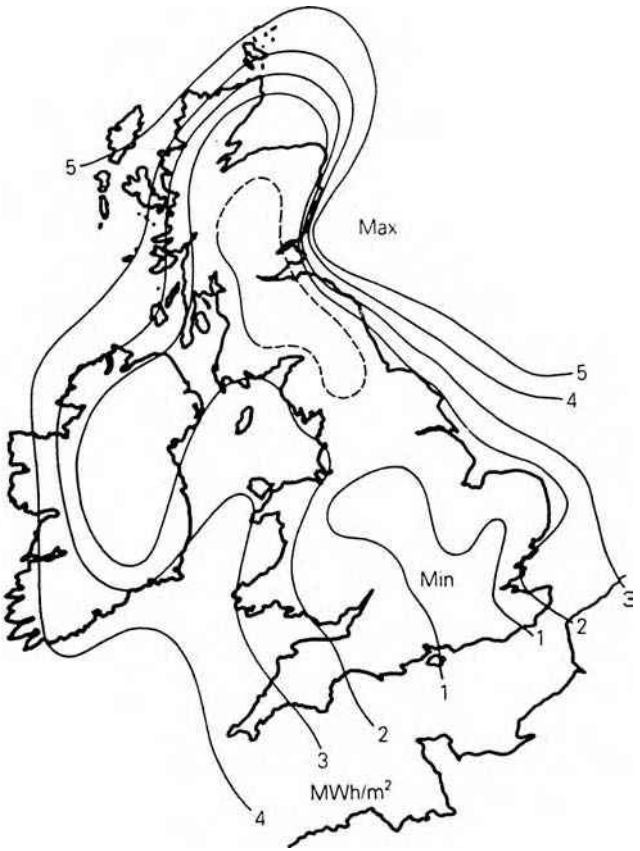

FIGURE 3.22 Wind energy map of the U.K. in MWh/m^2 per year at open sites, excluding hilltops. (From Freris, L.L., *Wind Energy Conversion Systems*, Prentice Hall, London, 1990.)

3.8.3 Mexico Wind Resource Map

The wind resource map of Mexico has been recently prepared under the Mexico–U.S. Renewable Energy Cooperation Program.[1] The data was collected at numerous city and airport sites spread throughout the country as shown in Figure 3.24. The maps were prepared based on the extensive data collected at those locations. They are reported separately for utility-scale power generation and for stand-alone remote power generation. This distinction is useful because the wind speed needed to make the wind farm economical for rural applications is less than that required for the utility-scale wind farm.

Figure 3.25 is the utility-scale wind resource map of Mexico. The highest wind potential for grid-connected power plants is in the Zacatecas and the southern Isthmus of Tehuantepec areas. The rural wind resource map in Figure 3.26 shows that areas suitable for stand-alone remote wind farms are widespread and include about half of Mexico.

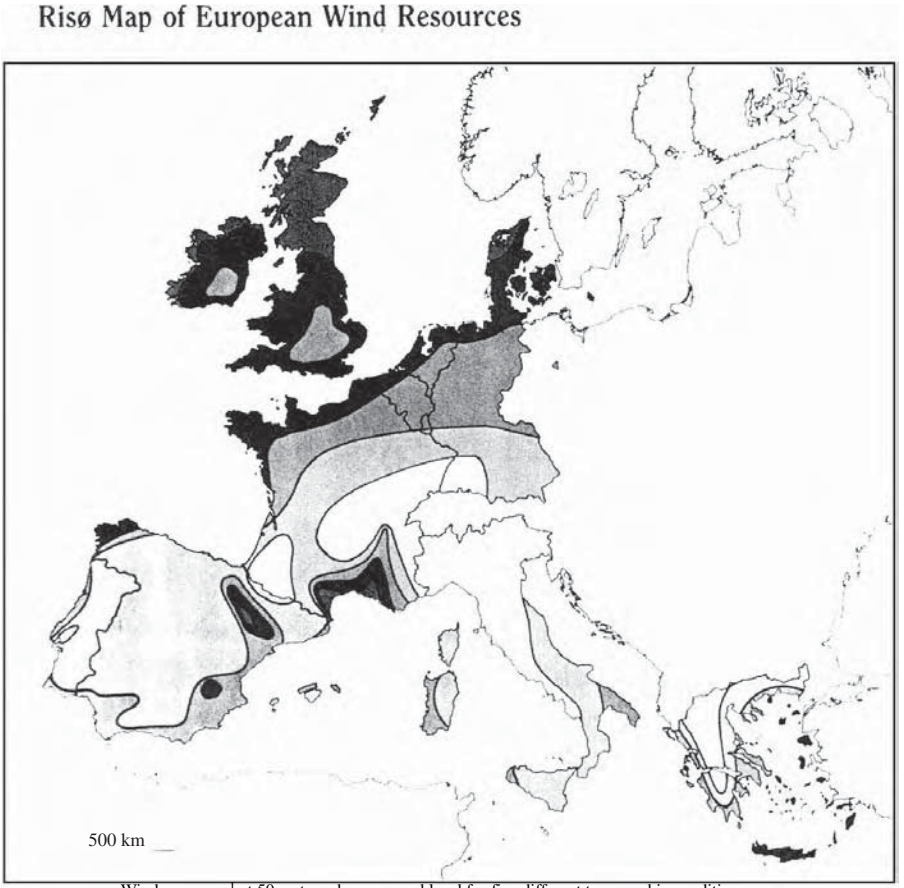

Wind resources[1] at 50 meters above ground level for five different topographic conditions

Sheltered terrain[2]		Open plain[3]		At a sea coast[4]		Open sea[5]		Hills and Ridge[6]	
ms^{-1}	Wm^{-2}	ms^{-1}	Wm^{-2}	ms^{-1}	Wm^{-2}	ms^{-1}	Wm^{-2}	ms^{-1}	Wm^{-2}
> 6.0	> 250	> 7.5	> 500	> 8.5	> 700	> 9.0	> 800	> 11.5	> 1800
5.0-6.0	150-250	6.5-7.5	300-500	7.0-8.5	400-700	8.0-9.0	600-800	10.0-11.5	1200-1800
4.5-5.0	100-150	5.5-6.5	200-300	6.0-7.0	250-400	7.0-8.0	400-600	8.5-10.0	700-1200
3.5-4.5	50-100	4.5-5.5	100-200	5.0-6.0	150-250	5.5-7.0	200-400	7.0-8.0	400-700
< 3.5	< 50	< 4.5	< 50	< 5.0	< 150	< 5.5	< 200	< 7.0	< 400

FIGURE 3.23 European wind resource map. (From RISO Laboratory, Denmark.)

3.8.4 Wind Mapping in India

Wind speed measurement stations in India have been in operation since the early 1980s at numerous locations.[11] Sites with high wind speeds are shown in Figure 3.27, and their annual mean speeds are listed in Table 3.7. Data have been collected at 10-m or 25-m tower height as indicated. It is seen that most of these sites have an annual mean wind speed exceeding 18 km/h, which generally makes the wind power plant economically viable. The states with high wind potential are Tamil Nadu, Gujarat (Figure 3.28), and Andhra Pradesh.

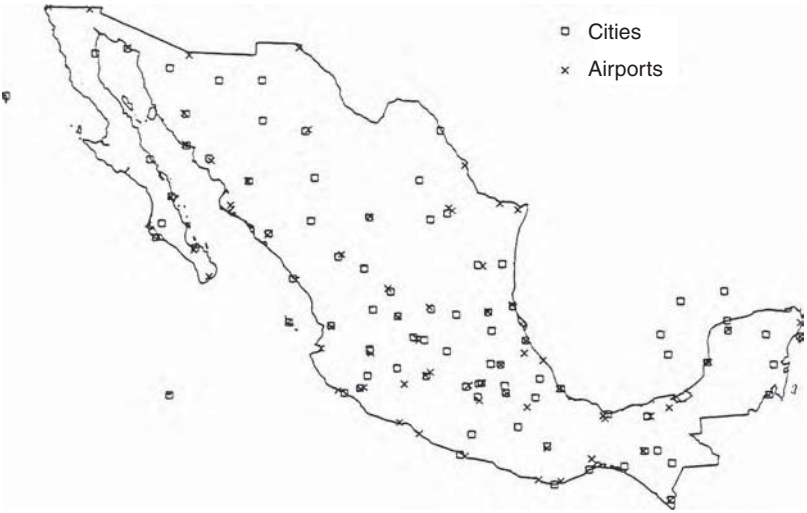

FIGURE 3.24 Locations in Mexico with surface wind data in DATSAV2 data set. (From Schwartz, M.N. and Elliott, D.L., "Mexico Wind Resource Assessment Project," DOE/NREL Report No. DE95009202, National Renewable Energy Laboratory, Golden, Colorado, March 1995.)

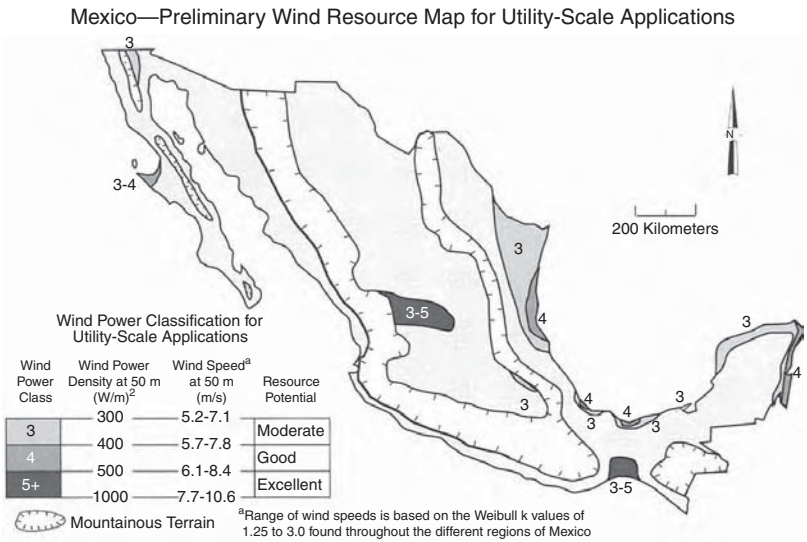

FIGURE 3.25 Annual average wind resource map of Mexico for utility-scale applications. (From Schwartz, M.N. and Elliott, D.L., "Mexico Wind Resource Assessment Project," DOE/NREL Report No. DE95009202, National Renewable Energy Laboratory, Golden, Colorado, March 1995.)

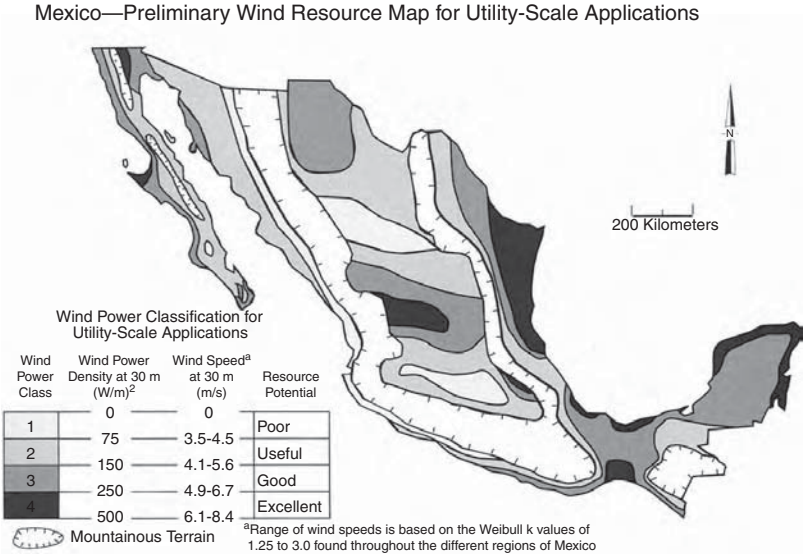

FIGURE 3.26 Annual average wind resource map of Mexico for rural power applications. (From Schwartz, M.N. and Elliott, D.L., "Mexico Wind Resource Assessment Project," DOE/NREL Report No. DE95009202, National Renewable Energy Laboratory, Golden, Colorado, March 1995.)

3.8.5 Wind Mapping — Other Countries

Wind resource maps in the following countries are already available from NREL/NWTC: Cambodia, Chile, China, Dominican Republic, Indonesia, Laos, Mexico, Mongolia, Philippines, Sri Lanka/Maldives, Thailand, and Vietnam, and more are added every year

In 2003, the United Nations also launched a program to map the solar and wind resources of 13 developing countries — Bangladesh, Brazil, China, Cuba, El Salvador, Ethiopia, Ghana, Guatemala, Honduras, Kenya, Nepal, Nicaragua, and Sri Lanka.

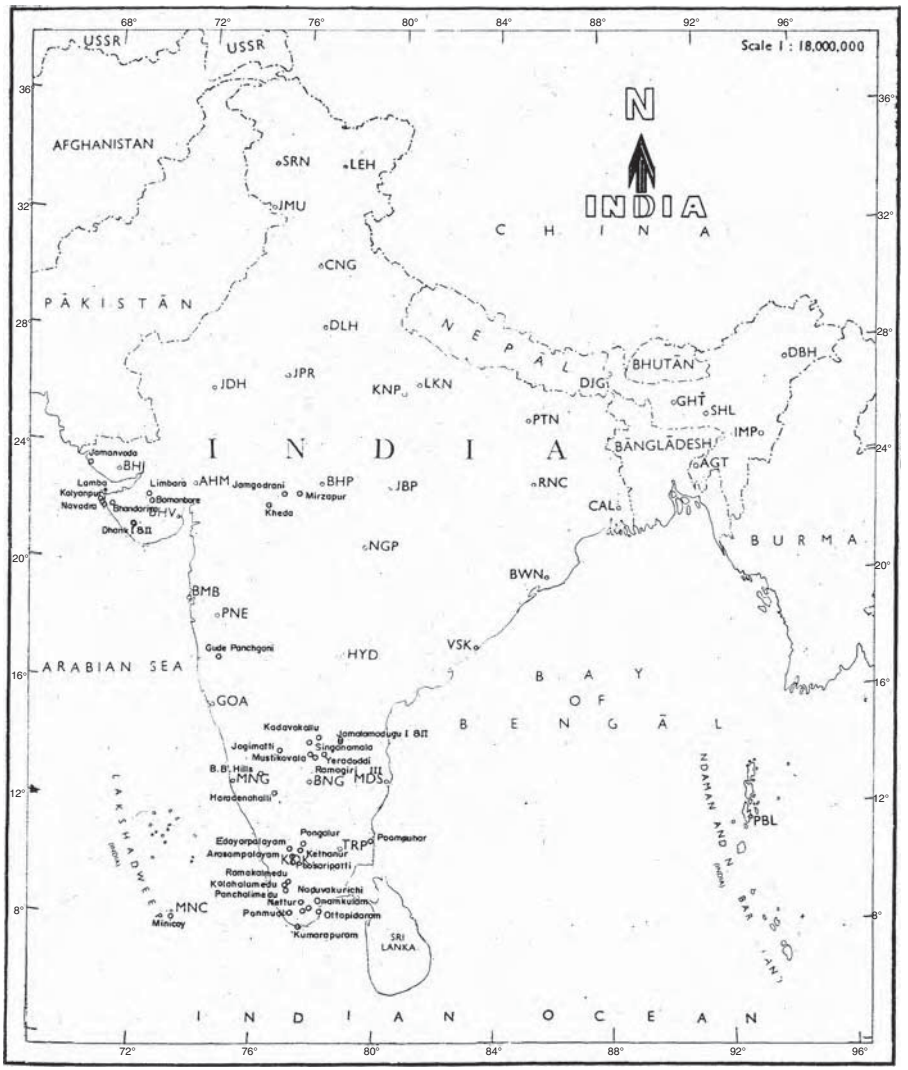

FIGURE 3.27 Wind-monitoring sites in India. (From Tata Energy Research Institute, New Delhi, India.)

TABLE 3.7
Mean Annual Wind Speed at Selected Sites in India

Site	km/h
Sites with 25–30 km/h Wind Speed	
Ramakalmedu	30.3
Jogmatti	30.0
B&H Hills	27.1
Dhank-2	25.1
Sites with 20–25 km/h Wind Speed	
Dhank-1	23.4
Singanamala	23.8
Edayarpalayam	22.4
Kadavakallu[a]	22.1
Kalyanpur	22.1
Kumarapuram[a]	22.0
Kethanur	21.1
Navadra	20.8
Arasampalayam	20.5
Bamambore-2	20.3
Mustikovala	20.2
Pancjalimedu	20.2
Lamda	20.0
Sites with 15–20 km/h Wind Speed	
Onamkulam[a]	19.9
Nettur[a]	19.9
Gude Panchgani	119.8
Bhandariya	19.5
Ramagiri-3	19.4
Poosaripatti[a]	19.3
Pongalur	19.1
Limbara	19.1
Jamalamadugu-2[a]	18.7
Ottapidaram	18.5
Ponmudi	18.3
Hardenahalli	18.2
Kheda	18.2
Jamgodrani	18.0
Jamalamadunga-1[a]	17.5
Poompuhar	17.2
Minicoy	17.0
Kolahalamendu	16.9
Naduvakkurichi	16.8
Yeradoddi[a]	15.8
Mirzapur	15.4

[a] Data at 25-m height, all others at 10-m height.

FIGURE 3.28 Lamda wind farm in Gujarat, India. (From Vestas Wind Systems, Denmark. With permission.)

References

1. Schwartz, M.N. and Elliott, D.L., Mexico Wind Resource Assessment Project, DOE/NREL Report No. DE95009202, National Renewable Energy Laboratory, Golden, CO, March 1995.
2. Alexiadis, M.C., Dokopoulos, P.S., and Sahsamanogdou, H.S., Wind Speed and Power Forecasting Based on Spatial Correlation Models, IEEE Paper No. PE-437-EC-0-03-1998.
3. Elliott, D.L., Holladay, C.G., Barchet, W.R., Foote, H.P., and Sandusky, W.F., Wind Energy Resources Atlas of the United States, DOE/Pacific Northwest Laboratory Report No. DE-86004442, April 1991.
4. Elliot, D.L., Synthesis of National Wind Assessment, DOE/Pacific Northwest Laboratory, NTIS Report No. BNWL-2220 Wind-S, 1997.
5. Rory, A., Minnesota Wind Resources Assessment Program, Minnesota Department of Public Service Report, 1994.
6. Freris, L.L., *Wind Energy Conversion Systems*, Prentice Hall, London, 1990.
7. Elliott, D.L. and Schwartz, M.N., Wind Energy Potential in the United States, Pacific Northwest Laboratory PNL-SA-23109, NTIS No. DE94001667, September 1993.
8. Elliott, D.L., Holladay, C.G., Barchet, W.R., Foote, H.P., and Sandusky, W.F, Wind Energy Resource Atlas of the United States, Report DOE/CH 10093-4, Solar Energy Research Institute, Golden, CO, 1987.
9. Elliott, D.L., Wendell, L.L., and Gower, G.L., An Assessment of the Available Windy Land Area and Wind Energy Potential in the Contiguous United States, Report PNL-7789, Pacific Northwest Laboratory, Richland, WA, 1991.
10. Schwartz, M.N., Elliott, D.L., and Gower, G.L., Gridded State Maps of Wind Electric Potential. Proceedings of the American Wind Energy Association's WindPower '92 Conference, October 19–23, Seattle, WA, 1992.
11. Gupta, A.K., Power Generation from Renewables in India, Ministry of Non-Conventional Energy Sources, New Delhi, India, 1997.

4 Wind Power Systems

The wind power system is fully covered in this and the following two chapters. This chapter covers the overall system-level performance, design considerations, and trades. The electrical generator is covered in the next chapter, and generator drives in Chapter 6.

4.1 SYSTEM COMPONENTS

The wind power system comprises one or more wind turbine units operating electrically in parallel. Each turbine is made of the following basic components:

- Tower structure
- Rotor with two or three blades attached to the hub
- Shaft with mechanical gear
- Electrical generator
- Yaw mechanism, such as the tail vane
- Sensors and control

Because of the large moment of inertia of the rotor, design challenges include starting, speed control during the power-producing operation, and stopping the turbine when required. The eddy current or another type of brake is used to halt the turbine when needed for emergency or for routine maintenance.

In a modern wind farm, each turbine must have its own control system to provide operational and safety functions from a remote location (Figure 4.1). It also must have one or more of the following additional components:

- Anemometers, which measure the wind speed and transmit the data to the controller.
- Numerous sensors to monitor and regulate various mechanical and electrical parameters. A 1-MW turbine may have several hundred sensors.
- Stall controller, which starts the machine at set wind speeds of 8 to 15 mph and shuts off at 50 to 70 mph to protect the blades from overstressing and the generator from overheating.
- Power electronics to convert and condition power to the required standards.
- Control electronics, usually incorporating a computer.
- Battery for improving load availability in a stand-alone plant.
- Transmission link for connecting the plant to the area grid.

FIGURE 4.1 Baix Ebre wind farm and control center, Catalonia, Spain. (From *Wind Directions*, Magazine of the European Wind Energy Association, London, October 1997. With permission.)

The following are commonly used terms and terminology in the wind power industry:

Low-speed shaft: The rotor turns the low-speed shaft at 30 to 60 rotations per minute (rpm).

High-speed shaft: It drives the generator via a speed step-up gear.

Brake: A disc brake, which stops the rotor in emergencies. It can be applied mechanically, electrically, or hydraulically.

Gearbox: Gears connect the low-speed shaft to the high-speed shaft and increase the turbine speed from 30 to 60 rpm to the 1200 to 1800 rpm required by most generators to produce electricity in an efficient manner. Because the gearbox is a costly and heavy part, design engineers are exploring slow-speed, direct-drive generators that need no gearbox.

Generator: It is usually an off-the-shelf induction generator that produces 50- or 60-Hz AC power.

Nacelle: The rotor attaches to the nacelle, which sits atop the tower and includes a gearbox, low- and high-speed shafts, generator, controller, and a brake. A cover protects the components inside the nacelle. Some nacelles are large enough for technicians to stand inside while working.

Pitch: Blades are turned, or pitched, out of the wind to keep the rotor from turning in winds that have speeds too high or too low to produce electricity.

Upwind and downwind: The upwind turbine operates facing into the wind in front of the tower, whereas the downwind runs facing away from the wind after the tower.

Vane: It measures the wind direction and communicates with the yaw drive to orient the turbine properly with respect to the wind.

Yaw drive: It keeps the upwind turbine facing into the wind as the wind direction changes. A yaw motor powers the yaw drive. Downwind turbines do not require a yaw drive, as the wind blows the rotor downwind.

The design and operating features of various system components are described in the following subsections.

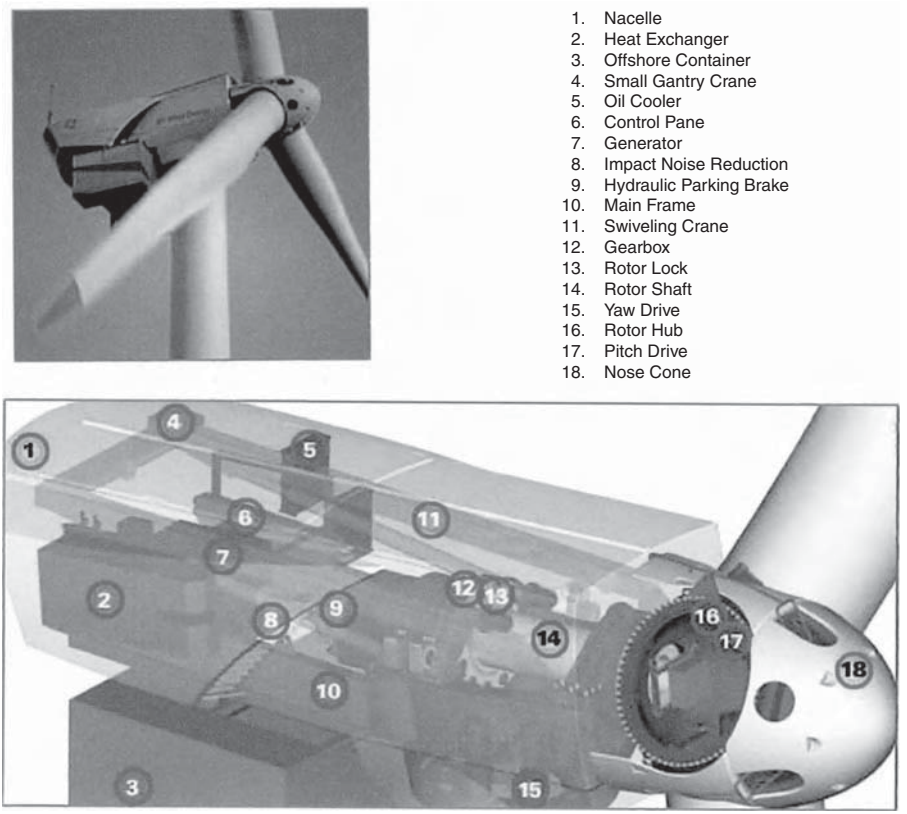

FIGURE 4.2 Nacelle details of a 3.6-MW/104-m-diameter wind turbine. (From GE Wind Energy. With permission.)

4.1.1 Tower

The wind tower supports the rotor and the nacelle containing the mechanical gear, the electrical generator, the yaw mechanism, and the stall control. Figure 4.2 depicts the component details and layout in a large nacelle, and Figure 4.3 shows the installation on the tower. The height of the tower in the past has been in the 20 to 50 m range. For medium- and large-sized turbines, the tower height is approximately equal to the rotor diameter, as seen in the dimension drawing of a 600-kW wind turbine (Figure 4.4). Small turbines are generally mounted on the tower a few rotor diameters high. Otherwise, they would suffer fatigue due to the poor wind speed found near the ground surface. Figure 4.5 shows tower heights of various-sized wind turbines relative to some known structures.

Both steel and concrete towers are available and are being used. The construction can be tubular or lattice. Towers must be at least 25 to 30 m high to avoid turbulence caused by trees and buildings. Utility-scale towers are typically twice as high to take advantage of the swifter winds at those heights.

FIGURE 4.3 A large nacelle under installation. (From Nordtank Energy Group, Denmark. With permission.)

The main issue in the tower design is the structural dynamics. The tower vibration and the resulting fatigue cycles under wind speed fluctuation are avoided by the design. This requires careful avoidance of all resonance frequencies of the tower, the rotor, and the nacelle from the wind fluctuation frequencies. Sufficient margin must be maintained between the two sets of frequencies in all vibrating modes.

The resonance frequencies of the structure are determined by complete modal analyses, leading to the eigenvectors and eigenvalues of complex matrix equations representing the motion of the structural elements. The wind fluctuation frequencies are found from the measurements at the site under consideration. Experience on a similar nearby site can bridge the gap in the required information.

Big cranes are generally required to install wind towers. Gradually increasing tower height, however, is bringing a new dimension in the installation (Figure 4.6). Large rotors add to the transportation problem as well. Tillable towers to nacelle and rotors moving upwards along with the tower are among some of the newer developments in wind tower installation. The offshore installation comes with its own challenge that must be met.

The top head mass (THM) of the nacelle and rotor combined has a significant bearing on the dynamics of the entire tower and the foundation. Low THM is generally a measure of design competency, as it results in reduced manufacturing and installation costs. The THMs of Vestas' 3-MW/90-m turbine is 103 t, NEG Micon's new 4.2-MW/110-m machine is 214 t, and Germany's REpower's 5-MW/125-m machine is about 350 t, which includes extra 15 to 20% design margins.

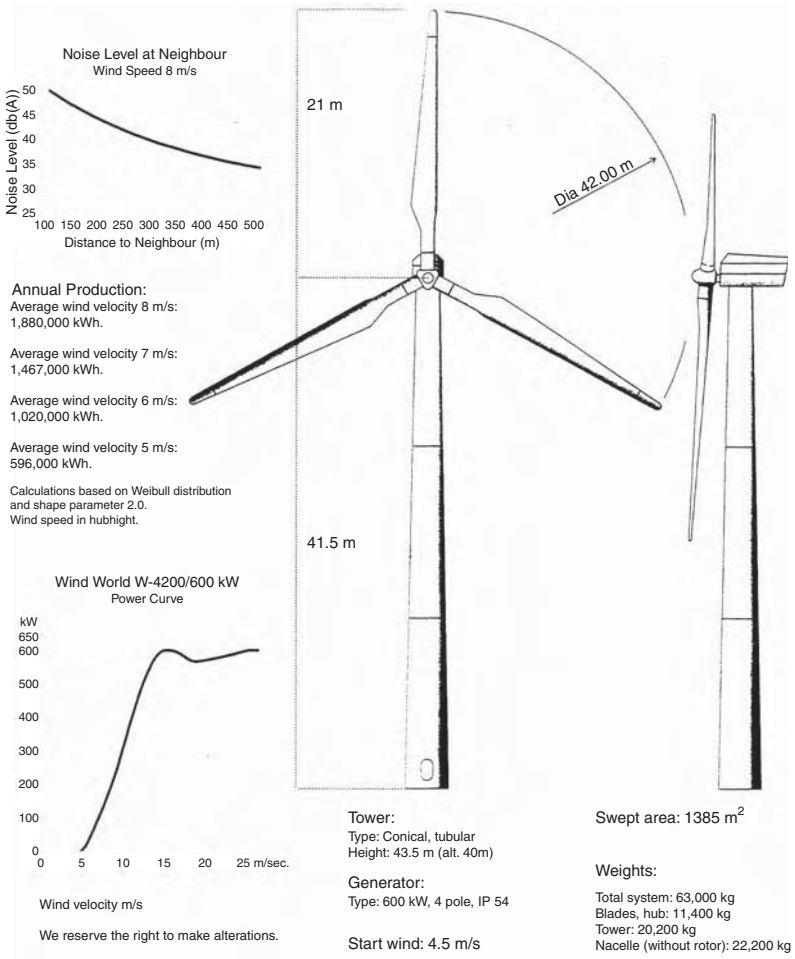

FIGURE 4.4 A 600-kW wind turbine and tower dimensions with specifications. (From Wind World Corporation, Denmark. With permission.)

4.1.2 Turbine

Wind turbines are manufactured in sizes ranging from a few kW for stand-alone remote applications to a few MW each for utility-scale power generation. The turbine size has been steadily increasing. The average size of the turbine installed worldwide in 2002 was over 1 MW. By the end of 2003, about 1200 1.5-MW turbines made by GE Wind Energy alone were installed and in operation. Today, even larger machines are being routinely installed on a large commercial scale, such as GE's new 3.6-MW turbines for offshore wind farms both in Europe and in the U.S. It offers lighter variable-speed, pitch-controlled blades on a softer support structure, resulting in a cost-effective foundation. Its rated wind speed is 14 m/sec with cut-in speed at 3.5 m/sec and the cutout at 25 m/sec. The blade diameter is 104 m with

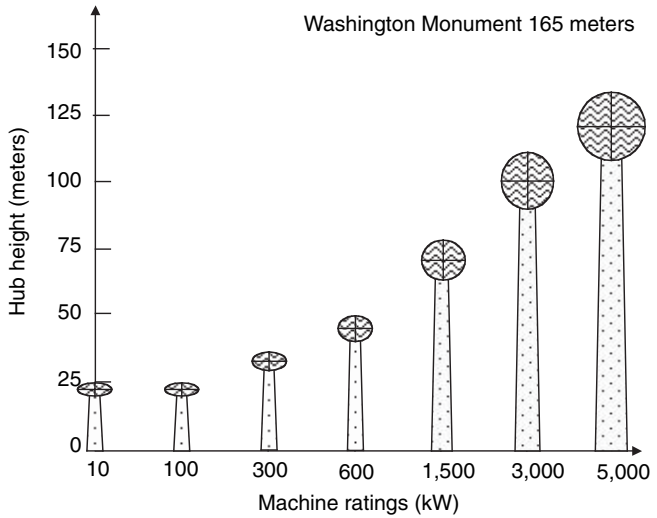

FIGURE 4.5 Tower heights of various capacity wind turbines.

hub height 100 m on land and 75 m offshore. In August 2002, Enercon's 4.5-MW wind turbine prototype was installed near Magdeburgh in eastern Germany. It has a 113-m rotor diameter, 124-m hub height, and an egg-shaped nacelle. Its reinforced concrete tower diameter is 12 m at the base, tapering to 4 m at the top. Today, even 5-MW machines are being installed in large offshore wind farms. The mass of a 5-MW turbine can vary from 150 to 300 t in nacelle and 70 to 100 t in the rotor blades, depending on the manufacturing technologies adopted at the time of design. The most modern designs would naturally be on the lighter side of the range.

Turbine procurement requires detailed specifications, which are often tailored from the manufacturers' specifications. The leading manufacturers of wind turbines in the world are listed in Table 4.1, with Denmark's Vestas leading with 22% of the world's market share. The major suppliers in the U.S. are GE Wind (52%), Vestas (21%), Mitsubishi (12%), NEG Micon (10%), and Gamesha (3%).

4.1.3 Blades

Modern wind turbines have two or three blades, which are carefully constructed airfoils that utilize aerodynamic principles to capture as much power as possible. The airfoil design uses a longer upper-side surface whereas the bottom surface remains somewhat uniform. By the Bernoulli principle, a "lift" is created on the airfoil by the pressure difference in the wind flowing over the top and bottom surfaces of the foil. This aerodynamic lift force flies the plane high, but rotates the wind turbine blades about the hub. In addition to the lift force on the blades, a drag force is created, which acts perpendicular to the blades, impeding the lift effect and slowing the rotor down. The design objective is to get the highest lift-to-drag ratio that can be varied along the length of the blade to optimize the turbine's power output at various speeds.

FIGURE 4.6 WEG MS-2 wind turbine installation at Myers Hill. (From Wind Energy Group, a Taylor Woodrow subsidiary and ETSU/DTI, U.K.)

TABLE 4.1
World's Major Wind Turbine Suppliers in 2004

Supplier	% Share of the World Market
Vestas, Denmark	22
GE Wind, U.S.	18
Enercon, Germany	15
Gamesha, Spain	12
NEG Micon, Denmark (Being acquired by Vestas, still separate trade names)	10

The rotor blades are the foremost visible part of the wind turbine, and represent the forefront of aerodynamic engineering. The steady mechanical stress due to centrifugal forces and fatigue under continuous vibrations make the blade design the weakest mechanical link in the system. Extensive design effort is needed to avoid premature fatigue failure of the blades. A swift increase in turbine size has been recently made possible by the rapid progress in rotor blade technology, including emergence of the carbon- and glass-fiber-based epoxy composites. The turbine blades are made of high-density wood or glass fiber and epoxy composites.

The high pitch angle used for stall control also produces a high force. The resulting load on the blade can cause a high level of vibration and fatigue, possibly leading to a mechanical failure. Regardless of the fixed- or variable-speed design, the engineer must deal with the stall forces. Researchers are moving from the 2-D to 3-D stress analyses to better understand and design for such forces. As a result, the blade design is continually changing, particularly at the blade root where the loading is maximum due to the cantilever effect.

The aerodynamic design of the blade is important, as it determines the energy-capture potential. The large and small machine blades have significantly different design philosophies. The small machine sitting on a tower relatively taller than the blade diameter, and generally unattended, requires a low-maintenance design. On the other hand, a large machine tends to optimize aerodynamic performance for the maximum possible energy capture. In either case, the blade cost is generally kept below 10% of the total installed cost.

4.1.4 Speed Control

The wind turbine technology has changed significantly in the last 25 yr.[1] Large wind turbines being installed today tend to be of variable-speed design, incorporating pitch control and power electronics. Small machines, on the other hand, must have simple, low-cost power and speed control. The speed control methods fall into the following categories:

No speed control whatsoever: In this method, the turbine, the electrical generator, and the entire system are designed to withstand the extreme speed under gusty winds.

Yaw and tilt control: The yaw control continuously orients the rotor in the direction of the wind. It can be as simple as the tail vane or more complex on modern towers. Theoretical considerations dictate free yaw as much as possible. However, rotating blades with large moments of inertia produce high gyroscopic torque during yaw, often resulting in loud noise. A rapid yaw may generate noise exceeding the local ordinance limit. Hence, a controlled yaw is often required and used, in which the rotor axis is shifted out of the wind direction when the wind speed exceeds the design limit.

Pitch control: This changes the pitch of the blade with changing wind speed to regulate the rotor speed. Large-scale power generation is moving towards variable-speed rotors with power electronics incorporating a pitch control.

Stall control: Yaw and tilt control gradually shifts the rotor axis in and out of the wind direction. But, in gusty winds above a certain speed, blades

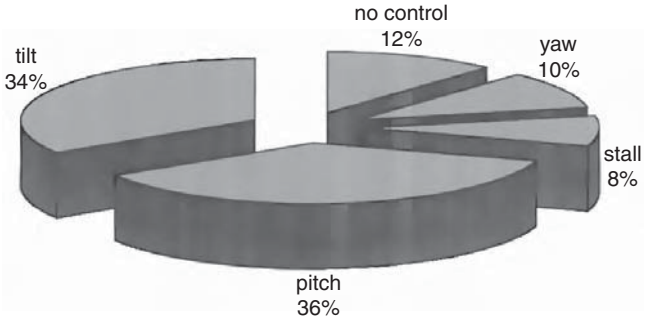

FIGURE 4.7 Speed control methods used in small- to medium-sized turbines.

are shifted (profiled) into a position such that they stall and do not produce a lift force. At stall, the wind flow ceases to be smooth around the blade contour, but separates before reaching the trailing edge. This always happens at a high pitch angle. The blades experience a high drag, thus lowering the rotor power output. This way, the blades are kept under the allowable speed limit in gusty winds. This not only protects the blades from mechanical overstress, but also protects the electrical generator from overloading and overheating. Once stalled, the turbine has to be restarted after the gust has subsided.

Figure 4.7 depicts the distribution of the control methods used in small wind turbine designs. Large machines generally use the power electronic speed control, which is covered in Chapter 6 and Chapter 11.

4.2 TURBINE RATING

The method of assessing the nominal rating of a wind turbine has no globally accepted standard. The difficulty arises because the power output of the turbine depends on the square of the rotor diameter and the cube of the wind speed. The rotor of a given diameter, therefore, would generate different power at different wind speeds. A turbine that can generate 300 kW at 7 m/sec would produce 450 kW at 8 m/sec wind speed. What rating should then be assigned to this turbine? Should we also specify the rated speed? Early wind turbine designers created a rating system that specified the power output at some arbitrary wind speed. This method did not work well because everyone could not agree on one speed for specifying the power rating. The "rated" wind speeds varied from 10 to 15 m/sec under this practice. Manufacturers quoted on the higher side to claim a greater output from the same design.

Such confusion in quoting the rating was avoided by some European manufacturers who quoted only the rotor diameter. But the confusion continued as to the maximum power the machine can generate under the highest wind speed in which the turbine can continuously and safely operate. Many manufacturers have, therefore,

adopted the combined rating designations x/y, the generator's peak electrical capacity followed by the wind turbine diameter. For example, a 300/30-kW/m wind system means a 300-kW electrical generator and a 30-m diameter turbine. The specific rated capacity (SRC) is often used as a comparative index of the wind turbine designs. It measures the power generation capacity per square meter of the blade-swept area, and is defined as follows in units of kW/m^2:

$$SRC = \frac{\text{Generator electrical capacity}}{\text{Rotor-swept area}} \tag{4.1}$$

The SRC for a 300/30 wind turbine is $300/\pi \times 15^2 = 0.42$ kW/m^2. It increases with diameter, giving favorable economies of scale for large machines, and ranges from approximately 0.2 kW/m^2 for a 10-m diameter rotor to 0.5 kW/m^2 for a 40-m diameter rotor. Some aggressively rated turbines have an SRC of 0.7 kW/m^2, and some reach as high as 1 kW/m^2. The higher-SRC rotor blades have higher operating stresses, which result in a shorter fatigue life. All stress concentration regions are carefully identified and eliminated in high-SRC designs. Modern design tools, such as the finite element stress analysis and the modal vibration analysis, can be of great value in rotor design.

Turbine rating is important as it indicates to the system designer how to size the electrical generator, the plant transformer, and the connecting cables to the substation and the transmission link interfacing the grid. The power system must be sized on the peak capacity of the generator. Because turbine power depends on the cube of the wind speed, the system-design engineer matches the turbine and the generator performance characteristics. This means selecting the rated speed of the turbine to match with the generator. As the gearbox and generator are manufactured only in discrete sizes, selecting the turbine's rated speed can be complex. The selection process goes through several iterations, trading the cost with benefit of the available speeds. Selecting a low rated speed would result in wasting much energy at high winds. On the other hand, if the rated speed is high, the rotor efficiency will suffer most of the time.

Figure 4.8 is an example of the technical summary data sheet of the 550/41-kW/m wind turbine manufactured by Nordtank Energy Group of Denmark. Such data is used in the preliminary design of the overall system. The SRC of this machine is 0.414. It has a cut-in wind speed of 5 m/sec, a cutout speed of 25 m/sec, and it reaches the peak power at 15 m/sec.

4.3 POWER VS. SPEED AND TSR

The typical turbine torque vs. rotor speed is plotted in Figure 4.9. It shows a small torque at zero speed, rising to a maximum value before falling to nearly zero when the rotor just floats with the wind. Two such curves are plotted for different wind speeds V_1 and V_2, with V_2 being higher than V_1. The corresponding power vs. rotor speed at the two wind speeds are plotted in Figure 4.10. As the mechanical power converted into the electric power is given by the product of the torque T and the

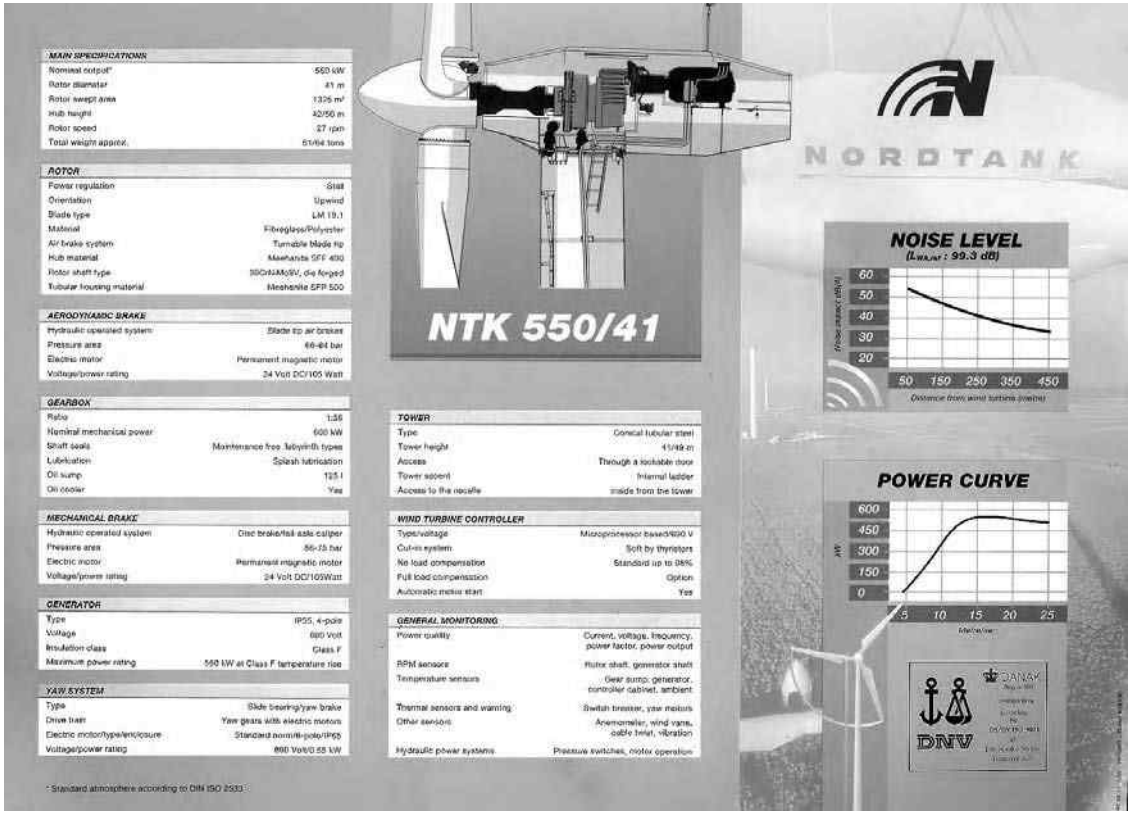

FIGURE 4.8 Technical data sheet of a 550-kW/41-m diameter wind turbine, with power level and noise level. (From Nordtank Energy Group, Denmark. With permission.)

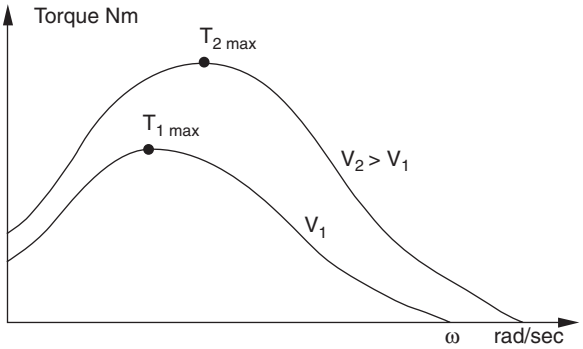

FIGURE 4.9 Wind turbine torque vs. rotor speed characteristic at two wind speeds, V_1 and V_2.

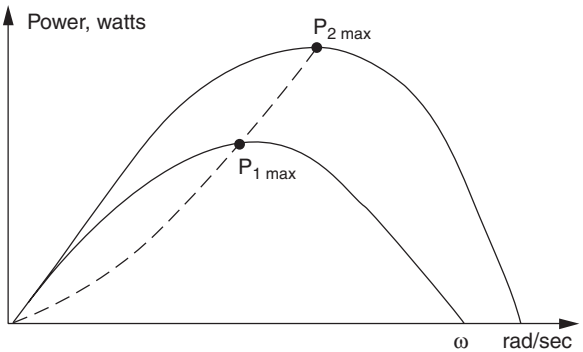

FIGURE 4.10 Wind turbine power vs. rotor speed characteristic at two wind speeds, V_1 and V_2.

angular speed, the power is zero at zero speed and again at high speed with zero torque. The maximum power is generated at a rotor speed somewhere in between, as marked by P_{1max} and P_{2max} for speeds V_1 and V_2, respectively. The speed at the maximum power is not the same speed at which the torque is maximum. The operating strategy of a well-designed wind power system is to match the rotor speed to generate power continuously close to the P_{max} points. Because the P_{max} point changes with the wind speed, the rotor speed must, therefore, be adjusted in accordance with the wind speed to force the rotor to work continuously at P_{max}. This can be done with a variable-speed system design and operation.

At a given site, the wind speed varies over a wide range from zero to high gust. We define tip speed ratio (TSR) as follows:

$$TSR = \frac{\text{Linear speed of the blade's outermost tip}}{\text{Free upstream wind velocity}} = \frac{\omega R}{V} \tag{4.2}$$

where R and ω are the rotor radius and the angular speed, respectively.

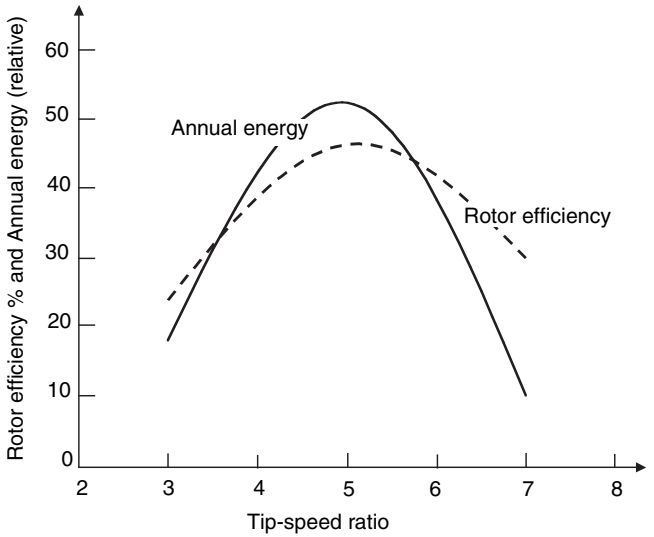

FIGURE 4.11 Rotor efficiency and annual energy production vs. rotor TSR.

For a given wind speed, the rotor efficiency C_p varies with TSR as shown in Figure 4.11. The maximum value of C_p occurs approximately at the same wind speed that gives peak power in the power distribution curve of Figure 4.10. To capture high power at high wind, the rotor must also turn at high speed, keeping TSR constant at the optimum level. However, the following three system performance attributes are related to TSR:

1. The maximum rotor efficiency C_p is achieved at a particular TSR, which is specific to the aerodynamic design of a given turbine. As was seen in Figure 3.4, the TSR needed for maximum power extraction ranges from nearly one for multiple-blade, slow-speed machines to nearly six for modern high-speed, two-blade machines.
2. The centrifugal mechanical stress in the blade material is proportional to the TSR. The machine working at a higher TSR is necessarily stressed more. Therefore, if designed for the same power in the same wind speed, the machine operating at a higher TSR would have slimmer rotor blades.
3. The ability of a wind turbine to start under load is inversely proportional to the design TSR. As this ratio increases, the starting torque produced by the blade decreases.

A variable-speed control is needed to maintain a constant TSR to keep the rotor efficiency at its maximum. At the optimum TSR, the blades are oriented to maximize the lift and minimize the drag on the rotor. The turbine selected for a constant TSR operation allows the rotational speed of both the rotor and generator to vary up to 60% by varying the pitch of the blades.

TABLE 4.2
Advantages of Fixed- and Variable-Speed Systems

Fixed-Speed System	Variable-Speed System
Simple and inexpensive electrical system	Higher rotor efficiency, hence, higher energy capture per year
Fewer parts, hence, higher reliability	Low transient torque
Lower probability of excitation of mechanical resonance of the structure	Fewer gear steps, hence, inexpensive gear box
No frequency conversion, hence, no current harmonics present in the electrical system	Mechanical damping system not needed; the electrical system could provide damping if required
Lower capital cost	No synchronization problems
	Stiff electrical controls can reduce system voltage sags

4.4 MAXIMUM ENERGY CAPTURE

The wind power system design must optimize the annual energy capture at a given site. The only operating mode for extracting the maximum energy is to vary the turbine speed with varying wind speed such that at all times the TSR is continuously equal to that required for the maximum power coefficient C_p. The theory and field experience indicate that the variable-speed operation yields 20 to 30% more power than with the fixed-speed operation. Nevertheless, the cost of variable-speed control is added. In the system design, this trade-off between energy increase and cost increase has to be optimized. In the past, the added costs of designing the variable-pitch rotor, or the speed control with power electronics, outweighed the benefit of the increased energy capture. However, the falling prices of power electronics for speed control and the availability of high-strength fiber composites for constructing high-speed rotors have made it economical to capture more energy when the speed is high. The variable-speed operation has an indirect advantage. It allows controlling the active and reactive powers separately in the process of automatic generation control. In fixed-speed operation, on the other hand, the rotor is shut off during high wind speeds, losing significant energy. The pros and cons of fixed- and variable-speed operations are listed in Table 4.2.

Almost all major suppliers now offer variable-speed systems in combination with pitch regulation. Potential advantages of the variable-speed system include active grid support, peak-power-tracking operation, and cheaper offshore foundation structure. The doubly fed induction generator is being used in some large wind turbines such as NEG Micon's 4.2-MW, 110-m diameter machines and multimegawatt GE machines. It is an emerging trendsetting technology in the variable-speed gear-driven systems, primarily because only the slip frequency power (20 to 30% of the total) has to be fed through the frequency converter. This significantly saves power electronics cost.

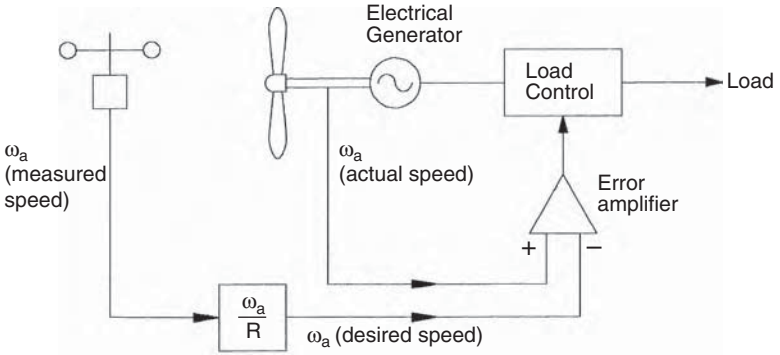

FIGURE 4.12 Maximum power operation using rotor tip speed control scheme.

4.5 MAXIMUM POWER OPERATION

As seen earlier, operating the wind turbine at a constant TSR corresponding to the maximum power point at all times can generate 20 to 30% more electricity per year. However, this requires a control scheme to operate with a variable speed to continuously generate the maximum power. Two possible schemes for such an operation are as follows:

4.5.1 Constant-TSR Scheme

In this scheme the machine is continuously operated at its optimum TSR, which is a characteristic of the given wind turbine. This optimum value is stored as the reference TSR in the control computer. The wind speed is continuously measured and compared with the blade tip speed. The error signal is then fed to the control system, which changes the turbine speed to minimize the error (Figure 4.12). At this time the rotor must be operating at the reference TSR, generating the maximum power. This scheme has the disadvantage of requiring the local wind speed measurements, which could have a significant error, particularly in a large wind farm with shadow effects. Being sensitive to the changes in the blade surface, the optimum TSR gradually changes with age and environment. The computer reference TSR must be changed accordingly many times, which is expensive. Besides, it is difficult to determine the new optimum TSR with changes that are not fully understood or easily measured.

4.5.2 Peak-Power-Tracking Scheme

The power vs. speed curve has a single well-defined peak. If we operate at the peak point, a small increase or decrease in the turbine speed would result in no change in the power output, as the peak point locally lies in a flat neighborhood. In other words, a necessary condition for the speed to be at the maximum power point is as follows:

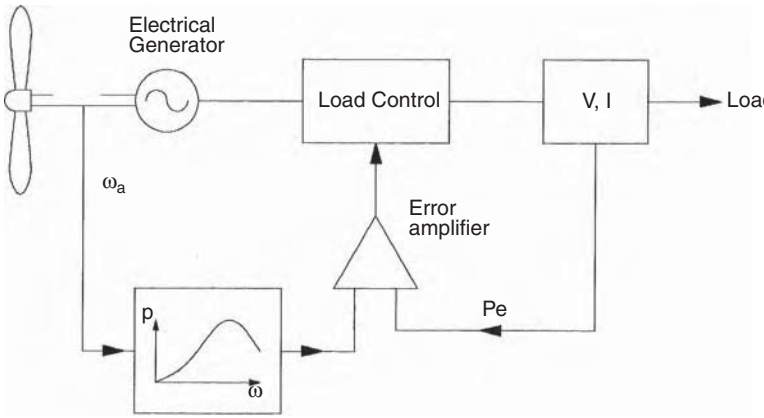

FIGURE 4.13 Maximum power operation using power control scheme.

$$\frac{dP}{d\omega} = 0 \tag{4.3}$$

This principle is used in the control scheme (Figure 4.13). The speed is increased or decreased in small increments, the power is continuously measured, and $\Delta P/\Delta\omega$ is continuously evaluated. If this ratio is positive — meaning we get more power by increasing the speed — the speed is further increased. On the other hand, if the ratio is negative, the power generation will reduce if we change the speed any further. The speed is maintained at the level where $\Delta P/\Delta\omega$ is close to zero. This method is insensitive to errors in local wind speed measurement, and also to wind turbine design. It is, therefore, the preferred method. In a multiple-machine wind farm, each turbine must be controlled by its own control loop with operational and safety functions incorporated.

4.6 SYSTEM-DESIGN TRADE-OFFS

When the land area is limited or is at a premium price, one optimization study that must be conducted in an early stage of the wind farm design is to determine the number of turbines, their size, and the spacing for extracting the maximum energy from the farm annually. The system trade-offs in such a study are as follows:

4.6.1 Turbine Towers and Spacing

Large turbines cost less per megawatt of capacity and occupy less land area. On the other hand, fewer large machines can reduce the megawatthour energy crop per year, as downtime of one machine would have larger impact on the energy output. A certain turbine size may stand out to be the optimum for a given wind farm from the investment and energy production cost points of view.

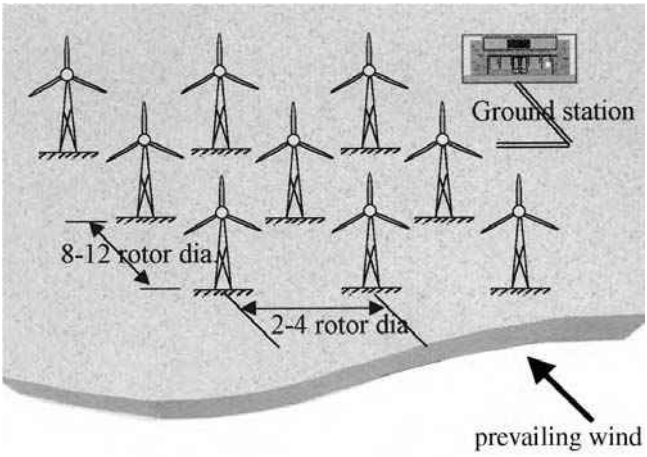

FIGURE 4.14 Optimum tower spacing in wind farms in flat terrain.

Tall towers are beneficial, but the height must be optimized with the local regulations and constrains of the terrain and neighborhood. Nacelle weight and structural dynamics are also important considerations.

When installing a cluster of machines in a wind farm, certain spacing between the wind towers must be maintained to optimize the energy crop over the year. The spacing depends on the terrain, wind direction, wind speed, and turbine size. The optimum spacing is found in rows 8 to 12 rotor diameters apart in the wind direction, and 2 to 4 rotor diameters apart in the crosswind direction (Figure 4.14). A wind farm consisting of 20 towers, rated at 500 kW each, needs 1 to 2 km^2 of land area. Of this, less than 5% of the land is actually required for turbine towers and access roads. The remaining land could continue its original use. Thus, wind turbines can co-exist with grazing, farming, fishing, and recreational use (Figure 4.15). The average number of machines in wind farms varies greatly, ranging from several to hundreds depending on the required power capacity of the farm. The preceding spacing rules would ensure that the turbines do not shield those further downwind. Some wind farms have used narrow spacing of five to six rotor diameters in the wind direction. One such farm in Mackinaw City, MI, has reported the rotors in downwind direction running slower due to the wake effect of the upwind rotors.

The wind power fluctuations and electrical transients on fewer large machines would cost more in the filtering of power and voltage fluctuations, or would degrade the quality of power, inviting penalty from the grid.

The optimization method presented by Roy[2] takes into account the preceding trades. Additionally, it includes the effect of tower height that goes with the turbine diameter, available standard ratings, cost at the time of procurement, and wind speed. The wake interaction and tower shadow are ignored for simplicity. Such optimization leads to a site-specific number and size of the wind turbines that will minimize the energy cost.

FIGURE 4.15 Original land use continues in a wind farm in Germany. (From Vestas Wind Systems, Denmark. With permission.)

4.6.2 Number of Blades

One can extract the power available in the wind with a small number of blades rotating quickly, or a large number of blades rotating slowly. More blades do not give more power, but they give more torque and require heavier construction. A few fast-spinning blades result in an economical system. Wind machines have been built with the number of blades ranging from 1 to 40 or more. A one-blade machine, although technically feasible, gives a supersonic tip speed and a highly pulsating torque, causing excessive vibrations. It is, therefore, hardly used in large systems. A very high number of blades were used in old low-TSR rotors for water pumping and grain milling, the applications requiring high starting torque. Modern high-TSR rotors for generating electric power have two or three blades, many of them with just two, although the Danish standard is three blades. The major factors involved in deciding the number of blades are as follows:

- The effect on power coefficient
- The design TSR
- The means of limiting yaw rate to reduce the gyroscopic fatigue

Compared to the two-blade design, the three-blade machine has smoother power output and a balanced gyroscopic force. There is no need to teeter the rotor, allowing the use of a simple rigid hub. Three blades are more common in Europe, where large machines up to a few MW are being built using the three-blade configuration. The practice in the U.S, however, has been to use the two-blade design. Adding the third blade increases the power coefficient only by about 5%, thus giving a diminished

rate of return for the 50% more blade weight and cost. The two-blade rotor is also simpler to erect, because it can be assembled on the ground and lifted to the shaft without complicated maneuvers during the lift. The number of blades is often viewed as the blade solidity. Higher solidity ratio gives higher starting torque and leads to low-speed operation. For electric power generation, the turbine must run at high speeds as the electrical generator weighs less and operates more efficiently at high speeds. That is why all large-scale wind turbines have low solidity ratio, with just two or three blades.

4.6.3 Rotor Upwind or Downwind

Operating the rotor upwind of the tower produces higher power as it eliminates the tower shadow on the blades. This results in lower noise, lower blade fatigue, and smoother power output. A drawback is that the rotor must constantly be turned into the wind via the yaw mechanism. The heavier yaw mechanism of an upwind turbine requires a heavy-duty and stiffer rotor compared to a downwind rotor.

The downwind rotor has the wake (wind shade) of the tower in the front and loses some power from the slight wind drop. On the other hand, it allows the use of a free yaw system. It also allows the blades to deflect away from the tower when loaded. Its drawback is that the machine may yaw in the same direction for a long period of time, which can twist the cables that carry current from the turbines.

Both types have been used in the past with no clear trend. However, the upwind rotor configuration has recently become more common.

4.6.4 Horizontal vs. Vertical Axis

In the horizontal-axis Danish machine, considered to be classical, the axis of blade rotation is horizontal with respect to the ground and parallel to the wind stream. Most wind turbines are built today with the horizontal-axis design, which offers a cost-effective turbine construction, installation, and control by varying the blade pitch.

The vertical-axis Darrieus machine has different advantages. First of all, it is omnidirectional and requires no yaw mechanism to continuously orient itself toward the wind direction. Secondly, its vertical drive shaft simplifies the installation of the gearbox and the electrical generator on the ground, making the structure much simpler. On the negative side, it normally requires guy wires attached to the top for support. This could limit its applications, particularly at offshore sites. Overall, the vertical-axis machine has not been widely used, primarily because its output power cannot be easily controlled in high winds simply by changing the blade pitch. With modern low-cost variable-speed power electronics emerging in the wind power industry, the Darrieus configuration may revive, particularly for large-capacity applications.

The Darrieus has structural advantages compared to a horizontal-axis turbine because it is balanced. The blades only “see” the maximum lift torque twice per revolution. Seeing maximum torque on one blade once per revolution excites many natural frequencies, causing excessive vibrations. Also a vertical-axis wind turbine configuration is set on the ground. Therefore, it is unable to effectively use higher wind speeds using a higher tower, as there is no tower here.

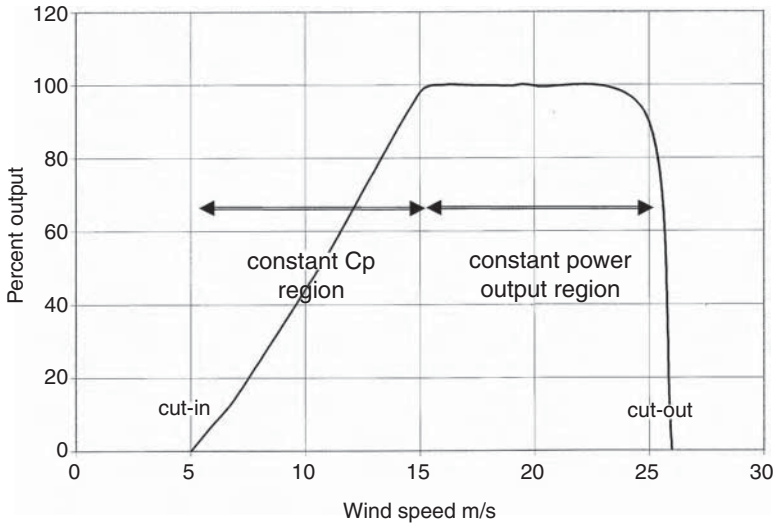

FIGURE 4.16 Five regions of turbine speed control.

4.7 SYSTEM CONTROL REQUIREMENTS

Both the speed and the rate of change must be controlled in a good system design.

4.7.1 Speed Control

The rotor speed must be controlled for three reasons:

- To capture more energy, as seen before.
- To protect the rotor, generator, and power electronic equipment from overloading during high-gust winds.
- When the generator is disconnected from the electrical load, accidentally or for a scheduled event. Under this condition, the rotor speed may run away, destroying it mechanically, if it is not controlled.

The speed control requirement of the rotor has five separate regions as shown in Figure 4.16:

1. The cut-in speed at which the turbine starts producing power. Below this speed, it is not worthwhile, nor efficient, to turn the turbine on.
2. The constant maximum C_p region where the rotor speed varies with the wind speed variation to operate at the constant TSR corresponding to the maximum C_p value.
3. During high winds, the rotor speed is limited to an upper constant limit based on the design limit of the system components. In the constant-speed region, the C_p is lower than the maximum C_p, and the power increases at a lower rate than that in the first region.

4. At still higher wind speeds, such as during a gust, the machine is operated at a controlled constant power to protect the generator and power electronics from overloading. This can be achieved by lowering the rotor speed. If the speed is decreased by increasing the electrical load, then the generator will be overloaded, defeating the purpose. To avoid generator overloading, some sort of a brake (eddy current or another type) must be installed on the rotor.
5. The cutout speed, at which the rotor is shut off to protect the blades, the electrical generator, and other components of the system beyond a certain wind speed.

4.7.2 Rate Control

The inertia of large rotors must be taken into account in controlling the speed. The acceleration and deceleration must be controlled to limit the dynamic mechanical stresses on the blades and hub, and the electrical load on the generator and power electronics. The instantaneous difference between the mechanical power produced by the blades and the electric power delivered by the generator will change the rotor speed as follows:

$$J\frac{d\omega}{dt} = \frac{P_m - P_e}{\omega} \tag{4.4}$$

where
J = polar moment of inertia of the rotor
ω = angular speed of the rotor
P_m = mechanical power produced by the blades
P_e = electric power delivered by the generator

Integrating Equation 4.4, we obtain:

$$\frac{1}{2}J(\omega_2^2 - \omega_1^2) = \int_{t_1}^{t_2}(P_m - P_e)\,dt \tag{4.5}$$

Let us examine this aspect for a sample rotor with the moment of inertia J = 7500 kg.m^2. Changing this rotor speed from 100 to 95 rpm in 5 sec requires ΔP of 800 kW. The resulting torque of 80 Nm would produce torsional stress on the rotor structure and hub components. If the same speed change were made in 1 sec, the required power would be 4000 kW, and the torque, 400 Nm. Such high torque can overstress and damage the rotor parts or shorten its life significantly. For this reason, the acceleration and deceleration must be kept within design limits, with adequate margins.

The strategy for controlling the speed of the wind turbine varies with the type of electrical machine used, i.e., the induction, synchronous, or DC machine.

TABLE 4.3
Noise Levels of Some Commonly Known Sources Compared with Wind Turbine

Source	Noise Level (dB)
Elevated train	100
Noisy factory	90
Average street	70
Average factory	60
Average office	50
Quiet conversation	30

4.8 ENVIRONMENTAL ASPECTS

The following aspects of environmental considerations enter the wind farm setting:

4.8.1 Audible Noise

The wind turbine is generally quiet. It poses no objectionable noise disturbance in the surrounding area. The wind turbine manufacturers supply the machine noise level data in dB(A) vs. the distance from the tower. A typical 600-kW machine noise level is shown in Figure 4.8. This machine produces 55-dB(A) noise at 50-m distance from the turbine and 40-dB(A) at 250-m distance. Table 4.3 compares the turbine noise level with other generally known noise levels. The table indicates that the turbine at a 50-m distance produces no noise higher than the average factory. This noise, however, is a steady noise. Additionally, the turbine makes a louder noise while yawing under the changing wind direction. In either case, the local noise ordinance must be complied with. In some instances, there have been cases of noise complaints reported by the nearby communities. Although noise pollution is not a major problem with offshore wind farms, it depends on the size whether or not one can hear the turbines while operating. It has also been suggested that the noise from the turbines travels underwater and disturbs sea life as well.

In general, there are two main sources of noise emitted from the wind turbine. One is mechanical, which is inherent in the gearing system. The other is created by the aerodynamics of the rotating blade, which emits a noise when passing the tower, known as the tower thump or simply the aerodynamic noise. The first may be at a somewhat low level, generally uniform over the year. The other — the tower thump — can be loud. It varies with the speed of blade rotation and may cause most of the problems and complaints. Some residents describe the tower thump noise as being like a boot in a tumble dryer. A large wind turbine can produce an aggregate noise level of up to 100 dB(A), which weakens to a normal level within a 1.5-km distance. The worst conditions are when the wind is blowing lightly and the back-

ground noise is minimal. Residents up to 1-km radius have complained to the Environmental Health Department about noise from such turbines.

4.8.2 Electromagnetic Interference (EMI)

Any stationary or moving structure in the proximity of a radio or TV tower interferes with the signals. The wind turbine tower, being a large structure, can cause objectionable EMI in the performance of a nearby transmitter or a receiver. Additionally, the rotating blades of an operating wind turbine may reflect impinging signals so that the electromagnetic signals in the neighborhood may experience interference at the blade passage frequency. The exact nature and magnitude of such EMIs depend on a number of parameters. The primary parameters are the location of the wind turbine tower relative to the radio or TV tower, physical and electrical properties of the rotor blades, the signal frequency modulation scheme, and the high-frequency electromagnetic wave propagation characteristics in the local atmosphere.[3]

EMI may be a serious issue with wind farm planning. For example, 5 of the 18 offshore wind farms planned around the U.K. coasts were blocked by the U.K. Ministry of Defense due to concerns that they may interfere with radar and flight paths to airfields close to the proposed sites. Detailed studies on the precise effects of wind turbines on radar and possible modifications in radar software may mitigate the concerns. The potential cost of such studies and legal appeals should be factored into the initial planning of large wind farms.

The University of Liverpool in the U.K. has investigated the effects of electromagnetic fields generated by offshore wind farm cables on the marine environment.

4.8.3 Effects on Birds

The effect of wind farms on wild life and avian population — including endangered species protected by federal laws — has created controversy and confusion within the mainstream environmental community. The breeding and feeding patterns of some birds may be disturbed. The wind turbine blade can weigh up to 1.5 t and the blade tips can travel at up to 200 mph, a lethal weapon against any airborne creature. The birds may be killed or at least injured if they collide with a blade. Often the suction draft created by the wind flowing to a turbine draws the birds into the airstream headed for the blades. Although less usual, birds are attracted by the tower hum (music!) and simply fly into the towers. On the other hand, studies at an inshore site near Denmark have determined that birds alter their flight paths 200 m around the turbine. Thus, a wind farm can significantly alter the flight paths of large avian populations. In another study, the population of water fowl declined 75 to 90% within 3 yr after installing an offshore wind farm in Denmark. Such a large decline could have a massive impact on the ecosystem of the surrounding area.

The initial high bird-kill rate of the 1980s has significantly declined with larger turbines having longer slower-moving blades, which are easier for the birds to see and avoid. Tubular towers have a lower bird-hit rate compared to lattice towers, which attract birds to nest. The turbines are now mounted on either solid tubular towers

or towers with diagonal bracing, eliminating the horizontal supports that attracted the birds for nesting. New wind farms are also sited away from avian flight paths.

Data from various sources on the birds killed follow:

- In Altamont Pass, CA, 200 to 300 red-tailed hawks and 40 to 60 golden eagles were killed annually by early wind farms in the 1980s. Bill Evans of Cornell University estimated that the bird kills due to wind farms may have exceeded 5,000,000/yr during the 1980s. Up to 10,000 have been killed by one turbine in one night. A 1994 estimate in Europe showed a significant number of 13 bird species, protected by European law, killed by turbines at Tarifa, Spain.
- Forest City School District in Iowa, which was buying electricity from a local utility at 4.5 cents/kWh, has installed wind turbines for self-sufficiency in energy. Their turbine sites have the most wind in the city, and are in the migratory path of many geese. Even then, neither bird kills nor noise complaints were reported over the first several years of operation.
- By way of comparison, U.S. hunters annually kill about 121 million birds, and about one billion birds are killed by flying into glass windows on their own each year in the U.S.

It is generally agreed that migration paths and nesting grounds of rare species of birds should be protected against the threat of wind farms. Under these concerns, obtaining permission from the local planning authorities can take considerable time and effort.

4.8.4 Other Impacts

The visual impact of the wind farm may be unpleasant to the property owners around the wind farm. This is more so for offshore wind farms, where the property owners are usually affluent people with significant influence on the area's policymaking organizations. The most publicized proposed project in Nantucket Sound became highly controversial by high-profiled owners of the waterfront estates.

Wind farm designers can minimize aesthetic complaints by installing identical turbines and spacing them uniformly.

Because wind is a major transporter of energy across the globe, the impact of the energy removed by many large wind farms on a grand scale may impact the climate. This may be a subject of future studies.

4.9 POTENTIAL CATASTROPHES

A fire or an earthquake can be a major catastrophe for a wind power plant.

4.9.1 Fire

Fire damage amounts to 10 to 20% of the wind plant insurance claims. A fire on a wind turbine is rare but difficult to fight. Reaching the hub height is slow, and water pressure is always insufficient to extinguish the fire. This generally leads to a total

loss of the turbine, leading to 9 to 12 months of downtime and lost revenue. The cost of replacing a single 30-m blade can exceed $100,000, and that of replacing the whole 3-MW turbine can exceed $2 million.

The following are some causes of fire in wind turbines:

Lightning strike: Lightning arresters are used to protect the turbine blades, nacelle, and tower assembly. However, if lightning is not properly snubbed, it can lead to local damage or total damage if it leads to sparks and subsequent turbine fire. Lightning occurrences depend on the location. Offshore turbines are more prone to lightning than land turbines. On land, lightning is rare in Denmark, whereas it is frequent in northern Germany and the Alps regions, and even more frequent in parts of Japan and the U.S., particularly in Florida and Texas. The growing trends of using electrically conducting carbon fiber-epoxy composites for their high strength and low weight in the blade construction make the blades more vulnerable to lightning. For this reason, some manufacturers avoid carbon fibers in their blades, more so in large, tall turbines for offshore installations.

Internal fault: Any electrical or mechanical fault leading to a spark with the transmission fluids or other lubricants is a major risk. The flammable plastic used in the construction, such as the nacelle covers, is also a risk. Typical internal faults that can cause excessive heat leading to a fire are as follows:

- Bearings running dry and failing
- Failing cooling system
- Brakes becoming hot under sustained braking
- Oil and grease spills
- Short circuit in the battery pack of the pitch-control system
- Cables running against rotating or vibrating components

Frequent physical checks of the entire installation, servicing and maintenance, and a condition-monitoring system, accessed remotely by computers used in modern installations, can detect potential fire hazards and avoid fires.

4.9.2 Earthquake

Lateral loads resulting from an earthquake are important data to consider in designing a tall structure in many parts of the world. The wind tower, being always tall, is especially vulnerable to seismic events. The seismic energy is concentrated in the 1- to 10-Hz frequency band. A dynamic analysis is required, as a dynamic response amplification is expected. However, because of the complexities in modeling and performing such analyses, it has been standard practice to represent seismic loads with equivalent static loads. The severity of the seismic loads, the potential failure modes, and the resulting effects require that design engineers make reasonable trade-offs between potential safety concerns and economics during the design phase. To alleviate this difficulty, the recent trend in the U.S. has been to require dynamic analyses to estimate seismic stresses. For example, all primary components of nuclear power plants in the U.S. must be dynamically analyzed for the specified seismic loadings. This is required even for plants located in seismically inactive areas.

4.10 SYSTEM-DESIGN TRENDS

Significant research and development work is underway at the NREL and the National Wind Technology Center in Golden, CO. The main areas of applied research conducted at the NWTC are as follows:

- Aerodynamics to increase energy capture and reduce acoustic impacts.
- Inflow and turbulence to understand the nature of wind.
- Structural dynamics models to minimize the need of prototypes.
- Controls to enhance energy capture, reduce loads, and maintain stable closed-loop behavior of these flexible systems are an important design goal.
- The wind turbine design progress includes larger turbines on taller towers to capture higher wind speed; the design difficulty increases as these machines become larger and the towers become taller.

References

1. Van Kuik, G., Wind turbine technology — 25 years' progress, *Wind Directions*, April 1998.
2. Roy, S., Optimal planning of wind energy conversion systems over an energy scenario, IEEE Transactions on Energy Conversion, September 1997.
3. Spera, D. A., *Wind Turbine Technology*, American Society of Mechanical Engineers, New York, 1994.

5 Electrical Generators

The mechanical power of a wind turbine is converted into electric power by an alternating current (AC) generator or a direct current (DC) generator. The AC generator can be either a synchronous machine or an induction machine, the latter being the most widely used in the wind power industry.

The electrical machine works on the principle of action and reaction of electromagnetic induction. The resulting electromechanical energy conversion is reversible. The same machine can be used as a motor for converting electric power into mechanical power or as a generator for converting mechanical power into electric power.

Figure 5.1 depicts common construction features of electrical machines. Typically, there is an outer stationary member (stator) and an inner rotating member (rotor). The rotor is mounted on bearings fixed to the stator. Both the stator and the rotor carry cylindrical iron cores, which are separated by an air gap. The cores are made of magnetic iron of high permeability and have conductors embedded in slots distributed on the core surface. Alternatively, the conductors are wrapped in the coil form around salient magnetic poles. Figure 5.2 is a cross-sectional view of a rotating electrical machine with the stator made of salient poles and the rotor with distributed conductors. The magnetic flux, created by the excitation current in one of the two coils, passes from one core to the other in a combined magnetic circuit always forming a closed loop. Electromechanical energy conversion is accomplished by interaction of the magnetic flux produced by one coil with the electrical current in the other coil. The current may be externally supplied or electromagnetically induced. The induced current in a coil is proportional to the rate of change in the flux linkage of that coil.

The various types of machines differ fundamentally in the distribution of the conductors forming the windings, and by their elements: whether they have continuous slotted cores or salient poles. The electrical operation of any given machine depends on the nature of the voltage applied to its windings. The narrow annular air gap between the stator and the rotor is the critical region of the machine operation, and the theory of performance is mainly concerned with the conditions in or near the air gap.

5.1 DC GENERATOR

All machines in the internal working are AC machines, because the conductors rotate in the magnetic flux of alternate north and south poles. The DC machine converts the inside AC into DC for outside use. It does so by using a mechanical commutator. The commutator performs this function by sliding carbon brushes along a series of copper segments. It switches the positive output terminal continuously to the conductor generating the positive polarity voltage, and likewise for the negative polarity

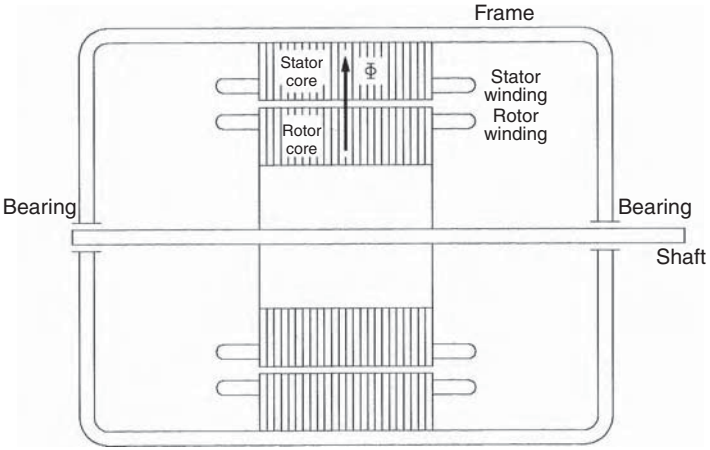

FIGURE 5.1 Common constructional features of rotating electrical machines.

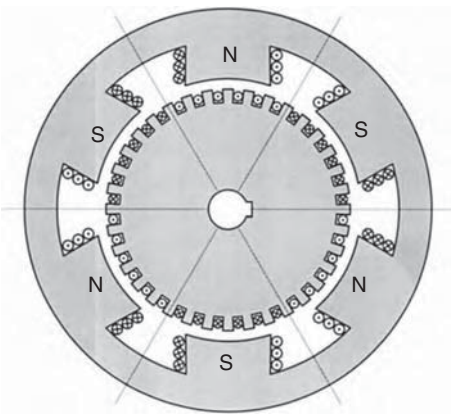

FIGURE 5.2 Cross section of the electrical machine stator and rotor.

terminal. The sliding contacts inherently result in low reliability and high maintenance cost. Despite this disadvantage, the DC machine was used extensively as a motor until the early 1980s because of its extremely easy speed control. It has been used as a generator in a limited number of wind power installations of small capacity, particularly where the electricity could be locally used in the DC form. However, the conventional DC machine with a mechanical commutator and sliding carbon brushes has fallen out of favor in the present day. Its brushless version is used where the DC machine gives a system advantage.

The conventional DC machine is either self-excited by shunt or by series coils carrying DC current to produce a magnetic field. The modern DC machine is often designed with permanent magnets to eliminate the field current requirement, hence, the commutator. It is designed in the "inside-out" configuration. The rotor carries

the permanent-magnet poles and the stator carries the wound armature. The stator produces AC current, which is then rectified using the solid-state semiconducting devices. Such a machine does not need the commutator and the brushes; hence, the reliability is greatly improved. The permanent-magnet DC machine is used with small wind turbines. However, due to limitations of the permanent-magnet capacity and strength, the brushless DC machine is generally limited to ratings below 100 kW.

5.2 SYNCHRONOUS GENERATOR

The synchronous generator produces most of the electric power consumed in the world. For this reason, the synchronous machine is an established machine. The machine works at a constant speed related to the fixed supply frequency. Therefore, it is not well suited for variable-speed operation in wind plants without power electronic frequency converters. Moreover, the conventional synchronous machine requires DC current to excite the rotor field, which has traditionally used sliding carbon brushes on slip rings on the rotor shaft. This introduces some unreliability in its use. The modern synchronous machines are made brushless by generating the required DC field current on the rotor itself. Reliability is greatly improved while reducing the cost. The DC field current need can be eliminated altogether by using a reluctance rotor,[1] in which the synchronous operation is achieved by the reluctance torque. The reluctance machine rating, however, is limited to tens of kW. It is being investigated at present for small wind generators.

The synchronous machine is ideally suited to constant-speed systems such as solar thermal power plants. It is, therefore, covered further in detail in Chapter 18.

The synchronous machine, when used in a grid-connected system, has some advantages over the induction machine. It does not require reactive power from the grid. This results in a better quality of power at the grid interface. This advantage is more pronounced when the wind farm is connected to a small-capacity grid using a long low-voltage transmission link. For this reason, California plants in the early 1980s used synchronous generators. Present-day wind plants connect to large grids using short lines and almost universally use the induction generator.

The synchronous generator is rarely used in gear-driven wind systems. However, the low-speed design of the synchronous generator is often found advantageous in the direct-drive variable-speed wind turbine. In such a design, the generator is completely decoupled from the grid by a voltage source power electronic converter connected to the stator, and the rotor is excited by an excitation winding or a permanent magnet. GE Wind's 2.X series of 2- to 3-MW generators has switched from the doubly fed induction generator to the synchronous generator, whereas the variable-speed pitch-control operating principle has remained unchanged.

5.3 INDUCTION GENERATOR

The electric power in industry is consumed primarily by induction machines working as motors driving mechanical loads. For this reason, the induction machine, invented by Nikola Tesla and financed by George Westinghouse in the late 1880s, represents

a well-established technology. The primary advantage of the induction machine is the rugged brushless construction that does not need a separate DC field power. The disadvantages of both the DC machine and the synchronous machine are eliminated in the induction machine, resulting in low capital cost, low maintenance, and better transient performance. For these reasons, the induction generator is extensively used in small and large wind farms and small hydroelectric power plants. The machine is available in numerous power ratings up to several megawatts capacity, and even larger.

For economy and reliability, many wind power systems use induction machines as electrical generators. The remaining part of this chapter is devoted to the construction and the theory of operation of the induction generator.

5.3.1 Construction

In the electromagnetic structure of the induction generator, the stator is made of numerous coils wound in three groups (phases), and is supplied with three-phase current. The three coils are physically spread around the stator periphery and carry currents, which are out of time phase. This combination produces a rotating magnetic field, which is a key feature in the working of the induction machine. The angular speed of the rotating magnetic field is called the *synchronous speed*. It is denoted by N_s and is given by the following in rpm:

$$N_s = 60\frac{f}{p} \tag{5.1}$$

where
f = frequency of the stator excitation
p = number of magnetic pole pairs

The stator coils are embedded in slots in a high-permeability magnetic core to produce the required magnetic field intensity with a small exciting current.

The rotor, however, has a completely different structure. It is made of solid conducting bars, also embedded in slots in a magnetic core. The bars are connected together at both ends by two conducting end rings (Figure 5.3). Because of its resemblance, the rotor is called a *squirrel cage rotor*, or the *cage rotor*, for short, and the motor is called the *squirrel cage induction motor*.

5.3.2 Working Principle

The stator magnetic field is rotating at the synchronous speed determined by Equation 5.1. This field is conceptually represented by the rotating magnets in Figure 5.3. The relative speed between the rotating field and the rotor induces the voltage in each closed loop of the rotor conductors linking the stator flux ϕ. The magnitude of the induced voltage is given by Faraday's law of electromagnetic induction, namely:

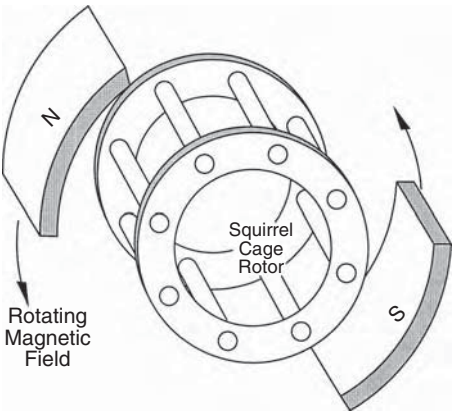

FIGURE 5.3 Squirrel cage rotor of the induction machine under rotating magnetic field.

$$e = -\frac{d\phi}{dt} \tag{5.2}$$

where ϕ = the magnetic flux of the stator linking the rotor loop.

This voltage in turn sets up the circulating current in the rotor. The electromagnetic interaction of the rotor current and stator flux produces the torque. The magnitude of this torque is given by the following:

$$T = k\Phi I_2 \cos\phi_2 \tag{5.3}$$

where
k = constant of proportionality
Φ = magnitude of the stator flux wave
I_2 = magnitude of induced current in the rotor loops
ϕ_2 = phase angle by which the rotor current lags the rotor voltage

The rotor accelerates under this torque. If the rotor were on frictionless bearings in a vacuum with no mechanical load attached, it would be completely free to rotate with zero resistance. Under this condition, the rotor would attain the same speed as the stator field, namely, the synchronous speed. At this speed, the current induced in the rotor is zero, no torque is produced, and none is required. Under these conditions, the rotor finds equilibrium and will continue to run at the synchronous speed.

If the rotor is now attached to a mechanical load such as a fan, it will slow down. The stator flux, which always rotates at a constant synchronous speed, will have a relative speed with respect to the rotor. As a result, electromagnetically induced voltage, current, and torque are produced in the rotor. The torque produced must equal that needed to drive the load at this speed. The machine works as a motor in this condition.

If we attach the rotor to a wind turbine and drive it faster than its synchronous speed via a step-up gear, the induced current and the torque in the rotor reverse the direction. The machine now works as the generator, converting the mechanical power of the turbine into electric power, which is delivered to the load connected to the stator terminals. If the machine were connected to a grid, it would feed power into the grid. Thus, the induction machine can work as an electrical generator only at speeds higher than the synchronous speed. The generator operation, for this reason, is often called the *supersynchronous operation* of the induction machine.

As described in the preceding text, an induction machine needs no electrical connection between the stator and the rotor. Its operation is entirely based on electromagnetic induction; hence, the name. The absence of rubbing electrical contacts and simplicity of its construction make the induction generator a very robust, reliable, and low-cost machine. For this reason, it is widely used in numerous industrial applications.

Engineers familiar with the theory and operation of the electrical transformer would see the working principle of the induction machine can be seen as the transformer with shorted secondary coil. The high-voltage coil on the stator is excited, and the low-voltage coil on the rotor is shorted on itself. The electrical or mechanical power from one to the other can flow in either direction. The theory and operation of the transformer, therefore, holds true when modified to account for the relative motion between the stator and the rotor. This motion is expressed in terms of the slip of the rotor relative to the synchronously rotating magnetic field.

5.3.3 Rotor Speed and Slip

The slip of the rotor is defined as the ratio of the speed of rotating magnetic field sweeping past the rotor and the synchronous speed of the stator magnetic field as follows:

$$s = \frac{N_s - N_r}{N_s} \tag{5.4}$$

where
s = slip of the rotor in a fraction of the synchronous speed
N_s = synchronous speed = 60 f/p
N_r = rotor speed

The slip is positive in the motoring mode and negative in the generating mode. In both modes, a higher rotor slip induces a proportionally higher current in the rotor, which results in greater electromechanical power conversion. In both modes, the value of slip is generally a few to several percent. Higher slips, however, result in greater electrical loss, which must be effectively dissipated from the rotor to keep the operating temperature within the allowable limit.

The heat is removed from the machine by the fan blades attached to one end-ring of the rotor. The fan is enclosed in a shroud at the end. The forced air travels

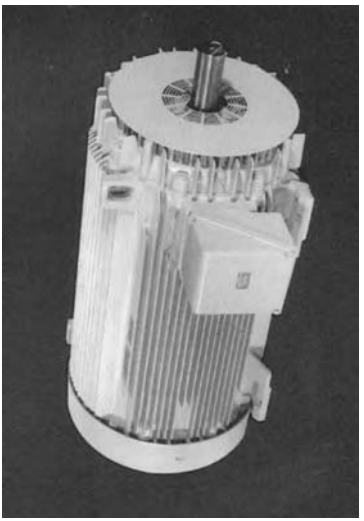

FIGURE 5.4 A 150-kW induction machine. (From General Electric Company, Fort Wayne, IN.)

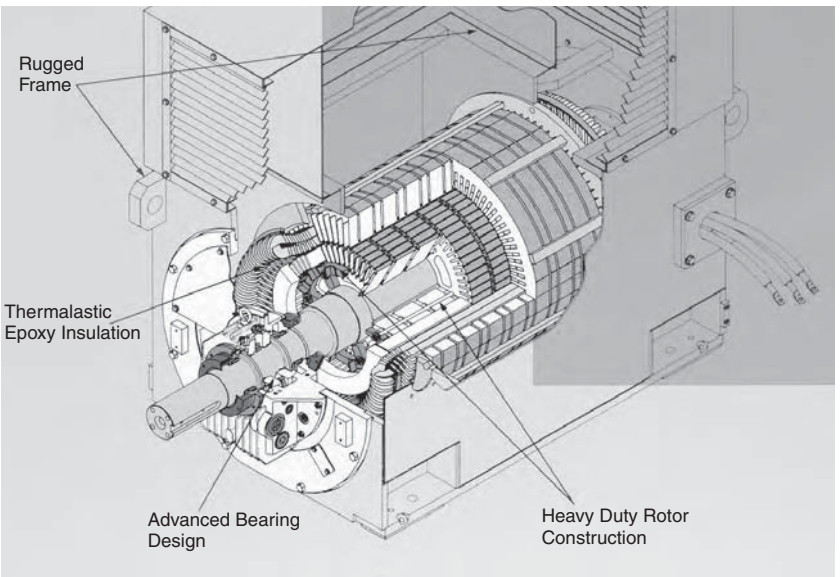

FIGURE 5.5 A 2-MW induction machine. (From Teco Westinghouse Motor Company, Round Rock, TX. With permission.)

axially along the machine exterior, which has fins to increase the dissipation area. Figure 5.4 is an exterior view of a 150-kW induction machine showing the end shroud and the cooling fins running axially. Figure 5.5 is a cutaway view of the machine interior of a 2-MW induction machine.

The induction generator feeding a 60-Hz grid must run at a speed higher than 3600 rpm in a 2-pole design, 1800 rpm in a 4-pole design, and 1200 rpm in a 6-pole design. The wind turbine speed, on the other hand, varies from a few hundred rpm in kW-range machines to a few tens of rpm in MW-range machines. The wind turbine, therefore, must interface the generator via a mechanical gear. As this somewhat degrades efficiency and reliability, many small stand-alone plants operate with custom-designed generators operating at lower speeds without any mechanical gear.

Under the steady-state operation at slip "*s*," the induction generator has the following operating speeds in rpm:

- Stator flux wave speed N_s
- Rotor mechanical speed $N_r = (1 - s)N_s$
- Stator flux speed with respect to rotor sN_s
- Rotor flux speed with respect to stator $N_r + sN_s = N_s$ (5.5)

Thus, the squirrel cage induction machine is essentially a constant-speed machine, which runs slightly slipping behind the rotating magnetic field of the three-phase stator current. The rotor slip varies with the power converted, and the rotor speed variations are within a few percent. It always consumes reactive power — undesirable when connected to a weak grid — which is often compensated by capacitors to achieve the systems power factor closed to one. Changing the machine speed is difficult. It can be designed to run at two different but fixed speeds by changing the number of poles of the stator winding.

The voltage usually generated in the induction generator is 690-V AC. It is not economical to transfer power at such a low voltage over a long distance. Therefore, the machine voltage is stepped up to a higher value between 10,000 V and 30,000 V via a step-up transformer to reduce the power losses in the lines.

5.3.4 Equivalent Circuit

The theory of operation of the induction machine is represented by the equivalent circuit shown in Figure 5.6(a). It is similar to that of the transformer. The left-hand side of the circuit represents the stator and the right-hand side, the rotor. The stator and rotor currents are represented by I_1 and I_2, respectively. The vertical circuit branch at the junction carries the magnetizing (also known as excitation or no-load) current I_o, which sets the magnetic flux required for the electromagnetic operation of the machine. The total stator current is then the sum of the rotor current and the excitation current. The air-gap separation is not shown, nor is the difference in the number of turns in the stator and rotor windings. This essentially means that the rotor is assumed to have the same number of turns as the stator and has an ideal 100% magnetic coupling. We calculate the performance parameters taking the stator winding as the reference. The actual rotor voltage and current would be related to the calculated values through the turn ratio between the two windings. Thus, the calculations are customarily performed in terms of the stator, as we shall do in this

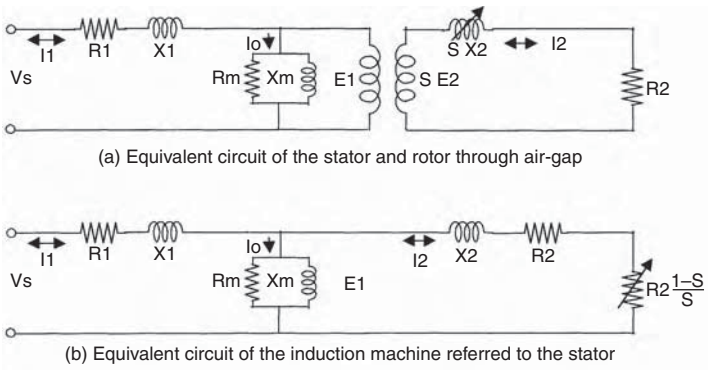

FIGURE 5.6 Equivalent electrical circuit of induction machine for performance calculations.

chapter. This matches the practice, as the performance measurements are always done on the stator side. The rotor is inaccessible for any routine measurements.

Most of the flux links both the stator and the rotor coils. The flux that does not link both the coils is called the leakage flux, and is represented by the leakage reactance in ohms per phase. One half of the total leakage reactance is attributed to each side, namely the stator leakage reactance X_1 and the rotor leakage reactance X_2 in Figure 5.6(b). The stator and rotor conductor resistance is represented by R_1 and R_2, respectively. The magnetizing parameters X_m and R_m represent the permeability and losses (hysteresis and eddy currents) in the magnetic circuit of the machine.

The slip-dependent electrical resistance $R_2(1 - s)/s$ represents the equivalent mechanical resistance on the shaft. Therefore, the electromechanical power conversion per phase is given by $I_2^2R_2(1 - s)/s$, and the three-phase power conversion is then given by the following in watts:

$$P_{em} = 3I_2^2R_2(1 - s)/s \tag{5.6}$$

If the machine is not loaded and has zero friction, it runs at the synchronous speed, the slip is zero, and the value of $R_2(1 - s)/s$ becomes infinite. The rotor current is then zero and P_{em} is also zero, as it should be. On the other speed extreme, when the rotor is standing still, the slip is unity, and the value of $R_2(1 - s)/s$ is zero. The rotor current is not zero, but the P_{em} is zero again, as the mechanical power delivered by the standstill rotor is zero. These two extreme operating points briefly validate the electromechanical power conversion given by Equation 5.6.

At any slip other than zero or unity, neither the rotor current nor the speed is zero, resulting in a nonzero value of P_{em}.

The machine's capacity rating is the power developed under rated conditions, that is:

$$\text{Machine rating} = \frac{P_{\text{em rated}}}{1000}\text{(kW)} \quad \text{or} \quad \frac{P_{\text{em rated}}}{746}\text{(hp)} \tag{5.7}$$

The mechanical torque is given by the power divided by the angular speed as follows:

$$T_{em} = P_{em}/\omega \tag{5.8}$$

where
T_{em} = electromechanical torque developed in the rotor in Nm
ω = angular speed of the rotor = $2\pi \cdot N_s(1 - s)/60$ in mechanical rad/sec

Combining Equation 5.6 and Equation 5.8, we obtain the torque at any slip s, as follows in units of Nm:

$$T_{em} = (180/2\pi N_s) I_2^2 R_2/s \tag{5.9}$$

The value of I_2 in Equation 5.9 is determined by the equivalent circuit parameters, and is slip-dependent. The torque developed by the induction machine rotor is, therefore, highly slip-dependent, as is discussed later in this chapter.

We take a note here that the performance of the induction machine is completely determined by the equivalent circuit parameters. The circuit parameters are supplied by the machine manufacturer, but can be determined by two basic tests on the machine. The full-speed test under no-load and the zero-speed test with blocked-rotor determine the complete equivalent circuit of the machine.[2–3]

Equivalent circuit parameters are generally expressed in fractions (per unit) of their respective rated values per phase. The rated impedance per phase is defined as follows in ohms:

$$Z_{rated} = \frac{\text{Rated voltage per phase}}{\text{Rated current per phase}} \tag{5.10}$$

For example, the per unit (pu) stator resistance is expressed in the following way:

$$R_{1\ \text{per unit}} = \frac{R_1(\text{ohms})}{Z_{rated}(\text{ohms})} \tag{5.11}$$

and similar expressions for all other circuit parameters. When expressed as such, X_1 and X_2 are equal, each a few to several percent, and R_1 and R_2 are also approximately equal, each a few percent of the rated impedance. The magnetizing parameters X_m and R_m are usually large, in several hundred percent of Z_{rated}, hence, drawing negligible current compared to the rated current. For this reason, the magnetizing branch of the circuit is often ignored in making approximations of the machine performance calculations.

All of the preceding performance equations hold true for both the induction motor and the induction generator by taking the proper sign of the slip. In the generator mode, the value of the slip is negative in the performance equations

wherever it appears. We must also remember that the real mechanical power output is negative, meaning that the shaft receives the mechanical power instead of delivering it. The reactive electric power drawn from the stator terminals remains leading with respect to the line voltage; hence, we say that the induction generator delivers a leading reactive power. Both of these mean that the magnetizing volt-amperes are supplied by an external source.

5.3.5 Efficiency and Cooling

The values of R_1 and R_2 in the equivalent circuit represent electrical losses in the stator and rotor, respectively. As seen later, for a well-designed machine, the magnetic core loss must equal the conductor loss. Therefore, with R_1 and R_2 expressed in pu of the base impedance, the induction machine efficiency is approximately equal to the following:

$$\eta = 1 - 2(R_1 + R_2) \tag{5.12}$$

For example, in a machine with R_1 and R_2 each 2%, we write $R_1 = R_2 = 0.02$ pu. The efficiency is then simply $1–2(0.02 + 0.02) = 0.92$ pu or 92%. Of the input power in this machine, 8% is lost in the electromechanical conversion process.

Losses taking place in the machine are minimized by providing adequate cooling. Small machines are generally air cooled. Large generators located inside the nacelle can be difficult to cool by air. Water cooling, being much more effective than air cooling in such situations, can be advantageous in three ways:

- Water cooling reduces the generator weight on the nacelle, thus benefiting the structural design of the tower.
- It absorbs and thus reduces noise and vibrations.
- It eliminates the nacelle opening by mounting the heat exchanger outside, making the nacelle more weatherproof.
- Overall, it reduces the maintenance requirement, a significant benefit in large machines usually sitting on tall towers in inclement weather.

5.3.6 Self-Excitation Capacitors

The induction machine needs AC excitation current. The machine is either self-excited or externally excited. Because the excitation current is mainly reactive, a stand-alone system is self-excited by shunt capacitors. An induction generator connected to the grid draws the excitation power from the network. The synchronous generators connected to the base-load network must be capable of supplying this reactive power.

As the generator, the induction machine has a drawback in requiring a leading reactive power for the excitation. For a stand-alone, self-excited induction generator, the exciting power can be provided by an external capacitor connected to the generator terminals (Figure 5.7). No separate AC supply is needed in this case. In the grid-connected generator, the reactive power is supplied from the base synchronous

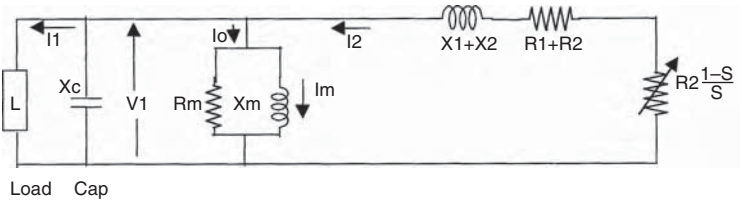

FIGURE 5.7 Self-excited induction generator with external capacitor.

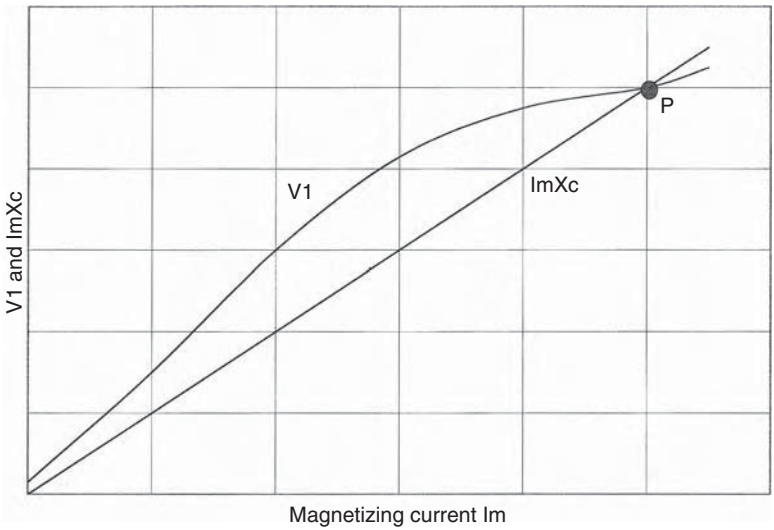

FIGURE 5.8 Determination of stable operation of self-excited induction generator.

generators working at the other end of the grid. Where the grid capacity of supplying the reactive power is limited, local capacitors can be used to partly supply the needed reactive power.

The induction generator can self-excite using the external capacitor only if the rotor has an adequate remnant magnetic field. In the self-excited mode, the speed, load, and capacitance value affect the generator output frequency and voltage. The operating voltage and frequency are determined in the following text in terms of the approximate equivalent circuit of Figure 5.7.

With no load on the machine terminals, the capacitor current $I_c = V_1/X_c$ must be equal to the magnetizing current $I_m = V_1/X_m$. The voltage V_1 is a function of I_m, linearly rising until the saturation point of the magnetic core is reached (Figure 5.8). The stable operation requires the line I_mX_c to intersect the V_1 vs. I_m curve. The operating point is fixed where V_1/X_c equals V_1/X_m, that is, when $1/X_c = 1/X_m$, where $X_c = 1/\omega C$. This settles the operating frequency in hertz. With the capacitor value C, the output frequency of the self-excited generator is therefore given by the following:

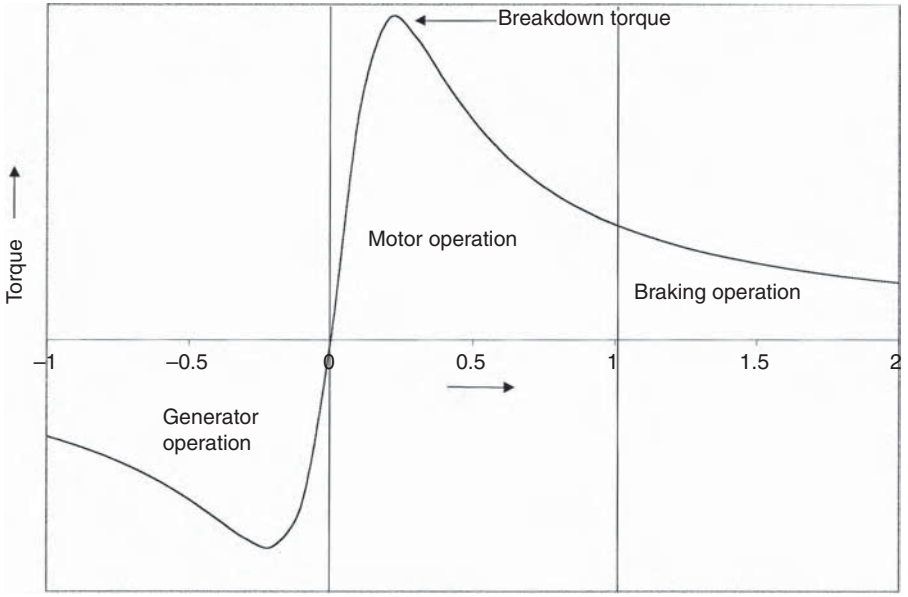

FIGURE 5.9 Torque vs. speed characteristic of the induction machine in three operating modes.

$$f = \frac{1}{2\pi C X_m} \quad \text{or} \quad \omega = \frac{1}{2\pi\sqrt{C L_m}} \tag{5.13}$$

Under load conditions, the generated power $V_1 I_2 \cos \phi_2$ provides for the power in the load resistance R and the loss in R_m, and the reactive currents must sum to zero, i.e.,

$$\frac{V_1}{X} + \frac{V_1}{X_m} + I_2 \sin \phi_2 = \frac{V_1}{X_c} \tag{5.14}$$

Equation 5.14 determines the output voltage under load.

Equation 5.13 and Equation 5.14 determine the induction generator output frequency and the voltage with a given value of the capacitance. Inversely, they can be used to determine the required value of the capacitance for the desired frequency and voltage.

5.3.7 Torque-Speed Characteristic

If we vary the slip over a wide range in the equivalent circuit, we get the torque-speed characteristic as shown in Figure 5.9. In the region of negative slips, the machine works as the generator powering the electrical load connected to its terminals.

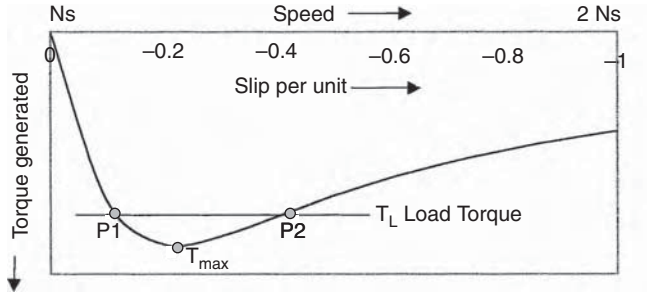

FIGURE 5.10 Torque vs. slip characteristic of induction generator under load.

In the region of positive slips, the machine works as the motor turning the mechanical load connected to its shaft. In addition to the motoring and generating regions, the induction machine has yet another operating mode, and that is the braking mode. If the machine is operated at slips greater than 1.0 by turning it backward, it absorbs power with a motoring torque. That is, it works as a brake. The power, in this case, is converted into I^2R loss in the rotor conductors, which must be dissipated as heat. The eddy current brake used with the wind turbine rotor works on this principle. As such, in case of emergencies, the grid-connected induction generator itself as a whole can be used as an eddy current brake by reversing the three-phase grid voltage sequence at the stator terminals. This reverses the direction of rotation of the magnetic flux wave with respect to the rotor. The torsional stress on the turbine blades and the hub, however, must be considered, which may limit such a high-torque braking operation only for emergencies.

The torque-slip characteristic in the generating mode is separately shown in Figure 5.10. If the generator is loaded at a constant load torque T_L, it has two possible points of operation, P_1 and P_2. Only one of these two points, P_1, is stable. Any perturbation in speed around P_1 will produce stabilizing torque to bring it back to P_1. The figure also shows the limit to which the generator can be loaded. The maximum torque it can support is called the *breakdown torque*, which is shown as T_{max}. If the generator is loaded under a constant torque above T_{max}, it will become unstable, stall, draw excessive current, and destroy itself thermally if not properly protected.

5.3.8 Transients

The induction generator may experience the following three types of transient currents:

Starting transient: In a grid-connected system, the induction generator is used as the motor for starting the turbine from rest to supersynchronous speeds. Only then is the machine switched to the generating mode, feeding power to the grid. If the full-rated voltage is applied for starting, the motor draws high starting current at zero speed when the slip is 1.0, and the rotor resistance is the least. Therefore, the starting inrush current can be 5 to 7 times the rated current, causing overheating problems, particularly in large machines. Moreover, as seen in Figure 5.11, the torque

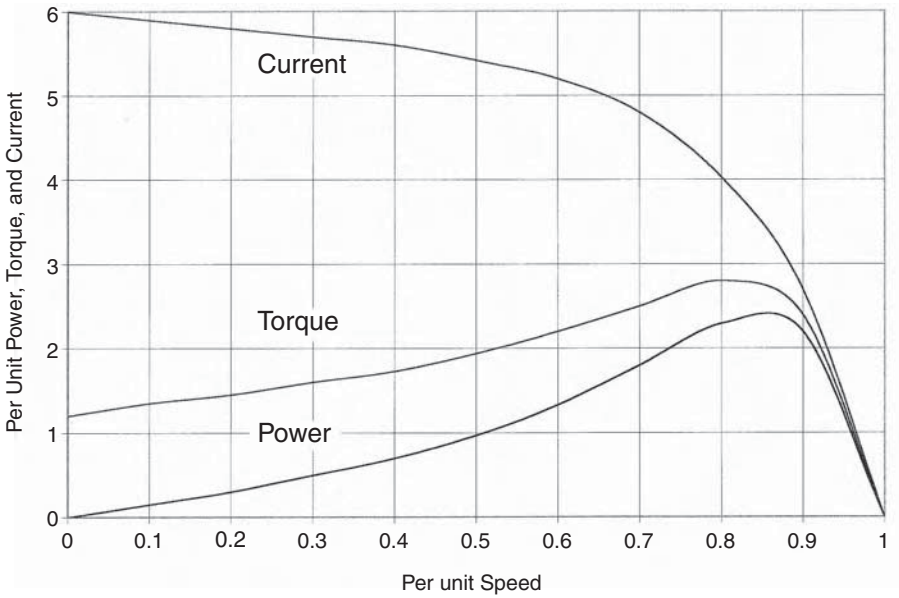

FIGURE 5.11 Induction machine starting and accelerating characteristics.

available to accelerate the rotor may be low, resulting in a slow start. This also adds to the heating problem. For this reason, the large induction motor is often started with a soft-start circuit, such as the voltage-reducing autotransformer or the star-delta starter. The modern method of starting is to apply a reduced voltage at reduced frequency, maintaining a constant volts-to-hertz ratio. This method starts the motor with the least mechanical and thermal stress.

Reswitching transient: A severe transient current can flow in the system if the induction generator operating in a steady state suddenly gets disconnected due to a system fault or some other reason, and then gets reconnected by automatic reswitching. The magnitude of the current depends on the phase angle of the voltage wave when the generator gets reconnected to the grid. The physical appreciation of this transient current comes from the constant flux linkage theorem. A coil having no resistance keeps its flux linkage constant. Because the winding resistance is small compared to the inductance in most electrical machines, the theorem of constant flux linkage holds after the fault. If the reswitching was done when the stator and rotor voltages were in phase opposition, large transient currents are established to maintain the flux linkage, which then decreases slowly to a small value after tens of milliseconds. Meanwhile, the transient electromechanical torque may be large enough to give the machine and the tower a severe jolt. The actual amplitude and sign of the first peak of the transient torque are closely dependent on the rotor speed and duration of the interruption. In the worst case, the first peak may reach 15 times the rated full-load torque. Frequent faults of this nature can cause shaft breakage due to fatigue stresses, particularly at the coupling with the wind turbine.

Short circuit: When a short-circuit fault occurs at or near the generator terminals, the machine significantly contributes to the system fault current, particularly if it is running on a light load. The short-circuit current is always more severe for a single-phase fault than a three-phase fault. The most important quantity is the first peak current as it determines the rating of the protective circuit breaker needed to protect the generator against such faults. The short-circuit current has a slowly decaying DC component superimposed on an AC component. The latter is larger than the direct online starting inrush current, and may reach 10 to 15 times the full-load-rated current.

The transient current and torque, in any case, are calculated using the generalized equivalent circuit of the machine in terms of the d-axis and q-axis transient and subtransient reactance and time constants.[4–7] The q-axis terms in the generalized theory do not enter in the induction generator transient analysis, as the d-axis and q-axis terms are identical due to the perfect circular symmetry in electromagnetic structure.

5.4 DOUBLY FED INDUCTION GENERATOR

The doubly fed induction generator is an emerging trendsetting technology, presently used in some large wind turbines with variable-speed operation. NEG Micon's 4.2-MW/100-m diameter machine and 2- to 3-MW GE machines are two examples. In the doubly fed induction motor, a voltage source frequency converter feeds slip frequency power to the three-phase rotor. Thus, the motor is fed from both sets of terminals, the stator as well as the rotor, hence the name. In the grid-connected wind turbine applications, the rotor speed and grid frequency are decoupled by using power electronic frequency converters.

The most attractive feature of the doubly fed induction generator is that only 20 to 30% of the power needs to pass through frequency conversion as compared with 100% in the variable-speed synchronous generator. This gives a substantial cost advantage in the power electronics cost. However, the fractional power conversion of the doubly fed induction generator introduces a grid-related problem. A new regulation requires that wind turbines remain connected to the grid in case of a voltage dip and that the built-in capacity of the wind turbine actively supports the grid. Instantly switching off a large wind-power-generating capacity during an emergency could lead to catastrophic grid blackout.[7]

5.5 DIRECT-DRIVEN GENERATOR

The wind turbine typically runs at tens of rpm, whereas the generator runs near 1800 or 3600 rpm in a 60-Hz system or near 1500 rpm or 3000 rpm in a 50-Hz system. In the conventional gear-driven system, a turbine running at 36 rpm, driving a four-pole generator must use a 1:50 gearbox. The cost, vibration, and noise associated with the gearbox can be eliminated by using a gearless direct-driven generator, which also improves the conversion efficiency.

Designing an electrical generator running at tens of rpm and yet having a comparable efficiency is a challenging task. It must have a very high-rated torque to convert the required power at such low speeds. Because the machine size and power losses depend on the rated torque, the low-speed design is inherently heavy and less efficient. This disadvantage is partly overcome by designing the machine with a large diameter and small pole pitch. Many types of direct-driven generators have been considered. For such applications, they are as follows:

- The conventional synchronous, switched-reluctance, and sector-induction generators among the electrically excited designs
- The radial-flux synchronous, axial-flux synchronous, and transverse-flux synchronous generators among the permanent-magnet designs

A variety of direct-driven generator designs in the 30-kW to 3-MW range have been compared with the conventional gear-driven generator designs by Grauers.[8] His design methodology is based on well-known analytical methods and lumped-parameter thermal models. The Grauers study concludes that a radial-flux permanent-magnet generator fits well with the direct-driven wind turbine. The design can be small and efficient for a grid-connected generator with a frequency converter if the rated torque is allowed to be close to the pull-out torque. Such design could be as efficient as the conventional gear-driven four-pole induction generator. That is, the generator must have a large number of poles. Such a machine must have a short pole pitch, resulting in a poor magnetic design. To circumvent such limitations, the permanent-magnet and wound-rotor synchronous machines are being considered for 1.5-MW direct-driven generators.

Another possible solution is the axial-gap induction machine. It can be designed with a large number of poles with less difficulty compared to the conventional radial-gap induction machine. The axial-gap machine is being considered for direct-drive marine propulsion, which is also inherently a low-speed system. For small gearless wind drives with the wind turbine, the axial-flux permanent-magnet generator may find some interest for its simplicity. A 5-kW, 200-rpm laboratory prototype of the axial-gap permanent-magnet design has been recently tested.[9] However, a significant research and development effort is needed before the variable-speed direct-driven systems can be commercially made available for large wind power systems.

The direct-drive is increasingly used along with the permanent-magnet generator up to 1.5-MW ratings. The simplified generator design and higher partial load efficiency are the principal benefits of the permanent-magnet generator.

References

1. Rahim, Y.H.A., Controlled Power Transfer from Wind Driven Reluctance Generators, IEEE Winter Power Meeting, Paper No. PE-230-EC-1-09, New York, 1997.
2. Say, M.G., *Alternating Current Machines*, John Wiley & Sons, New York, 1983.
3. Alger, P.L., *The Nature of Induction Machines*, Gordon and Breach, New York, 1965.

4. Adkins, B., *The General Theory of Electrical Machines*, Chapman and Hall, London, 1964.
5. Kron, G., *Equivalent Circuits of Electrical Machines*, Dover Publications, New York, 1967.
6. Yamayee, Z.A. and Bala, J.L., *Electromechanical Devices and Power Systems*, John Wiley & Sons, New York, 1994.
7. Slootweg, J.G., Wind Power Modeling and Impact on Power System Dynamics, Ph.D. thesis in Electric Power Systems, TU Delft, The Netherlands, 2003.
8. Grauers, A., Design of Direct-Driven Permanent-Magnet Generators for Wind Turbines, Ph.D. thesis, Chalmers University of Technology, Goteborg, Sweden, October 1996.
9. Chalmers, B.J. and Spooner, E., Axial Flux Permanent Magnet Generator for Gearless Wind Energy Systems, IEEE Paper No. PE-P13-EC-02, July 1998.

6 Generator Drives

The turbine speed is much lower than the desired speed for the electrical generator. For this reason, the turbine speed is stepped up using a gear drive. The system can be fixed speed or variable speed, as described in this chapter.

The wind power equation as derived in Chapter 3 is as follows:

$$P = \frac{1}{2}\rho A V^3 C_p \tag{6.1}$$

where C_p = rotor power coefficient.

As seen earlier, the value of C_p varies with the ratio of the rotor tip speed to the wind speed, termed as the tip speed ratio (TSR). Figure 6.1 depicts a typical relationship between the power coefficient and the TSR. The TSR and the power coefficient vary with the wind speed. The C_p characteristic has a single maximum at a specific value of TSR, around 5 in this case. Therefore, when operating the rotor at a constant speed, the power coefficient can be maximum at only one wind speed. However, for achieving the highest annual energy yield, the value of the rotor power coefficient must be maintained at the maximum level at all times, regardless of the wind speed.

The value of C_p varies not only with the TSR but also with the construction features of the rotor. The theoretical maximum value of C_p is 0.59, but the practical limit may be 0.5. Attaining C_p above 0.4 is considered good. Whatever maximum value is attainable with a given wind turbine, it must be maintained constant at that value. Therefore, the rotor speed must change in response to the changing wind speed. This is achieved by incorporating a speed control in the system design to run the rotor at high speed in high wind and at low speed in low wind. Figure 6.2 illustrates this principle. For given wind speeds V_1, V_2, or V_3, the rotor power curves vs. the turbine speed are plotted in solid curves. For extracting the maximum possible energy over the year, the turbine must be operated at the peak power point at all wind speeds. In the figure, this happens at points P_1, P_2, and P_3 for wind speeds V_1, V_2, and V_3, respectively. The common factor among the peak power production points P_1, P_2, and P_3 is the constant high value of TSR around 5.

Operating the machine at the constant TSR corresponding to the peak power point means turning the rotor at high speed in gusty winds. The centrifugal forces produced in the rotor blades above a certain top speed can mechanically destroy the rotor. Moreover, the electrical machine producing power above its rated capacity may overheat and thermally destroy itself. For these reasons, the turbine speed and the generator power output must be controlled.

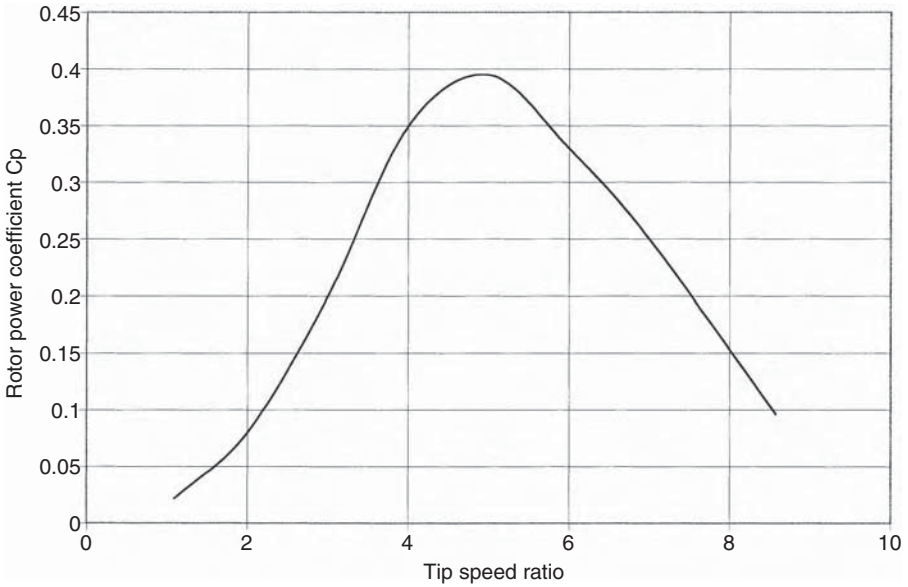

FIGURE 6.1 Rotor power coefficient vs. tip speed ratio has a single maximum.

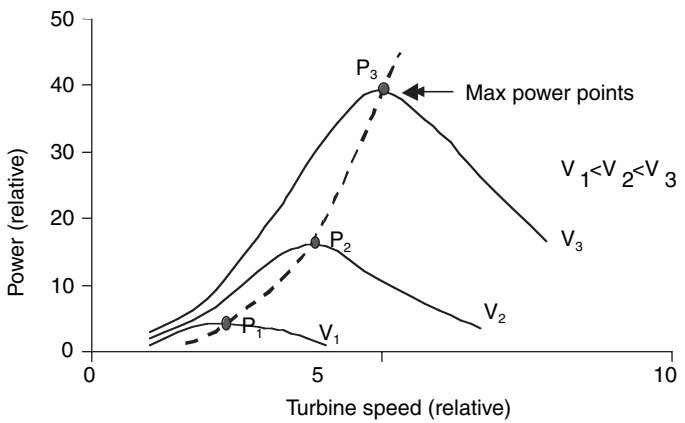

FIGURE 6.2 Turbine power vs. rotor speed characteristics at different wind speeds. The peak power point moves to the right at higher wind speed.

6.1 SPEED CONTROL REGIONS

The speed and power controls in wind power systems have three distinct regions as shown in Figure 6.3, where the solid curve is the power and the dotted curves, the rotor efficiency. They are as follows:

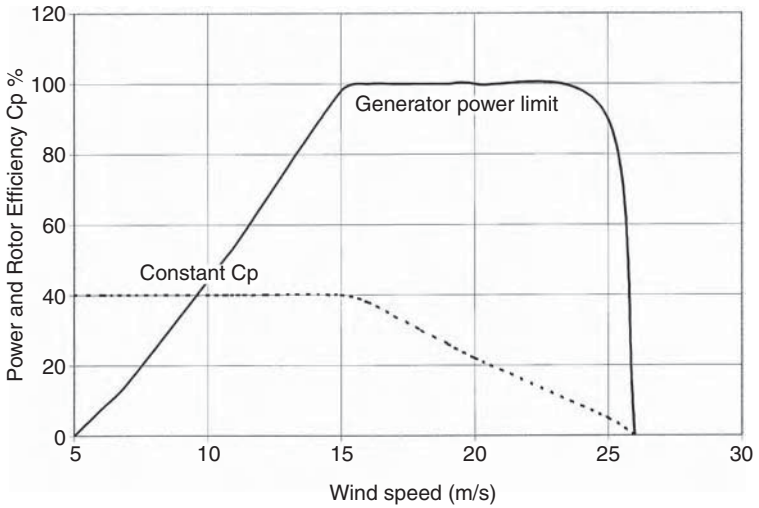

FIGURE 6.3 Three distinct rotor speed control regions of the system.

- The optimum constant C_p region, generating linearly increasing power with increasing wind speed
- The power-limited region, generating a constant power even at higher winds, by decreasing the rotor efficiency C_p
- The power-shut-off region, where the power generation is ramped down to zero as the wind speed approaches the top cutout limit

Typically, the turbine starts operating (cut-in) when the wind speed exceeds 4 to 5 m/sec, and is shut off at speeds exceeding 25 to 30 m/sec. In between, it operates in one of the above three regions. At a typical site, the wind turbine may operate about 70 to 80% of the time. Other times, it is off because wind speed is too low or too high.

The constant C_p region is the normal mode of operation, where the speed controller operates the system at the optimum constant C_p value stored in the system computer. Two alternative schemes of controlling the speed in this region were described in Section 4.4.

To maintain a constant C_p, the control system increases the rotor speed in response to the increasing wind speed only up to a certain limit. When this limit is reached, the control shifts into the speed-limiting region. The power coefficient C_p is no longer at the optimum value, and the rotor power efficiency suffers.

If the wind speed continues to rise, the system approaches the power limitation of the electrical generator. When this occurs, the turbine speed is reduced, and the power coefficient C_p moves farther away from the optimum value. The generator output power remains constant at the design limit. When the speed limit and power limit cannot be maintained under an extreme gust of wind, the machine is cut out of the power-producing operation.

Two traditional methods of controlling the turbine speed and generator power output are as follows:

1. *Pitch control:* The turbine speed is controlled by controlling the blade pitch by mechanical and hydraulic means. The power fluctuates above and below the rated value as the blade pitch mechanism adjusts with the changing wind speed. This takes some time because of the large inertia of the rotor. Figure 6.4 depicts the variation in wind speed, the pitch angle of the blades, the generator speed, and the power output with respect to time in a fluctuating wind based on the actual measurements on a Vestas 1.65-MW wind turbine with OptiSlip® (registered trade name of Vestas Wind Systems, Denmark). The generator power output is held constant even with a 10% fluctuation in the generator speed. This minimizes the undesired fluctuations on the grid. The "elasticity" of such a system also reduces the stress on the turbine and the foundation.
2. *Stall control:* The turbine uses the aerodynamic stall to regulate the rotor speed in high winds. The power generation peaks somewhat higher than the rated limit and then declines until the cutout wind speed is reached. Beyond that point, the turbine stalls and the power production drops to zero (Figure 6.5).

In both methods of speed regulation, the power output of most machines in practice is not as smooth. Theoretical considerations give only approximations of the powers produced at any given instant. For example, the turbine can produce different powers at the same speed depending on whether the speed is increasing or decreasing.

6.2 GENERATOR DRIVES

Selecting the operating speed of the generator and controlling it according to changing wind speed must be determined early in the system design. This is important, as it determines all major components and their ratings. The alternative generator drive strategies and the corresponding speed control methods fall in the following categories.

6.2.1 One Fixed-Speed Drive

The fixed-speed operation of the generator offers a simple system design. It naturally fits well with the induction generator, which is inherently a fixed-speed machine. However, the turbine speed is generally low, whereas the electrical generator works more efficiently at high speed. The speed match between the two is accomplished by the mechanical gear. The gearbox reduces the speed and increases the torque, thus improving the rotor power coefficient C_p. Under varying wind speed, the increase and decrease in the electromagnetically converted torque and power are accompanied by the corresponding increase or decrease in the rotor slip with respect to the stator. The wind generator generally works at a few percent slip. The higher

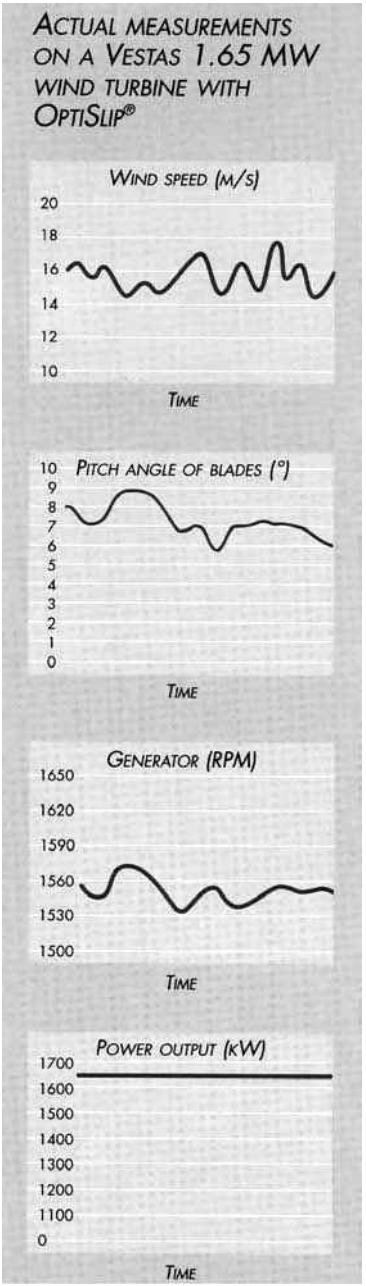

FIGURE 6.4 Wind speed, pitch angle, generator speed, and power output under fluctuating wind speed in 1650-kW turbine. (From Vestas Wind Systems, Denmark. With permission.)

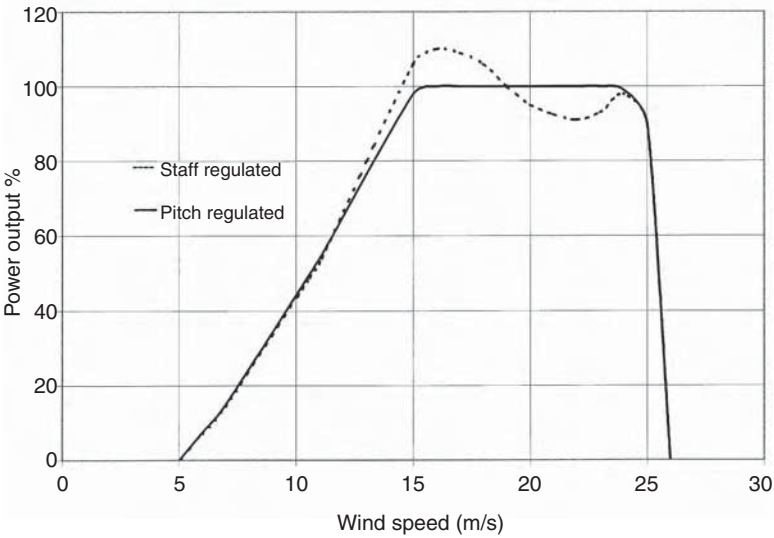

FIGURE 6.5 Generator output power variation with wind speed in blade pitch-regulated and stall-regulated turbines.

value benefits the drive gear, but increases the electrical loss in the rotor, which leads to a cooling difficulty.

The annual energy yield for a fixed-speed wind turbine must be analyzed with the given wind speed distribution at the site of interest. Because the speed is held constant under this scheme, the turbine running above the rated speed is not a design concern. But, the torque at the generator shaft must be higher. Therefore, it is possible to generate electric power above the rated capacity of the generator. When this happens, the generator is shut off by opening the circuit breaker, thus shedding the load and dropping the system power generation to zero.

The major disadvantage of one fixed-speed operation is that it almost never captures the wind energy at the peak efficiency in terms of the rotor coefficient C_p. The wind energy is wasted when the wind speed is higher or lower than a certain value selected as the optimum.

With the generator operating at a constant speed, the annual energy production depends on the wind speed and the gear ratio. Figure 6.6 depicts the annual energy vs. gear ratio relation typical of such a system. It is seen that the annual energy yield is highly dependent on the selected gear ratio. For the given wind speed distribution in the figure, the energy production for this turbine would be maximum at the gear ratio of 25. When choosing the gear ratio, it is therefore important to consider the average wind speed at the specific site. The optimum gear ratio for the operation of the wind turbine varies from site to site.

Because of the low energy yield over the year, the fixed-speed drives are generally limited to small machines.

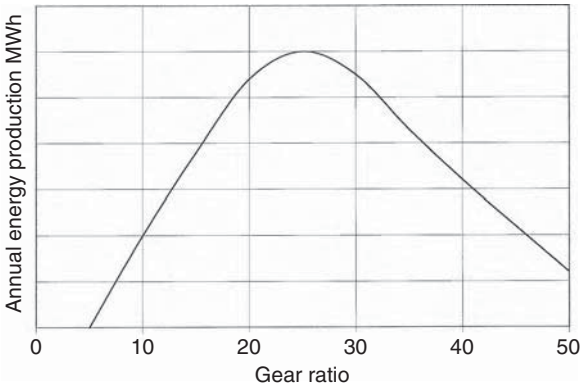

FIGURE 6.6 Annual energy production strongly varies with gear ratio for a given wind speed in one fixed-speed drive.

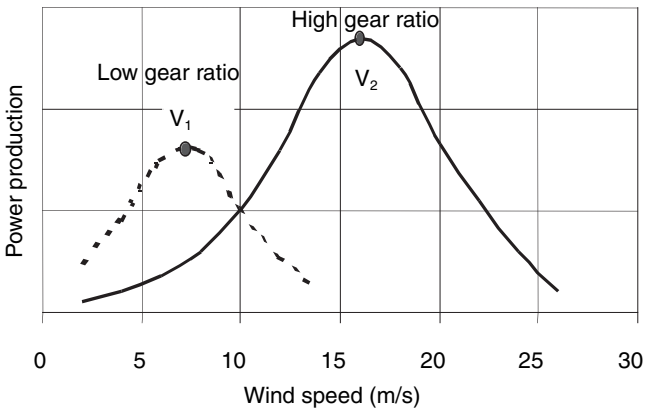

FIGURE 6.7 Power production probability distribution for various wind speeds with low and high gear ratios.

6.2.2 Two Fixed-Speed Drive

The two-speed machine improves energy capture and reduces electrical loss in the rotor and gear noise. The speed is changed by changing the gear ratio. The two operating speeds are selected to optimize the annual energy production with the expected wind speed distribution at the site. Obviously, the wind speeds V_1 and V_2 that would generate peak powers with two gear ratios must be on the opposite side of the expected annual average wind speed. In the specific example of Figure 6.7, the system is operated on the low gear ratio for wind speeds below 10 m/sec, and on the high gear ratio for wind speeds above 10 m/sec. The gear ratio would be changed during operation at 10 m/sec in this example.

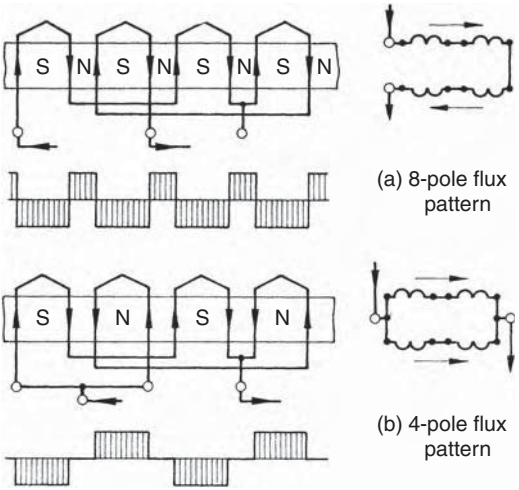

FIGURE 6.8 Pole-changing stator winding for a speed ratio of 2:1.

In some early American designs, two speeds were achieved by using two separate generators and switching between the generators with a belt drive. An economic and efficient method is to design the induction generator to operate at two speeds. The cage motor with two separate stator windings of different pole numbers can run at two or more integrally related speeds. The pole-changing motor, on the other hand, has a single stator winding, the connection of which is changed to give a different number of poles. Separate windings that match with the system requirement may be preferred where the speed change must be made without losing control of the machine. Separate windings are, however, difficult to accommodate.

In the pole-changing method with one winding, the stator is wound with coils that can be connected either in P or 2P number of poles. No changes are needed, nor are they possible, in the squirrel cage rotor. The stator connection, which produces a higher pole number for low-speed operation, is changed to one half as many poles for high-speed operation. This maintains the TSR near the optimum to produce a high rotor power coefficient C_p. The machine, however, operates with only one speed ratio of 2:1.

Figure 6.8 shows one phase of a pole-changing stator winding. For the higher pole number, the coils are in series. For the lower number, they are in series–parallel. The resulting magnetic flux pattern corresponds to eight and four poles, respectively. It is common to use a double-layer winding with 120° electrical span for the higher pole number. An important design consideration in such a winding is to limit the space harmonics, which may decrease the efficiency in the generating mode and may also produce a tendency to crawl when using the machine as a motor during the start-up operation.

The coil pitch of the stator winding is fixed once wound, but its electrical span depends on the number of poles. A coil pitch one eighth of the circumference provides full-pitch coils for an 8-pole connection, two thirds for a 6-pole, and one half for a 4-pole connection. Too narrow a coil span must be avoided. For a 2:1

speed-ratio generator, a possible coil span is 1.33-pole pitch for the larger and 0.67 for the smaller pole number. In each case, the coil span factor would be 0.86. Using the spans near 1 and 0.5, with span factors of 1.0 and 0.71, one can avoid an excessive leakage reactance in the lower-speed operation.

Two-speed technology using a fixed-blade rotor with stalled type design is still available in small (<1 MW) machines.

6.2.3 Variable-Speed Gear Drive

The variable-speed operation using a variable gear ratio has been considered in the past but has been found to add more problems than benefits. Therefore, such drives are not generally used at present.

6.2.4 Variable-Speed Power Electronics

The advanced electronic control systems in some wind machines continually adjust the wind turbine's blade pitch angle to enable it to achieve optimum rotational speed and maximum lift-to-drag at each wind speed. This variable-speed operation maximizes the turbine's ability to remain at the highest-level efficiency. Whereas constant-speed rotors must be designed to deflect high-wind-gust loads, variable-speed operation enables the loads from the gust to be absorbed and converted to electric power. Generator torque is controlled through the frequency converter. This control strategy allows the turbine rotor to speed up operation in strong, gusty winds, thereby reducing torque loads in the drive train. The variable-speed turbine's operating speed range is notably wider than the "slip" range used by other technologies, which produce heat rather than electric power when regulating power in strong, gusty winds. The variable-speed system also provides active damping of the entire wind turbine system. This results in considerably less tower oscillation when compared to constant-speed wind turbines. Active damping of the machine also limits peak torque, providing greater drive train reliability, reduced maintenance cost, and longer turbine life.

The modern variable-speed drive uses power electronics to convert the variable-voltage and variable-frequency output of the generator into a fixed-voltage, fixed-frequency output. The technology is similar to that used in the aircraft power system. The trend of using such a system is driven by the declining cost of power semiconductors. Conventional silicon-controlled rectifiers and inverters can be used, but the modern design in the wind industry appears to prefer pulse-width-modulated thyristors. The speed ratio is not limited in theory, but practical considerations limit the ratio to 3:1, which is wider than that obtainable using the pole-changing method described earlier and the Scherbius machine described in the following subsection. The energy yield of the variable-speed system is higher. However, the added cost and the electrical loss in the power electronics partially offset the benefit. The cost and benefit trade-off is generally positive in large systems.

In addition to higher annual energy production, the variable-speed power electronic system offers remotely adjustable and controllable quality of power. This has two major benefits not available in other systems:

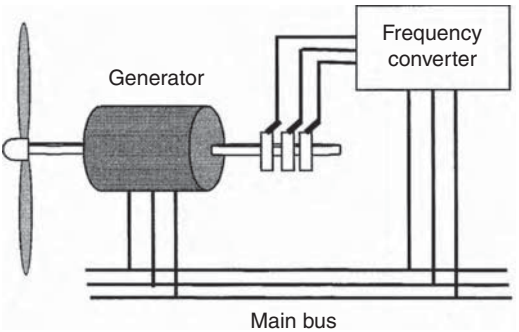

FIGURE 6.9 Scherbius variable-speed drive with doubly fed induction generator.

- Opportunity for remote control: This makes it attractive for offshore applications.
- Fine-tuning for superior grid connection: This makes it better suited for meeting the demand of weak grids in developing countries such as China and India.

The power electronics-based variable-speed system introduces some system-level issues not found in other systems. It produces high-frequency harmonics (electrical noise) in the network, which degrades the quality of power. Alternatively, for the same quality of power, it requires a higher degree of electrical filtering to meet the grid-quality requirement.

6.2.5 Scherbius Variable-Speed Drive

Compared to the variable-speed system using power electronics, the Scherbius machine offers a lower-cost alternative that also eliminates the power-quality disadvantage. It has been used in hoist applications in factories and mines. Extending the analysis of the equivalent circuit described in Chapter 5, the speed of the induction machine can be changed by changing the rotor resistance or by injecting an external voltage of the frequency corresponding to the desired rotor slip. The squirrel cage construction does not allow such an injection. Therefore, the wound-rotor construction with slip rings is used (Figure 6.9). The rotor circuit is connected to an external variable-frequency source via slip rings, and the stator is connected to the grid system. For this reason, the Scherbius machine is also called the *doubly fed induction machine*. It is fed from both the stator and the rotor. The speed is controlled by adjusting the frequency of the external source of the rotor current. The range of variable-speed control using the Scherbius machines is generally limited to 2:1.

This concept was used in early turbines. The decreased reliability due to the rubbing electrical contacts at the slip rings had been a concern. However, some manufacturers appear to have resolved this concern and are implementing the system in turbines in MW ratings. The need of the variable-frequency source for the rotor adds into the cost and complexity. For large systems, however, the added cost is less than the benefit of greater energy production of the variable-speed operation.

In the doubly fed Scherbius variable-speed drive, a power electronic converter — a pulse width or a cycloconverter type — linked to the controlled main grid line converts the frequency and the voltage to the values necessary to maintain the desired rotor speed. The control is done through two different control circuits: the main bus frequency controller and the injection voltage controller. The control circuitry of the main bus frequency controller measures the frequency of the grid (or rpm of the generator) and compares this frequency to a given set point (50 or 60 Hz). A signal is then sent to the injection voltage controller, depending on how far away the frequency is from the set point.

The injection voltage controller receives this signal from the bus frequency controller and compares it to the set point, which corresponds to 50 or 60 Hz. A subsequent adjustment on the injection voltage by the action of the frequency converter will make the injection voltage and frequency output match the set point. This action makes the variable-speed, variable-voltage AC generator produce a constant voltage and frequency output at the grid terminals.

Datta and Ranganathan[1] compared the benefits of a doubly fed, wound rotor induction generator with fixed-speed and variable-speed schemes using the cage rotor. The comparison was made on the basis of major hardware required, operating region, and energy output for a practical wind speed distribution. The comparison shows that the wound rotor generator of similar rating can significantly enhance energy capture due to its ability to operate with the rated torque even at supersynchronous speeds. The power is then generated out of the rotor as well as the stator. Moreover, with a rotor side control, the voltage rating of the power electronic devices and DC bus filter capacitor bank is reduced. The size of the line side inductor filter coil is also decreased.

A combination of the variable-speed scheme with pitch control is increasingly becoming the dominant choice in larger turbines. The two-speed active-stall combination and the classic-stall version with fixed blades also remain in use.

6.2.6 Variable-Speed Direct Drive

A generator that operates directly at the turbine speed is extremely attractive. It is possible particularly for small machines where the rotor speed is high. The direct drive eliminates the mechanical gear altogether and needs no power electronics. This results in multiple benefits:

- Lower nacelle weight
- Reduced noise and vibration
- Lower power loss by several percent
- Less frequent servicing requirement at the nacelle

The last benefit is particularly attractive for offshore installation.

In large turbines, the low rotor speed imposes a design limitation on the direct-drive generator. However, research and developments are underway to resolve the generator design issues as discussed in Chapter 5. For example, Vensys of Germany installed a 1.2-MW prototype in 2003. It uses a permanent-magnet generator with

a belt-driven pitch system. MTorres of Spain and Zephyros of Amsterdam are pursuing other types of direct-drive systems.

A low-speed, direct-drive machine — without a gearbox or with just a simple gearbox — is a very desirable design. The multibrid technology developed in Germany is described as a compact drive with a single-stage gearbox and a medium-speed (150 rpm), permanent-magnet marine-type generator. A 5-MW multibrid prototype has been developed and tested successfully.

6.3 DRIVE SELECTION

The constant-speed system allows a simple, robust, and low-cost drive train. The variable-speed system, on the other hand, brings the following advantages:

- 20 to 30% higher energy yield
- Lower mechanical stress — a wind gust accelerating the blades instead of a torque spike
- Less fluctuation in electric power because the rotor inertia works as the energy buffer
- Reduced noise at lower wind speed

The current and/or voltage harmonics introduced by the power electronics in the variable-speed design may be of concern.

The variable-speed operation can capture theoretically about a third more energy per year than the fixed-speed system.[2] The actual improvement reported by the variable-speed system operators in the field is lower, around 20 to 30%. However, an improvement of even 15 to 20% in the annual energy yield can make the variable-speed system commercially viable in a low-wind region. This can open an entirely new market for the wind power installations, and this is happening at present in many countries. Therefore, the newer installations are more likely to use the variable-speed systems.

The approximate distribution of the system design at present is 30% one fixed-speed, 40% two fixed-speed, and 30% variable-speed power electronic systems (Figure 6.10). The market share of the variable-speed systems, however, is increasing every year.[3]

6.4 CUTOUT SPEED SELECTION

In any case, it is important that the machine is operated below its top speed and power limits. Exceeding either one above the design limit can damage and even destroy the machine.

In designing the variable-speed system, an important decision must be made for the top limit of the operating speed. For the energy distribution shown in Figure 6.11, if the wind plant is designed to operate up to 18 m/sec, it can capture energy E_1 integrated over the year (area under the curve). On the other hand, if the system is designed to operate at a variable speed up to 25 m/sec, it can capture energy E_2

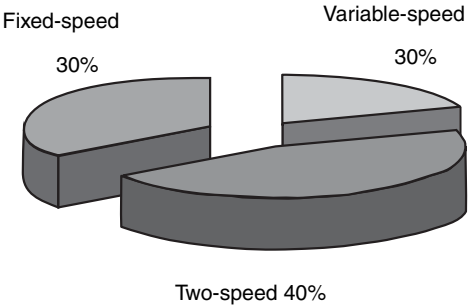

FIGURE 6.10 Design choices in generator drive systems.

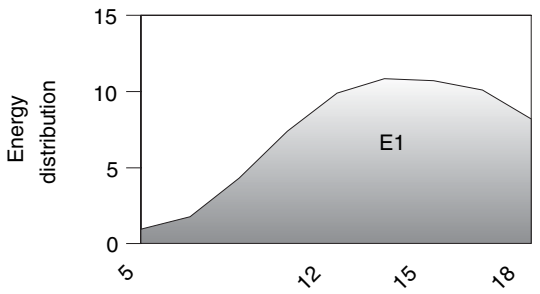

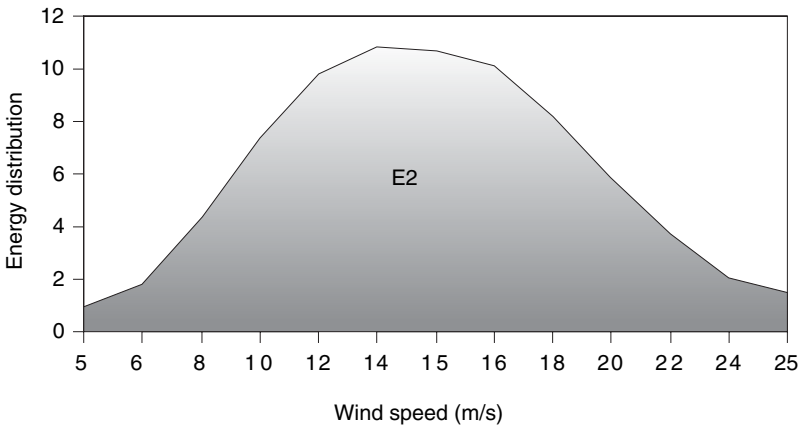

FIGURE 6.11 Probability distribution of annual energy production at two cutout speeds.

over the same period. The latter, however, comes with an added cost of designing the wind turbine and the generator to handle a higher speed and a higher power. The benefit and cost must be traded off for the given site to arrive at the optimum upper limit on the rotor speed.

On one side of the trade-off is additional energy $(E_2 - E_1)$ that can be captured over the year. If the revenue of the generated electricity is valued at p \$/kWh, the added benefit per year is $p(E_2 - E_1)$ dollars. The present worth PW of this yearly benefit over the life of n years at the annual cost of capital i is as follows:

$$PW = p\left(E_2 - E_1\right)\left[\frac{\left(1+i\right)^n - 1}{i\left(1+i\right)^n}\right] \tag{6.2}$$

In the present example, if the initial capital cost is C_1 for the variable-speed system with cutout speed of 25 m/sec, and C_2 for that with 18 m/sec, then the variable-speed system with 25 m/sec cutout speed will be financially beneficial if the following is true:

$$PW > (C_2 - C_1) \tag{6.3}$$

Such trade-offs should account for other incidental but important issues, such as potential noise concerns at higher cutout speeds.

References

1. Datta, R. and Ranganathan, V.T., Variable-Speed Wind Power Generation Using a Doubly Fed Wound Rotor Induction Machine: A Comparison with Alternative Schemes, IEEE Transactions on Energy Conversion, Paper No. PE-558EC, September 2002.
2. Zinger, D.S. and Muljadi, E., Annualized wind energy improvement using variable-speed, IEEE Transactions on Industry Applications, Vol. 33–6, pp. 1444–47, 1996.
3. Gardner, P., Wind turbine generator and drive systems, *Wind Directions*, Magazine of the European Wind Energy Association, London, October 1996.

7 Offshore Wind Farms

The oceans cover two thirds of the earth's surface, contain energy resources far greater than the entire human race could possibly use, and offer open space for deploying new energy technologies on a grand scale without significant interference with the environment or normal human activities. As for wind farms, the wind speed in the ocean is higher than on land — 30 to 40% higher in the open ocean and 15 to 20% higher near the shore. An offshore wind farm, therefore, can generate up to 50 to 70% more power and reduce its electricity costs, even with a higher cost of installation in water. For this reason, many large offshore wind farms have been installed in Europe (Figure 7.1), and more are under construction. Governments in many countries in Europe, Asia, and the Americas are evaluating new proposals every year. Germany has a goal of installing 30-GW offshore wind farms by 2020, the U.K. has plans for 6-GW offshore capacity by 2010, France aims at 5-GW offshore capacity by 2010, Winergy of Long Island has applied for 12-GW capacity off the U.S. east coast, and Australia's Tasmanian coast is being seriously explored for large wind farms.

The U.S. east coast, being thousands of miles long, has more promise as compared to many European countries with hundreds of miles of coastline. Among the main attractions along the northeast coast of the U.S. are strong, steady winds, shallow waters, low wave height, and a growing regional market for renewable energy. The southern New England shore is viewed as a potential Saudi Arabia of wind energy. It is the most heavily populated urban region with heavy transmission constraints. Power produced elsewhere cannot necessarily be transmitted for use in the cities. Although there are good wind regimes along the coast, both over and off water, the wind speed dramatically drops off within just 30 to 60 km inland. For these reasons, developers are considering large wind farms offshore of the northeast U.S.

Offshore wind projects are generally large, often costing $100 to $300 million. To reduce the cost per megawatt of capacity, wind turbines built for offshore applications are larger than those used onshore. The Vestas 2-MW and GE's 3.6-MW turbine are just two examples. Even larger turbines in the 5 to 7 MW range are being developed for offshore installations. At present, a 300-MW onshore wind farm would probably use 150 to 200 wind turbines, whereas an offshore wind farm of the same capacity would probably use fewer than 100 turbines. The project construction cost decreases with turbine size because a smaller number of barges, ships, and cranes are required per megawatt installed.

Offshore wind farms fall into two broad categories: near shore (<6 km) and far shore (>6 km). Most existing European farms are less than 10 km offshore in water of less than 10-m depth, on average, but new larger far-shore ones are planned. Public opinion favors locations far out to sea even though extra cost is involved.

FIGURE 7.1 Vindeby offshore wind farm in Denmark. (From Vestas Wind Systems, Denmark. With permission.)

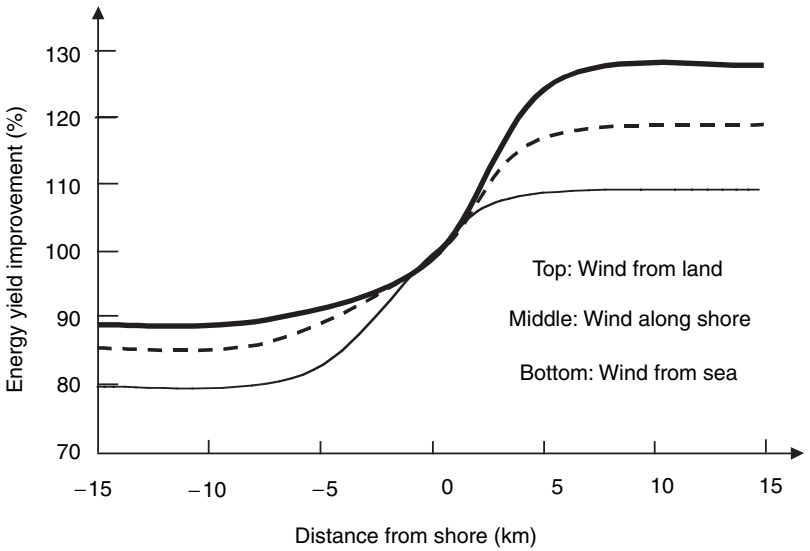

FIGURE 7.2 Energy-yield improvement with distance from the shore in a 3-MW turbine at 80-m hub height. (Adapted from H. Bjerregaard, *Renewable Energy World,* James & James Ltd., London, March–April 2004, p. 102.)

The wind speed and the resulting energy yield improve with distance from the shore as seen in Figure 7.2 for a 3-MW turbine on an 80-m tall tower. With wind coming from the land, the energy yield can be 25 to 30% higher 5 to 6 km from the shore,

TABLE 7.1
Existing Offshore Wind Farms in Europe

Location[a, b]	Country	Online	MW	No	Rating
Vindeby	Denmark	1991	5.0	11	Bonus 450 kW
Lely (Ijsselmeer) (close onshore)	Holland	1994	2.0	4	NedWind 500 kW
Tunø Knob	Denmark	1995	5.0	10	Vestas 500 kW
Irene Vorrink (close to shore)	Denmark	1996	16.8	28	Nordtank 600 kW
Dronten (Ijsselmeer) (close onshore)	Holland	1996	11.4	19	Nordtank 600 kW
Gotland (Bockstigen)	Sweden	1997	2.75	5	Wind World 550 kW
Blyth Offshore	U.K.	2000	3.8	2	Vestas 2 MW
Middelgrunden, Copenhagen (cooperative)	Denmark	2001	40	20	2 MW
Uttgrunden, Kalmar Sound	Sweden	2001	10.5	7	Enron 1.5 MW
Horns Rev	Denmark	2002	160	80	Vestas 2 MW
Samso	Denmark	2003	23	10	Bonus 2.3 MW
Frederikshavn (close to shore)	Denmark	2003	5.3	2	Vestas >3 MW Bonus 2.2 MW
Nysted, Rodsand	Sweden	2003	158	72	Bonus 2.2 MW

[a] Minimum distance to shore 0 to 14 km with an average of 7 km.
[b] Water depth varies from 0 to 20 m with an average of 8 m.

Source: From British Wind Energy Association.

whereas it is 12 to 15% lower 5 to 6 km inland. Similar gains are seen with wind coming from the sea or along the shore. Thus, the difference between 5 km offshore and 5 km inland can be 30 to 45% in energy yield. Ten kilometers from the shore, the wind speed is typically 1 m/sec (10 to 15%) higher. This gives 30 to 50% higher energy yields. Moreover, wind is less turbulent at sea, which improves the quality of power and extends the life of the blades. On the negative side of being farther out at sea are the deeper seabed, higher construction and operating costs, and higher grid connection cost, all of which partially offset the higher energy yield.

7.1 OFFSHORE PROJECTS

Offshore wind farms currently operational in Europe are listed in Table 7.1. The early projects were relatively small, and located in shallow or sheltered waters. Not until Blyth came online, exposed to the full force of the North Sea, could any project be described as truly offshore. At present, more than 100 offshore wind farms are being planned worldwide, with the highest concentration in northern Europe. In the 4-yr period from 2004 to 2007, new offshore installations planned in Europe alone amount to almost 4000 MW.

In the U.K. three wind farms are planned, one off the northwest cost and two off the east coast, with the first one to start in 2005. It will have 38 2-MW turbines on 60-m-high towers 3 km off the coast of Great Yarmouth and would cost $109 million. A 500-MW farm is planned off the Irish coast.

Germany's Borkum West has planning permission for construction outside the 12-km zone at a water depth of about 30 m. It will initially have 12 5-MW turbines in a pilot plant 45 km north of Borkum Island in the North Sea, connected to the onshore transformer station via 100-kV AC cable over a 115-km distance. After 3 yr of the pilot operation, further developments may upgrade it to full 1000-MW capacity at a cost of 1.5 billion euros.

The largest offshore wind farm in operation in 2002 was the 160-MW Horns Rev installed in Danish waters at a total cost of 268 million euros. It is built in the harsh environment of the North Sea, and has 80 2-MW Vestas turbines on 62-m towers. The mean wind speed is 9.7 m/sec. The site is 17 km offshore, where the water depth is 6.5 to 13.5 m, and the seabed consists of firm sand and gravel. The farm layout is rectangular in rows 560 m apart. The electric energy yield is estimated to exceed 600 GWh/yr.

Along the U.S. northeast coast, a proposed 420-MW project, Cape Wind, will be located 8 km off Hyannis village in a 40-km^2 shallow area in Nantucket Sound. It consists of 130 3.6-MW turbines placed 0.5 km apart and connected to the New England power grid by two 130-kV submarine cables through an electrical substation on Cape Cod. Although this project holds great wind power potential, it has met with both legislative and environmental opposition.

A study funded by New York State[1] found that about 5200 MW of capacity could be installed in an 800-km^2 band 5 to 10 km off the south shore of Long Island. About 2500 MW of capacity could be installed even by placing the wind turbines in a smaller 400-km^2 band where the water depth is typically 15 m or less deep. The Long Island Power Authority has been inviting proposals and meeting with interested developers and environmental groups for a final approval in a 2005 to 2007 time frame for an initial 100-MW capacity. The cost estimates are $150 to 180 million for 100-MW wind turbines and $40 to 70 million for the grid-interconnecting substation. The energy cost estimate is 6 to 9 cents/kWh — about half of what the local consumers are paying. The initial 100-MW capacity would use 35 3-MW turbines 5 to 10 km offshore. The rotor would be 50-m diameter on a 80-m hub above the water surface, with the rotor tip reaching out 130 m above the surface of the water. Jones beach has been mentioned as a possible location along with Montauk. Further detailed studies are underway for specific site locations. The permitting process, due to multiple oversight entities, may take 3 to 5 yr.

7.2 LEGAL ASPECTS IN THE U.S

The government policies on issues pertaining to this new type of energy generation must be addressed before offshore wind farms are built in any country. The rush of offshore wind projects in the early 2000s highlighted the regulatory holes that exist in identifying and understanding the applicable laws. In the U.S., for example,

currently there is no federal framework that exists to evaluate any aspect of the proposed projects on Cape Cod, Long Island, or elsewhere. Because no such project has ever been formally approved or sited in U.S. waters, historical case law, statutory interpretation, and administrative guidance are nonexistent. Therefore, analyses are based upon statutory interpretation of the current federal, state, and local regulatory schemes, reviews of analogous projects (i.e., dredge and fill actions), and communications with appropriate regulatory authorities.

It is generally recognized that offshore wind farm permits are required from at least seven federal and state agencies, such as:

- Army Corps of Engineers, under their authority derived from the Rivers and Harbors Acts
- Coast Guard, as almost any offshore wind farm would be in navigable waters
- Federal Aviation Administration, as the wind towers may impact navigable airspace
- State and local governments, to comply with local planning and zoning ordinances
- Many federal agencies, which may also require various reviews under their jurisdiction, *vis-a-vis* the Clean Water Act, Endangered Species Act, Tidal Wetland Act, etc.

Major federal regulations that must be reviewed and complied with are as follows:

Rivers and Harbors Appropriation Act of 1899 (33 USC 403; Chapter 425, March 3, 1899; 30 Stat. 1151): This act prohibits the construction of any bridge, dam, dike, or causeway over or in navigable waterways of the U.S. without Congressional approval. Administration of section 9 has been delegated to the Coast Guard. Structures authorized by state legislatures may be built if the affected navigable waters are totally within one state, provided that the plan is approved by the chief of engineers and the secretary of the army (33 USC 401). Under section 10 of the act, the building of any wharfs, piers, jetties, and other structures is prohibited without Congressional approval. Excavation or fill within navigable waters requires the approval of the chief of engineers. Service concerns include contaminated sediments associated with dredge or fill projects in navigable waters. Section 13 of the act was modified by the Federal Water Pollution Control Act Amendments of 1972, which established the National Pollutant Discharge Elimination System Permits for the discharge of refuse matter into or affecting navigable waters.

The Fish and Wildlife Coordination Act (16 USC 661-667e; 48 Stat. 401): This provides authority for the U.S. Fish and Wildlife Service to review and comment on the effects on fish and wildlife of activities proposed to be undertaken or permitted by the Corps of Engineers.

The Deepwater Port Act of 1974 (P.L. 93-627): This authorizes the secretary of transportation, after consultation with the secretary of the interior, to waive the removal requirements for a deepwater port if its components can be used in conjunction with a mineral lease sale.

Outer Continental Shelf (OCS) Lands Act of 1953 (43 USC 1331-1356, P.L. 212, Ch. 345, as amended in 1975, 1978, and 1984): Numerous amendments were incorporated in the Outer Continental Shelf Lands Act amendments of 1978 (P.L. 95-372):

- Title II of these amendments provides for the cancellation of leases or permits if continued activity is likely to cause serious harm to life, including fish and other aquatic life. It also stipulates that the economic, social, and environmental value of renewable and nonrenewable resources be considered in management of the OCS.
- Title III of these amendments established an Offshore Oil Spill Pollution Compensation Fund to be financed by a tax on oil obtained from the OCS and stipulated the damages for which claims could be made against the fund.
- Title IV of the amendments established a Fishermen's Contingency Fund to compensate fishermen for damage to fishing gear by materials, equipment, tools, containers, or other items associated with oil and gas exploration.
- Title V amended the 1972 Coastal Zone Management Act to authorize grants to coastal states under a Coastal Energy Impact Program.

Amendments enacted in 1984 provided for changes to certain administrative provisions in the Fishermen's Contingency Fund.

The Army Corps of Engineers relies on the Rivers and Harbors Act of 1899 and the OCS Lands Act (OCSLA) of 1953 as the legal authorities to evaluate OCS wind power plant proposals. Although the Corps has claimed jurisdiction over OCS wind farm development, its jurisdiction under the Rivers and Harbors Act is limited to 3 nmi from shore. Most wind power plant proposals are on lands outside this 3-nmi limit. Corps approval is not sufficient to support development of this nature. In addition, the OCS Lands Act, which initially was enacted to regulate extraction activities for resources such as gas, oil, and minerals, is the only federal statute concerning the activities on OCS lands; it has absolutely no application to wind farm development projects.

OCS lands are a valuable natural resource the federal government holds in trust for all U.S. citizens. This means that the government cannot allow the appropriation and development of these lands by private business interests without first carefully considering and protecting the public interest in the lands and their resources. The public interest includes its environmental, aesthetic, recreational, and historic interests in each location proposed for development. The sacrifice of those interests is potentially justifiable only if the benefits to the public will outweigh the losses from the industrialization of a natural resource.

Congress, however, has not yet passed any law or authorized any agency to govern wind energy development on OCS lands.

7.3 ENVIRONMENTAL IMPACT

Under the National Environmental Policy Act, an environmental impact assessment of the entire project must be conducted before a private company is allowed to erect any structure on OCS lands. The environmental study must include the Migratory Bird Treaty Act, the Marine Mammal Protection Act, the Endangered Species Act, and the National Environmental Policy Act. It must also include the initial data-gathering structures and work offshore such as localized disturbance of the seabed and possible pollution. Mathematical simulation programs developed by British Maritime Technology to evaluate the environmental impacts of offshore installations and their waste, such as drill cuttings, lubricants, and other chemicals, may be of help here.

It has not been investigated yet whether or not large wind farms could affect the local wave patterns and/or weather patterns by extracting more than a third of the wind energy from the region. As for shipping traffic, the individual turbines could be spaced such that small vessels could sail through the array. However, the proposed site may interfere with shipping routes or large pleasure craft. The wind turbines could lie in the way of fishing areas or even migrating/mating whale habitats. The underground cable may also interfere with fishing areas.

The environmental issues involved in the placement of offshore wind farms include the impact on the avian population and underwater ecosystems. This is especially a factor when birds of known endangered and threatened species reside in or migrate through the area. Avian collisions with turbines resulting in death are a major concern along with the disruption of feeding, nesting, and migrating habits. Though avian deaths by blades had been seen on a large scale at the Altamont Pass, CA, location, it has not been experienced offshore.[2]

Several species of endangered birds have been considered in the proposed Long Island project: the bald eagle, piping plover, least tern, roseate tern, common loon, and osprey. These birds rarely appear along the south shore and usually stay within a mile of the shoreline. They migrate up the Atlantic Coast through the Montauk area from New England. Migratory birds consisting of sea ducks, waterfowl, and gulls pass in large numbers through the Montauk area. Scoters number over 100,000, eiders in thousands, and other species in tens of thousands. Because of such significant bird population migration through Montauk, the far eastern shore is unsuitable for installing wind farms.

For underwater ecosystems, the south shore of Long Island is protected by the state and federal wildlife reserve. The South Shore Estuary Reserve is mostly an inland bay protected from the Atlantic Ocean by island barriers. This provides an environment of mixed freshwater and saltwater where many species of plants and animals flourish. To protect and preserve the underwater sea life here, no site closer than 1.5 mi to the shore may be allowed. However, due to avian migration and nesting in the area, the desirable distance could probably be increased to 2 mi at the minimum.

Sound propagation both in the air and underwater must be considered. The turbines are usually placed at a far enough distance from where the sound propagating through air cannot be heard onshore. Studies have shown that sound propagation

TABLE 7.2
Installation Cost Breakdown for Large Wind Farms

Cost Element	Cost on Land (Percentage of Total)	Cost Offshore (Percentage of Total)
Wind turbines	70	50
Foundations	6	16
Internal connections	7	5
Grid connection	7	18
Engineering	3	4
All others	7	7

Source: From Offshore Wind Energy: Ready to Power a Sustainable Europe, final report for European Commission, 2002.

through water from the turbine may not affect sea life as long as creatures in that area are used to the sound of passing motorboats, which emit a similar sound. That the shadow of the rotating blades may frighten some fishes is another consideration. Studies have shown that the population of fish around the area of the installed turbines actually increases once installed. This is due to the new area provided on which marine growth can attach and develop.

Although offshore wind farms do not use valuable real estate, they pose a potential visual interference. Waterfront residents, who have paid high prices for ocean-view property, do not want to see an offshore wind farm from their windows. The Cape Cod proposal met resistance from many residents fighting against the development. Vacation resorts may be concerned that tourists could see the wind farm from the shore and hear the turbine noise from the beach on a low-wind day.

7.4 OFFSHORE COSTS

Generally, offshore wind farms cost 50 to 100% more to install compared to those on land. Even on land, the investment cost breakdown is highly site specific. The cost varies considerably with the location, particularly for remote sites where the cost of grid connection may be very high. A 2002 study on the cost breakdown of wind farms being installed currently onshore and offshore is summarized in Table 7.2.

The offshore costs vary over a wide range between 1000 and 2000 euros/kW, and the energy cost varies between 0.04 and 0.06 euros/kWh. The primary cost parameters are the distance from the shore, water depth, and the wind speed. The foundation and interconnect costs can exceed the wind turbine cost. The operation and maintenance costs are also difficult to predict with a high degree of confidence. Thus, possibilities of large cost variations pose an investment risk and make the project financing difficult unless the risk can be adequately insured. However, the offshore wind farm market is relatively new for both the financing companies and the insurance companies. Therefore, potential investors must first obtain adequate

and reliable data to determine how best to maximize profitability and minimize the investment risk. Data collection includes stationary data towers pile-driven into the seabed at the proposed site.

7.5 POWER TRANSMISSION TO SHORE

Offshore wind farm power is transmitted to the shore by cables running under water. Most individual wind generators produce 690-V AC. Without an electrical substation in the water next to the tower to step up voltage, the cable voltage must be the same as the generator voltage. This would significantly increase the transmission loss. However, as on land, the offshore wind farm as a whole operates at a distribution substation voltage level. A transformer is installed under each tower to step up the generator voltage to the substation level. The substation, typically farther away from the farm, requires a high voltage — 35 kV or even higher — to minimize power losses.

A very large wind farm above 300-MW capacity may require the transmission voltage to be even greater than 150 kV, possibly around 350 kV. However, the cost of the transformer and switchgear increases with the voltage level. As reported by Ackerman,[3] the 160-MW Danish Hornes Rev wind farm uses 36 kV for the collecting substation offshore. It is then stepped up to 150 kV for feeding a 15-km AC cable to the shore. The offshore substation is built as a tripod structure. The 20-m × 28-m steel building is placed 14 m above the mean sea level. The platform accommodates the 36/150 kV step-up transformer and the switchgear on the sides, emergency diesel generator, controls and instrumentation, staff and service facilities, helipad, crane, and a boat. Such high-voltage offshore substations are new developments, although the oil and gas industry has been using 135-kV power systems for a long time.

The high-voltage offshore system improves the energy efficiency but also contributes to high capital cost. Because the energy cost at the mouth of the wind farm is much lower than that at the customer meter, an economic trade-off exists for using a low distribution voltage, which would be less efficient but also low in capital cost.

Turbines in a typical offshore wind farm are connected in the radial configuration shown in Figure 7.3. The number of turbines in one radial arm determines the cable capacity. This configuration is less reliable, as a damaged cable would disable all the turbines connected to it. A ring configuration may be preferred for reliability. The cable is typically buried 1 to 2 m deep in offshore ground to protect it from ship anchors and sea currents. This may not be enough near busy ports, where anchors of large ships can go 10 to 12 m deep into the ground. It is not practical to bury cables at such depths. Good reliability can be achieved only by having a redundant cable on a separate route. Getting permission for one cable route is difficult enough, so most offshore wind farms accept the reliability achievable with one cable.

Burying cables and pipes underwater requires underwater earthmoving equipments, many of them made by Soil Machine Dynamics (Newcastle upon Tyne, U.K). Umbilical lines provide power up to 1 MW to pump seawater to create a 3-m-deep fluidized trench behind the vehicle in which the cable is buried while moving between towers. For a rocky seabed, a chain cutter is used to cut a vertical slot of about 1.5 m below the vehicle.

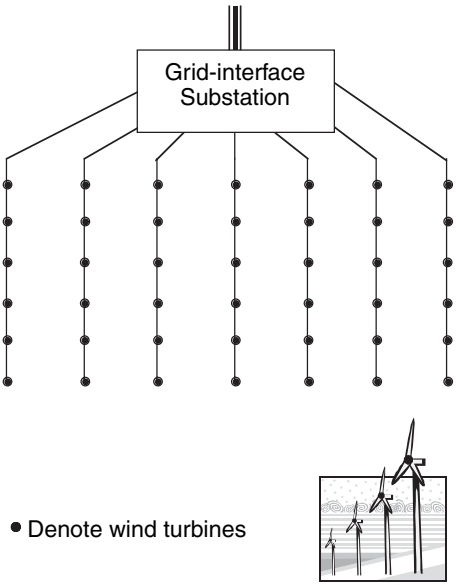

FIGURE 7.3 Radial layout of wind farm turbines.

Instead of using electrical cables, it is possible to produce hydrogen offshore using wind power and to transmit it onshore by pipelines. Such a proposal has been considered in Germany, where no tax is levied on hydrogen produced by offshore wind farms. However, initial studies indicate that it would be less expensive to transmit power to the shore than to use it for producing and transmitting hydrogen to the shore.

7.5.1 AC Cable

All wind farms to date transmit power to shore using AC cables. For large megawatt ratings and long transmission distances, AC has the following disadvantages:

- Power losses increase significantly.
- VAR compensation is required at both ends of the cable, whether by using synchronous machines or static power electronic compensators.
- Cable capacity may be limited. For example, polyethylene-insulated XLPE cable is limited to 200 MW with one 150-kV three-phase cable. A 1000-MW wind farm would require five such cables in parallel, with possibly one more for reliability.

7.5.2 DC Cable

High-voltage DC (HVDC) cable can eliminate the preceding disadvantages. Moreover, it significantly reduces the fault current contribution to the onshore network.

HVDC cable in the ocean is an established technology. The first such 100-km, 20-MW, 100-kV submarine cable was installed between the Swedish island of Gotland and the Swedish mainland in 1954. Since then, many HVDC links have been built around the world — in the U.S., Canada, Japan, New Zealand, Brazil, and Paraguay — for power ratings up to 6300 MW and voltages up to ±600 kV.

The use of HVDC requires AC–DC and DC–AC conversions at the two ends of the transmission cable. This can use conventional or voltage source converter-based technology. However, it adds significant capital cost and operating cost, and there is power loss. The capital cost can be several times that with conventional AC cables. It is estimated that traditional HVDC transmission to the shore may not be economical for power ratings below 400 to 500 MW and distances below 50 km. However, the new voltage source converter (VSC) technology offered by ABB (HVDC Lite™) and by Siemens (HVDC Plus™) has been found to be economical. Both are based on PWM designs using IGBTs, as opposed to the line-commutated converters using thyristors. In the VSC, the current can be switched off without costly commutating circuits, and the active and reactive powers can be controlled independently. The VSC is bipolar — the DC circuit is not connected to ground — so it uses a two-conductor cable. The first VSC link, a 70-km, 50-MW, ±80-kV link, was built for voltage support for a large wind capacity installed in the south of Sweden at Gotland. Many other VSC links are being built onshore around the world today.

As for the cables' insulation, XLPE can be used for AC as well as DC power. It gives the flexibility of converting the shore connection from AC to DC, if and when the offshore wind farm gradually expands from pilot phase to full capacity.

The cost of 150-mm^2 grid connection cable is about $100 per meter of 35-kV-class cable. The voltage drop and power loss would be about 0.15% per km distance from the wind farm to the grid connection on land.

7.6 OCEAN WATER COMPOSITION

About three quarters of the earth's surface is covered by oceans. The average ocean depth is 3,800 m, and the maximum depth is 11,524 m in the Mindanao Trench in the Pacific Ocean. In comparison, the average land elevation is 840 m, and the highest elevation is 8,840 m at the top of Mount Everest. Figure 7.4 is the cross section of the ocean floor, depicting the general terminology of the shore and the continental shelf. About 8% of the ocean floor is shallower than 1,000 m and 5% is shallower than 200 m, where the majority of offshore oil and gas platforms are located. Most offshore wind farms in Europe have been installed in water less than 15 to 20 m in depth.

The ocean shore and shelf material generally consists of sand and gravel coming from land via rivers and blown in by wind. The ocean water density of seawater at atmospheric pressure and 10°C is 1027 kg/m^3. It contains 35 g of salt per kilogram of seawater, which is expressed as the salinity of 35 ppt (parts per thousand). The salinity is measured by measuring the electrical conductivity of seawater, as the two are related. Seawater salt composition by percentage is shown in Figure 7.5: 55% chlorine, 31% sodium, and 14% all others.

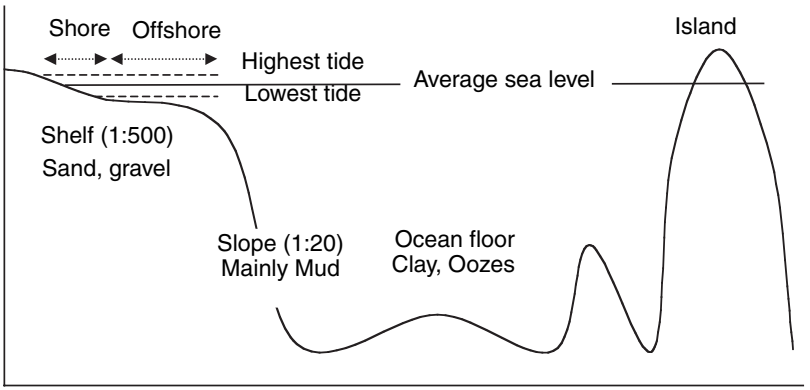

FIGURE 7.4 Ocean-floor terminology.

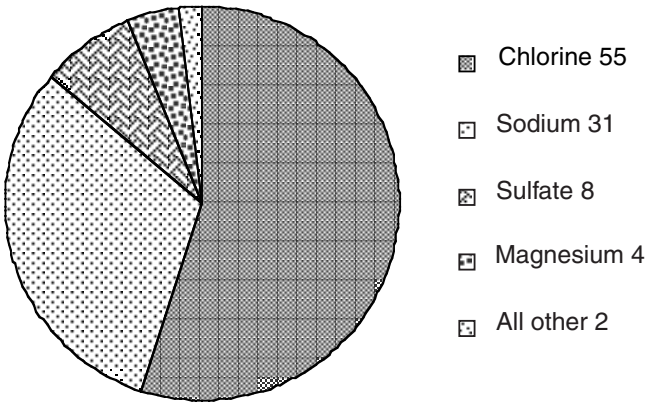

FIGURE 7.5 Salt composition of ocean water (by percentage).

7.7 WAVE ENERGY AND POWER

The primary wave-generating forces are the wind, storms, earthquakes, the moon, and the sun. Figure 7.6 ideally represents a typical ocean wave in shallow offshore water. It is characterized by the following expressions:

$$\frac{2\pi}{d} < 0.25 \quad \text{and} \quad \frac{d}{gT^2} < 0.0025 \tag{7.1}$$

where d = water depth and T = wave period.

As shown in Figure 7.7, the water particles under the wave travel in orbits that are circular in deep water, gradually becoming horizontal-elliptical (flat-elliptical) near the surface. The kinetic energy in the wave motion is determined by integrating the incremental energy over the depth and averaging over the wavelength:

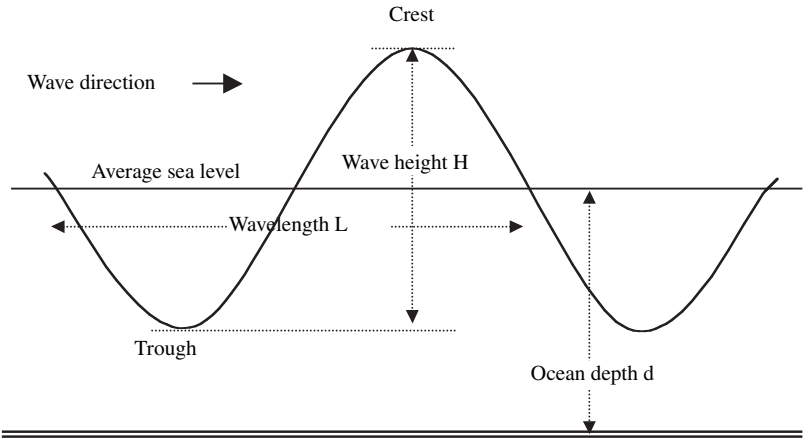

FIGURE 7.6 Ideal representation of ocean waves in shallow offshore water.

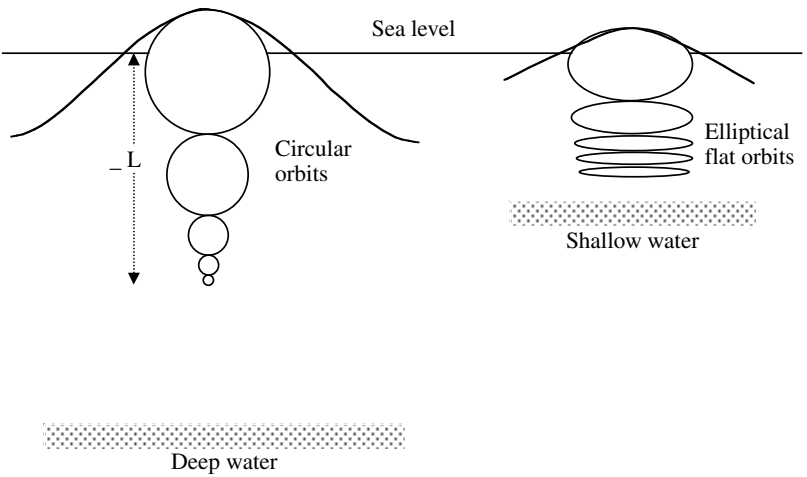

FIGURE 7.7 Orbits of water particles in deep and shallow waters.

$$\text{wave kinetic energy} \quad E_k = \frac{\rho g H^2}{16} \tag{7.2}$$

The potential energy of the wave is determined by integrating the incremental potential energy in the height of a small column width over one wavelength:

$$\text{wave potential energy} \quad E_p = \frac{\rho g H^2}{16} \tag{7.3}$$

Note that the wave's potential energy and kinetic energy are equal in magnitude, which is expected in an ideal wave with no energy loss. Therefore, the total energy per unit length of the wave, E_l, is twice that value, i.e.:

$$\text{total energy per unit length } E_l = E_k + E_p = \frac{\rho g H^2}{8} \tag{7.4}$$

The total energy E in one wavelength L is given by the following:

$$\text{total energy in one wave } E = E_l L = \frac{\rho g H^2}{8} L \tag{7.5}$$

The mechanical power in the wave is the energy per unit time. It is obtained by multiplying the energy in one wavelength by the frequency (number of waves per second) as follows:

$$\text{wave power } P = \frac{\rho g H^2}{8} Lf \tag{7.6}$$

The energy in a wave thus depends on the frequency, which is a random variable. Ocean wave energy is periodic, with the frequency distribution in ocean surface waves as shown in Figure 7.8. The actual waves may have long waves superimposed

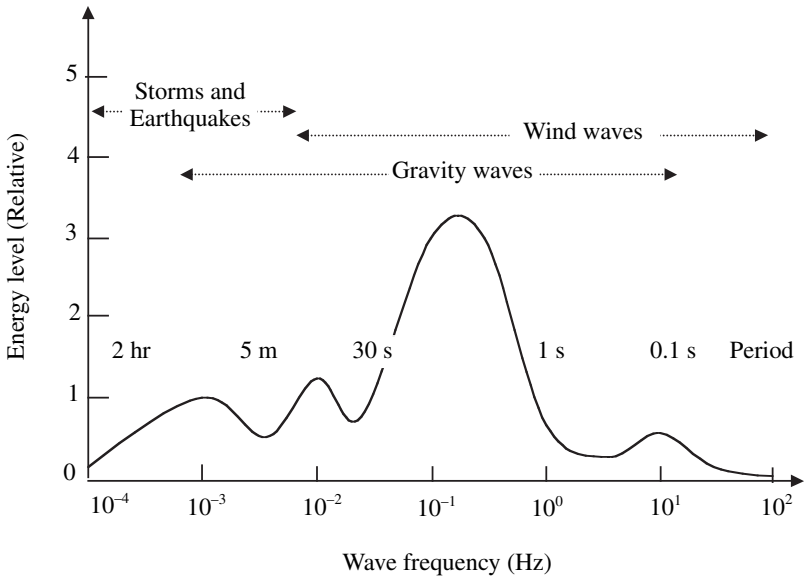

FIGURE 7.8 Approximate energy distribution in ocean surface waves.

on short waves from different directions. A simple linear one-frequency wave theory may be superimposed for an approximate estimate of the total effect.

7.8 OCEAN STRUCTURE DESIGN

Wind-generated waves with a period of 1 to 30 sec are the most important in determining the wave power and force acting on ocean structures.

7.8.1 Forces on Ocean Structures

The offshore structure must withstand mechanical forces exerted by the ocean waves, currents, wind, storms, and ice. The wave force is the most dominant of all. The structure must absorb, reflect, and dissipate wave energy without degradation in performance over a long lifetime.

Offshore platforms have been built around the world since the early 1950s to drill for oil and gas, along with undersea pipelines. Offshore mining is also being developed now, and the offshore wind farm is the latest addition to such structures installed to provide a means of producing energy resources and transporting energy to the shore.

The weight and cost of a fixed platform that will withstand wave forces, currents, and wind increase exponentially with the depth of water as seen in Figure 7.9. The offshore cable or pipelines carrying the cable must withstand forces due to inertia, drag, lift, and friction between the floor and the pipe. The water drag and lift forces for an underwater structure in a somewhat streamlined water current can be derived from classical hydrodynamic considerations. They depend on the water velocity near the floor, which follows the one seventh power law, namely

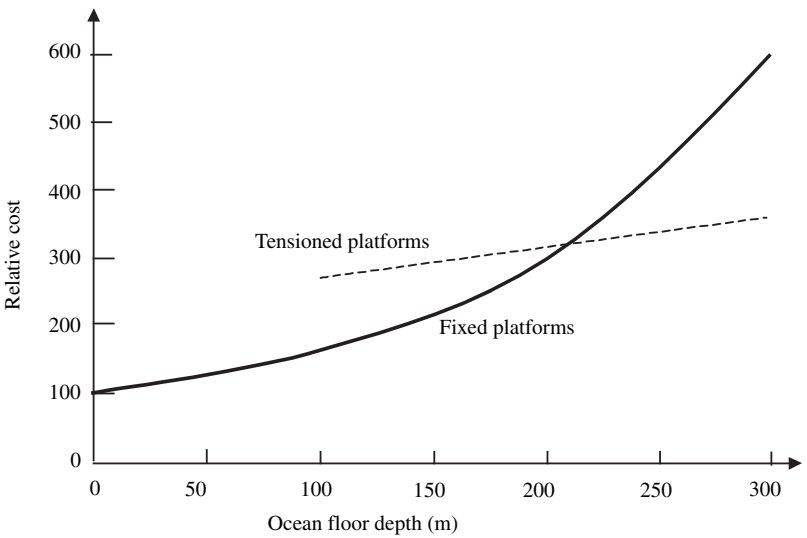

FIGURE 7.9 Cost of offshore structures at various depths.

TABLE 7.3
Corrosion Rate of Various Materials in Seawater

Material	Average Corrosion Rate (μm/yr)
Titanium	None
Stainless steel, Nichrome	<2.5
Nickel and nickel-copper alloys	<25
Copper	10–75
Aluminums alloys	25–50
Cast iron	25–75
Carbon steel	100–175

$$\frac{V}{V_o} = \left(\frac{Y}{Y_o}\right)^{1/7} \tag{7.6}$$

where V and V_o are the water velocities at heights Y and Y_o, respectively, above the seabed.

The friction coefficient between the pipe surface and the seabed varies with the sediment type. The concrete-coated pipes commonly used offshore have a friction coefficient of 0.3 to 0.6 in clay, about 0.5 in gravel, and 0.5 to 0.7 in sand.

7.9 CORROSION

Corrosion is caused by the electrochemical reaction in which a metal anode corrodes by oxidation and a cathode undergoes reduction reaction. The seawater works as an electrolyte for the transfer of ions and electrons between the two electrodes. The corrosion rate must be accounted for in the design. Table 7.3 lists the corrosion rates of commonly used metals.

Two types of cathodic protection are widely used for corrosion protection of materials submerged in seawater. The impressed current system gives more permanent protection, but requires electric power. Galvanic protection employs aluminum, magnesium, or zinc anodes attached to the steel structure in seawater. Under the cathodic protection principle, a metal receiving electrons becomes a cathode, which can no longer corrode. The zinc anode is most widely used as a sacrificial material to protect steel hulls of ships. When it has deteriorated, it is replaced for continued protection. Zinc provides about 1000-Ah charge-transfer capacity per kilogram. The sacrificial anode design follows basic electrical circuit principles.[4]

7.10 FOUNDATION

The tower foundation design depends on water depth, wave height, and the seabed type. The foundation for an offshore turbine and its installation is a significant cost

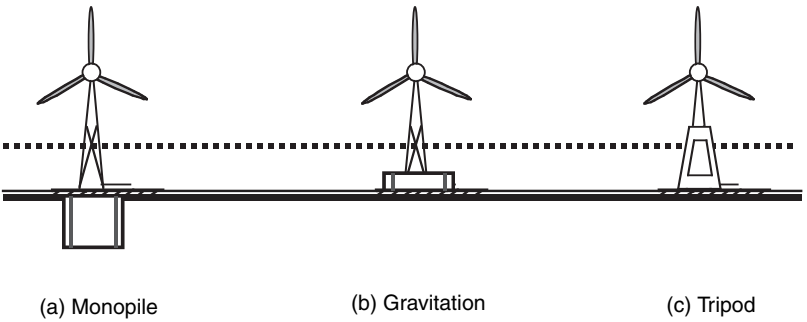

FIGURE 7.10 Foundation types for offshore wind turbines.

component of the overall project, 20 to 30% of the cost of the turbine. The height and consequently the depth of installation are determining factors in choosing the farm location. Turbines installed on land generally have a tower height equal to the rotor diameter to overcome wind shear from ground obstacles. However, the offshore tower height can be 70% of the rotor diameter due to the low shear effect of water.

The most favorable water depth for an offshore wind farm is 2 to 30 m. Depths less than 2 m are not accessible by ship, and those greater than 30 m make the foundation too expensive. In this range, three possible foundation designs are shown in Figure 7.10. They are: monopile for 5 to 20 m depths, gravity for 2 to 10 m depths, and tripod or jacket for 15 to 30 m depths.[5]

7.10.1 Monopile

The cylindrical steel monopile is the most common and cost-effective foundation in 5 to 20 m deep water. It is driven into the seabed up to a depth of 1.1 times the water depth, depending on the seabed conditions. It does not need seabed preparation, and erosion is not a problem. However, boulders and some layers of bedrock may require drilling or blasting, which would increase the installation cost. The monopile construction is limited to water depths of 20 m due to the stability considerations. A monopile foundation including installation for a 1.5-MW turbine in 15-m deep water could cost about $450,000 in 2005.

7.10.2 Gravitation

The gravitation foundation is made of concrete and steel that sits on the seabed. It is often used in bridges and low-depth turbine installations. It is less expensive in shallow water (2 to 10 m deep), but is extremely expensive in water deeper than 15 m.

7.10.3 Tripod

The tripod foundation is suitable for 15 to 30 m deep water. It utilizes a lightweight, three-legged steel jacket to support the foundation. The jacket is anchored to the seafloor by piles driven into each leg. Each pile is driven up to 20 to 25 m into the seafloor, depending on seabed conditions. Boulders in the pile area are the only

concern, which may be blasted or drilled if necessary. The tripod foundation cannot be used in depths less than 10 m due to the legs' possible interference with vessels. However, in water deeper than 10 m, the tripod is very effective as has been tested in oil rig foundations. Preparation of the seafloor is not necessary, and erosion is not a concern with this installation. For a 1.5-MW turbine utilizing a tripod foundation at a water depth of 15 m, the foundation cost including installation would be about $400,000 in 2005. (Source: Danish Wind Industry Association report, Offshore Foundations: Tripod.)

Other foundations under development for the offshore towers include the following:

- Lightweight foundations guyed for stability
- Floating foundations with the turbine, tower, and foundation in one piece
- Bucket-type foundation

The bucket-type foundation design is used to support Vestas 3-MW turbines. The 135-t structure has the shape of an upturned bucket and is sucked into the seabed through a vacuum process. Early indications are that such a design makes the fabrication, handling, installation, and subsequent removal easier and less expensive. Figure 7.11 depicts a typical wind tower foundation structure.

The most economical way to install turbines in terms of manpower, equipment, and time is to install the turbine and tower as a single unit. The foundation is placed first, and then the turbine, tower, and the rotor are lifted and attached to the foundation in that sequence. A jack-up lift barge is the most likely vessel to be used for installing the foundation as it can carry the foundation and drive the piles in.

Typical foundation cost is about $50 per kW on land and $300 per kW offshore in 10-m deep water, increasing by roughly 2% per meter of additional water depth. These costs vary with the seabed and water conditions.

Approximate costs of foundation installation have been compiled in a chart by the Danish Wind Industry Association.[5] The chart plots the price of the foundation, including installation in water with an average depth of around 25 m. It does not include the cost of installing the turbine tower, nacelle, and rotor.

The issues of remoteness from the onshore facilities and crews to construct and maintain offshore installations are being addressed by developing wind turbines fitted with integrated assembly cranes, helicopter pads, and emergency shelters capable of sustaining crews for several days of harsh weather offshore.

7.11 MATERIALS

Offshore equipment is necessarily made to withstand the marine environment. They have marine-grade material, components, seals, and coatings to protect them from the corrosive environment.

Table 7.4 lists materials commonly used in seawater along with their mechanical strengths and relative costs. The marine environment is harsh enough to cause rapid and sometimes unanticipated degradation of equipment. For example, all 81 of the 2-MW turbines at Denmark's Horns Rev — the largest wind farm built to date —

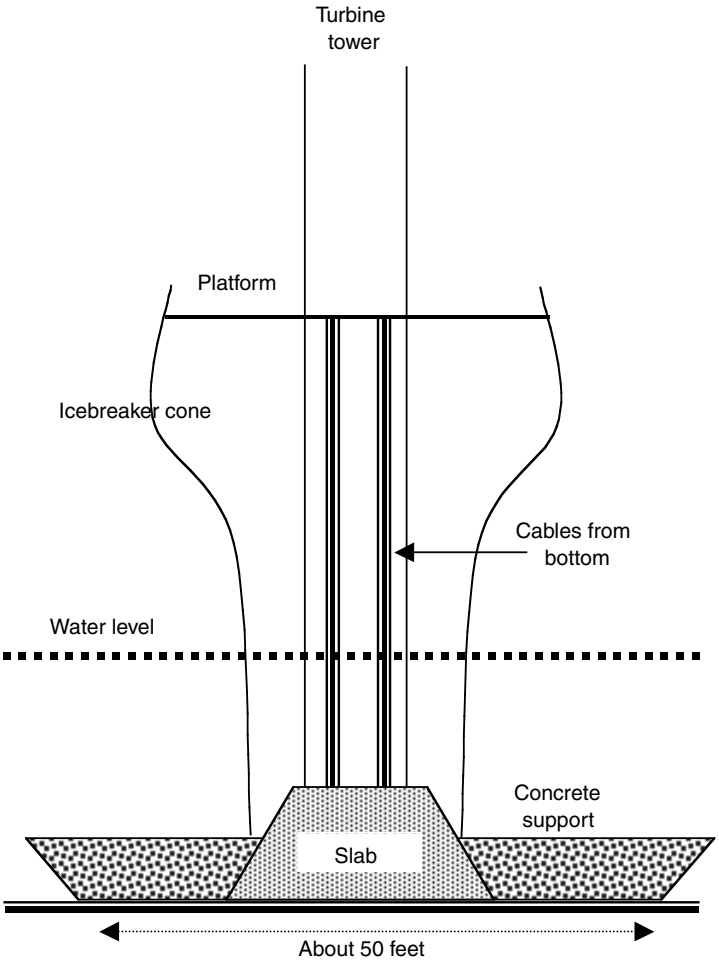

FIGURE 7.11 Typical foundation structure.

were moved back to the shore within a couple of years after installation to repair or modify the generators and transformers at a considerable expense (to remove and reinstall the turbines). It was believed that the equipment design and material would not have withstood the harsh marine environment for a long duration. Similar problems have been encountered before in other offshore farms.

The coatings on the wind turbine must last over its design life of 20 to 25 yr. Because the turbines are highly visible on tall towers, they need to be pleasing in appearance for public acceptance. A typical coating system on the onshore wind turbine is a three-coat system. It consists of 50 to 80 μm epoxy-zinc-rich primer, 100 to 150 μm epoxy midcoat, and 50 to 80 μm polyurethane topcoat. Protection for offshore wind turbines in highly corrosive marine environments is defined in the EN-ISO-12944 standard. It is necessarily different for parts under water and for the tower parts above water.

TABLE 7.4
Mechanical Strength of Various Materials Commonly Used in Structures in Seawater

Material	Yield Strength (ksi)	Ultimate Strength (ksi)	Elongation (Percent)	Relative Cost
Mild steels	30–50	50–80	15–20	1
Medium-strength steels	80–180	100–200	15–20	3–5
High-strength steel	200–250	250–300	12–15	10–15
Stainless steels 302 and 316	35–45	80–90	55–60	5–10
Aluminum alloys	30–70	45–75	10–15	7–8
Titanium alloys	100–200	125–225	5–15	20

7.12 MAINTENANCE

Maintenance of the wind turbine and foundation is important for its longevity and for keeping the energy cost down. Regularly scheduled inspections are absolutely necessary, particularly because offshore towers do not get incidental periodic visits. No federal regulations exist in regard to inspecting the equipment in offshore wind farms. The Naval Facilities Engineering Command outlines procedures for inspecting offshore structures based on good engineering practices. Although not mandatory, their implementation would reduce the maintenance cost in the long run. The inspections must be planned taking into consideration weather conditions and the wave height.

Presently wind farms are built to operate for 20 yr with minimal maintenance. Visual inspections of the turbine and tower should be conducted periodically during the plant's lifetime to search for apparent physical signs of deterioration, damage, etc. The procedures for inspecting the tower follow those laid out for inspecting the underwater foundation.

Inspections of the foundation and the tower at the splash line are important as this part of the structure is exposed to corrosion due to galvanic action. A level-one inspection is conducted annually for the underwater structures. A level-two inspection is conducted biannually for the underwater structures, and a level-three inspection is made every 6 yr. The procedures and equipment used to carry out these inspections are listed in the Underwater Inspection Criteria published by the Naval Facilities Engineering Service Center.

Generally, visual inspections allow detection and documentation of most forms of deterioration of steel structures. Some types of corrosion may not be detected by visual inspections. For example, inside steel pipe piling, anaerobic bacterial corrosion caused by sulfate-reducing bacteria is especially difficult to detect. Fatigue distress can be recognized by a series of small hairline fractures perpendicular to the line of stress but these are difficult to locate by visual inspection. Cathodic

protection systems must be closely monitored both visually and electrically for wear of anodes, disconnected wires, damaged anode suspension systems, and/or low voltage. A nondestructive test plan may be developed and tailored to any specific area of concern at a particular wind farm site.

References

1. Long Island Power Authority. Long Island's Offshore Wind Energy Development Potential: A Preliminary Assessment. Report for New York State Energy Research and Development Authority by AWS Scientific, Inc., Albany, NY, 2002.
2. Krohn, S., 2000. Offshore Wind Energy: Full Speed Ahead, Danish Wind Industry Association Report, 2002.
3. Ackerman, T., 2000. Transmission Systems for Offshore Wind Farms, *IEEE Power Engineering Review*, December 2000, pp. 23–28.
4. Randall, R.E., 1997. *Elements of Ocean Engineering*, The Society of Naval Architects and Marine Engineers, Jersey City, NJ, 1997.
5. Danish Wind Industry Association, 2003. Wind Turbine Offshore Foundations, April 2003.

Part B

Photovoltaic Power Systems

8 Photovoltaic Power

Photovoltaic (PV) power technology uses semiconductor cells (wafers), generally several square centimeters in size. From the solid-state physics point of view, the cell is basically a large-area pn diode with the junction positioned close to the top surface. The cell converts sunlight into DC. Numerous cells are assembled in a module to generate the required power (Figure 8.1). Unlike the dynamic wind turbine, the PV installation is static, does not need strong tall towers, produces no vibration or noise, and needs no active cooling. Because much of current PV technology uses crystalline semiconductor material similar to that of integrated circuit chips, the production costs have been high. However, between 1980 and 2004, the capital cost of PV modules per watt of power capacity has declined from more than $20 per watt to less than $4 per watt (Figure 8.2). During the same period, the cost of energy has declined from almost $1 to about 20 cents per kWh at present (Figure 8.3), and is expected to decline to less than 15 cents per kWh by the year 2010. The cumulative installed capacity in the U.S. has risen from nearly zero in 1980 to approximately 200 MW in 1996, and exceeded 1000 MW in 2004 (Figure 8.4). The world's cumulative installed capacity of PV systems was about 300 MW in 1996, which grew to 800 MW by 2000 and 1330 MW by the end of 2002 (Figure 8.4). The annual growth rate of PV installation rose from 20% in 1994 to 40% in 2000.

The European PV Industry Association reports that the total global PV cell production worldwide in 2002 was over 560 MW and has been growing at about 30% annually in recent years.

Figure 8.5 depicts the annual production of PV modules in 2002. Out of a total of 562 MW worldwide, Japan led the way with 251 MW, followed by 135 MW in Europe, 121 MW in the U.S., and 55 MW in the rest of the world. Germany is expecting 50% growth in PV in 2004 with 120 MW of new solar parks.

The strong growth in PV has continued, with grid-connected plants dominating. The IEA estimates that by the end of 2000 about two thirds will be off-grid and one third, grid-connected. Since 2000, the price of PV systems has decreased by more than 20%. Several new fully automated module plants have started production, and the factory prices of single crystals and polycrystalline silicon modules — making up over 80% of the world PV module market — fell below $3.50 per watt in 2004. Worldwide, solar PV is now a $7 billion annual business, mainly driven by Germany.

The present PV energy cost is still higher than the price utility customers pay in most countries. For that reason, PV applications have been limited to remote locations not connected to utility lines. With the declining prices, the market of new modules has been growing at 25 to 30% annually during the last 5 yr. The U.S., U.K., Germany, Japan, China, India, and other countries have established new programs or have expanded existing ones. It has been estimated that the potential

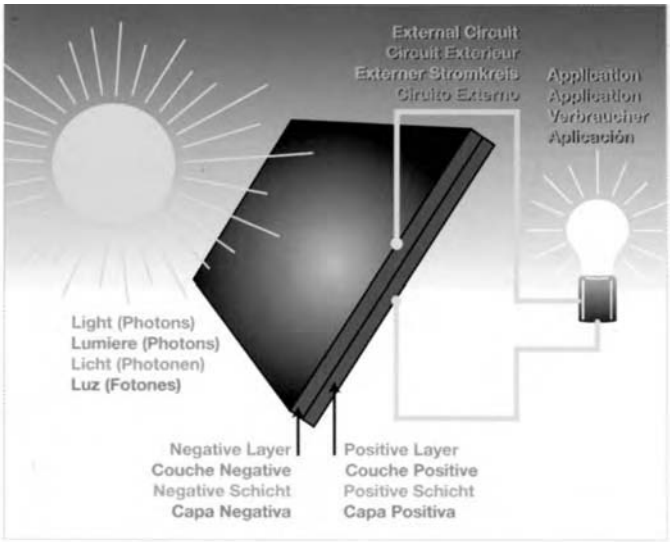

FIGURE 8.1 PV module in sunlight generates DC. (From Solarex/ BP Solar, Frederick, MD. With permission.)

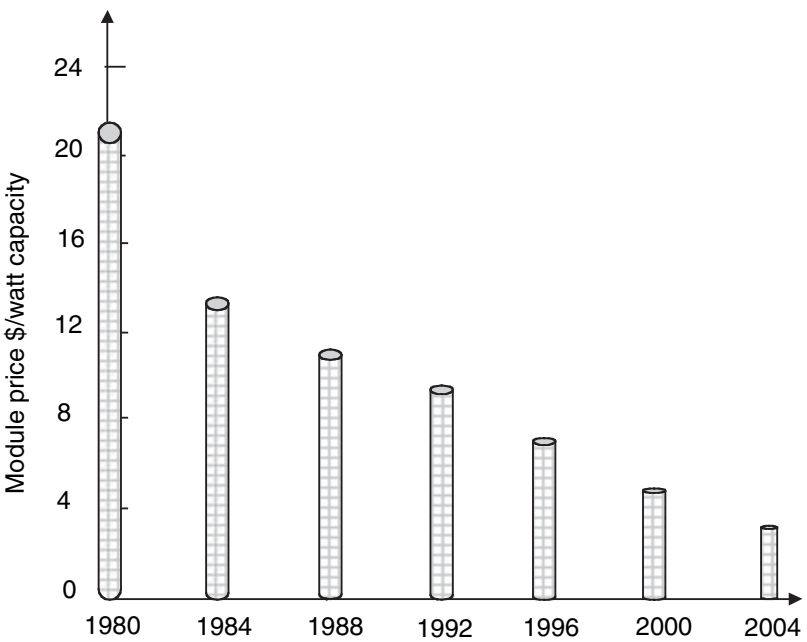

FIGURE 8.2 PV module price trends.

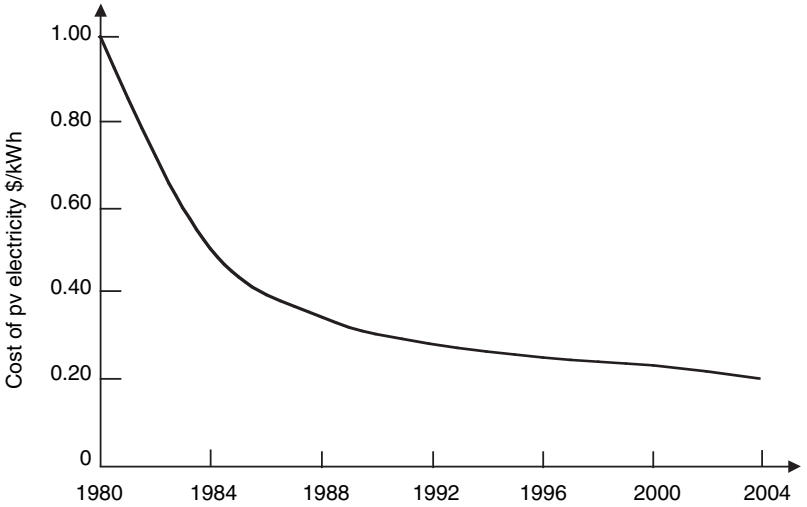

FIGURE 8.3 PV energy price trends.

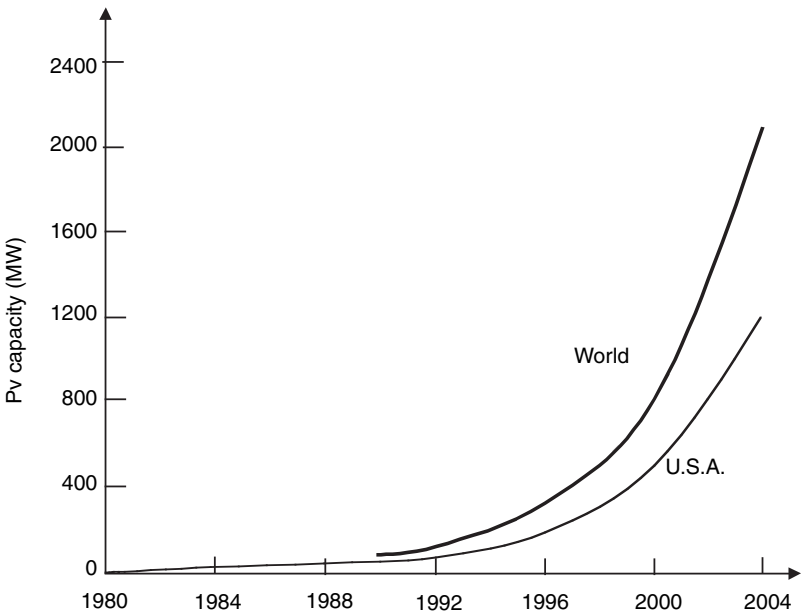

FIGURE 8.4 Cumulative capacity of PV installations in the world and in the U.S.

PV market, with new programs coming in, could be as large as 1600 MW by 2010. This is a significant growth projection, largely attributable to new manufacturing plants installed in the late 1990s and early 2000s to manufacture low-cost PV cells and modules to meet the growing demand.

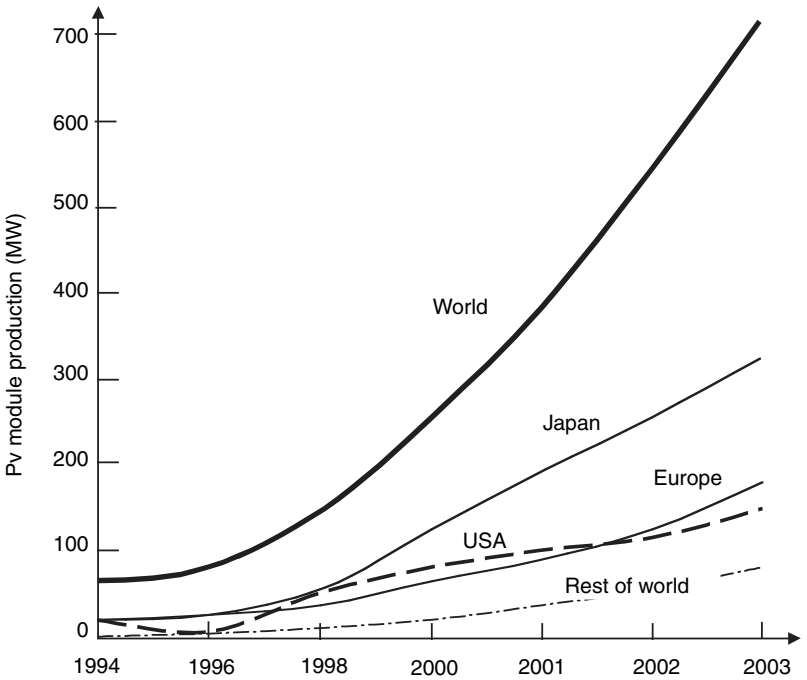

FIGURE 8.5 Annual production of PV cells and modules. (From Renewable Energy World, July–August 2003, p. 86.)

TABLE 8.1
Production Capacities of Various PV Technologies in 2002

PV Technology	Production in 2002	
	MW of Capacity	Percentage of Total
Crystalline silicon	162	29
Polycrystalline silicon	306	55
Amorphous silicon	33	6
Ribbon silicon	17	3
All others	44	7
TOTAL	562	100

Source: Renewable Energy World, James & James Ltd., London, July–August 2003, p. 86.

The annual production of various PV cells in 2002 is shown in Table 8.1. About 90% of the production has been in the crystalline silicon and amorphous silicon technologies, with 10% of all other types still in the development stage. The major

TABLE 8.2
Top PV Cell Producers in the World

Manufacturer	Production in 2002	
	MW of Capacity	Percentage of Total
Sharp	123	21.9
BP Solar	74	13.2
Kyocera	60	10.7
Shell Solar	58	10.3
Sanyo	35	6.2
GE (AstroPower)	30	5.3
All others	182	32.4
World Total	562	100

Source: PV News, Vol. 22, No. 3, 2003.

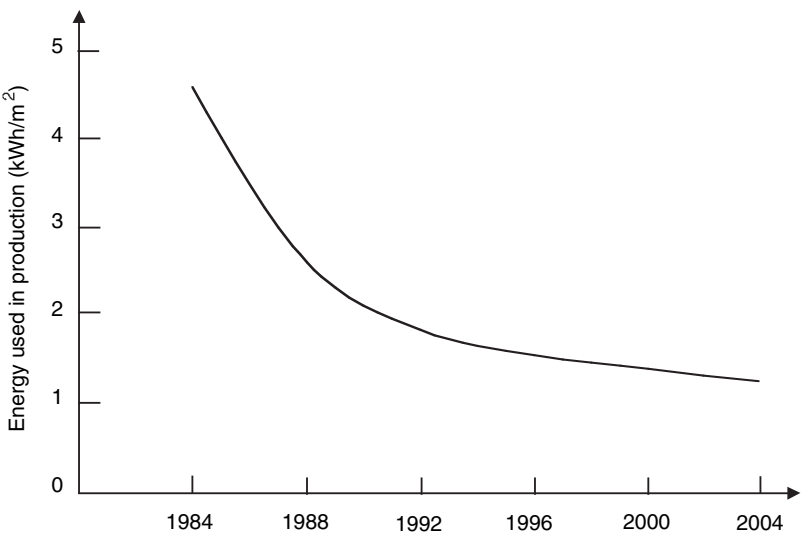

FIGURE 8.6 Energy consumption per square centimeter of PV cell manufactured. (From U.S. Department of Commerce and Dataquest, Inc.)

PV cell producers in the world are listed in Table 8.2. Sharp, BP Solar, Koycera, and Shell Solar supplied more than 50% of the world market.

The PV-cell-manufacturing process is energy intensive. Every square centimeter of cell area consumes more than a kWh before it faces the sun and produces the first kWh of energy. However, the energy consumption during manufacturing is steadily declining with continuous implementation of new production processes (Figure 8.6).

Major advantages of PV power are:

- Short lead times to design, install, and start up a new plant
- Highly modular; hence, the plant economy is not strongly dependent on size
- Power output matches very well with peak-load demands
- Static structure, no moving parts; hence, no noise
- High power capability per unit of weight
- Longer life with little maintenance because of no moving parts
- Highly mobile and portable because of light weight

At present, PV power is extensively used in stand-alone power systems in remote villages around the world, particularly in hybrid systems with diesel power generators. It is expected that this application will continue to find expanding markets in many countries. The driving force is the energy need in developing countries and the environmental concerns in developed countries.

8.1 PV PROJECTS

U.S. electric utilities have started programs to develop power plants using the newly available low-cost PV modules. Idaho Power has a program to supply power to selected customers not yet connected to the grid. Other utilities such as Southern California Edison, the municipal utility of Austin, Delmarva Power and Light, and New York Power Authority are installing PV systems to meet peak demands. Pacific Gas and Electric's utility-scale 500-kW plant at Kerman, California is designed to deliver power during local peak demand, generating 1.1 MWh of energy annually.

City planners are recognizing the favorable overall economics of PV power for urban applications. Tens of thousands of private, federal, state, and commercial PV systems have been installed over the last 25 yr. More than 65 cities in 25 states have installed such systems for a variety of necessary services. These cities, shown in Figure 8.7, are located in all regions of the country, dispelling the myth that PV systems require a sunbelt climate to work efficiently and generate returns. State subsidies in California, New York, Arizona, and North Carolina have accelerated PV power growth to 25 to 30% annually during 2000 to 2004. California's PV buy-down program resulted in an 8-MW added capacity in 2002 at a cost of $3.50 per watt to customers. Arizona added 3 MW of PV power in 2002.

A 5-MW PV plant in the Mojave Desert consists of 20 250-kW modules occupying a 40-acre site around Barstow. Southern California Edison has contracted to purchase the entire energy production of 11 million kWh annually. The plant capacity was the world's largest in 2004. A 1.2-MW PV system was built on the roof of Santa Rita jail in Dublin, CA.

The roof of the Aquatic Center in Atlanta (Figure 8.8), venue of the 1996 Olympic swimming competition, was one of the largest grid-connected power plants when built. It generates 345 kW of electric power, and is tied into the Georgia Power grid lines. Its capacity is enough to power 70 homes connected to the network. It saves

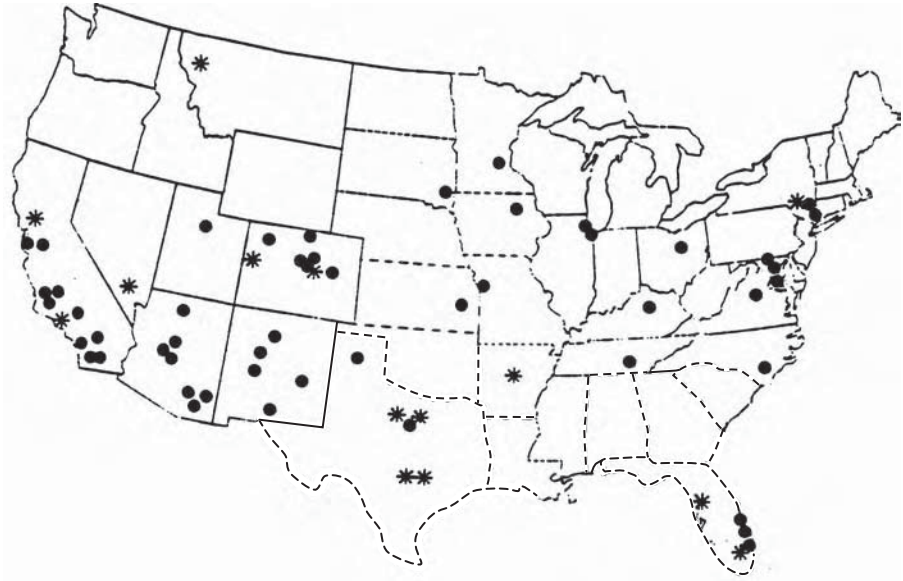

FIGURE 8.7 U.S. cities with PV installations. (From U.S. Department of Energy.)

FIGURE 8.8 Roof of Atlanta's Aquatic Center with 345-kW grid-connected PV power system. (From Georgia Institute of Technology. With permission.)

330 t of CO_2, 8.3 t of SO_2, and 1.2 t of NOx yearly. A similar 500-kW grid-connected system was installed to power the Olympics Games of 2000 in Sydney, Australia.

The Long Island Power Authority offers $4 per watt installed up to 10 kW to both commercial and residential customers under the Solar Pioneer Program started in early 2002. Under this program, 30 families were selected for free installation of 300-W systems.

Germany's 100,000-roof Solar Power Program offered a guaranteed 0.50 euros/kWh feed-in tariff and attractive financing to encourage 100-MW PV installation, beginning January 2000. It surpassed the goal by adding 325 MW of capacity by July 2003.

Shell Solar GmbH and Gesellschaft announced in 2004 plans to build the largest 5-MW solar PV park, south of Leipzig in Germany. The power will be fed directly into the grid. It will consist of 33,500 modules made from the new Shell SQ series of PV cells with the inverters, transformer, and switchgear supplied by Siemens AG.

India is implementing perhaps the highest number of PV systems in the world for remote villages. The energy-deprived population lives mostly in rural India, where extending the national power grid is prohibitively expensive. Solar PV is becoming a powerful solution in such areas. Studies by the Arid Zone Research Institute, Jodhpur, indicate that significant solar energy reaches the earth's surface in India. About 30% of the electric energy used in India is for agricultural needs. Because the availability of solar power for agricultural needs is not time critical (within a few days), India is expected to lead the world in PV installations in the near future.

The state of Rajasthan has initiated a policy to purchase PV electricity at an attractive rate equivalent to U.S. $0.08 per kWh. In response, a consortium of U.S. companies proposed installing a 50-MW plant using thin-film cells. When completed, this will be the largest PV power plant in the world.

In the remote mountain region of Ladakh on the Tibetan and Pakistani border in the north, India in 2003 launched a 5-yr plan for 2-MW PV plants. The altitude ranges from 2500 to 7000 m. The plan involves numerous solar home systems, each with a 40-W module, 75-Ah deep-cycle battery with an oversized electrolyte reservoir, an electronic charge controller, and two 11-W fluorescent lamps. This allows 3 h of light every night in winters even without the sun shining for 2 d. To avoid the battery freezing at –30C at night, the battery has thermal insulation and a high-density electrolyte.

In the state of Madhya Pradesh, 700-kW and 425-kW grid-connected PV plants were commissioned. The state of West Bengal converted Sagar Island into a PV island with 26-kW solar PV plants to meet the entire electricity need of the island. The island has about 200,000 inhabitants in 16 villages spread out over an area of about 300 km^2. The island previously relied on diesel generation, which was expensive and was causing severe environmental problems. Similar initiatives have been pursued in villages in southern India.

China has been the fastest-growing economy in the world for the last 15 yr, with the GDP growing annually at 8%. Much of the population in rural China living in remote villages in the western and southwestern regions cannot be economically connected to the existing power grid, which is at least 50 km away. If power is not supplied to these people, they may migrate to the cities and create serious problems for the governments. A major project was begun in 1996 to power off-grid villages, and PV is playing a major role in this process. The solar potential in these regions is high — about 3000 h of sunlight per year, yielding about 1700 kWh/m^2.

Worldwide, the total installed PV capacity by the end of 2004 is estimated to be 100 MW, about 40% grid-connected and the rest stand-alone. The total PV system

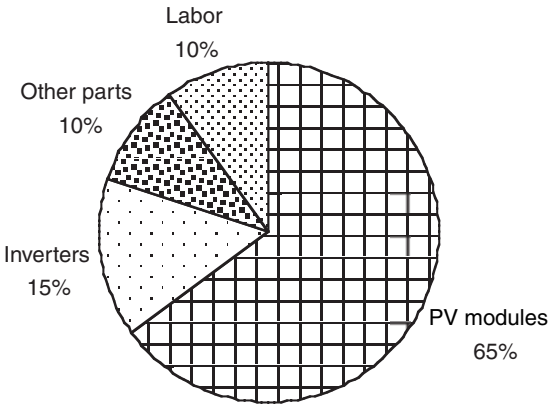

FIGURE 8.9 Component cost breakdown in PV power systems.

cost runs to about $8/W for a 1-kW stand-alone system, $6/kW for a 100-kW system, and $5/kW for a 1000-kW grid-connected system. Typical component costs are about 60 to 70% in PV modules, 10 to 15% in inverters, 10% in other parts, and 10% in labor (Figure 8.9).

8.2 BUILDING-INTEGRATED PV SYSTEM

The near-term potentially large application of PV technology is for cladding buildings to power air-conditioning and lighting loads. One of the attractive features of the PV system is that the power output matches very well with the peak-load demand. It produces more power on a sunny summer day when the air-conditioning load strains the grid lines (Figure 8.10). Figure 8.11 shows a PV-clad building in Germany with an integrated grid-connected power system.

In the mid-1990s, the DOE launched a 5-yr cost-sharing program with Solarex (now BP Solar) in Maryland to develop and manufacture low-cost, easy to install, preengineered building-integrated photovoltaic (BIPV) modules. Such modules made in shingles and panels can replace traditional roofs and walls. The building owners have to pay only the incremental cost of these components. The land is paid for, the support structure is already installed, the building is already wired, and developers may finance the BIPV modules as part of their overall project. The major advantage of the BIPV system is that it produces distributed power generation at the point of consumption. The BIPV system, therefore, offers the first potentially widespread commercial implementation of PV technology in the industrialized countries.

On the consumer side, the DOE also initiated the Million Solar Roofs Initiative to place one million solar power systems on homes and buildings across the U.S. by the year 2010.

Japan added about 150 MW of BIPV systems between 1995 and 2000. The existing programs in Europe, Japan, and the U.S. could add 200 MW of installations by the year 2010, and the Netherlands plans to install 250 MW by 2010.

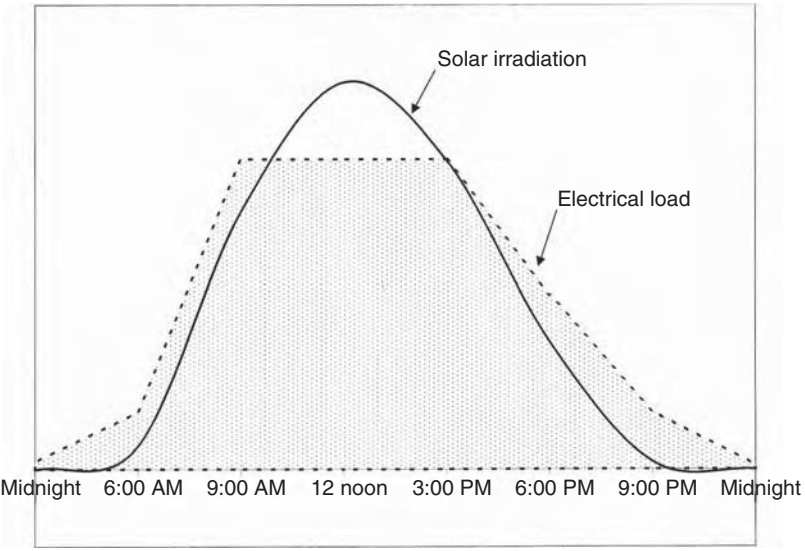

FIGURE 8.10 Power usage in a commercial building on a typical summer day.

project	Flachglas building
location	Wernberg, Germany
architect	Kiermeier
date completed	July 1995
area of solar facade	140m^2
electricity generated	7,000 kWh/year
cell material	polycrystalline
efficiency	11.5%
number of panels	330
orientation	south west/south east
angle of orientation	90°
grid connected	yes

FIGURE 8.11 Building-integrated PV systems in Germany. (From *Professional Engineering*, publication of the Institution of Mechanical Engineers, April 1997, U.K. With permission.)

8.3 PV CELL TECHNOLOGIES

In comparing alternative power generation technologies, the most important measure is the energy cost per kilowatthour delivered. In PV power, this cost primarily depends on two parameters: the PV energy conversion efficiency, and the capital cost per watt capacity. Together, these two parameters indicate the economic competitiveness of the PV electricity.

The conversion efficiency of the PV cell is defined as follows:

$$\eta = \frac{\text{electrical power output}}{\text{solar power impinging on the cell}}$$

The primary goals of PV cell research and development are to improve the conversion efficiency and other performance parameters to reduce the cost of commercial solar cells and modules. The secondary goal is to significantly improve manufacturing yields while reducing the energy consumption and manufacturing costs, and reducing the impurities and defects. This is achieved by improving our fundamental understanding of the basic physics of PV cells. The continuing development efforts to produce more efficient low-cost cells have resulted in various types of PV technologies available in the market today in terms of the conversion efficiency and the module cost. The major types are discussed in the following subsections.[1]

8.3.1 Single-Crystalline Silicon

Single-crystal silicon is the most widely available cell material and has been the workhorse of the industry. Its energy conversion efficiency ranges from 14 to 18%. In the most common method of producing it, the silicon raw material is first melted and purified in a crucible. A seed crystal is then placed in the liquid silicon and drawn at a slow constant rate. This results in a solid, single-crystal cylindrical ingot (Figure 8.12). The manufacturing process is slow and energy intensive, resulting in high raw material cost, presently at $20 to $25 per pound. The ingot is sliced using a diamond saw into 200- to 400-μm (0.005 to 0.010 in.)-thick wafers. The wafers are further cut into rectangular cells to maximize the number of cells that can be mounted together on a rectangular panel. Unfortunately, almost half of the expensive silicon ingot is wasted in slicing the ingot and forming square cells. The material waste can be minimized by making full-sized round cells from round ingots (Figure 8.13). Using such cells would be economical when panel space is not at a premium. Another way to minimize waste is to grow crystals on ribbons. Some U.S. companies have set up plants to draw PV ribbons, which are then cut by laser beam to reduce waste.

8.3.2 Polycrystalline and Semicrystalline Silicon

This is a relatively fast and low-cost process to manufacture crystalline cells. Instead of drawing single crystals using seeds, the molten silicon is cast into ingots. In the process, it forms multiple crystals. The conversion efficiency is lower, but the cost is much lower, giving a low cost per watt of power. Because the crystal structure is somewhat random (imperfect) to begin with, it cannot degrade further with imperfections in the manufacturing process or in operation. It comes in both thick- and thin-film cells and is overtaking the cell market in commercial applications.

8.3.3 Thin-Film Cell

These are new types of PV entering the market. Copper indium diselenide ($CuInSe_2$ or CIS), cadmium telluride (CdTe), and gallium arsenide (GaAs) are all thin-film

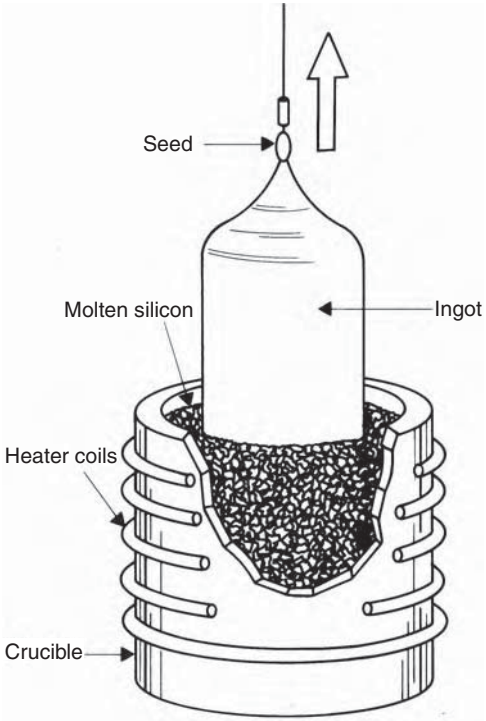

FIGURE 8.12 Single-crystal ingot making by Czochralski process. (From Photovoltaic Fundamentals, DOE/NREL Report DE91015001, February 1995.)

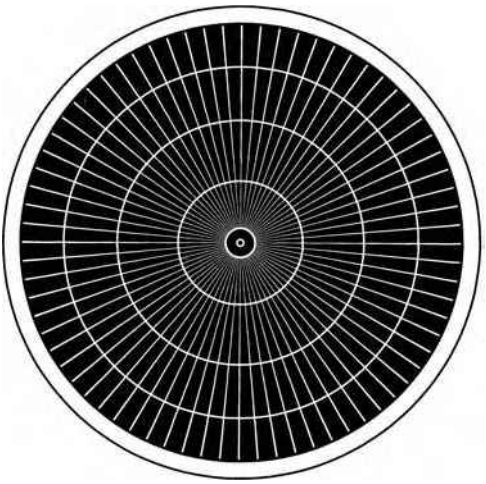

FIGURE 8.13 Round-shaped PV cell reduces material waste typically found in rectangular cells. (Depiction based on cell used by Applied Solar Energy Corporation.)

materials, typically a few micrometers or less in thickness, directly deposited on a glass, plastic, stainless steel, ceramic, or other compatible substrate material. In this manufacturing process, layers of different PV materials are applied sequentially to a substrate. This technology uses much less material per square area of the cell, and hence, is less expensive per watt of power generated.

Cadmium telluride appears to be a promising thin-film technology for low-cost-per-watt capacity. Researchers at NREL are also developing efficient and low-cost CIS cells. This work has been focused on processes that are capable of being inexpensive while maintaining high performance. NREL in 2004 achieved a record thin-film solar cell efficiency of 18% for a CIS cell.

The DOE-funded research at NREL is also directed at developing reproducible processes for making high-efficiency thin-film CdS/CdTe devices, as well as developing alternative processes that can improve device performance, reproducibility, and manufacturability through improvements in five areas. They are transparent conducting oxide layers, CdS/window layers, absorbers and junctions, back contacts, and nanoparticle devices.

8.3.4 Amorphous Silicon

In this technology, a 2-μm-thick amorphous silicon vapor film is deposited on a glass or stainless steel roll, typically 2000 ft long and 13 in. wide. Compared to crystalline silicon, this technology uses only about 1% of the material. Its efficiency is about half that of crystalline silicon technology at present, but the cost per watt is significantly lower. On this premise, two large plants to manufacture amorphous silicon panels started in the U.S. in 1996.

The DoE-funded research concentrates on stabilizing a-Si module efficiency through four tasks:

- Improving thin-film deposition through promising new techniques
- Developing materials with lower band gaps to better balance photon utilization in multijunction devices
- Understanding light-induced metastability to deposit more stable a-Si material
- Developing low-temperature epitaxy

Table 8.3 compares amorphous silicon and crystalline silicon technologies.

8.3.5 Spheral Cell

This is yet another technology that is being explored in the laboratories. The raw material is low-grade silicon crystalline beads, presently costing about $1 per pound. The beads are applied on typically 4-in squares of thin perforated aluminum foil. In the process, the impurities are pushed to the surface, where they are etched away. Because each sphere works independently, the individual sphere failure has a negligible impact on the average performance of the bulk surface. The Southern California Edison Company estimates that a 100-ft^2 spheral panel can generate 2000 kWh per year in an average Southern California climate.

TABLE 8.3
Comparison of Crystalline and Amorphous Silicon Technologies

	Crystalline Silicon	Amorphous Silicon
Present Status	Workhorse of terrestrial and space applications	New rapidly developing technology, tens of MW of yearly production facilities were commissioned in 1996 to produce low-cost cells
Thickness	200-400 μm (0.004–0.008 in.)	2 μm (less then 1% of that in crystalline silicon)
Raw Material	High	About 3% of that in crystalline silicon
Conversion Efficiency	16–20%	8–10%
Module costs (2004)	$3–5 per watt, expected to fall slowly due to the maturation of this technology	$3–5 per watt, expected to fall rapidly to $2 per watt due to substantial DOE funding to fully develop this new technology

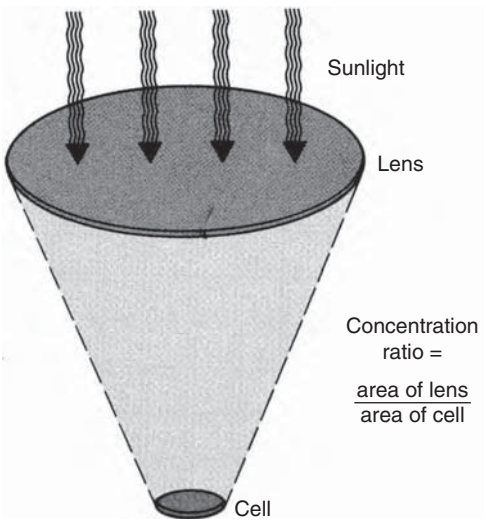

FIGURE 8.14 Lens concentrating the sunlight on a small area reduces the need for active cell material. (From Photovoltaic Fundamentals, DOE/NREL Report DE91015001, February 1995.)

8.3.6 Concentrator Cell

In an attempt to improve conversion efficiency, sunlight is concentrated tens or hundreds of times the normal intensity by focusing on a small area using low-cost lenses (Figure 8.14). A primary advantage of this is that such a cell requires a small

fraction of area compared to the standard cells, thus significantly reducing the PV material requirement. However, the total sunlight collection area remains approximately the same for a given power output. Besides increasing the power and reducing the size or number of cells, the concentrator cell has the additional advantage that the cell efficiency increases under concentrated light up to a point. Another advantage is its small active cell area. It is easier to produce a high-efficiency cell of small area than to produce large-area cells with comparable efficiency. An efficiency of 37% has been achieved in a cell designed for terrestrial applications, which is a modified version of the triple-junction cell that Spectrolab developed for space applications. On the other hand, the major disadvantage of the concentrator cell is that it requires focusing optics, which adds to the cost. Concentrator PV cells have seen a recent resurgence of interest in Australia and Spain.

8.3.7 Multijunction Cell

The single-junction n-on-p silicon cell converts only red and infrared light into electricity, but not blue and ultraviolet. The PV cell converts light into electricity most efficiently when the light's energy matches the semiconductor's energy level, known as its band gap. The layering of multiple semiconductors with a wide range of band gaps converts more energy levels (wavelengths) of light into electricity. The multijunction cell uses multiple layers of semiconductor materials to convert a broader spectrum of sunlight into electricity, thus improving the efficiency. With the gallium indium phosphide/gallium arsenide/germanium (GaInP/GaAs/Ge) triple-junction cell, NREL and Spectrolab have reported a record 34% efficiency under concentrated sunlight. The cell captures infrared photons as well. Efficiencies up to 40% in triple-junction space-qualified cells have been measured by Spectrolab, Inc.

Under NASA and NREL funding, Tecstar (now Emcore) and Spectrolab (now Boeing) developed multijunction solar cells in 2000 for space power systems. The GaInP/GaAs dual-junction solar cell formed the basis of the triple-junction GaInP/GaAs/Ge solar cell, which achieved yet another record efficiency of 34%. This cell was the first triple-junction cell designed for terrestrial applications and the first monolithic solar cell to reach an efficiency of a third of the sun. Currently, the GaInP/GaAs/Ge cell is being widely used in satellite power systems but may soon trickle down to terrestrial applications.

8.4 SOLAR ENERGY MAPS

The solar energy impinging on the surface of the earth is depicted in Figure 8.15, where the white areas get more solar radiation per year. The yearly 24-h average solar flux reaching the horizontal surface of the earth is shown in Figure 8.16, whereas Figure 8.17 depicts that in the month of December. Note that the 24-h average decreases in December. This is due to the shorter days and the presence of clouds, and not due to the low altitude of the sun and cold temperatures. As will be seen later, the PV cell actually converts more solar energy into electricity at a low temperature.

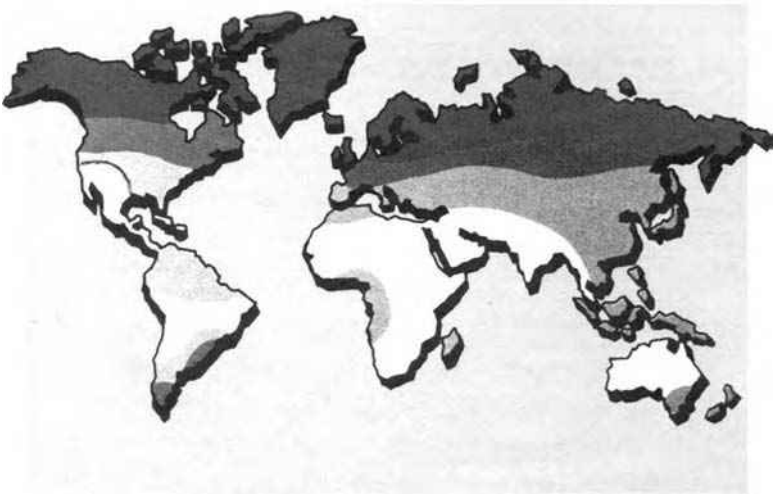

FIGURE 8.15 Solar radiation by regions of the world (higher energy potential in the white areas).

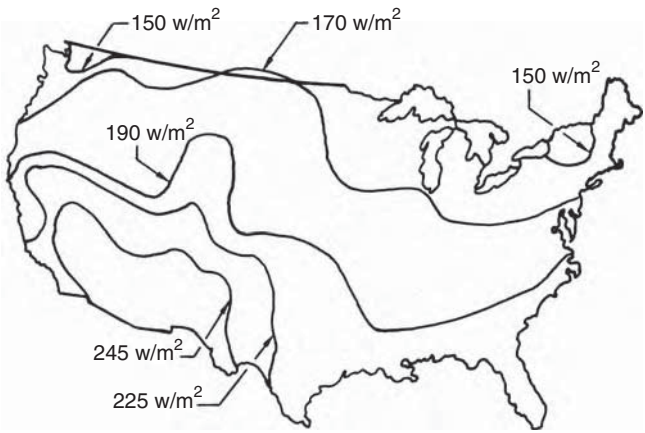

FIGURE 8.16 Yearly 24-h average solar radiation in watts/m^2 reaching the horizontal surface of the earth. (From Profiles in Renewables Energy, DOE/NREL Report No. DE-930000081, August 1994.)

It is the total yearly energy-capture potential of the site that determines the economical viability of installing a power plant. Figure 8.18 is useful in this regard, as it gives the annual average solar energy per day impinging on the surface always facing the sun at 90°. Modules mounted on a sun-tracking structure receive this energy. The electric energy produced per day is obtained by multiplying the map number by the photoconversion efficiency of the modules installed at the site.

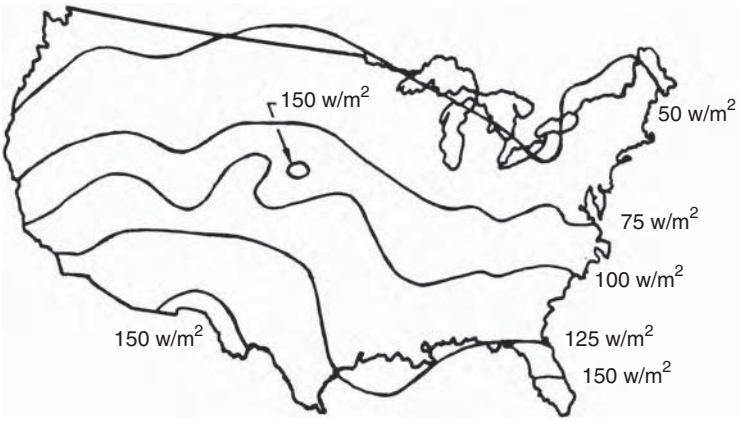

FIGURE 8.17 December 24-h average solar radiation in watts/m^2 reaching the horizontal surface of the earth. (From Profiles in Renewables Energy, DOE/NREL Report No. DE-930000081, August 1994.)

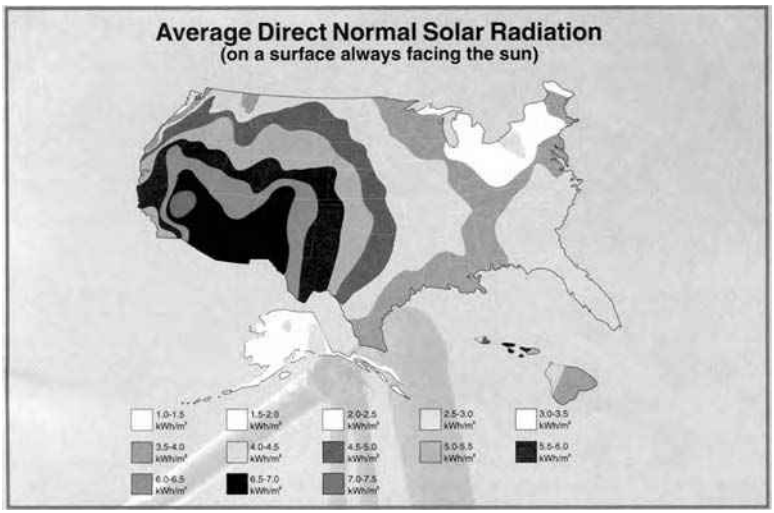

FIGURE 8.18 Yearly 24-h average solar energy in kWh/m^2 reaching the surface always facing the sun at 90°. (From Profiles in Renewables Energy, DOE/NREL Report No. DE-930000081, August 1994.)

8.5 TECHNOLOGY TRENDS

Technology developments continue primarily to increase the conversion efficiency and decrease the modules' cost per watt. The improvements in traditional single-crystal silicon cells have been incremental until now, from 10% in the early 1950s

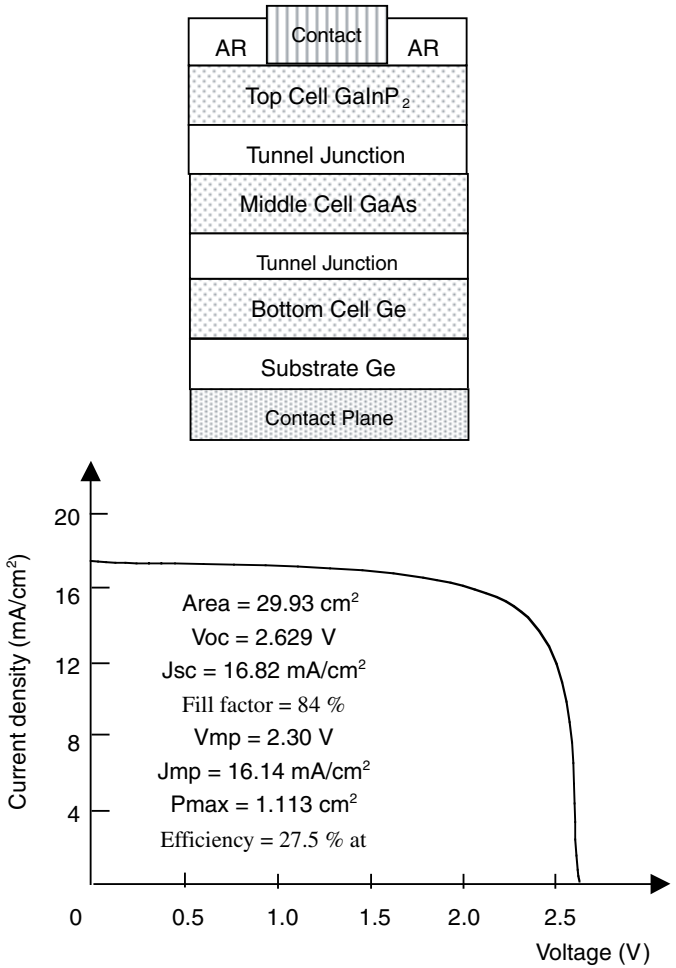

FIGURE 8.19 Triple-junction cell construction and I-V curve.

to 15% in 2005. In 2004, SunPower Corporation produced a high-performance cell with 20% efficiency. This new cell has another advantage, as well. Its positive and negative contacts are at the back of the cell, leaving the front clear of the silver wires and keeping its shadow from falling on the active cell area in the front.

The present energy-intensive manufacturing processes of the PV cell are being replaced by new energy-efficient processes. Newer processes are being developed and continuously implemented to lower the energy use per square centimeter of the finished cell. In the present manufacturing process, the front and the back of the cells are diffused separately, taking 1 to 3 h of manufacturing time. Researchers at the Georgia Institute of Technology are considering rapid-thermal-processing technology. This process simultaneously forms the front and the back of the cell in several minutes, and the metal contacts are applied by screen printing. It not only

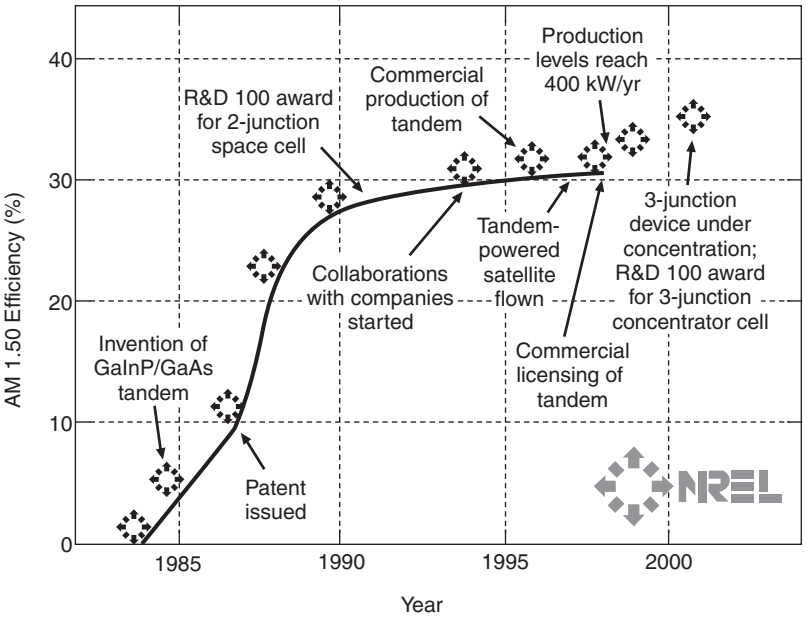

FIGURE 8.20 PV cell efficiency improvement trends.

cuts the processing time but also lowers the temperature and energy needed for fabrication.

The next major efficiency improvement has come from the triple-junction cell shown in Figure 8.19. In the multijunction GaAs cell, one cell consists of two tandem GaAs cells separated by a thin-tunnel junction of GaInP, followed by a third tandem GaInP cell, and separated by an AlInP tunnel junction. Triple-junction cell efficiency has been tested up to 40% in controlled laboratory conditions, and up to 34% in production cells. The present cost of these cells limits its application to spacecraft power systems only, but it would eventually become cost-effective for terrestrial use.

The improvement trends of PV cell efficiency over the last two decades are shown in Figure 8.20. The next generation of multijunction solar cells might have four layers. The most direct path to achieving this is to develop a 1.0-eV band-gap material that is lattice-matched with the GaInP, GaAs, and Ge of the present NREL-designed triple-junction solar cell. The NREL scientists estimate that the multijunction PV cell efficiency has a theoretical limit of 50%, which is like capturing 50% of the incident solar energy.

Reference

1. Carlson, D. E., 1995. Recent Advances in Photovoltaics, Proceedings of the Intersociety Engineering Conference on Energy Conversion, 1995, pp. 621–626.

9 Photovoltaic Power Systems

The photovoltaic (PV) effect is the electrical potential developed between two dissimilar materials when their common junction is illuminated with radiation of photons. The PV cell, thus, converts light directly into electricity. A French physicist, Becquerel, discovered the PV effect in 1839. It was limited to the laboratory until 1954, when Bell Laboratories produced the first silicon cell. It soon found application in U.S. space programs for its high power-generating capacity per unit weight. Since then, it has been extensively used to convert sunlight into electricity for earth-orbiting satellites. Having matured in space applications, PV technology is now spreading into terrestrial applications ranging from powering remote sites to feeding utility grids around the world.

9.1 PV CELL

The physics of the PV cell is very similar to that of the classical diode with a pn junction (Figure 9.1). When the junction absorbs light, the energy of absorbed photons is transferred to the electron–proton system of the material, creating charge carriers that are separated at the junction. The charge carriers may be electron–ion pairs in a liquid electrolyte or electron–hole pairs in a solid semiconducting material. The charge carriers in the junction region create a potential gradient, get accelerated under the electric field, and circulate as current through an external circuit. The square of the current multiplied by the resistance of the circuit is the power converted into electricity. The remaining power of the photon elevates the temperature of the cell and dissipates into the surroundings.

The origin of the PV potential is the difference in the chemical potential, called the *Fermi level*, of the electrons in the two isolated materials. When they are joined, the junction approaches a new thermodynamic equilibrium. Such equilibrium can be achieved only when the Fermi level is equal in the two materials. This occurs by the flow of electrons from one material to the other until a voltage difference is established between them, which has a potential just equal to the initial difference of the Fermi level. This potential drives the photocurrent in the PV circuit.

Figure 9.2 shows the basic cell construction.[1] Metallic contacts are provided on both sides of the junction to collect electrical current induced by the impinging photons. A thin conducting mesh of silver fibers on the top (illuminated) surface collects the current and lets the light through. The spacing of the conducting fibers in the mesh is a matter of compromise between maximizing the electrical conductance and minimizing the blockage of the light. Conducting-foil (solder) contact is provided over the bottom (dark) surface and on one edge of the top surface. In

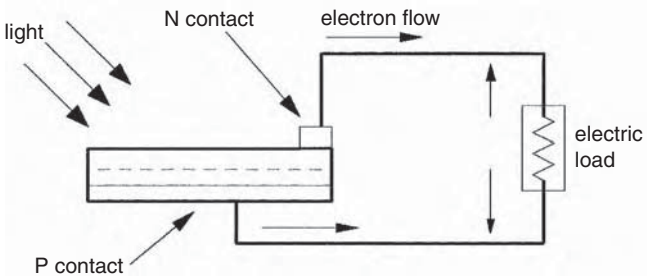

FIGURE 9.1 PV effect converts the photon energy into voltage across the pn junction.

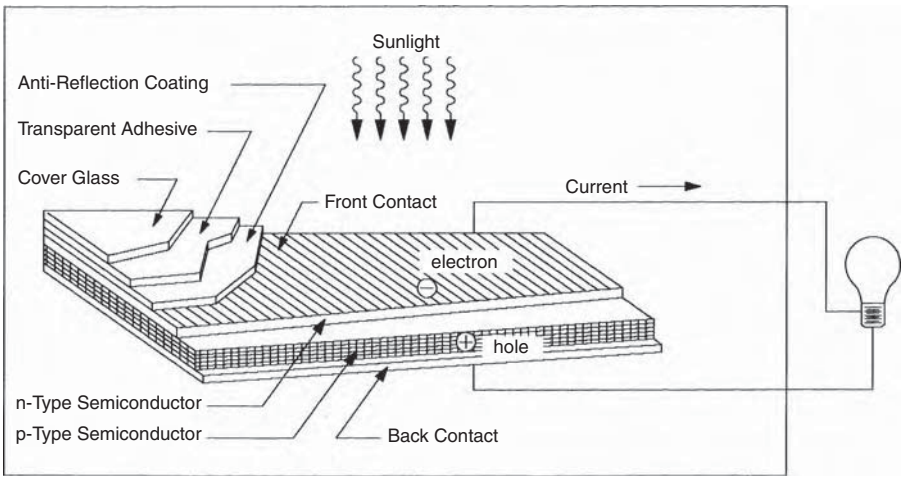

FIGURE 9.2 Basic construction of PV cell with performance-enhancing features (current-collecting silver mesh, antireflective coating, and cover-glass protection).

addition to the basic elements, several enhancement features are also included in the construction. For example, the front face of the cell has an antireflective coating to absorb as much light as possible by minimizing the reflection. The mechanical protection is provided by a cover glass applied with a transparent adhesive.

9.2 MODULE AND ARRAY

The solar cell described in the preceding subsection is the basic building block of the PV power system. Typically, it is a few square inches in size and produces about 1 W of power. To obtain high power, numerous such cells are connected in series and parallel circuits on a panel (module) area of several square feet (Figure 9.3). The solar array or panel is defined as a group of several modules electrically connected in a series–parallel combination to generate the required current and voltage. Figure 9.4 shows the actual construction of a module in a frame that can be mounted on a structure.

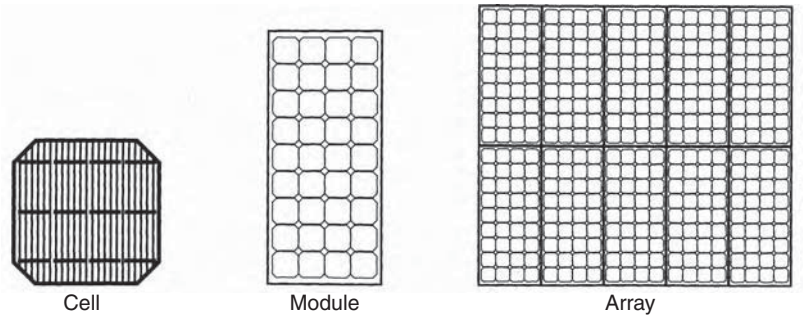

FIGURE 9.3 Several PV cells make a module, and several modules make an array.

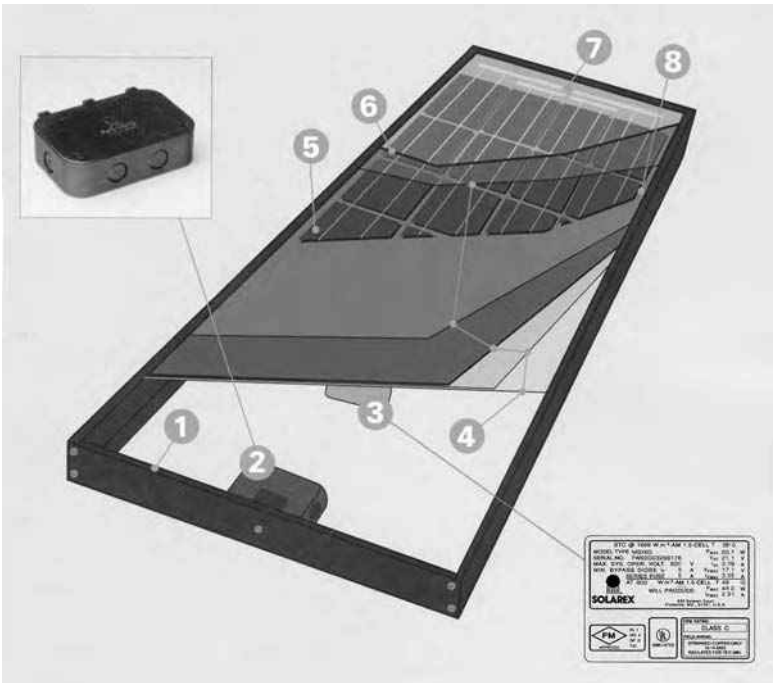

FIGURE 9.4 Construction of PV module: (1) frame, (2) weatherproof junction box, (3) rating plate, (4) weather protection for 30-yr life, (5) PV cell, (6) tempered high-transmittivity cover glass, (7) outside electrical bus, (8) frame clearance. (From Solarex/BP Solar, Frederick, MD. With permission.)

Mounting of the modules can be in various configurations as seen in Figure 9.5. In roof mounting, the modules are in a form that can be laid directly on the roof. In the newly developed amorphous silicon technology, the PV sheets are made in shingles that can replace the traditional roof shingles on a one-to-one basis, providing better economy in regard to building material and labor.

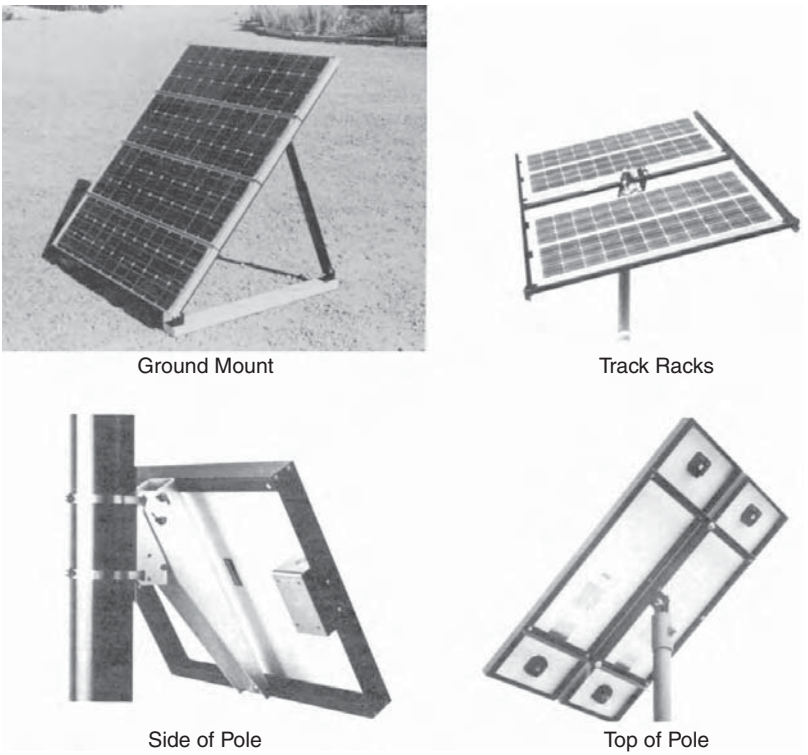

FIGURE 9.5 PV module mounting methods.

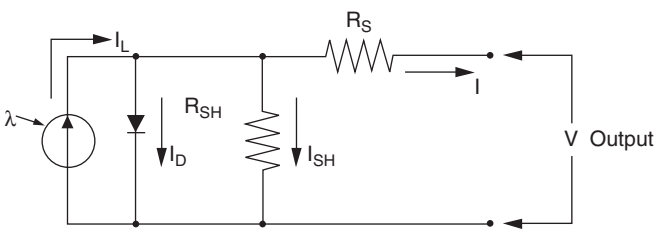

FIGURE 9.6 Equivalent circuit of PV module showing the diode and ground leakage currents.

9.3 EQUIVALENT ELECTRICAL CIRCUIT

The complex physics of the PV cell can be represented by the equivalent electrical circuit shown in Figure 9.6. The circuit parameters are as follows. The current I at the output terminals is equal to the light-generated current I_L, less the diode current I_d and the shunt-leakage current I_{sh}. The series resistance R_s represents the internal resistance to the current flow, and depends on the pn junction depth, impurities, and contact resistance. The shunt resistance R_{sh} is inversely related to the leakage current

to ground. In an ideal PV cell, $R_s = 0$ (no series loss), and $R_{sh} = \infty$ (no leakage to ground). In a typical high-quality 1 in.^{2} silicon cell, R_s varies from 0.05 to 0.10 Ω and R_{sh} from 200 to 300 Ω. The PV conversion efficiency is sensitive to small variations in R_s, but is insensitive to variations in R_{sh}. A small increase in R_s can decrease the PV output significantly.

In the equivalent circuit, the current delivered to the external load equals the current I_L generated by the illumination, less the diode current I_d and the shunt-leakage current I_{sh}. The open-circuit voltage V_{oc} of the cell is obtained when the load current is zero, i.e., when $I = 0$, and is given by the following:

$$V_{oc} = V + IR_{sh} \tag{9.1}$$

The diode current is given by the classical diode current expression:

$$I_d = I_D\left[e^{\frac{QV_{oc}}{AkT}} - 1\right] \tag{9.2}$$

where
I_D = the saturation current of the diode
Q = electron charge = 1.6×10^{-19} C
A = curve-fitting constant
k = Boltzmann constant = 1.38×10^{-23} J/°K
T = temperature on absolute scale °K

The load current is therefore given by the expression:

$$I = I_L - I_D\left[e^{\frac{QV_{oc}}{AkT}} - 1\right] - \frac{V_{oc}}{R_{sh}} \tag{9.3}$$

The last term is the leakage current to the ground. In practical cells, it is negligible compared to I_L and I_D and is generally ignored. The diode-saturation current can therefore be determined experimentally by applying a voltage V_{oc} to the cell in the dark and measuring the current going into the cell. This current is often called the *dark current* or the *reverse diode-saturation current*.

9.4 OPEN-CIRCUIT VOLTAGE AND SHORT-CIRCUIT CURRENT

The two most important parameters widely used for describing cell electrical performance are the open-circuit voltage V_{oc} and the short-circuit current I_{sc} under full illumination. The short-circuit current is measured by shorting the output terminals and measuring the terminal current. Ignoring the small diode and ground leakage currents under zero terminal voltage, the short-circuit current under this condition is the photocurrent I_L.

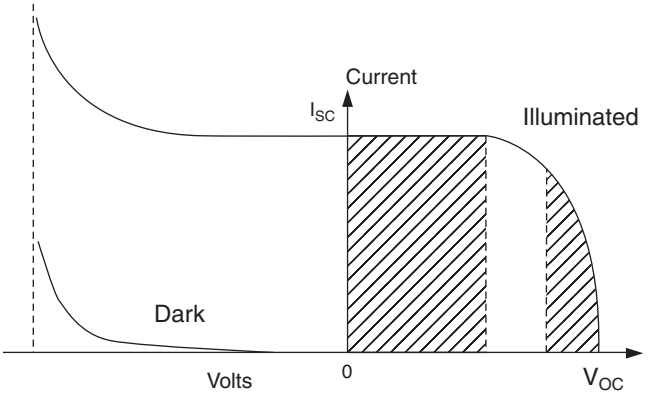

FIGURE 9.7 Current vs. voltage (I-V) characteristic of the PV module in sunlight and in the dark.

The maximum photovoltage is produced under the open-circuit voltage. Again, by ignoring the ground leakage current, Equation 9.3 with $I = 0$ gives the open-circuit voltage as follows:

$$V_{oc} = \frac{AkT}{Q} \text{Log}_n \left(\frac{I_L}{I_D} + 1 \right) \tag{9.4}$$

The term kT/Q is expressed in voltage (0.026 V at 300°K). In practical photocells, the photocurrent is several orders of magnitude greater than the reverse saturation current. Therefore, the open-circuit voltage is many times the kT/Q value. Under conditions of constant illumination, I_L/I_D is a sufficiently strong function of the cell temperature, and the solar cell ordinarily shows a negative temperature coefficient of the open-circuit voltage.

9.5 I-V AND P-V CURVES

The electrical characteristic of the PV cell is generally represented by the current vs. voltage (I-V) curve. Figure 9.7 shows the I-V characteristic of a PV module under two conditions, in sunlight and in the dark. In the first quadrant, the top left of the I-V curve at zero voltage is called the short-circuit current. This is the current we would measure with output terminals shorted (zero voltage). The bottom right of the curve at zero current is called the *open-circuit voltage*. This is the voltage we would measure with output terminals open (zero current). In the left-shaded region, the cell works as a constant current source, generating a voltage to match with the load resistance. In the shaded region on the right, the current drops rapidly with a small rise in the voltage. In this region, the cell works like a constant voltage source with an internal resistance. Somewhere in the middle of the two shaded regions, the curve has a knee point.

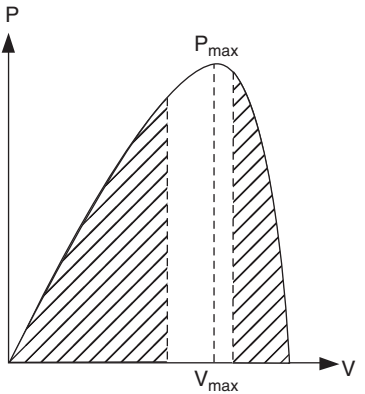

FIGURE 9.8 Power vs. voltage (P-V) characteristic of the PV module in sunlight.

If a voltage is externally applied in the reverse direction, for instance, during a system fault transient, the cell current remains flat, and the power is absorbed by the cell with a negative voltage and positive current. However, beyond a certain negative voltage, the junction breaks down as in a diode, and the current rises to a high value. In the dark, the current is zero for any voltage up to the breakdown voltage, which is the same as in the illuminated condition.

The power output of the panel is the product of the voltage and current outputs. In Figure 9.8, the power is plotted against the voltage. Note that the cell produces no power at zero voltage or zero current, and produces the maximum power at the voltage corresponding to the knee point of the I-V curve. This is why the PV power circuit is always designed to operate close to the knee point with a slight slant on the left-hand side. The PV circuit is modeled approximately as a constant current source in the electrical analysis of the system.

Figure 9.9 is the I-V characteristic of a 22-W panel at two solar illumination intensities, 1000 W/m^2 and 500 W/m^2. These curves are at AM1.5 (air mass 1.5). The AM0 (air mass zero) represents the outer-space conditions (vacuum), in which the solar radiation is 1350 W/m^2. AM1 represents conditions normal to the sun in a clear unpolluted atmosphere of the earth on a dry noon. Thus, AM1 represents ideal conditions in pure air when sunlight experiences the least resistance to reach the earth. AM1.5 represents average quality air with average humidity and pollution at an average inclination. AM1.5 is, therefore, taken as a reference value for terrestrial PV designs. In northern altitudes with the sun at 15° from the horizon, the AM index can be as high as 4 when sunlight has a high resistance to cut through before reaching the earth surface.

Solar power impinging on a normal surface on a bright day with AM1.5 is about 1000 W/m^2, and it would be low on a cloudy day. The 500 W/m^2 solar intensity is another reference condition the industry uses to report I-V curves.

The photoconversion efficiency of the PV cell is defined by the following ratio:

$$\eta = \frac{\text{electrical power output}}{\text{solar power impinging the cell}} \tag{9.5}$$

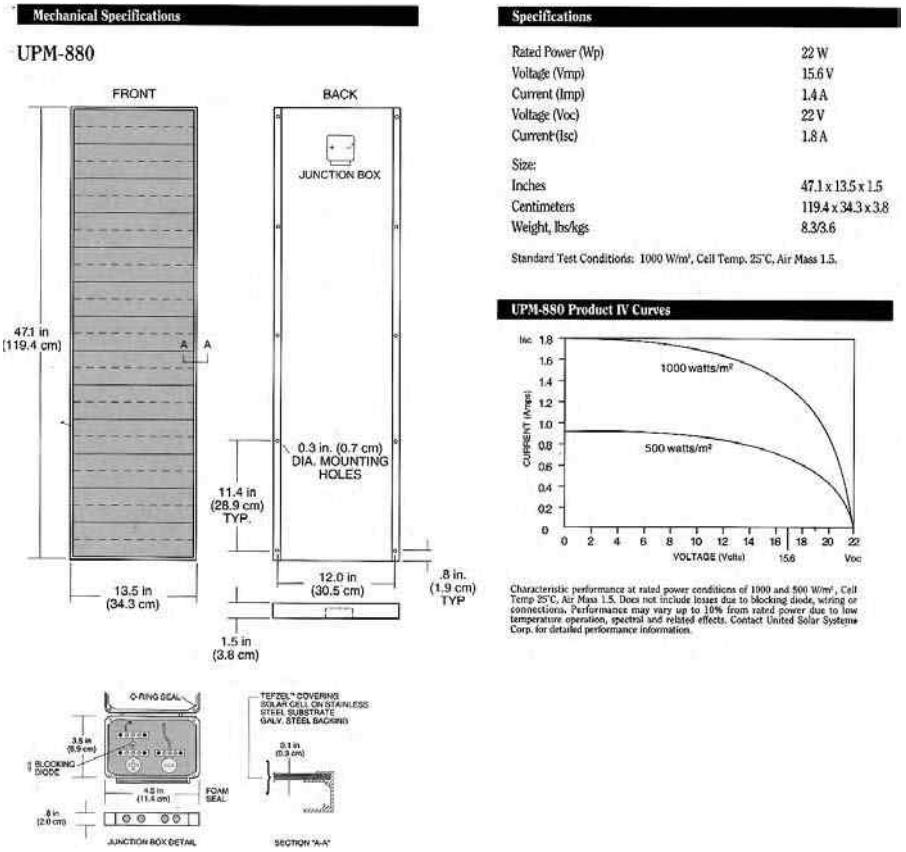

FIGURE 9.9 I-V characteristic of a 22-W PV module at full and half sun intensities. (From United Solar Systems, San Diego, CA. With permission.)

Obviously, the higher the efficiency, the higher the output power we get under a given illumination.

9.6 ARRAY DESIGN

The major factors influencing the electrical design of the solar array are as follows:

- The sun intensity
- The sun angle
- The load matching for maximum power
- The operating temperature

These factors are discussed in the following subsections.

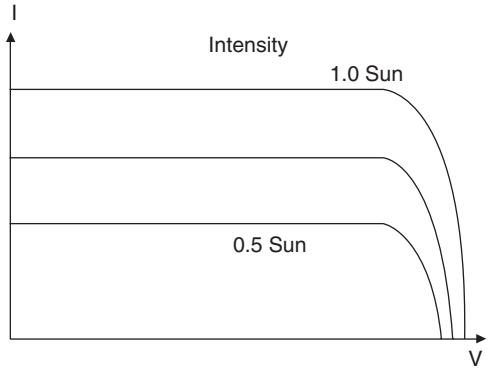

FIGURE 9.10 I-V characteristic of PV module shifts down at lower sun intensity, with small reduction in voltage.

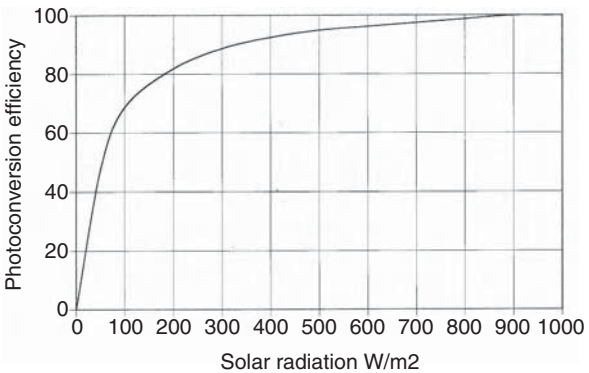

FIGURE 9.11 Photoconversion efficiency vs. solar radiation (practically constant over a wide range of radiation).

9.6.1 Sun Intensity

The magnitude of the photocurrent is maximum under a full bright sun (1.0 sun). On a partially sunny day, the photocurrent diminishes in direct proportion to the sun intensity. At a lower sun intensity, the I-V characteristic shifts downward as shown in Figure 9.10. On a cloudy day, therefore, the short-circuit current decreases significantly. The reduction in the open-circuit voltage, however, is small.

The photoconversion efficiency of the cell is insensitive to the solar radiation in the practical working range. For example, Figure 9.11 shows that the efficiency is practically the same at 500 W/m^2 and at 1000 W/m^2. This means that the conversion efficiency is the same on a bright sunny day as on a cloudy day. We get a lower power output on a cloudy day only because of the lower solar energy impinging on the cell.

TABLE 9.1
Kelly Cosine Values of the Photocurrent in Silicon Cells

Sun Angle Degrees	Mathematical Cosine Value	Kelly Cosine Value
30	0.866	0.866
50	0.643	0.635
60	0.500	0.450
80	0.174	0.100
85	0.087	0

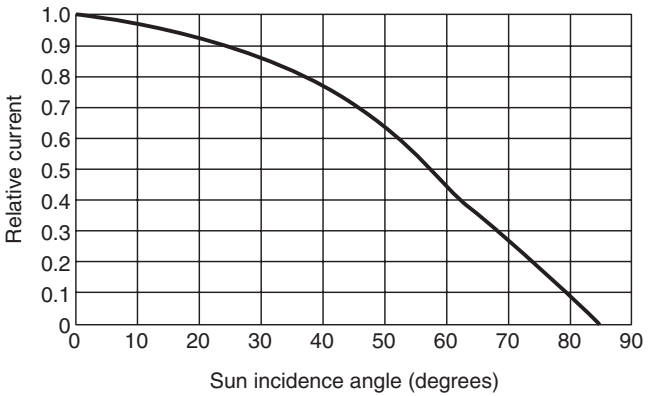

FIGURE 9.12 Kelly cosine curve for PV cell at sun angles form 0 to 90°.

9.6.2 Sun Angle

The cell output current is given by $I = I_o\cos\theta$, where I_o is the current with normal sun (reference), and θ is the angle of the sun line measured from the normal. This cosine law holds well for sun angles ranging from 0 to about 50°. Beyond 50°, the electrical output deviates significantly from the cosine law, and the cell generates no power beyond 85°, although the mathematical cosine law predicts 7.5% power generation (Table 9.1). The actual power-angle curve of the PV cell, called the *Kelly cosine*, is shown in Figure 9.12.

9.6.3 Shadow Effect

The array may consist of many parallel strings of series-connected cells. Two such strings are shown in Figure 9.13. A large array may get partially shadowed due to a structure interfering with the sun line. If a cell in a long series string gets completely shadowed, it loses the photovoltage but still must carry the string current by virtue of its being in series with all other cells operating in full sunlight. Without internally generated voltage, the shadowed cell cannot produce power. Instead, it acts as a load, producing local I^2R loss and heat. The remaining cells in the string must work

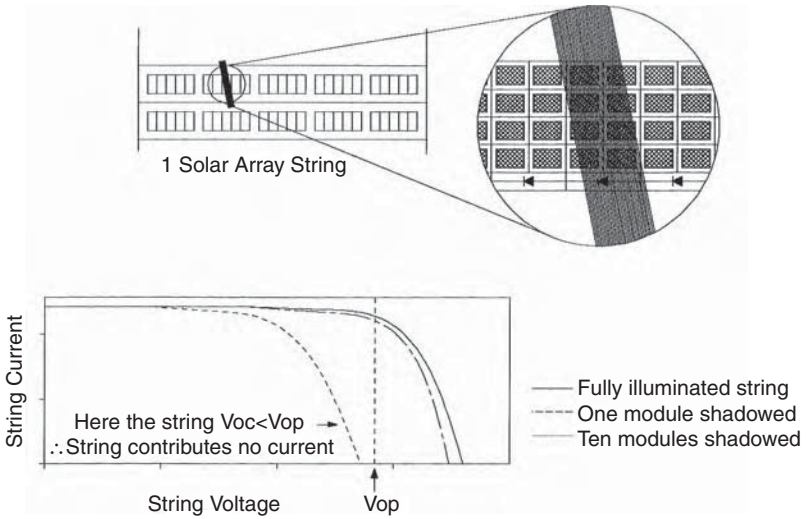

FIGURE 9.13 Shadow effect on one long series string of an array (power degradation is small until shadow exceeds the critical limit).

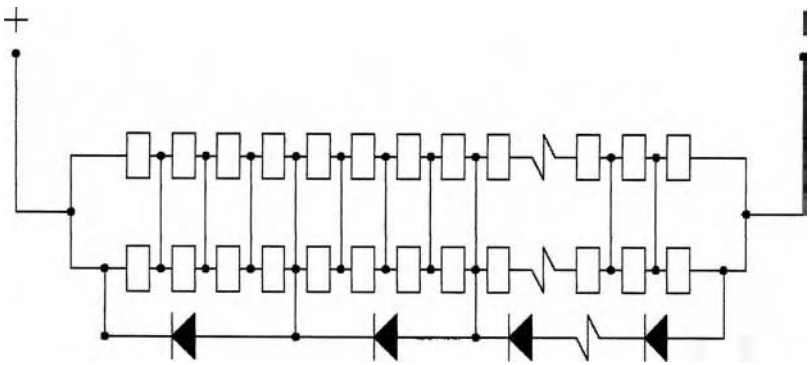

FIGURE 9.14 Bypass diode in PV string minimizes power loss under heavy shadow.

at higher voltage to make up the loss of the shadowed cell voltage. A higher voltage in healthy cells means a lower string current as per the I-V characteristic of the string. This is shown in the bottom left of Figure 9.13. The current loss is not proportional to the shadowed area, and may go unnoticed for a mild shadow on a small area. However, if more cells are shadowed beyond the critical limit, the I-V curve goes below the operating voltage of the string, making the string current fall to zero, losing all the power of the string. This causes loss of one whole string from the array.

The commonly used method to eliminate loss of string power due to a possible shadow is to subdivide the circuit length in several segments with bypass diodes (Figure 9.14). The diode across the shadowed segment bypasses only that segment

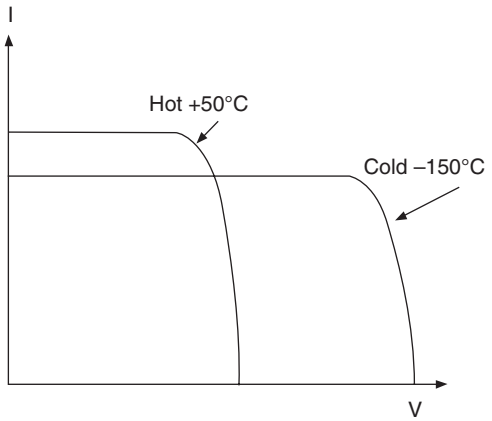

FIGURE 9.15 Effect of temperature on I-V characteristic (cell produces less current but greater voltage, with net gain in the power output at cold temperatures).

of the string. This causes a proportionate loss of the string voltage and current, without losing the whole-string power. Some modern PV modules come with such internally embedded bypass diodes.

9.6.4 Temperature Effects

With increasing temperature, the short-circuit current of the cell increases, whereas the open-circuit voltage decreases (Figure 9.15). The effect of temperature on PV power is quantitatively evaluated by examining the effects on the current and the voltage separately. Suppose I_o and V_o are the short-circuit current and the open-circuit voltage at the reference temperature T, and α and β are their respective temperature coefficients. If the operating temperature is increased by ΔT, then the new current and voltage are given by the following:

$$I_{sc} = I_o(1 + \alpha \cdot \Delta T) \text{ and } V_{oc} = V_o(1 - \beta \cdot \Delta T) \tag{9.6}$$

Because the operating current and the voltage change approximately in the same proportion as the short-circuit current and open-circuit voltage, respectively, the new power is as follows:

$$P = VI = I_o(1 + \alpha \cdot \Delta T)V_o(1 - \beta \cdot \Delta T) \tag{9.7}$$

This can be simplified in the following expression by ignoring a small term:

$$P = P_o[1 + (\alpha - \beta)\ \Delta T] \tag{9.8}$$

For a typical single-crystal silicon cell, α is about 20 μu/°C and β is about 5 mu/°C, where u stands for unit. The power is, therefore, given by the following:

$$P = P_o[1 + (20 \times 10^{-6} - 5 \times 10^{-3})\ \Delta T] \text{ or } P = P_o[1 - 0.005 \cdot \Delta T] \tag{9.9}$$

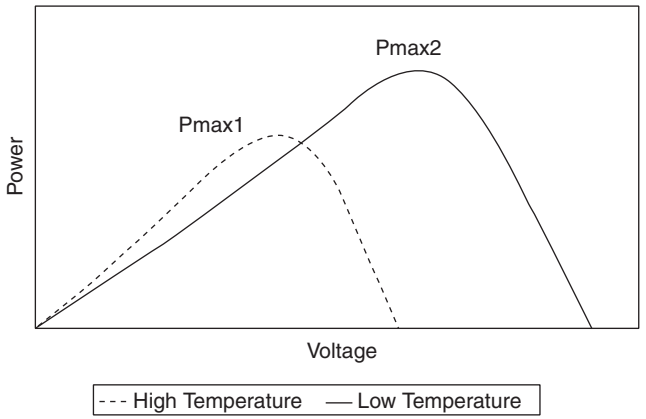

FIGURE 9.16 Effect of temperature on P-V characteristic (cell produces more power at cold temperatures).

This expression indicates that for every degree centigrade rise in the operating temperature above the reference temperature, the silicon cell power output decreases by about 0.5%. Because the increase in current is much less than the decrease in voltage, the net effect is a decrease in power at a higher operating temperature.

The effect of temperature on the power output is shown in the power vs. voltage characteristics at two operating temperatures in Figure 9.16. The figure shows that the maximum power available at a lower temperature is higher than that at a higher temperature. Thus, a cold day is actually better for the PV cell, as it generates more power. However, the two P_{max} points are not at the same voltage. In order to extract maximum power at all temperatures, the PV system must be designed such that the module output voltage can increase to V_2 for capturing P_{max2} at a lower temperature and can decrease to V_1 for capturing P_{max1} at a higher temperature. This adds to the system-design complexity.

9.6.5 Effect of Climate

On a partly cloudy day, the PV module can produce up to 80% of its full sun power. It can produce about 30% power even with heavy clouds on an extremely overcast day. Snow does not usually collect on the module, because it is angled to catch the sun. If snow does collect, it quickly melts. Mechanically, the module is designed to withstand golf-ball-size hail.

9.6.6 Electrical Load Matching

The operating point of any power system is the intersection of the source line and the load line. If the PV source having the I-V and P-V characteristics shown in Figure 9.17(a) is supplying power to a resistive load R_1, it will operate at point A_1. If the load resistance increases to R_2 or R_3, the operating point moves to A_2 or A_3, respectively. The maximum power is extracted from the module when the load resistance is R_2 (Figure 9.17b). Such a load that matches with the source is always necessary for the maximum power extraction from a PV source.

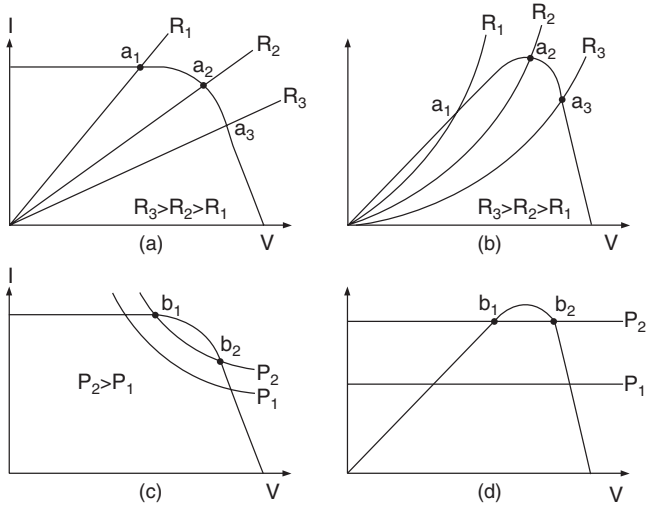

FIGURE 9.17 Operating stability and electrical load matching with constant-resistive load and constant-power load.

The operation with a constant-power load is shown in Figure 9.17(c) and Figure 9.17(d). The constant-power load line has two points of intersection with the source line, denoted by B_1 and B_2. Only the point B_2 is stable, as any perturbation from it generates a restoring power to take the operation back to B_2, and the system continues to operate at B_2 with an inherent stability.

Therefore, the necessary condition for the electrical operating stability of the solar array is as follows:

$$\left[\frac{dP}{dV}\right]_{load} > \left[\frac{dP}{dV}\right]_{source} \tag{9.10}$$

Some loads such as heaters have constant resistances, which absorb power that varies with the square of the voltage. Other loads such as induction motors behave more like constant-power loads. They draw more current at lower voltage and *vice versa*. In most large systems with mixed loads, the power varies approximately in a linear proportion with voltage.

9.6.7 Sun Tracking

More energy is collected by the end of the day if the PV module is installed on a tracker with an actuator that follows the sun. There are two types of sun trackers:

- One-axis tracker, which follows the sun from east to west during the day.
- Two-axis tracker, which follows the sun from east to west during the day, and from north to south during the seasons of the year (Figure 9.18).

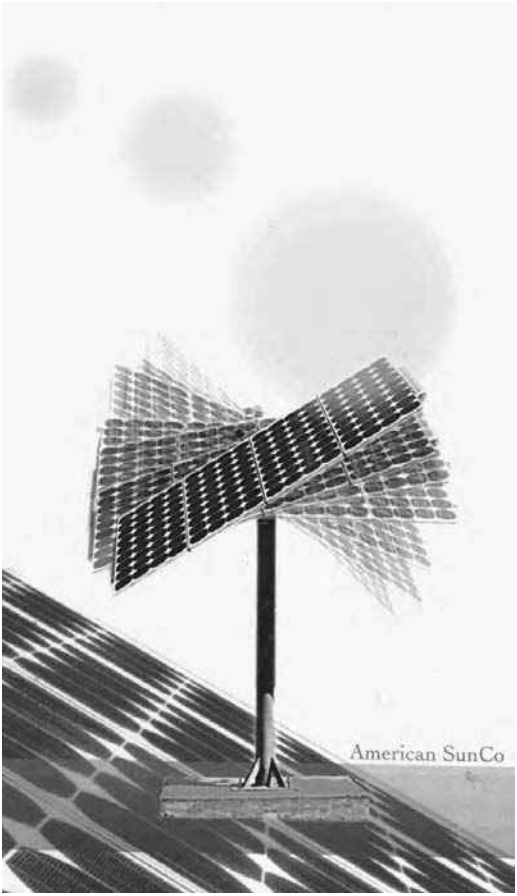

FIGURE 9.18 Dual-axis sun tracker follows the sun throughout the year. (From American Sun Company, Blue Hill, Maine. With permission.)

A sun-tracking design can increase the energy yield up to 40% over the year compared to the fixed-array design. Dual-axis tracking is done by two linear actuator motors, which follow the sun within one degree of accuracy (Figure 9.19). During the day, it tracks the sun east to west. At night it turns east to position itself for the next morning's sun. Old trackers did this after sunset using a small nickel-cadmium battery. The new design eliminates the battery requirement by doing the turning in the weak light of the dusk and/or dawn. The Kelly cosine presented in Table 9.1 is useful in assessing accurately the power available in sunlight incident at extreme angles in the morning or evening.

When a dark cloud obscures the sun, the tracker may aim at the next brightest object, which is generally the edge of a cloud. When the cloud is gone, the tracker aims at the sun once again, and so on and so forth. Such sun hunting is eliminated in newer sun trackers.

FIGURE 9.19 Actual motor of the sun tracker. (From American Sun Company, Blue Hill, Maine. With permission.)

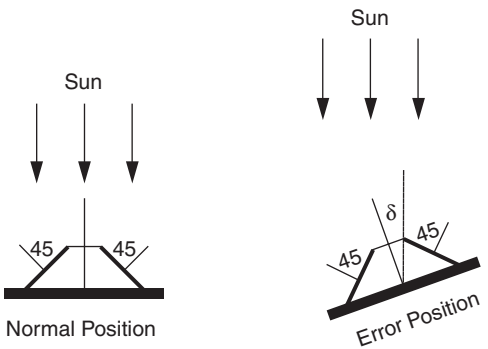

FIGURE 9.20 Sun-tracking actuator principle. (Two differentially connected sensors at 45° generate signals proportional to the pointing error.)

One method of designing the sun tracker is to use two PV cells mounted on two 45° wedges (Figure 9.20), and connecting them differentially in series through an actuator motor. When the sun is normal, the currents on both cells are equal to $I_o\cos 45°$. As they are connected in series opposition, the net current in the motor is zero, and the array stays put. On the other hand, if the array is not normal to the sun, the sun angles on the two cells are different, giving two different currents as follows:

$$I_1 = I_o\cos(45 + \delta) \text{ and } I_2 = I_o\cos(45 - \delta) \tag{9.11}$$

The motor current is therefore:

$$I_m = I_1 - I_2 = I_o\cos(45 + \delta) - I_o\cos(45 - \delta) \tag{9.12}$$

Using Taylor series expansion:

$$f(x+h) = f(x) + hf'(x) + \frac{h^2}{2!}f''(x) + \cdots$$

we can express the two currents as follows:

$$I_1 = I_o\cos 45 - I_o\delta \sin 45 \text{ and } I_2 = I_o\cos 45 + I_o\delta \sin 45 \tag{9.13}$$

The motor current is then

$$I_m = I_1 - I_2 = 2I_o\delta \sin 45° = \sqrt{2}I_o\delta \text{ if } \delta \text{ is in radians} \tag{9.14}$$

A small pole-mounted panel can use one single-axis or dual-axis sun tracker. A large array, on the other hand, is divided into small modules, each mounted on its own sun tracker. This simplifies the structure and eliminates the problems related to a large movement in a large panel.

9.7 PEAK-POWER OPERATION

The sun tracker drives the module mechanically to face the sun to collect the maximum solar radiation. However, that in itself does not guarantee the maximum power output from the module. As was seen in Figure 9.16, the module must operate electrically at a certain voltage that corresponds to the peak power point under a given operating condition. First we examine the electrical principle of peak-power operation.

If the array is operating at any point at voltage V and current I on the I-V curve, the power generation is $P = VI$ watts. If the operation moves away from the preceding point such that the current is now $I + \Delta I$, and the voltage is $V + \Delta V$, then the new power is as follows:

$$P + \Delta P = (V + \Delta V)(I + \Delta I) \tag{9.15}$$

which, after ignoring a small term, simplifies to the following:

$$\Delta P = \Delta V \cdot I + \Delta I \cdot V \tag{9.16}$$

ΔP would be zero if the array were operating at the peak power point, which necessarily lies on a locally flat neighborhood. Therefore, at the peak power point, the preceding expression in the limit becomes:

$$\frac{dV}{dI} = -\frac{V}{I} \tag{9.17}$$

We note here that dV/dI is the dynamic impedance of the source, and V/I the static impedance. Thus, at the peak power point, the following relation holds:

$$\text{Dynamic impedance } Z_d = -\text{static impedance } Z_s \tag{9.18}$$

There are three electrical methods of extracting the peak power from a PV source, as described in the following text:

1. In the first method, a small signal current is periodically injected into the array bus, and the dynamic bus impedance ($Z_d = dV/dI$) and the static bus impedance ($Z_s = V/I$) are measured. The operating voltage is then increased or decreased until Z_d equals $-Z_s$. At this point, the maximum power is extracted from the source.
2. In another method, the operating voltage is increased as long as dP/dV is positive. That is, the voltage is increased as long as we get more power. If dP/dV is sensed negative, the operating voltage is decreased. The voltage stays the same if dP/dV is near zero within a preset deadband.
3. The third method makes use of the fact that for most PV cells, the ratio of the voltage at the maximum power point to the open-circuit voltage (i.e., V_{mp}/V_{oc}) is approximately constant, say K. For example, for high-quality crystalline silicon cells, K = 0.72. An unloaded cell is installed on the array and kept in the same environment as the power-producing cells, and its open-circuit voltage is continuously measured. The operating voltage of the power-producing array is then set at $K \cdot V_{oc}$, which will produce the maximum power.

9.8 SYSTEM COMPONENTS

The array by itself does not constitute the PV power system. We may also need a structure to mount it, a sun tracker to point the array to the sun, various sensors to monitor system performance, and power electronic components that accept the DC power produced by the array, charge the battery, and condition the remaining power in a form that is usable by the load. If the load is AC, the system needs an inverter to convert the DC power into AC at 50 or 60 Hz.

Figure 9.21 shows the necessary components of a stand-alone PV power system. The peak-power tracker senses the voltage and current outputs of the array and continuously adjusts the operating point to extract the maximum power under varying climatic conditions. The output of the array goes to the inverter, which converts the DC into AC. The array output in excess of the load requirement is used to charge the battery. The battery charger is usually a DC–DC buck converter. If excess power is still available after fully charging the battery, it is shunted in dump heaters, which may be a room or water heater in a stand-alone system. When the sun is not available, the battery discharges to the inverter to power the load. The battery discharge diode Db is to prevent the battery from being charged when the charger is opened after a full charge or for other reasons. The array diode Da is to isolate the array from the

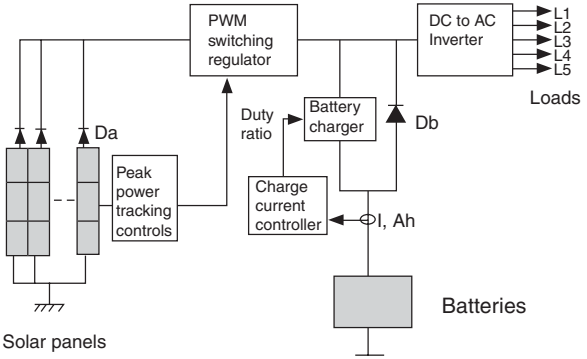

FIGURE 9.21 Peak-power-tracking PV power system showing major components.

battery, thus keeping the array from acting as the load on the battery at night. The mode controller collects system signals, such as the array and the battery currents and voltages, and keeps track of the battery state of charge by bookkeeping the charge/discharge ampere-hours. It uses this information to turn on or off the battery charger, discharge converter, and dump loads as needed. Thus, the mode controller is the central controller of the entire system.

In the grid-connected system, dump heaters are not required, as all excess power is always fed to the grid lines. The battery is also eliminated, except for a few small critical loads, such as the start-up controller and the computer. DC power is first converted into AC by the inverter, ripples are filtered, and only then is the filtered power fed into the grid lines.

In the PV system, the inverter is a critical component, which converts the array DC power into AC for supplying the loads or interfacing with the grid. A new product line recently introduced into the market is the AC PV module, which integrates an inverter directly into module design. It is presently available in a few hundred watts capacity. It provides utility-grade 60-Hz power directly from the module junction box. This greatly simplifies PV system design.

Reference

1. Cook, G., Billman, L., and Adcock R., Photovoltaic Fundamentals, DOE/Solar Energy Research Institute Report No. DE91015001, February 1995.

Part C

System Integration

10 Energy Storage

Electricity is more versatile in use than other types of power, because it is a highly ordered form of energy that can be converted efficiently into other forms. For example, it can be converted into mechanical form with efficiency near 100% or into heat with 100% efficiency. Heat energy, on the other hand, cannot be converted into electricity with such high efficiency, because it is a disordered form of energy in atoms. For this reason, the overall thermal-to-electrical conversion efficiency of a typical fossil thermal power plant is less than 50%.

A disadvantage of electricity is that it cannot be easily stored on a large scale. Almost all electric energy used today is consumed as it is generated. This poses no hardship in conventional power plants, in which fuel consumption is continuously varied with the load requirement. Wind and photovoltaics (PVs), both being intermittent sources of power, cannot meet the load demand at all times, 24 h a day, 365 d a year. Energy storage, therefore, is a desired feature to incorporate with such power systems, particularly in stand-alone plants. It can significantly improve the load availability, a key requirement for any power system.

The present and future energy storage technologies that may be considered for stand-alone wind or PV power systems fall into the following broad categories:

- Electrochemical battery
- Flywheel
- Compressed air
- Superconducting coil

10.1 BATTERY

The battery stores energy in an electrochemical form and is the most widely used device for energy storage in a variety of applications. The electrochemical energy is in a semiordered form, which is in between the electrical and thermal forms. It has a one-way conversion efficiency of 85 to 90%.

There are two basic types of electrochemical batteries:

The *primary battery*, which converts chemical energy into electric energy. The electrochemical reaction in a primary battery is nonreversible, and the battery is discarded after a full discharge. For this reason, it finds applications where a high energy density for one-time use is required.

The *secondary battery*, which is also known as the *rechargeable battery*. The electrochemical reaction in the secondary battery is reversible. After a discharge, it can be recharged by injecting a direct current from an external source. This type of battery converts chemical energy into electric energy

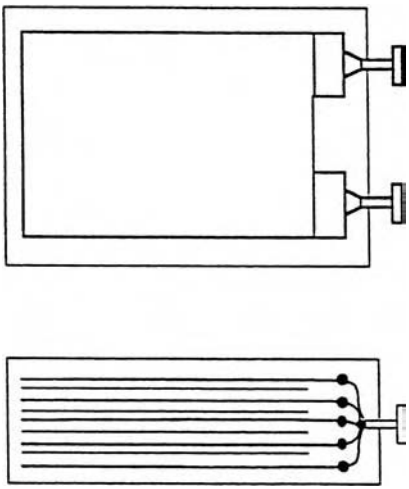

FIGURE 10.1 Electrochemical energy storage cell construction.

in the discharge mode. In the charge mode, it converts the electric energy into chemical energy. In both modes, a small fraction of energy is converted into heat, which is dissipated to the surrounding medium. The round-trip conversion efficiency is between 70 and 80%.

The internal construction of a typical electrochemical cell is shown in Figure 10.1. It has positive and negative electrode plates with insulating separators and a chemical electrolyte in between. The two groups of electrode plates are connected to two external terminals mounted on the casing. The cell stores electrochemical energy at a low electrical potential, typically a few volts. The cell capacity, denoted by C, is measured in ampere-hours (Ah), meaning it can deliver C A for one hour or C/n A for n hours.

The battery is made of numerous electrochemical cells connected in a series–parallel combination to obtain the desired battery voltage and current. The higher the battery voltage, the higher the number of cells required in series. The battery rating is stated in terms of the average voltage during discharge and the ampere-hour capacity it can deliver before the voltage drops below the specified limit. The product of the voltage and ampere-hour forms the watthour (Wh) energy rating the battery can deliver to a load from the fully charged condition. The battery charge and discharge rates are stated in units of its capacity in Ah. For example, charging a 100-Ah battery at $C/10$ rate means charging at 100/10 = 10 A. Discharging that battery at $C/2$ rate means drawing 100/2 = 50 A, at which rate the battery will be fully discharged in 2 h. The state of charge (SOC) of the battery at any time is defined as the following:

$$SOC = \frac{\text{Ah capacity remaning in the battery}}{\text{Rated Ah capacity}}$$

TABLE 10.1
Average Cell Voltage during Discharge in Various Rechargeable Batteries

Electrochemistry	Cell Volts	Remark
Lead-acid	2.0	Least-cost technology
Nickel-cadmium	1.2	Exhibits memory effect
Nickel-metal hydride	1.2	Temperature sensitive
Lithium-ion	3.6	Safe, contains no metallic lithium
Lithium-polymer	3.0	Contains metallic lithium
Zinc-air	1.2	Requires good air management to limit self-discharge rate

10.2 TYPES OF BATTERY

There are at least six major rechargeable electrochemistries available today. They are as follows:

- Lead-acid (Pb-acid)
- Nickel-cadmium (NiCd)
- Nickel-metal hydride (NiMH)
- Lithium-ion (Li-ion)
- Lithium-polymer (Li-poly)
- Zinc-air

New electrochemistries are being developed by the United States Advanced Battery Consortium for a variety of applications, such as electric vehicles, spacecraft, utility load leveling and, of course, for renewable power systems.[1]

The average voltage during discharge depends on the electrochemistry, as shown in Table 10.1. The energy densities of various batteries, as measured by the Wh capacity per unit mass and unit volume, are compared in Figure 10.2. The selection of the electrochemistry for a given application is a matter of performance and cost optimization.

Some construction and operating features of these electrochemistries are presented in the following sections.

10.2.1 LEAD-ACID

This is the most common type of rechargeable battery used today because of its maturity and high performance-over-cost ratio, even though it has the least energy density by weight and volume. In a Pb-acid battery under discharge, water and lead sulfate are formed, the water dilutes the sulfuric acid electrolyte, and the specific gravity of the electrolyte decreases with the decreasing *SOC*. Recharging reverses the reaction, in which the lead and lead dioxide are formed at the negative and positive plates, respectively, restoring the battery into its originally charged state.

The Pb-acid battery comes in various versions. The shallow-cycle version is used in automobiles, in which a short burst of energy is drawn from the battery to

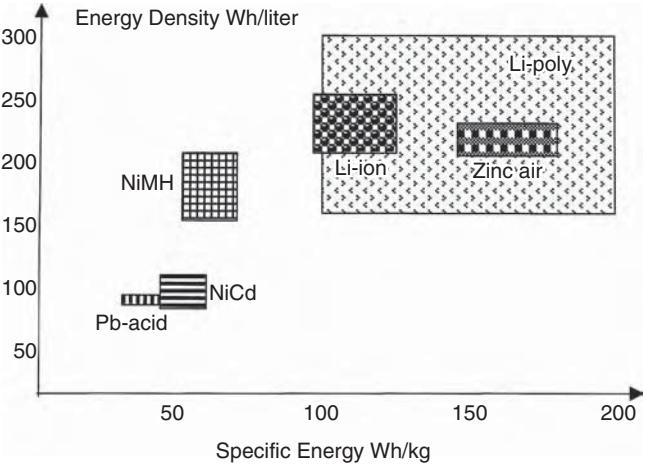

FIGURE 10.2 Specific energy and energy density of various electrochemistries.

start the engine. The deep-cycle version, on the other hand, is suitable for repeated full charge and discharge cycles. Most energy storage applications require deep-cycle batteries. The Pb-acid battery is also available in a sealed "gel-cell" version with additives, which turns the electrolyte into nonspillable gel. The gel-cell battery, therefore, can be mounted sideways or upside down. The high cost, however, limits its use in military avionics.

10.2.2 Nickel-Cadmium

The NiCd is a matured electrochemistry, in which the positive electrode is made of cadmium and the negative electrode of nickel hydroxide. The two electrodes are separated by Nylon™ separators and placed in potassium hydroxide electrolyte in a stainless steel casing. With a sealed cell and half the weight of the conventional Pb-acid, the NiCd battery has been used to power most rechargeable consumer applications. It has a longer deep-cycle life and is more temperature tolerant than the Pb-acid battery. However, this electrochemistry has a memory effect (explained later), which degrades the capacity if not used for a long time. Moreover, cadmium has recently come under environmental regulatory scrutiny. For these reasons, NiCd is being replaced by NiMH and Li-ion batteries in laptop computers and other similar high-priced consumer electronics.

10.2.3 Nickel-Metal Hydride

NiMH is an extension of the NiCd technology and offers an improvement in energy density over that in NiCd. The major construction difference is that the anode is made of a metal hydride. This eliminates the environmental concerns of cadmium. Another performance improvement is that it has a negligible memory effect. NiMH, however, is less capable of delivering high peak power, has a high self-discharge rate, and is susceptible to damage due to overcharging. Compared to NiCd, NiMH

is expensive at present, although the price is expected to drop significantly in the future. This expectation is based on current development programs targeted for large-scale application of this technology in electric vehicles.

10.2.4 Lithium-Ion

The Li-ion technology is a new development, which offers three times the energy density over that of Pb-acid. Such a large improvement in energy density comes from lithium's low atomic weight of 6.9 vs. 207 for lead. Moreover, Li-ion has a higher cell voltage, 3.5 V vs. 2.0 V for Pb-acid and 1.2 V for other electrochemistries. This requires fewer cells in series for a given battery voltage, thus reducing the manufacturing cost.

On the negative side, the lithium electrode reacts with any liquid electrolyte, creating a sort of passivation film. Every time the cell is discharged and then charged, the lithium is stripped away, a free metal surface is exposed to the electrolyte, and a new film is formed. This is compensated for by using thick electrodes or else the battery life would be shortened. For this reason, Li-ion is more expensive than NiCd.

In operation, the Li-ion electrochemistry is vulnerable to damage from over-charging or other shortcomings in battery management. Therefore, it requires more elaborate charging circuitry with adequate protection against overcharging.

10.2.5 Lithium-Polymer

This is a lithium battery with solid polymer electrolytes. It is constructed with a film of metallic lithium bonded to a thin layer of solid polymer electrolyte. The solid polymer enhances the cell's specific energy by acting as both the electrolyte and the separator. Moreover, the metal in solid electrolyte reacts less than it does with a liquid electrolyte.

10.2.6 Zinc-Air

The zinc-air battery has a zinc negative electrode, a potassium hydroxide electrolyte, and a carbon positive electrode, which is exposed to the air. During discharge, oxygen from the air is reduced at the carbon electrode (the so-called air cathode), and the zinc electrode is oxidized. During discharge, it absorbs oxygen from the air and converts it into oxygen ions for transport to the zinc anode. During charge, it evolves oxygen. Good air management is essential for the performance of the zinc-air battery.

10.3 EQUIVALENT ELECTRICAL CIRCUIT

For steady-state electrical performance calculations, the battery is represented by an equivalent electrical circuit shown in Figure 10.3. In its simplest form, the battery works as a constant voltage source with a small internal resistance. The open-circuit (or electrochemical) voltage E_i of the battery decreases linearly with the Ah discharged (Q_d), and the internal resistance R_i increases linearly with Q_d. That is, the battery open-circuit voltage is lower, and the internal resistance is higher in a partially

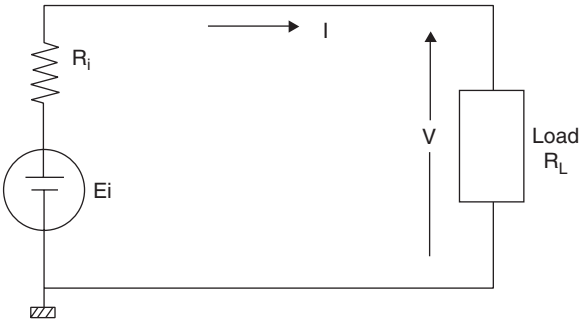

FIGURE 10.3 Equivalent electrical circuit of the battery showing internal voltage and resistance.

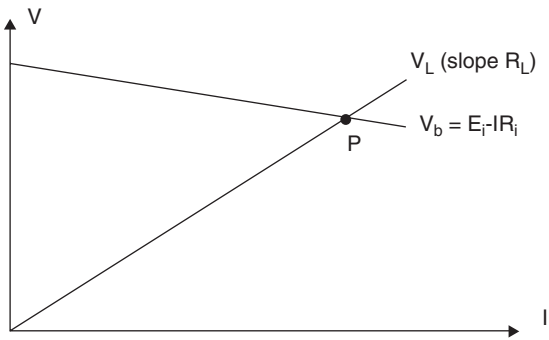

FIGURE 10.4 Battery source line intersecting with load line at the operating point.

discharged state as compared to the E_0 and R_0 values in a fully charged state. These parameters are expressed quantitatively as follows:

$$E_i = E_0 - K_1 Q_d$$
$$R_i = R_0 + K_2 Q_d \tag{10.1}$$

where K_1 and K_2 are constants found by curve-fitting the test data.

The terminal voltage drops with increasing load as shown by the V_b line in Figure 10.4, in which the operating point is the intersection of the source line and the load line (point P). The power delivered to the external load resistance is I^2R_L.

In a fast-discharge application, such as for starting a heavily loaded motor, the battery may be required to deliver the maximum possible power for a short time. The peak power it can deliver is derived using the maximum power transfer theorem in electrical circuits. It states that the maximum power can be transferred from the source to the load when the internal impedance of the source equals the conjugate of the load impedance. The battery can deliver the maximum power to a DC load when $R_L = R_i$. This gives the following:

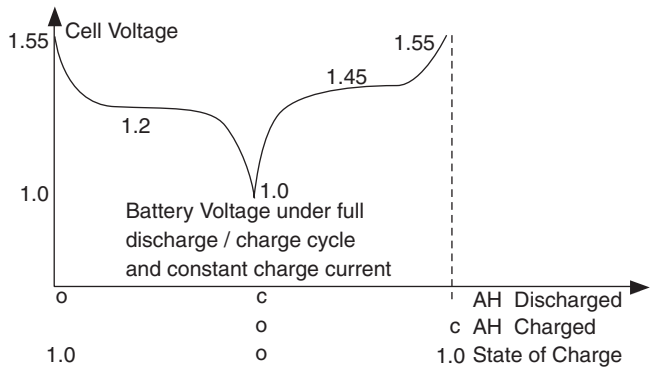

FIGURE 10.5 Voltage variation during C/D cycle of NiCd cell with nominal voltage of 1.2 V.

$$P_{max} = \frac{E_i^2}{4R_i} \tag{10.2}$$

Because E_i and R_i vary with the *SOC*, the P_{max} also varies accordingly. The internal loss is I^2R_i. The efficiency at any *SOC* is therefore:

$$\eta = \frac{R_L}{R_L + R_i} \tag{10.3}$$

The efficiency decreases as the battery is discharged, thus generating more heat at a low *SOC*.

10.4 PERFORMANCE CHARACTERISTICS

The basic performance characteristics, which influence the battery design, are as follows:

- Charge/discharge (C/D) voltages
- C/D ratio
- Round-trip energy efficiency
- Charge efficiency
- Internal impedance
- Temperature rise
- Life in number of C/D cycles

10.4.1 C/D Voltages

The cell voltage variation during a typical C/D cycle is shown in Figure 10.5 for a cell with nominal voltage of 1.2 V, such as NiMH and NiCd. The voltage is maximum when the cell is fully charged (*SOC* = 1.0 or Ah discharged = 0). As the cell is

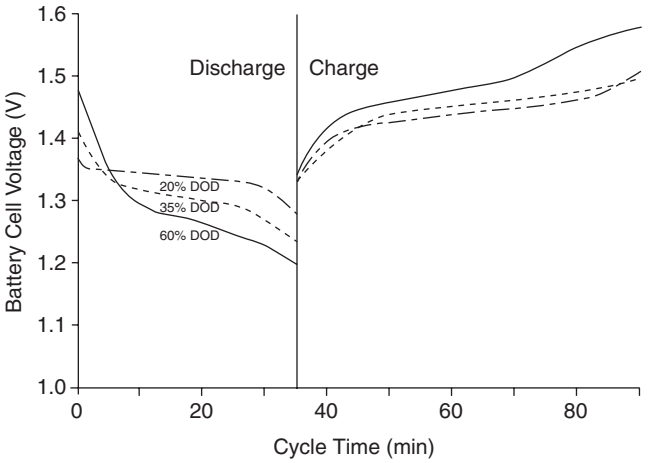

FIGURE 10.6 Cell voltage curves at different C/D rates.

discharged, the cell voltage (V_c) drops quickly to a plateau value of 1.2 V, which holds for a long time before dropping to 1.0 at the end of capacity ($SOC = 0$). In the reverse, when the cell is recharged, the voltage quickly rises to a plateau value of 1.45 V and then reaches a maximum value of 1.55 V. The C/D characteristic also depends on how fast the battery is charged and discharged (Figure 10.6).

10.4.2 C/D Ratio

After discharging a certain Ah to load, the battery requires more Ah of charge to restore the full *SOC*. The C/D ratio is defined as the Ah input over the Ah output with no net change in the *SOC*. This ratio depends on the charge and discharge rates and also on temperature, as shown in Figure 10.7. At 20°C, for example, the C/D ratio is 1.1, meaning the battery needs 10% more Ah charge than that which was discharged for restoring to its fully charged state.

10.4.3 Energy Efficiency

The energy efficiency over a round trip of a full charge and discharge cycle is defined as the ratio of the energy output over the energy input at the electrical terminals of the battery. For a typical battery of capacity C with an average discharge voltage of 1.2 V, average charge voltage of 1.45 V, and C/D ratio of 1.1, the efficiency is calculated as follows:

The energy output over the full discharge = $1.2 \times C$
The energy input required to restore full charge = $1.45 \times 1.1 \times C$

Therefore, the round-trip energy efficiency is as follows:

$$\eta_{\text{energy}} = \frac{1.2 \times C}{1.45 \times 1.1 \times C} = 0.75 \text{ or } 75\%$$

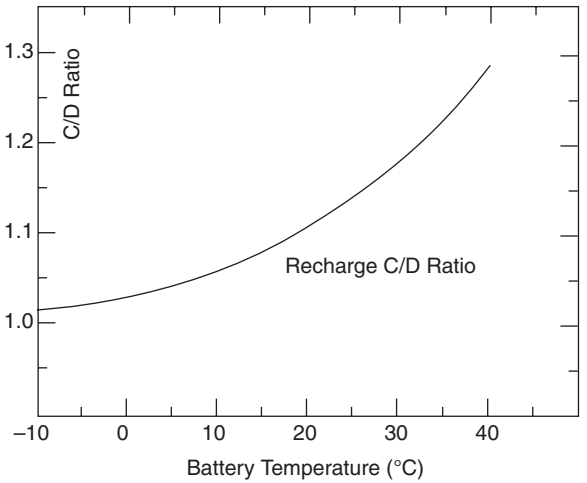

FIGURE 10.7 Temperature effect on C/D ratio.

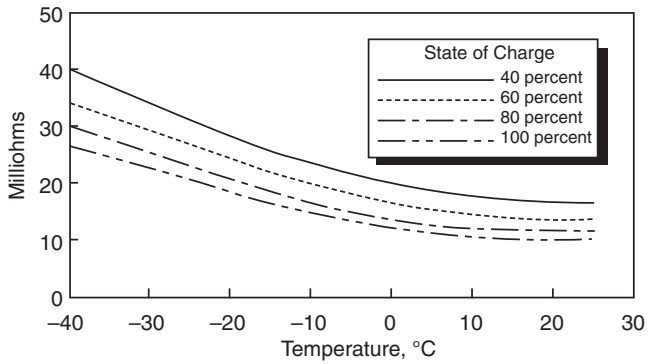

FIGURE 10.8 Temperature effect on internal resistance in 25-Ah NiCd cell.

10.4.4 Internal Resistance

The efficiency calculations in the preceding text indicate that 25% of the energy is lost per C/D cycle, which is converted into heat. This characteristic of the battery can be seen as having an internal resistance R_i. The value of R_i is a function of the battery capacity, operating temperature, and the *SOC*. The higher the cell capacity, the larger the electrodes and the lower the internal resistance. R_i varies with *SOC* as per Equation 10.1. It also varies with temperature as shown in Figure 10.8, which is for a high-quality 25-Ah NiCd cell.

10.4.5 Charge Efficiency

Charge efficiency is defined as the ratio of the Ah being deposited internally between the plates over that delivered to the external terminals during the charging process.

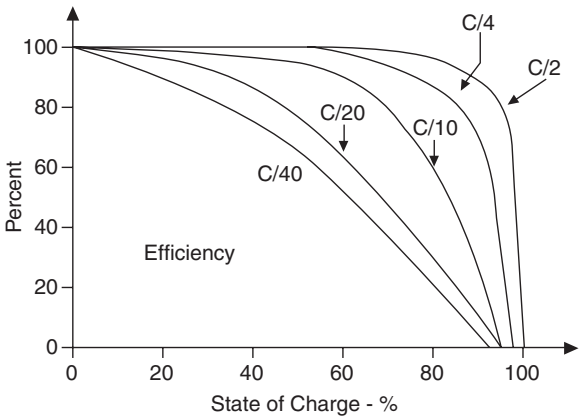

FIGURE 10.9 Charge efficiency vs. SOC at various charge rates.

It is different from energy efficiency. The charge efficiency is almost 100% when the cell is empty of charge, the condition in which it converts all Ah received into useful electrochemical energy. As the *SOC* approaches one, the charge efficiency tapers down to zero. The knee point at which the charge efficiency starts tapering off depends on the charge rate (Figure 10.9). For example, at *C*/2 charge rate, the charge efficiency is 100% up to about 75% *SOC*. At a fast charge rate of *C*/40, on the other hand, the charge efficiency at 60% *SOC* is only 50%.

10.4.6 Self-Discharge and Trickle-Charge

The battery slowly self-discharges even with no load on its terminals (open circuit). To maintain full *SOC*, it is continuously trickle-charged to counter the self-discharge rate. This rate is usually less than 1% per day for most electrochemistries in normal working conditions.

After the battery is fully charged, the charge efficiency drops to zero. Any additional charge will be converted into heat. If overcharged at a higher rate than the self-discharge rate for an extended period of time, the battery would overheat, posing a safety hazard of potential explosion. Excessive overcharging produces excessive gassing, which scrubs the electrode plates. Continuous scrubbing at high rate produces excessive heat and wears out electrodes, leading to shortened life. For this reason, the battery charger should have a regulator to cut back the charge rate to the trickle rate after the battery is fully charged. Trickle charging produces a controlled amount of internal gassing. It causes mixing action of the battery electrolyte, keeping it ready to deliver the full charge.

10.4.7 Memory Effect

One major disadvantage of the NiCd battery is the memory effect. It is the tendency of the battery to remember the depth at which it has delivered most of its capacity in the past. For example, if the NiCd battery is repeatedly charged and discharged 25% of its capacity to point M in Figure 10.10, it will remember point M. Subsequently, if

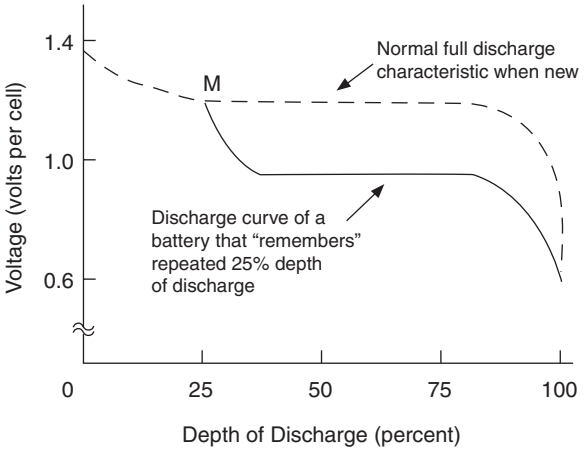

FIGURE 10.10 Memory effect degrades discharge voltage in NiCd cell.

the battery is discharged beyond point M, the cell voltage will drop much below its original normal value shown by the dotted line in Figure 10.10. The end result is the loss of full capacity after repeatedly using many shallow discharge cycles. The phenomenon is like losing a muscle due to lack of use over a long time. A remedy for restoring the full capacity is "reconditioning," in which the battery is fully discharged to almost zero voltage once every few months and then fully charged to about 1.55 V per cell. Other types of batteries do not have this memory effect.

10.4.8 Effects of Temperature

As seen in the preceding sections, the operating temperature significantly influences the battery performance as follows:

- The capacity and charge efficiency decrease with increasing temperature.
- The capacity drops at temperatures above or below a certain range, and drops sharply at temperatures below freezing.
- The self-discharge rate increases with temperature.
- The internal resistance increases with decreasing temperature.

Table 10.2 shows the influence of temperature on the charge efficiency, discharge efficiency, and self-discharge rate in the NiCd battery. The process of determining the optimum operating temperature is also indicated in the table. It is seen that different attributes have different desirable operating temperature ranges shown by the boldfaced numbers. With all attributes jointly considered, the most optimum operating temperature is the intersection of all the desirable ranges. For example, if we wish to limit the self-discharge rate below 1%, discharge efficiency at 100%, and charge efficiency at 90% or higher, Table 10.2 indicates that the optimum working-temperature range is between 10°C and 25°C, which is the common belt through the boldfaced parts of the three columns.

TABLE 10.2
Optimum Working-Temperature Range for NiCd Battery

Operating Temperature (°C)	Charge Efficiency (%)	Discharge Efficiency (%)	Self-Discharge Rate (% Capacity/Day)
–40	0	72	0.1
–35	0	80	0.1
–30	15	85	0.1
–25	40	90	0.2
–20	75	95	0.2
–15	85	97	0.2
–10	**90**	**100**	**0.2**
–5	**92**	**100**	**0.2**
0	**93**	**100**	**0.2**
5	**94**	**100**	**0.2**
10	**94**	**100**	**0.2**
15	**94**	**100**	**0.3**
20	**93**	**100**	**0.4**
25	**92**	**100**	**0.6**
30	91	100	1.0
35	90	100	1.4
40	88	100	2.0
45	85	100	2.7
50	82	100	3.6
55	79	100	5.1
60	75	100	8.0
65	70	100	12
70	60	100	20

10.4.9 Internal Loss and Temperature Rise

The battery temperature varies over the C/D cycle. Taking NiCd as an example, the heat generated in one such cycle with 1.2 h of discharge and 20.8 h of charge every day is shown in Figure 10.11. Note that the heat generation increases with the depth of discharge (DoD) because of the increased internal resistance at higher DoD. When the battery is put to charge, the heat generation is negative for a while, meaning that the electrochemical reaction during the initial charging period is endothermic (absorbing heat), as opposed to the exothermic reaction during other periods with a positive heat generation. The temperature rise during the cycle depends on the cooling method used to dissipate the heat by conduction, convection, and radiation.

Different electrochemistries, however, generate internal heat at different rates. The heat generation of various batteries can be meaningfully compared in terms of the adiabatic temperature rise during discharge, which is given by the following relation:

$$\Delta T = \frac{WH_{\mathrm{d}}}{MC_{\mathrm{p}}}\left[1 - \eta_v + \frac{E_{\mathrm{d}}}{E_{\mathrm{o}}}\right] \tag{10.4}$$

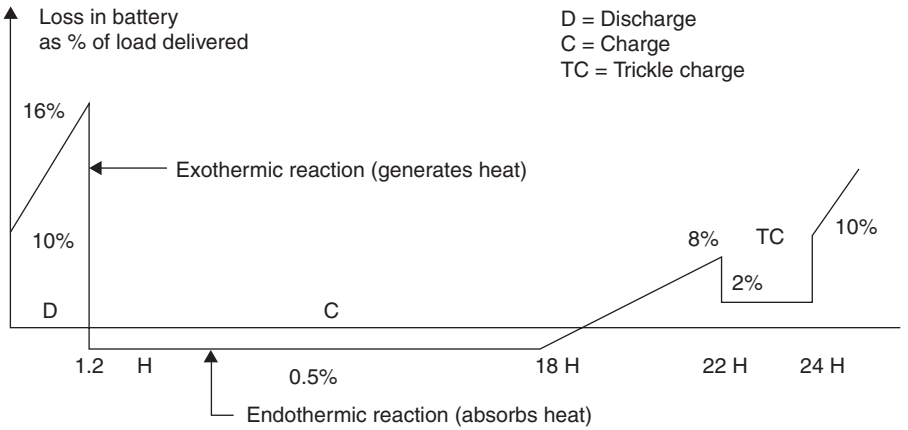

FIGURE 10.11 Internal energy loss in battery during C/D cycle showing endothermic and exothermic periods.

TABLE 10.3
Battery Characteristics Affecting Thermal Design

Electrochemistry	Operating Temperature Range (°C)	Overcharge Tolerance	Heat Capacity (Wh/kg-K)	Mass Density (kg/l)	Entropic Heating on Discharge W/A
Lead-acid	–10 to 50	High	0.35	2.1	–0.06
Nickel-cadmium	–20 to 50	Medium	0.35	1.7	0.12
Nickel-metal hydride	–10 to 50	Low	0.35	2.3	0.07
Lithium-ion	10 to 45	Very low	0.38	1.35	0
Lithium-polymer	50 to 70	Very low	0.40	1.3	0

where

ΔT = adiabatic temperature rise of the battery, °C
WH_d = watthour energy discharged, Wh
M = mass of the battery, kg
C_p = battery-specific heat, Wh/kg·C
η_v = voltage efficiency factor on discharge
E_d = average cell entropy energy per coulomb during discharge, i.e., average power loss per ampere of discharge, W/A
E_o = average cell open-circuit voltage, V

For full discharge, the WH_d/M ratio in Equation 10.4 becomes the specific energy. This indicates that a higher specific energy cell would also tend to have a higher temperature rise during discharge, requiring an enhanced cooling design. Various battery characteristics affecting the thermal design are listed in Table 10.3. Figure

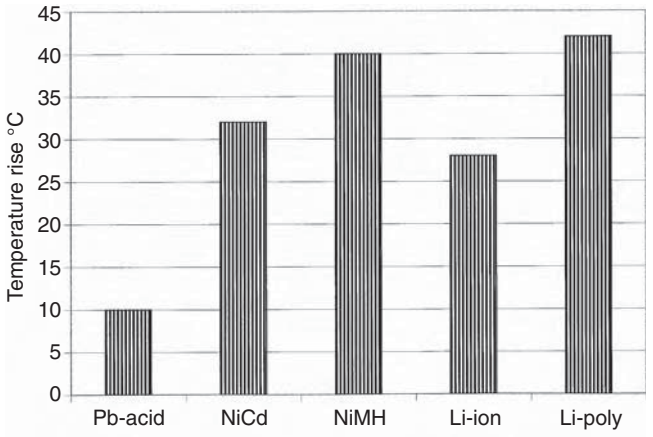

FIGURE 10.12 Adiabatic temperature rise for various electrochemistries.

10.12 depicts the adiabatic temperature rise ΔT for various electrochemistries after a full discharge in short bursts.

10.4.10 Random Failure

The battery fails when at least one cell in a series fails. *Cell failure* is theoretically defined as the condition in which the cell voltage drops below a certain value before discharging the rated capacity at room temperature. The value is generally taken as 1.0 V in cells with nominal voltage of 1.2 V. This is a very conservative definition of battery failure. In practice, if one cell shows less than 1.0 V, other cells can make up the difference without detecting the failure at the battery level. Even if all cells show stable voltage below 1.0 V at full load, the load can be reduced to maintain the desired voltage for some time until the voltage degrades further.

The cell can fail in open, short, or be in some intermediate state (a soft short). A short that starts soft eventually develops into a hard short. In a low-voltage battery, any attempt to charge with a shorted cell may result in physical damage to the battery or the charge regulator. On the other hand, the shorted cell in a high-voltage battery with numerous series-connected cells may work forever. It, however, loses the voltage and ampere-hour capacity, and hence, would work as a load on the healthy cells. An open cell, on the other hand, disables the entire battery of series-connected cells.

In a system having two parallel batteries (a common design practice), if one cell in one battery gets shorted, the two batteries would have different terminal characteristics. Charging or discharging such batteries as a group can result in highly uneven current sharing, subsequently overheating one of the batteries. Two remedies are available to avoid this. One is to charge and discharge both batteries with individual current controls such that they both draw their rated share of the load. The other is to replace the failed cell immediately, which can sometimes be impractical.

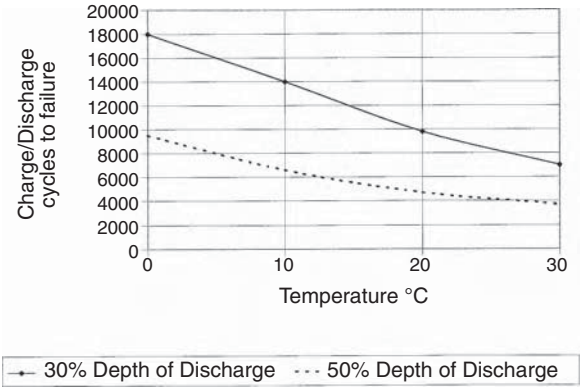

FIGURE 10.13 C/D cycle life of sealed NiCd battery vs. temperature and DoD.

In general, an individual C/D control for each battery is the best strategy. It may also allow replacement of any one battery with a different electrochemistry or different age, which would have different load-sharing characteristics. Batteries are usually replaced several times during the economic life of a plant.

10.4.11 Wear-Out Failure

In addition to a random failure, the battery cell eventually wears out and fails. This is associated with the electrode wear due to repeated C/D cycles. The number of times the battery can be discharged and recharged before the electrodes wear out depends on the electrochemistry. The battery life is measured by the number of C/D cycles it can deliver before a wear-out failure. The life depends strongly on the depth of discharge and the temperature as shown in Figure 10.13, which is for a high-quality NiCd battery. The life also depends, to a lesser degree, on the electrolyte concentration and the electrode porosity. The first two factors are application related, whereas the others are construction related.

It is noteworthy from Figure 10.13 that the life at a given temperature is an inverse function of the depth of discharge. At 20°C, the life is 10,000 cycles at 30% DoD and about 6,000 cycles at 50% DoD. This makes the product of the number of cycles until failure and the DoD remain approximately constant. This product decreases with increasing temperature. This is true for most batteries. This means that the battery at a given temperature can deliver the same number of equivalent full cycles of energy regardless of the depth of discharge. The total Wh energy the battery can deliver over its life is approximately constant. Such observation is useful in comparing the costs of various batteries for a given application.

The life consideration is a dominant design parameter in battery sizing. Even when the load may be met with a smaller capacity, the battery is oversized to meet the life requirement as measured in number of C/D cycles. For example, with the same Wh load, the battery that must charge or discharge twice as many cycles over its life needs approximately double the capacity to have the same calendar life.

TABLE 10.4
Specific Energy and Energy Density of Various Batteries

Electrochemistry	Specific Energy (Wh/kg)	Energy Density (Wh/l)	Specific Power (W/kg)	Power Density (W/l)
Lead-acid	30–40	70–75	~200	~400
Nickel-cadmium	40–60	70–100	150–200	220–350
Nickel-metal hydride	50–65	140–200	~200	450–500
Lithium-ion	90–120	200–250	>500	500–600
Lithium-polymer	100–200	150–300	>200	>350
Zinc-air	140–180	200–200	~150	~200

TABLE 10.5
Life and Cost Comparison of Various Batteries

Electrochemistry	Cycle Life in Full Discharge Cycles	Calendar Life in Years	Self-Discharge (%/month at 25°C)	Relative Cost ($/kWh)
Lead-acid	500–1000	5–8	3–5	200–300
Nickel-cadmium	1000–2000	10–15	20–30	1500
Nickel-metal hydride	1000–2000	8–10	20–30	400–600
Lithium-ion	1500–2000	—	5–10	500–800
Lithium-polymer	1000–1500	—	1–2	>2000
Zinc-air	200–300	—	4–6	—

10.4.12 Battery Types Compared

The performance characteristics and properties of various electrochemistries presented in the preceding sections are summarized and compared in Table 10.4 and Table 10.5. Note that the overall cost of the Pb-acid battery is low compared to NiCd, NiMH, and Li-ion batteries. Because of its least cost per Wh delivered over the life, the Pb-acid battery has been the workhorse of industry.[2]

10.5 MORE ON THE LEAD-ACID BATTERY

The Pb-acid battery is available in small to large capacities in various terminal voltages, such as 6 V, 12 V, and 24 V. As in other batteries, the ampere-hour capacity of the Pb-acid battery is sensitive to temperature. Figure 10.14 shows the capacity variations with temperature for deep-cycle Pb-acid batteries. At 20°F, for example, the high-rate battery capacity is about 20% of its capacity at 100°F. The car is hard to start in winter for this reason. On the other hand, the self-discharge rate decreases significantly at cold temperatures, as seen in Figure 10.15.

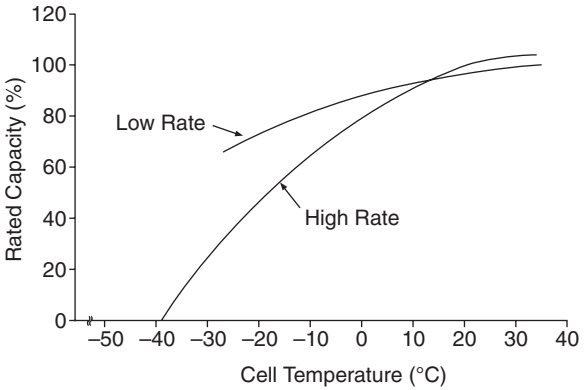

FIGURE 10.14 Pb-acid battery capacity variations with temperature.

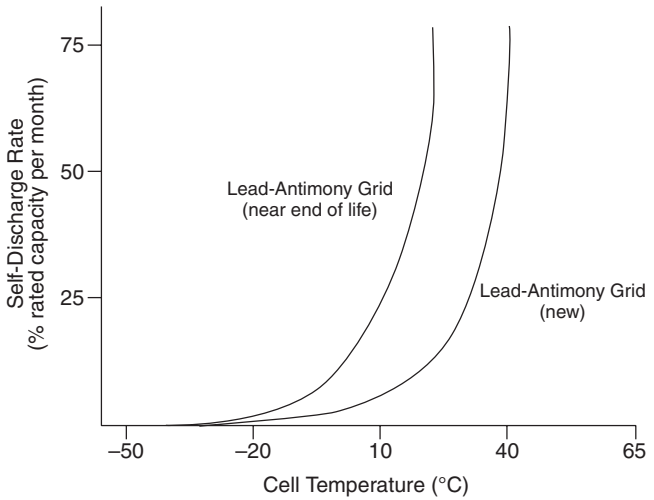

FIGURE 10.15 Pb-acid battery self-discharge rate vs. temperature.

Table 10.6 shows the effect of *SOC* on the voltage, specific gravity, and freezing point of the Pb-acid battery. The electrolyte in a fully charged battery has a high specific gravity and freezes at 65°F. On the other hand, a fully discharged battery freezes at +15°F. The table shows the importance of keeping the battery fully charged on cold days.

The cycle life vs. DoD for the Pb-acid battery is depicted in Figure 10.16, again showing the "half-life at double the DoD" rule of thumb.

The discharge rate influences the Pb-acid battery capacity, as shown in Figure 10.17. The shorter the discharge time (i.e., higher the discharge rate), the lower the ampere-hour capacity the battery can deliver.

TABLE 10.6
Effects of *SOC* on Specific Gravity and Freezing Point of Lead-Acid Battery

State of Charge	Specific Gravity	Freezing Point	120-V Battery Voltage
1 (Fully Charged)	1.27	–65°F	128
75%	1.23	–40°F	124
50%	1.19	–10°F	122
25%	1.15	+5°F	120
0 (Fully Discharged)	1.12	+15°F	118

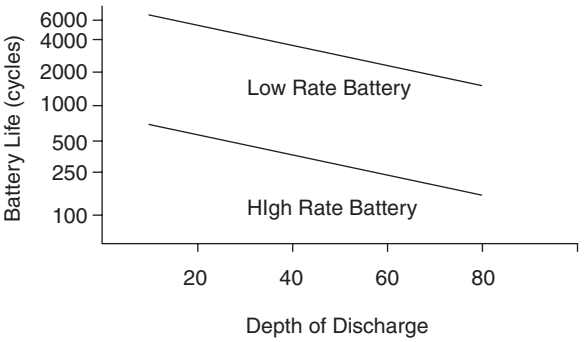

FIGURE 10.16 Pb-acid battery life in cycles to failure vs. DoD.

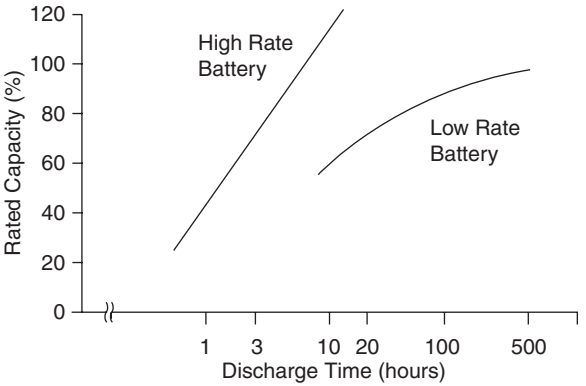

FIGURE 10.17 Pb-acid battery capacity with discharge time.

The Pb-acid cell voltage is 2.0 V nominal, and the internal resistance is around 1 mΩ per cell. The cycle life is 500 to 1000 full C/D cycles for medium-rated batteries. The ranges of operating temperature are between –20 and 50°C and the survival temperature between –55 and 60°C.

10.6 BATTERY DESIGN

The battery design for a given application depends on the following system requirements:

- Voltage and current
- C/D and duration
- Operating temperature during C/D
- Life in number of C/D cycles
- Cost, size, and weight constraints

Once these system-level design parameters are identified, the battery design proceeds in the following steps:

1. Select the electrochemistry suitable for the overall system requirements.
2. Determine the number of series cells required to meet the voltage requirement.
3. Determine the ampere-hour discharge required to meet the load demand.
4. For the required number of C/D cycles, determine the maximum allowable DoD.
5. Ampere-hour capacity of the battery is then determined by dividing the ampere-hour discharge required by the allowable DoD calculated earlier.
6. Determine the number of battery packs required in parallel for the total ampere-hour capacity.
7. Determine the temperature rise and thermal controls required.
8. Provide the C/D rate controls as needed.

Each cell in the battery pack is electrically insulated from the others and from the ground. The electrical insulation must be a good conductor of heat to maintain a low temperature gradient between the cells and also to the ground.

The battery performs better under slow C/D rates. It accepts less energy when charged at a faster rate. Also, the faster the discharge rate, the faster the voltage degradation and lower the available capacity to the load. For these reasons, high-C/D-rate applications require different design considerations from the low-rate applications.

Because the battery design is highly modular, built from numerous cells, there is no fundamental technological limitation on the size of the energy storage system that can be designed and operated using electrochemical batteries. The world's largest 40-MW peak-power battery was commissioned in 2003 at a cost of $30 million. The system used 14,000 sealed NiCd cells manufactured from recycled cadmium by Saft Corporation at a total cell cost of $10 million. The cells will be recycled again after their 20-yr life. The battery system is operated by Golden Valley Electric Association in Fairbanks for an Alaskan utility company. The spinning energy reserve of the battery provides continuous voltage support and cuts down on blackout possibilities.

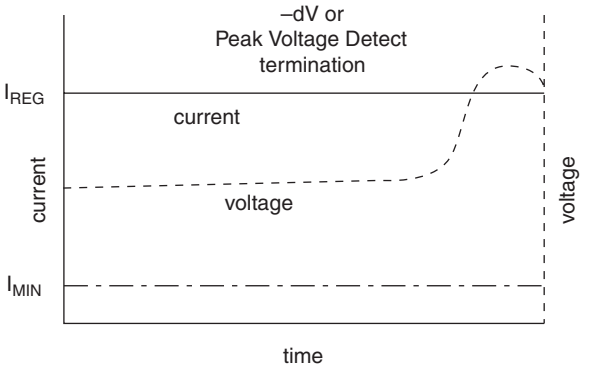

FIGURE 10.18 Constant current charging of NiCd and NiMH batteries.

10.7 BATTERY CHARGING

During battery charging, the energy management software monitors the *SOC*, the overall health, and safe termination criteria. The continuously monitored operating parameters are the battery voltage, current, and temperature. The charging timer is started after all initial checks are successfully completed. Charging may be suspended (but not reset) if it detects any violation of critical safety criteria. The timer stops charging if the defect persists beyond a certain time limit.

Normal charging has the following three phases:

- Bulk (fast) charge, which deposits 80 to 90% of the drained capacity
- Taper charge, in which the charge rate is gradually cut back to top off the remaining capacity
- Trickle (float) charge after the battery is fully charged to counter the self-discharge rate

The bulk-charge and the taper-charge termination criteria are preloaded in the battery management software to match the battery electrochemistry and system-design parameters. For example, the NiCd and NiMH batteries are generally charged at a constant current (Figure 10.18), terminating the charging when the continuously monitored ΔV is detected negative. On the other hand, the Li-ion battery, being sensitive to overcharging, is charged at a constant voltage, tapering off the charge current as needed (Figure 10.19).

10.8 CHARGE REGULATORS

For safety reasons, it is extremely important that excessive charging of the battery be avoided at all times. Overcharging causes internal gassing, which causes loss of water in the Pb-acid battery and premature aging. The charge regulator allows the maximum rate of charging until the gassing starts. Then the charge current is tapered off to the trickle-charge rate so that the full charge is approached gently.

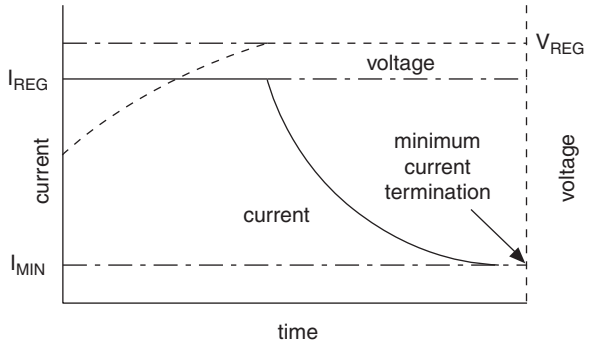

FIGURE 10.19 Constant voltage charging of Li-ion battery.

The batteries are charged in the following three different manners:

10.8.1 Multiple Charge Rates

This is the best method, in which the battery is charged gently in multiple steps. First the battery is charged at a full charge rate until 80 to 90% of the capacity is achieved. The charge current is then cut back in steps until the battery is fully charged. At this time, the charge current is further reduced to a trickle-charge rate, keeping it fully charged until the next load demand comes on the battery. This method, therefore, needs at least three charge rates in the charge regulator design.

10.8.2 Single-Charge Rate

This method uses a simple low-cost regulator, which is either on or off. The regulator is designed for only one charge rate. When the battery is fully charged, as measured by its terminal voltage, the charger is turned off by a relay. When the battery voltage drops below a preset value, the charger is again connected in full force. Because the charging is not gentle in this method, full charge is difficult to achieve and maintain. An alternate version of this charging method is the multiple pulse charging. Full current charges the battery up to a high preset voltage just below the gassing threshold. At this time, the charger is shut off for a short time to allow the battery chemicals to mix and the voltage to fall. When the voltage falls below a low preset threshold, the charger is reconnected, again passing full current to the battery.

10.8.3 Unregulated Charging

This least-cost method can be used in PV power systems. It uses no charge regulator. The battery is charged directly from a solar module dedicated just for charging. The charging module is properly designed for safe operation with a given number of cells in the battery. For example, in a 12-V Pb-acid battery, the maximum PV module voltage is kept below 15 V, making it impossible to overcharge the battery. When the battery is fully charged, the array is fully shunted to ground by a shorting switch (transistor). The shunt transistor switch is open when the battery voltage drops below

a certain value. The isolation diode blocks the battery that powers the array or shunt at night, as discussed in Section 9.8.

10.9 BATTERY MANAGEMENT

Drawing electric power from the battery when needed, and charging it back when access power is available, requires a well-controlled charge and discharge process. Otherwise, the battery performance could suffer, life could be shortened, and maintenance would increase. Some common performance problems are as follows:

- Low charge efficiency, resulting in low *SOC*
- Loss of capacity, disabling the battery to hold the rated ampere-hour charge
- Excessive gassing and heating, leading to a short life
- Unpredictable premature failure, leading to loss of load availability
- Positive plate corrosion, shortening the life
- Stratification and sulfation, degrading the performance

The following features incorporated into battery management can avoid the problems given in the preceding text:

- Controlled voltage charging, preferably at a constant voltage
- Temperature-compensated charging, in which the charge termination occurs earlier if the battery temperature is higher than the reference temperature
- Individual charge control if two or more batteries are charged in parallel
- Accurate set points to start and stop the charge and discharge modes

10.9.1 Monitoring and Controls

The batteries in modern power systems are managed by dedicated computer software. The software monitors and controls the following performance parameters:

- Voltage and current
- Temperature and pressure (if applicable)
- Ampere-hour in and out of the battery
- *SOC* and discharge
- Rate of charge and discharge
- Depth of discharge
- Number of charge and discharge cycles

An ampere-hour-integrating meter is commercially available, which keeps track of the ampere-hour in and out of the battery and sends the required signals to the mode controller.

The temperature-compensated maximum battery voltage and the *SOC* can improve battery management, particularly in extreme cold temperatures. It can allow

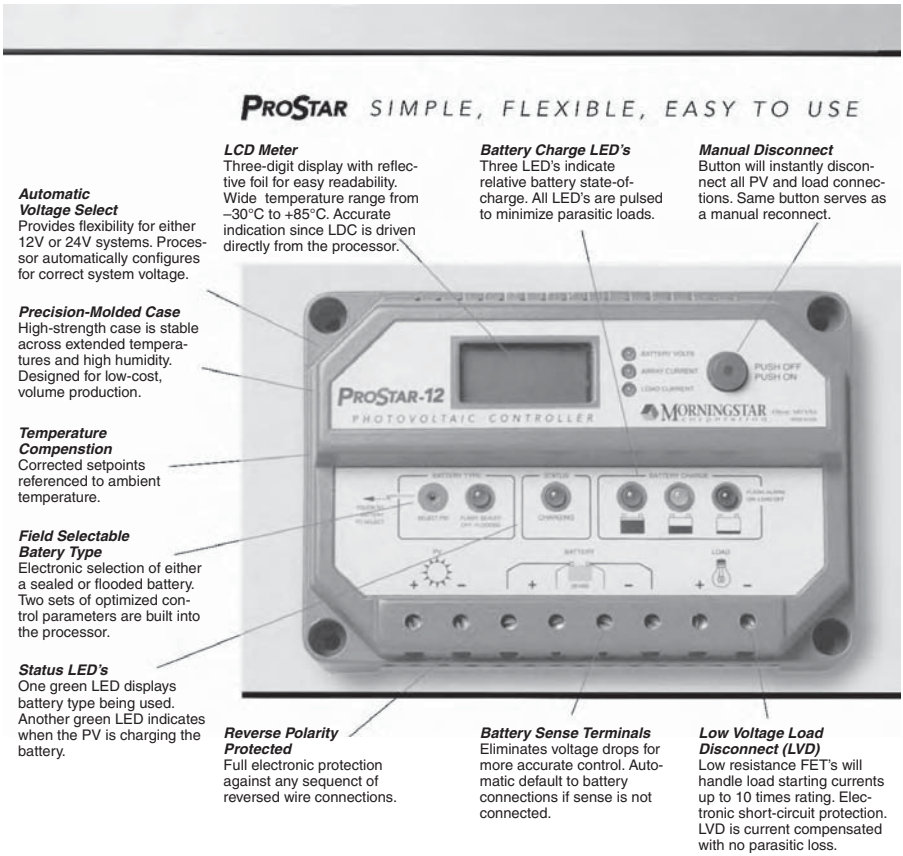

FIGURE 10.20 Battery management microprocessor for PV power system. (From Morningstar Corporation, Newtown, PA. With permission.)

an additional charging during cold periods when the battery can accept more charge. The low-voltage alarm is a good feature to have, as discharging below the threshold low voltage can cause a cell voltage to reverse (become negative). The negative voltage of the cell makes it a load, leading to overheating and a premature failure. The alarm can be used to shed noncritical loads from the battery to avoid potential damage.

Figure 10.20 depicts a commercially available battery management system incorporating a dedicated microprocessor with software.

10.9.2 Safety

The battery operation requires certain safety considerations. The most important is not to overcharge the battery. Any overcharge above the trickle-charge rate is converted into heat, which, if beyond a certain limit, can cause the battery to explode. This is particularly critical when the battery is charged directly from a PV module

without a charge regulator. In such a case, the array is sized below a certain safe limit. As a rule of thumb, the PV array rating is kept below the continuous overcharge current that can be tolerated by the battery. This is typically below *C*/15 A for Pb-acid batteries.

10.10 FLYWHEEL

The flywheel stores kinetic energy in a rotating inertia. This energy can be converted from and to electricity with high efficiency. The flywheel energy storage is an old concept, which has now become commercially viable due to advances made in high-strength, lightweight fiber composite rotors, and the magnetic bearings that operate at high speeds. The flywheel energy storage system is being developed for a variety of potential applications, and is expected to make significant inroads in the near future. The round-trip conversion efficiency of a large flywheel system can approach 90%, much higher than that of a battery.

The energy storage in a flywheel is limited by the mechanical stresses due to the centrifugal forces at high speeds. Small- to medium-sized flywheels have been in use for years. Considerable development efforts are underway around the world for high-speed flywheels to store large amounts of energy. The present goal of these developments is to achieve five times the energy density of the currently available secondary batteries. This goal is achievable with the following enabling technologies, which are already in place in their component forms:

- High-strength fibers having ultimate tensile strength of over one million pounds per square inch
- Advances made in designing and manufacturing fiber-epoxy composites
- High-speed magnetic bearings, which eliminate friction, vibrations, and noise

The flywheel system is made of a fiber-epoxy composite rotor, supported on magnetic bearings, rotating in a vacuum, and mechanically coupled with an electrical machine that can work as a motor or a generator. Two counter-rotating wheels are placed side by side where gyroscopic effects must be eliminated, such as in a city transit bus, train, or an automobile.

10.10.1 Energy Relations

The energy stored in a flywheel having the moment of inertia J and rotating at an angular speed ω is given by the following:

$$E = \frac{1}{2} J\omega^2 \tag{10.5}$$

The centrifugal force in the rotor material of density ρ at radius r is given by $\rho(r\omega)^2$, which is supported by the hoop stress in the rotor rim. Because the linear

velocity $V = 2\pi r\omega$, the maximum centrifugal stress in the rotor is proportional to the square of the outer tip velocity. The allowable stress in the material places an upper limit on the rotor tip speed. Therefore, a smaller rotor can run at a high speed and *vice versa*. The thin-rim-type rotor has a high inertia-to-weight ratio and stores more energy per kilogram weight. For this reason, the rotor, in all practical flywheel system designs, is a thin-rim configuration. For such a rotor with inner radius R_1 and outer radius R_2, it can be shown that the maximum energy that can be stored for an allowable rotor tip velocity V is as follows:

$$E_{\max} = K_1 V^2 \left[1 + \left(\frac{R_1}{R_2} \right)^2 \right] \tag{10.6}$$

where K_1 is the proportionality constant. The thin-rim flywheel with R_1/R_2 ratio approaching unity results in a high specific energy for a given allowable stress limit. The higher the ultimate strength of the material, the higher the specific energy. The lower the material density, the lower the centrifugal stress produced, which leads to a higher allowable speed and specific energy. The maximum energy storage $E_{\max}$, therefore, can be expressed as follows:

$$E_{\max} = K_2 \frac{\sigma_{\max}}{\rho} \tag{10.7}$$

where
K_2 = another proportionality constant
$\sigma_{\max}$ = maximum allowable hoop stress
ρ = density of the rotor material

A good flywheel design therefore has a high $\sigma_{\max}/\rho$ ratio for high specific energy. It also has a high E/ρ ratio for rigidity, where E is the Young's modulus of elasticity.

The metallic flywheel has low specific energy because of a low $\sigma_{\max}/\rho$ ratio, whereas high-strength polymer fibers such as graphite, silica, and boron, having much higher $\sigma_{\max}/\rho$ ratio, store an order of magnitude higher energy per unit weight. Table 10.7 compares the specific energy of various metallic and polymer fiber composite rotors. In addition to a high specific energy, the composite rotor has a safe mode of failure, as it disintegrates to fluff rather than fragmenting like the metal flywheel.

Figure 10.21 shows a rotor design recently developed at the Oakridge National Laboratory. The fiber-epoxy composite rim is made of two rings. The outer ring is made of high-strength graphite, and the inner ring of low-cost glass fiber. The hub is made of single-piece aluminum in the radial spoke form. Such a construction is cost-effective because it uses the costly material only where it is needed for strength, that is, in the outer ring where the centrifugal force is high, resulting in a high hoop stress.

TABLE 10.7
Maximum Specific Energy Storable in a Thin-Rim Flywheel with Various Rim Materials

Rotor Wheel Material	Maximum Specific Energy Storable (Wh/kg)
Aluminum alloy	25
Maraging steel	50
E-glass composite	200
Carbon fiber composite	220
S-glass composite	250
Polymer fiber composite	350
Fused silica fiber composite	1000
Lead-acid battery	30–40
Lithium-ion battery	90–120

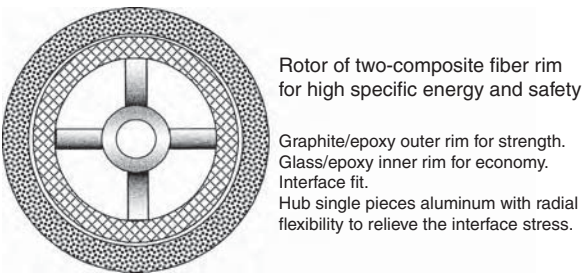

FIGURE 10.21 Flywheel rotor design using two composite rings. (Adapted from the DOE/Oakridge National Laboratory's prototype design.)

Figure 10.22 shows a prototype 5-kWh flywheel weight and specific energy (watthour per pound) vs. σ_{max}/ρ ratio of the material. It is noteworthy that the weight decreases inversely and the specific energy increases linearly with the σ_{max}/ρ ratio.

10.10.2 Flywheel System Components

The complete flywheel energy storage system requires the following components:

- High-speed rotor attached to the shaft via a strong hub
- Bearings with good lubrication system or with magnetic suspension in high-speed rotors
- Electromechanical energy converter, usually a machine that can work as a motor during charging and as a generator while discharging the energy
- Power electronics to drive the motor and to condition the generator power
- Control electronics for controlling the magnetic bearings and other functions

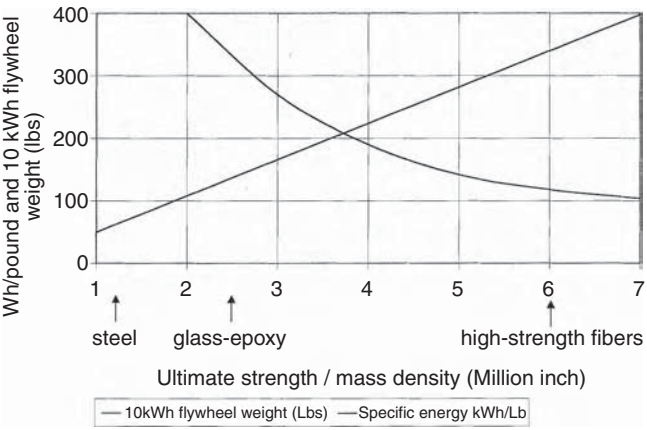

FIGURE 10.22 Specific energy vs. specific strength in flywheel design.

Good bearings have low friction and vibration. Conventional bearings are used up to speeds in a few tens of thousands rpm. Speeds approaching 100,000 rpm are possible only by using magnetic bearings, which support the rotor by magnetic repulsion and attraction. The mechanical contact is eliminated, thus eliminating friction. Running the rotor in a vacuum eliminates windage.

The magnetic bearing comes in a variety of configurations using permanent magnets and dynamic current actuators to achieve the required restraints. A rigid body can have 6 degrees of freedom. The bearings retain the rotor in 5 degrees of freedom, leaving 1 degree free for rotation. The homopolar configuration is depicted in Figure 10.23. Permanent magnets are used to provide free levitation support for the shaft and to help stabilize the shaft under a rotor drop. The electromagnet coils are used for stabilization and control. The control coils operate at low-duty cycle, and only one servo-controller loop is needed for each axis. The servo-control coils provide active control to maintain shaft stability by providing restoring forces as needed to maintain the shaft in the centered position. Various position and velocity sensors are used in an active feedback loop. The electric current variation in the actuator coils compels the shaft to remain centered in position with desired clearances.

Small flux pulsation as the rotor rotates around the discrete actuator coils produces a small electromagnetic loss in the metallic parts. This loss, however, is negligible compared to the friction loss in conventional bearings.

In the flywheel system configuration, the rotor can be located radially outward, as shown in Figure 10.24. It forms a volume-efficient packaging. The magnetic bearing has permanent magnets inside. The magnetic flux travels through the pole shoes on the stator and a magnetic feedback ring on the rotor. The reluctance lock between the pole shoes and the magnetic feedback ring provides the vertical restraint. The horizontal restraint is provided by the two sets of dynamic actuator coils. The currents in the coils are controlled in response to a feedback loop controlling the rotor position.

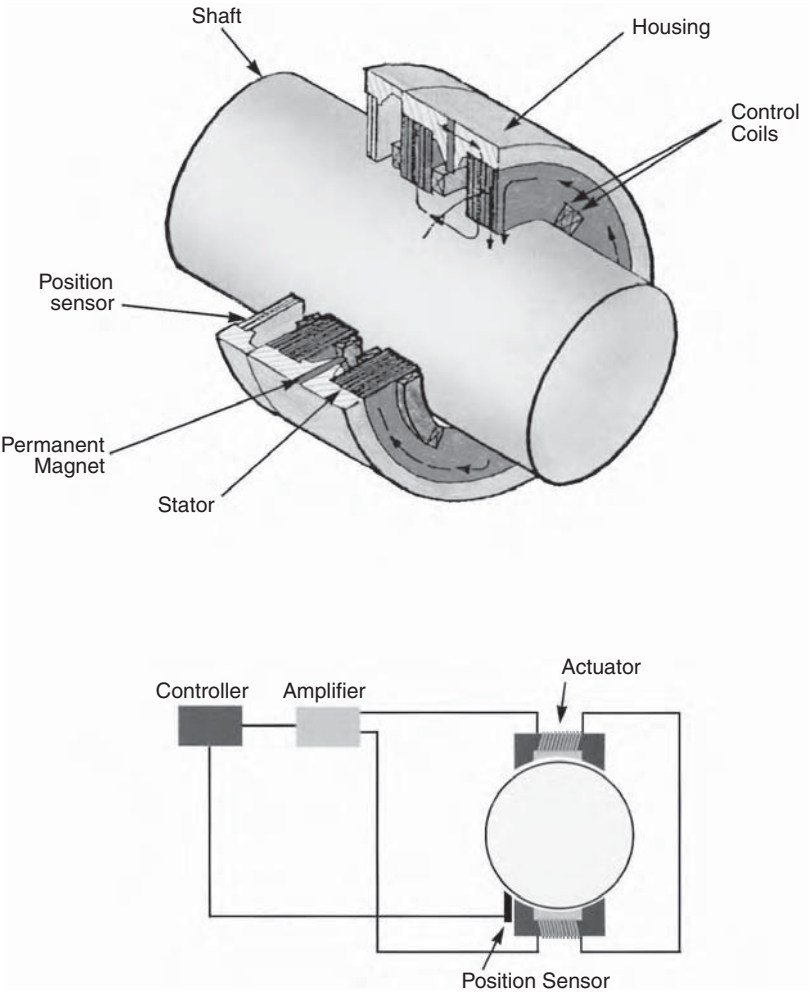

FIGURE 10.23 Avcon's patented homopolar permanent-magnet active bearing. (From Avcon Inc., Woodland Hills, CA. With permission.)

The electromechanical energy conversion in both directions is achieved with one electrical machine, which works as a motor for spinning up the rotor for energy charge, and as a generator while decelerating the rotor for a discharge. Two types of electrical machines can be used, the synchronous machine with variable-frequency converter or the permanent-magnet brushless DC machine.

The machine voltage varies over a wide range with speed. The power electronic converters provide an interface between the widely varying machine voltage and the fixed bus voltage. It is possible to design a discharge converter and a charge converter with input voltage varying over a range of 1 to 3. This allows the machine speed to vary over the same range. That is, the low rotor speed can be one third of the full speed. Because the energy storage is proportional to the speed squared, the flywheel

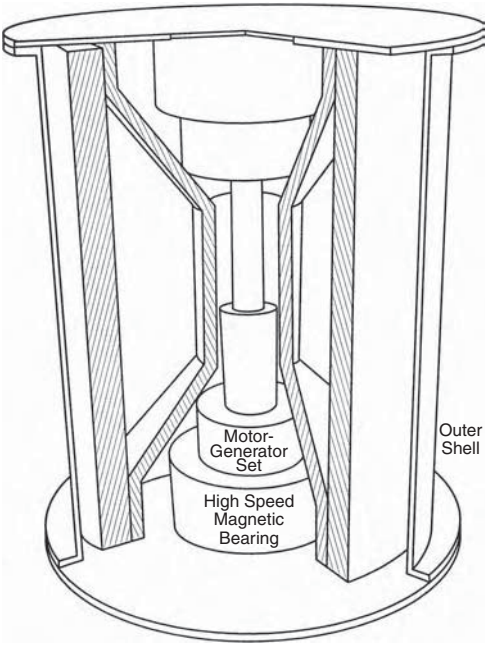

FIGURE 10.24 Flywheel configuration with rotor outside enclosing the motor generator and the bearing.

SOC at low speed can be as low as 0.10. This means 90% of the flywheel energy can be discharged with no hardship on the power electronics, or other components of the system.

As to the number of charge-discharge cycles the flywheel can withstand, the fatigue life of the composite rotor is the limiting factor. Experience indicates that the polymer fiber composites in general have a longer fatigue life than solid metals. A properly designed flywheel, therefore, can last much longer than a battery and can discharge to a much deeper level. Flywheels made of composite rotors have been fabricated and tested to demonstrate more than 10,000 cycles of full charge and discharge. This is an order of magnitude more than any battery can deliver at present.

10.10.3 Benefits of Flywheel over Battery

The main advantages of the flywheel energy storage over the battery are as follows:

- High energy storage capacity per unit of weight and volume
- High DoD
- Long cycle life, which is insensitive to the DoD
- High peak-power capability without concerns about overheating
- Easy power management, as the *SOC* is simply measured by the speed
- High round-trip energy efficiency

- Flexibility in design for a given voltage and current
- Improved quality of power as the electrical machine is stiffer than the battery

These benefits have the potential of making the flywheel the least-cost energy storage alternative per watthour delivered over its operating life.

10.11 SUPERCONDUCTING MAGNET

The superconductor technology for storing energy has started yielding highly promising results. In its working principle, the energy is stored in the magnetic field of a coil, and is given by the following expression:

Energy E stored in a coil carrying current I is given by the following:

$$E = \tfrac{1}{2}B^2/\mu \text{ (J/m}^3\text{) or } E = \tfrac{1}{2}I^2L \text{ (J)} \tag{10.8}$$

where
B = magnetic field density produced by the coil (T)
μ = magnetic permeability of air = $4\ \pi \cdot 10^{-7}$ (H/m)
L = inductance of the coil (H)

The coil must carry current to produce the required magnetic field. The current requires a voltage to be applied to the coil terminals. The relation between the coil current I and the voltage V is as follows:

$$V = RI + L\frac{\mathrm{d}i}{\mathrm{d}t} \tag{10.9}$$

where R and L are the resistance and inductance of the coil, respectively. For storing energy in a steady state, the second term in Equation 10.9 must be zero. Then the voltage required to circulate the needed current is simply $V = RI$.

The resistance of the coil is temperature dependent. For most conducting materials, it is higher at higher temperatures. If the temperature of the coil is reduced, the resistance drops as shown in Figure 10.25. In certain materials, the resistance abruptly drops to a precise zero at some critical temperature. In the figure, this point is shown as T_c. Below this temperature, no voltage is required to circulate current in the coil, and the coil terminals can be shorted. The current continues to flow in the shorted coil indefinitely, with the corresponding energy also stored indefinitely in the coil. The coil is said to have attained the superconducting state, one that has zero resistance. The energy in the coil then "freezes."

Although the superconducting phenomenon was discovered decades ago, the industry interest in developing practical applications started in the early 1970s. In the U.S., the pioneering work has been done in this field by the General Electric Company, Westinghouse Research Center, University of Wisconsin, and others.

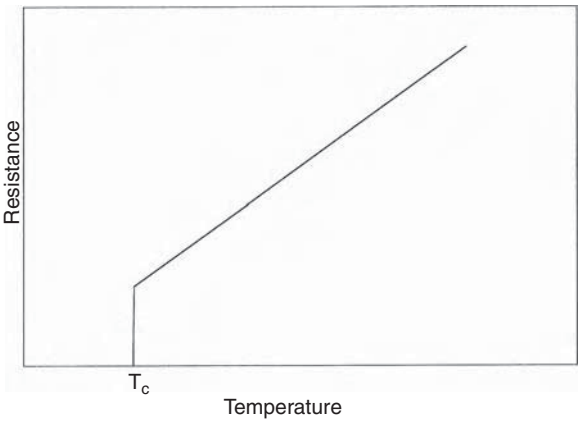

FIGURE 10.25 Resistance vs. temperature with abrupt loss of resistance at the critical superconducting temperature.

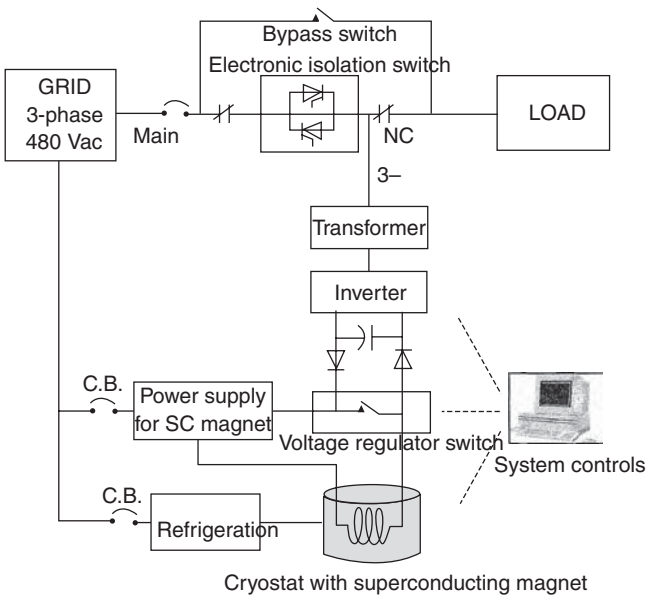

FIGURE 10.26 Superconducting energy storage system schematic.

During the 1980s, a grid-connected 8-kWh superconducting energy storage system was built with funding from the Department of Energy, and was operated by the Bonneville Power Administration in Portland, OR. The system demonstrated over one million charge-discharge cycles, meeting its electrical, magnetic, and structural performance goals. Conceptual designs of large superconducting energy storage systems up to 5000 MWh energy for utility applications have been developed.

The main components in a typical superconducting energy storage system are shown in Figure 10.26. The superconducting magnet coil is charged by an AC-to-DC converter in the magnet power supply. Once fully charged, the converter continues providing the small voltage needed to overcome losses in the room temperature parts of the circuit components. This keeps a constant DC current flowing (frozen) in the superconducting coil. In the storage mode, the current is circulated through a normally closed switch.

The system controller has three main functions.

- It controls the solid-state isolation switch.
- It monitors the load voltage and current.
- It interfaces with the voltage regulator that controls the DC power flow to and from the coil.

If the system controller senses the line voltage dropping, it interprets that the system is incapable of meeting the load demand. The switch in the voltage regulator opens in less than 1 msec. The current from the coil now flows into a capacitor bank until the system voltage recovers the rated level. The capacitor power is inverted into 60- or 50-Hz AC and is fed to the load. The bus voltage drops as the capacitor energy is depleted. The switch opens again, and the process continues to supply energy to the load. The system is sized to store the required energy to power a specified load for a specified duration.

The superconducting energy storage has several advantages over other technologies:

- The round-trip efficiency of the charge-discharge cycle is high at 95%. This is higher than that attainable by any other technology.
- It has a much longer life, up to about 30 yr.
- The charge and discharge times can be extremely short, making it attractive for supplying large power for a short time if needed.
- It has no moving parts in the main system, except in the cryogenic refrigeration components.

In the superconducting energy storage system, a major cost is to keep the coil below the critical superconducting temperature. Until now, the niobium–titanium alloy has been extensively used, which has a critical temperature of about 9°K. This requires liquid helium as a coolant at around 4°K. The 1986 discovery of high-temperature superconductors has accelerated the industry interest in this technology. Three types of high-temperature superconducting materials are available now, all made from bismuth or yttrium–cuprate compounds. These superconductors have the critical temperature around 100°K. Therefore, they can be cooled by liquid nitrogen, which needs significantly less refrigeration power. As a result, numerous programs around the world have started to develop commercial applications. Toshiba of Japan, GEC-Alsthom along with Electricite de France, and many others are actively pursuing development in this field.[3–4]

10.12 COMPRESSED AIR

Compressed air stores energy in a pressure–volume relation. It can store excess energy of a power plant — thermal, nuclear, wind, or PV — and supply it when needed during lean periods or peak demands. The compressed air energy storage system consists of:

- Air compressor
- Expansion turbine
- Electric motor–generator
- Overhead storage tank or an underground cavern

If P and V represent the air pressure and volume, respectively, and if the air compression from pressure P_1 to P_2 follows the gas law PV^n = constant, then the work required during this compression is the energy stored in the compressed air. It is given by the following:

$$\text{Energy stored} = \frac{n(P_2V_2 - P_1V_1)}{n-1} \tag{10.10}$$

And the temperature at the end of the compression is given by the following:

$$\frac{T_2}{T_1} = \left(\frac{P_2}{P_1}\right)^{\frac{n-1}{n}} \tag{10.11}$$

The energy stored is smaller with a smaller value of n. The isentropic value of n for air is 1.4. Under normal working conditions, n is about 1.3. When air at an elevated temperature after constant-volume pressurization cools down, a part of the pressure is lost with a corresponding decrease in the stored energy.

Electric power is generated by venting the compressed air through an expansion turbine that drives a generator. The compressed air system may work under a constant volume or constant pressure.

In constant-volume compression, the compressed air is stored in pressure tanks, mine caverns, depleted oil or gas fields, or abandoned mines. One million cubic feet of air stored at 600 psi provides an energy storage capacity of about 0.25 million kWh_e. This system, however, has a disadvantage. The air pressure reduces as compressed air is depleted from the storage, and the electric power output decreases with decreasing air pressure.

In constant-pressure compression, the air storage may be in an above-ground variable-volume tank or an underground aquifer. One million cubic feet of air stored at 600 psi provides an energy storage capacity enough to generate about 0.10 million kWh. A variable-volume tank maintains a constant pressure by a weight on the tank cover. If an aquifer is used, the pressure remains approximately constant whereas

the storage volume increases because of water displacement in the surrounding rock formation. During electrical generation, water displacement of the compressed air causes a decrease of only a few percent in the storage pressure, keeping the electrical generation rate essentially constant.

The operating-energy cost would include cooling the compressed air to dissipate the heat of compression. Otherwise, air temperature may rise as high as 1000°C — in effect, shrinking the storage capacity and adversely affecting the rock wall of the mine. Energy is also lost to the cooling effect of expansion when the energy is released.

The energy storage efficiency of the compressed-air storage system is a function of a series of component efficiencies, such as the compressor efficiency, motor–generator efficiency, heat losses, and compressed air leakage. The overall round-trip energy efficiency of about 50% has been estimated.

The compressed air can be stored in the following:

- Salt caverns
- Mined hard rock
- Depleted gas fields
- Buried pipes

The current capital cost estimate of a compressed air power system varies between $1000 and 1500 per kW, depending on the air storage systems used.

Compressed air power plants of 300-MW capacities have also been built in Israel, Morocco, and other countries. Two 150-MW plants, one in Germany and one in Alabama, have been in operation for more than a decade. Both these installations operate reliably, although on a single generator. They occupy salt caverns created by dissolving salt and removing brine.

A 200-MW compressed air energy storage plant is being planned by a consortium of electrical and gas utilities near Fort Dodge, IA, to support the new rapidly developing wind power generation in the area. This $200-million project is planned for completion in 2007. The plant will use energy from a 100-MW wind farm to store compressed air in an underground aquifer and then blend it with natural gas to fire turbines for power generation.

A Houston-based company, CAES, has proposed the use of abandoned limestone mines in Norton, OH (Figure 10.27). The 10-million-m^3 mines can store enough compressed air to drive 2700-MW-capacity turbines. The Ohio power sitting board approved the proposal in 2001 for the operation to start before 2005. A Sandia National Laboratory study found the rock structure dense enough to prevent air leakage and solid enough to handle the working pressures from 11 MPa down to 5.5 MPa. The air from the mine after the expansion cooling is heated with natural gas to drive the turbines at an optimal temperature. This operation would use less than one third of the fuel of a gas-fired generator and would reduce the energy cost and emission levels. The Ohio system is designed with nine 300-MW generators and uses 18 compressors to pressurize the mines.

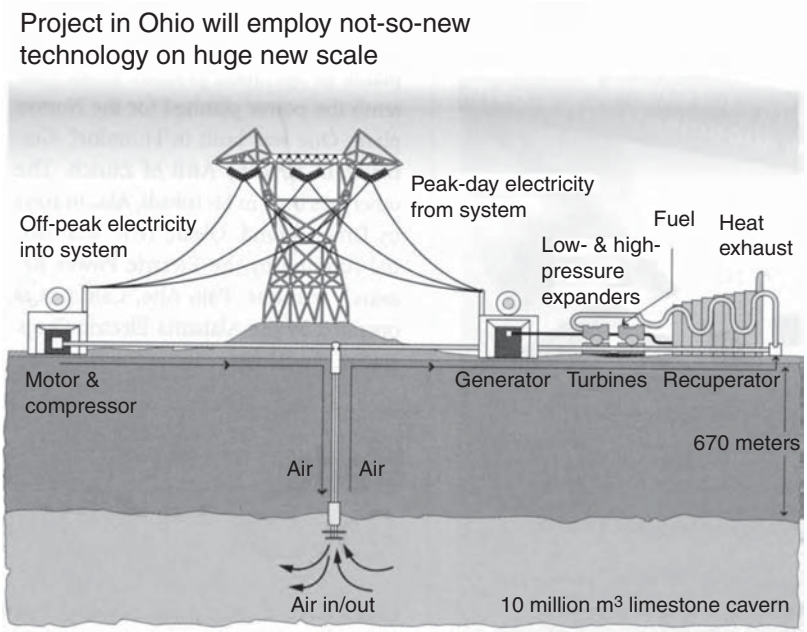

FIGURE 10.27 2700-MW power system to be installed for utility load leveling using compressed air energy storage at an Ohio mine. (From *IEEE Spectrum*, August 2001, p. 27. © IEEE. With permission.)

10.13 TECHNOLOGIES COMPARED

For a very large-scale energy storage, Enslin et al.[5] of KEMA investigated the feasibility of a 20-MWh energy storage system for a 100-MW Dutch wind farm. A minimum of 10-MWh capacity was found necessary for this wind farm, and a 10-MWh additional capacity was allowed to meet the losses during discharge with some margin. Water pump storage, compressed air pumped storage, and Pb-acid batteries were considered and compared for this project. They also conducted a parametric study with the storage capacity for potential applications in the 20 to 160 MWh range. The results of this study are shown in Figure 10.28. It shows that the Pb-acid battery is the least-cost option, followed by the pumped water, and then the compressed air systems. These trades, however, are extremely site-specific. The nature of air storage and its cost (e.g., free use of old mines) can alter the trades and the final installation decision.

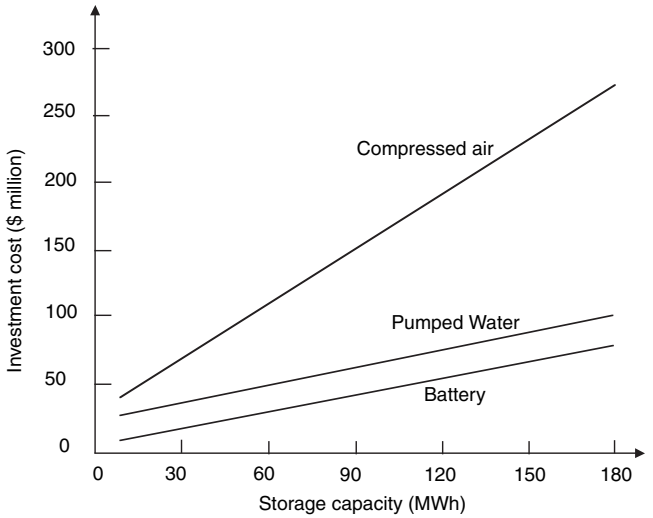

FIGURE 10.28 Energy storage capacity vs. investment cost of various alternative technologies. (Adapted from Enslin et al., *Renewable Energy World*, James & James, London, January–February 2004, p. 108.)

References

1. Riezenman, M.J., In search of better batteries, *IEEE Spectrum*, pp. 51–56, May 1995.
2. Wicks, F. and Halls, S., Evaluating performance enhancement of lead-acid batteries by force circulation of the electrolytic, Proceedings of the Intersociety Engineering Conference on Energy Conversion, Paper No. 180, 1995.
3. DeWinkel, C.C. and Lamopree, J.D., Storing power for critical loads, *IEEE Spectrum*, pp. 38–42, June 1993.
4. Balachandran, U., Super Power, Progress in developing the new superconductors, *IEEE Spectrum*, pp. 18–25, July 1997.
5 Enslin, J., Jansen, C., and Bauer, P., In store for the future, Interconnection and energy storage for offshore wind farms, *Renewable Energy World*, James & James Ltd., London, January–February 2004, pp. 104–113.

11 Power Electronics

Power electronic circuits in wind and photovoltaic (PV) power systems basically perform the following functions:

- Convert alternating current (AC) to direct current (DC)
- Convert DC to AC
- Control voltage
- Control frequency
- Convert DC to DC

These functions are performed by solid-state semiconductor devices periodically switched on and off at a desired frequency. Device costs in 2005 have declined to about a tenth of those in 1990, fueling an exponential growth in applications throughout the power industry. No other technology has brought about a greater change in power engineering, or holds a greater potential for bringing improvements in the future, than power electronic devices and circuits. In this chapter, we review the power electronic equipment used in modern wind and PV power systems.

11.1 BASIC SWITCHING DEVICES

Among a great variety of solid-state devices available in the market, some commonly used devices are as follows:

- Bipolar junction transistor (BJT)
- Metal-oxide semiconductor field effect transistor (MOSFET)
- Insulated gate bipolar transistor (IGBT)
- Silicon controlled rectifier (SCR), also known as the thyristor
- Gate turn-off thyristor (GTO)

For a specific application, the choice of device depends on the power, voltage, current, and frequency requirement of the system. A common feature of these devices is that all are three-terminal devices, as shown in their (generally used) circuit symbols in Figure 11.1. The two power terminals 1 and 0 are connected in the main power circuit, and the third terminal G, known as the gate terminal, is connected to an auxiliary control circuit. In a normal conducting operation, terminal 1 is generally at a higher voltage than terminal 0.

Because these devices are primarily used for switching power on and off as required, they are functionally represented by a gate-controlled switch (shown in the last row in Figure 11.1). In the absence of a control signal at the gate, the device resistance between the power terminals is large — a functional equivalent of an

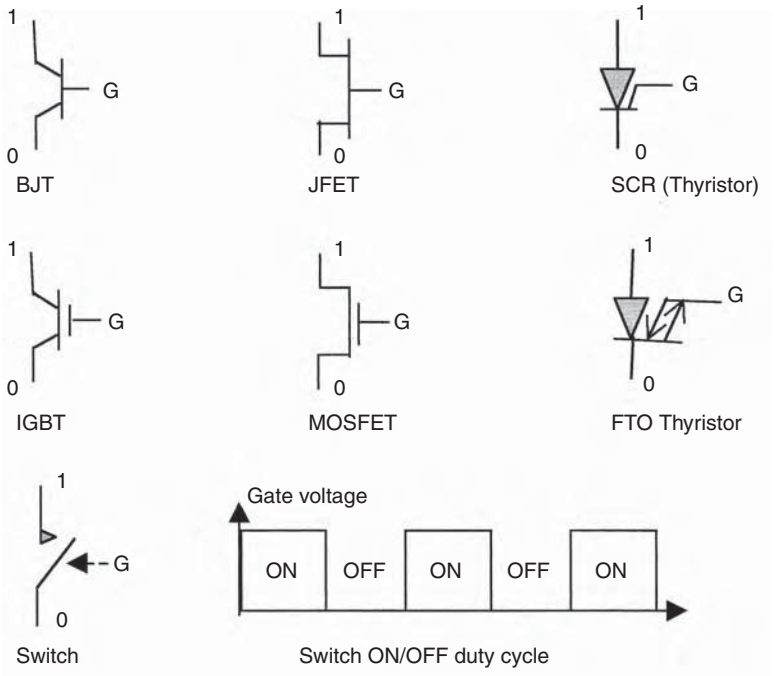

FIGURE 11.1 Basic semiconductor switching devices.

open switch. When the control signal is applied at the gate, the device resistance approaches zero, making the device behave like a closed switch. The device in this state lets the current flow freely through it.

The characteristics of switching devices commonly available in the market are listed in Table 11.1. The maximum voltage and current ratings along with unique operating features of transistors and SCRs commonly used in high-power applications, such as in wind and PV power systems, are listed in Table 11.2.

Thyristor technology has advanced dramatically into a variety of devices such as forced-commutated and line-commutated thyristors. GTO and static induction thyristors (SITHs) get turned on by a positive pulse to the thyristor gate and turned off by a negative pulse. They offer good forced-commutation techniques. GTOs are available in ratings of up to 4500 V/3000 A and SITHs up to 1200 V/300 A. Both have high flexibility and can be easily controlled. SITHs have a high-frequency switching capability greater than that of the GTOs, which are limited to about 10 kHz. The SCRs and IGBTs are limited to 100 Hz at present. IGBTs are less common but could give good control flexibility.

In general, BJTs (1200 V/400 A) have lower power-handling capabilities than thyristors, but they have good control characteristics and high-frequency switching capabilities.

MOSFETs are controlled by a gate voltage as opposed to other transistors controlled by a gate current and can be used at even higher switching frequencies but in low power ranges.

TABLE 11.1
Characteristics of Power Electronic Semiconductor Devices

Type	Function	Voltage	Current	Upper Frequency (kHz)	Switching Time (μsec)	On-State Resistance (mΩ)
Diode	General purpose	5000	5000	1	100	0.1–0.2
	High speed	3000	1000	10	2–5	1
	Schottky	<100	<100	20	0.25	10
Forced-turned-off thyristor	Reverse blocking	5000	5000	1	200	0.25
	High speed	1200	1500	10	20	0.50
	Reverse blocking	2500	400	5	40	2
	Reverse conducting	2500	1000	5	40	2
	GATT	1200	400	20	8	2
	Light triggered	6000	1500	1	200–400	0.5
TRIAC	—	1200	300	1	200–400	3–4
Self-turned-off thyristor	GTO	4500	3000	10	15	2–3
	SITH	1200	300	100	1	1–2
Power transistor	Single	400	250	20	10	5
		400	40	20	5	30
		600	50	25	2	15
	Darlington	1200	400	10	30	10
Power MOSFET	Single	500	10	100	1	1
		1000	5	100	1	2
		500	50	100	1	0.5
IGBT	Single	1200	400	100	2	60
MCT	Single	600	60	100	2	20

TABLE 11.2
Maximum Voltage and Current Ratings of Power Electronic Switching Devices

Device	Voltage Rating (volts)	Current Rating (amperes)	Operating Features
BJT	1500	400	Requires large current signal to turn on
IGBT	1200	400	Combines the advantages of BJT, MOSFET, and GTO
MOSFET	1000	100	Higher switching speed
SCR	6000	3000	Once turned on, requires heavy turn-off circuit

Power diode ratings can be as high as 5000 V/5000 A, with leakage currents in the off state reaching up to 100 A.

MOS controlled thyristor (MCT), reverse conducting thyristor (RCT), gate-assisted turn-off thyristor (GATT), and light-activated silicon controlled rectifier (LASCR) are other example of specialty devices, each having its niche application.

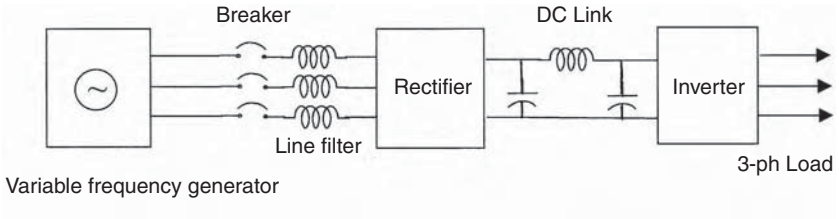

FIGURE 11.2 Variable-speed constant-frequency wind power system schematic.

Switching transistors of any type in power electronic equipment are triggered periodically on and off by a train of gate signals of suitable frequency. The gate signal may be of rectangular or any other wave shape and is generated by a separate triggering circuit, which is often called the *firing circuit*. Although the firing circuit has a distinct identity and many different design features, it is generally incorporated in the main component assembly.

The output frequency and voltage of a variable-speed wind power generator vary with the wind speed. The output is converted into a fixed voltage at 60 or 50 Hz to match with the utility requirement. In modern plants, this is accomplished by the power electronics scheme shown in Figure 11.2. The variable frequency is first rectified into a DC, which is then inverted back into a fixed-frequency AC. The increase in energy production from the variable-speed wind turbine over the lifetime of the plant more than offsets the added cost of the power electronic equipment.

In a PV power system, the DC power output of the PV array is inverted into 60 or 50 Hz AC using the inverter. The inverter circuit in the PV system is essentially the same as that used in the variable-speed wind power system.

The main power electronic components of the wind and PV power systems are, therefore, the rectifier and the inverter. Their circuits and the AC and DC voltage and current relationships are presented in the following sections.

11.2 AC–DC RECTIFIER

The circuit diagram of the full-bridge, three-phase, AC–DC rectifier is shown in Figure 11.3. The power switch generally used in the rectifier is the SCR. The average DC output voltage is given by:

$$V_{dc} = \frac{3\sqrt{2}}{\pi} V_L \cos\alpha \tag{11.1}$$

where

V_L = line-to-line voltage on the three-phase AC side of the rectifier and

α = angle of firing delay in the switching.

The delay angle is measured from the zero crossing in the positive half of the AC voltage wave. Equation 11.1 shows that the output DC voltage can be controlled

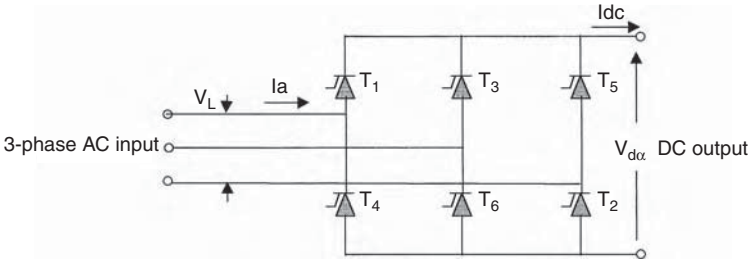

FIGURE 11.3 Three-phase, full-bridge, AC–DC controlled rectifier circuit.

by varying the delay angle α, which in turn controls the conduction (on-time) of the switch.

Superimposed on the DC voltage at the rectifier output are high-frequency AC harmonics (ripples). A harmonic filter is, therefore, needed to reduce the AC component of the output voltage and increase the DC component. An L–C filter does this with an inductor connected in series and a capacitor in parallel with the rectified output voltage.

The load determines the DC-side current as:

$$I_{DC} = \frac{\text{DC load power}}{V_{DC}} \tag{11.2}$$

In steady-state operation, the balance of power must be maintained on both AC and DC sides. That is, the power on the AC side must be equal to the sum of the DC load power and the losses in the rectifier circuit. The AC-side power is therefore:

$$P_{AC} = \frac{\text{DC load power}}{\text{Rectifier efficiency}} \tag{11.3}$$

Moreover, as we will see in Chapter 14, the three-phase AC power is given by:

$$P_{AC} = \sqrt{3}\, V_L I_L \cos\phi \tag{11.4}$$

where $\cos\phi$ is the power factor on the AC side. With a well-designed power electronic converter, the power factor on the AC side is approximately equal to that of the load.

From Equation 11.3 with Equation 11.4, we obtain the AC-side line current I_L.

11.3 DC–AC INVERTER

The power electronic circuit used to convert DC into AC is known as the inverter. The term "converter" is often used to mean either the rectifier or the inverter. The DC input to the inverter can be from any of the following sources:

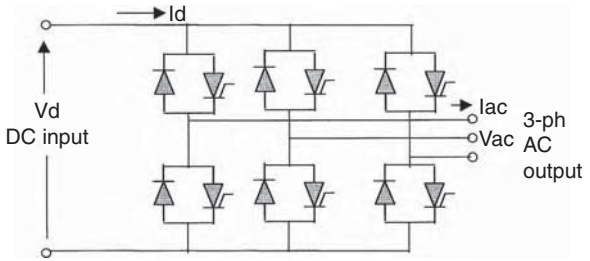

FIGURE 11.4 DC-to-three-phase AC inverter circuit.

- Variable-speed wind power system (rectified DC output)
- PV power modules
- Battery used in the wind or PV power system

Figure 11.4 shows the DC-to-three-phase AC inverter circuit diagram. The DC source current is switched successively in a 60-Hz three-phase time sequence so as to power the three-phase load. The AC current contains significant harmonics, as discussed in Section 14.7. The fundamental frequency (60 or 50 Hz) phase-to-neutral voltage is as follows:

$$V_{\text{ph}} = \frac{2\sqrt{2}}{\pi}\cos\left(\frac{\pi}{6}\right)V_{\text{dc}} \tag{11.5}$$

The line-to-line AC voltage is given by $\sqrt{3}\cdot V_{\text{ph}}$.

Unlike in BJT, MOSFET, and IGBT, the thyristor current once switched on must be forcefully switched off (commutated) to terminate conduction. If the thyristor is used as a switching device, the circuit must incorporate an additional commutating circuit to perform this function. The commutating circuit is a significant part of the inverter circuit. There are two main types of inverters, the line-commutated and the forced-commutated.

The line-commutated inverter must be connected to the AC system they feed power to. The design method is well developed and has been extensively used in high-voltage DC (HVDC) transmission line inverters. This inverter is simple and inexpensive, and can be designed for any size. The disadvantage is that it acts as a sink for reactive power and generates high content of high-frequency harmonics. Therefore, its output needs a heavy-duty harmonic filter to improve the quality of power at the AC output. This is done by an inductor connected in series and a capacitor in parallel to the inverted output voltage, similar to that done in the rectification process.

The poor power factor and high harmonic content in the line-commutated inverter significantly degrade the quality of power at the grid interface. This problem has been recently addressed by a series of design changes. Among them are the 12-pulse inverter circuit and increased harmonic filtering. These new design features have resulted in today's inverter operating with near-unity power factor and less than

3 to 5% total harmonic distortion. The quality of power at the utility interface at many modern wind power plants now exceeds that of the grid they interface.

The forced-commutated inverter does not have to supply load and can be free-running as an independent voltage source. The design is relatively complex and expensive. The advantage is that it can be a source of reactive power and the harmonic content is low.

Among the inverters commonly used for high-power applications, the 12-pulse line-commutated bridge topology prevails. However, with the advent of GTOs and high-power IGBTs, the voltage source inverter with shunt capacitors in the DC link is emerging as a preferred topology.

There are three basic approaches to inverter design:

- One inverter inverts all DC power (central inverter).
- Each string or multistring unit has its own inverter (string inverter).
- Each module has a built-in inverter (module inverter).

Economies of scale would dictate the most economical design for a given system. Present inverter prices are about $1500/kW for ratings below 1 kW, $1000/kW for 1 to 10 kW, $600/kW for 10 to 100 kW, and $400/kW for ratings near 1000 kW. The DC–AC efficiency with the transformer at full load is typically 85 to 90% in small ratings and 92 to 95% in large ratings.

Most PV inverters incorporate active and/or passive islanding protection. Islanding, in which a section of the PV system is disconnected from the grid and still supplies the local loads, is undesirable for personnel safety and quality of power, and because of the possibility of equipment damage in the event of automatic or manual reclosure of the power island with the grid. With islanding, an electrical generating plant essentially operates without an external voltage and frequency reference. Operating in parallel is the opposite of islanding. Islanding prevention is therefore included in the inverter design specification. A grid computer could offer an inexpensive and efficient means for participants to cooperate in reliable operation.

The inverter is a key component of the grid-connected PV system. In addition to high efficiency in DC–AC conversion and peak-power tracking, it must have low harmonic distortion, low electromagnetic interference (EMI), and high power factor. Inverter performance and testing standards are IEEE 929-2000 and UL 1741 in the U.S., EN 61727 in the EU, and IEC 60364-7-712 (the international standards).

The total harmonic distortion (THD) generated by the inverter is regulated by international standard IEC-61000-3-2. It requires that the full-load current THD be less than 5% and the voltage THD be less than 2% for the harmonic spectra up to the 49th harmonic. At partial loads, the THD is usually much higher.

11.4 CYCLOCONVERTER

The cycloconverter, a direct frequency changer, converts AC power of one frequency to AC power of another frequency by AC–AC conversion. By adding control circuitry capable of measuring the voltage and frequency of the bus bar and by comparing them with the desired voltage and frequency, we can obtain a constant voltage and

frequency output. The cycloconverter used to be more economical than the DC-link inverter but has been gradually replaced by the rectifier–inverter setup because of its high harmonic content and the decreasing price of power semiconductors. However, advances in fast switching devices and control microprocessors are increasing the efficiency and power quality of the cycloconverter.

Large three-phase cycloconverters use GTOs as semiconductors. The same thyristor commutating techniques are used in the cycloconverter as in the AC–DC rectifier. The cycloconverter uses one SCR for positive wave voltages and another for negative wave voltages. The firing angle of the thyristors controls the AC root mean square (rms) voltage, and the firing frequency controls the output frequency. However, the frequency control is complex.

11.5 GRID INTERFACE CONTROLS

At the utility interface, the power flow direction and magnitude depend on the voltage magnitude and the phase relation of the site voltage with respect to the grid voltage. The grid voltage being fixed, the site voltage must be controlled both in magnitude and phase in order to feed power to the grid when available and to draw from the grid when needed. If the inverter is already included in the system for frequency conversion, the magnitude and phase control of the site voltage is done with the same inverter at no additional hardware cost. The controls are accomplished as described in the following subsections.

11.5.1 Voltage Control

For interfacing with the utility grid lines, the renewable power system output voltage at the inverter terminals must be adjustable. The voltage is controlled by using one of the following two methods:

The first is controlling the alternating voltage output of the inverter using a tap-changing autotransformer at the inverter output (Figure 11.5). The tap changing is automatically obtained in a closed-loop control system. If the transformer has a

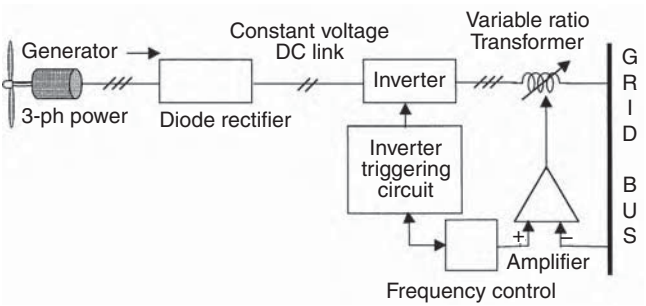

FIGURE 11.5 Voltage control by means of uncontrolled rectifier and variable-ratio tap-changing transformer.

phase-changing winding also, complete control of the magnitude and phase of the site voltage can be achieved. The advantages of this scheme are that the wave shape of the site output voltage does not vary over a wide range, and a high input power factor is achieved by using uncontrolled diode rectifiers for the DC-link voltage. The added cost of the transformer, however, can be avoided by using the following method.

Because the magnitude of the AC voltage output from the static inverter is proportional to the DC voltage input from the rectifier, voltage control can be achieved by operating the inverter with a variable DC-link voltage. Such a system also maintains the same output voltage, frequency, and wave shape over a wide range. However, in circuits deriving the load current from the commutating capacitor voltage of the DC link, the commutating capability decreases when the output voltage is reduced. This could lead to an operational difficulty when the DC-link voltage varies over a wide range, such as in a motor drive controlling the speed in a ratio exceeding 4:1. In renewable power applications, such a commutation difficulty is unlikely because the speed varies over a narrow range.

The variable DC-link voltage is obtained in two ways. One is to connect a variable-ratio transformer on the input side of the rectifier. The secondary tap changing is automatically obtained in a closed-loop control system. The other way is to use the phase-controlled rectifier in place of the uncontrolled rectifier in Figure 11.5. At reduced output voltages, this method gives a poor power factor and high harmonic content and requires filtering of the DC voltage before feeding to the inverter.

11.5.2 Frequency Control

The output frequency of the inverter solely depends on the rate at which the switching thyristors or transistors are triggered into conduction. The triggering rate is determined by the reference oscillator producing a continuous train of timing pulses, which are directed by logic circuits to the thyristor gating circuits. The timing-pulse train is also used to control the turn-off circuits. The frequency stability and accuracy requirements of the inverter dictate the selection of the reference oscillator. A simple temperature-compensated R–C relaxation oscillator gives frequency stability within 0.02%. When better stability is needed, a crystal-controlled oscillator and digital counters may be used, which can provide stability of .001% or better. Frequency control in a stand-alone power system is an open-loop system. Steady-state or transient load changes do not affect the frequency. This is a major advantage of the power electronic inverter over the old electromechanical means of frequency control.

11.6 BATTERY CHARGE/DISCHARGE CONVERTERS

The stand-alone PV power system uses the DC–DC converter for battery charging and discharging. DC–DC conversion techniques have undergone rapid development in recent decades. Over 500 different topologies currently exist, with more being developed each year. However, we will briefly cover a few basic topologies, leaving the details to advanced books dedicated to the subject.

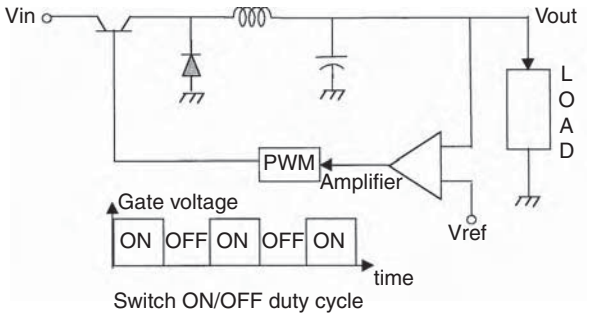

FIGURE 11.6 Battery charge converter for PV systems (DC–DC buck converter).

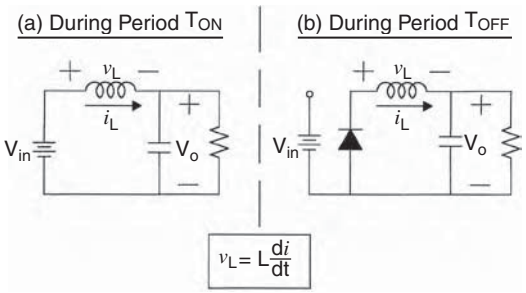

FIGURE 11.7 Charge converter operation during switch on-time and off-time.

11.6.1 Battery Charge Converter

Figure 11.6 is the most widely used DC–DC battery charge converter circuit, also called the *buck converter*. The switching device used in such a converter may be a BJT, MOSFET, or IGBT. The buck converter steps down the input bus voltage to the battery voltage during charging. The transistor switch is turned on and off at a high frequency (in tens of kHz). The duty ratio D of the switch is defined as:

$$D = \frac{\text{on-time}}{\text{Period}} = \frac{T_{on}}{T} = T_{on} \cdot \text{Switching frequency} \tag{11.6}$$

The operation of a charge converter during one complete cycle of the triggering signal is shown in Figure 11.7. During the on-time, the switch is closed and the circuit operates as in Figure 11.7(a). The DC source charges the capacitor and supplies power to the load via an inductor. During the off-time, the switch is opened and the circuit operates as in Figure 11.7(b). The power drawn from the DC source is zero. However, full-load power is supplied by the energy stored in the inductor and the capacitor, with the diode providing the return circuit. Thus, the inductor and the capacitor provide the required energy storage to ride through the off-period of the switch.

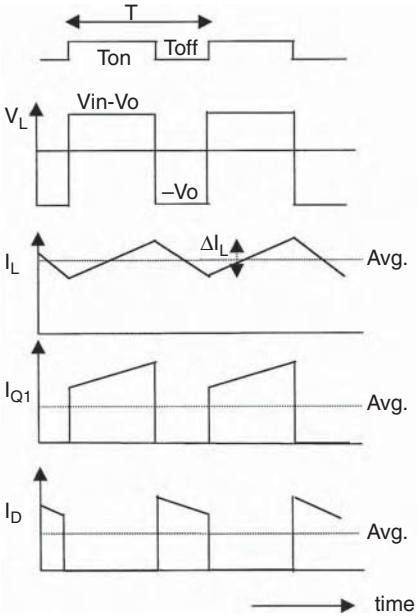

FIGURE 11.8 Current and voltage waveforms in the buck converter.

A simple analysis of this circuit is carried out in the following text. It illustrates the basic methodology of analyzing all power electronic circuits of this nature. It is based on the energy balance over one period of the switching signal as follows:

Energy supplied to the load over one complete period (i.e., $T_{on} + T_{off}$) = Energy drawn from the source during the on-time.
Energy supplied to the load during the off-time = Energy drawn from the inductor and capacitor during off-time.

Alternatively, the volt-second balance method is used. In essence, it gives the energy balance stated in the preceding text.

The voltage and current waveforms over one complete period are displayed in Figure 11.8. In the steady-state condition, the inductor volt-second balance during the on- and off-period must be maintained. Because the voltage across the inductor must equal $L\ dI_L/dt$,

$$\text{During on-time, } \Delta I_L L = (V_{in} - V_{out})T_{on} \tag{11.7}$$

$$\text{and during off-time, } \Delta I_L L = V_{out}T_{off} \tag{11.8}$$

If the inductor is large enough, as is usually the case in a practical design, the change in the inductor current is small, and the peak value of the inductor current is given by the following:

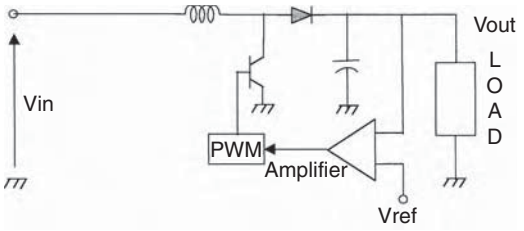

FIGURE 11.9 Battery discharge converter circuit for PV system (DC–DC boost converter).

$$I_{peak} = I_o + \tfrac{1}{2}\,\Delta I_L \tag{11.9}$$

where the load current $I_o(V_{out}/R_{load})$ is the average value of the inductor current.

The algebraic manipulation of the preceding equations leads to:

$$V_{out} = V_{in}D \tag{11.10}$$

It is seen from Equation 11.9 that the output voltage is controlled by varying the duty ratio D. This is done in a feedback control loop with the required battery charge current as the reference. The duty ratio is controlled by modulating the pulse width of T_{on}. Such a converter is, therefore, also known as the *pulse-width-modulated (PWM) converter.*

11.6.2 Battery Discharge Converter

The battery discharge converter circuit is shown in Figure 11.9. It steps up the sagging battery voltage during discharge to the required output voltage. When the transistor switch is on, the inductor is connected to the DC source. When the switch is off, the inductor current is forced to flow through the diode and the load. The output voltage of the boost converter is derived again from the volt-second balance in the inductor. With a duty ratio D of the switch, the output voltage is given by the following:

$$V_{out} = \frac{V_{in}}{1-D} \tag{11.11}$$

For all values of D less than 1, the output voltage is always greater than the input voltage. Therefore, the boost converter can only step up the voltage. On the other hand, the buck converter presented in the preceding section can only step down the input voltage. Combining the two converters in a cascade, therefore, gives a buck–boost converter, which can step down or step up the input voltage. A modified buck–boost converter often used for this purpose is shown in Figure 11.10. The voltage relation is obtained by combining the buck–boost converter voltage relations:

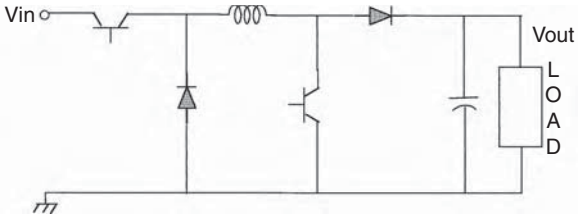

FIGURE 11.10 Buck–boost converter circuit (general DC–DC converter for PV systems).

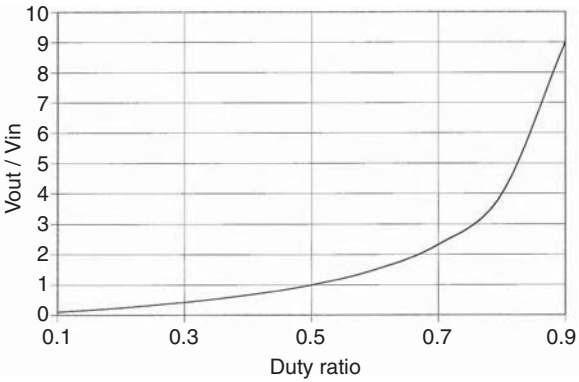

FIGURE 11.11 Buck–boost converter output-to-input ratio vs. duty ratio.

$$V_{\text{out}} = \frac{V_{\text{in}} D}{1 - D} \tag{11.12}$$

Equation 11.12 for the buck–boost converter shows that the output voltage can be higher or lower than the input voltage, depending on the duty ratio D (Figure 11.11).

In addition to its use in battery charging and discharging, the buck–boost converter is capable of four-quadrant operation with a DC machine when used in the variable-speed wind power systems. The converter is used in the step-up mode during the generating operation and in the step-down mode during the motoring operation.

11.7 POWER SHUNTS

In a stand-alone PV system, the power generation in excess of the load and battery-charging requirements must be dissipated in a dump load in order to control the output bus voltage. The dump load may be resistance heaters. However, when heaters cannot be accommodated in the system operation due to thermal limitations, dissipation of excess power can pose a problem. In such situations, shorting (shunting) the PV module to ground forces the module to operate under the short-circuit

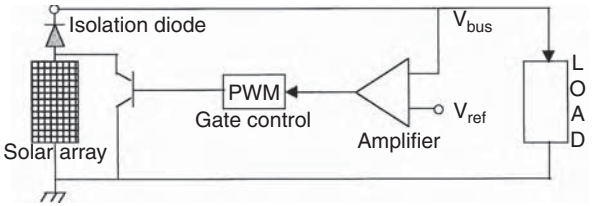

FIGURE 11.12 Power shunt circuit for shorting the module.

condition, delivering I_{sc} at zero voltage. No power is delivered to the load. The solar power remains on the PV array, raising the array temperature and ultimately dissipating the excess power in the surrounding air. The array area is essentially used here as a heat dissipater.

The circuit used for shunting the PV array is shown in Figure 11.12. A transistor is used as a switch. When the excess power is available, the bus voltage will rise above the rated value. This is taken as a signal to turn on the shunt circuits across the required number of PV modules. The shunt circuit is generally turned on or off by a switch controlled by the bus voltage reference. An electromechanical relay can perform this function, but the moving contacts have a much shorter life than a transistor switch. Therefore, such a relay is seldom used except in a small system.

Another application of the power shunt circuit is in a PV module dedicated to directly charging the battery without a charge regulator. When the battery is fully charged, the module is shunted to ground by shorting the switch. This way, the battery is always protected from overcharging.

For an array with several modules in parallel, the basic configuration shown in Figure 11.12 is used for each module separately, but the same gate signal is supplied to all modules simultaneously. For shunting large amounts of power, multiple shunt circuits can be switched on and off in sequence to minimize switching transients and EMI with neighboring equipment. For fine power control, one segment can be operated in the PWM mode.

Power electronics has a very wide scope and is a developing subject. The intent of this chapter is to present an overview of the basic circuits used in wind and PV power systems. Further details can be obtained from many excellent books on power electronics.[1–3]

References

1. Bose. B., *Power Electronics and Variable Frequency Drives*, IEEE Press, New York, 1996.
2. Dewan, S.B. and Straughen, A., *Power Semiconductor Circuits*, John Wiley & Sons, New York, 1975.
3. Mohan, N. and Undeland, T., *Power Electronics Converters, Applications and Design*, IEEE and John Wiley & Sons, New York, 1995.

12 Stand-Alone Systems

The stand-alone power system is used primarily in remote areas where utility lines are uneconomical to install due to the terrain, right-of-way difficulties, or environmental concerns. Building new transmission lines is expensive even without these constraints. A 230-kV line costs more than $1 million per mile. A stand-alone wind system would be more economical for remote villages that are farther than a couple of miles from the nearest transmission line. The break-even distance for a stand-alone photovoltaic (PV) system, however, is longer because PV energy is more expensive than wind energy at present.

Solar and wind power outputs can fluctuate on an hourly or daily basis. The stand-alone system, therefore, must have some means of storing excess energy on a sunny day for use on a rainy day. Alternatively, wind, PV, or both can be used in a hybrid configuration with a diesel engine generator in remote areas or with a fuel cell in urban areas.

According to the World Bank, more than 2 billion people live in villages that are not yet connected to utility lines. These villages are the largest potential market for stand-alone hybrid systems using a diesel generator with wind or PV for meeting their energy needs. Additionally, wind and PV systems create more jobs per dollar invested than many other industries. This, on top of bringing much needed electricity to rural areas, helps minimize migration to already strained cities in most countries.

Because power sources having significantly different performance characteristics must be used in parallel, the stand-alone hybrid system is technically more challenging and expensive to design than the grid-connected system that simply augments the existing utility network.

12.1 PV STAND-ALONE

The typical PV stand-alone system consists of a solar array and a battery connected as shown in Figure 12.1. The PV array supplies power to the load and charges the battery when there is sunlight. The battery powers the load otherwise. An inverter converts the DC power of the array and the battery into 60 or 50 Hz power. Inverters are available in a wide range of power ratings with efficiencies ranging from 85 to 95%. The array is segmented with isolation diodes for improving reliability. In such a design, if one string of the solar array fails, it does not load or short the remaining strings. Multiple inverters are preferred for reliability. For example, three inverters, each with a 35% rating, are preferred to one with a 105% rating. If one such inverter fails, the remaining two can continue supplying most loads until the failed one is repaired or replaced. The same design approach also extends to using multiple batteries.

Most stand-alone PV systems are installed in developing countries to provide basic necessities such as lighting and pumping water. Others go a step further (Figure 12.2).

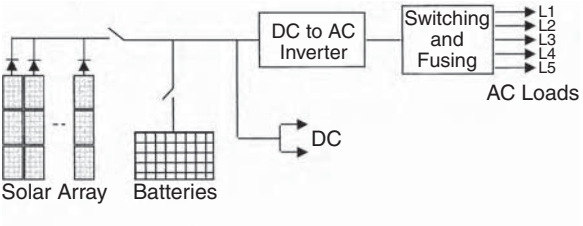

FIGURE 12.1 PV stand-alone power system with battery.

FIGURE 12.2 A traveling clinic uses photovoltaic electricity to keep vaccines refrigerated in the African desert area. (From Siemens Solar Industries. With permission.)

12.2 ELECTRIC VEHICLE

The solar electric car developed in the U.S. and in many other countries is an example of a stand-alone (or rather a "move-alone") PV power system. The first solar car was built in 1981 and driven across the Australian outback by Hans Tholstrup of Australia. A modern-day solar car has been developed and is commercially available, although it is more expensive than the conventional car at present. However, continuing development is closing the price gap every year.

A new sport at U.S. universities these days is the biennial solar car race. The Department of Energy (DOE) and several car manufacturers sponsor the race every 2 yr. It is open to all engineering and business students, who design, build, and run their cars across the heartland of America. The first U.S. solar car race was organized in 1990. Figure 12.3 shows one such car built at the University of Michigan in 1993. It finished first in the 1100-mi "Sunrayce" that started from Arlington, TX, and cruised through Oklahoma, Kansas, Missouri, and Iowa, and ended in Minnesota. It covered 1102 mi in six and a half days. In 1994, the same solar car finished the 1900-mi-long World Solar Challenge from Darwin to Adelaide across the Australian outback. Several dozens of teams participate in these races. Much more than just holding a race, the goal of this DOE program is to provide a hands-on, "minds-on" experience for young students in renewable power sources to display their

FIGURE 12.3 The University of Michigan solar car raced 1100 mi in the U.S. and 1900 mi in Australia. (From Patel, K.M., 1993 Sunrayce Team, University of Michigan.)

TABLE 12.1
Design Characteristic Range of Solar Race Cars Built by U.S. University Students for the Biennial 1100-mi "Sunrayce"

Design Parameters	Parameter Range
Solar array power capability (silicon crystalline, gallium arsenide)	750–1500 W
Battery (lead-acid, silver-zinc)	3.5–7 kWh
Electric motor (DC PM brushless)	4–8 hp
Car weight	500–1000 lb
Car dimensions	≈20-ft long × 7-ft wide × 3.5-ft high

inventiveness and use of the latest technology on wheels across the country. This biennial DOE-sponsored solar car race taps the bright young brains across the country.

The solar cars entering such university races generally have a wide range of design characteristics as listed in Table 12.1. The Michigan car was designed with silicon cells and a lead-acid battery, which was changed to a silver-zinc battery later on. With a permanent-magnet (PM) brushless DC motor, it reached a peak speed of 50 mph. The Gallium Arsenide PV cells are often used by many in the Australian race, but these are not allowed in the U.S. race. A few race cars have been designed with a Stirling engine driven by helium heated by solar energy instead of using PV cells. The design considerations include trading off among hundreds of technical parameters covered in this book and meeting their constraints *vis-a-vis* a vehicle design. But certain key technical elements are essential for winning. They are as follows:

- PV cells with high conversion efficiency
- Peak-power-tracking design
- Lightweight battery with high specific energy

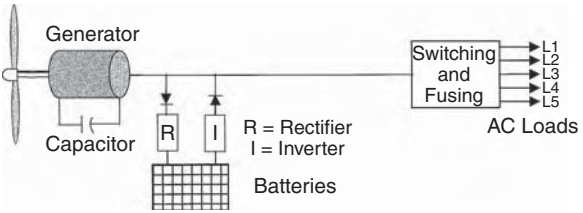

FIGURE 12.4 Stand-alone wind power system with battery.

- Energy-efficient battery charging and discharging
- Low aerodynamic drag
- High reliability without adding weight

The zinc-air battery discussed in Chapter 10 is an example of a lightweight battery. Chapter 9 covered the use of isolation diodes in a solar array for achieving reliability without adding weight, as well as the peak-power-tracking principle for extracting the maximum power out of the PV array for a given solar radiation.

After the car is designed and tested, developing a strategy to optimize solar energy capture and to use it efficiently, while maintaining the energy balance for the terrain and the weather on the day of the race, becomes the final test. The energy balance analysis methods for sizing the solar array and the battery are described later in this chapter.

12.3 WIND STAND-ALONE

A simple stand-alone wind system using a constant-speed generator is shown in Figure 12.4. It has many features that are similar to the PV stand-alone system. For a small wind system supplying local loads, a PM DC generator makes the system simple and easier to operate. The induction generator, on the other hand, gives AC power, which is used by most consumers these days. The generator is self-excited by shunt capacitors connected to the output terminals. The frequency is controlled by controlling the turbine speed. The battery is charged by an AC–DC rectifier and discharged through a DC–AC inverter.

The wind stand-alone power system is often used for powering farms (Figure 12.5). In Germany, nearly half the wind systems installed on farms are owned either by individual farmers or by an association. The performance of turbines under the "250 MW Wind" program is monitored and published by ISET, the Institute of Solar Energy and Technology at the University of Kassel.[1] The performance reports are also available from the German Wind Energy Institute. The reports list all installations, their performance, and any technical problems.

The steady-state performance of the electrical generator is determined by the theory and analyses presented in Chapter 5. This includes determining the capacitor rating needed to self-excite the generator for the desired voltage and frequency. The power factor of load has a great effect on both the steady-state and the transient performance of the induction generator. The load power factor can be unity, lagging,

FIGURE 12.5 Remote farms are a major market for the stand-alone power systems. (From World Power Technologies, Duluth, MN. With permission.)

or leading, depending on the load's being resistive, inductive, or capacitive, respectively. Most loads in the aggregate are inductive with a power factor of about 0.9 lagging. Unlike in the synchronous generator, the induction generator output current and power factor for a given load are determined by the generator parameters. Therefore, when the induction generator delivers a certain load, it also supplies a certain in-phase current and a certain quadrature current. The quadrature current is supplied by the capacitor bank connected to the terminals. Therefore, the induction generator is not suitable for supplying a low-power-factor load.

The transient performance of the stand-alone, self-excited induction generator, on the other hand, is more involved. The generalized d-q axis model of the generator is required. Computer simulation using a d-q axis model shows the following general transient characteristics:[2]

- Under sudden loss of self-excitation due to tripping-off of the capacitor bank, the resistive and inductive loads cause the terminal voltage to quickly reach the steady-state zero. A capacitive load takes a longer time before the terminal voltage decays to zero.
- Under sudden loading of the generator, resistive and inductive loads result in a sudden voltage drop, whereas a capacitive load has little effect on the terminal voltage.
- Under sudden loss of resistive and inductive loads, the terminal voltage quickly rises to its steady-state value.
- At light load, the magnetizing reactance changes to its unsaturated value, which is large. This makes the machine performance unstable, resulting in terminal-voltage collapse. To remedy this instability problem, the stand-alone induction generator must always have a minimum load, a dummy if necessary, permanently connected to its terminals.

12.4 HYBRID SYSTEMS

12.4.1 Hybrid with Diesel

The certainty of meeting load demands at all times is greatly enhanced by hybrid systems, which use more than one power source. Most hybrids use a diesel generator

FIGURE 12.6 A 300-kW PV–diesel hybrid system in Superior Valley, California. (From ASE Americas, Inc., Billerica, MA. With permission.)

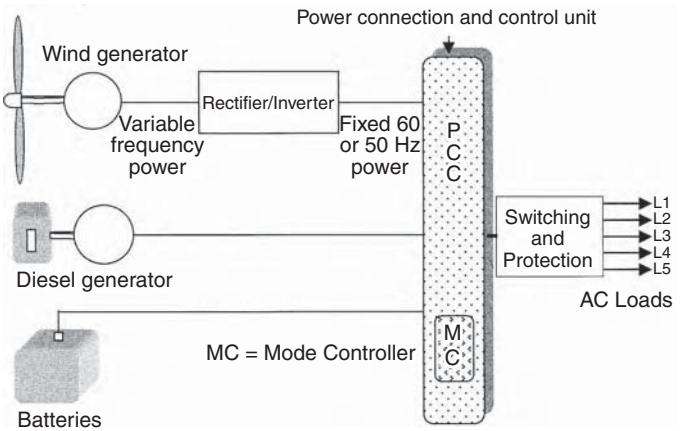

FIGURE 12.7 Wind–diesel–battery hybrid system.

with PV or wind, because diesel provides more predictable power on demand. A battery is used in addition to the diesel generator in some hybrids. The battery meets the daily load fluctuation, and the diesel generator takes care of the long-term fluctuations. For example, the diesel generator is used in the worst-case weather condition, such as an extended period of overcast skies or when there is no wind for several weeks.

Figure 12.6 shows a large PV–diesel hybrid system installed in California. The project was part of the Environmental Protection Agency's PV-Diesel program. Figure 12.7 is a schematic layout of a wind–diesel–battery hybrid system. The power connection and control unit (PCCU) provides a central place to make organized connections of most system components. In addition, the PCCU houses the following components:

FIGURE 12.8 Integrated power connection and control unit for wind–PV–battery hybrid system. (From World Power Technologies, Duluth, MN. With permission.)

- Battery charges and discharge regulators
- Transfer switches and protection circuit breakers
- Power flow meters
- Mode controller

Figure 12.8 shows a commercially available PCCU for hybrid power systems. The transient analysis of the integrated wind–PV–diesel requires an extensive model that takes the necessary input data and event definitions for computer simulation.[3]

12.4.2 Hybrid with Fuel Cell

In stand-alone renewable power systems of hybrid design, the fuel cell has the potential to replace the diesel engine in urban areas, where the diesel engine is undesirable due to its high carbon emissions. The airborne emission of a fuel cell power plant is negligible, about 25 g per MWh delivered. Factories and hospitals have started replacing the diesel generator with the fuel cell in their uninterruptible power supply (UPS) systems. Electric utility companies are considering the use of the fuel cell for meeting peak demand and for load leveling between day and night, and during the week.

On a small scale, a fuel cell about the size of a dishwasher can power a 3000 to 5000 ft^2 house without a grid connection. The mass-production cost of such a unit could be $2500 to $4000. The first fuel cells for use in residential areas were installed in 80 locations in New York state from 1998 to 2000. On a larger scale, New York Power Authority has installed 12 2.4-MW grid-connected fuel cell plants.

On a grander scale, Reykjavik, home to about 120,000 people in Iceland, plans to be the world's first hydrogen city. The first commercial hydrogen filling station opened in Iceland at an existing Shell retail station in Reykjavik. It dispenses hydrogen produced by electrolysis technology using renewable energy. A Mercedes car was the first to use this station, and three Daimler-Chrysler hydrogen-powered buses were placed in service in late 2003. As proposed by the University of Iceland,

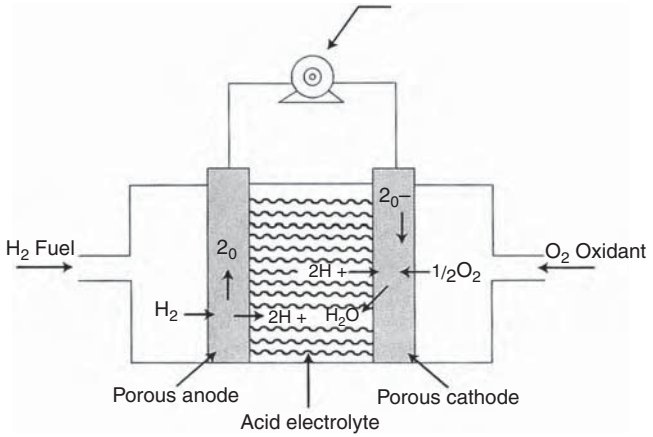

FIGURE 12.9 Fuel cell principle: hydrogen and oxygen in, electric power and water out.

the government hopes to transform the entire country into a hydrogen economy by 2050.

German car manufacturer Daimler-Benz and Ballard Power Systems of Canada have developed a solid polymer fuel cell for automobiles as an alternative to the battery. The first commercial fuel-cell-powered vehicle is already on the market.

The fuel cell is an electrochemical device that generates electricity by a chemical reaction that does not alter the electrodes and the electrolyte materials. This distinguishes the fuel cell from the electrochemical battery, in which the electrodes wear out. The concept of the fuel cell is the reverse of the electrolysis of water, in that hydrogen and oxygen are combined to produce electricity and water. Thus, the fuel cell is a static device that converts the chemical energy of fuel directly into electric energy. Because this process bypasses the thermal-to-mechanical conversion, and also because its operation is isothermal, the conversion efficiency is not Carnot limited. In this way, it differs from the diesel engine.

The fuel cell, developed by NASA as an intermediate-term power source for space applications, was first used in a moon buggy and continues to be used in the fleet of space shuttles. It also finds other niche applications at present. Providing electric power for a few days or a few weeks is not practical using the battery, but is effectively done with the fuel cell.

The basic constructional features of the fuel cell are shown in Figure 12.9. Hydrogen is combined with oxygen from the air to produce electricity. The hydrogen "fuel," however, does not burn as in the internal combustion engine; rather, it produces electricity by an electrochemical reaction. Water and heat are the only byproducts of this reaction if the fuel is pure hydrogen. With natural gas, ethanol, or methanol as the source of hydrogen, the byproducts include some carbon dioxide and traces of carbon monoxide, hydrocarbons, and nitrogen oxides. However, they are all less than 1% of that emitted by the diesel engine. The superior reliability, with no moving parts, is an additional benefit of the fuel cell as compared to the diesel generator. Multiple fuel cells stack up in a series–parallel combination for the required voltage and current, just as the electrochemical cells do in a battery.

TABLE 12.2
Characteristics of Various Fuel Cells

Fuel Cell Type	Working Temperature °C	Power Density W/cm²	Projected Life Hours	Projected Cost $/kW
PAFC	150–200	0.2–0.25	40,000	1000
AFC	60–100	0.2–0.3	10,000	200
MCFC	600–700	0.1–0.2	40,000	1000
SOFC	900–1000	0.25–0.3	40,000	1500
SPFC	50–100	0.35–0.6	40,000	200
DMFC	50–100	0.05–0.25	10,000	200

Note: PAFC = Phosphoric acid fuel cell; AFC = Alkaline fuel cell; MCFC = Molten carbonate fuel cell; SOFC = Solid-oxide fuel cell; SPFC = Solid-polymer fuel cell (also known as proton-exchange membrane fuel cell); and DMFC = Direct methanol fuel cell.

Source: From *IEEE Power and Energy*, November–December 2004, pp. 27–28.

The several types of fuel cells are as follows:

Phosphoric acid: This is the most established type of fuel cell for relatively small applications, such as in hospitals.
Alkaline: This is NASA's space shuttle fuel cell, too expensive for commercial use.
Proton-exchange membrane: This is the most promising fuel cell for small-scale applications such as homes.
Molten carbonate: This fuel cell works at high temperature (so it can be used for heating as well) and has a high efficiency of around 80%. It uses zirconium oxide. Although expensive, it is the most likely fuel cell to be used in large-scale applications.

The operating characteristics and projected costs of various fuel cell technologies under development at present are summarized in Table 12.2. Among the various alternative fuel cell types available, the optimum fuel cell for a specific application depends on the specific requirements, including the capital cost limitations.

Low-temperature (under 200°C) fuel cells are now commercially available from several sources. They use phosphoric acid as the electrolytic solution between the electrode plates. A typical low-temperature fuel cell with a peak-power rating of 200 kW costs under $1000 per kW at present, which is over twice the cost of the diesel engine. The fuel cell price, however, is falling with new developments being implemented every year.

High-temperature (over 1000°C) fuel cells yield a high electric energy per kilogram of fuel, but at a relatively high cost, limiting its use to special applications at present. Solid-oxide and molten carbonate fuel cells fall in this category. The industry interest in such cells is in large capacity for use in utility-scale power plants.

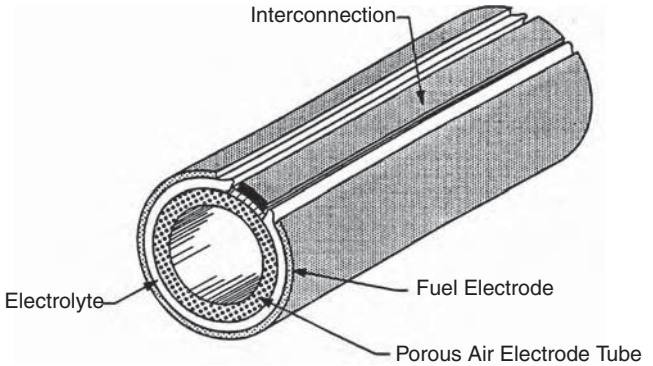

FIGURE 12.10 Air-electrode-supported-type tubular solid-oxide fuel cell design. (From Westinghouse Electric Co., a division of CBS Corp., Pittsburgh, PA. Reprinted with permission.)

The Fuel Cell Commercialization Group in the U.S. recently field-tested 2-MW molten carbonate direct fuel cells. The test results were a qualified success. Based on the results, multimegawatt commercial fuel cell power plants have been designed and installed in New York and other cities.

Solid-oxide fuel cells of several different designs, consisting of essentially similar materials for the electrolyte, the electrodes, and the interconnections, are being investigated worldwide. Most of the success to date has been achieved with the tubular geometry being developed by Westinghouse Electric in the U.S. and Mitsubishi Heavy Industries in Japan. The cell element in this geometry consists of two porous electrodes separated by a dense oxygen ion-conducting electrolyte as depicted in Figure 12.10.[4] It uses a ceramic tube operating at 1000°C. The fuel cell is an assembly of such tubes. SureCELL™ (Trademark of Westinghouse Electric Corporation, Pittsburgh, PA) is a solid-oxide high-temperature tubular fuel cell and is shown in Figure 12.11. It has been developed for multimegawatt combined cycle gas turbine and fuel cell plants, and is targeted at distributed power generation and cogeneration plants of up to 60-MW capacity. It is well suited for utility-scale wind and PV power plants. Inside SureCELL, natural gas or other fuels are converted to hydrogen and carbon monoxide by internal reformation. No external heat or steam is needed. Oxygen ions produced from an air stream react with the hydrogen and carbon monoxide to generate electric power and high-temperature exhaust gas.

Because of the closed-end tubular configuration, no seals are required and the relative cell movement due to differential thermal expansions is not restricted. This enhances the thermal cycle capability. The tubular configuration solves many of the design problems facing other high-temperature fuel cells. The overall efficiency of the SureCELL design is about 75%, compared to the 60% maximum possible using only the gas turbine (Figure 12.12). Environmentally, the solid-oxide fuel cell produces much lower CO_2, NOx, and virtually zero SOx compared with other fuel cell technologies.

These cells have shown good voltage stability with operating hours in service. During the 8 yr of failure-free steady-state operation of the early prototypes, they maintained the output voltage within 0.5% per 1,000 h of operation. The second

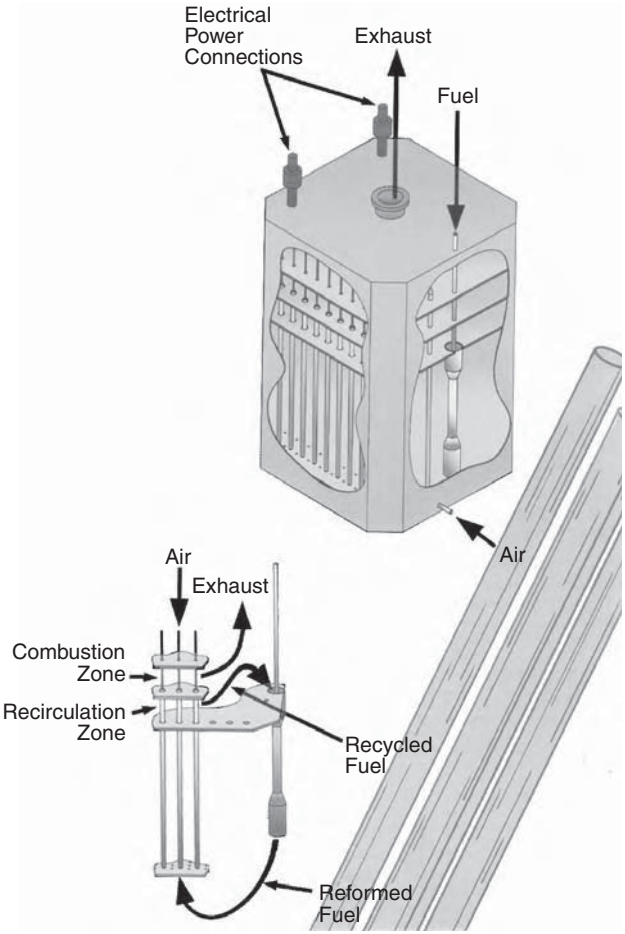

FIGURE 12.11 Seal-less solid-oxide fuel cell power generator. (From Westinghouse Electric Co., a division of CBS Corp., Pittsburgh, PA. Reprinted with permission.)

generation of the Westinghouse fuel cell shows even less voltage degradation, less than 0.1% per 1,000 h of operation. The SureCELL prototype has been tested for over 1,000 thermal cycles with zero performance degradation, and for 12,000 h of operation with less then 1% performance degradation. The estimated life is in tens of thousands of hours of operation.

The transient electrical performance model of the fuel cell includes electrochemical, thermal, and mass flow elements that affect the electrical output.[5] The electrical response of the cell to a load change is of primary interest. To design for the worst case, the performance is calculated for both constant reactant flow and constant inlet temperature.

When hydrogen is passed across the anode and a catalyst, it is possible to separate hydrogen into protons and electrons. The electrons will pass through an external circuit with a current and a voltage while the protons will go through the electrolyte.

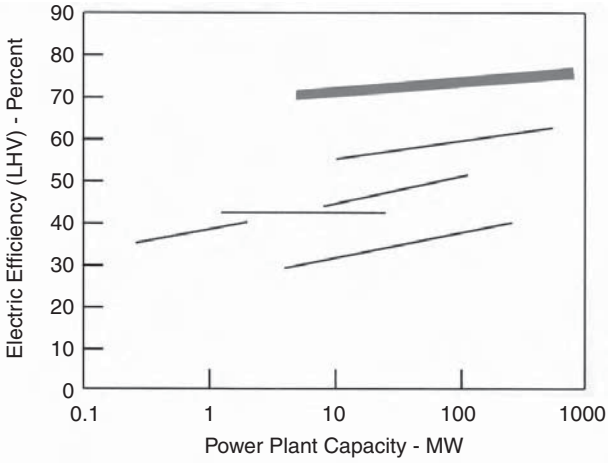

FIGURE 12.12 Natural gas power generation system efficiency comparison. (From Westinghouse Electric Co., a division of CBS Corp., Pittsburgh, PA. Reprinted with permission.)

The electrons come back from the electrical external circuit and they recombine with the protons and oxygen to produce water and heat. The reactions are described as follows:[6]

Anode reaction: $H_2 \longrightarrow 2H^+ + 2e^-$
Cathode reaction: $\frac{1}{2}O_2 + 2H^+ \longrightarrow H_2O$

Fuel cell efficiency is described by the thermodynamic efficiency as follows:

$$\eta_{th} = \Delta G/\Delta H \tag{12.1}$$

where
$\Delta G = nFE$ = Gibb's free energy of reaction (kJ/mol),
ΔH = reaction enthalpy (kJ/mol),
n = number of electrons involved,
F = Faraday's constant = 96485 C/mol, and
E = theoretical cell potential.

The number of electrons involved with hydrogen–oxygen is 4, and the theoretical cell potential 1.23 V. After meeting the various losses in the reaction, we get less than 1 V at the output terminals under load. The current, however, is proportional to the electrode area, which can be made large to provide a high current capability. Thus, each cell generates a low voltage and a high current. High operating voltage and current are obtained by placing multiple fuel cells in series–parallel combination, known as the *fuel cell stack*.

Hydrogen fuels can be stored in any one of the following ways, depending on the amount and duration of the storage:

- Underground, for large quantities of gas and also for long-term storage
- As liquid hydrogen for large quantities of gas, long-term storage, low electricity costs, or for applications requiring liquid hydrogen
- As compressed gas for small quantities of gas, high cycle times, or short storage times
- As metal hydrides for small quantities of gas

12.4.3 Mode Controller

The overall power system must be designed for a wide performance range to accommodate the characteristics of the diesel generator (or fuel cell), the wind generator, and the battery. As and when needed, switching to the desired mode of generation is done by the mode controller. Thus, the mode controller is the central monitor and controller of the system. It houses the microcomputer and software for the source selection, the battery management, and load-shedding strategy. The mode controller performs the following functions:

- Monitors and controls the health and state of the system
- Monitors and controls the battery state of charge
- Brings up the diesel generator when needed and shuts it off when not needed
- Sheds low-priority loads in accordance with the set priorities

The battery comes online by an automatic transfer switch, which takes about 5 msec to connect to the load. The diesel, on the other hand, is generally brought online manually or automatically after going through a preplanned strategy algorithm stored in the system computer. Even with an automatic transfer switch, the diesel generator takes a relatively long time to come online, typically about 20 sec.

The mode controller is designed and programmed with deadbands to avoid frequent changeover between sources for correcting small variations on the bus voltage and frequency. The deadbands avoid chatter in the system. Figure 12.13 is an example of a 120-V hybrid system's voltage-control regions. The deadbands are along the horizontal segments of the control line.

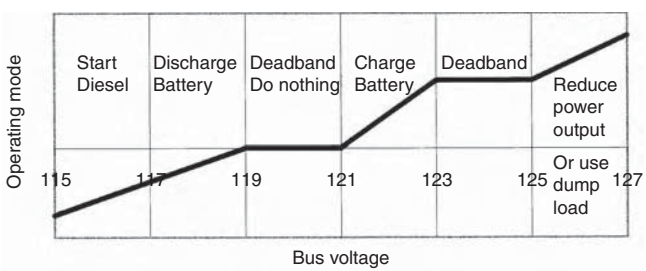

FIGURE 12.13 Mode controller deadbands eliminate system chatter.

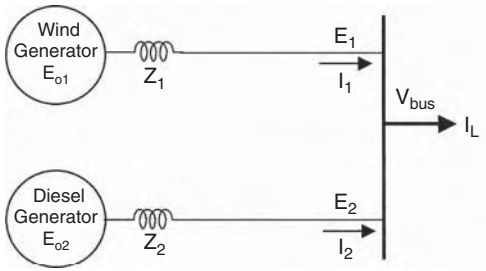

FIGURE 12.14 Thevenin's equivalent model of two sources in a hybrid power system.

As a part of the overall system controller, the mode controller may incorporate the maximum power extraction algorithm. The dynamic behavior of the closed-loop system, following common disturbances such as changes in sunlight due to clouds, wind fluctuation, sudden load changes, and short-circuit faults, is taken into account in a comprehensive design.[7]

12.4.4 Load Sharing

Because the wind, PV, battery, and diesel (or fuel cell) in various combinations are designed to operate in parallel, as is often the case, the load sharing between them is one of the key design aspects of the hybrid system. For example, in the wind–diesel hybrid system (Figure 12.14), the electrical properties of the two systems must match so that they share the load in proportion to their rated capacities.

For determining the load sharing, the two systems are first reduced to their respective Thevenin equivalent circuit model, in which each system is represented by its internal voltage and the series impedance. This is shown in Figure 12.14. The terminal characteristics of the two generators are then given by the following:

$$E_1 = E_{01} - I_1 Z_1$$
$$E_2 = E_{02} - I_2 Z_2 \tag{12.2}$$

where subscripts 1 and 2 represent systems 1 and 2, respectively,
E_0 = internally generated voltage,
Z = internal series impedance, and
E = terminal voltage of each system.

If the two sources are connected together, their terminal voltages E_1 and E_2 must be equal to the bus voltage V_{bus}. Additionally, the sum of the component loads I_1 and I_2 must be equal to the total load current I_L. Thus, the conditions imposed by the terminal connection are as follows:

$$E_1 = E_2 = V_{bus} \text{ and } I_1 + I_2 = I_L \tag{12.3}$$

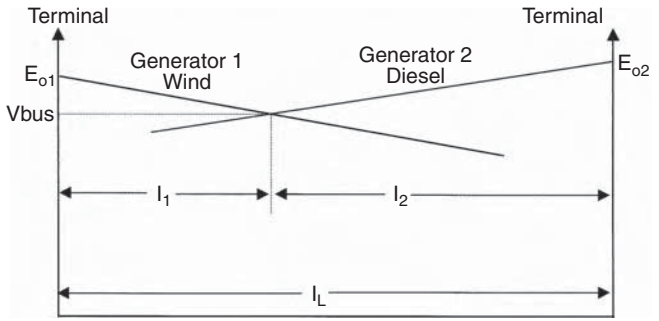

FIGURE 12.15 Graphical determination of load shared by two sources in a hybrid power system.

These imposed conditions, along with the machines' internal characteristics E_0 and Z, would determine the load sharing I_1 and I_2. The loading on an individual source is determined algebraically by solving the two simultaneous equations for the two unknowns, I_1 and I_2. Alternatively, the solution is found graphically as shown in Figure 12.15. In this method, the E vs. I characteristics of the two power sources are first individually plotted on the two sides of the current axis (horizontal). The distance between the two voltage axes (vertical) is kept equal to the total load current I_L. The power sources feeding power in parallel to a common bus share the load such that their terminal voltages are exactly equal. This condition, imposed by connecting them together at the bus, is met at the point of intersection of the two load lines. The point P in the figure, therefore, decides the bus voltage and the load sharing. The currents I_1 and I_2 in the two generators are then read from the graph.

Controlling the load sharing requires controlling the E vs. I characteristics of the sources. This may be easy in the case of the separately excited DC or the synchronous generator used with the diesel engine. It is, however, difficult in the case of the induction machine. Usually the internal impedance Z is fixed once the machine is built. Care must be exercised in hybrid design to ensure that sufficient excitation control is built in for the desired load sharing between the sources.

The load-sharing strategy can vary depending on the priority of loads and the cost of electricity from alternative sources. In a wind–diesel system, for example, diesel electricity is generally more expensive than wind (~25 vs. 5 cents/kWh). Therefore, all priority-1 (essential) loads are met first by wind as far as possible and then by diesel. If the available wind power is more than priority-1 loads, wind supplies part of priority-2 loads and the diesel is not run. If wind power now fluctuates on the downside, the lower-priority loads are shed to avoid running the diesel. If wind power drops further to cut into the priority-1 load, the diesel is brought online again. Water pumping and heater loads are examples of priority-2 loads.

12.5 SYSTEM SIZING

For determining the required capacity of the stand-alone power system, estimating the peak-load demand is only one aspect of the design. Estimating the energy

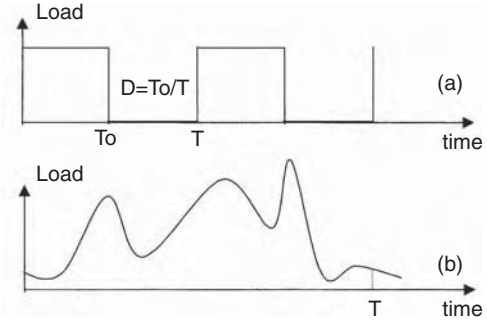

FIGURE 12.16 Duty ratio and peak power of intermittent loads.

required over the duration selected for the design is discussed in the following subsections.

12.5.1 Power and Energy Estimates

System sizing starts with compiling a list of all loads that are to be served. Not all loads are constant or are connected at all times. Therefore, all loads are expressed in terms of the peak watts they consume and the duty ratio. The peak power consumption is used in determining the wire size connecting to the source. The duty ratio is used in determining the contribution of an individual load in the total energy demand. If the load has clean on–off periods as shown in Figure 12.16(a), then the duty ratio D is defined as $D = T_o/T$, where T_o is the time the load is on and T is the period of repetition. For the irregularly varying loads shown in Figure 12.16(b), the duty ratio is defined as the actual energy consumed in one period over the peak power multiplied by the period, i.e.:

$$D = \frac{\text{energy in watthours consumed in one repetition period}}{\text{peak power in watts} \cdot \text{repetition period in hours}} \tag{12.4}$$

Once the peak power consumption and the duty ratio of all loads are compiled, the product of the two is the actual share of the energy requirement of that load on the system during one repetition period. If there are distinct intervals in the period, for instance, between the battery discharge and charge intervals, then the peak power and duty ratio of each load are computed over the two intervals separately. As a simple example of this in a solar power system, one interval may be from 8 a.m. to 6 p.m. and the other from 6 p.m. to 8 a.m. The power table is then prepared as shown in Table 12.3.

In a community of homes and businesses, not all connected loads draw power simultaneously. The statistical time staggering in their use results in the average power capacity requirement of the plant's being significantly lower than the sum of the individually connected loads. The National Electrical Code® provides factors for determining the average community load in normal residential and commercial areas (Table 12.4). The average plant capacity is then determined as follows:

TABLE 12.3
Power and Energy Compilation Table for Energy Balance Analysis

Load	8 a.m. to 6 p.m. (Interval A) (Battery on Charge)			6 p.m. to 8 a.m. (Interval B) (Battery on Discharge)		
	Peak Watts	Duty Ratio	Energy per Period (Wh)	Peak Watts	Duty Ratio	Energy per Period (Wh)
Load $_1$	P_{1a}	D_{1a}	E_{1a}	P_{1b}	D_{1b}	E_{1b}
Load $_2$	P_{2a}	D_{2a}	E_{2a}	P_{2b}	D_{2b}	E_{2b}
…	…	…	…	…	…	…
Load $_n$	P_{na}	D_{na}	E_{na}	P_{nb}	D_{nb}	E_{nb}
Total	ΣP_a		ΣE_a	ΣP_b		ΣE_b

Note: Total battery discharge required = ΣE_b wattshours.

TABLE 12.4
NEC® Demand Factors

Number of Dwellings	Demand Factor
3	0.45
10	0.43
15	0.40
20	0.38
25	0.35
30	0.33
40	0.28
50	0.26
>62	0.23

Source: Adapted from *National Electrical Code® Handbook*, 7th ed., 1996, Table 220–232.

$$\text{Required power system capacity} = \text{NEC® factor from Table 12.4} \times \text{Sum of connected loads} \tag{12.5}$$

12.5.2 Battery Sizing

The battery ampere-hour capacity to support the load energy requirement of E_{bat} as determined in Table 12.3 or equivalent is given by the following:

$$Ah = \frac{E_{bat}}{\eta_{disch}\left[N_{cell}V_{disch}\right]DoD_{allowed}N_{bat}} \tag{12.6}$$

where

E_{bat} = energy required from the battery per discharge,
η_{disch} = efficiency of discharge path, including inverters, diodes, and wires, etc.,
N_{cell} = number of series cells in one battery,
V_{disch} = average cell voltage during discharge,
$DoD_{allowed}$ = maximum DoD allowed for the required cycle life, and
N_{bat} = number of batteries in parallel.

Example: The following example illustrates the use of this formula to size the battery. Suppose we want to design a battery for a stand-alone power system, which charges and discharges the battery from a 110-V DC solar array. For the DC–DC buck converter that charges the battery, the maximum available battery-side voltage is 70 V for it to work efficiently in the pulse-width-modulated (PWM) mode. For the DC–DC boost converter discharging the battery, the minimum required battery voltage is 45 V. Assuming that we are using NiMH electrochemistry, the cell voltage can vary from 1.55 V when fully charged to 1.1 V when fully drained to the maximum allowable DoD. Then, the number of cells needed in the battery is less than 45 (70/1.55) and more than 41 (45/1.1). Thus, the number of cells in the battery, estimated from voltage considerations, must be between 41 and 45. It is generally more economical to use fewer cells of a higher capacity than to use more lower-capacity cells. We, therefore, select 41 cells in the battery design.

Now, let us assume that the battery is required to discharge a total of 2 kW load for 14 h (28,000 Wh) every night for 5 yr before replacement. The lifetime requirement is, therefore, $5 \times 365 = 1{,}825$ cycles of deep discharge. For the NiMH battery, the cycle life at full depth of discharge is 2,000. Because this is greater than the 1,825 cycles required, we can fully discharge the battery every night for 5 yr. If the discharge efficiency is 80%, the average cell discharge voltage is 1.2 V, and we require three batteries in parallel for reliability, each battery ampere-hour capacity calculated from the above equation is as follows:

$$Ah = \frac{28000}{0.80 \times \left[41 \times 1.2\right] \times 1.0 \times 3} = 237 \tag{12.7}$$

Three batteries, each having 41 series cells of ampere-hour capacity 237, therefore, will meet the system requirement. We must also allow some margin to account for the uncertainty in estimating the loads.

12.5.3 PV Array Sizing

The basic tenet in sizing a stand-alone "power system" is to remember that it is really a stand-alone "energy system." It must, therefore, maintain the energy balance over the specified period. The energy drained during lean times must be made up by the positive balance during the remaining time of the period if there is no other source of energy in parallel. A simple case of a constant load on a PV system using

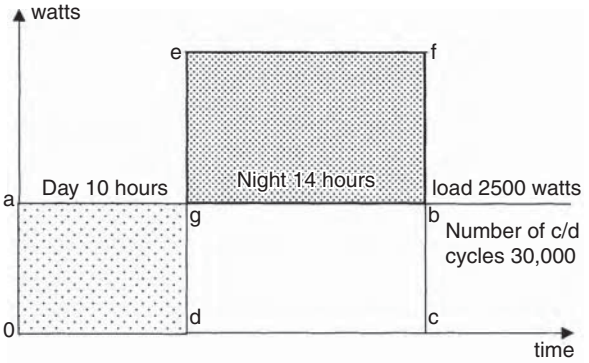

FIGURE 12.17 Energy balance analysis over one load cycle.

solar arrays perfectly pointed toward the sun for 10 h of the day is shown in Figure 12.17 to illustrate the point. The solar array is sized such that the two shaded areas on the two sides of the load line must be equal. That is, the area *oagd* must be equal to the area *gefb*. The system losses in the round-trip energy transfers, e.g., from and to the battery, adjust the available load to a lower value.

In general, the stand-alone system must be sized so as to satisfy the following energy balance equation over one period of repetition:

$$\int_{8\text{ a.m.}}^{6\text{ p.m.}} (\text{solar radiation} \cdot \text{conversion efficiency})\,dt = \int_{8\text{ a.m.}}^{6\text{ p.m.}} (\text{loads} + \text{losses} + \text{charge power} + \text{shunt power})\,dt + \int_{6\text{ p.m.}}^{8\text{ a.m.}} (\text{loads} + \text{losses})\,dt \tag{12.8}$$

Or, in discrete time intervals of constant load and source power,

$$\sum_{8\text{ a.m.}}^{6\text{ p.m.}} (\text{solar radiation} \cdot \text{conversion efficiency})\,\Delta t = \sum_{8\text{ a.m.}}^{6\text{ p.m.}} (\text{loads} + \text{losses} + \text{charge power} + \text{shunt power})\,\Delta t + \sum_{6\text{ p.m.}}^{8\text{ a.m.}} (\text{loads} + \text{losses})\,\Delta t \tag{12.9}$$

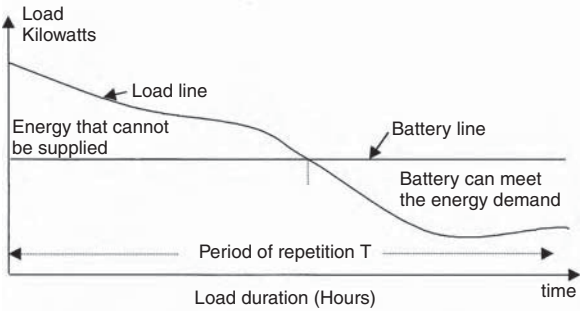

FIGURE 12.18 Effect of battery size on load availability for given load duration curve.

12.6 WIND FARM SIZING

In a stand-alone wind farm, selecting the number of towers and the battery size depends on the load power availability requirement. A probabilistic model can determine the number of towers and the size of the battery storage required for meeting the load with a required certainty. Such a model can also be used to determine the energy to be purchased from, or injected into, the grid if the wind power plant were connected to the grid. In the probabilistic model, wind speed is taken as a random variable. The load is treated as an independent variable. The number of wind turbines and the number of batteries are also variables in the analysis. Each turbine in a wind farm may or may not have the same rated capacity and the same outage rate. In any case, the hardware failure rates in individual turbines are independent of each other. The resulting model has a joint distribution of the available wind power (wind speed variations) and the operating mode (each turbine working or not working). The events of these two distributions are independent. For a given load duration curve over a period of repetition, the expected energy not supplied to the load by the hybrid system clearly depends on the size of the battery, as shown in Figure 12.18. The larger the battery, the higher the horizontal line, thus decreasing the duration of the load not supplied by the system.

With such a probabilistic model, the time for which the load is not supplied by the system is termed as the *Expected Energy Not Supplied* (*EENS*). This is given by the shaded area on the left-hand side. The Energy Index of Reliability (*EIR*) is then given by the following:

$$EIR = 1 - \frac{EENS}{E_o} \tag{12.10}$$

where E_o is the energy demand on the system over the period under consideration, which is the total area under the load duration curve. The results of such a probabilistic study[7,8] are shown in Figure 12.19, which indicates the following:

- The higher the number of wind turbines, the higher the *EIR*

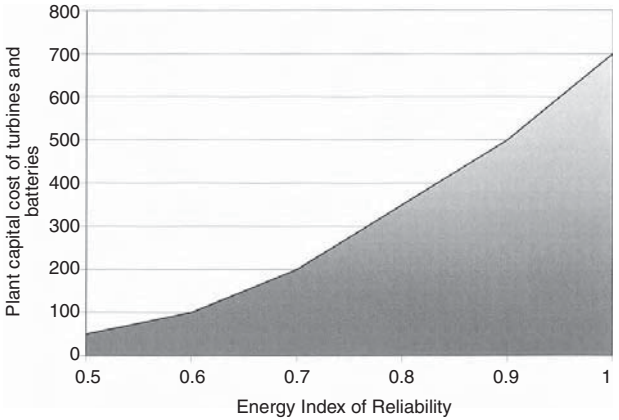

FIGURE 12.19 Relative capital cost vs. *EIR* with different numbers of wind turbines and battery sizes.

- The larger the battery size, the higher the *EIR*
- The higher the *EIR* requirement, the higher the number of required towers and batteries, with a higher project capital cost

Setting an unnecessarily high *EIR* requirement can make the project uneconomical. For this reason, *EIR* must be set after a careful optimization of the cost and the consequences of not meeting the load requirement during some portion of the time period.

References

1. Institute of Solar Energy and Technology Annual Report, Kassel, Germany, 1997.
2. Wang, L. and Su, J., Dynamic Performance of an Isolated Self-Excited Induction Generator under Various Load Conditions, IEEE Power Engineering Paper No. PE-230-EC-1-09, 1997.
3. Bonarino, F., Consoli, A., Baciti, A., Morgana, B., and Nocera, U., Transient Analysis of Integrated Diesel-Wind-Photovoltaic Generation Systems, IEEE Paper No. PE-425-EC-104, July 1998.
4. Singhal, S.C., Status of solid oxide fuel cell technology, Proceedings of the 17th Riso International Symposium on Material Science, High Temperature Electrochemistry, Ceramics and Metals, Roskilde, Denmark, September 1996.
5. Hall, D.J. and Colclaser, R.G., Transient Modeling and Simulation of a Tubular Solid Oxide Fuel Cell, IEEE Paper No. PE-100-EC-004, July 1998.
6. Appleby, A.J., *Fuel Cells: Trends in Research and Applications*, Hemisphere Publishing, New York, 1985, p. 146.
7. Abdin, E.S., Asheiba, A.M., and Khatee, M.M., Modeling and Optimum Controllers Design for a Stand-Alone Photovoltaic-Diesel Generating Unit, IEEE Paper No. PE-1150-0-2, 1998.
8. Baring-Gould, E.I., Hybrid2, The Hybrid System Simulation Model User Manual, NREL Report No. TP-440-21272, June 1996.

13 Grid-Connected Systems

Wind and photovoltaic (PV) power systems have made a successful transition from small stand-alone sites to large grid-connected systems. The utility interconnection brings a new dimension to the renewable power economy by pooling the temporal excess or the shortfall in the renewable power with the connecting grid that generates base-load power using conventional fuels. This improves the overall economy and load availability of the renewable plant site — the two important factors of any power system. The grid supplies power to the site loads when needed or absorbs the excess power from the site when available. A kilowatthour meter is used to measure the power delivered to the grid, and another is used to measure the power drawn from the grid. The two meters are generally priced differently on a daily basis or on a yearly basis that allows energy swapping and billing the net annual difference.

Figure 13.1 is a typical circuit diagram of the grid-connected PV power system. It interfaces with the local utility lines at the output side of the inverter as shown. A battery is often added to meet short-term load peaks. In the U.S., the Environmental Protection Agency sponsors grid-connected PV programs in urban areas where wind towers would be impractical. In recent years, large building-integrated PV installations have made significant advances by adding grid connections to the system design. For example, Figure 13.2 shows the building-integrated PV system on the roof of the Northeastern University Student Center in Boston. The project was part of the EPA PV DSP program. The system produces 18 kW power and is connected to the grid. In addition, it collects sufficient research data using numerous instruments and computer data loggers. The vital data are sampled every 10 sec, and are averaged and stored every 10 min. The incoming data includes information about air temperature and wind speed. The performance parameters include direct current (DC) voltage and current generated by the PV roof and the alternating current (AC) power at the inverter output side.

In the U.K., a 390-m^2 building-integrated PV system has been in operation since 1995 at the University of Northumbria, Newcastle (Figure 13.3). The system produces 33,000 kWh electricity per year and is connected to the grid. The PV panels are made of monocrystalline cells with a photoconversion efficiency of 14.5%.

On the wind side, most grid-connected systems are large utility-scale power plants. A typical equipment layout in such a plant is shown in Figure 13.4. The wind generator output is at 690-V AC, which is raised to an intermediate level of 35 kV by a pad-mounted transformer. An overhead transmission line provides a link to the site substation, where the voltage is raised again to the grid level. The site computer, sometimes using multiplexers and remote radio links, controls the wind turbines in response to the wind conditions and load demand.

Large wind systems being installed now generally operate at variable speeds to maximize the annual energy yield. The power schematic of such a system is shown in Figure 13.5. The variable-frequency generator output is first rectified into DC and then inverted into a fixed-frequency AC. Before the inversion, harmonics in rectified

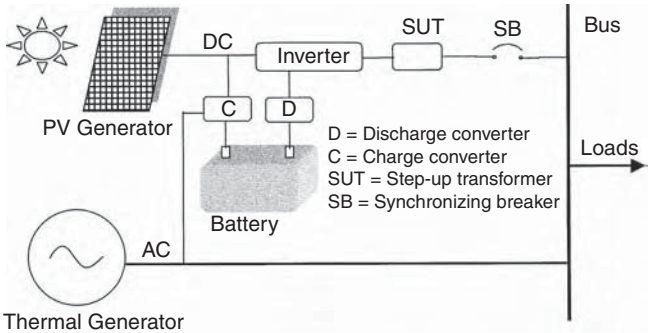

FIGURE 13.1 Electrical schematic of the grid-connected PV system.

FIGURE 13.2 18 kW grid-connected PV system on the Northeastern University Student Center in Boston. (Source: ASE Americas, Billerica, MA. With permission.)

DC are filtered out by an inductor and a capacitor. The frequency reference for inverter firing and the voltage reference for rectifier phase-angle control are taken from the grid lines. The rotor tip speed ratio (TSR) computed with the measured wind speed is continuously compared with the optimum reference value stored in the computer. The turbine speed is accordingly changed to assure maximum power generation at all times.

Most utility-scale wind turbines require a minimum wind speed of about 5 m/sec (12 mph). Therefore, 30 to 40% of the time, they run feeding the grid. Other times, the grid acts as a backup power source for local loads.

13.1 INTERFACE REQUIREMENTS

Both the wind and PV systems interface the grid at the output terminals of a synchronizing breaker after the inverter. The power flows in either direction depending on the site voltage at the breaker terminals. The fundamental requirements on the site voltage for interfacing with the grid are as follows:

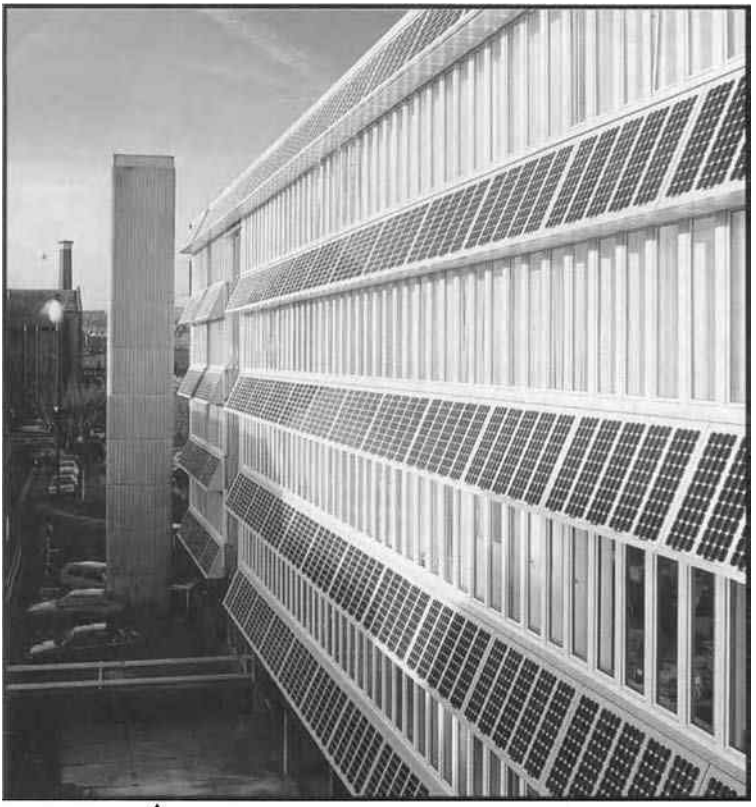

▲

project	University of Northumbria
location	Newcastle
consulting engineer	Ove Arup and Partners
date completed	October 1995
area of solar facade	390m^2
electricity generated	33,000 kWh/year
cell material	monocrystalline
efficiency	14.5%
number of panels	465
orientation	16° east of south
angle of orientation	25°
grid connected	yes

FIGURE 13.3 Grid-connected PV system at the University of Northumbria, Newcastle, U.K. The 390-m^2 monocrystalline modules produce 33,000 kWh per year. (From *Professional Engineer*, publication of the Institution of Mechanical Engineers, London. With permission.)

- The voltage magnitude and phase must equal that required for the desired magnitude and direction of the power flow. The voltage is controlled by the transformer turn ratio or the power electronic converter firing angle in a closed-loop control system.
- The frequency must be exactly equal to that of the grid or else the system will not work. To meet the exacting frequency requirement, the only

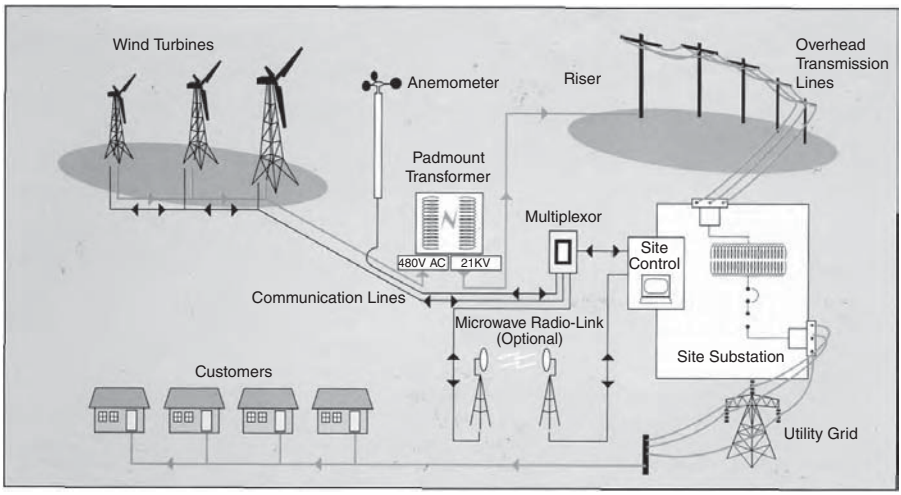

FIGURE 13.4 Electrical component layout of the grid-connected wind power system. (From AWEA/IEA/CADDET Technical Brochure, 1995.)

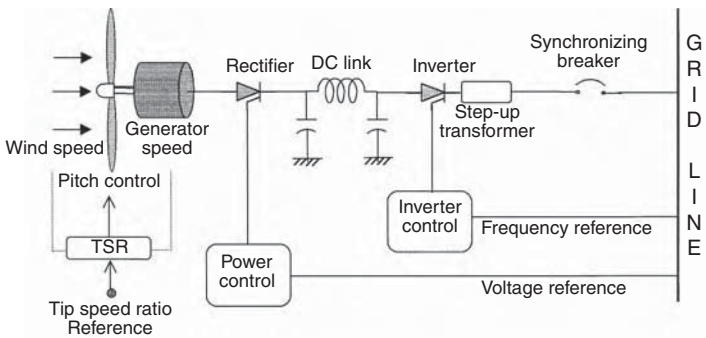

FIGURE 13.5 Electrical schematic of the grid-connected variable-speed wind power system.

effective means is to use the utility frequency as the inverter switching frequency reference.

- In the wind system, the base-load synchronous generators in the grid provide the magnetizing current for the induction generator.

The interface and control issues are similar in many ways in the PV and wind systems. The wind system, however, is more involved. The electrical generator and turbine, due to their large inertia, introduce certain dynamic issues not applicable in the static PV system. Moreover, wind plants generally have much greater power capacity than the PV plants. For example, many wind plants that have been already installed around the world have capacities of hundreds of megawatts each. More wind plants exceeding 300-MW capacity are being installed, and even larger plants are being planned.

13.2 SYNCHRONIZING WITH THE GRID

The synchronizing breakers in Figure 13.1 and Figure 13.5 have internal voltage and phase-angle sensors to monitor the site and grid voltages and signal the correct instant for closing the breaker. As a part of the automatic protection circuit, any attempt to close the breaker at an incorrect instant is rejected by the breaker. Four conditions that must be satisfied before the synchronizing switch permits the closure are as follows:

1. The frequency must be as close as possible to the grid frequency, preferably about one third of a hertz higher.
2. The terminal-voltage magnitude must match with that of the grid, preferably a few percent higher.
3. The phase sequences of both three-phase voltages must be the same.
4. The phase angle between the two voltages must be within 5°.

Taking the wind power system as an example, the synchronizing process runs as follows:

1. With the synchronizing breaker open, the wind power generator is brought up to speed by using the electrical machine in the motoring mode.
2. The machine is changed to the generating mode, and the controls are adjusted so that the site and grid voltages match to meet the requirements as closely as possible.
3. The match is monitored by a synchroscope or three synchronizing lamps, one in each phase (Figure 13.6). The voltage across the lamp in each phase is the difference between the renewable site voltage and the grid voltage at any instant. All three lamps are dark when the site and grid voltages are exactly equal in all three phases. However, it is not enough for the lamps to be dark at any one instant. They must remain dark for a long time. This condition is met only if the generator and grid voltages have nearly the same frequency. If not, one set of the two three-phase voltages will rotate faster relative to the other, and the phase difference between the two voltages will light the lamps.
4. The synchronizing breaker is closed if the lamps remain dark for ¼ to ½ sec.

Following the closure, any small mismatch between the site voltage and grid voltage circulates an inrush current from one to the other until the two voltages equalize and come to a perfect synchronous operation.

13.2.1 Inrush Current

A small unavoidable difference between the site and grid voltages results in an inrush current flowing between the site and the grid. The inrush current eventually decays to zero at an exponential rate that depends on the internal resistance and inductance.

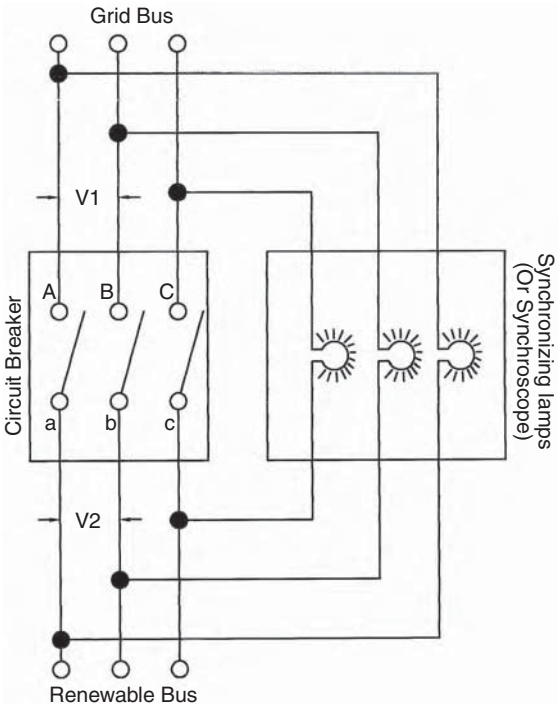

FIGURE 13.6 Synchronizing circuit using three synchronizing lamps or the synchroscope.

The initial magnitude of this current at the instant of the circuit breaker closing depends on the degree of mismatch between the two voltages. This is not completely disadvantageous as it produces the synchronizing power, which brings the two systems into a synchronous lock. However, it produces a mechanical torque step, setting up electromechanical oscillations before the two sides come into synchronism and get locked with each other at one voltage. The magnitude of the inrush current is calculated as follows:

Let ΔV be the difference between the site voltage and the grid voltage at the instant of closing. Because this voltage is suddenly applied to the system, the resulting inrush current is determined by the subtransient reactance X_d'' of the generators:

$$I_{\text{inrush}} = \frac{\Delta V}{X_d''} \tag{13.1}$$

The inrush current is primarily reactive as it is solely determined by X_d''. Its magnitude is kept within the allowable limit or else thermal or mechanical damage may result.

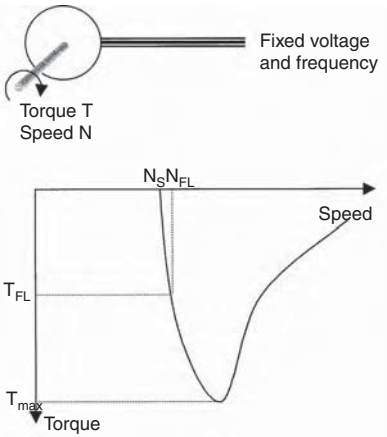

FIGURE 13.7 Resilience in the torque vs. speed characteristic of induction generator.

The synchronizing power produced by the inrush current brings the wind system and the grid in synchronism after the oscillations decay out. Once synchronized, the wind generator has a natural tendency to remain in synchronism with the grid, although it can fall out of synchronous operation if excessively loaded or a large load step is applied or during a system fault. Small load steps induce swings in the load angle decay out over time, restoring the synchronous condition. The magnitude of the restoring power, also known as the synchronizing power, is high if the wind generator is running at a light load and is low if it is running near the steady-state stability limit.

13.2.2 Synchronous Operation

Once synchronized, the voltage and frequency of the wind system need to be controlled. The grid serves as the frequency reference for the generator output frequency when the induction generator is directly connected to the grid. The grid also acts as the excitation source supplying the reactive power. Because the torque vs. speed characteristic of the induction generator has a steep slope near zero slip (Figure 13.7), the speed of the wind turbine remains approximately constant within a few percentages. A higher load torque is met by a proportionately increased slip, up to a certain point beyond which the generator becomes unstable. If the load torque is immediately reduced, the generator returns to the stable operation. From the operating point of view, the induction generator is softer, as opposed to a relatively stiff operation of the synchronous generator, which works at an exact constant speed or falls out of stability.

If the synchronous generator is used, as in wind farms installed in California in the 1980s, the voltage is controlled by controlling the rotor field excitation current. The frequency control, however, is not required on a continuous basis. Once synchronized and connected with the lines, the synchronous generator has an inherent tendency to remain in synchronous lock with the grid. The synchronism can be lost

only during severe transients and system faults. The generator must be resynchronized after such an event.

In the variable-speed induction generator system using the inverter at the interface, the inverter gate signal is derived from the grid voltage to assure synchronism. The inverter stability depends a great deal on the design. For example, there is no stability limit with a line-commutated inverter. The power limit in this case is the steady-state load limit of the inverter with any short-term overload limit.

13.2.3 Load Transient

The grid will pick up the area load during steady-state operation if the renewable power system output is fully or partially lost. The effect of this is felt in two ways:

- The grid generators slow down slightly to increase their power angle under the increased load. This results in a momentary drop in frequency until the governors allow more fuel.
- The grid conductors now carry more load, resulting in a small voltage drop throughout the system.

The same effects are felt if a large load is suddenly switched on. Because starting the wind turbine as the induction motor draws a large current, it also results in the aforementioned effect. Such load transients are minimized by soft-starting large machines. In wind farms consisting of many generators, individual generators are started in sequence, one after another.

13.2.4 Safety

Safety is a concern when renewable power is connected to the utility grid lines. The interconnection may endanger the utility repair crew working on the lines by continuing to feed power into the grid even when the grid itself is down. This issue has been addressed by including an internal circuit that takes the inverter off-line immediately if the system detects a grid outage. Because this circuit is critical for human safety, it has a built-in redundancy.

The grid interface breaker can get suddenly disconnected either accidentally or to meet an emergency situation. The high-wind-speed cutout is a usual condition when the power is cut off to protect the generator from overloading. In a system with large capacitors connected at the wind site for power factor improvement, the site generator would still be in the self-excitation mode, drawing excitation power from the capacitors and generating terminal voltage. In the absence of such capacitors, one would assume that the voltage at the generator terminals would come down to zero. The line capacitance, however, can keep the generator self-excited. The protection circuit is designed to avoid both of these situations, which are potential safety hazards to unsuspecting site crew.

When the grid is disconnected for any reason, the generator will experience a loss of frequency regulation as the frequency-synchronizing signal derived from the grid lines is now lost. When a change in frequency is detected beyond a certain

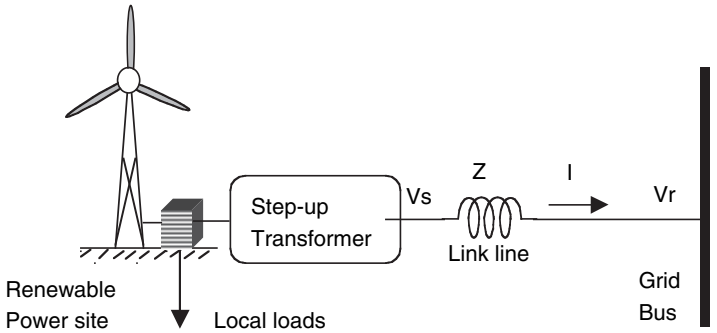

FIGURE 13.8 Equivalent circuit of renewable power plant connected to grid *via* transmission line link.

limit, the automatic control can shut down the system, cutting off all possible sources of excitation.

In new systems, however, the wind generator is designed to remain safely connected to the grid and ride through all transients. This is discussed later in this chapter.

13.3 OPERATING LIMIT

The link connecting a renewable power site with the area grid introduces an operating limit in two ways, the voltage regulation and the stability limit. In most cases, the link can be considered as an electrically short transmission line. The ground capacitance and the ground leakage resistance are generally negligible. The equivalent circuit of such a line, therefore, reduces to a series leakage impedance Z (Figure 13.8). Such an approximation is valid in lines up to 50 mi long. The line carries the renewable power to the grid or from the grid to the renewable site during local peak demand. There are two major effects of the transmission line impedance, one on the voltage regulation and the other on the maximum power transfer capability of the link, as discussed in the following text.

13.3.1 Voltage Regulation

The phasor diagram of the voltage and current at the sending and receiving ends is shown in Figure 13.9. Because the shunt impedance is negligible, the sending-end current I_s is the same as the receiving-end current I_r, i.e., $I_s = I_r = I$. The voltage at the sending end is the vector sum of the receiving-end voltage and the voltage drop $I{\cdot}Z$ in the line:

$$V_s = V_r + I(R + jX) \tag{13.2}$$

where Z is the line impedance, equal to $R + j\,X$ (per phase).

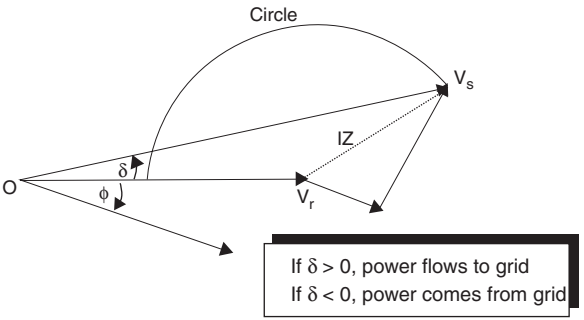

FIGURE 13.9 Phasor diagram of the link line carrying rated current.

The voltage regulation is defined as the rise in the receiving-end voltage, expressed in percent of the full-load voltage, when full load at a specified power factor is removed, holding the sending-end voltage constant. That is as follows:

$$\text{percent voltage regulation} = \frac{V_{nl} - V_{fl}}{V_{fl}} \times 100 \tag{13.3}$$

where
V_{nl} = magnitude of receiving-end voltage at no load = V_s
V_{fl} = magnitude of receiving-end voltage at full load = V_r

With reference to the phasor diagram of Figure 13.9, $V_{nl} = V_s$ and $V_{fl} = V_r$.

The voltage regulation is a strongly dependent function of the load power factor. For the same load current at a different power factor, the voltage drop in the line is the same but is added to the sending-end voltage at a different phase angle to derive the receiving-end voltage. For this reason, the voltage regulation is greater for a more lagging power factor and is the least or even negative with a leading power factor.

In Figure 13.9, if the magnitude of V_r and I are held constant and the power factor of the load is varied from zero lagging to zero leading, the vector V_s varies such that its end point lies on a semicircle because the magnitude $I(R + jX)$ is constant. Such a circle diagram is useful for plotting the sending-end voltage vs. load power factor for a given load voltage and kilovoltampere.

If the voltages at both ends of the lines are held constant in magnitude, the receiving-end real power and reactive power points plotted for several loads would lie on a circle known as the power circle diagram. The reader is referred to Stevenson[1] for further information on the transmission line circle diagrams.

13.3.2 Stability Limit

The direction of power flow depends on the sending- and receiving-end voltages and the electrical phase angle between the two. However, the maximum power the

line can transfer while maintaining a stable operation has a certain limit. We derive in the following text the stability limit, assuming that the power flows from the renewable site to the grid, although the same limit applies in the reverse direction as well. The series resistance in most lines is negligible and hence is ignored here.

The power transferred to the grid via the link line is as follows:

$$P = V_r I \cos \phi \tag{13.4}$$

Using the phasor diagram of Figure 13.9, the current I can be expressed as follows:

$$I = \frac{V_s - V_r}{jX} = \frac{V_s \angle \delta - V_r \angle o}{jX} = \frac{V_s(\cos\delta + j\sin\delta) - V_r}{jX} \tag{13.5}$$

The real part of this current is as follows:

$$I_{real} = \frac{V_s \sin\delta}{X} \tag{13.6}$$

This, when multiplied with the receiving-end voltage V_r, gives the following power:

$$P = \frac{V_s V_r}{X} \sin\delta \tag{13.7}$$

Thus, the magnitude of the real power transferred by the line depends on the power angle δ. If $\delta > 0$, the power flows from the site to the grid. On the other hand, if $\delta < 0$, the site draws power from the grid.

The reactive power depends on $(V_s - V_r)$. If $V_s > V_r$, the reactive power flows from the site to the grid. If $V_s < V_r$, the reactive power flows from the grid to the site.

Obviously, the power flow in either direction is maximum when δ is 90° (Figure 13.10). Beyond P_{max}, the link line becomes unstable and falls out of synchronous operation. That is, it loses its ability to synchronously transfer power from the renewable power plant to the utility grid. This is referred to as the *steady-state stability limit*. In practice, the line loading must be kept well below this limit to allow for transients such as sudden load steps and system faults. The maximum power the line can transfer without losing the stability even during system transients is referred to as the *dynamic stability limit* (P'_{max} in the figure). In a typical system, the power angle must be kept below 15 or 20° to maintain dynamic stability at all times.

Because the generator and the link line are in series, the internal impedance of the generator is added in the line impedance for determining the link's maximum power transfer capability, dynamic stability, and steady-state performance.

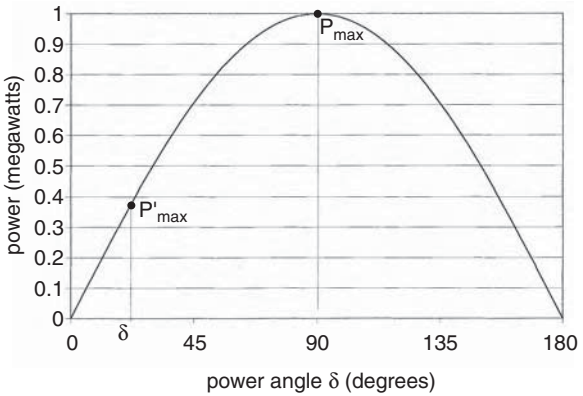

FIGURE 13.10 Power vs. power angle showing static and dynamic stability limits of the link line.

If an area has many large wind farms, each connecting to the grid via short links, the utility company needs a major transmission line to carry the bulk of the wind power to a major load center. The maximum power transfer and the dynamic stability limits we discussed for a short link also apply to the transmission line. New lines are needed if the existing lines are near their limits. For example, the California Independent Systems Operators, which manage the flow of electric power through the grid, is building new transmission lines to carry wind power from the Tehachapi and Antelope Valleys to other parts of the state. This 40-km Antelope–Pardee line will cost about $100 million and may be commissioned by 2006.

13.4 ENERGY STORAGE AND LOAD SCHEDULING

A wind farm sized to meet an average community load with average wind speed cannot meet 100% of the load demand at all times. The options for making the power availability nearly 100% are as follows:

- Interconnecting with the area grid to draw power from the grid or to feed power back to the grid, depending on the wind speed
- A diesel generator or a fuel cell of needed size, which would burn fuel only when the wind speed is below average. At high wind, the excess power is wasted by deflecting the blades away from the optimum position
- A rechargeable energy storage, such as a battery, pumped water, or compressed air

Even with a grid connection, large wind and PV plants may find it economical to store some energy locally in a battery. The short-term peak demand is met by the battery without drawing from the grid and paying the demand charge. For formulating an operating strategy for scheduling and optimizing the use of grid power,

TABLE 13.1
Production Cost of 300-MW Thermal–PV–Battery System

System Configuration	Battery Depletion MWh/d	Production Cost $/d	Savings $/d
Thermal only	—	750,000	—
Thermal + PV	—	710,000	40,000
Thermal + PV + battery	344	696,000	54,000

major system constraints are first identified. The usual constraints are the battery size, the minimum on/off times and ramp rates for thermal power plants, the battery charge and discharge rates, and the renewable power capacity limits. For arriving at the best short-term and long-term scheduling, the optimization problem is formulated to minimize the cost of all thermal and renewable plants combined subject to the constraints. Such an optimization process determines the hours for which the base-load thermal units of the utility company should be taken either off-line or online. The traditional thermal scheduling algorithms, augmented by Lagrangian relaxation, branch and bound, successive dynamic programming, or heuristic method (genetic algorithms and neural networks), can be used for minimizing the cost of operating the thermal units with a given renewable-battery system. Marwali et al.[2] have recently utilized the successive dynamic programming to find the minimum cost trajectory for battery and the augmented Langrangian to find thermal unit commitment. In a case study of a 300-MW thermal–PV–battery power plant, the authors have arrived at the total production costs shown in Table 13.1 that a battery hybrid system saves $54,000 per day compared to the thermal power plants alone.

13.5 UTILITY RESOURCE PLANNING TOOLS

Wind and PV power, in spite of their environmental, financial, and fuel diversity benefits, have been slow to enter utility resource planning because of the planners' lack of familiarity with them, and analytical tools for nondispatchable sources of such power are not available on demand. The energy laboratory at the Massachusetts Institute of Technology (MIT) has developed an analytical tool to analyze the impact of nondispatchable renewables on New England's power systems operation. Cardell and Connors[3] applied this tool for analyzing two hypothetical wind farms totaling 1500-MW capacity for two sites, one in Maine and the other in Massachusetts. The average capacity factor at these two sites is estimated to be 0.25. This is good, although many sites have achieved the capacity factor of 0.35 or higher. The MIT study shows that the wind energy resource in New England is comparable to that in California. The second stage of their analysis developed the product-cost model, demonstrating the emission and fuel cost risk mitigation benefits of the utility resource portfolios incorporating wind power.

13.6 WIND FARM–GRID INTEGRATION

With restructuring and technological changes in the utility sector, electric utilities have begun to include wind farms and PV parks in their resource mix. The issues the power industry must deal with in integration of these new power sources are the following:[4–5]

- Branch power flows and node voltages
- Protection scheme and its ratings
- Harmonic distortion and flicker
- Power system dynamics and dynamic stability
- Reactive power control and voltage control
- Frequency control and load dispatch from conventional generators

The first three have primarily local impacts, whereas the last three have broad grid-level impacts. In addressing these issues, however, there is an increased need for independent analysis of the technical and economic aspects. Projects funded by the National Renewable Laboratory's (NREL) National Wind Technology Center (NWTC) and its partners in the utility and wind industries developed new information on integration and valuation issues and the reliability of new wind turbine products. The program output has become a catalyst in a national outreach effort (with investor-owned utilities, electric cooperatives, public power organizations, energy regulators, and consumers) encouraging the use of wind power in generation portfolios and the purchase of wind-generated power using market-based activities. Numerous reports[6–8] are available on these issues that can be downloaded from the Internet.

As for modeling the system performance, different wind farms are connected to different kinds of utility grids. The NWTC studies the behavior of power systems under different conditions to identify grid stability and power quality factors that enter into the development of wind farms throughout the U.S. Again, numerous reports[9–13] are available on these issues that can be downloaded from the Internet.

As for the planning models and operations, researchers are studying how multiple wind farms or multiple wind generators in one large farm can smooth out each other's output in a variable wind environment. Power output fluctuations are also being studied in the context of wind farm integration into utility grids. Hand and Madsen reports[14–15] are just two examples of such studies.

Certification and standards are of equal importance when the country as a whole must deal with a new technology. The NREL/NWTC conducts a certification process and provides guidelines to help users prepare for certification. Underwriters Laboratory (UL) is NREL's partner in this process. NREL has developed checklists to help designers understand what the certification body is likely to be looking for in their documentation. These are the same checklists that NREL and UL would use when evaluating their design documentation. Sign-offs on these checklists are used as a report of compliance or resolution on each design issue. Also offered is a checklist to help users comply with the International Electrotechnical Commission (IEC)'s requirements. NWTC has documented the general quality management, design evaluation, and testing procedures related to the certifications.

13.7 GRID STABILITY ISSUES

With today's wind turbine technology, wind power could supply 20% of the electricity needs of the U.S. A study by GE Energy concluded that the New York State power grid can handle 3300 MW of power from future utility-scale wind farms with proper procedures installed. Although the U.S. has some way to go in that direction, Europe has wind capacity already up to 20% in certain regions and up to 60% in some extremely large wind farm areas. As a result, grid stability is becoming a major concern in the European wind industry. Until recently, wind turbines were disconnected during faults on the grids, but this led to dynamic instability and blackouts. A new requirement is that the wind turbines remain connected with the grid, ride through the problems, and have a built-in capacity for active grid support. Functionally, this means that wind turbines must behave as conventional thermal and nuclear power plants.

13.7.1 Low-Voltage Ride-Through

Wind turbines in the past were designed to trip off-line in the event of major system disturbances such as lightning strikes, equipment failures, or downed power lines. However, this loss of generation impacts system stability and can lead to cascaded tripping and loss of revenue. Today, many utilities are requiring that wind farms ride through grid disturbances while remaining online to continue supporting the system. The new wind systems are designed to deliver ride-through capability at or below 15% of the grid voltage for up to 500 msec. This requires upgrading the wind turbine's main control cabinet, low-voltage distribution panel, pitch system, uninterruptible power supply, and power converter to ensure compliance with the low-voltage ride-through requirements.

With recent advances in power electronics, the low-voltage ride-through (LVRT) capability that enables wind turbines to stay connected to the grid during system disturbances is among the technologies introduced in the market during 2003 by many manufacturers. For example, the LVRT capability is now being built into all of GE Wind's new turbines, ranging from 1.5-MW units to the 5-MW units designed for offshore applications to meet more stringent transmission standards. On land, the 200-MW Taiban Mesa Wind Farm in New Mexico was the first project to install the ride-through capability.

With this new feature, wind turbines remain online and feed reactive power to the electric grid right through major system disturbances. This meets the transmission reliability standards similar to those demanded of thermal power plants. The LVRT adds significant new resiliency to wind farm operations at the time when more utilities require it.

Another power electronics technology that has been recently introduced is the dynamic power conversion system with optional reactive power control to provide support and control to local grid voltage, improve transmission efficiencies, provide the utility grid with reactive power (VARs), and increase grid stability. For example, GE's WindVAR® technology automatically maintains defined grid voltage levels and power quality within fractions of a second. This feature is particularly beneficial with weaker grids or larger turbine installations.

TABLE 13.2
10-MWh Energy Storage Alternatives for Grid Support

Technology	Round Trip Efficiency Percent	Storage Element Life Years	Power Equipment Cost (Euros/kWh)	Energy Storage Cost (Euros/KWh)
Water-pumped storage	75	40	1800	300
Compressed-air-pumped storage	60	30	1400	700
Lead-acid batteries	70	5	100	350

Source: From Enslin, J., Jansen, C., and Bauer, P., In Store for the Future, Interconnection and Energy Storage for Offshore Wind Farms, *Renewable Energy World*, James & James Ltd., London, January–February 2004, pp 104–113.

13.7.2 Energy Storage for Stability

Recent experience in the Scandinavian countries indicates that large-scale wind farms can cause grid stability problems if the wind capacity exceeds 10 to 20% of the instantaneous load. Innovative solutions are needed to avoid such possibilities, such as Flexible AC transmission systems (FACTS), high-voltage direct current (HVDC), and energy storage. The peak loading in the Netherlands at present approaches 10%, at the threshold of the stability problem area. The fundamental issues to be addressed are the dynamic stability, short-circuit power, and the grid upgrades. The power balancing between wind farms and other independent power producers, export and import, and natural loading on high-voltage grids are also of concern. Regulations are being prepared to ensure that these large fluctuating power sources can be handled without sacrificing power stability and quality. Large wind farms' output can vary more than ±50% around the average value over a one-week period due to fluctuating wind speed. Such variation can be smoothed out to a constant power output by energy storage using one of the following options: electrochemical batteries (least expensive), pumped water storage (medium cost), and compressed air (most expensive). KEMA investigated the storage requirement for a large-scale offshore wind farm. Their study, reported by Enslin, Jansen, and Bauer,[16] estimates that a 100-MW wind farm may require a 20-MW peak power and a 10-MWh energy storage capacity. The results of the plant economy are summarized in Table 13.2. The energy storage option, however, may become more economical if implemented for more than one function.

Rodriguez et al.[17] have addressed the impact of high wind power penetration in grid planning and operation, with a particular reference to the 15,000-MW wind capacity planned in the Spanish grid system over the next 5 yr. The key problems studied are those related to the stability of the power systems. Their analysis is based on results of the dynamic simulation. Dynamic models of the wind farms using squirrel cage and doubly fed induction generators have been developed and used in simulations for arriving at recommendations for integrating the new wind capacity of such a large magnitude.

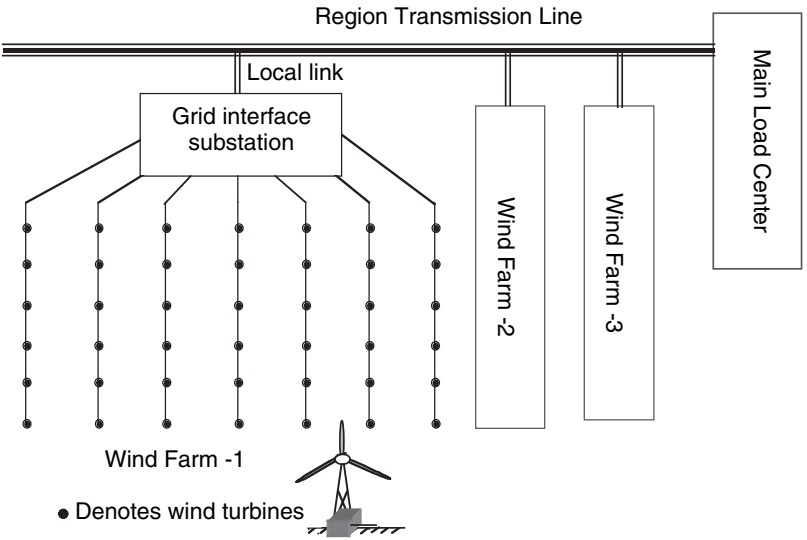

FIGURE 13.11 Distributed power generation with wind farms.

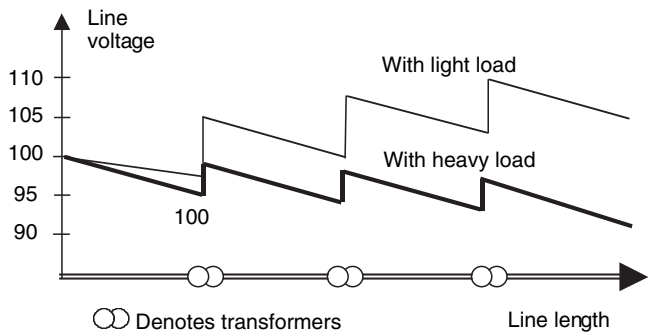

FIGURE 13.12 Voltage drops and rises along power lines with distributed generators and transformers for voltage boosts.

13.8 DISTRIBUTED POWER GENERATION

In a classical power system, the power flows from the central generating station to the end users via transmission and distribution lines using many step-down transformers. The voltage drops gradually from the highest value at the generating end to the lowest value at the user end, with some boosts at the substation transformers by adjusting the turns ratio. However, with distributed power generation using PV parks and wind farms, power is injected all along the lines in a distributed pattern (Figure 13.11). In such a system, the voltage does not drop gradually; rather, it rises at the point of injection and then drops again (Figure 13.12). The European Standard EN-50160 requires that the supply voltage at the delivery point of the low voltage network be within ±10% of the nominal value. However, generally acceptable

voltage is typically between 90 and 106%. The voltage variation between the no-load and full-load conditions is generally kept below ±2% by regulating the voltage by automatic tap-changing transformers or other means. Povlsen[18] has recently studied these problems in some detail.

The system voltage can rise above the limits if the power is injected in between no- and full-load conditions by PV or wind farms. The two distributed power sources, however, influence the grid differently. Compared with wind farms, distributed PV parks generally hold the system voltage well, as its high output coincides with high demand on a hot, bright summer day. PV power injection is less suitable for grids in cold regions, where use of air conditioners is limited. In such regions, high power output from PV farms generally coincides with low demands from both residential and industrial sectors, as during holiday seasons. Similar situations exist even in warm countries during summer holidays when the load is light.

It is possible that PV injection has to be limited to keep the voltage from rising above the specified limit when the system is operating at the minimum load. The minimum load is typically set at 25% of the maximum load in residential areas in many countries. No PV injection can be tolerated at the minimum load when the voltage is already at the maximum value, and the PV power injection would raise it even higher. On the other hand, at the maximum load, a significant amount of PV power (up to 70%) could be acceptable if well distributed, or even higher (up to 140% of load on that line) if injected into one low-voltage (LV) line. If the system is lightly loaded to only 25%, these limits may be 0 and 20%, respectively. The PV injection limits rise linearly from the lightly loaded to fully loaded systems.

It is uneconomical not to produce PV because the maximum allowable PV injected is limited by the systems load. The maximum PV injection can be increased by using tap changers on the distribution transforms. This can be done by off-load tap changing by hand on the LV side, or by automatic on-load on the high-voltage (HV) side. The automatic tap changers are expensive, whereas manual tap changing would require power interruption twice a year.

REFERENCES

1. Stevenson, W.D., *Elements of Power System Analysis*, McGraw-Hill Book Company, New York, 1962.
2. Marwali, M.K.C., Halil, M., Shahidehpour, S.M., and Abdul-Rahman, K.H., Short-Term Generation Scheduling in Photovoltaic-Utility Grid with Battery Storage, IEEE paper No. PE-184-PWRS-16-09, 1997.
3. Cardell, J.B. and Connors, S.R., Wind power in New England, Modeling and Analyses of Nondispatchable Renewable Energy Technologies, IEEE Paper No. PE-888-PWRS-2-06, 1997.
4. Riso National Laboratory, Power Quality and Grid Connection of Wind Turbines Summary Report R-853, Denmark, October 1996.
5. Gardner, P., Wind Farms and Weak Networks, *Wind Directions, Magazine of the European Wind Energy Association*, London, July 1997.
6. Smith, J.W., DOE/NREL Wind Farm Monitoring: Annual Report, NICH Report No. SR-500-31188, 2002.

7. Wan, Y.H., Wind Power Plant Monitoring Project Annual Report, NICH Report No. TP-500-30032, 2001.
8. Cadogan, J., Milligan, M., Wan, Y., and Kirby, B., Short-Term Output Variations in Wind Farms — Implications for Ancillary Services in the United States, NICH Report No. CP-500-29155, 2000.
9. Muljadi, E., Wan, Y., Butterfield, C.P., and Parsons, B., Study of a Wind Farm Power System, NICH Report No. CP-500-30814, 2002.
10. Muljadi, E. and McKenna, H.E., Power Quality Issues in a Hybrid Power System, NICH Report No. CP-500-30412, 2001.
11. Milligan, M.R., Modeling Utility-Scale Wind Power Plants, Part 1: Economics, NICH Report No. TP-500-27514, 2000.
12. Milligan, M.R., Modeling Utility-Scale Wind Power Plants, Part 2: Capacity Credit, NICH Reports No. TP-500-29701, 2002.
13. Schwartz, M. and Elliott, D., Remapping of the Wind Energy Resource in the Midwestern United States, NICH Report No. AB-500-31083, 2001.
14. Hand, M. M. and Balas, M. J., Systematic Controller Design Methodology for Variable-Speed Wind Turbines, NICH Report No. TP-500-29415, 2002.
15. Madsen, P. H., Pierce, K., and Buhl, M., Predicting Ultimate Loads for Wind Turbine Design, NICH Report No. CP-500-25787, 1998.
16. Enslin, J., Jansen, C., and Bauer, P., In Store for the Future, Interconnection and Energy Storage for Offshore Wind Farms, *Renewable Energy World*, James & James Ltd., London, January–February 2004, pp. 104–113.
17. Rodriguez, J.M. et al., Incidence on Power System Dynamics of High Penetration of Fixed-Speed and Doubly-Fed Wind Energy Systems: Study of the Spanish Case, IEEE Power & Energy, Paper No. PE-165PRS, September 2002.
18. Povlsen, A.F., Distributed Power Using PV, Challenges for the Grid, *Renewable Energy World*, James & James Ltd., London, April 2003, pp. 63–73.

14 Electrical Performance

14.1 VOLTAGE CURRENT AND POWER RELATIONS

Power systems worldwide are 3-phase, 60 Hz or 50 Hz AC. The three phases (coils) of the generator are connected in Y or Δ as shown in Figure 14.1. In balanced three-phase operation, the line-to-line voltage, the line current, and the three-phase power $P_{3\text{-ph}}$ in terms of the phase voltage V_{ph}, phase current I_{ph}, and load power factor pf are given by the following expression, with notations marked in Figure 14.1.

In a Y-connected system:

$$V_{\text{L}} = \sqrt{3} V_{\text{ph}}$$

$$I_{\text{L}} = I_{\text{ph}}$$

$$P_{3\text{-ph}} = \sqrt{3} V_{\text{L}} I_{\text{L}} pf \tag{14.1}$$

In a Δ-connected system:

$$V_{\text{L}} = V_{\text{ph}}$$

$$I_{\text{L}} = \sqrt{3} I_{\text{ph}}$$

$$P_{3\text{-ph}} = \sqrt{3}\ V_{\text{L}} I_{\text{L}} pf \tag{14.2}$$

For steady-state or dynamic performance studies, the system components are modeled to represent the entire system. The components are modeled to represent the conditions under which the performance is to be determined. Electrical generators, rectifiers, inverters, and batteries were discussed in earlier chapters. This chapter concerns system-level performance.

A one-line diagram often represents the three phases of the system. Figure 14.2 is an example of a one-line diagram of a grid-connected system. On the left-hand side are two Y-connected synchronous generators, one grounded through a reactor and the other through a resistor, supplying power to load A. On the right-hand side is a wind power site with one Δ-connected induction generator supplying power to load B. The remaining power is fed to the grid via a step-up transformer, circuit breakers, and the transmission line.

The balanced three-phase system is analyzed on a single-phase basis. The neutral wire in the Y-connection does not enter the analysis in any way, because it is at zero voltage and carries zero current.

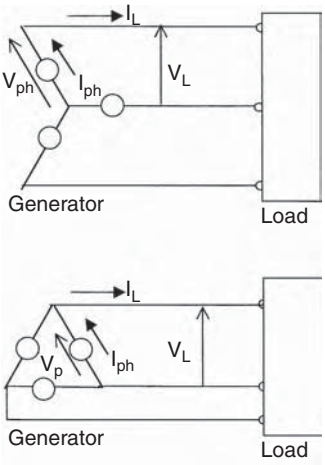

FIGURE 14.1 Three-phase AC systems connected in Y or Δ.

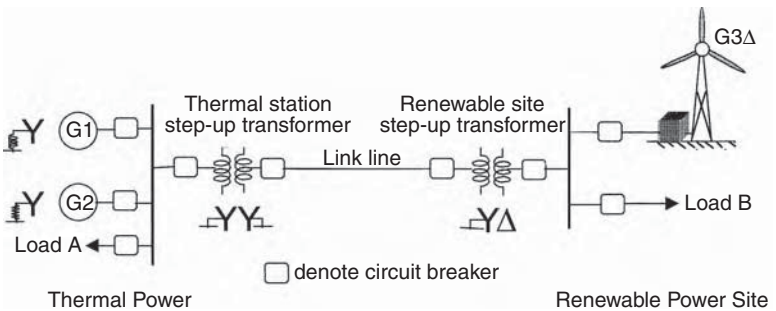

FIGURE 14.2 One-line schematic diagram of grid-connected wind farm.

An unbalanced system, with balanced three-phase voltage on unbalanced three-phase load or with unbalanced faults, requires advanced methods of analyses, such as the method of symmetrical components.

14.2 COMPONENT DESIGN FOR MAXIMUM EFFICIENCY

An important performance criterion of any system is the efficiency, which is the power output expressed as a percentage of the power input. Because the system is only as efficient as its components, designing an efficient system means designing each component to operate at its maximum efficiency.

The electrical and electronic components, while transferring power from the input side to the output side, lose some power in the form of heat. In practical designs, a maximum efficiency of 90 to 98% is typical in large power equipment of hundreds of kW ratings, and 80 to 90% in small equipment of tens of kW ratings.

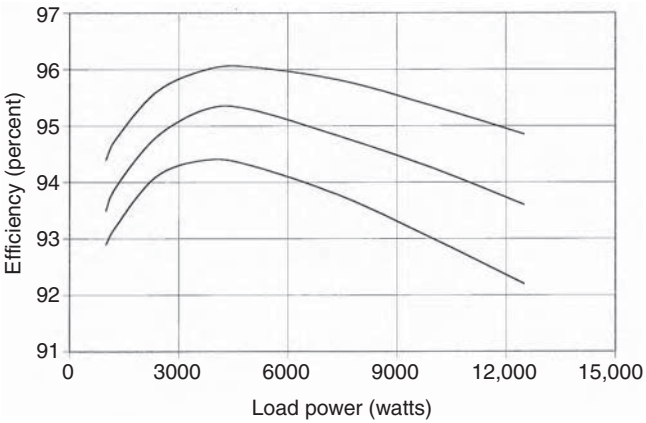

FIGURE 14.3 Power equipment efficiency varies with load with a single maximum.

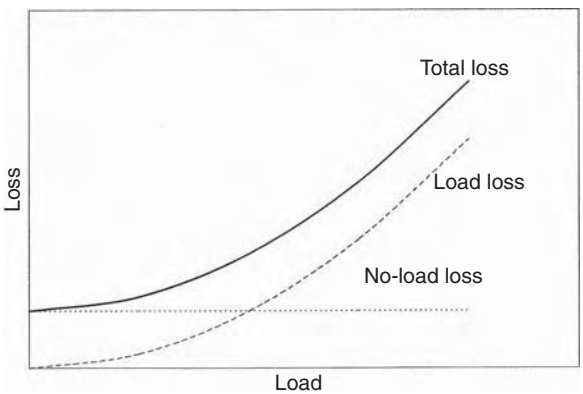

FIGURE 14.4 Loss components varying with load in typical power equipment.

The component efficiency, however, varies with load as shown in Figure 14.3. The efficiency increases with load up to a certain point, and then it decreases. A good design maximizes the efficiency at the load that the equipment supplies most of the time. For example, if the equipment is loaded at 70% of its rated capacity most of the time, it is beneficial to have the maximum efficiency at 70% load. The method of achieving the maximum efficiency at a desired load level is presented in the following text.

The total loss in any power equipment generally has two components. The one that represents the quiescent no-load power consumption remains fixed. It primarily includes eddy and hysteresis losses in the magnetic parts. The other component, representing ohmic loss in the conductors, varies with the square of the current. For a constant voltage system, the conductor loss varies with the square of the load power. The total loss (Figure 14.4) is therefore expressed as the following:

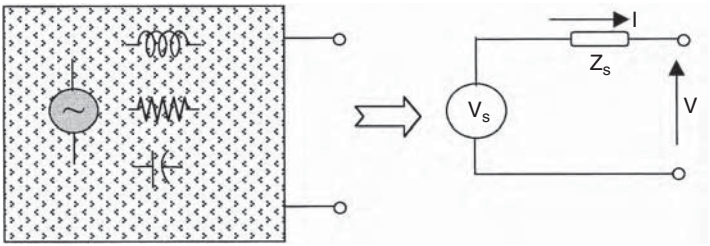

FIGURE 14.5 Thevenin equivalent circuit model of a complex power system.

$$\text{loss} = L_o + kP^2 \tag{14.3}$$

where P is the output power delivered to the load, L_o the fixed loss, and k the proportionality constant. The efficiency is given by the following:

$$\eta = \frac{\text{output}}{\text{input}} = \frac{\text{output}}{\text{output} + \text{loss}} = \frac{P}{P + L_o + kP^2} \tag{14.4}$$

For the efficiency to be maximum at a given load, its derivative with respect to the load power must be zero at that load:

$$\frac{d\eta}{dP} = \frac{P(1+2kP) - (P + L_o + kP^2)}{(P + L_o + kP^2)^2} = 0 \tag{14.5}$$

This equation reduces to $L_o = kP^2$. Therefore, the component efficiency is maximum at the load under which the fixed loss is equal to the variable loss. This is an important design rule, which can result in significant savings in electric energy in large power systems. Power electronic components using diodes have an additional loss that is linearly proportional to the current. Inclusion of such a loss in the preceding analysis does not change the maximum efficiency rule just derived.

14.3 ELECTRICAL SYSTEM MODEL

An electrical network of any complexity can be reduced to a simple Thevenin equivalent circuit consisting of a single internal source voltage V_s and impedance Z_s in series (Figure 14.5). The two parameters are determined as follows:

With the system operating at no load and with all other parameters at rated values, the internal voltage drop is zero and the voltage at the open-circuit terminals equals the internal source voltage; that is, V_s = open-circuit voltage of the system.

For determining the source impedance, the terminals are shorted together and the terminal current is measured. Because the internal voltage is now totally consumed in driving the current through the source impedance only, we have the following:

$$Z_s = \text{open-circuit voltage/short-circuit current.} \tag{14.6}$$

If Z_s is to be determined by an actual test, the general practice is to short the terminals with a small open-circuit voltage that is only a small percentage of the rated voltage. The low-level short-circuit current is measured and the full short-circuit current is calculated by scaling to the full-rated voltage. Any nonlinearity, if present, is accounted for.

The equivalent circuit is developed on a per-phase basis and in percent or per-unit basis. The source voltage, current, and impedance are expressed in units of their respective base values at the terminal. The base values are defined as follows:

V_{base} = rated output voltage,
I_{base} = rated output current, and
Z_{base} = rated output voltage/rated output current.

14.4 STATIC BUS IMPEDANCE AND VOLTAGE REGULATION

If the equivalent circuit model of Figure 14.5 is derived under steady-state static conditions, then Z_s is called the static bus impedance. The steady-state voltage rise on removal of full-load-rated current is then $\Delta V = I_{base}Z_s$.

Under a partial or full-load step transient, as in the case of a loss of load due to accidental opening of the load-side breaker, the bus voltage oscillates until the transient settles to a new steady-state value. If the load current rises in step as shown in Figure 14.6, the voltage oscillates before settling down to a lower steady-state value. The steady-state change in the bus voltage is then given by $\Delta V = \Delta I\, Z_s$. Then, the percent voltage regulation is given by the following:

$$\text{Voltage Regulation } (\%) = \frac{\Delta V}{V_{base}} \times 100 \tag{14.7}$$

The feedback voltage-control system responds to bring the bus voltage deviation back to the rated value. However, in order not to flutter the system more than necessary, the control system is designed with suitable deadbands. For example, Figure 14.7 shows a 120-V photovoltaic (PV)-battery system with two deadbands in its control system.

Often we need to calculate the voltage drop across an impedance Z, such as that of a generator, transformer, and/or a transmission cable, to determine the required generator voltage. It is given by the following:

$$V_{drop} = IZ \tag{14.8}$$

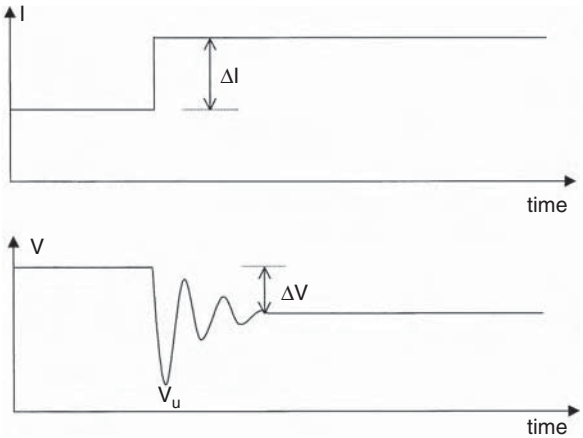

FIGURE 14.6 Transient response of the system voltage under sudden load step.

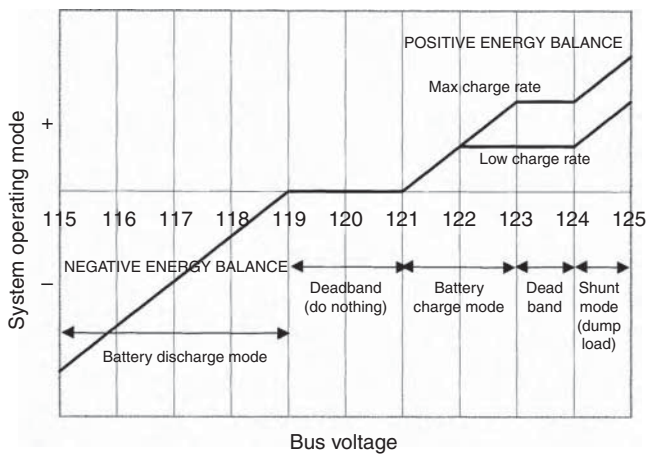

FIGURE 14.7 Deadbands in the feedback voltage-control system avoid system flutter.

where V and I are voltage and current phasors, and $Z = Z_{gen} + Z_{transformer} + Z_{cable}$.

Because the voltage drop in the cable is proportional to the length and inversely proportional to the cross-sectional area of the conductor, the cable size is selected to have a relatively low voltage drop, generally below 3%. Temperature limitation is another factor that may determine the cable size in some cases. Standard tables for cable gauge include the impedance, and the temperature and current limitations.

If the load is to be powered at voltage V_L and power factor cosθ, the generator must generate voltage given by the following phasor sum:

$$V_{gen} = V_L + V_{drop} \tag{14.9}$$

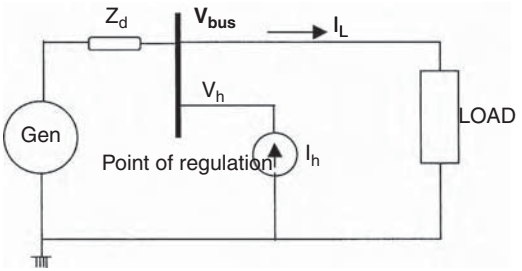

FIGURE 14.8 Harmonic and dynamic source impedance test measurement setup.

If Z is expressed as resistance and reactance, i.e., $Z = R + jX$, the generator voltage is given by the following relationship:

$$V_{gen} = \sqrt{(V_L \cos\theta + IR)^2 + (V_L \sin\theta + IX)^2} \tag{14.10}$$

All calculations are done in a per-phase analysis. Note that the generated voltage depends on the load power factor also. A power factor of 0.85 lagging is common in many systems. Capacitors can improve the power factor to close to 1.0, with a subsequent reduction in the voltage drop.

14.5 DYNAMIC BUS IMPEDANCE AND RIPPLES

If the circuit model of Figure 14.5 is derived for dynamic conditions, i.e., for an incremental load, the source impedance is called the dynamic bus impedance and is denoted by Z_d. It can be either calculated or measured as follows: With the bus in operational mode supplying rated load, a small high-frequency AC current I_h is injected into the bus using an independent grounded current source (Figure 14.8). The high-frequency voltage perturbation in the bus voltage is measured and denoted by V_h. The dynamic bus impedance at that frequency is given by:

$$Z_d = \frac{V_h}{I_h} \tag{14.11}$$

Ripples is the term used to describe periodic high-frequency glitches in the current or the voltage. Ripples are commonly found in systems with power electronic components, such as rectifiers, inverters, and battery chargers. Transistors switching on and off cause the ripples, the frequencies of which are integral multiples of the switching frequency. The ripples are periodic but not sinusoidal, and are superimposed on the fundamental wave.

The ripple voltage induced on the bus due to ripple current is given by the following:

$$V_{ripple} = I_{ripple} Z_d \tag{14.12}$$

The ripple content is minimized by capacitors connected to the bus or preferably at the load terminals of the component causing ripples. The ripple current is then supplied or absorbed by capacitors, rather than by the bus, thus improving the quality of power.

14.6 HARMONICS

Harmonics is the term used to describe higher-frequency sine wave currents or voltages superimposed on the fundamental sine wave. Phase-controlled power switching is one source of harmonics. Harmonics are also generated by magnetic saturation in power equipment. The generator and transformer behave linearly, but not with saturation present in the magnetic circuit. The saturated magnetic circuit requires non-sine-wave magnetizing current.

The usual method of analyzing a system with harmonics is to determine the system performance for each harmonic separately and then to superimpose the results. For such an analysis, the system is represented by the equivalent circuit for each harmonic separately.

The fundamental equivalent circuit of the electrical generator is represented by the d-axis and q-axis.[1,2] The inductance L_n in the nth harmonic equivalent circuit, being for high frequency, is the average of the subtransient inductance in the d and q axes:

$$L_n = \frac{(L_d'' + L_q'')}{2} \tag{14.13}$$

The reactance for the harmonic of order n is given by the following:

$$X_n = 2\pi f_n L_n = 2\pi n f L_n \tag{14.14}$$

where f_n is the nth harmonic frequency and f the fundamental frequency.

In AC current having symmetrical positive and negative portions of the cycle, an odd number of harmonics is always absent. That is, $I_n = 0$ for $n = 2, 4, 6, 8$, and so on. In three-phase load circuits fed by transformers having the primary windings connected in delta, all triple harmonics are also absent in the line currents, that is, $I_n = 0$ for $n = 3, 9, 15$, and so on. The m-pulse full-bridge inverter circuit contains harmonics of the order $n = mk \pm 1$, where $k = 1, 2, 3, 4$, and so on. For example, the harmonics present in a 6-pulse inverter are 5, 7, 11, 13, 17, and 19. On the other hand, the harmonics present in a 12-pulse inverter are 11, 13, 23, and 25. The approximate magnitude and phase of the harmonic currents are found to be inversely proportional to the harmonic order n:

$$I_n = \frac{I_1}{n} \tag{14.15}$$

TABLE 14.1
Harmonic Content of 6-Pulse and 12-Pulse Converters

Harmonic Order (n)	6-Pulse Converter (Equation 14.15)	12-Pulse Converter (Equation 14.15)	3-Pulse and 6-pulse Converters (IEEE Standard 519)
5	20	—	17.5
7	14.5	—	11.1
11	9.1	9.1	4.5
13	7.7	7.7	2.9
17	5.9	5.9	1.5
19	5.3	5.3	1.0

where I_1 is the fundamental current. This formula gives the approximate harmonic content in 6- and 12-pulse inverters, which are given in the first two columns of Table 14.1 and clearly show the benefits of using a 12-pulse converter. The actually measured harmonic currents are lower than those given approximately by Equation 14.15. IEEE Standard 519 gives the current harmonic spectrum in a typical 6-pulse converter as listed in the last column of Table 14.1.

The harmonic currents induce a harmonic voltage on the bus. A harmonic voltage of order n is given by $V_n = I_n Z_n$, where Z_n is the nth harmonic impedance. Harmonic impedance can be derived in a manner similar to dynamic impedance, in which a harmonic current I_n is injected into or drawn from the bus and the resulting harmonic voltage V_n is measured. A rectifier circuit drawing harmonic current I_n provides a simple circuit, which works as the harmonic current load. If all harmonic currents are measured, then the harmonic impedance of order n is given by the following:

$$Z_n = V_n/I_n, \text{ where } n = mk \pm 1,\ k = 1, 2, 3, \ldots \tag{14.16}$$

14.7 QUALITY OF POWER

The quality of power at the grid interface is a part of the power purchase contracts between the utility and the renewable power plant. The rectifier and inverter are the main components influencing power quality. The grid-connected power system, therefore, must use converters, which are designed to produce high-quality, low-distortion AC power. Power quality concerns become more pronounced when the renewable power system is connected to small-capacity grids using long low-voltage links.

There is no generally acceptable definition of the quality of power. However, the International Electrotechnical Commission and the North American Reliability Council have developed working definitions, measurements, and design standards. Broadly, power quality has three major components for measurement:

- Total harmonic distortion, primarily generated by power electronic rectifier and inverter
- Transient voltage sags caused by system disturbances and faults
- Periodic voltage flickers

14.7.1 Harmonic Distortion Factor

Any nonsinusoidal alternating voltage $V(t)$ can be decomposed by the following Fourier series:

$$V(t) = V_1 \sin \omega t + \sum_{n=2}^{\infty} V_n \sin(n\omega t + \alpha_n) \tag{14.17}$$

The first component on the right-hand side of the preceding equation is the fundamental component, whereas all other higher-frequency terms (n = 2, 3, ... ∞) are harmonics.

The total harmonic distortion (*THD*) factor is defined as follows:

$$THD = \frac{\left[V_2^2 + V_3^2 + \ldots V_n^2\right]^{\frac{1}{2}}}{V_1} \tag{14.18}$$

The *THD* is useful in comparing the quality of AC power at various locations of the same power system, or of two or more power systems. In a pure sine wave AC source, *THD* = 0. The greater the value of *THD*, the more distorted the sine wave, resulting in more I^2R loss for the same useful power delivered; this way, the quality of power and the efficiency are related.

As seen earlier, the harmonic distortion on the bus voltage caused by harmonic current I_n drawn by any nonlinear load is given by $V_n = I_n Z_n$. It is this distortion in the bus voltage that causes the harmonic current to flow even in a pure linear resistive load, called the *victim load*. If the renewable power plant is relatively small, a nonlinear electronic load may cause significant distortion on the bus voltage, which then supplies distorted current to the linear loads. The harmonics must be filtered out before feeding power to the grid. For a grid interface, having a *THD* less than 3% is generally acceptable. IEEE Standard 519 limits the *THD* for utility-grade power to less than 5%.

Harmonics do not contribute to the delivery of useful power but produce I^2R heating. Such heating in generators, motors, and transformers is more difficult to dissipate due to their confined designs, as compared to open conductors. The National Electrical Code® requires all distribution transformers to state their k ratings on the permanent nameplate. This is useful in sizing the transformer for use in a system having a large *THD*. The k-rated transformer does not eliminate line harmonics. The k rating merely represents the transformer's ability to tolerate harmonics. A k rating of unity means that the transformer can handle the rated load drawing

pure sine wave current. A transformer powering only electronic loads may require a high k rating from 15 to 20.

A recent study funded by the Electrical Power Research Institute reports the impact of two PV parks on the power quality of the grid-connected distribution system.[3] The harmonic current and voltage waveforms were monitored under connection/disconnection tests over a 9-month period in 1996. The current injected by the PV park had a total distortion below the 12% limit set by IEEE standard 519. However, the individual even harmonics of orders between 18 and 48, except the 34th, exceeded IEEE standard 519. The total voltage distortion, however, was minimal.

A rough measure of quality of power is the ratio of the peak voltage to rms voltage measured by the true rms voltmeter. In a pure sine wave, this ratio is $\sqrt{2}$, i.e., 1.414. Most acceptable bus voltages will have this ratio in the 1.3 to 1.5 range, which can be used as a quick approximate check of the quality of power at any location in the system.

14.7.2 Voltage Transients and Sags

The bus voltage can deviate from the nominally rated value due to many reasons. The deviation that can be tolerated depends on its magnitude and the time duration. Small deviations can be tolerated for a longer time than large deviations. The tolerance band is generally defined by voltage vs. time (V–t) limits. Computers and business equipment using microelectronic circuits are more susceptible to voltage transients than rugged power equipment such as motors and transformers. The power industry has developed an array of protective equipment. Even then, some standard of power quality must be maintained at the system level. For example, the system voltage must be maintained within the V–t envelope shown in Figure 14.9, where

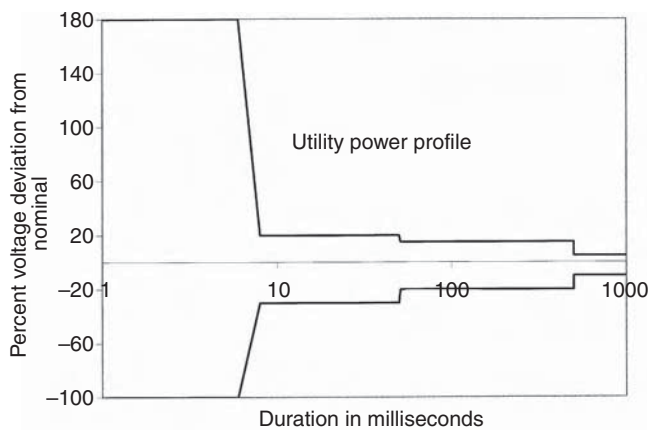

FIGURE 14.9 Allowable voltage deviation in utility-grade power vs. time duration of the deviation. (Adapted from the American National Standards Institute.)

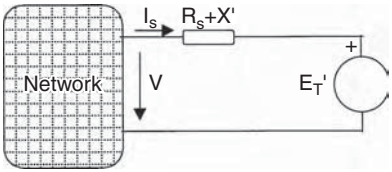

FIGURE 14.10 Thevenin equivalent circuit model of induction generator for voltage-flicker study.

the solid line is that specified by the American National Standard Institute (ANSI), and the dotted line is that specified by the Computer and Business Equipment Manufacturers Associations (CBEMA). The right-hand side of the band comes primarily from the steady-state performance limitations of motors and transformer-like loads, the middle portion comes from visible lighting flicker annoyance considerations, and the left-hand side of the band comes from the electronic load susceptibility considerations. The CBEMA curve allows larger deviations in the microsecond range based on the volt-second capability of the power supply magnetics. ANSI requires the steady-state voltage of the utility source to be within 5%, and short-time frequency deviations to be less than 0.1 Hz.

Capacitors are often used to economically create reactive power VARs. However, in wind farm applications, each capacitor-switching event creates a voltage transient that causes excessive torque on the wind turbine's gear mechanism, leading to excessive wear and tear on the gearbox. Moreover, the high volume of switching necessary for system voltage maintenance leads to early failures of the capacitors, resulting in higher maintenance costs. A new product in the industry, such as GE's D-VAR™ system, when used in conjunction with capacitors, drastically reduces the number of required capacitor switchings. One such system has been used for the SeaWest project in Wyoming.

14.7.3 Voltage Flickers

Turbine speed variation under fluctuating wind conditions causes slow voltage flickers and current variations that are large enough to be detected as flickers in fluorescent lights. The relation between the fluctuation of mechanical power, rotor speed, voltage, and current is analyzed by using the dynamic d- and q-axis model of the induction generator or the Thevenin equivalent circuit model shown in Figure 14.10. If we assume:

R_1, R_2 = resistance of stator and rotor conductors, respectively,
x_1, x_2 = leakage reactance of stator and rotor windings, respectively,
x_m = magnetizing reactance,
x = open-circuit reactance,
x = transient reactance,
τ_o = rotor open-circuit time constant = $(x_2 + x_m)/(2\pi f R_2)$,
s = rotor slip,

f = frequency,
E_T = machine voltage behind the transient reactance,
V = terminal voltage,
I_s = stator current,

then the value of E_T is obtained by integrating the following differential equation:

$$\frac{dE_T}{dt} = -j2\pi fsE_T - \frac{1}{\tau_o}\left[E_T - j(x - x')I_s\right] \tag{14.19}$$

And the stator current from:

$$I_s = \frac{V - E_T}{R_l + jX'} \tag{14.20}$$

The mechanical equation, taking into account rotor inertia, is as follows:

$$2H\frac{ds}{dt} = P_e - \frac{P_m}{1-s} \tag{14.21}$$

where
P_e = electric power delivered by the generator,
P_m = mechanical power of the wind turbine,
H = rotor inertia constant in seconds = $\frac{1}{2}J\omega^2/P_{rated}$,
J = moment of inertia of the rotor, and
$\omega = 2\pi f$.

The electric power is the real part of the product of E_T and I_s*:

$$P_e = \text{real part of } [E_T \cdot I_S^*] \tag{14.22}$$

where I_s* is the complex conjugate of the stator current.

The mechanical power fluctuations can be expressed by a sine wave superimposed on the steady value of P_{mo} as follows:

$$P_m = P_{mo} + \Delta P_m \sin \omega_1 t \tag{14.23}$$

where ω_1 = rotor speed fluctuation corresponding to the wind power fluctuation.

Solving these equations by an iterative process on the computer, Feijoo and Cidras[4] showed that fluctuations of a few hertz could cause noticeable voltage and current fluctuations. Fluctuations on the order of several hertz are too small to be detected at the machine terminals. The high-frequency fluctuations, in effect, are

filtered out by the wind turbine inertia, which is usually large. That leaves only a band of fluctuations that can be detected at the generator terminals.

The flickers caused by wind fluctuations may be of concern in low-voltage transmission lines connecting to the grid. The voltage drop related to power swing is small in high-voltage lines because of the small current fluctuation for a given wind fluctuation.

The power quality regulations in Denmark require all grid-connected power plants — onshore or offshore — to be capable of reducing the power output by 20% within 2 sec of a fault to keep the network stable during a fault. German and Swedish grid authorities are also considering imposing such regulations on all grid interconnections.

The flickers are also caused by frequent switching of the wind generator on and off at the wind speed around the cut-in speed. This problem is aggravated when the area grid has many wind generators distributed along the lines. The grid company usually allows such switching no more often than three to four times per hour. A desirable solution is to keep the rotor switched off until the wind reaches a stable speed beyond the cut-in value, with some deadband hysteresis built into the control process.

The wind generator's low-frequency mode of oscillation may be excited by random wind fluctuation, wind shear, and tower shadow, producing large ripples in the driving torque as well as in generated electric power, which can be noticed as an approximately 0.5% voltage flicker at a frequency between 2 and 4 Hz. Several control strategies of static converters have been designed to provide damping of such oscillations and voltage flickers.

Flicker limits are specified in IEEE standards 141-1993 and 519-1992, which have served the industry well for many years. Cooperative efforts between IEC, UIE, EPRI, and IEEE have resulted in updated standards as documented in IEC standards 61000-3.

14.8 RENEWABLE CAPACITY LIMIT

A recent survey made by Gardner[5] in the European renewable power industry indicates that the grid interface issue is one of the economic factors limiting full exploitation of available wind resources. The regions with high wind-power potentials have weak existing electrical grids. In many developing countries such as India, China, and Mexico, engineers are faced with problems in locating sites that are also suitable for interfacing with the existing grid from the point of view of power quality. The basic consideration in such decisions is the source impedance before and after making the connection. Another way of looking at this issue is the available short-circuit megavoltampere (*MVA*) at the point of proposed interconnection. The short-circuit *MVA* capacity is also known as the *system stiffness* or the *fault level*.

14.8.1 System Stiffness

One way of evaluating the system stiffness after making the interconnection is by using the Thevenin equivalent circuit of the grid and the renewable plant separately, as shown in Figure 14.11. If we assume

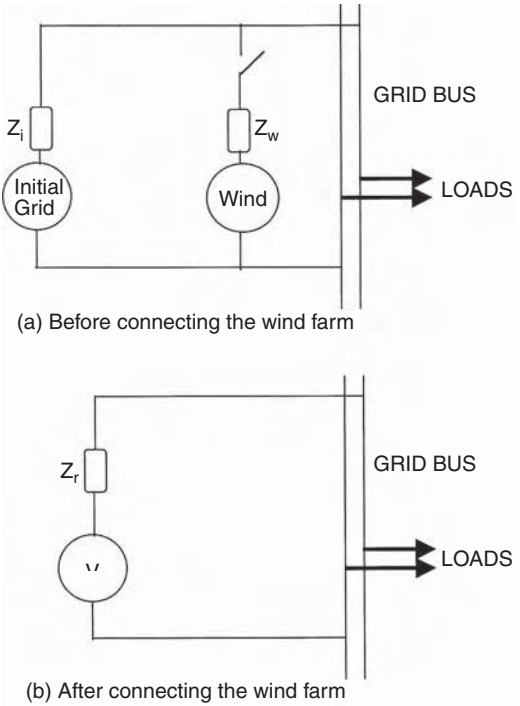

FIGURE 14.11 Thevenin equivalent circuit model of the grid and wind farm for evaluation of the grid interface performance for evaluating system stiffness at the interface.

V = network voltage at the point of the proposed interconnection,
Z_i = source impedance of the initial grid before the interconnection,
Z_w = source impedance of the wind farm,
Z_l = impedance of the interconnecting line from the wind farm to the grid, and
Z_T = total combined source impedance of the two systems,

then, after connecting the system with the proposed wind capacity to the grid, the combined equivalent Thevenin network would be as shown in (b), where:

$$\frac{1}{Z_T} = \frac{1}{Z_i} + \frac{1}{Z_w + Z_l} \tag{14.24}$$

The combined short-circuit *MVA* at the point of the interconnection is then:

$$MVA_{sc} = \frac{\text{Rated MVA Capacity}}{Z_{T\text{per unit}}} \tag{14.25}$$

The higher the short-circuit *MVA*, the stiffer the network. A certain minimum grid stiffness in relation to the renewable power capacity is required to maintain the

power quality of the resulting network. This consideration limits the total wind capacity that can be added at a site. A wind capacity exceeding that limit may be a difficult proposal to sell to the company in charge of the grid.

Not only is the magnitude of Z_T important, the resistance R and the reactance X, which are components of Z_T, have their individual importance. Fundamental circuit theory dictates that the real and reactive power in any electrical network must be separately maintained in balance. Therefore, the real and reactive components of the wind generator impedance would impact the network, more so in a weaker grid. The R/X ratio is often found to be 0.5, which is generally satisfactory for fixed-speed wind generators. Lower R/X ratios may pose another limitation when designing the system.

The fault current decays exponentially as $e^{-R/X}$. A low R/X ratio causes the fault current to persist, making fault protection relaying more difficult. Voltage regulation (variation from zero to full load on the wind farm) is yet another design consideration that is impacted by the R/X ratio. The estimated voltage regulation of the wind farm must be compared with the contractual limit of the utility. In doing so, the actual continuous maximum load the wind farm can deliver must be taken into account, and not the nominal rating, which can be much higher. The acceptable voltage regulation is typically 5% in industrialized countries and 7% in developing countries.

Starting the wind generator as induction motor causes an inrush of current from the grid, resulting in a sudden voltage drop for a few seconds. This can be outside the tolerance limits of the grid line. Most countries limit this transient voltage dip to 2 to 5%, the higher value prevailing in developing countries. Fortunately, for wind farms with many machines, the machines can be started in sequence to minimize this effect. For a very weak system, however, this issue can limit the number of machines that can be connected to the grid. The voltage-flicker severity increases as the square root of the number of machines. The flicker caused by starting one machine varies inversely with the fault level at the point of grid connection, and hence can be an issue on weaker grids.

Harmonics are generated by the power electronics employed for soft-start of large wind turbines and for speed control during energy-producing operations. The former can be generally ignored due to its short duration and because of the use of sequential starts.

The operating harmonics, however, need to be filtered out. The total harmonic content of the wind farm is empirically found to depend on the square root of the number of machines. Because the high-voltage grid side has a lower current, using pulse-width-modulated converters on the grid side can be advantageous. Utility grids around the world are not consistent in the way they limit harmonics. Some grids limit harmonics in terms of the absolute current in amperes, whereas others set limits proportional to the grid's short-circuit *MVA* at the point of interconnection.

Utilities find it convenient to meet power quality requirements by limiting the total renewable power rating to less than a small percentage of the short-circuit *MVA* of the grid at the proposed interface. The limit is generally 2 to 3% in developed countries and 5% in developing countries. This becomes restrictive because a strong wind area is usually available in a nonurbanized area, where the grid is usually weak.

It is more restrictive than the overall power quality requirement imposed in accordance with national standards.

14.8.2 Interfacing Standards

Wind farms connected to the grid may pose problems in regard to the following system-level issues, especially for large-capacity wind farms on a weak grid:

- Electrical stiffness
- Short-circuit *MVA* capacity
- Quality of power
- National standards

The maximum capacity the renewable power plant can install is primarily determined from system stability (discussed in Chapter 13) and power quality considerations (presented in this chapter). A rough rule of thumb to control power quality has been to keep the renewable power plant capacity in MW less than the grid line voltage in kV if the grid is stiff (large). On a weak grid, however, only 10 or 20% of this capacity may be allowed. The regulations generally imposed on renewable power farms these days are in terms of the short-circuit capacity at the proposed interface site.

The major power quality issues discussed in this chapter are as follows:

- Acceptable voltage variation range on the distribution system
- Step change in voltage due to step loading
- Steady-state voltage regulation
- Voltage flickers caused by wind speed fluctuation
- *THD* factor of harmonics

The generally acceptable voltage variations in the grid voltage at the distribution point in four countries are given in Table 14.2. The limit on the step change a customer can trigger on loading or unloading is listed in Table 14.3. It is difficult to determine the maximum renewable capacity that can be allowed at a given site that will meet all these complex requirements. It may be even more difficult to demonstrate such compliance. In this situation, some countries impose limits as percentages of the grid short-circuit capacity. For example, such limits in Germany and Spain are listed in Table 14.4. These limits, however, are continuously evolving in most countries at present.

The International Electrotechnical Commission (IEC) is drafting the power quality standards applicable specifically to grid-connected wind farms. It is expected that these standards will be more realistic than the rigid criteria based on the ratio of the wind turbine capacity to the short-circuit *MVA* of the grid. It may ultimately provide a consistent and predictable understanding of the power quality requirements for designing wind farms that comply with power quality requirements.

TABLE 14.2
Acceptable Voltage Variation at Distribution Points

Country	Acceptable Range (%)
U.S.	±5
France	±5
U.K.	±6
Spain	±7

Note: Low-voltage consumers may see wider variations.

TABLE 14.3
Allowable Step Change in Voltages a Customer Can Trigger by Step Loading or Unloading

Country	Allowable Range (%)
France	±5
U.K.	±3
Germany	±2
Spain	±2 for wind generators ±5 for embedded generators

TABLE 14.4
Renewable Power Generation Limits as Percentages of the Grid Short-Circuit Capacity at the Point of Interface

Country	Allowable Limit (%)
Germany	2
Spain	5
Other countries	Evolving

Voltage dips, interruptions, and variations in consumer power networks have been measured and quantified by several organizations, including Eurelectric. Table 14.5 is a typical assessment of power quality within European power distribution networks.

TABLE 14.5
Voltage Dips, Interruptions, and Variations on European Power Distribution Networks

Voltage Drop (%)	Duration of Disturbance and Number of Events per Year			
	10 msec to 100 msec	100 msec to ½ sec	1.2 sec to 1sec	1 sec to 3 sec
10–30	61	66	12	6
30–60	8	36	4	1
60–100	2	17	3	2
100	0	12	24	5

Source: From Lutz, M. and Nicholas, W., *Conformity Magazine*, November 2004, p. 12.

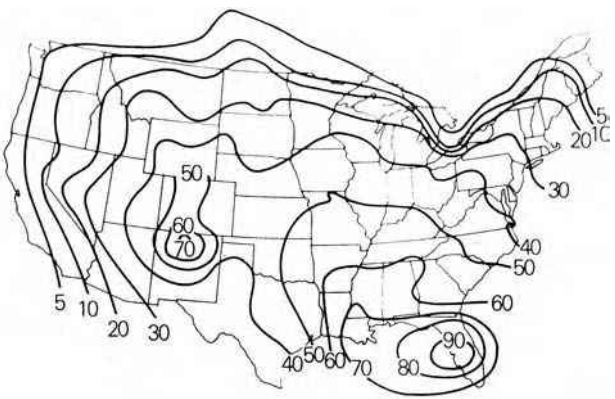

FIGURE 14.12 Thunderstorm frequency in the U.S. and southern Canada. The contour lines indicate the average number of days per year on which thunderstorms occur.

14.9 LIGHTNING PROTECTION

The risk of mechanical and thermal damage to the blades and electrical systems due to lightning is minimized by a coordinated protection scheme using lightning arresters and spark gaps[6] in accordance with international standards. IEC Standard 1024-1 covers the requirements for protection of structures against lightning. The electrical generator and transformer are designed with a certain minimum Basic Insulation Level (BIL) consistent with the lightning risk in the area. The risk is proportional to the number of thunderstorms per year in the area, which is depicted in Figure 14.12 for the U.S. and southern Canada.

Tall towers in open spaces are more vulnerable to lightning risk. A new development in the wind power industry is that offshore wind power towers experience a higher-than-average incidence of lightning strikes. System manufacturers have addressed this issue with design changes. Figure 14.13 is one such solution developed

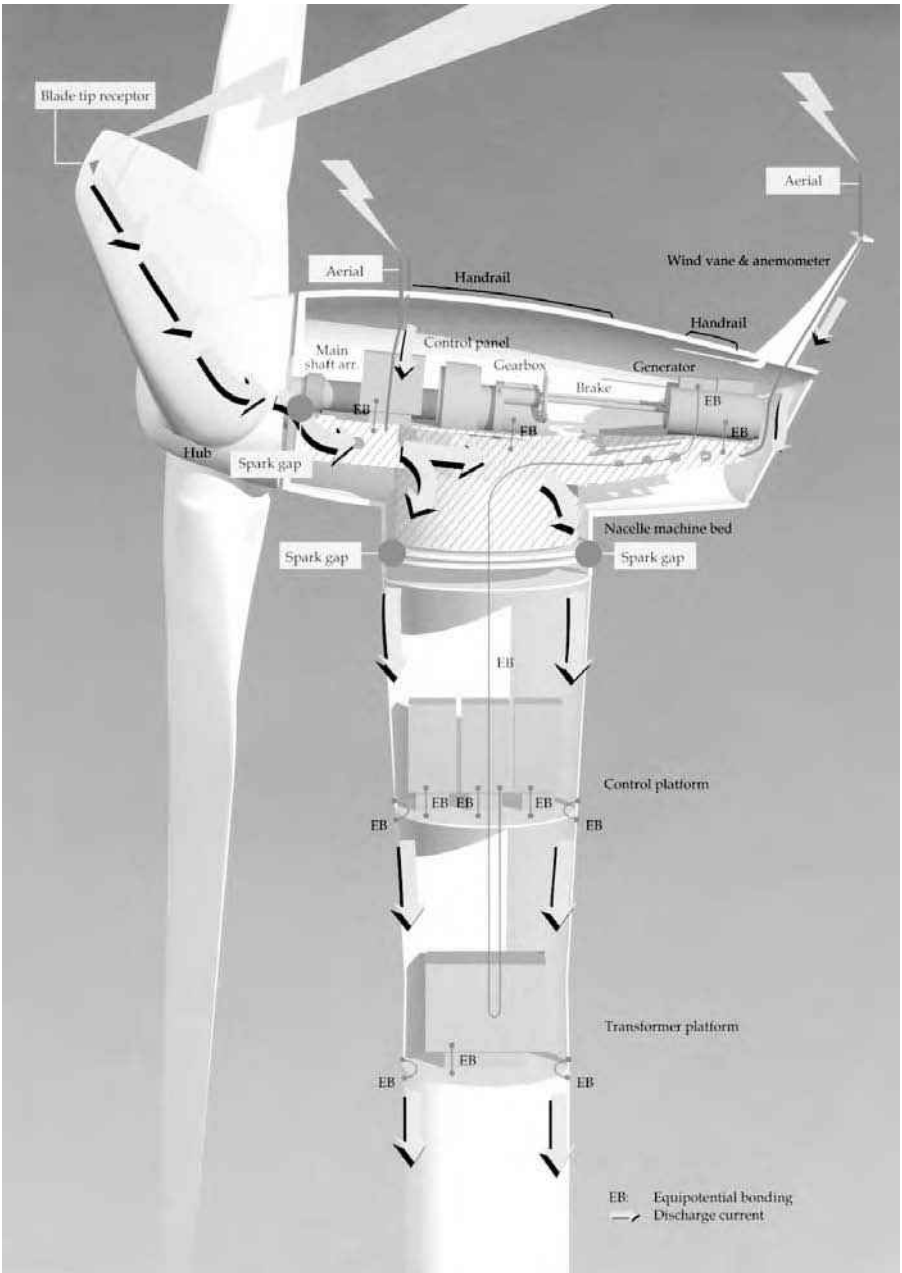

FIGURE 14.13 Lightning protection of the wind tower. (From Vestas Wind Systems, Denmark. With permission.)

by Vestas Wind Systems (Randers, Denmark). The lightning current is conducted to the ground through a series of spark gaps and equipotential bonding at joints. The transformer is protected by placing it inside the tower.

14.10 NATIONAL ELECTRICAL CODE®

The National Electrical Code[7] has recently established electrical system requirements for wind and PV power systems. The PVs are covered in Article 690. Article 705 covers all renewable and cogeneration power systems, including wind, which has been reproduced in Appendix 1 of this book.

REFERENCES

1. Adkins, B., *The General Theory of Electrical Machines*, Chapman and Hall, London, 1964.
2. Kron, G., *Equivalent Circuits of Electrical Machines*, Dover Publications, New York, 1967.
3. Oliva, A.R., Balda, J.C., McNabb, D.W., and Richardson, R.D., Power quality monitoring of a PV generator, IEEE paper No. PE-507-EC0-07, 1997.
4. Feijoo, A. and Cidras, J., Analyses of mechanical power fluctuations in asynchronous WECs, IEEE paper No. PE-030-EC-0-1 0, 1997.
5. Gardner, P., Wind farms and weak networks, *Wind Directions*, Magazine of the European Wind Energy Association, London, July 1997.
6. Lewis, W.W., *The Protection of Transmission Systems Against Lightning*, Dover Publications, New York, 1965.
7. *National Electrical Code Handbook*, 7th ed., National Fire Protection Association, Quincy, MA, 2004.

15 Plant Economy

The economic viability of a proposed plant is influenced by several factors that contribute to its profitability. The plant proposal is generally initiated with some expected values of the contributing factors. As the expected profitability would vary with deviations in these factors, the sensitivity of profitability to such variances around their expected values is analyzed. Such a sensitivity analysis determines the range of profitability and raises the confidence level of potential investors. This is important for both wind and photovoltaic (PV) systems but more so for wind systems, in which profitability is extremely sensitive to wind speed variations.

The primary factors that contribute to the economic viability of a wind farm or PV park are discussed in this chapter. The results are displayed in easy-to-use charts for screening the profitability of the proposed plant. Such charts can be used for a quick estimate of profitability and its sensitivity to deviations in wind speed, solar radiation, and other contributing factors.

15.1 ENERGY DELIVERY FACTOR

The key economic performance measure of a power plant is the electric energy it delivers over the year. Not all power produced is delivered to the paying customers. A fraction of it is used internally to power the control equipment, in meeting power equipment losses, and in housekeeping functions such as lighting. In a typical wind farm or PV park, about 90% of the power produced is delivered to the paying customers, and the remaining is self-consumed in plant operations.

The quantity of energy delivered depends on the peak power capacity of the site and how fully that capacity is utilized. A normalized measure of the power plant performance is the energy delivery factor (*EDF*). It is defined as the ratio of the electric energy delivered to customers to the energy that could have been delivered if the plant were operated at full installed capacity during all the 8760 h of the year. It is expressed as follows:

$$\text{average annual } EDF = \frac{\text{kWh delivered over the year}}{\text{installed capacity} \times \text{number of hours in the year}} \tag{15.1}$$

Because the load power varies over time, *EDF* takes the following integral form:

$$\text{average annual } EDF = \frac{\int_{\text{year}} P_o(t)\,dt}{P_{max} \cdot 8760} \tag{15.2}$$

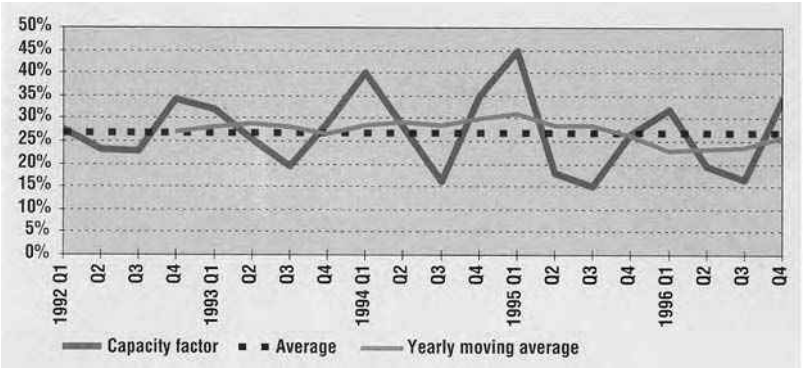

FIGURE 15.1 Capacity factors of operating wind farms in England and Wales. (From U.K. Department of Trade and Industry, Renewable Energy Technology Status Report, August 1997. With permission.)

where
P_{max} = Plant capacity (maximum power the plant can deliver)
$P_o(t)$ = Power delivered to the customers at any time t.

EDF is usually determined by recording and summing the energy delivered over a continuous series of small discrete time intervals as follows:

$$\text{average annual } EDF = \frac{\sum^{\text{year}} P_{\text{avg}}(\Delta t)}{P_{\max} \cdot 8760} \tag{15.3}$$

where P_{avg} = average power delivered over a small time interval Δt.

Thus, *EDF* is a figure of merit that measures how well the plant is utilized to deliver the maximum possible energy. Not only does it include the energy conversion efficiencies of various components, it also accounts for the overall reliability, maintainability, and availability of the plant over the entire year. Therefore, *EDF* is useful in comparing the economic utilization of one site over another, or to assess the annual performance of a given site. Wind plants operate at an annual average *EDF* of around 30%, with some plants reporting an *EDF* as high as 40%. This compares with 40 to 80% for conventional power plants, the peak-power plants near 40%, and the base-load plants near 80%.

It must be taken into account that the wind farm *EDF* varies with the season. As an example, the quarterly average *EDF* of early wind plants in England and Wales are shown in Figure 15.1. The operating data show rather wide variations, ranging from 15 to 45%. The *EDF* is high in the first quarter and low in the last quarter of every year. Even with the same kilowatthours produced per year, the average price per kilowatthour that the plant may fetch could be lower if the seasonal variations are wide.

TABLE 15.1
Capital Cost for Various Power Technologies

Plant Technology	Capital Cost (US$/kW)
Wind turbine	400–700
Solar PV	1500–3000
Solar thermal (Solar-II type)	3000–5000 (land ~15 acres/MW)
Coal thermal (steam turbine)	400–600 (land ~10 acres/MW)
Combined cycle (gas turbine)	800–1200

TABLE 15.2
Wind Power System Component Cost Contribution in Total Capital Cost

Cost Item	Contribution (%)
Rotor assembly	25
Nacelle structure and auxiliary equipment	15
Electric power equipment	15
Tower and foundation	10
Site preparation and roads	10
Ground equipment stations	8
Maintenance equipment and initial spares	5
Electrical interconnections	4
Other nonrecurring costs	3
Financing and legal	5
Total	100

Note: Land cost is not included.

15.2 INITIAL CAPITAL COST

The capital cost depends on the size, site, and technology of the plant. Typical ranges for various types of large power plants are given in Table 15.1. The costs of technologically matured coal and gas turbine plants are rising with inflation, whereas wind and PV plant costs are falling with new developments in the field. Therefore, renewable-power-plant costs must be estimated along with their component costs current at the time of procurement, which may be lower than at the time of planning.

The percentage breakdown of the component costs in the total initial capital cost of a typical wind farm is given in Table 15.2. As expected, the single-largest cost item is the rotor assembly (blades and hub).

15.3 AVAILABILITY AND MAINTENANCE

The rates and effects of failure determine the maintenance cost of the plant and its availability to produce power. The data from past operating experiences are used for learning lessons and making improvements. In the wind power industry, failures, their causes, and their effects are recorded and periodically published by ISET, the solar energy research unit of the University of Kassel in Germany. Figure 15.2 summarizes ISET's early database.[1] The statistics show that the plants were nonoperational for 67%

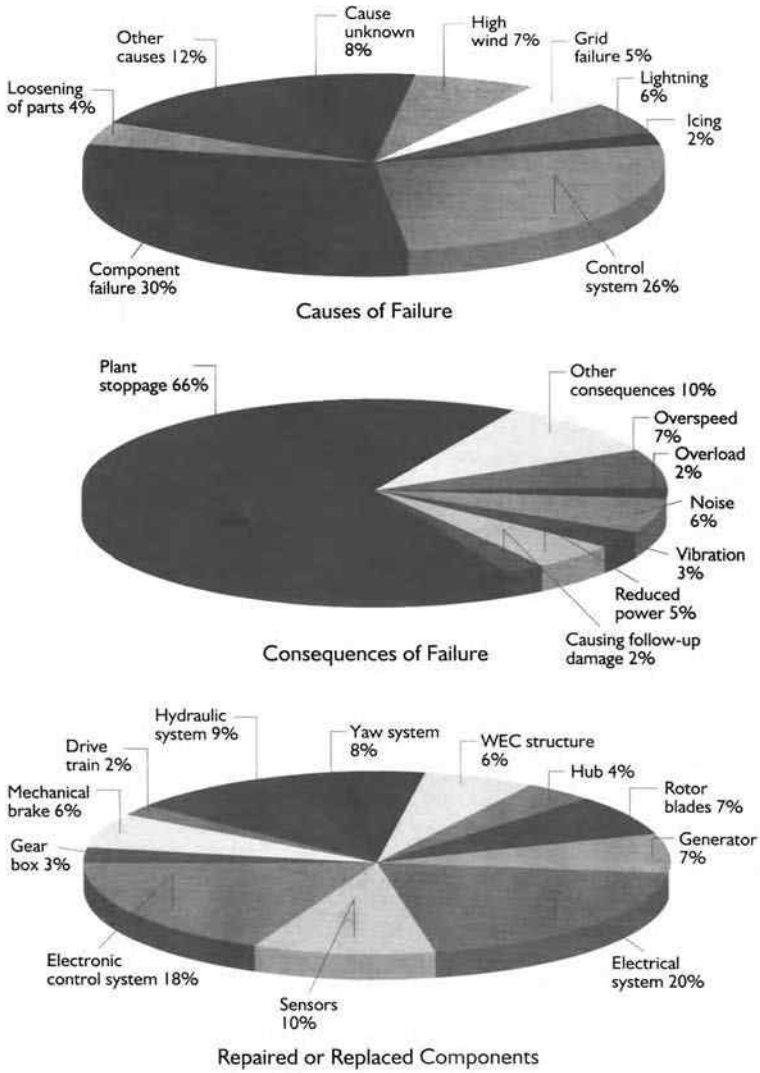

FIGURE 15.2 Wind power plant failure, cause, effect, and repair statistics. (From Institute of Solar Energy and Technology, University of Kassel, Germany. With permission.)

of the time during the reported period. Among the repairs needed to bring the plants back to operation, 20% was in the electric power equipment and 19% in the electronic controls. The major causes of failure were related to the control systems (28%) and component defects (24%). The failure rates have declined from those levels with the design improvements made since then. The wind power industry has developed a database that records specific failures, their causes, and their effects. In modern systems, however, with many components incorporating computers of some sort, almost 80% of the problems are computer related.

The overall availability of the plant is defined as the ratio of hours in a year that the plant is available to deliver power to the total hours in the year. It is impacted by downtimes due to repairs and routine maintenance, which are reflected in the EDF. Significant improvements in reliability and maintainability have pushed the availability of modern renewable power plants up to 95% in recent years. However, data shows that, for about 50% of the time during an average year, the plant undergoes an outage or is not operational because of low wind speeds.

The PV systems, being static, require a much lower level of maintenance relative to the wind systems, which have moving parts. With proper maintenance, most wind turbines are designed to operate for 20 to 30 yr, which translate to about 200,000 h of operation. However, the actual life and optimum maintenance schedule depend on the climatic conditions and the quality of design and construction. Climatic conditions include wind turbulence and the stress cycles on the turbine. Offshore wind turbines experience low wind turbulence compared to their counterparts on land.

As for maintaining wind turbines, many factors go into setting an optimum maintenance strategy and schedule. Too little maintenance can cost in downtime, whereas too much would in itself be expensive. The industry-average normal maintenance period has been once every 6 months for onshore turbines and once every year for offshore turbines. With regular, periodic oil change, the life of the gearbox is 5 to 7 yr, and the overall life of the turbine is 20 to 30 yr.

Maintenance cost is low when the machine is new and increases with time. For large wind turbines in megawatt capacities, the annual maintenance costs range from 1.5 to 2% of the original turbine cost. In plants with EDF of 30 to 40%, this translates as ½ to 1 cent/kWh in energy costs.

When a wind turbine nears the end of its life, the overall structure, including the foundation and tower, may be in good shape, but the rotor and gearbox may need to be replaced. The price of a new set of rotor blades and gearbox is usually 15 to 20% of the turbine price.

15.4 ENERGY COST ESTIMATES

A key parameter of performance of an electric power plant is the unit cost of energy (*UCE*) per kilowatthour delivered to the paying consumers. It takes into account all economic factors discussed in the preceding sections and is given by the following:

$$UCE = \frac{ICC(AMR + TIR) + OMC}{EDF \cdot KW \cdot 8760} \tag{15.4}$$

TABLE 15.3
Cost of Electricity with Various Power Technologies in 2003

Plant Technology	Direct Generation Cost[a] Fuel + Capital (cents/ kWh)	Indirect External Costs[b] (cents/ kWh)	Total Cost to the Society (cents/ kWh)
Wind turbine	3–5	0.1–0.3	3.1–5.3
Solar PV	15–25	0.5–1	15.5–26
Solar thermal (Solar-II type)	8–10	0.1–0.3	8.1–10.3
Biomass	7–9	0.2–3	7.2–12
Hydro	3–7	0–1	3–8
Coal thermal (steam turbine)	3–4	2–15	5–19
Nuclear	10–14	0.2–1	10.2–15
Natural gas	3–5	1–4	4–9
Combined cycle (gas turbine)	5–7	2–6	7–13

[a] Generation cost estimates are for the U.S. and Europe.

[b] External costs are for meeting the U.S. and European environment and health standards, converted in U.S. cents/kWh at $1 = 0.90 euros.

Source: From Mainstreaming Renewable Energy in the 21st Century.

where

ICC = initial capital cost, including the land cost and startup cost up to the time the first unit of energy is sold
AMR = amortization rate per year as a fraction of the ICC
TIR = tax and insurance rate per year as a fraction of the ICC
OMC = operating and maintenance costs per year
EDF = energy delivery factor over 1 yr
KW = kilowatt electric power capacity installed

The amortization rate reflects the cost of capital. It is generally taken as the mortgage interest rate applicable to the project. The *EDF* accounts for variations in the impinging energy (sun intensity or wind speed) at the proposed site and all downtimes — full or partial. It is also a strong function of the reliability and maintainability of the plant through the year.

The insurance on a wind farm project covers delays or damages during construction or operation whether because of technical reasons or the forces of nature. The costs of insurance necessary for financing wind projects have significantly increased in recent years. Offshore wind farms, being relatively new, are exposed to even more unknown factors and therefore charged higher premiums.

The present costs of various energy sources are summarized in Table 15.3. It shows the direct generation cost and the indirect external costs for meeting environmental and health standards in the U.S. and Europe. The table shows that wind power now compares well with the conventional coal thermal and other types of power plants.

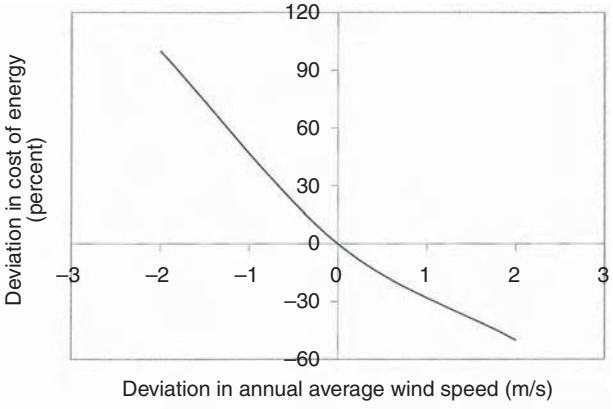

FIGURE 15.3 Sensitivity analysis of wind electricity cost with variation in wind speed around the expected annual mean of 10 m/sec.

15.5 SENSITIVITY ANALYSIS

It is not sufficient to accurately estimate the cost of electricity produced. Project planners must also carry out a sensitivity analysis, in which the energy cost is estimated with a series of input parameters deviating on both sides of the expected values. The sensitivity of the energy cost to variations in two primary economic factors — wind speed in wind farms and solar radiation in PV parks — is discussed in the following subsections.

15.5.1 Effect of Wind Speed

Because the energy output of a wind plant varies with the cube of wind speed, a change in speed by several percentage points can have a significant impact on plant economy. For example, if the annual average wind speed is 10 m/sec, the unit cost of energy is calculated for wind speeds ranging from 8 to 12 m/sec. The plant site is considered economically viable only if the plant can be profitable at the low end of the range. Figure 15.3 illustrates the result of a sensitivity study. It shows that the cost of electricity can be as low as half or as high as twice the expected value if the wind speed turns out to be higher or lower by 2 m/sec than the expected value of 10 m/sec.

15.5.2 Effect of Tower Height

The tower height varies from approximately four times the rotor diameter for small turbines (kW ratings) to a little over one diameter for large turbines (MW ratings). For small turbines, it is determined by the wind speed at the hub. The higher the hub, the greater the wind speed. For large turbines, it is primarily determined by the tower structure and the foundation design.

As seen in Table 15.2, the turbine cost constitutes 25% of the total wind farm cost. Because wind speed increases with tower height, a given turbine can produce more energy and reduce the cost of energy if installed on a taller tower. To study the influence of tower height on energy cost, we define E_1 as the contribution of the turbine cost in the total energy cost per square meter of the rotor-swept area. E_1 is, therefore, measured in \$/kWh·m^2. The power is proportional to the square of the rotor diameter and the cube of the wind speed as follows:

$$P \propto D^2V^3 \tag{15.5}$$

The energy captured over the life of the turbine is also proportional to the same parameters, i.e., D^2 and V^3. In a matured, competitive market, the rotor cost would be proportional to the swept area, hence D^2, although it is far from that stage in the rapidly evolving market at present. However, assuming a competitive market, E_1 is as follows:

$$E_1 \propto D^2/D^2V^3 \propto 1/V^3 \tag{15.6}$$

As seen earlier in Equation 3.34, the wind speed varies with tower height in the exponential relation:

$$V \propto H^{\alpha} \tag{15.7}$$

where H = tower height at the hub and α = terrain friction coefficient.

Combining Equation 15.6 and Equation 15.7, we obtain:

$$E_1 \propto \frac{1}{H^{3\alpha}} \tag{15.8}$$

The parameter α varies with the terrain. Table 3.3 in Chapter 3 gives these parameter values — 0.10 over the ocean, 0.40 over urban areas with tall buildings, and the often-used average of 0.15 (~1/7) in areas with foot-high grass on flat ground. Even a higher value of 0.43 was estimated for a New England site at Stratton, Mt. Vermont.[2] With such wide variations in α, the wind speed can vary with tower height over a wide range from $H^{0.3}$ to $H^{1.3}$.

Equation 15.8 clearly indicates that the turbine contribution in cost of energy per unit swept area decreases at least with the square root of the tower height. With the average value of $\alpha = 0.15$, the turbine cost contribution is approximately given by the following:

$$\text{turbine cost per kWh per m}^2 \qquad E_1 = \frac{\text{constant}}{\sqrt{\text{tower height}}} \tag{15.9}$$

In rough terrains, the tower height can be extremely beneficial as shown by the following equation with $\alpha = 0.40$:

$$\text{turbine cost per kWh per m}^2 \qquad E_1 = \frac{\text{constant}}{H^{1.2}} \tag{15.10}$$

Equation 15.9 and Equation 15.10 indicate that there is not much benefit in increasing the tower height in offshore installations that have low α values. However, on rough terrains that have high α, increasing the tower height from 30 to 60 m would decrease the contribution of the turbine cost per kWh/m^2 by 56%, a significant reduction. Therefore, determining the α parameter accurately for a specific site is extremely important in determining the tower height and plant economy. An uneconomical site using short towers or a conservative estimate of an average value of α can turn out to be profitable with tall towers and/or the site-specific value of α obtained by actual measurements. In the early data-collection period, therefore, anemometers are installed on multiple towers at two or more heights on the same tower to determine the α at the site.

15.6 PROFITABILITY INDEX

As with conventional projects, profitability is measured by the profitability index (*PI*), defined as follows:

$$PI = \frac{\text{present worth of future revenues} - \text{initial project cost}}{\text{initial project cost}} \tag{15.11}$$

By definition, a *PI* of zero gives the break-even point.

Profitability obviously depends on the price at which a plant can sell the energy it produces. In turn, it depends on the prevailing market price that the utilities are charging the area customers. Installations in regions with high energy cost could be more profitable if the capital cost is not high in the same proportion. Table 15.4 lists the average electricity prices in 2004 in certain regions of the U.S. The average price in the U.K. is about 10 pence/kWh (about 17 cents/kWh).

Inputs to the renewable power plant profitability analysis include the following:

- Anticipated energy impinging the site, that is, the wind speed at hub height for a wind farm or the solar radiation rate for a PV park
- Expected initial capital cost of the installation
- Cost of capital (usually the interest rate on the loans)
- Expected economic life of the plant
- Operating and maintenance costs
- Average selling price of the energy generated by the plant

TABLE 15.4
Average Electricity Prices for U.S. Residential Customers in High-Cost Areas in 2004

Utility Area	Cents/kWh
Long Island Lighting, New York	22
Consolidated Edison, New York	21
Public Service of New Hampshire	20
New York State Electric and Gas	18
Commonwealth Energy Systems, MA	18
Central Maine Power, ME	17
PECO Energy, PA	17
Public Service Electric, NJ	17

Note: Average price in the U.K. ≈ 10 pence/kWh ≈ 17 cents/kWh.

A detailed multivariable profitability analysis with these parameters is always required before making financial investments. Potential investors can make initial profitability assessments using screening charts. The following subsections present easy-to-use charts for initial profitability screening of the wind and PV power plant sites.

15.6.1 Wind Farm Screening Chart

Figure 15.4 is a wind farm profitability-screening chart based on an initial cost of €1100 per kW capacity, cost of capital (discount rate) of 8%, a project life of 15 yr, and operating and maintenance costs of 3% of the initial project cost.[3] The chart takes into account a flat rate of inflation, i.e., costs and revenues rising at the same rate. Taxes on sales, if any, must be deducted from the average selling price before it is entered while reading the chart.

Example: To illustrate the use of Figure 15.4, consider a site with 7.5 m/sec wind speed at hub height; the *PI* would be zero (the break-even point) if the energy can be sold at €0.069/kWh. If the energy price were €0.085/kWh, the *PI* would be 0.30, generally an attractive value for private investors. At a site with only 7 m/sec wind speed, the same profitability can be achieved if the energy can be sold at €0.097/kWh.

15.6.2 PV Park Screening Chart

Similar screening charts for PV stand-alone or grid-connected systems are shown in Figure 15.5 and Figure 15.6.[4] For these charts, the yearly energy delivery E_y in kWh/yr is defined as follows:

$$E_y = K_p H_y P_{pk} \tag{15.12}$$

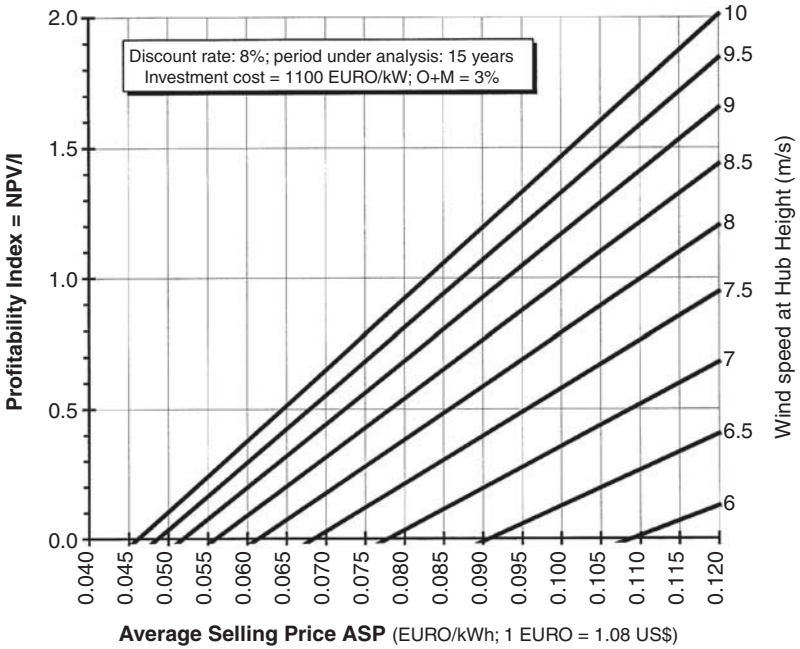

FIGURE 15.4 Profitability chart for wind farms. (From Chabot, B., L'analyse economique de l'energie ecolienne, *Revue de l'Energie*, ADME, France, No. 485, February 1997; *Wind Directions*, magazine of the European Wind Energy Association, London, October 1997. With permission.)

where

K_p = performance ratio of the system

H_y = yearly solar irradiation in the plane of the modules, kWh/m^2/yr

P_{pk} = installed peak power under the standard test conditions of 1 kW/m^2 solar irradiation, cell-junction operating temperature of 25°C, and air mass of 1.5.

The PV energy conversion efficiency of the modules is included in $P_{pk.}$ A typical value of K_p is 0.7 to 0.8 for a grid-connected system without battery and delivering alternating current (AC) and 0.5 to 0.6 for a stand-alone system using battery and delivering direct current (DC) power.

The inputs to the figures are the initial project cost of the PV system in dollars or euros per peak watt capacity I_{up}, cost of capital, plant life, operating and maintenance costs K_{om}, yearly solar radiation H_y, and the performance parameter K_p as defined earlier. With these inputs, Figure 15.5 gives the overall discounted cost (ODC) of electricity delivered. The life of the plant, n years, can be the desired payback period to recover the initial investment or the full economic life of the plant. In the latter case, the ODC is known as the life cycle cost (LCC) of the energy delivered. The chart is prepared with typical values for large PV farms, such as K_p of 0.75, cost of capital of 8%, a life of 20 yr, and operating and maintenance costs of 2%.

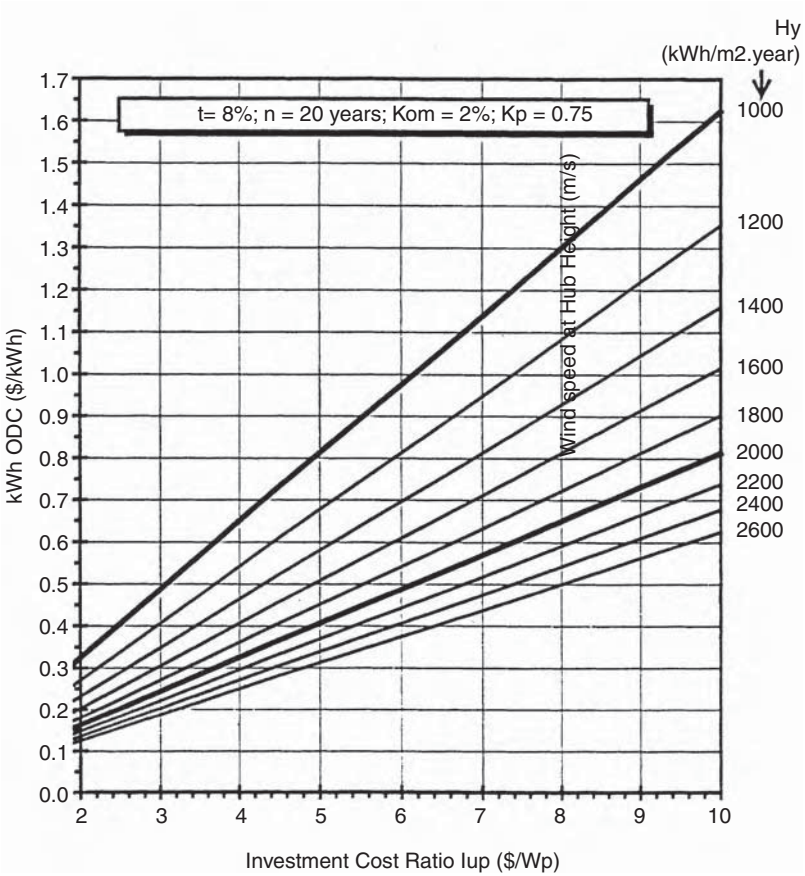

FIGURE 15.5 Overall discounted cost of PV energy. (From Chabot, B., From costs to prices: economic analyses of photovoltaic energy and services, *Progress in Photovoltaic Research and Applications*, Vol. 6, p. 58, 1998. John Wiley & Sons, Bristol, U.K. With permission.)

Example: To illustrate the use of Figure 15.5, we consider a PV site with H_y of 2000 kWh/m^2/yr and a capital cost of \$5 per peak watt (W_p) and see that the energy cost would be \$0.40 per kWh delivered. For the cost of energy to be below \$0.20/kWh, the capital cost of the plant must be \$2.50 per W_p. With new PV technologies being developed and made commercially available at lower costs, a capital cost below \$3/W_p is realizable.

Being costlier than wind power, PV systems at present are more likely to be installed in remote areas where a higher cost can be justified and partially offset by low-interest loans. Figure 15.6 is cast in terms of the *PI* defined earlier. The parameters for this chart are a project cost of \$4/W_p, cost of capital of 3%, an economic life of 30 yr, operating and maintenance costs of 1%, and a performance parameter of 0.75%. For a solar irradiation of 2000 kWh/m^2/yr and an average selling price of 20 cents/kWh, the *PI* would be 0.25, a reasonable number for private investors.

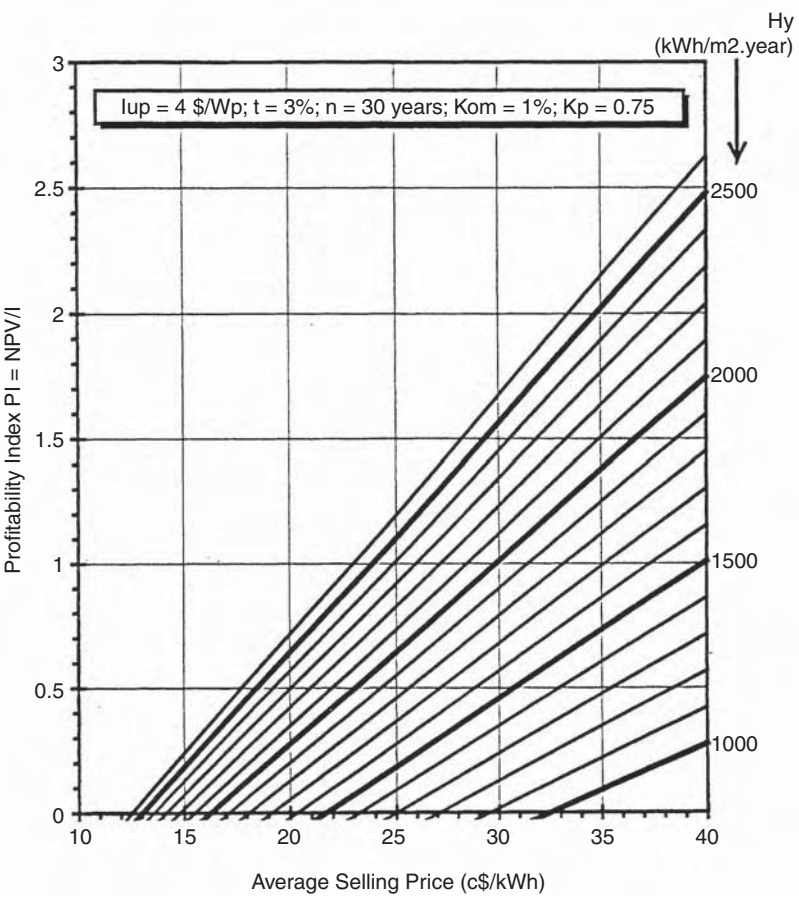

FIGURE 15.6 Profitability chart for photovoltaic power. (From Chabot, B., L'analyse economique de l'energie ecolienne, *Revue de l'Energie*, ADME, France, No. 485, February 1997; Chabot, B., From costs to prices: economic analyses of photovoltaic energy and services, *Progress in Photovoltaic Research and Applications*, Vol. 6, p. 62, 1998. John Wiley & Sons, Bristol, U.K. With permission.)

15.6.3 Stand-Alone PV vs. Grid Line

In remote areas, where grid power is not available and wind power is not an option, a customer who wants electricity has two options:

- Paying the utility company for extending the line
- Installing a PV power plant at the site

The cost of extending the line may be prohibitive if the stretch is long. The line cost is fixed for a given distance of extension. The economy of electric energy, therefore, clearly depends on the energy demand in kWh per day. Figure 15.7 is a

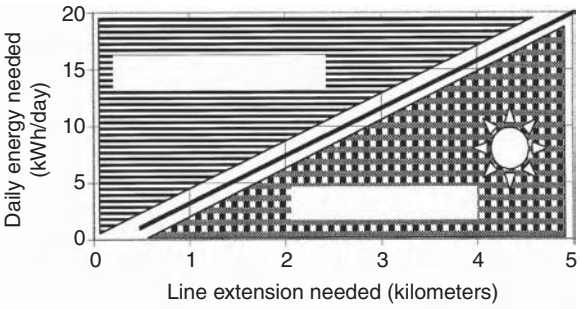

FIGURE 15.7 Stand-alone PV plant or line extension costs for various levels of energy needs based on average 2000 costs in the U.S.

screening chart for making an economic choice between a line extension and installing a PV plant at the site. It has been developed using average utility charges for line extension and PV modules at prices in 2000. As an example of using the chart, if a customer needs 10 kWh/d and lives 3 mi away from the nearest power line, a stand-alone PV at the site would be economical. However, if the distance were 1 mi, the line extension would be economical. The break-even distance for this customer is about 1.7 mi. For another customer who needs 20 kWh/d, the break-even distance would be 3 mi.

In selected low-population-density areas in the U.S., some utility companies offer customers a choice of installing a PV system at the site as an alternative to line extension and costly emergency service of the line that serves one or a few customers. In these areas, however, rural utilities and their customers have conflicting interests. The utility is interested in controlling the cost, whereas the customer is interested in reliable power. The following sequence shows how some U.S. utility companies in rural areas respond to potential PV customers:

1. A customer interested in electric power contacts the utility company.
2. It is determined whether the point-of-service will be economically served by extending a line or installing a PV system at the site.
3. The utility company develops a PV design.
4. The system is installed by an independent contractor.
5. The total capital cost is paid by the utility company.
6. The utility company is responsible for maintenance of the system.
7. The customer is billed a fixed monthly rate, rather than the amount based on the energy consumed. This approach spreads out the burden of the initial capital cost on the customer.

15.7 HYBRID ECONOMICS

A detailed analytical tool to evaluate the economics of hybrid systems has been developed by the National Renewable Energy Laboratory. A newer version, Hybrid-2,[5] allows the user to determine basic economic figures of a particular simulation

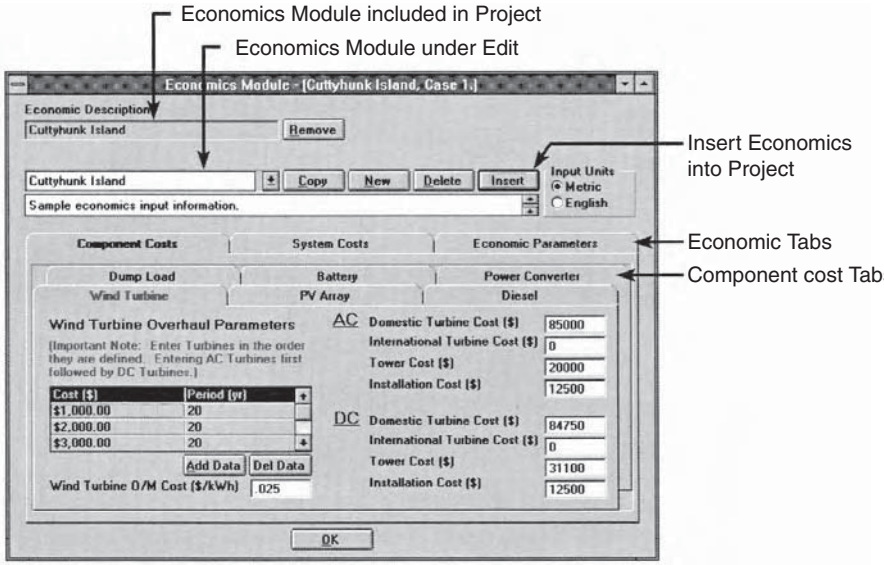

FIGURE 15.8 Hybrid-2 economic simulation model. (From Ian Baring-Gould, National Renewable Energy Laboratory, Golden, CO. With permission.)

run. The economics module uses information from the performance simulation run and economic data supplied by the user. It computes parameters such as the payback period, internal rate of return, cash flow, and equipment replacement expenses. The user has wide versatility in determining the expense of the project and what inputs to include. Parameters such as grid extension, import tariffs, system administration costs, and taxes can be included in the analysis. The user may conduct comparisons between different hybrid possibilities and power solutions and their approximate costs. Figure 15.8 shows the computer screen displaying the choices available to a user. As indicated by the menu buttons, it includes wind, PV, diesel, and battery systems.

Hybrid-2 allows the user to conduct parametric analyses on certain cost parameters such as the fuel cost, discount rate, and inflation rate to help determine how the values of certain parameters can affect the viability of the project.

15.8 PROJECT FINANCE

The project financing and economic viability of a proposed wind or PV power plant depends a great deal on the electricity prices prevailing in the region. The average electricity prices to household customers in various countries in 2002 are listed in Table 15.5. They averaged 3.6 cents/kWh in India, 8.5 cents/kWh in the U.S., and 20.7 cents/kWh in Japan. The high prices in Germany and Japan partly explain the high rate of growth in wind and solar power in those countries. The average U.S. price for the commercial sector in 2004 was 9 cents/kWh.

TABLE 15.5
Average 2002 Residential Electricity Prices in Various Countries

Country	Equivalent U.S. cents per kWh
India	3.6
Mexico	5.5
Poland	6.2
Thailand	7.4
Turkey	8.0
Australia	8.0
U.S.	8.5
South Korea	9.4
Chile	12.1
U.K.	12.5
The Netherlands	13.0
France	13.4
Argentina	13.9
Germany	16.1
Japan	20.7

Source: From *Renewable Energy World*, James & James, London, November 2002, p. 26.

The capital cost is also a factor. For large wind power plants in MW capacity, the total capital cost is about $1/W, including the cost of the last switch to turn on the power. For small wind plants of around 100-kW capacity, it is about $2/W. The capital cost of wind plants in relation to capacity varies as shown in Figure 15.9 (approximate values).

As mentioned earlier, with the new net-metering law in the U.S., school districts are getting interested in installing wind power plants. An example of a 1-MW project for a school district of typical size is shown in Table 15.6. It involves a total capital cost of $1.125 million, produces 2732 MWh electricity per year, and has a payback period of 6.7 yr at a 4.5% project financing cost (discount rate).

As for the project funding, there have been strong financial incentives for renewable power in many countries around the world. However, the incentives have been declining because the renewables are becoming economically competitive on their own merits. More projects are being funded strictly on a commercial basis. Enviro-Tech Investment Funds in the U.S. is a venture capital fund supported by Edison Electric Institute (an association of investor-owned electric utility companies providing 75% of the nation's electricity). The World Bank now includes wind and PV projects in its lending portfolios. Several units in the World Bank group are jointly developing stand-alone projects in many developing countries.

Because wind power and PV power are intermittent, nondispatchable, and unpredictable, they have less economic value than power from fuel sources that can deliver steady, predictable power on demand. Utilities obligated to provide service with

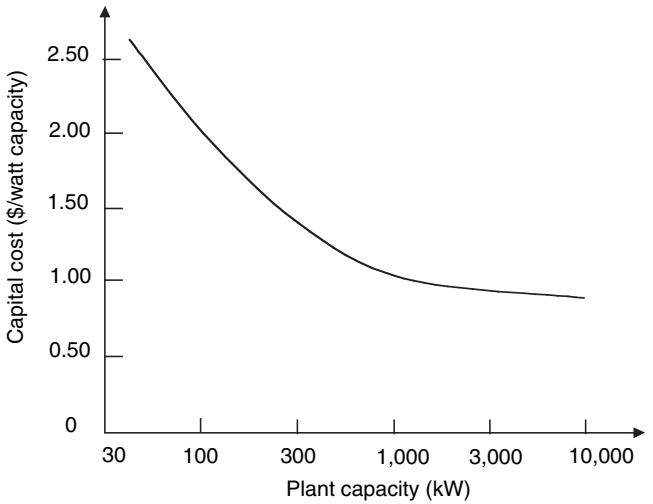

FIGURE 15.9 Declining cost of capital with increasing wind power plant capacity.

TABLE 15.6
Example of Profitability of 1-MW Wind Plant for School Districts

Total capital cost C	$1,125,000
Total yearly cost	$135,235
20-yr mortgage on C @ 4.5%	$86,485
Operating + Maintenance + Insurance costs @ 3 % of C	$33,750
Maintenance contract @ $15,000/MW	$15,000
Plant installed at a wind site in class 5–6 range	
Average wind 8 m/sec at 50-m height (to be verified by data)	
Yearly average power (with k = 2, 80-m hub)	346.6 kWe
Energy production per year with 90% availability	2,732 MWh
Swapping up to 3,150 MWh/yr consumption is allowed	
So, feedback to a grid with 1-MW plant is not needed	
Yearly savings in energy bill at 9 cents/kWh	$245,860
Yearly cost with 100% debt financing	$135,235
Net savings per year after debt servicing	$110,625
Yearly reward for risking capital C	9.8%
Yearly cost with 100% equity financing	$48,750
Net savings per year without debt servicing	$197,110
Payback period at 4.5% discount rate	6.7 yr

almost 100% availability must either back up the intermittent power at a premium, estimated to be between ½ and 1 cent/kWh, or penalize the provider of interruptible power by ½ to 1 cent/kWh price differential. Also, because of the uncertainty of output, lenders impose higher financing costs compared to those for more predictable power generation.

References

1. Institute of Solar Energy and Technology, Annual Report, University of Kassel, Germany, 1997.
2. Cardell, J.B. and Connors, S.R., Wind Power in New England, Modeling and Analyses of Non-dispatchable Renewable Energy Technologies, IEEE Paper No. Power Engineering-888-PWRS-2-06, 1997.
3. Chabot, B., L'analyse economique de l'energie ecolienne, *Revue de l'Energie*, ADME, France, No. 485, February 1997.
4. Chabot, B., From costs to prices: economic analyses of photovoltaic energy and services, *Progress in Photovoltaic Research and Applications*, Vol. 6, pp. 55–68, 1998.
5. Baring-Gould, E.I., *Hybrid-2, The Hybrid System Simulation Model User Manual*, NREL Report No. TP-440-21272, June 1996.

16 The Future

The future of wind and photovoltaic (PV) power and its projected growth, expressed as a percentage of the total electricity demand in the world, are discussed in this chapter. The historical data on market developments in similar basic-need industries and the Fisher–Pry market growth model indicate that PV and wind power may reach their full potential in the year 2065. The probable impact of the U.S. utility restructuring on renewable energy sources is reviewed.

16.1 WORLD ELECTRICITY DEMAND UP TO 2015

According to the U.S. Department of Energy (DOE), electric power is expected to be the fastest-growing source of energy for end users throughout the world over the next two decades. Electricity demand is projected to grow to 19 trillion kWh by the year 2015 (Figure 16.1) at an annual growth rate of 2.6%.[1] The electricity demand in industrial and developing countries projected to 2015 is shown in Figure 16.2, indicating a fast growth rate in developing countries. Table 16.1 shows the per capita consumption by region and country. The Organization for Economic Cooperation and Development (OECD) countries constitute 20% of the world's population but consume over 60% of the world's electricity. The electricity demand of non-OECD Asia is expected to grow faster than that of the Eastern European and former Soviet Union (EE/FSU) countries. This is a result of the relatively high economic growth rate projected for non-OECD Asia. Although the U.S. is the largest consumer of electricity in the world, it has the lowest projected growth rate of 1.3% vs. the world average of 2.6%. Mexico has the highest projected growth rate of 4.7% per year up to the year 2015.

Developing Asia is expected to experience the strongest growth compared to any other region in the world, with a projected growth rate of 5% per year (Figure 16.3). As electricity demand grows, coal will remain the primary fuel for power generation, especially in China and India. The share of nuclear power generation worldwide has reached a peak, and is expected to decline in the future. Coal, natural gas, and renewables are all expected to grow to replace the retiring nuclear power plants. However, the renewables are expected to contribute a greater percentage of the growth. For example, the Swedish government in 1997 started to gradually shut down the country's large nuclear power industry, whose plants supply 50% of Sweden's electricity. This was in response to a referendum vote to end nuclear power in Sweden. To compensate, the government is to step up intervention in the energy market and force a switch to the greater use of nonfossil fuel alternatives. Other industrial countries also have serious commitments to reducing pollution of the environment.

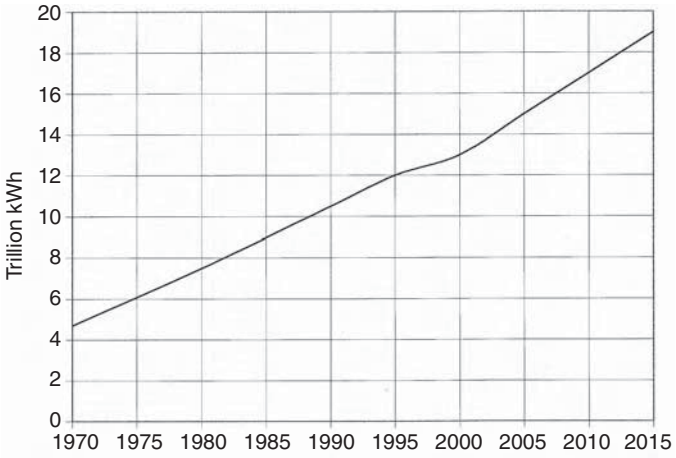

FIGURE 16.1 World electricity consumption for 1970–2015. (From U.S. Department of Energy, International Energy Outlook with Projections to 2015, DOE Office of Integrated Analysis and Forecasting, 2004.)

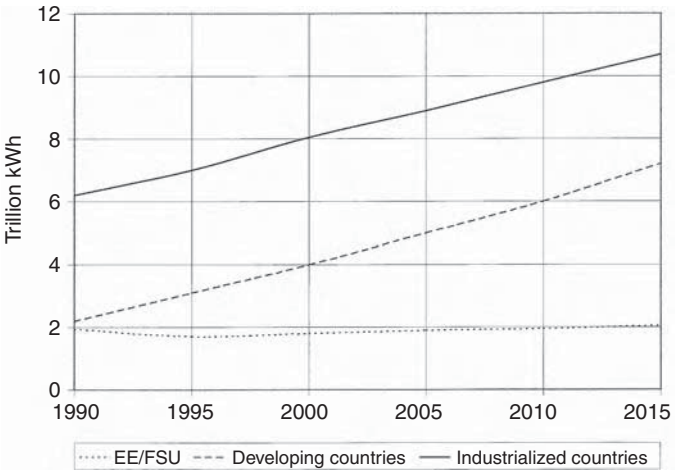

FIGURE 16.2 Electricity consumption by industrialized and developing countries for 1990–2015. (From U.S. Department of Energy, International Energy Outlook with Projections to 2015, DOE Office of Integrated Analysis and Forecasting, 2004.)

16.2 KYOTO TREATY

According to the Environmental Protection Agency (EPA) of the U.S., the electric power industry is the nation's largest polluter. It is responsible for emitting 66% of the SO_2, 29% of the NOx, 36% of man-made CO_2, and 21% of the mercury. The European Union (EU) generates about 15% of the global CO_2 emission. The 160

TABLE 16.1
Electricity Consumption per Capita by Region for 1980, 1995, and 2015 in MWh per Person

Region/Country	1980	1995	2015 (Projected)
OECD North America			
U.S.	9.2	11.1	12.6
Canada	12.6	15.4	19.2
Mexico	0.9	1.2	2.5
Other Regions			
OECD Europe	4.0	5.0	7.8
EE/FSU	4.0	4.0	5.1
Japan	4.4	6.3	10.3
Non-OECD Asia	0.3	0.5	1.2
Middle East	0.9	1.3	1.6
Africa	0.4	0.4	0.5
Central and South America	0.9	1.3	1.7

Source: From U.S. Department of Energy, International Energy Outlook with Projections to 2015, DOE Office of Integrated Analysis and Forecasting, Report No. DE-97005344, April 1997.

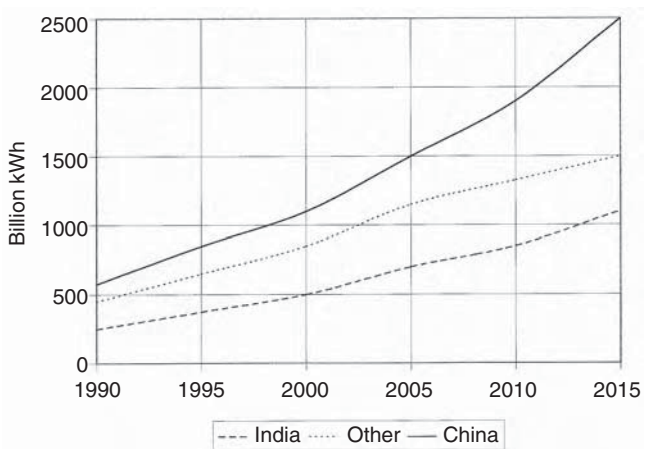

FIGURE 16.3 Electricity consumption in developing Asia for 1990–2015. (From U.S. Department of Energy, International Energy Outlook with Projections to 2015, DOE Office of Integrated Analysis and Forecasting, 2004.)

countries that gathered in Kyoto, Japan, in December 1997 under the UN Convention on Climate Change agreed to work on reducing emissions of CO_2 and other greenhouse gases as per the national and regional goals depicted in Figure 16.4. The U.S.

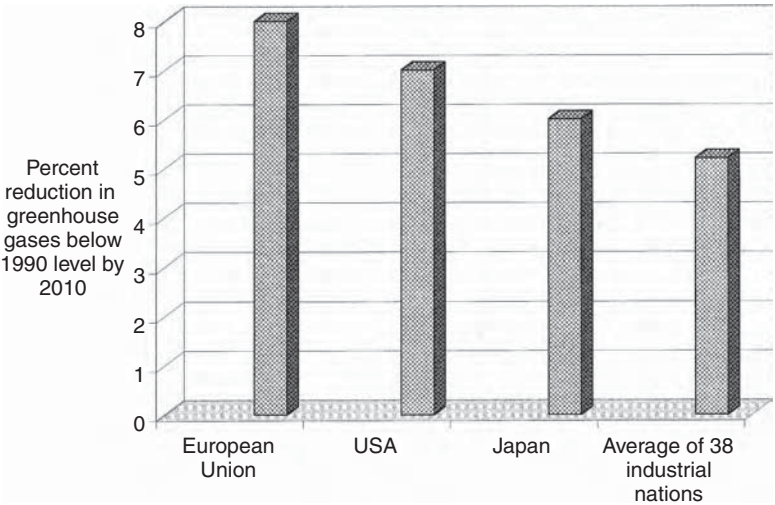

FIGURE 16.4 Cutting emissions under Kyoto treaty. (From United Nations.)

initially promised a 7% cut by the years 2008–2012, as measured against the base year of 1990. Because the U.S. economy would have grown by then, the real cut required would be over 30% of the current level of emissions. This is a significant challenge and will certainly require an aggressive policy on the promotion of renewable energy sources.

The U.S. pulled out of the protocol in 2001, but the EU member countries in 2002 once again ratified the Kyoto Protocol targets set for industrialized countries. The Russian Duma (parliament) ratified the treaty in 2004, moving it forward on the path to becoming a global law . Having been endorsed by 121 countries, the Kyoto treaty on global warming now formally goes into effect. The developed world has come to terms with the need for carbon reductions with commitments to respond accordingly. The Kyoto Protocol now has the endorsement of the developed nations responsible for 55% of the global greenhouse gas emissions. This provides a framework for addressing the issue of global warming. However, the U.S., which is responsible for 36% of the total emission of greenhouse gases, has not endorsed the pact as yet.

Developing countries have an additional reason for promoting wind and PV programs. With a significant rural population and inadequate transmission systems, they would benefit from distributed power generation near the loads. At the 2003 World Summit on Sustainable Development in Johannesburg, although the Kyoto Protocol on reducing greenhouse gases was discussed again, no worldwide target for renewable energy was established.

16.3 FUTURE OF WIND POWER

The U.S. DOE reports that wind is experiencing the strongest growth among the renewable energy sources with a decreasing generation cost. The wind power cost has dropped below 4 cents per kWh, and the DOE projections suggest that further

TABLE 16.2
Wind Power Technology, Past, Present, and Future

Technology Status	1980	2000	Near Future
Cost per kWh[a]	$0.35–$0.40	$0.04–$0.06	<$0.04
Capital cost per kW	$2000–$3000	$400–$600	<$400
Operating life	5–7 yr	20 yr	30 yr
Capacity factor (Average)	15%	25–30%	>30%
Availability	50–65%	95%	>95%
Size range	50–150 kW	500–1,500 kW	1–5 MW

[a] For wind sites with average annual wind speed of 7 m/sec (15.6 mph) at 30-m (100-ft) hub height.

decline to below 3 cents is possible by 2010 with favorable financing. The American Wind Energy Association forecasts that the top five growth markets for wind energy through 2005 have been Germany, Spain, U.S., India, and China. Table 2.1 in Chapter 2 lists the cumulative installed wind power capacity in major regions of the world.

Renewable power sources are clean, abundant, and do not need to be imported. However, they must be economical on their own merits. New developments are meeting this challenge on two fronts, the initial capital cost and the cost per unit of electricity generated. As seen in Table 16.2, wind power capital costs over the last two decades have declined by 80%, operation and maintenance costs have also dropped by 80%, and the availability factor of grid-connected plants has risen to 95%. For the wind plants at present, the capital cost has dropped below $600 per kW and the electricity cost below 4 cents per kWh. The goal of current research programs is to reduce wind power cost below 3 cents per kWh by the year 2010. This will be highly competitive as compared to the cost of conventional power plant technologies. The capital cost in the range of $400 to $600 per kW is also comparable to conventional power plant costs. According to the Electrical Power Research Institute (EPRI), continuing technology developments and production economy have already made wind the least-cost source of new electric power in the U.S.

More than 3000 MW of new wind capacity will be added in the U.S. from 2005 to 2010. The DOE's Wind Powering America Initiative aims at providing 5% of the nation's electricity through wind power by 2020. This would amount to 100,000 MW of accumulated wind capacity by 2020. In California — the fourth largest economy in the world — the support for renewables is growing. The current goal of meeting 20% of the electricity requirement from renewables (including hydro) by 2017 is likely to be met 7 yr earlier, and now a new goal of 33% of power from renewables by 2020 is being discussed.

World Market Update 2003 by BTM Consult (Ringkøbing, Denmark) reported the following for wind power:

- The world's cumulative wind capacity passed the 40,000-MW mark, supplying 0.5% of the world's electric energy, with 67% of the new installations being in Europe.

TABLE 16.3
Past, Present, and Future Growth Rate in Wind Power Capacity

Period	Growth Rate (%)
1993–1998	40
1999–2001	35
2002–2007	25
2008	20
2013	15
2016	10

TABLE 16.4
Future Electricity Demand and Available Wind Resources in the World

Region	Average Annual Growth in Electricity Demand (2000–2020)	Electricity Demand by 2020	20% of 2020 Demand (TWh/ Yr)	Available Wind Resource (TWh/Yr)	Resource Exceeding 20% Demand (Factor)
OECD Europe	1.9%	4,515	903	943	1
OECD North America	1.3%	5,729	1,146	14,000	12
South America	3.8%	2,041	408	5,400	13
OECD Pacific	1.5%	1,745	349	3,600	10
East Asia	4.5%	2,081	416		
South Asia	5.1%	1,695	339	4,600	3
China	5.1%	3,691	738		
Middle East	4.0%	907	181	n/a	n/a
Africa	3.4%	864	173	10,600	61
All others	2.6%	2,615	523	10,600	20
Total World	2.7%	25,883	5,176	49,743	10

Source: From IEA World Energy Outlook 2000.

- 8,344 MW of new capacity was installed worldwide in 2003.
- Average growth rate from 1998 to 2003 was 26%.
- Predicted growth from 2004 to 2009 is around 12 to 15%.
- By 2010, the cumulative installed capacity is expected to be 200,000 MW, which will supply 2% of the world's electric energy.

The past, present, and future growth rates in wind power are shown in Table 16.3. It was as high as 40% in the recent past, is 20 to 25% at present, and is expected to slow down to 10% by 2015 as the industry moves to a degree of maturity.

The available wind resources and future electricity demand in the world projected up to 2020 are shown in Table 16.4. The forecast for alternative electric energy

TABLE 16.5
Forecasts for Alternative Electric Energy Generation Costs

Technology	Generation Cost (Cents/ kWh)
Onshore wind	3–4
Gas turbine	3–4
Offshore wind	3–5
Coal thermal	3–5
Nuclear	4–6
Biomass	4–6
Ocean Wave	4–8
Photovoltaic	15–20

Note: U.S. cents/kWh by 2020 based on 2004 price index.

Source: From Milborrow, D., On track as the cheapest in town, *Wind Power Monthly*, January 2002.

generation cost by 2020 is shown in Table 16.5.[2] The table shows that wind will remain the least expensive source of new electricity in the future, as it is at present. The industry experts make this forecast based on the following ongoing research programs:

- More efficient airfoil and blade design and manufacture
- Better understanding of the structure and foundation loads under turbulence, operating fatigue loads, and their effects on the life of the turbine
- Computer prototyping by accurate system modeling and simulation
- Integrated variable-speed electrical generators and power electronics to eliminate the mechanical gearbox
- Efficient low-cost energy storage on a large scale
- Better wind speed characterization, particularly within a large wind farm

Successful design, development, and demonstration based on the results of these research programs are expected to increase the share of wind power throughout the world.

Offshore wind potential is much greater than onshore owing to good wind speed and the large area available for commercial installations. It is limited only by practical working depth and other maritime activities near the shore. Fishing and shipping routes and military test grounds are some of the activities that may conflict with wind farms. A water depth of 30 m is practical. Taking only the water depth as a constraint, the accessible offshore wind resource in the U.K. is estimated to be 380 TWh per year. Taking other constraints also into account, this estimate is reduced to 120 TWh per year.

TABLE 16.6
European Wind Energy Association Target for the Future

Year	Installed Wind Capacity Target	Annual Growth rate
1998 (actual)	5,000 MW	Reference
2010	40,000 MW	17.5%
2020	100,000 MW	10%

Source: From Wind Directions, Magazine of the European Wind Energy Association, London.

A study commissioned by the EU has suggested that offshore wind farms in the coastal regions of Germany, Holland, and Denmark could meet all the electricity demand in those countries. Denmark's ambitious offshore plan announced in the government's latest Energy-21 report aims to have at least 2300 MW by 2015 and 4000 MW by the year 2030. This will amount to about 50% of that country's electricity coming from wind, which may be the practical maximum for any intermittent source of power.

The offshore wind speed is generally higher, typically 8 to 10 m/sec. However, due to lack of long-term data, these estimates must take into account the inherent variability and the associated effect on the cost of generated electricity. Onshore wind technology is applicable to offshore installations. The major difference, however, is the hostile environment and the associated increase in the installation cost. Electrical loss in transmitting power to the shore also needs to be accounted for. Overall, it is estimated that offshore wind power plant costs can be at least 30% higher than those for comparable inland plants.

Europe's present wind capacity by country is shown in Figure 2.5. Germany and Denmark lead in Europe in wind power. Both have achieved phenomenal wind energy growth through a guaranteed tariff based on the domestic electricity prices, perhaps a model for the rest of the world to follow. The 2003 draft amendment of Germany's Renewable Energy Law targets 12.5% of all power generation from renewable sources by 2010, 20% by 2020, and 50% by 2050. In 2003, the share was 9%, including hydro.

As for the future, the European Wind Energy Association (EWEA) adopted an ambitious target of 40,000 MW of wind capacity in Europe by the year 2010 and 100,000 MW by 2020 (Table 16.6). Each European country would be obligated to meet its committed share of renewable electricity, including the wind energy obligation, toward the overall target of 12% of the primary energy from wind in Europe by the year 2020. The European Conference for Renewable Energy: Intelligent Policy Options held in Berlin, Germany, unanimously set a revised target of 20% renewable energy by 2020 as part of a strategy for sustainable economic development, climate change prevention, and social cohesion.

TABLE 16.7
Present Wind Capacity and Future Targets in Selected Countries

Country	Capacity
Germany	>5,000 MW was operational in 2000
Netherlands	2,750 MW target by 2020
Denmark	750 MW target by 2005
Offshore target	2,300 MW target by 2015
	4,000 MW target by 2030
U.K.	>500 MW was operational in 2000
Ireland	Government target 500 MW by 2010
	IWEA target 1,000 MW by 2010
Italy	100 MW was operational as of November 1997
U.S.	>2,000 MW was operational in 2000
	6,000 MW target by 2006
	12,000 MW target by 2015
India	1,000 MW was operational as of December 1997

The EWEA and Greenpeace have released a new global blueprint, Wind Force 12, for producing 12% of the world's electricity from wind by 2020. Meeting this target would require 1,260 GW of wind capacity generating 3,100 billion kWh of electric energy around the globe. It is not a forecast, but a feasibility study. Its implementation depends on decisions taken by governments around the world. To reach the 12% goal by 2020, manufacturing capacity must gradually increase to 150,000 MW/yr, about 20 times that of 2001. By that time, an installed capacity of 1,260 GW should have been achieved. This installed capacity would generate electricity equivalent to that of today's hydropower plants. Much more wind capacity would be required to achieve the same annual energy output as hydro because of the 30% capacity factor for wind vs. 60% for hydropower plants. The Wind Force 12 study assumes an investment cost of $765 per kW installed capacity and a generation cost of 3.6 cents/kWh in 2001, which then declines by the classical learning curves as the market matures by 2020 and beyond.

The present wind capacity and the future targets in selected countries are listed in Table 16.7, and the present and future targets for meeting the total electricity demand by wind capacity are listed in Table 16.8. Based on these targets, it is reasonable to expect that wind may contribute 10 to 25% of the total electricity demand in some countries by 2010.

Environmental benefit is generally the primary contributing factor to the development of wind and PV systems. Wind plants, however, involve one area of concern, i.e., the effect on birds and their habitats. This issue is being studied by DOE and wind-industry-funded research to define the magnitude of the problem and ways to prevent bird kills. The noise factor and the impact on the rural landscape are other concerns that may adversely affect wind market development. These factors have

TABLE 16.8
Present and Future Target for Percent of Total Electricity Demand Met by Wind Capacity

Country	Wind as Percent of Total Electricity Demand
Denmark	Was 6% as of June 1997
	Target 50% by 2030 (aggressive)
Germany	Was 10% as of June 1997
	Target 20–25% by 2010
Ireland	Government target 5% by 2010
	IWEA target 10% by 2010
U.S.	Was < 1% in 1997
	EPRI estimate 10% by 2020

Source: From Wind Directions, Magazine of the European Wind Energy Association, London. With permission.

begun to contribute to making the planning process difficult in some countries. The sheer speed of the new developments has far outpaced the capacities and capabilities of decision makers. The regulations are inadequate to cover the installations of wind turbines in rural areas. Some governments have started publishing clear guidelines in order to help local authorities in the planning procedures. However, as expected, the closer the wind turbines are located and the smaller the local benefits in terms of jobs and tax revenue, the stronger the opposition from the local community. Future developments will have to deal with these inherent human factors.

16.4 PV FUTURE

The cost of solar PV electricity is still high, in the neighborhood of 20 cents per kWh. With the consumer cost of utility power averaging from 10 to 15 cents per kWh nationwide, PV cannot economically compete with utility power as yet, except in remote markets where utility power is not available and the transmission line cost is prohibitive. Many developing countries have large areas falling in this category. With research programs jointly funded by DOE and the National Renewable Energy Laboratory (NREL), and the ongoing research in PV technologies around the world, PV energy cost is expected to fall below 15 cents per kWh by 2010 as the learning curve and economies of scale come into play.

Total worldwide production of PV modules was 287 MW in 2000 and 561 MW in 2002. The cumulative capacity installed in the world was 800 MW in 2000, 1330 MW in 2002, and 2030 MW in 2004, which amounts to 25% annual growth (Figure 16.5).

Among the other advances underway in PV technology, the *thin film* is expected to lead. Amorphous silicon particularly holds the most promise of quickly penetrating the market due to its low material and manufacturing costs. In this technology, 2-μm thick amorphous silicon vapor is deposited on glass or stainless steel rolls,

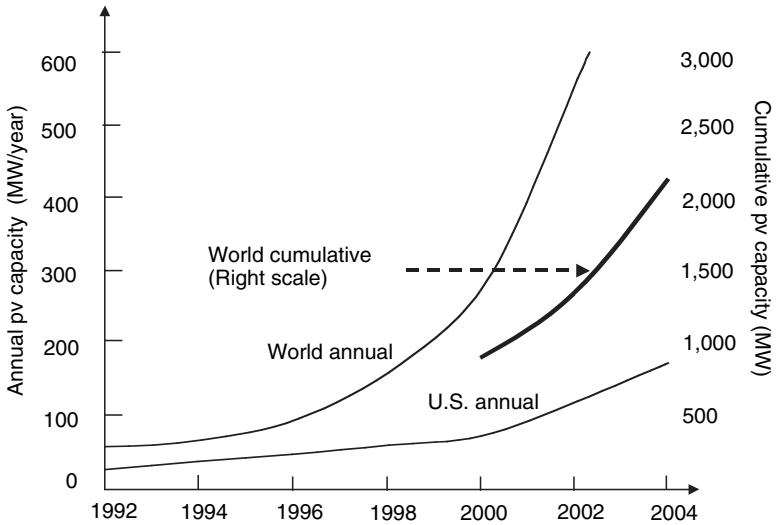

Figure 16.5 PV annual and cumulative installed capacities worldwide.

typically 2000-ft long and 13-in. wide. Compared to thick crystalline silicon cells, amorphous silicon technology uses less than 1% of the material. Sheet manufacturing, compared to single cells from ingots, offers a low-cost base. The disadvantage in single-junction amorphous silicon is that the cell efficiency degrades about 20% in the first several months under sunlight before stabilizing. At present, the stabilized efficiency is half that of crystalline silicon cells and the retail price is also half, thus keeping the price per watt the same. However, this is the market-based price and not the technology-based price. Crystalline silicon technology has been available in the U.S. for several decades and has entered the plateau of a slow learning curve. On the other hand, amorphous silicon technology is new and, hence, a steep learning curve is expected. The expected result is a rapid decline in amorphous silicon price per watt, brought about by increasing efficiency and decreasing manufacturing cost. On this premise, two large plants manufacturing amorphous silicon panels started production in the U.S. in 1997. The concentrator PV cell is another breakthrough on the horizon. The PV energy cost per kilowatthour with these new technologies is expected to follow declining-cost curves as shown in Figure 16.6, and to benefit the industry in the long run.

16.5 WIND AND PV GROWTH

Many governments around the world have set national goals for growth in renewable energy sources. Wind and PV are expected to benefit most from these goals and the incentives under various programs and initiatives. Many U.S. states have adopted the Renewable Portfolios Standards (RPS) that are summarized in Table 16.9.

A 2002 survey of professional engineers in the U.K. asked which of the renewable power generation technologies had the greatest potential to be major contributors to Britain's power needs in the medium to long term. The result based on 306

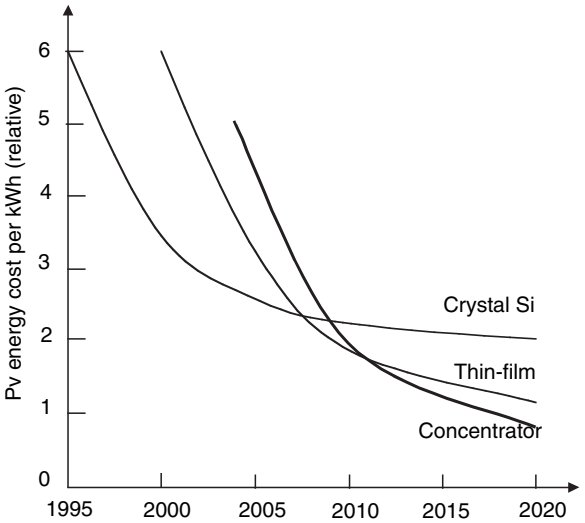

FIGURE 16.6 Future PV technologies for cost-competitive electric power.

TABLE 16.9
Renewable Portfolio Targets of U.S. States

U.S. State	Renewable Portfolio Standards
California	20% by 2010 (on target)
	30% by 2020 (being discussed)
Connecticut	13% by 2009, and continuing at 1% per year thereafter
New York	25% by 2012
Massachusetts	New 0.5% per year to reach 4.5% by 2009, 1% per year thereafter
New Jersey	6.5% by 2012
Maine	30% by 2000 (achieved)
Wisconsin	2.2% by 2011
Iowa	105 MW accumulated (MW_a) by 2009
Minnesota	825 MW_a by 2012
Texas	2880 MW_a by 2009
Arizona	1.1% by 2007
Nevada	15% by 2013
New Mexico	5% by 2006, then add 1% per year,
	10% in 2010

responses placed wind in the first place as shown in Figure 16.7. To additional questions, 69% of the respondents said they did not consider the presence of a wind turbine to be visually or acoustically intrusive. A British Wind Energy Association survey of over 2500 customers found 74% in favor of the government's ambition of generating 20% of its electricity from renewable energy sources by 2020.

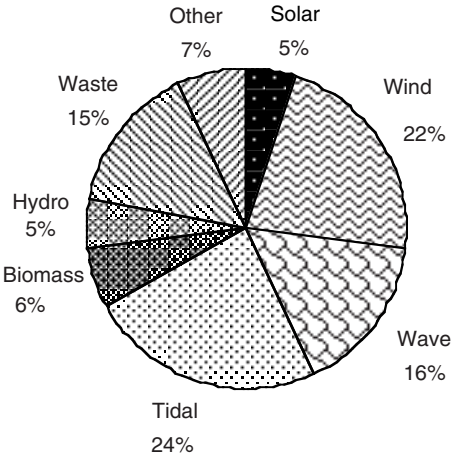

FIGURE 16.7 Engineers' view on future power technologies.

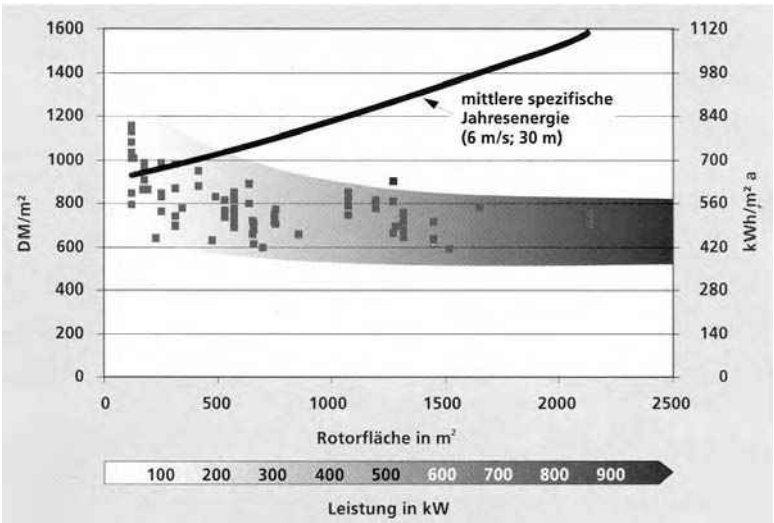

FIGURE 16.8 Economies-of-scale trends for capital cost in DM/m^2 and annual energy produced in kWh/m^2 vs. blade-swept area. (From Institute of Solar Energy and Technology, University of Kassel, Germany. With permission.)

16.6 DECLINING PRODUCTION COST

Economies of scale are expected to continue to contribute to declining prices. Future wind plants will undoubtedly be larger than those installed in the past, and the cost per square meter of the blade-swept area will decline with size. Figure 16.8 shows the year 2000 costs of wind turbines of various sizes in Germany. The price is in DM/m^2 of the blade area, falling from 800 to 1200 DM/m^2 for small turbines to 500

to 800 DM/m^2 for large turbines of 50-m diameter. The line showing the annual energy potential per square meter rises from 630 kWh/m^2 in small turbines to 1120 kWh/m^2 in large turbines of 46-m diameter.

With the advances in technology and the economies of scale combined, the manufacturing cost of new technologies has historically shown declining patterns. The growth of a new product eventually brings with it a stream of competitors, and the learning curve decreases the cost. A learning-curve hypothesis has been commonly used to model such cost declines in new technologies. The cost is modeled as an exponentially decreasing function of the cumulative number of units produced up to that time. A standard form for a cost decline is constant doubling, in which the cost is discounted by a fraction λ when the cumulative production doubles. For renewable electricity, the production units are megawatts of capacity produced and kilowatthours of electricity produced. If we want to monitor only one production unit, kilowatt hours is preferred because it includes both the megawatts capacity installed and the length of the operating experience, thus making it an inclusive unit of production.

For new technologies, the price keeps declining during the early phase of a new product at a rate that depends on the nature of the technology and the market. The pattern varies widely as seen in new technologies such as those in the computer, telephone, and airline industries. For the early wind turbines, the cost per kW capacity has declined with the number of units produced, as seen in Figure 16.9. The declining electricity price was seen earlier in Figure 2.2.

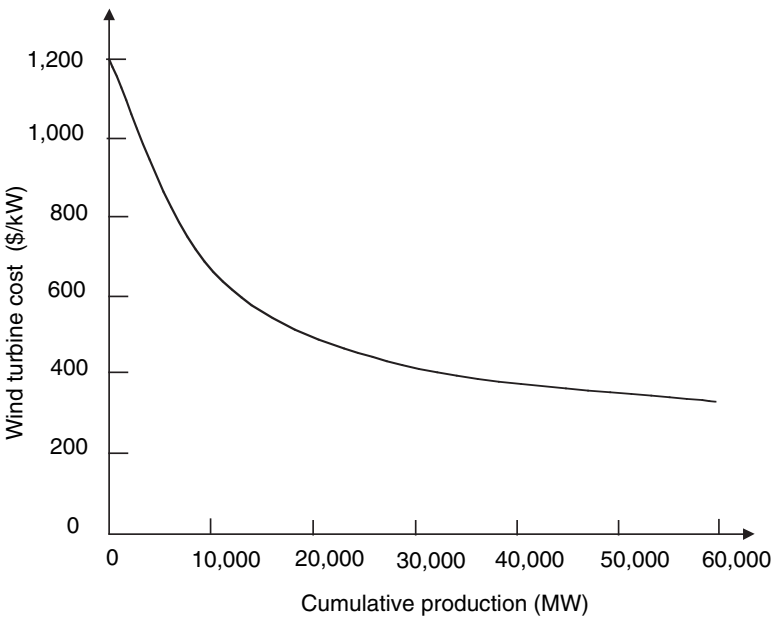

FIGURE 16.9 Learning curve of the wind turbine costs.

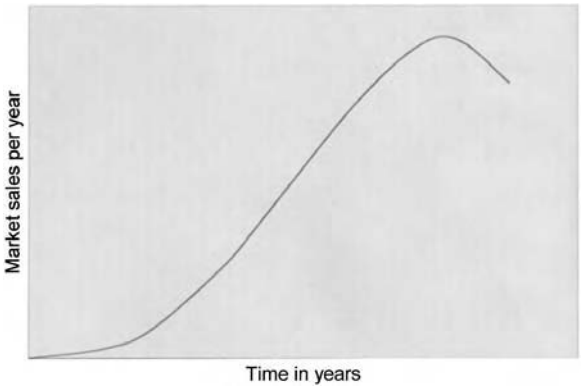

FIGURE 16.10 S-shaped growth and maturity of new products.

In general, the future cost of a new product can be expressed as follows:

$$C(t) = C_o \lambda^{\log_2 (N_t/N_o)} \quad 0 < \lambda < 1 \tag{16.1}$$

where
$C(t)$ = cost at time t
C_o = cost at the reference time
N_t = cumulative production at time t
N_o = cumulative production at reference time.

Estimating the parameter λ based on historical data is complex, and the estimate itself may be open to debate. However, the expression itself has been shown to be valid for new technologies time and again in the past. It may be used to forecast future trends in the capital cost decline in any new technology, including wind and PV power.

16.7 MARKET PENETRATION

With all market forces combined and working freely, the penetration of a new technology over a period of time takes the form of an S-shaped curve, as shown in Figure 16.10. It is characterized by a slow initial rise, followed by a period of more rapid growth, leveling off to a saturation plateau, and finally declining to make room for a newer technology. The S-shape hypothesis is strongly supported by empirical evidence.

One model available for predicting the market penetration of a new product is the diffusion model proposed by Bass.[3] However, it can be argued that renewable energy is not really a new product. It merely substitutes for an existing product. The Bass model, therefore, may not be appropriate for renewable power. Because electricity is a basic need of society, the penetration of renewable power technologies is better compared with similar substitutions in the past, such as in the steel-making

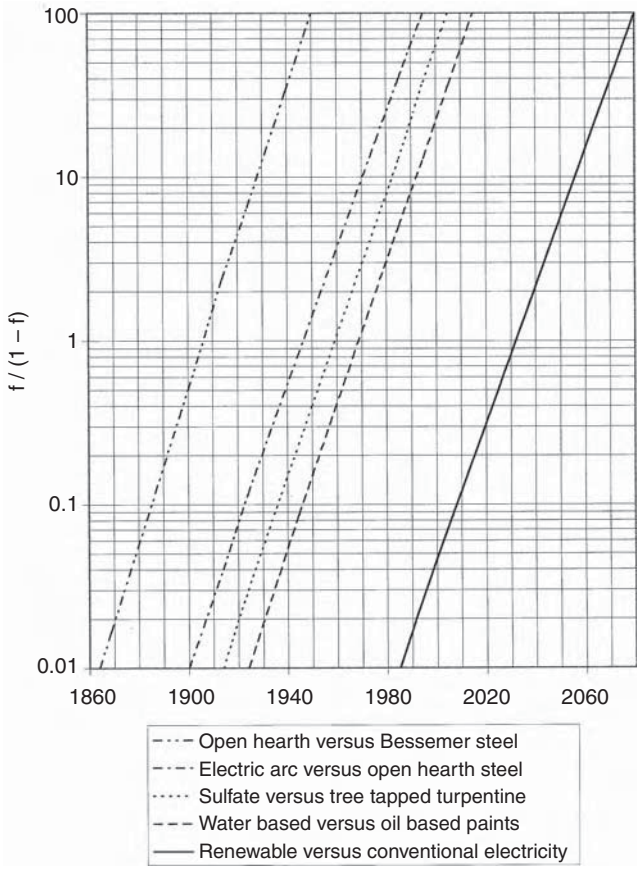

FIGURE 16.11 Market penetration of a new product substituting for existing products. Wind and PV shown in parallel with historical data. (From Fisher, J.C. and Pry, R.H., A simple substitution model of technological change, *Technology Forecasting and Social Change*, Vol. 3, 79–88, 1971.)

industry, as shown in Figure 16.11. The solid lines are the actual penetration rates seen in those industries.

With ongoing developments in wind and PV power technology and with adjustments in social attitudes, the market penetration rate may follow a line parallel to the historical experience with similar products as depicted in Figure 16.11. It can be analytically represented by the Fisher–Pry substitution model.[4] In this model, the rate at which wind and PV energy may penetrate the market can be expressed as a fraction of the total megawatthour energy consumed every year.

If f is the fraction of the market captured by the renewables at time t, and t_o the time when f equals ½, then f can be expressed as follows:

$$f = \frac{1}{1+e^{[-b(t-t_o)]}} \quad \text{or} \quad \frac{f}{1-f} = e^{-b(t-t_o)} \tag{16.2}$$

Here b is the growth constant, which characterizes the growth to the potential associated with a particular technology. The equation gives log-linear straight lines, as shown in Figure 16.11.

We must mention here that wind power was successfully demonstrated to be commercially viable in the 1970s and commercial production started in 1985, when a group of wind farms in California were installed and operated for profit by private investors. Based on this, and on the Fisher–Pry model just described, we can draw the dotted line in Figure 16.11, beginning in 1985 and then running parallel to the lines followed by similar substitution products in the past. That is the rate of market penetration we can expect wind power to follow in the future.

At the rate indicated by the dotted line, the full 100% potential of wind will perhaps be realized around 2065. Wind power's reaching 100% potential in the year 2065 does not mean that it will completely replace thermal and other power. It merely means that wind power will attain its full potential. Experts will argue about the upper limit of this potential for a given country. However, wind and PV power, being intermittent sources of energy, cannot be the base-load provider. They can augment a base-load plant, thermal or other type, which can dispatch energy on demand. Such reasoning puts the upper limit of wind and PV power at well below 50%, perhaps around 25%. According to a 1997 study published in the U.K. by the Royal Institute of International Affairs, all renewable sources could together provide between 25 and 50% of European electricity by the year 2030. The contributions of wind and PV in meeting the total electricity demand, however, will largely depend on the operating experience gained with grid-connected plants and energy storage technologies developed during the next few decades that can remedy the nondispatchable nature of wind and PV energy. New energy storage products are being developed that incorporate battery, flywheel, fuel cell, and superconducting magnet into system solutions for the power industry, such as load leveling and power quality improvements. Electric utility restructuring and the subsequent increase in competition are creating new and higher-value markets for energy storage. Wind and PV power are the new market opportunities for large-scale energy storage products.

Sophisticated prediction models have been developed by the DOE, NREL, and others based on mathematical considerations and regression analyses of applicable data. However, there is a limit to how much such models can be confidently used to commit huge sums of capital investment. Small errors in data can cause large errors in projections, particularly decades in the future. Time-proven data on how people make investment decisions when faced with long-term uncertainties can also help. Experience indicates that investors commit funds only if the payback period is less than 5 yr; the shorter it is, the quicker the investment commitments are made. The upper limit of the payback period with significant market penetration is 4 to 5 yr, and large market penetration requires a payback period of less than 3 yr.

16.8 EFFECT OF UTILITY RESTRUCTURING

Although the U.S. electricity market approached $300 billion in 2004, the electric utilities had grown into regulated monopolies, with no competition at the consumer level. Since the inception of the power industry, both the generation and the transmission

of electricity remained with one company. Even when electricity could be produced by other sources, transmission access to the loads was denied, or the owners set the price so high that the access was effectively denied, to protect their own position in the generation market.

The Public Utility Regulatory Policy Act of 1978 (PURPA) required utilities to purchase electricity from power generators using renewable energy sources or cogeneration. PURPA also required the utilities to pay the *qualifying facilities* (QFs) at rates based on their *avoided cost.* Congress defined avoided cost as the incremental cost of electric energy the utility would incur if it generated the energy itself or purchased it from another source. This definition is vague in at least one sense: Does the incremental cost include the share of the capital cost needed to generate the incremental unit of energy? For example, if the plant cost is taken as sunk cost, the avoided cost would primarily mean the fuel cost, which for thermal power plants may be 2 cents per kWh. On the other hand, if a new plant has to be built to meet the added demand, which a renewable power plant can supply, the avoided cost would include the capital cost of about 5 to 6 cents per kWh, making the total avoided cost 7 to 8 cents per kWh. Congress left the exact definition of avoided cost and the implementation of PURPA to the states. Nevertheless, with the regulatory advantage of PURPA, renewable and cogeneration power plants started coming up across the nation.

16.8.1 Energy Policy Act of 1992

By passing the Energy Policy Act (EPAct) of 1992, Congress encouraged even greater wholesale competition by reducing the market barriers for independent generators interested in selling electric power. This act permits wholesale customers to have a choice of generators and obliges utilities to wheel power over their transmission lines at the same cost that they would charge all others, including themselves. For effective implementation of the act, the utilities were required to break up the generation, transmission, and distribution businesses into separate companies that would own the generating plants and the wires. In the past, electricity was sold as a delivered product. The new restructuring merely unbundled the product price and the delivery charge, with the wires owned and operated separately as common carriers obligated to charge the same rate to all customers. Thus, the new law separated the power industry into two parts: (1) the generation and/or sale of electricity by a licensed power supplier and (2) the delivery of electricity to consumers by regulated companies.

In the new retail competition, all customers choose their energy supplier (the generating company). Each supplier has direct open access to the transmission and distribution wires. The concept is similar to what happened in the telephone industry in the 1980s. The idea is as old as American free enterprise — open, unrestricted competition at the consumer level. The U.K., Chile, Norway, and parts of Australia have systems similar to that implemented in the U.S. power industry in the late 1990s. This was the biggest restructuring of the electric utility industry in the U.S. since the beginning of the industry some 100 yr ago. The uncertainty and skepticism around the EPAct of 1992 initially caused significant confusion and uncertainty for new investors in the industry.

As with PURPA, the implementation of the EPAct of 1992 was also left to individual states. The states with relatively higher energy costs at the time (12 to 16 cents per kWh), such as California, Illinois, Massachusetts, Michigan, New Hampshire, and Pennsylvania, started with active pilot programs. For example, in 1996, New Hampshire started a pilot project in which 16,500 customers were selected randomly and allowed to choose their electricity producer. This 2-yr experiment led to full implementation by the end of 1998. In late 1997, Pennsylvania became the largest state in the U.S. to implement an extensive program of encouraging competition among electric power sources. The state, home to 12 million people, licensed 47 companies to sell power to the public; this included four major established conventional utility companies (Philadelphia Electric Company, PECO; Pennsylvania Power and Light, PP&L; General Power Utilities, GPU; and American Electric Power, AEP). Approximately one million customers volunteered for the pilot program, in which they were guaranteed savings. Full-scale competition began in 1999, resulting in rate cuts averaging about 8% initially, and about 15% in the years that followed.

In Massachusetts, the most immediate effect of the restructuring was an automatic 10% savings beginning in 1998, which increased to 15 to 18% later. New Jersey introduced a pilot program in 1999 and full implementation in 2003. Fact finding and investigations were undertaken in midrange-cost states, but no significant activity took place in states having low energy cost (6 to 8 cents per kWh).

The 1992 EPAct, when fully implemented, is estimated to have saved end users 10 to 20% in electricity price.[5] A 2002 estimate made by the U.S. government indicates that retail competition saves the consumers about $200 billion a yr, averaging about $232 per household. This was achieved partly by promoting competition among utility and nonutility power generators, and partly by the most efficient use of the generation and transmission assets through generating and wheeling the power as dictated by regional economies. This becomes rather evident when viewed from an operational research point of view. In finding an optimized solution with constraints, the farther the constraint boundaries are, the more economical is the solution. The absence of constraints results in the most economical solution.

With the expected decline in electricity prices, some of the high-cost power plants became uneconomical compared to new power plants, including the renewables. One of the debated issues in the power industry at present is about who will pay the "stranded cost" of these uneconomical plants, which has not been recovered in the new competitive market. Examples of stranded costs are the cost of nuclear plants, which is not recovered as yet, and the cost of locked-in power contracts with independent generators at a higher market price. According to the Competitive Enterprises Institute, the stranded cost in the U.S. power industry is estimated to be more than $200 billion.

Another issue debated in the renewable power industry is the definition of the "avoided cost" that is paid by utility companies. The issue is complex, as illustrated by the following example: For a utility company, the sunk cost of generation is, say, 10 cents per kWh. This includes 2 cents for the fuel cost, and 8 cents for the capital and administrative costs of generation and transmission. If that utility has excess capacity, its incremental avoided cost is only 2 cents — the cost of adding a customer

or the savings by deleting a customer. This is what it would pay to the renewable power generator. On the other hand, it charges its average consumer 12 cents per kWh. If the cost of self-generation using a wind power plant is 5 cents per kWh, the customer would save 7 cents by self-generation, but society at large would lose 3 cents per kWh (because the utility would save 2 cents in fuel cost but the self-generating customer would spend 5 cents). However, in situations in which the energy demand is growing but generation and transmission capacities cannot keep up, the avoided cost includes the capital cost also. For example, the Pacific Gas and Electric Company (San Francisco, CA) found that by purchasing power to meet loads at the end of heavily loaded lines, it could avoid having to construct new generation and transmission capacity. The avoided cost in this situation is 10 cents per kWh, and society at large would gain 5 cents (the utility saves 10 cents but the self-generator would spend 5 cents). This example highlights the basic difficulty in accounting the benefits of renewable power. In such common situations, the impact of electric utility restructuring on renewable power will depend on how fairly it is treated in regard to defining some of the costs of both the conventional and renewable electricity.

16.8.2 Impact on Green Power

Industry leaders expect the generating businesses, conventional and renewable, to become more profitable in the long run under the EPAct of 1992. The reasoning is that the generation business will be freed from regulated prices and opened to competition between electricity producers and resellers. The transmission and distribution business, on the other hand, would still be regulated. The American experience indicates that free businesses have historically made more profits than regulated businesses. This has been the experience in the U.K. and Chile, where the electric power industry has been structured along lines similar to that proposed by the EPAct of 1992. The generating companies in these countries make good profits as compared to the transmission and distribution companies.

As for the renewable electricity producers, they are likely to benefit as much as other producers of electricity, as they will be able to freely sell power to end users through truly open access to the transmission lines (Figure 16.12). Another benefit is that the renewable power price will fall as technology advances, whereas the price of conventional power will rise with inflation, making renewable power even more attractive in the future.

16.8.3 Green-Power Marketing

Unless the cost of renewable electricity matches the cost of conventional electricity, the market penetration of renewable power may be slow. On the other hand, under the restructured electricity market, it is possible that environmentally conscious consumers may opt for green power even at a higher price. Surveys strongly indicate that they would.[6] In 1995, several utility companies in the U.S. surveyed 300 customers of each company. Of these, 64% said that renewable power is very important, and 36% said that they would pay more for electricity from such sources. 24% said they would pay at least 10% more. An extensive survey of Massachusetts

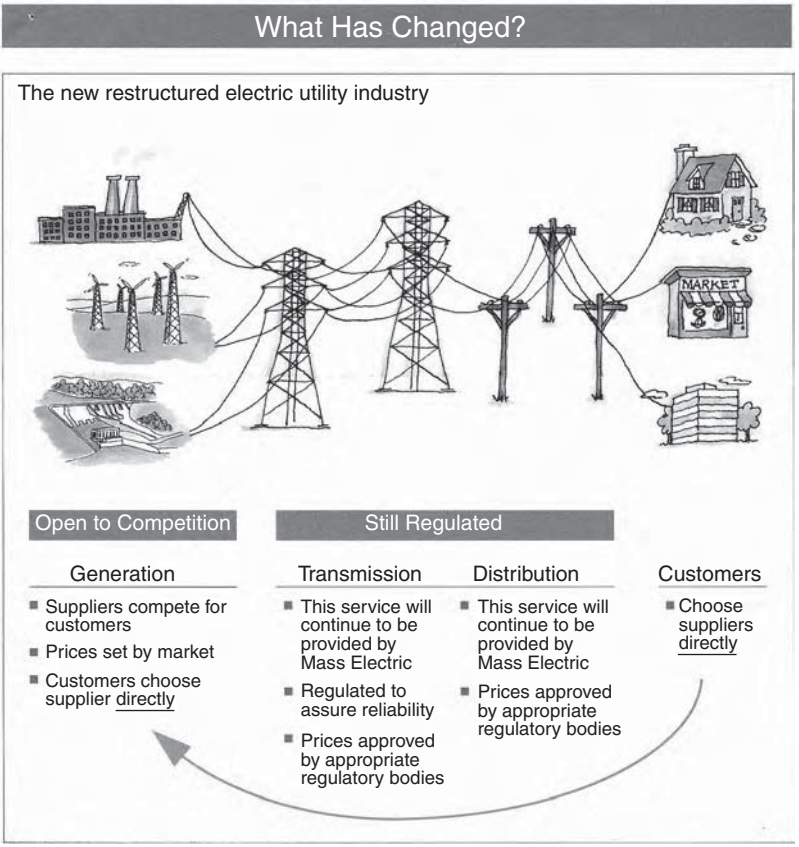

FIGURE 16.12 Newly restructured electric utility industry in the U.S. (Courtesy of Massachusetts Electric, Boston.)

residents in 2002 showed that 90% favored buying their electricity from renewable sources. Some 57% were willing to pay $10 more per month to buy green electricity; this figure rose to 70% if a tax deduction was made available for this. Almost two million consumers across Europe have signed up for green electricity under a new label EUGENE.

Under this premise, several U.S. utilities developed marketing programs for green electricity under which they allow their customers to voluntarily pay premiums for renewable power. For example, a pilot program called ClearChoice was initiated in the city of San Angelo, TX, beginning in October 1997. Today, in 2005, many utilities offer the green-power option at a premium price.

16.9 STRAINED GRIDS

The U.S. grid's 200,000 mi of high-voltage lines work as superhighways for transporting electric energy. They are operating at near their maximum capacity at present.

This problem is not expected to ease soon, considering that the U.S. is expected to add 14% more electrical capacity by 2012, but only 6% new grid lines.

North America's worst blackout, in August 2003, affected some 50 million people in the northeastern U.S. and Canada. The cost of the outage to the U.S. economy was estimated to be around $10 billion, excluding personal losses. The estimated cost of upgrading the grid system to avoid such outages in the future is about $50 billion. Because the blackout was caused by overloaded transmission lines, and it would take decades before new lines can be planned and built, it has created a window of opportunity for distributed power generation from wind and PV. For example, independent system operators have agreed to support a study proposed by AWEA for transmission planning of the 10,000 MW of wind power being developed in the nine states of the western Midwest region by 2007.

The shift from centralized mainframe computers to decentralized personal computers in the late 1980s can become a model for distributed power generation. A host of improvements in microcomputer technology, new-material research, and energy-efficient designs are helping in distributed generation and production of clean energy at the same time. However, such a transformation is not easy to achieve. It means developing technologies for massive energy storage because electric energy cannot be stored like data packets in computing networks for local use or for transmission to other users on the Internet. Transmitting excess energy from one locality to another can choke up the grid lines, leading to blackouts. Even a 15-sec power outage at a critical manufacturing plant can cost as much as $10 million in lost production. Moreover, how to effectively connect numerous power resources to the grid without giving rise to power quality issues is a challenge for the power industry.

As with distributed computing, distributed power generation is likely to involve a broad mix of new technologies, such as smart control systems and software designed to maximize the grid's ability to handle distributed generation efficiently and reliably. Even then, the depth and breadth of a shift from the highly centralized power grid of the present to a super-grid that can accommodate small, distributed, and renewable power systems based on power sources such as wind, PV, and fuel cells are difficult to predict.

REFERENCES

1. U.S. Department of Energy, Office of Integrated Analysis and Forecasting, International Energy Outlook with Projections to 2015, Report No. DE-97005344, April 1997.
2. Milborrow, D., On track as the cheapest in town, *Wind Power Monthly*, January 2002.
3. Bass, F. M., A new product growth model, *Management Science*, Vol. 15, 215–227, 1969.
4. Fisher, J. C. and Pry, R. H., A simple substitution model of technological change, *Technology Forecasting and Social Change*, Vol. 3, 79–88, 1971.
6. Backus, G. and Baylis, S., Dynamics of U.S. electrical utility deregulation, DOE Office of Utility Technology, Report No. DE-9600052, December 1996.
7. Puttgen, H. B., Truly, R., Hyde, D. G., Walker, R., Terrado, E., Cohen, G., and Hurwitch, J.W., Realization of alternative energy generation and storage, *IEEE Power Engineering Review*, 5–18 May 1998.

Part D

Ancillary Power Technologies

17 Solar Thermal System

The solar thermal power system collects the thermal energy in solar radiation and uses it at high or low temperatures. Low-temperature applications include water and room heating for commercial and residential buildings.[1] High-temperature applications concentrate the sun's heat energy to produce steam for driving electrical generators. Concentrating solar power (CSP) technology has the ability to store thermal energy from sunlight and deliver electric power during dark or peak-demand periods. Its usefulness has been demonstrated on a commercial scale, with research-and-development funding primarily from the government and active participation of some electric utility companies. Therefore, CSP technology promises to deliver low-cost, high-value electricity on a large scale. This chapter covers such high-temperature solar thermal power systems.

Figure 17.1 is a schematic of a large-scale solar thermal power station developed, designed, built, tested, and operated with Department of Energy (DOE) funding. In such a plant, solar energy is collected by thousands of sun-tracking mirrors, called *heliostats*, which reflect the sun's energy to a single receiver atop a centrally located tower. This enormous amount of energy that is focused on the receiver tower is used to melt a salt at high temperature. The hot molten salt is stored in a storage tank and used when needed to generate steam and drive a turbine generator. After generating steam, the used molten salt, now at low temperature, is returned to the cold-salt storage tank. From here, the salt is pumped to the receiver tower to be heated again for the next thermal cycle. The usable energy extracted during such a thermal cycle depends on the working temperatures. The maximum thermodynamic conversion efficiency that can be theoretically achieved with the hot-side temperature T_{hot} and the cold-side temperature T_{cold} is given by the Carnot cycle efficiency, which is as follows:

$$\eta_{carnot} = \frac{T_{hot} - T_{cold}}{T_{hot}} \tag{17.1}$$

where the temperatures are in degrees Kelvin. A higher hot-side working temperature and a lower cold-side exhaust temperature give higher plant efficiency for converting the captured solar energy into electricity. The hot-side temperature, however, is limited by the properties of the working medium. The cold-side temperature is largely determined by the cooling method and the environment available to dissipate the exhaust heat.

A major benefit of this scheme is that it incorporates thermal energy storage for several hours with no degradation in performance or for longer with some degradation. This feature makes this technology capable of producing high-value electricity for meeting peak demands. Moreover, compared with the solar photovoltaic (PV) system, the solar thermal system is economical and more efficient because it eliminates

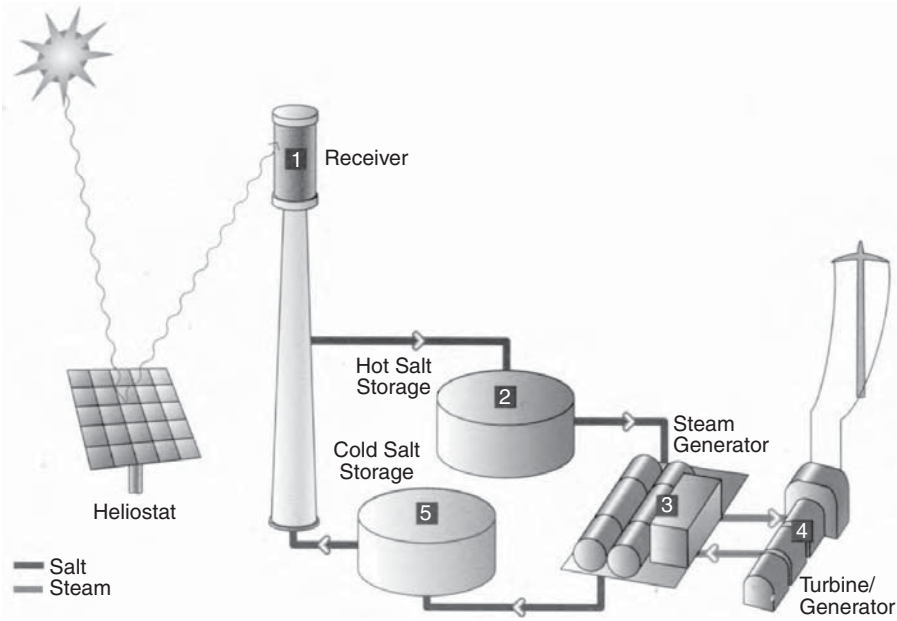

FIGURE 17.1 Solar thermal power plant schematic for generating electricity.

use of costly PV cells and alternating current (AC) inverters. It is, however, limited to large-scale applications.

17.1 ENERGY COLLECTION

CSP research and development focuses on three types of concentrators, which use different kinds of concentrating mirrors to convert the sun's energy into high-temperature heat energy. The three alternative configurations of the concentrators are shown in Figure 17.2. Their main features and applications are as described in the following subsections:

17.1.1 Parabolic Trough

The parabolic trough system is by far the most commercially matured of the three technologies. It focuses sunlight on a glass-encapsulated tube running along the focal line of a collector. The tube carries a heat-absorbing liquid, usually oil, that heats water to generate steam. More than 350 MW of parabolic trough capacity has been in operation in the California Mojave Desert since the early 1990s. It is connected to Southern California Edison's utility grid.

17.1.2 Central Receiver

In the central receiver system, an array of field mirrors focus sunlight on a central receiver mounted on a tower. To focus sunlight on the central receiver at all times, each heliostat is mounted on a dual-axis sun tracker to seek a position in the sky

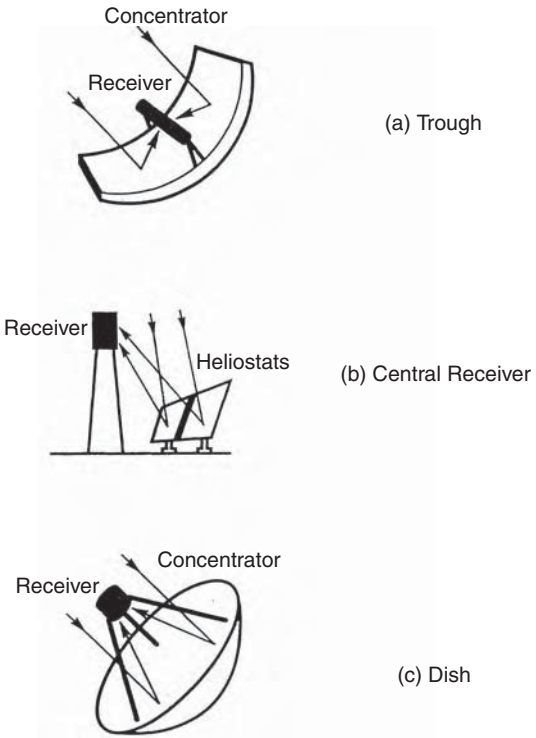

FIGURE 17.2 Alternative thermal-energy collection technologies.

that is midway between the receiver and the sun. Compared with the parabolic trough, this technology produces a much higher concentration and hence a higher temperature of the working medium, usually a salt. Consequently, it yields higher Carnot efficiency and is well suited for utility-scale power plants of tens of hundreds of megawatt capacity.

17.1.3 Parabolic Dish

A parabolic dish tracks the sun to focus heat, which drives a Stirling heat engine that is connected to an electrical generator. This technology has applications in relatively small capacity (tens of kilowatts) due to available engine size and wind load on the collector dishes. Because of their small size, they are more modular than other solar thermal power systems and can be assembled in capacities ranging from a few hundred kilowatts to a few megawatts. This technology is particularly attractive for small stand-alone remote applications. The three alternative solar thermal technologies are compared in Table 17.1.

17.2 SOLAR-II POWER PLANT

Central receiver power tower technology with a solar power tower, having a higher potential of generating low-cost electricity on a large scale, is getting a new developmental

TABLE 17.1
Comparison of Alternative Solar Thermal Power System Technologies

Technology	Solar Concentration (x Suns)	Operating Temperature (Hot Side)	Thermodynamic Cycle Efficiency
Parabolic trough receiver	100	300–500°C	Low
Central receiver power tower	1000	500–1000°C	Moderate
Dish receiver with engine	3000	800–1200°C	High

FIGURE 17.3 Solar-II plant site view. (From: U.S. Department of Energy.)

thrust in the U.S. An experimental 10-MW_e power plant using this technology was built and commissioned in 1996 by the DOE in partnership with the Solar-II Consortium of private investors led by Southern California Edison, the second-largest electric utility company in the U.S. It is connected to the grid and has enough capacity to power 10,000 homes. The plant is designed to operate commercially for 25 to 30 yr. Figure 17.3 is a photograph of this plant site located east of Barstow, CA. It uses some components of the Solar-I plant, which was built and operated at this site using central receiver power tower technology. The Solar-I plant, however, generated steam directly to drive the generator without the thermal storage feature of the Solar-II plant.

The Solar-II central receiver (Figure 17.4) was developed by the Sandia National Laboratory. It raises the salt temperature to 1050°F. The most important feature of the Solar-II design is its innovative energy collection and storage system. It uses a salt that has excellent heat-retention and heat-transfer properties. The heated salt can be used immediately to generate steam and electric power. Or it can be stored for use during cloudy periods or to meet the evening load demand on the utility grid

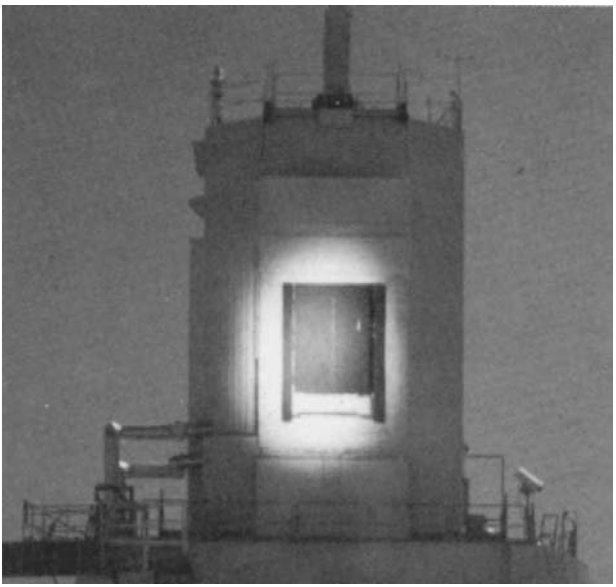

FIGURE 17.4 Experimental 1050°F thermal receiver tower for Solar-II power plant. (From: DOE/Sandia National Laboratory.)

after the sun has set. Because of this unique energy storage feature, power generation is decoupled from energy collection. For an electric utility, this storage capability is crucial, in that the energy is collected when available and used to generate high-value electricity when most needed to meet peak demands. The salts selected by the Sandia laboratory for this plant are sodium nitrate and potassium nitrate, which work as a single-phase liquid that is colorless and odorless. It has the needed thermal properties up to the operating temperature of 1050°F. Moreover, it is inexpensive and safe.

Table 17.2 and Table 17.3 give the technical design features of the experimental Solar-II power plant. The operating experience to date indicates an overall plant capacity factor of 20%, and an overall thermal-to-electrical conversion efficiency of 16%. It is estimated that 25% overall efficiency can be achieved in a commercial plant design using this technology.

17.3 SYNCHRONOUS GENERATOR

The electromechanical energy conversion in the solar thermal power system is accomplished by the synchronous machine, which runs at a constant speed to produce 60-Hz electricity. This power is then directly used to meet the local loads and/or to feed the utility grid lines.

The electromagnetic features of the synchronous machine are shown in Figure 17.5. The stator is made of conductors, consisting of three interconnected phase coils, placed in slots of magnetic iron laminations. The rotor consists of magnetic poles created by the field coils carrying direct current (DC). The rotor is driven by

TABLE 17.2
Solar-II Design Features

Site
Mojave desert in California
1,949 ft above sea level
7.5 kWh/m^2 annual average daily insolation
95 acres of land

Tower
Reused from Solar-I plant
277 ft to top of the receiver
211 ft to top of BCS deck

Heliostats
1,818 Solar-I heliostats, 317.1 m^2, 91% reflectivity
108 new Lug heliostats, 95.1 m^2, 93% reflectivity
81,000 m^2 total reflective surface
Can operate in winds up to 35 mph

Receiver
New for Solar-II plant
Supplier: Rockwell
42.2-MW thermal power rating
Average flux 429 suns (429 kW/m^2)
Peak flux 800 suns
24 panels, 32 tubes per panel
20-ft tall and 16.6-ft diameter
0.8125-in. tube OD
0.049-in. tube wall thickness
Tubes 316H stainless steel

Thermal Storage System
Supplier: Pitt Des Moines
Two new 231,000-gal storage tanks, 38-ft ID
Cold tank carbon steel, 25.8-ft high, 9-in. insulation
Hot tank 304 stainless steel, 27.5-ft high, 18-in. insulation
3 h of storage at rated turbine output

Nitrate Salt–Chilean Nitrate
60% $NaNO_3$, 40% KNO_3
Melting temperature 430°F
Decomposing temperature 1,100°F
Energy storage density two thirds that of water
Density two times that of water
Salt inventory 3.3 million lb

Steam Generator
Supplier: ABB Lummus
New salt-in-shell superheater
New slat-in-tube kettle boiler
New salt-in-shell preheater

Turbine Generator
Supplier: General Electric Company
Refurbished from Solar-I plant
10 MW_e net
12 MW_e gross

Source: From U.S. Department of Energy and Southern California Edison Company.

a steam turbine to create a rotating magnetic field. Because of this rotation, the conventional rotor field coils use slip rings and carbon brushes to supply DC power from a stationary source. Modern rotors, however, are made brushless by using self-excitation with rotating diodes on the same shaft.

The stator conductors are wound in three groups connected in a three-phase configuration. Under the rotating magnetic field of the rotor, the three phase coils generate AC voltages that are 120° out of phase with each other. If the electromagnetic structure of the machine has p pole pairs and it is required to generate electricity at frequency f, then the rotor must rotate at N revolutions per minute given by the following:

$$N = 60\frac{f}{p} \tag{17.2}$$

TABLE 17.3
Solar-II Operating Features

Thermodynamic Cycle	Electric Power Generator
Hot-salt temperature: 1,050°F	Capacity: 10 MW_e
Cold-salt temperature: 550°F	Capacity factor: 20%
Steam temperature: 1,000°F	Overall solar electric efficiency: 16%
Steam pressure: 1,450 psi	Cost of conversion from Solar-I: $40 million
Receiver salt flow rate: 800,000 lb/h	
Steam generator flow rate: 660,000 lb/h	

Source: From U.S. Department of Energy and Southern California Edison Company.

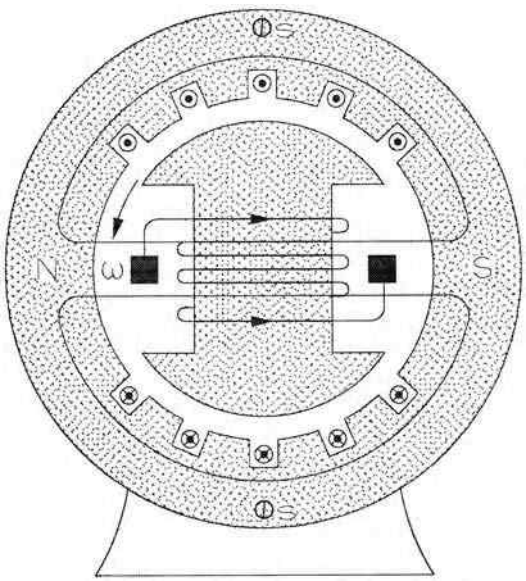

FIGURE 17.5 Cross-sectional view of the synchronous generator.

The synchronous machine must operate at this constant speed to generate power at the specified frequency. In a stand-alone solar thermal system, small speed variations can be tolerated within the frequency tolerance band. If the generator is connected to the grid, it must be synchronous with the grid frequency and must operate exactly at this grid frequency at all times. Once synchronized, such a machine has an inherent tendency to remain synchronous. However, a large, sudden disturbance such as a step load can force the machine out of synchronism, as discussed in Subsection 17.3.4.

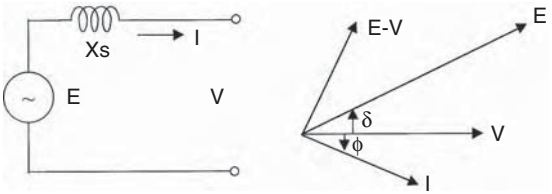

FIGURE 17.6 Equivalent electrical circuit and phasor diagram of the synchronous machine.

17.3.1 Equivalent Electrical Circuit

The equivalent electrical circuit of the synchronous machine is represented by a source of alternating voltage E and an internal series resistance R_s and reactance X_s representing the stator winding. The resistance, being much smaller than the reactance, can be ignored to reduce the equivalent circuit to a simple form, as shown in Figure 17.6. If the machine supplies a load current I that lags behind the terminal voltage V by phase angle ϕ, it must internally generate the voltage E, which is the phasor sum of the terminal voltage and the internal voltage drop IX_s. The phase angle between V and E is called the power angle. At zero power output, the load current is zero and so is the IX_s phasor, making V and E in phase with zero power angle. Physically, the power angle represents the angle by which the rotor's magnetic field leads the stator-induced rotating magnetic field. The output power can be increased, up to a certain limit, by increasing the power angle. Beyond this limit, the rotor and stator fields would no longer follow each other in a lockstep and will step out of the synchronous mode of operation. In the nonsynchronous mode, steady power cannot be produced.

17.3.2 Excitation Methods

The synchronous machine's excitation system is designed to produce the required magnetic field in the rotor, which is controllable, in order to control the voltage and reactive power of the system. In modern high-power machines, X_s can be around 1.5 times the base impedance of the machine. With reactance of this order, the phasor diagram in Figure 17.6 shows that the rotor field excitation required at the rated load (100% load at 0.8 lagging power factor) is more than twice that at no load with the same terminal voltage. The excitation system has the corresponding current and voltage ratings, with capability of varying the voltage over a wide range of 1 to 3, or even more, without undue saturation in the magnetic circuit. Excitation power, which is required primarily to overcome the rotor winding I^2R loss, ranges from ½ to 1% of the generator rating. Most excitation systems operate at 200 to 1000 V DC.

For large machines, four types of excitation systems — DC, AC, static, and brushless — are possible. In the DC system, a suitably designed DC generator supplies the main field winding excitation through conventional slip rings and brushes. Due to low reliability and high maintenance requirements, the conventional DC machine is seldom used in the synchronous machine excitation system.

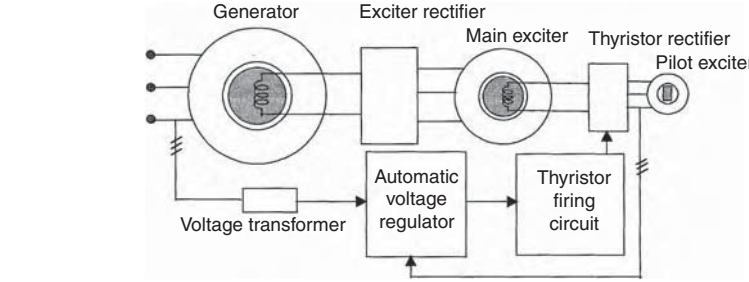

FIGURE 17.7 AC excitation system for the synchronous generator.

Many utility-scale generators use the AC excitation system shown in Figure 17.7. A pilot exciter excites the main exciter. The AC output of a permanent-magnet pilot exciter is converted into DC by a floor-standing rectifier and supplied to the main exciter through slip rings. The main exciter's AC output is converted into DC by means of a phase-controlled rectifier whose firing angle is changed in response to the terminal-voltage variations. After filtering the ripples, this DC is fed to the synchronous generator field winding.

An alternative scheme is static excitation, as opposed to dynamic excitation described in the preceding paragraph. In static excitation, the controlled DC voltage is obtained in a rectified and filtered form from a suitable stationary AC source. The DC voltage is then fed to the main field winding through slip rings. This excitation scheme has a fast dynamic response and is more reliable because it has no rotating exciters.

Modern utility-scale generators use the brushless excitation system. The exciter is placed on the same shaft as the main generator. The AC voltage induced in the exciter is rectified and filtered to a DC voltage by rotating diodes on the shaft. The DC is then fed directly into the rotor field coil. Such a design eliminates the need for slip rings and brushes.

The excitation control system model in analytical studies must be carefully done as it forms a multiple feedback control system that can become unstable. IEEE has developed industry standards for modeling excitation systems. The model must account for the nonlinearity due to magnetic saturation present in all practical designs. Stability can be improved by supplementing the main control signal with auxiliary signals such as for speed and power.

17.3.3 Electric Power Output

The electric power output per phase of the synchronous machine is as follows in units of W/phase:

$$P = VI\cos\phi \tag{17.3}$$

Using the phasor diagram in Figure 17.6, the current can be expressed as follows:

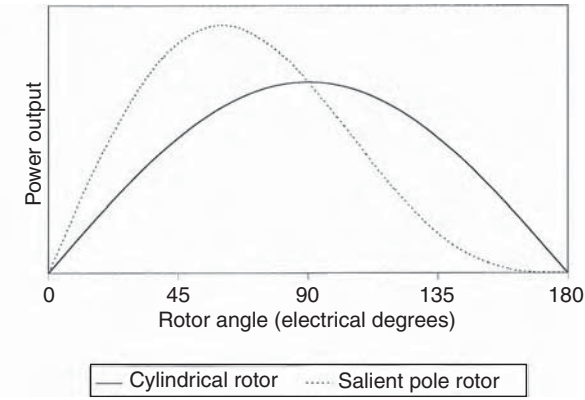

FIGURE 17.8 Power vs. power angle of cylindrical rotor and salient-pole synchronous machine.

$$I = \frac{E - V}{jX_s} = \frac{E\angle\delta - V\angle o}{jX_s} = \frac{E(\cos\delta + j\sin\delta) - V}{jX_s} \tag{17.4}$$

The real part of this current is $I_{real} = E\sin\delta/X_s$

This part, when multiplied with the terminal voltage *V*, gives the output power per phase in units of W/phase:

$$P = \frac{VE}{X_s}\sin\delta \tag{17.5}$$

Output power vs. power angle is a sine curve shown by the solid line in Figure 17.8, having the maximum value at $\delta = 90°$. The maximum power in W/phase that can be generated by the machine is therefore given by:

$$P_{max} = \frac{VE}{X_s} \tag{17.6}$$

Some synchronous machine rotors have magnetic saliency in the pole structure. The saliency produces a small reluctance power superimposed on the main power, modifying the power-angle curve as shown by the dotted line in Figure 17.8.

The electromechanical torque required at the shaft to produce this power is the power divided by the angular velocity of the rotor in units of N·m/phase:

$$T_e = \frac{VE}{\omega X_s}\sin\delta \tag{17.7}$$

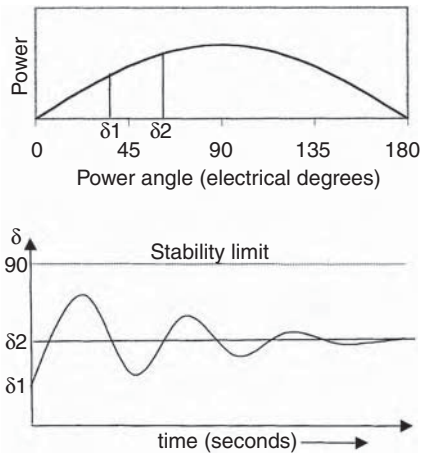

FIGURE 17.9 Load step transient and stability limit of the synchronous machine.

The torque also has a maximum limit corresponding to the maximum power limit and is given by the following in units of N·m/phase:

$$T_{\max} = \frac{VE}{\omega X_s} \tag{17.8}$$

17.3.4 Transient Stability Limit

The maximum power limit described earlier is called the *steady-state stability limit*. Any load beyond this value will cause the rotor to lose synchronism and hence affects the power generation capability. The steady-state limit must not be exceeded under any condition, including those that can be encountered during transients. For example, if a sudden load step is applied to a machine initially operating at a steady-state load power angle δ_1 (Figure 17.9), the rotor power angle would increase from δ_1 to δ_2, corresponding to the new load that it must supply. This takes some time, depending on the electromechanical inertia of the machine. No matter how long it takes, the rotor inertia and the electromagnetic restraining torque will set the rotor in a mass-spring type of oscillatory mode, swinging the rotor power angle beyond its new steady-state value. If the power angle exceeds 90° during this swing, machine stability and power generation are affected. For this reason, the machine can be loaded only to the extent that even under the worst-case load step, planned or accidental, or during all possible faults, the power angle swing will remain sufficiently below 90°. This limit on loading the machine is called the *transient stability limit*.

Equation 17.5 shows that the stability limit at given voltages can be increased by designing the machine with low synchronous reactance X_s, which is largely due to the stator armature reaction component.

TABLE 17.4
Comparison of 10-MW_e Solar-II and 100-MW_e Prototype Design

Performance Parameter	Solar-II Plant 10 MW_e (in %)	Commercial Plant 100 MW_e (in %)
Mirror reflectivity	90	94
Field efficiency	73	73
Mirror cleanliness	95	95
Receiver efficiency	87	87
Storage efficiency	99	99
Electromechanical conversion efficiency of generator	34	43
Auxiliary components efficiency	90	93
Overall solar-to-electric conversion efficiency	16	23

Source: From U.S. Department of Energy and Southern California Edison Company.

17.4 COMMERCIAL POWER PLANTS

Commercial power plants using the solar thermal system are being explored in capacities of a few hundred MW_e. Based on the experience of operating Solar-II, the design studies made by the National Renewable Energy Laboratory (NREL) have estimated the performance parameters that are achievable for a 100-MW_e commercial plant. Table 17.4 summarizes these estimates and compares them with those achieved in an experimental 10-MW_e Solar-II power plant. The 100-MW_e prototype design studied showed that an overall (solar radiation to AC electricity) conversion efficiency of 23% could be achieved in a commercial plant using existing technology. For comparison, conventional coal thermal plants typically operate at 40% overall efficiency, and the PV power systems have an overall efficiency of 6 to 8% with amorphous silicon, 12 to 15% with crystalline silicon, and 20 to 25% with new thin-film multijunction PV cell technologies.

The major conclusions of the studies to date are the following:

1. Designing and building plants with capacities as large as 200 MW_e is possible, based on the demonstrated technology to date. Future plants could be larger. A 200-MW_e plant would require about 3 mi^2 of land.
2. The plant capacity factors up to 65% are possible.
3. About 20% of the conversion efficiency of solar radiation to AC electricity is achievable annually.
4. The thermal energy storage feature of the technology can meet peak demand on utility lines.
5. Leveled energy cost is estimated to be 7 to 9 cents/kWh.
6. The capital cost of \$2000/kW_e for the first few commercial plants, and less for future plants, is estimated. The fuel (solar heat) is free.
7. A comparable combined-cycle gas turbine plant would initially cost \$1000/kW_e, and then the fuel cost would be added every year.

Compared with PV and wind power, solar thermal power technology is less modular. Its economical size is estimated to be in the range of 100 to 300 MW_e. The cost studies at NREL have shown that a commercially designed utility-scale power plant using central receiver power tower technology can produce electricity at a cost of 6 to 10 cents/kWh, depending on the size.

17.5 RECENT TRENDS

As of January 2004, the total collection area of installed solar thermal systems in all countries was 95 million m^2, and that in developing countries was 62 million m^2. At 1 kW/m^2 power in full sun, this amounts to collecting 95 GW of power in full sun. Assuming 50% sun and 20% conversion efficiency on average, this amounts to about 10 GW of end-use electricity. Most of this is in low-temperature applications in developing countries. The total installed capacity of the solar-driven steam power plants in the world today, however, is less than 500 MW but is rapidly growing. The high-temperature applications have yet to develop on a commercial scale.

At present, solar thermal power plants are found to be economical in regions with an annual minimum direct normal solar energy of around 2000 kWh/m^2. The capital cost of a complete midsize (around 100 MW) power plant ranges between \$3 and \$5/W, and the energy costs between 10 and 15 cents/kWh.

Solar Millennium AG of Germany plans to build two 50-MW grid-connected solar thermal power plants near Granada in Spain. The estimated cost is \$400 million (\$8/watt), with a completion target of 2006. The design uses parabolic trough concentrator technology (similar to that used in the Kramer Junction plant of U.S. Duke Solar Energy, Raleigh, NC) and plans to build and operate a 50-MW solar thermal power plant in Nevada using a nontracking parabolic concentrator, which collects almost 60% of the solar energy and reaches temperatures up to 160°C, high enough to produce steam.

Solarmundo in Belgium has developed low-cost concentrators to generate steam using flat rather than conventional parabolic mirrors, which are more expensive to manufacture. In a 2500-m^2 pilot program, the mirrors were arranged as in a Fresnel lens, i.e., fanned out in a number of different segments, each positioned at the optimum angle to the sun. The modular design is scalable up to 200 MW_e. A conceptual design study indicates that a 200-MW plant using this technology in a suitable site in North Africa could generate electricity at 4 to 8 cents/kWh.

Solar heat not being available on demand, solar–fossil hybrids are the next step in development of this technology. For example, an integrated combined cycle of 40-MW_e solar thermal with a 100-MW_e gas turbine power plant is proposed at Jodhpur in Rajasthan, India. According to the Indian Renewable Energy Development Agency, India has a target to install 1500 MW_e by 2012.

A long-term forecast was prepared in 2003 by Teske[3] for Greenpeace International and European Solar Thermal Power Industry Association. The forecast for the next two decades is shown in Table 17.5,[3] with the present installations in some selected countries. The forecast projects the cumulative capacity to reach 21,540 MW in 2020 and would avoid 154 million tons of CO_2 emission during the 2000 to 2020 period. This would require a cumulative investment of U.S. \$42 billion.

TABLE 17.5
Projections for Solar Thermal Power Plants 2005–2020

Year	Cumulative Capacity (MW)	Annual Electricity Generation (Million kWh)	Annual Emissions Avoided (Million Tons)
2005	505	1,058	0.63
2010	1,550	6,095	3.66
2015	6,000	15,200	9.12
2020	21,500	54,600	32.8

Present Plants:

Algeria	140-MW ISCC plant with 35-MW solar capacity
Australia	35-MW compact linear Fresnel reflector to preheat steam for a 2000-MW coal thermal plant
Egypt	127-MW ISCC plant with 29-MW solar capacity
Greece	50-MW solar capacity using steam cycle
India	140-MW ISCC plant with 35-MW solar capacity
Israel	100-MW solar hybrid operation
Italy	40-MW solar capacity using steam cycle
Mexico	300-MW ISCC plant with 29-MW solar capacity
Morocco	230-MW ISCC plant with 26-MW solar capacity
Spain	2 × 50-MW solar capacity using steam cycle and storage in solar-only mode
U.S.	50-MW solar capacity using steam cycle; 1-MW parabolic trough using Organic Rankine Cycle (ORC) engine.

(* ISCC = Integrated Solar Combine Cycle.)

REFERENCES

1. Mancini, T., *Solar Thermal Power Today and Tomorrow*, Mechanical Engineering, Publication of the Institution of Mechanical Engineers, London, August 1994.
2. Technology Report No. 14, Southern California Edison Company, Irwindale, CA, Fall 1995.
3. Teske, S., Solar Thermal Power 2020, *Renewable Energy World*, January–February 2004, pp. 120–124.

18 Ancillary Power Systems

There are various ways, other than conventional wind and photovoltaic (PV) systems, to generate electric power. The ultimate source of energy is, of course, the sun. This energy comes primarily in the form of heat. The sun's heat, in turn, produces wind in the air, marine currents in the ocean, and waves on the ocean surface. All of these carry energy derived from solar energy, which can be converted into electricity using various energy conversion technologies such as the wind and PV systems discussed in the preceding chapters. This chapter covers several other concepts that are being developed. Some have been successfully demonstrated by prototypes and have been proposed for large-scale power generation, seeking potential investors.

18.1 HEAT-INDUCED WIND POWER

The solar-heat-induced wind power schematic shown in Figure 18.1 uses a tall chimney surrounded by a large solar-heat-collecting roof made of glass or plastic sheets supported on a framework. Toward the center, the roof curves upward to join the chimney, thus creating a funnel. The sun heats the air underneath the roof. The heated air follows the upward incline of the roof until it enters the chimney, through which it flows at high speed and drives the wind turbines installed at the top exit. Electrical generators can be installed at the top or bottom of the chimney by means of a shaft and a gear. The large thermal time constant of the ground generates power even several hours after sunset. The overall efficiency of the plants is 3 to 5%, primarily depending on the chimney height. Because the capital cost is high, such a power plant is economical only in large capacities (>1 MW) in desert regions where the land is free or very cheap. However, the plant can be made more economical by using the land under the roof as a greenhouse for agricultural purposes.

In the arid flat land of southeastern Australia, EnviroMission of Melbourne has plans for a solar wind tower (Figure 18.2). The sun-capture area is a 11-km^2 glass-roof enclosure. The concrete chimney is 140 m in diameter and 1000 m tall. At the top, 32 wind turbines add to a total capacity of 200 MW of electric power. The estimated cost of $380 million is twice the cost of a conventional wind farm of similar capacity, but the tower is more reliable for power generation because even on a cloudy day, half of the sun's energy reaches the earth, as compared to that on a sunny day. EnviroMission is also evaluating sunny sites in the southwestern U.S. for similar power plants.

18.2 MARINE CURRENT POWER

Among the many forms of ocean energy, tidal or marine currents and waves offer two prominent short- to medium-term prospects for renewable power. The U.K. Department of Trade and Industry, in 2004, funded £50 million for marine research

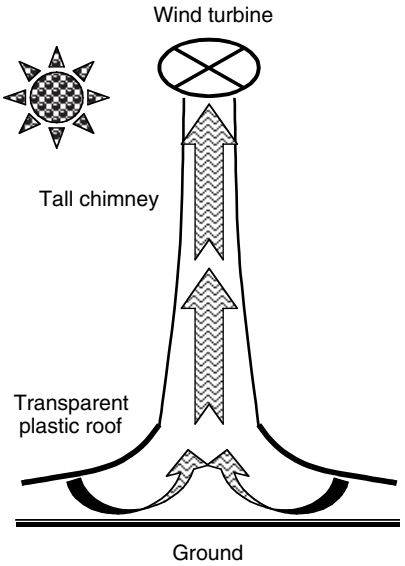

FIGURE 18.1 Solar-heat-induced wind chimney power plant schematic.

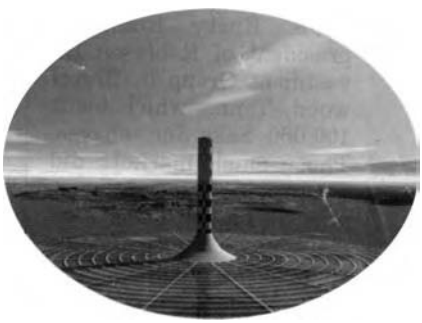

FIGURE 18.2 Proposed solar-heat-induced wind chimney power plant. (From EnviroMission Ltd, Melbourne, Australia.)

on harnessing wave and tidal stream power. Scotland is leading the way in this research, with the first such plant in operation on the island of Islay. The European Marine Energy Center in Orkney, Scotland, offers development, testing, and monitoring of grid-connected wave energy conversion systems.

Three options available for power generation from the ocean are:

- Wave energy
- Tidal energy
- Marine currents

FIGURE 18.3 The 300-kW marine current power generator installed near Devon, U.K. (From Marine Current Turbines Ltd., Bristol, U.K., the European Commission, and *Professional Engineering, Professional Engineering Publications,* p. 7, February 13, 2002.)

Wave energy is ultimately a form of solar energy, which generates pressure differences in air and, hence, wind. The wind, in turn, generates waves on the ocean surface. Marine currents also result from solar heat. Tidal energy, on the other hand, results from the enormous movement of water due to gravitational forces of the sun and the moon on the seas.

Interest in marine current power has emerged only since 1990. Successful prototypes have been demonstrated using the conventional horizontal-axis turbine, although a Darrieus turbine can also be used. After a few successful demonstrations, work is underway on two commercial grid-connected power generators; one, rated 300 kW with a horizontal-axis turbine in the U.K., and another, rated 250 kW with a vertical-axis turbine in Canada. A 300-kW tidal current turbine has been installed 1 km off the shore of Devon, U.K., funded by the U.K., Germany, and the European Commission (Figure 18.3). The machine is built by the Marine Current Turbine Company and partly funded by London Electricity. It is mounted on steel pipes set into the seabed. Its 11-m-diameter blades generate 300 kW of power under tidal currents of 2.7 m/sec. The top end of the whole installation stands a few meters above the water surface. Another design is also being developed that does not require anchorage to the seabed.

Marine current speeds tend to be maximum near the surface, so the turbine rotor must intercept as much of the depth as possible near the surface. The rotor can be secured in position in several ways similar to those used in the offshore oil-drilling and oil-mining platforms (Figure 18.4).

A study[1] funded by the European Commission estimated 48 TWh/yr of exploitable tidal current energy potential at more than 100 locations around Europe. Similar

FIGURE 18.4 A proposed marine current tidal power system. (From Frankel, P., Marine Currents Turbine Ltd., Bristol, U.K. With permission.)

studies around the world have shown such energy potentials of 70 TWh/yr in the Sibulu Passage in the Philippines and 37 TWh/yr near the Chinese coasts.

The principle of converting this kinetic energy into electricity is similar to that in the wind turbine. The analytical methods covered in Chapter 3 are valid, except for the density and speed difference between the tidal current and the wind. No new theory is needed to design a tidal turbine. Density of water is 800 times that of air, but the current speed is about half that of air, so the theoretical tidal current power density per square meter of the blade-swept area is approximately 100 times higher than that in wind.

Tidal current turbines have two advantages over wind turbines:

- Higher power density per unit blade area.
- Tidal currents are more predictable.

For example, a marine current of 3 m/sec (6 kn) represents an impinging mechanical power of 14 kW/m^2 of the blade-swept area. A minimum current of about 1.25 m/sec, bringing 1 kW/m^2 of mechanical power, is practically required for a power plant. Thus, a potential site must have a sustained current exceeding 1 m/sec at sufficient depth for installation of a turbine of a required diameter for the desired electrical capacity.

18.3 OCEAN WAVE POWER

Ocean waves bring enormous amounts of energy to the shore, day and night, all year round. Tapping a small percentage of this energy can provide all the energy required worldwide.

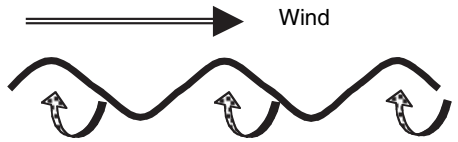

(a) Storm generates waves by friction of wind against the water surface.

(b) As waves move farther, they become rolling swells. Water appears to be moving forward, but it only goes around in circles.

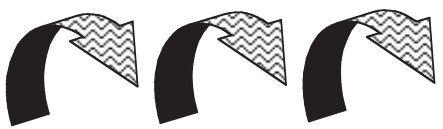

(c) An underwater reef or seamount breaks the wave, distorts the circular motion, and the wave basically trips over itself.

FIGURE 18.5 Ocean wave generation mechanism.

The wind acting on the ocean surface generates waves. Hence, wave power is essentially wind power. The energy extracted from waves is replenished by the wind. Wave energy is thus a renewable source, more so than other renewable energy sources.

Large waves are generated by huge windstorms. Wave heights of 70 to 100 ft are possible in 70 to 100 mph storms. A wave generation mechanism, depicted in Figure 18.5, is as follows:[2]

1. Waves are generated due to the friction between the wind and the surface of the ocean. The stronger and longer the wind blows over wide, deep water, the higher the waves.
2. As the waves spread from the storm area, they become rolling swells. The water appears to be moving some distance, but it really just goes in circles. The energy of the waves, however, moves on in a domino-effect pattern.
3. When the wave hits an underwater obstruction, such as a reef or seamount, the shear friction due to the obstruction distorts the circular motion of the water, and the wave breaks up (trips over itself).

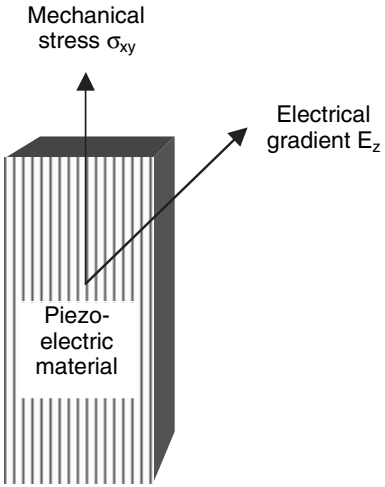

FIGURE 18.6 Piezoelectric phenomenon.

An estimated 2 to 3 million MW of power are contained in the waves breaking up on shores worldwide. At favorable coastlines, the power density could be 30 to 50 MW/km. A number of companies in the U.S., Europe, Canada, and around the world are engaged in extracting marine power to generate electricity. A dedicated facility for testing electricity generation from wave power has been established in Blyth, U.K. A 70-m × 18-m testing tank with wave-generating machines has been made from a dry dock.

A few alternative technologies can be considered for converting wave energy into electricity. One scheme uses the circulating water particles in the waves to create local currents to drive a turbine. A prototype built and connected to the Danish grid in 2002 is working well, even with irregular waves as small as 20 cm. A combination of Wells turbine and Darrieus rotor is used to capture the wave energy from both up-and-down and back-and-forward currents.[3] It works on a complex principle by which lift in a circulating flow is created using hydrofoil blades.

Another scheme, developed by Ocean Power Technologies (Princeton, NJ) uses the newly developed piezoelectric polymer sheets to convert wave energy directly into electricity[4,5] and is described in the following section.

18.4 PIEZOELECTRIC GENERATOR

Piezoelectric material, when subjected to mechanical stress over an area, generates an electrical field in the transverse direction (Figure 18.6). The *piezoelectric coupling coefficient* is defined as the ratio of the electrical field across the thickness to the longitudinal mechanical stress,[6] i.e., in units of V/m per N/m^2:

$$\alpha = \frac{E_z}{\sigma_{xy}} \tag{18.1}$$

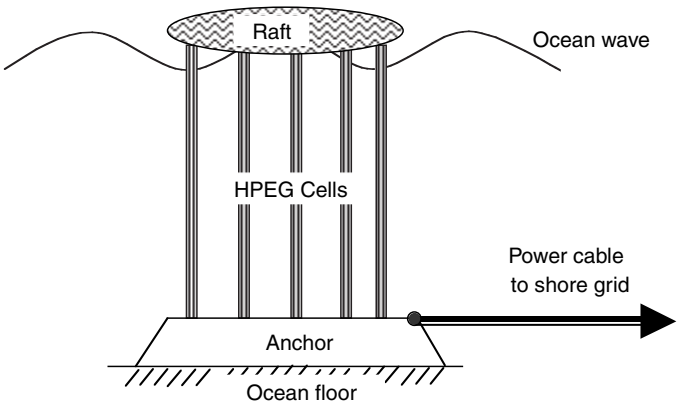

FIGURE 18.7 Hydropiezoelectric generator.

Piezoelectric crystals have been in use for many years for acceleration and mechanical stress measurements. The most commonly used crystals are expensive and have α less than 0.5 V/m per N/m^2. However, low-cost piezoelectric polymers having high α have been recently developed by companies such as AMP for generating large-scale electric power from the mechanical power of ocean waves.

The hydropiezoelectric generator (HPEG) converts ocean wave energy directly into electricity. It uses many piezoelectric cells, each cell made of many piezoelectric polymer sheets laminated together. The cells are hung from a raft in the ocean and anchored to the ocean floor (Figure 18.7).

The sheets stretch when a wave lifts the raft, and the resulting strain generates electric power.[7,8] A power electronic circuit converts the low-frequency power into direct current (DC), and then to a standard 60-Hz or 50-Hz power. The characteristic low frequency of ocean wave power poses a significant design challenge in power electronic frequency converters.

The HPEG concept differs from other ocean power conversion schemes, which generally involve large moving parts and rotating turbine generators. The HPEG, although having a conversion efficiency of around 2%, has many potential applications in providing power for remote islands, coastal communities, lighthouses, offshore platforms, buoys, etc.

18.5 JET-ASSISTED WIND TURBINE

Stand-alone wind turbines depend on the wind blowing favorably at all times. The availability of electric power during low-wind conditions can be assured only if an extremely large energy storage battery is incorporated in the system, or if a diesel generator is available on the ground in addition to the wind generator on the tower. However, a jet-assisted wind turbine with fuel jets located at the tips of the rotor blades can assist the turbine in low wind or drive it when there is no wind. On remote farms, diesel is always available for use in farm equipment. In the absence of adequate wind, the diesel is burned and ejected in jets at the rotor tip to assist

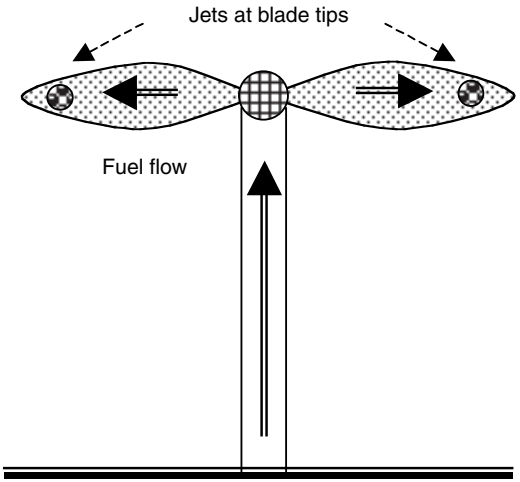

FIGURE 18.8 Jet-assisted wind turbine generator.

the wind turbine in maintaining the desired speed (Figure 18.8). Thus, fuel drums are sturdy, low-cost, and extremely reliable means of energy storage at power plants. The main savings come not from having an independent diesel generator but instead from using the same electrical generator in the wind turbine tower. Research funding has been granted by the California Energy Commission for such a scheme being developed by Appa Technology Initiatives (Lake Forest, CA).

18.6 SOLAR THERMAL MICROTURBINE

In this scheme, the sun's energy is collected in the form of heat using a concentrator. The heat, in turn, is used to generate steam and drive a rotating microturbine generator (Figure 18.9). The scheme basically uses a thermodynamic cycle. The usable energy extracted during a thermal cycle depends on the working temperatures. The maximum thermodynamic conversion efficiency that can be theoretically achieved with a hot-side temperature T_{hot} and a cold-side temperature T_{cold} is given by the Carnot cycle efficiency as:

$$\eta_{carnot} = \frac{T_{hot} - T_{cold}}{T_{hot}} \tag{18.2}$$

where the temperatures are in degrees Kelvin. A high hot-side working temperature and a low cold-side exhaust temperature give a high efficiency of converting the captured solar energy into electricity.

Compared to the solar PV system, the solar thermal microturbine system is economical, as it eliminates the costly PV cells and battery. The solar dynamic concentrator with a turbo alternator also offers significant advantage in efficiency and weight and hence in the overall cost over the solar PV technology.

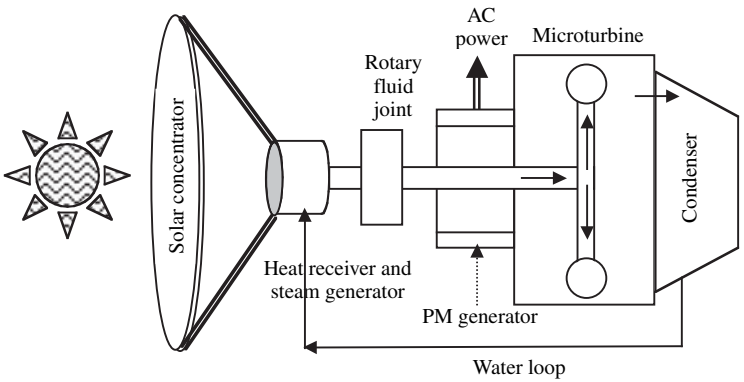

FIGURE 18.9 Solar thermal microturbine generator.

Research funding has been granted by the California Energy Commission for developing such a turbine proposed by Appa Technology Initiatives. The age-old Hero's steam engine concept has been found effective and affordable in designing a small 10 to 25 kW system suitable for residential or small-farm use. The engine consists of a single rotating composite disk having many steam jet nozzles embedded tangentially into its rim. The spinning disk drives a lightweight, high-speed electrical generator, the output of which is converted into utility-quality power by power electronics. Steam pressure in the range of 500 to 2,000 kPa yields thermodynamic efficiencies of 20 to 30% at disk speeds of 3,000 to 10,000 rpm. Simplicity and fewer components are key features of this scheme. The sun-to-electricity energy conversion efficiency is 15 to 20%, which is in the range of normal PV cell efficiency. On a sunny day, with solar radiation of 1,000 W/m^2, a parabolic dish of 5-m diameter can generate 3 kW of electric power using this scheme. However, the cost of such a power source is estimated to be around $5,000. A 3-kW PV power system in 2005 would cost about $25,000, which is 5 times more than the solar thermal microturbine system.

18.7 THERMOPHOTOVOLTAIC SYSTEM

In the thermophotovoltaic (TPV) system, the solar heat is directed onto PV cells. The system can have a cylindrical or flat configuration, as shown in Figure 18.10. A heated surface radiates infrared (heat) onto an array of PV cells sensitive in the infrared range. A part of the energy is converted into DC, and some is reflected back and dissipated as heat. The energy conversion process is different from that in the conventional PV cell. The efficiency varies with the radiator temperature.

Most current TPVs use low-bandgap PV cells (0.55-eV InGaAs or 0.73-eV GaSb) to optimize the cell response to energy sources in the 1 to 2 μm range. The low bandgap of these cells leads to low open-circuit voltage (0.25 to 0.45 V) and poor fill factor caused by high intrinsic carrier concentration. The cell is operated at low temperatures, generally below 60°C, to have adequate output voltage.

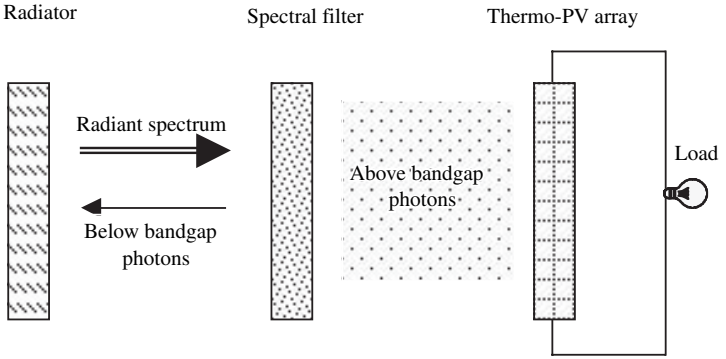

FIGURE 18.10 Thermophotovoltaic conversion scheme.

The TPV concept has recently seen renewed interest with new developments in semiconductor technology. Recent advances have produced low-bandgap (0.50 to 0.55 eV) material that is lattice-matched to GaSb substrates. At relatively low radiator temperatures, there are many viable options for the heat source, and a number of applications become attractive. Using the waste heat of a cogeneration power plant is one example. TPV ensures that power plants can generate electricity day and night, rain or shine. The extra energy collected during a sunny day is stored in a hot liquid, which is then used in TPV systems at night or on a cloudy day. The energy storage, thus, is inherent to the system design.

REFERENCES

1. Frankel, P., Energy from the Oceans, Preparing To Go On-Stream, *Renewable Energy World*, James & James, London, August 2002, pp. 223–227.
2. Myers, J.J., Holm, C.H., and McAllister, R.F., *Handbook of Ocean and Underwater Engineering*, McGraw-Hill, New York, 1968.
3. Temeev, A.A. et al., Natural-Artificial Power-Industrial System Based on Wave Energy Conversion, Proceedings of the 34th Intersociety Energy Conversion Engineering Conference, Vancouver, BC, Canada, SAE, 2000, Paper No. 1-2556.
4. Mario, C., Ocean Power Envisions a Piezoelectric Energy Farm, U.S. 1 Business, Princeton, NJ, January 18, 1995, pp. 223–227.
5. Taylor, G.W. et al., *Piezoelectricity*, Gordon and Breach Science Publishers, New York, 1985.
6. Gross, N., Jolt of Electrical Juice from Choppy Seas, *Business Week*, November 28, 1994, p. 149.
7. Patel, M.R., Piezoelectric Conversion of Ocean Wave Energy, Proceedings of the 1st International Energy Conversion Engineering Conference, Portsmouth, VA, AIAA, 2003, Paper No. 6073.
8. Patel, M.R., Optimized Design of Piezoelectric Conversion of Ocean Wave Energy, Proceedings of the 2nd International Energy Conversion Engineering Conference, Providence, RI, AIAA, 2003, Paper No. 5703.

19 Contrarotating Wind Turbines

New developments in any technology usually take incremental steps forward, but the research presented here may potentially improve wind turbine efficiency by 30 to 40% in one step.[1] It may significantly enhance the energy density per acre of wind farms in constrained areas or may make wind farms in low-wind regions economically viable. Both theoretical considerations and the prototype construction and tests are presented in detail, which may help professionals and university researchers carry it forward to commercial realization in the future.

19.1 INTRODUCTION

As seen in Section 3.2, the maximum theoretical efficiency of a single rotor is 59% when the downstream wind velocity is a third of the upstream velocity. Albert Betz established this in 1926.[2] In practice, it is difficult to achieve a two-thirds velocity reduction with one rotor and, therefore, most wind turbines hardly achieve better than 40% conversion efficiency.

Charles Gordon Curtis, while working on steam turbines in the 1880s, had realized that a single-rotor system could not efficiently produce large changes in enthalpy or velocity. Therefore, he introduced the principle of velocity compounding, in which multiple pairs of rotor and stator disks are mounted in tandem to improve the energy conversion efficiency up to 80%. In 1903, General Electric (GE) funded Curtis to build and demonstrate the first American 500-kW steam turbine using tandem disks, which became a landmark invention in steam and gas turbines.[3] Lately, a number of patents have been issued on methods of improving wind energy conversion efficiency. U.S. Patent No. 5,419,683, issued to Peace, is for a method of installing multiple wind turbines on chimneys, towers, and so forth. Two rotors with their axes horizontal were mounted back-to-back on a ring that revolved about a chimney. The primary concept of this invention, however, is to utilize existing tall structures to mount multiple wind turbines to simulate large wind farms.

As an alternate approach, Appa Technology Initiatives recently built several contrarotating wind turbine models and conducted wind tunnel and field tests with funding from the California Energy Commission. These studies have shown that contrarotating rotors in tandem can extract an additional 30 to 40% of wind energy compared to a corresponding single-rotor system. On the basis of this study, three U.S. patents, 6,127,739, 6,278,197 B1, and 6,492,743, were issued. A schematic outline of the contrarotating wind turbine system is depicted in Figure 19.1.

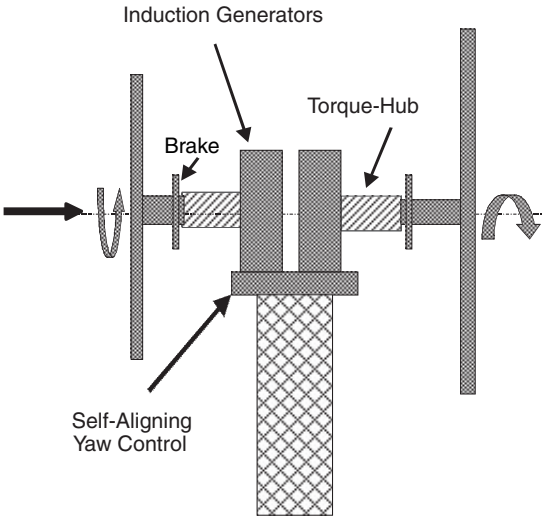

FIGURE 19.1 Contrarotating rotors with dedicated generators.

19.2 POTENTIAL APPLICATIONS

If the contrarotating rotor system could extract an additional 30 to 40% energy, why the wind turbine industry has not adopted this concept is a frequently asked question. A possible explanation is that by extending the rotor diameter, the same amount of power could be generated without the need for a more complex contrarotating rotor design. This argument may be valid when considering a single turbine in an open field, but in the case of a wind farm with a limited land area, the space required for a single tower and the maximum number of towers that can be installed would limit the power output of the farm. Based on aerodynamic performance considerations, the minimum space required between turbines in a wind farm is about 8 to 12 rotor diameters in the wind direction. So, increasing the rotor diameter does not help, as it reduces the number of towers, diminishing the power density per acre. Energy production and revenue depend on the power density of the wind farm. Energy-dense wind farms are rare but are becoming necessary under the current environmental constraints in siting new wind farms. The contrarotating rotor arrangement increases the electric energy production and revenue from a wind farm. Achieving 30 to 40% more power from the same farm may make class-3 and class-4 category wind speeds economically viable for wind power generation, which is a new thrust area of the U.S. Department of Energy (DOE) and the National Renewable Energy Laboratory (NREL).

Thus, two potential applications of the contrarotating rotor system are:

1. To maximize the annual energy output of a large wind farm where the land or offshore ocean area is constrained by environmental or economical reasons
2. To make a wind farm in low-wind-speed regions of class-3 and class-4 categories economically viable

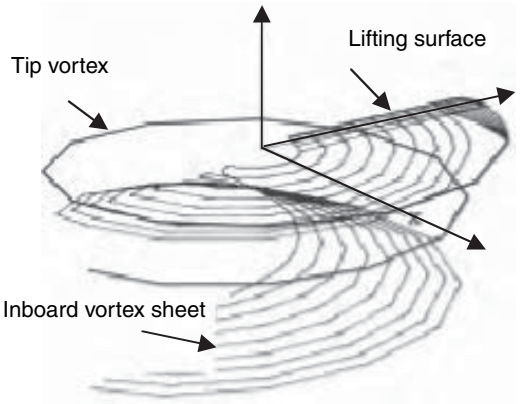

FIGURE 19.2 Vortex sheet shed behind the front rotor.

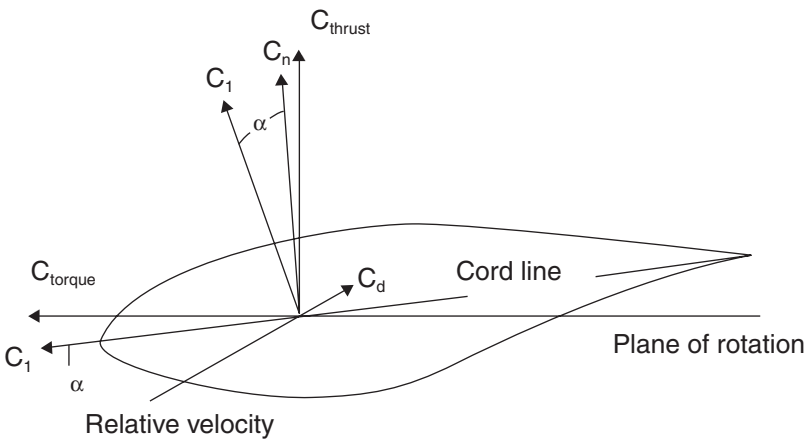

FIGURE 19.3 Typical force components on an airfoil section.

19.3 MATHEMATICAL MODEL

Modeling of the windward and leeward rotor blades as lifting surfaces requires a complete understanding of the vortex sheet shed behind the rotors. Figure 19.2 depicts a schematic outline of the vortex sheet.[4] A certain amount of wind energy is transformed into rotational energy. It is, therefore, possible to recover this vortex energy by means of the contrarotating rotor system. As will be seen later, the counter-rotating leeward rotor straightens out the vortex flow. In doing so, the momentum due to the tangential velocity component is transformed into mechanical work. Thus, the energy conversion efficiency of a wind turbine system could be improved. Figure 19.3 shows the orientation of a blade section at any radial station of a moving rotor. The aerodynamic force components with respect to the relative wind are also shown there.

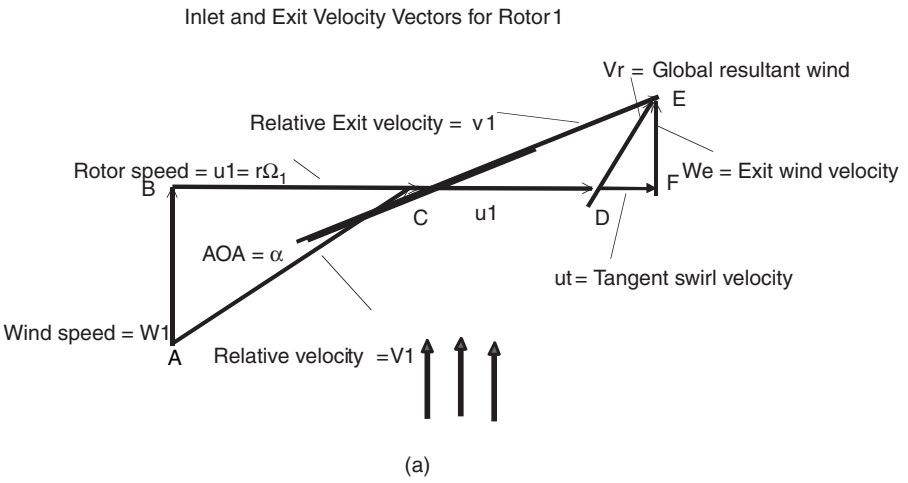

FIGURE 19.4(a) Inlet and exit velocity vectors for windward rotor (rotor 1).

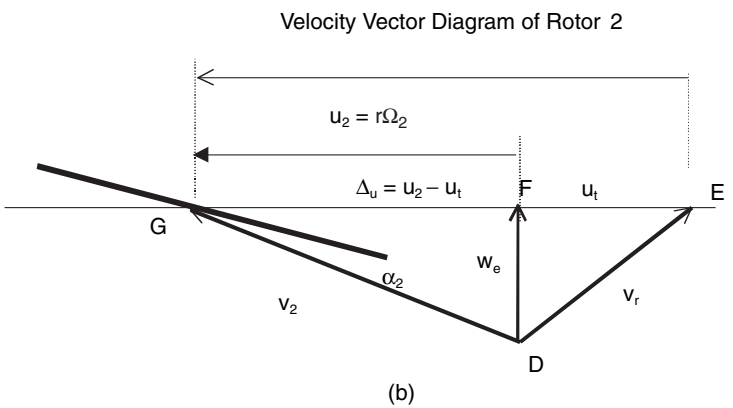

FIGURE 19.4(b) Velocity vector diagram for leeward rotor (rotor 2).

19.3.1 Velocity Components

Let us consider the blade sections pertaining to the windward rotor and the leeward rotor. The blades of these rotors are set to rotate in opposite directions. Figure 19.4(a) depicts the velocity vectors for the windward rotor 1, in which AB denotes the wind speed w_1, BC the tangential rotor speed u_1, and AC the relative velocity v_1. The blade incidence is set at α_1. If the blade surface is considered frictionless, then the flow leaves the trailing edge tangentially with exit velocity v_1. The global exit velocity v_r is then denoted by DE, having a tangential (swirl) component u_t, and an axial exit-wind velocity w_e.

The velocity components of the leeward rotor are shown in Figure 19.4(b), in which DE denotes the onset wind speed v_r, EG the tangential velocity u_2, and DG

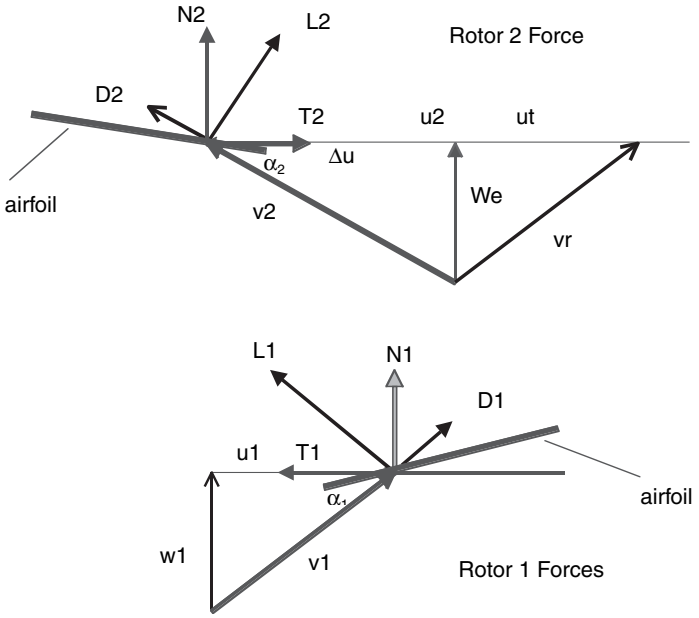

FIGURE 19.5 Force vector diagram in a contrarotating wind turbine system.

the relative velocity v_2. It is noteworthy that if the rotor speeds Ω_1 and Ω_2 are equal and opposite, i.e., $\Omega_2 = -\Omega_1$, the relative velocity v_2 is almost equal to v_1 (because α_1 is small), and consequently the torques of rotor 1 and rotor 2 balance each other, resulting in zero net torque load on the supporting structure. This is an incidental benefit but has great value in tower design.

19.3.2 Force Components

The corresponding force vectors of the two counter-rotating rotors are shown in Figure 19.5, in which L_1, D_1 and L_2, D_2 denote the lift and drag components of rotors 1 and 2, respectively. On resolving these forces along the normal and tangential directions, the thrust and tangential forces for each rotor are denoted by N_1, T_1 and N_2, T_2, respectively.

The torque per unit strip dS of each rotor blade is given by the following:

$$d\tau_1 = \frac{1}{2}\rho w^2 \sqrt{(1+t_1^2\xi^2)}[C_L - C_D t_1 \xi]dS \cdot r \tag{19.1}$$

$$d\tau_2 = -\frac{1}{2}\rho w^2 \sqrt{(1+(\Delta t\xi)^2)}[C_L - C_D \Delta t \xi]dS \cdot r \tag{19.2}$$

Power per unit strip dS is given by the following:

$$dP_1 = \frac{1}{2}\rho w^3 t_1 \xi \sqrt{(1+t_1^2\xi^2)}[C_L - C_D t_1 \xi]\,dS \tag{19.3}$$

$$dP_2 = -\frac{1}{2}\rho w^3 t_2 \xi \sqrt{(1+(\Delta t\xi)^2)}[C_L - C_D \Delta t \xi]\,dS \tag{19.4}$$

where
C_D and C_L = drag and lift coefficients of the blade foil, respectively
$dS = C_r\,dr$ = area of the blade strip

$t_1 = \dfrac{\Omega_1 R}{w_1}$ = rotor 1 tip speed ratio

$t_2 = \dfrac{\Omega_2 R}{w_e}$ = rotor 2 tip speed ratio

$\xi = r/R$, R = rotor tip radius

$\Delta t = t_1 + t_2$

The net power production from the contrarotating wind turbine system is given by:

$$dP_{CRWT} = dP_1 + dP_2 \tag{19.5}$$

The power in the wind stream, according to momentum theory, is given by:

$$dP_w = \frac{1}{2}\rho w^3 (2\pi r\,dr) \tag{19.6}$$

The wind power conversion efficiency, integrated over the radius of the rotor, can be written as follows:

$$C_p = \frac{P_{CRWT}}{P_w} \tag{19.7}$$

A few illustrative calculations are performed here for a small rotor to determine the power conversion efficiency of a contrarotating system. The tip speed ratio (TSR) was selected as 6 so that the tip speed does not exceed 75 m/sec at 330 rpm of the rotor speed. The computed power curves for rotors 1 and 2 are shown in Figure 19.6. The available wind stream power is shown by the top curve, whereas the curve below denotes the net power from both rotors. This data suggests that at low rotor speeds, a counter-rotating system is able to extract nearly 70% of the usable power, which is about twice that of a practical single-rotor system. This implies that utility-scale machines, which

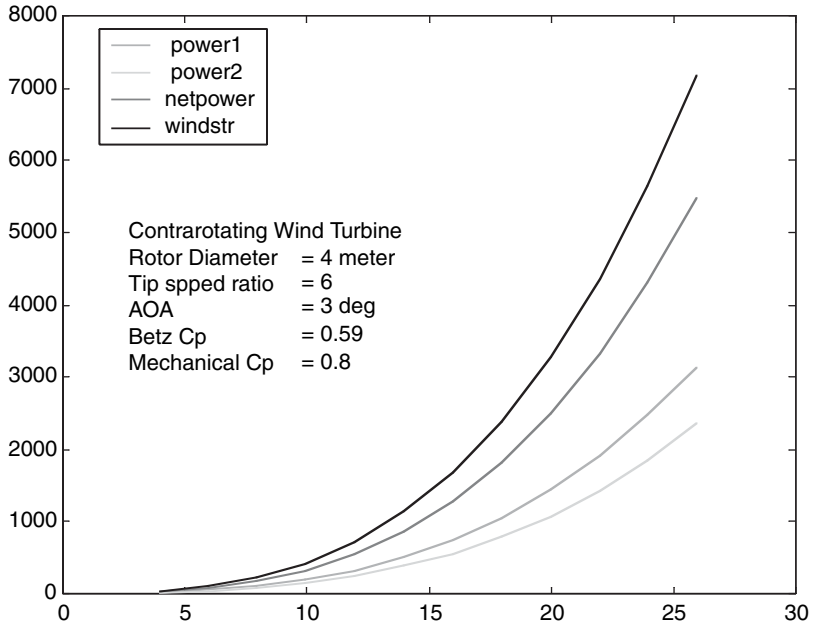

FIGURE 19.6 Power from 4-m-diameter contrarotating rotors.

normally rotate at 18 to 30 rpm, may produce almost twice the amount of energy, quite a remarkable theoretical improvement.

19.4 PROTOTYPE DESIGN

To demonstrate the concept, a simple configuration consisting of two 3-kW permanent-magnet (PM) generators in tandem was fabricated. Two two-blade, 4-m-diameter rotors were directly attached to the magnetic drums of each generator. The leeward rotor blade was set to rotate in a direction opposite to that of the windward rotor.

A variable-speed wind turbine, being more efficient than a constant-speed system, was chosen in building two PM generators. Figure 19.7 shows the magnetic drum rotor. The drum was made of a 267-mm-diameter steel tube having 9.5-mm wall thickness. The mean flux path diameter of the drum was 223 mm. There were 16 C8-type magnets, each of 102-mm length, 40-mm width, and 12.5-mm thickness. Two bearings were used to mount the drum on a stationary armature shaft. The armature shown in Figure 19.8 had 48 skewed slots, which housed 48 coils having 1.15-mm-thick film-insulated copper wire. There were six groups of inductive coils, each having eight 10-turn coils connected in series. The three phases of the stators were connected in parallel inside and in a Y configuration outside. The measured impedance of the armature consisted of a resistance R equal to 1.13 Ω and an inductance L equal to 7.5 mH per phase.

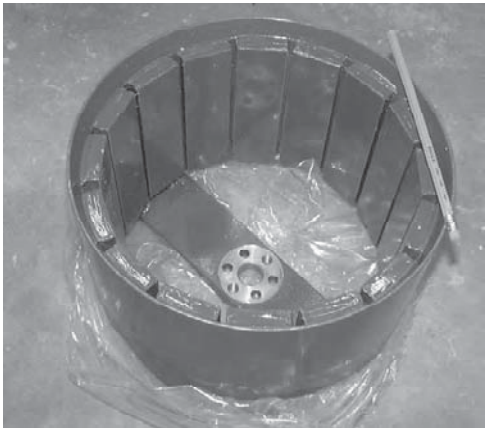

FIGURE 19.7 PM drum rotor.

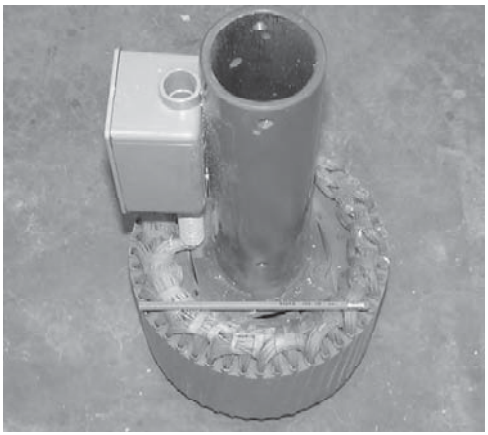

FIGURE 19.8 Laminated stationary armature.

19.4.1 Design Method

For an average wind speed w at a given site, the design engineer can select the rotor diameter of a contrarotating wind turbine system for the desired design power using the following expression:

$$D = \sqrt{\frac{\text{Power}}{C_{\text{pnet}}(\pi\rho w^3)}} \tag{19.8}$$

where
D = rotor diameter
$Power$ = design power
C_{pnet} = net power coefficient
w = average wind speed at a given site
ρ = air density

Once the rotor diameter has been selected, it is necessary to select the chord distribution. Gasch[5] has reported two methods proposed by Betz and Schmitz. Betz's approach uses the average of the upstream and downstream velocities, whereas Schmitz also considers the influence of the rotational flow. Both methods yield the same chord distribution at the tip stations, but at the blade root sections, Schmitz's method yields a more realistic distribution of the chord. Hence we chose to use Schmitz's chord distribution, which is given by:

$$\text{Chord}(\xi) = \left(\frac{16\ R}{C_L N}\right)\xi \sin^2\left(\frac{\alpha_1}{3}\right) \tag{19.9}$$

where
N = number of blades
C_L = lift coefficient at C_L/C_D max
R = rotor radius
ξ = blade radial station.

The relative wind velocity direction with respect to the rotor plane is given by:

$$\alpha_1 = \tan^{-1}\left(\frac{w}{\Omega r}\right) \tag{19.10}$$

Next, we select the blade setting β given by the following:

$$\beta = \frac{\alpha_1}{3} - \alpha_{AOA} \tag{19.11}$$

where α_{AOA} is the airfoil angle of attack, which may be kept constant along the blade.

The airfoil of interest in this study was the 21%-thick S809 from the NREL thick-airfoil family for horizontal-axis wind turbine applications. For this purpose the airfoil was designed to have a sustained maximum lift, minimal sensitivity of lift to roughness, and a low profile drag. Typical airfoil sections of the windward and leeward rotors are presented in Figure 19.9 and Figure 19.10, respectively. An extensive experimental database for this airfoil was developed at Ohio State University.

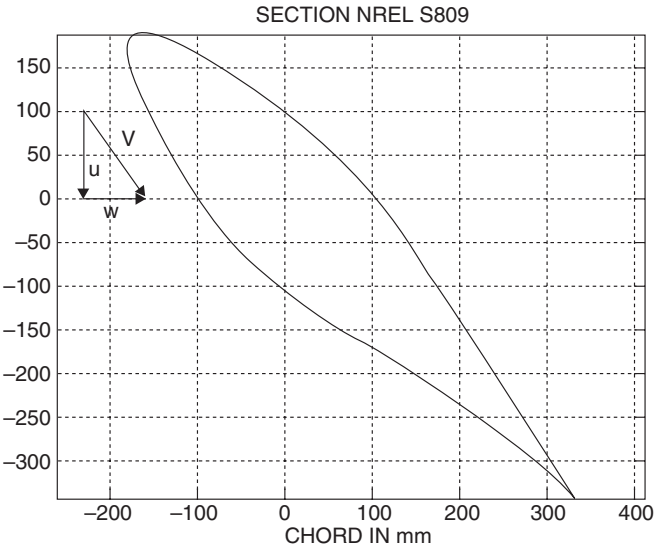

FIGURE 19.9 Windward rotor at root section, rotated at elastic axis at 35% chord.

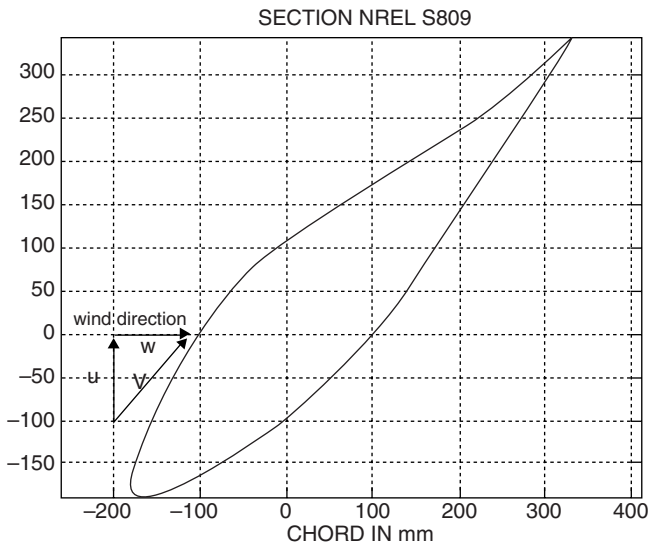

FIGURE 19.10 Leeward rotor at root section, rotated at elastic axis at 35% chord.

The experimental C_L and C_D curves for S809 are presented in Figure 19.11 and Figure 19.12.

The windward and leeward rotors consisted of two blades each. Clockwise- and counterclockwise-spinning blades were fabricated using carbon composite fabrics. The assembled contrarotating wind turbine prototype is shown in Figure 19.13. A

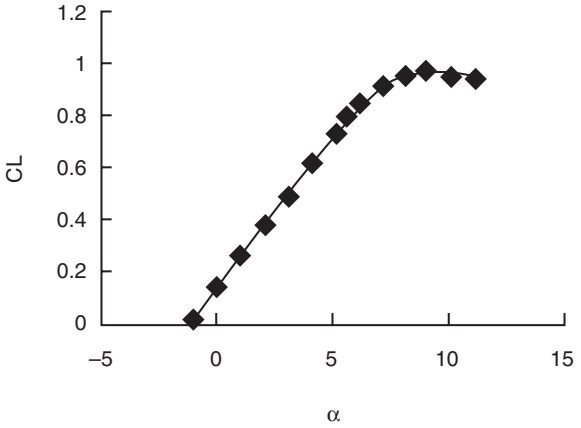

FIGURE 19.11 Experimental lift coefficient vs. alpha.

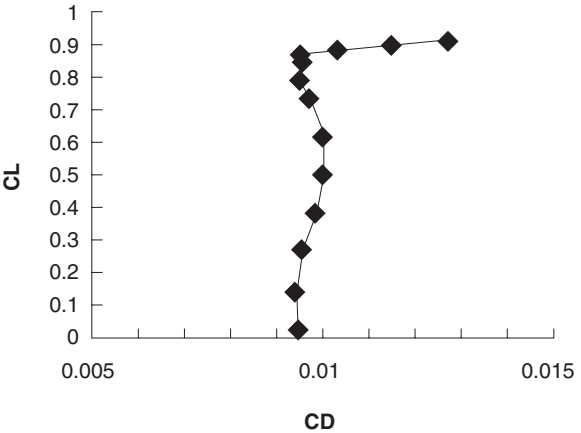

FIGURE 19.12 Experimental drag coefficient vs. C_L.

tail boom was used to turn the rotors into the wind direction. However, in a dual-rotor system, it is possible to eliminate the tail boom by providing a longer lever arm to the leeward rotor, so that the unbalanced rotor drag would be able to point the rotor into the wind. Short-circuiting of the armature was used to park the system on brake when required.

19.4.2 Selection of Sensors

The PM generator is a variable-speed system and generates power at varying voltage and frequency depending on the wind speed. The AC electric power is first rectified into DC, which is inverted into AC of the required voltage and frequency. The AC power was dissipated by means of heaters in these prototype tests. The following

FIGURE 19.13 Assembled contrarotating wind turbine system.

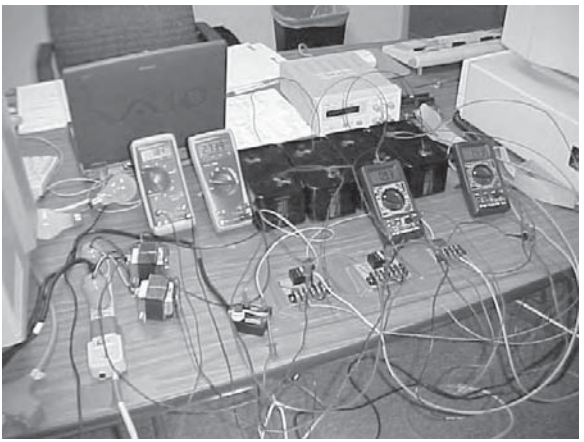

FIGURE 19.14 Calibration of sensors.

sensors were used to measure the performance characteristics of the contrarotating system:

- Two voltage sensors to measure voltage and rotor speed in rpm
- Two watt sensors to measure three-phase power
- One anemometer to measure wind speed
- One acceleration sensor to measure the vibration of the system

In addition to the sensors, two clamp current meters and two digital multimeters were used to monitor the current and voltage of the generators. The calibration setup of the sensors is shown in Figure 19.14 and Figure 19.15.

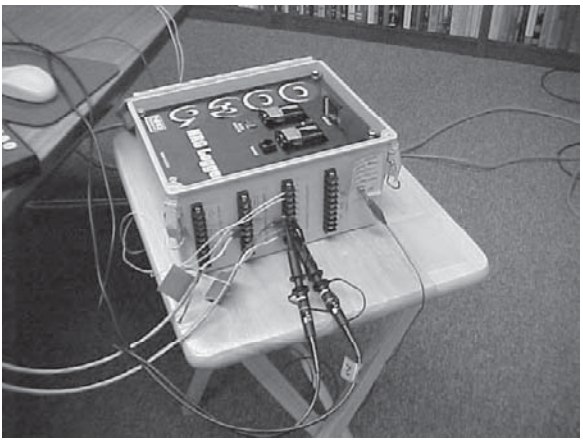

FIGURE 19.15 NRG system instrumentation and verification.

The current sensors used the Hall effect principle. A current-carrying conductor is passed through a hole. A DC supply voltage is applied perpendicular to the plane of the magnetic field generated by the current. The resulting effect is an induced voltage proportional to the conductor current. Winding several turns of the conductor through the meter can increase the magnetic field strength. The schematic of the watt sensor built by Load Controls, Inc., is shown in Figure 19.16. This unit was used to record power at various voltages and frequencies in the range of 3 Hz to 1 kHz. The output is an analog signal in 0 to 5 V DC range representing the full-scale power of 3118 W. Each conductor may carry as much as 40 A at 60-V AC.

19.5 PROTOTYPE TESTS

The prototype tests were first performed on the generators and then on the assembled turbine.

19.5.1 Generator Performance Tests

The PM generator performance was calibrated by bench tests. A vertical milling machine was used to drive the PM rotor at various speeds. Several lamps were used as resistive load. Plots of armature voltage and current vs. PM rotor speed are shown in Figure 19.17 and Figure 19.18, respectively. These tests established the relation between voltage and rpm or the frequency, which is given by the following expressions:

$$\textit{Voltage} = 7.5 \times \textit{frequency} \text{ in hertz or } \textit{Voltage} = 0.3 \times \textit{speed} \text{ in rpm} \qquad (19.12)$$

19.5.2 Turbine Performance Tests

The assembled wind turbine unit was installed on a 50-ft-high tower at the Oak Creek Energy Systems test site at Tehachapi pass in Mojave, CA (Figure 19.19).

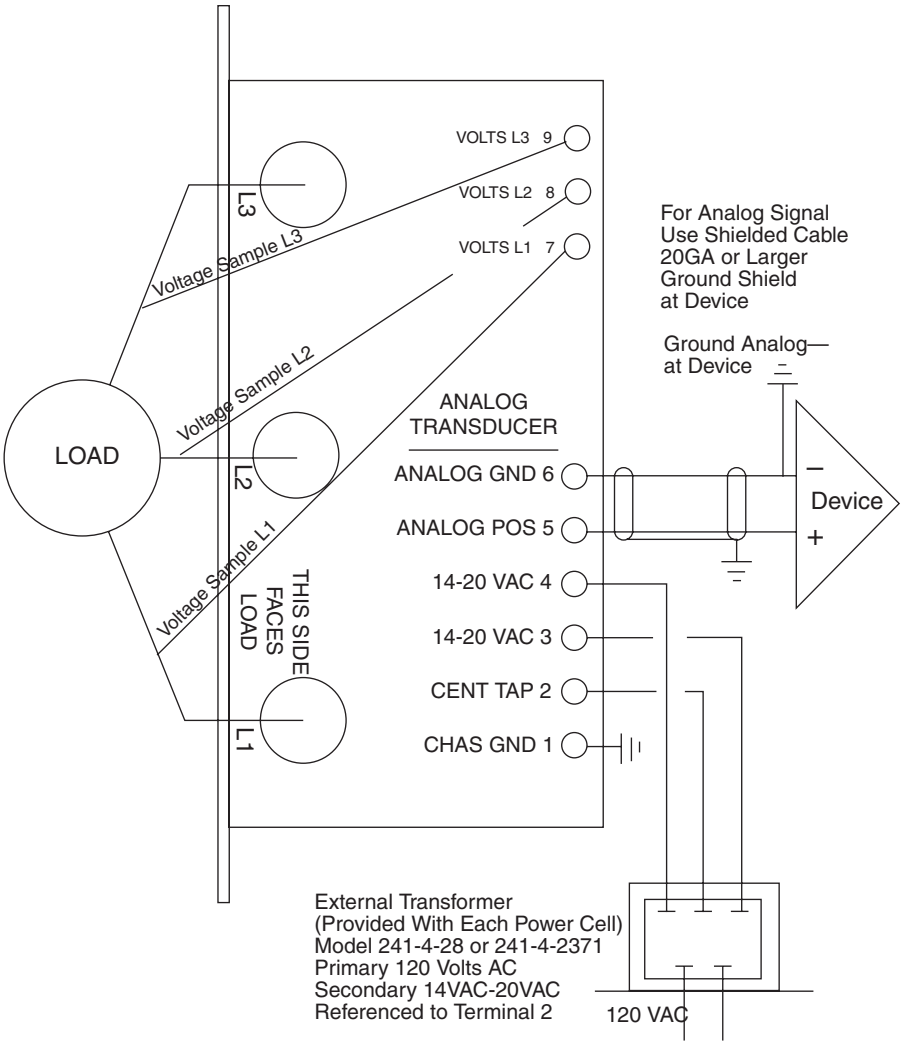

FIGURE 19.16 Three-phase watt sensor PH-3A built by Load Controls, Inc.

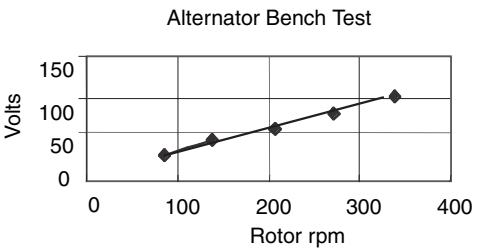

FIGURE 19.17 Armature voltage vs. PM rotor rpm.

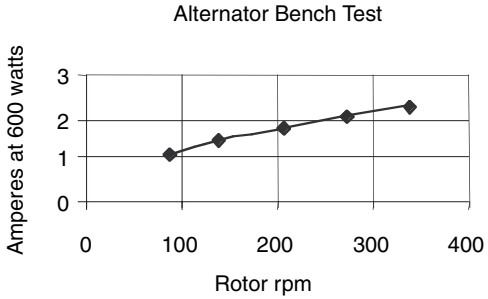

FIGURE 19.18 Armature current vs. PM rotor rpm.

FIGURE 19.19 Contrarotating turbine installation on a 50-ft tower at Oak Creek Energy Systems test site in Mojave, CA.

The system was provided with a set of three-position toggle switches. The short-circuit position was used to hold the rotor on brake, whereas the no-load and load positions were used to start and load the turbine. PM machines are difficult to start on load even in high-wind conditions. Therefore, first the switch was set at no-load until the armature voltage reached 60 V and then the toggle switch was thrown to the load position. The single-rotor test cases were performed with one rotor on brake (by short-circuiting, making it a magnetic brake), while the other was on load. Figure 19.20 shows the wind speed and power availability at the test site. The field tests were conducted from December 2001 to April 2002. Winter months are the high-wind season at this site.

19.5.3 Field-Test Instrumentation

Figure 19.21 shows the conventional approach used in the operation of a stand-alone wind turbine with PM generators. The AC power is converted into DC to charge a

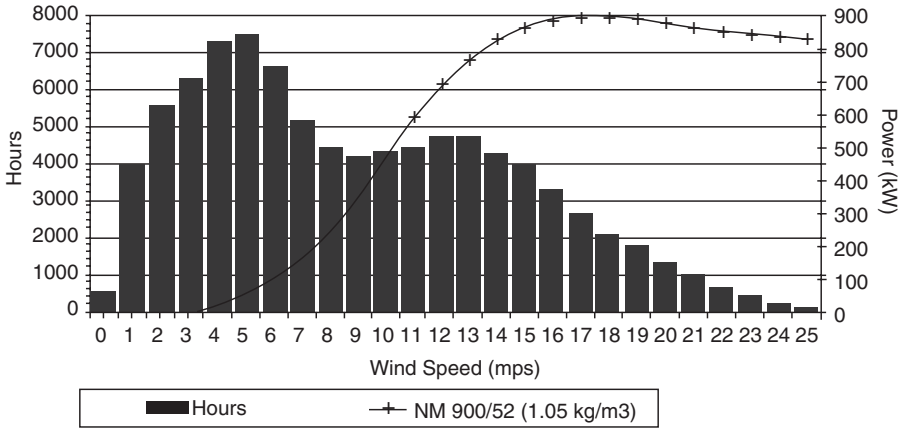

FIGURE 19.20 Wind speed characteristics at the test site. (Over 92,500 h at 20-m hub height, mean speed 9.2 m/sec.)

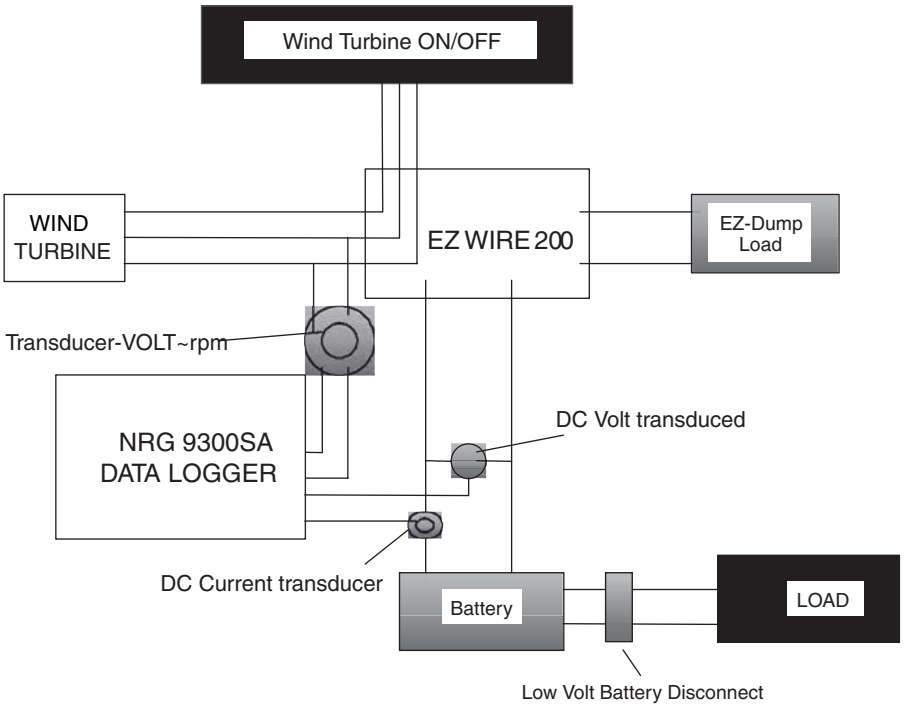

FIGURE 19.21 Conventional operation of stand-alone wind turbine.

battery bank or is directed to a load. This system dissipates energy in a set of low-cost dump heaters as depicted in Figure 19.22. The generator phases are Y-connected, whereas the load is Δ-connected. Each heater is rated at 1500 W with three steps of

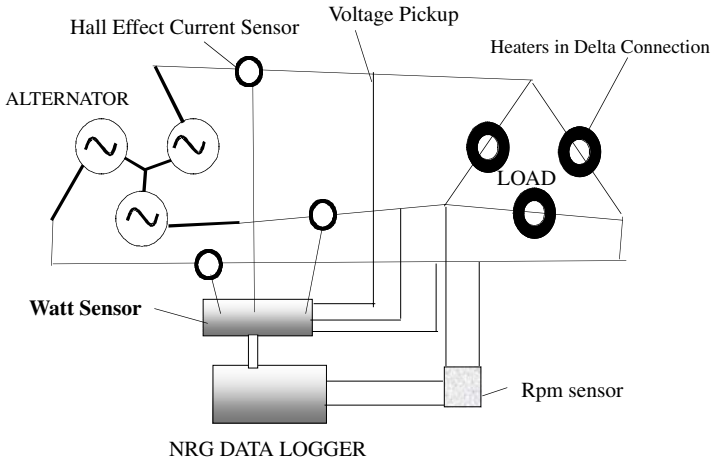

FIGURE 19.22 Load and sensor connection.

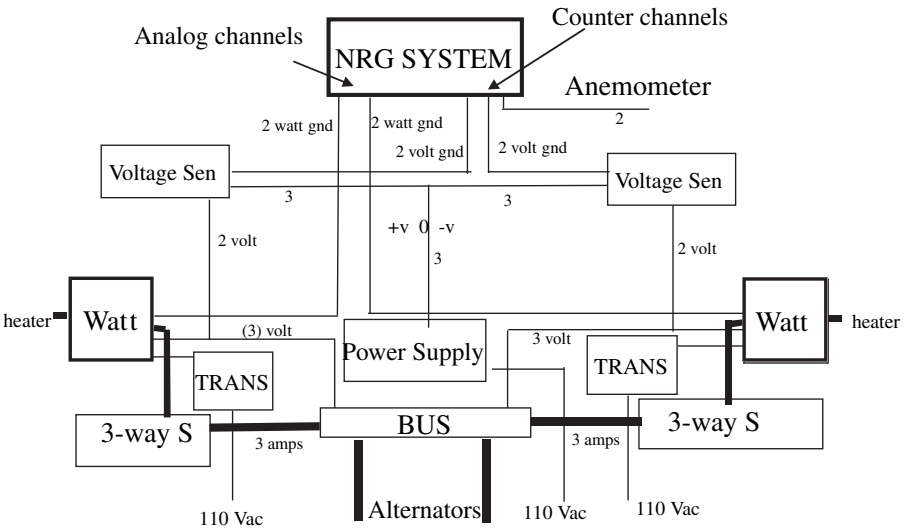

FIGURE 19.23 Field-test instrumentation.

load control. The control panel has a provision to add three more heaters in parallel. It was necessary to do so whenever the turbines ran too fast when wind speeds were above the design speed. Figure 19.23 shows specific details of the instrumentation used in the data collection procedure. 110-V AC supply was made available at the test site to operate the sensors and data loggers.

Anemometers and two generator voltage sensors were connected to the three counter channels of the NRG system, whereas two power signals and one acceleration signal were connected to the analog channels. A nonvolatile PCMCIA card

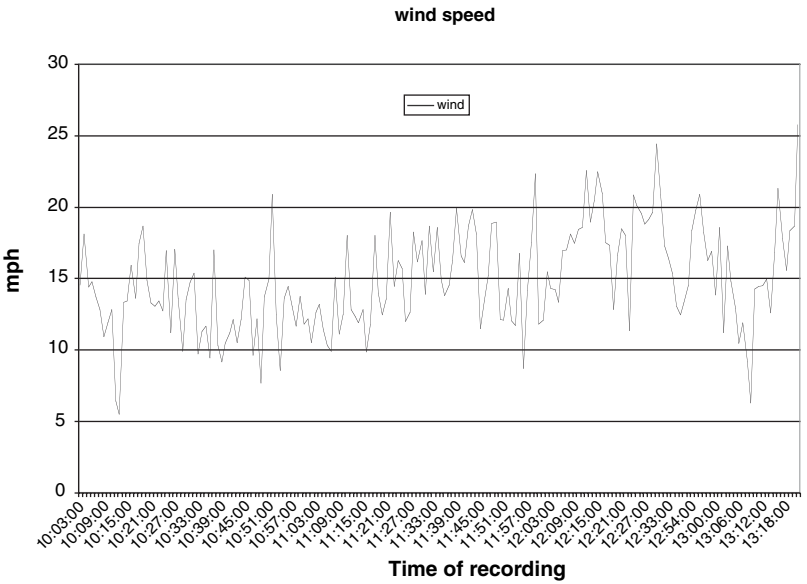

FIGURE 19.24 Histogram of wind speed (February 18, 2002).

was used to store the data. At the end of the test day, the card data were downloaded and processed using NRG-provided software. Sample data strips are presented in the following subsection.

19.5.4 Discussion of Field-Test Data

Figure 19.24 shows the histogram of the wind speed vs. time of the day. The average wind speed is around 15 mph, increasing to 25 mph and above. At wind speeds of 25 mph and above, both rotors spin faster than 360 rpm, with the current and voltage exceeding the design limit by a factor of 3 to 4 as seen in Figure 19.25. The armature design voltage is 60 V, but voltages exceeding 250 V were observed. Figure 19.26 shows the angular speed of generator 2. The relationship between voltage and angular speed (in rpm) was determined in the laboratory calibration test and is given by Equation 19.12.

The power histogram of both generators is shown in Figure 19.27. The data shown by the thin line corresponds to the front rotor (generator 1), whereas the data denoted by the thick line corresponds to the rear rotor (generator 2). At each gust, the power generated by the rear rotor is found to be in the range of 35 to 50% of the front rotor. Each data point represents an average value taken over 1 min. Similarly, data recorded on different test schedules are shown in Figure 19.28, Figure 19.29, and Figure 19.30. It is noteworthy that the power conversion efficiency of the leeward rotor increases with lower rotor speed. Figure 19.28, corresponding to the low rotor angular speed (rpm), shows a power ratio of around 50%, whereas Figure 19.30, for the higher angular speed (rpm) data, shows a power ratio of around 25%. The probable reason could be that at very high rotor speeds, the blade tips may stall and/or the front rotor might have a blanketing effect on the leeward rotor.

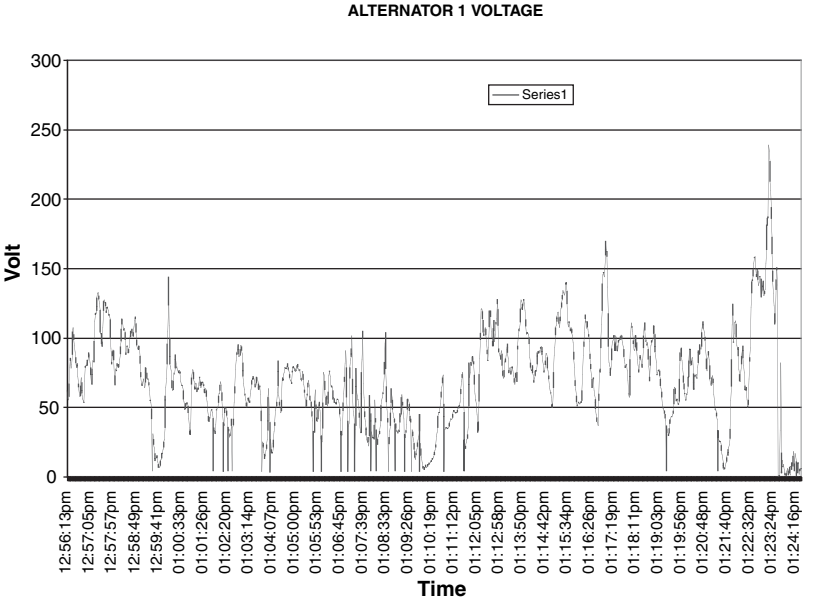

FIGURE 19.25 Voltage of generator 1.

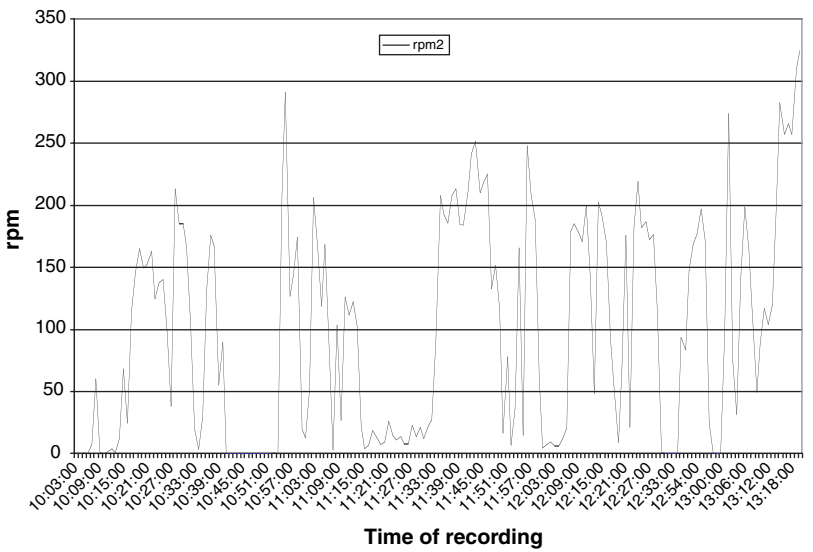

FIGURE 19.26 Angular speed in rpm of generator 2.

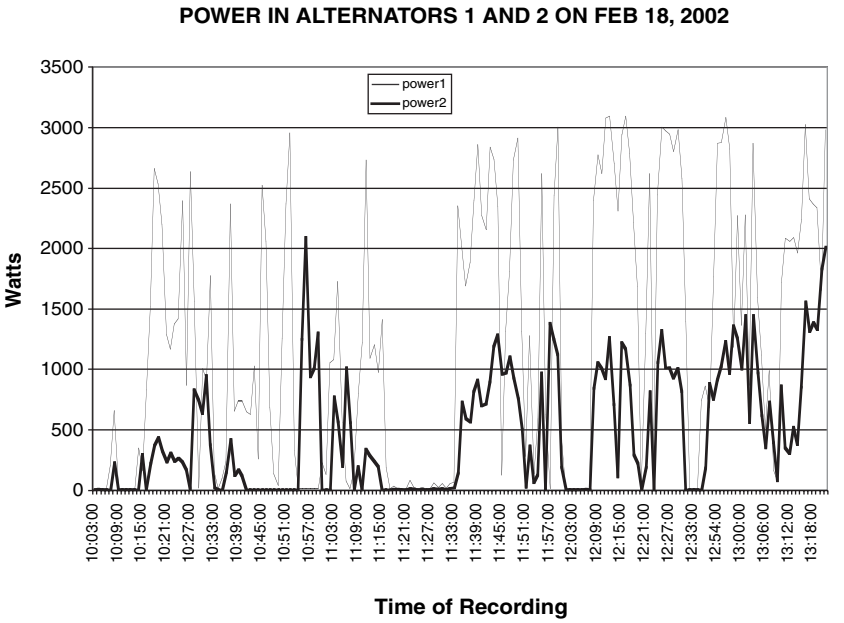

FIGURE 19.27 Power histogram of generators 1 and 2.

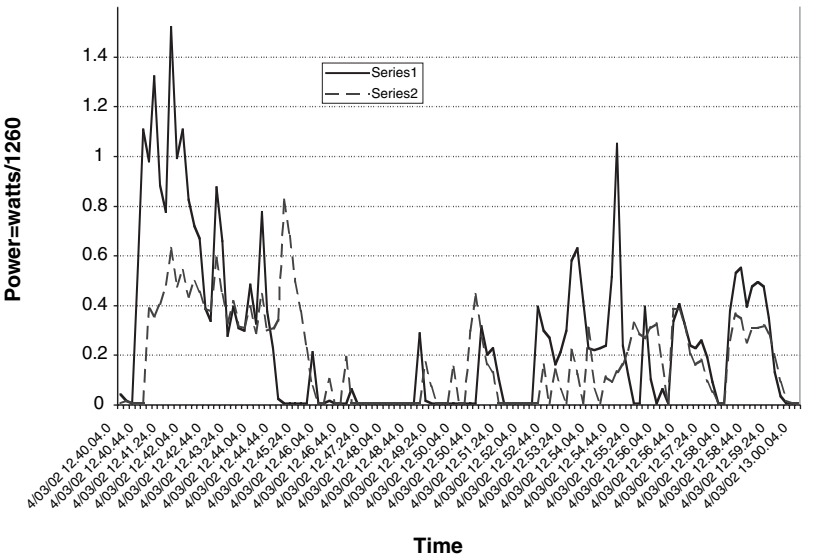

FIGURE 19.28 Comparison of power output in low rotor angular speed (rpm) condition.

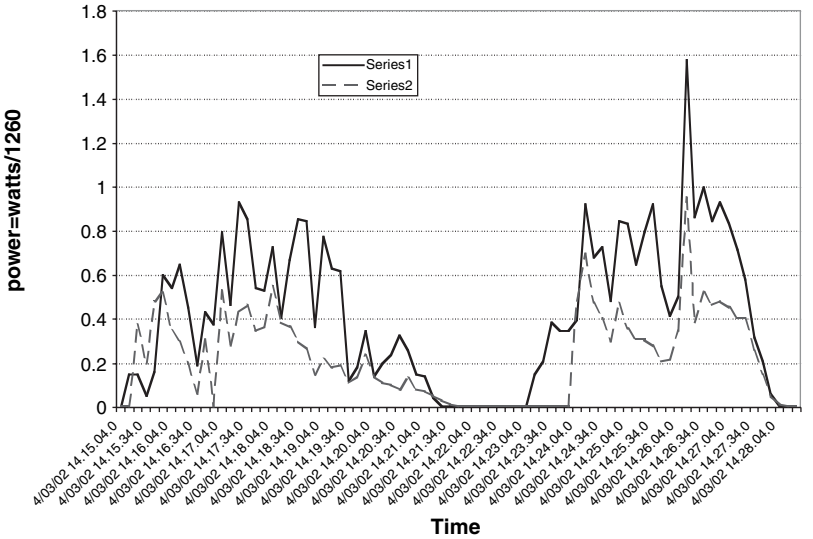

FIGURE 19.29 Comparison of power output in medium rotor angular speed (rpm) condition.

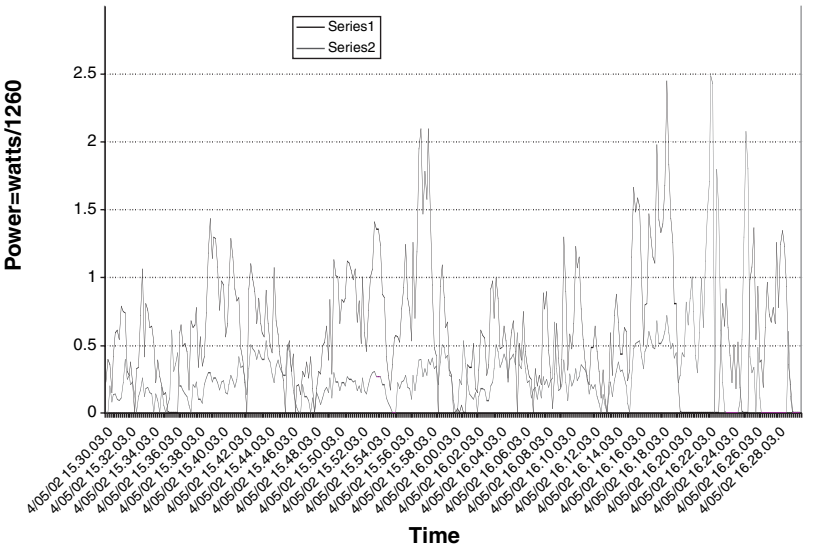

FIGURE 19.30 Comparison of power output in high rotor angular speed (rpm) condition.

The wind turbine performance data are generally best viewed as power vs. wind speed. In field tests, however, such information is available only as time history data. Therefore, there is a need to compute the mean power at any specific wind speed. The following procedure was used to compute the mean power:

Using the wind speed vs. time and power vs. time data, an incremental velocity band V_k was selected and the number of times T_n the velocity band V_k was encountered. Next, the power P_i at each T_i, (i =1, n) was determined. Then the mean value is given by

$$p_{\mathrm{m}}(k) = \left(\frac{1}{n} \sum_i P_i \right) \tag{19.13}$$

where P_i is the interpolated power data at velocity V_k, and n the number of encounters at that velocity in a strip of data that represents the dual-rotor operation. Then $p_{\mathrm{m}}(k)$ vs. V_k represents power vs. wind speed. To evaluate the performance characteristics of the contrarotating wind turbine, an analytical prediction based on elementary blade theory was also performed.

Figure 19.31 presents five sets of power curves. The field-test data for rotors 1 and 2 are denoted by diamond and square symbols, respectively, whereas the net power is represented by circular symbols. The prediction of elementary blade theory is shown by the dash–dot curve, whereas the wind stream power is given by the dotted curve. At low rotor speeds, the net power output agrees well with blade theory. But at higher rotor speeds, the departure is obvious due to two possible reasons: (1) stalling of the blade tip and (2) blanketing of the second rotor.

The performance of the contrarotating rotor system can be better judged by comparing the power coefficients presented in Figure 19.32. The power coefficient is defined as the ratio of the total power generated by the rotors to the wind stream power. According to Betz's disc theory, the maximum theoretical power coefficient is limited to 59% with one rotor. With two contrarotors, the power coefficient of the windward rotor (rotor 1) is seen to be around 40%, whereas the leeward rotor (rotor 2) produces up to 20 to 30% more power. The net power coefficient is found to be more than 60% at low rotor speeds and levels off to 40% at high rotor speeds. The power coefficient from the blade theory of two rotors is 76%, which is the same at low and high rotor speeds. One possible explanation for the field tests deviating from blade theory is that the tangential velocity momentum conversion into mechanical power is more efficient at low than at high rotor speeds. This suggests that a large utility-grade wind turbine, which rotates at low speeds of 15 to 25 rpm, may produce 40 to 50% more power with the contrarotating dual-rotor concept. This observation requires more field testing, preferably on a large, grid-connected, contrarotating wind turbine.

19.5.5 Buffeting

Having discussed the power conversion efficiency of dual rotors, let us next review the buffeting problem of the dual-rotor system, which is a widespread cause for

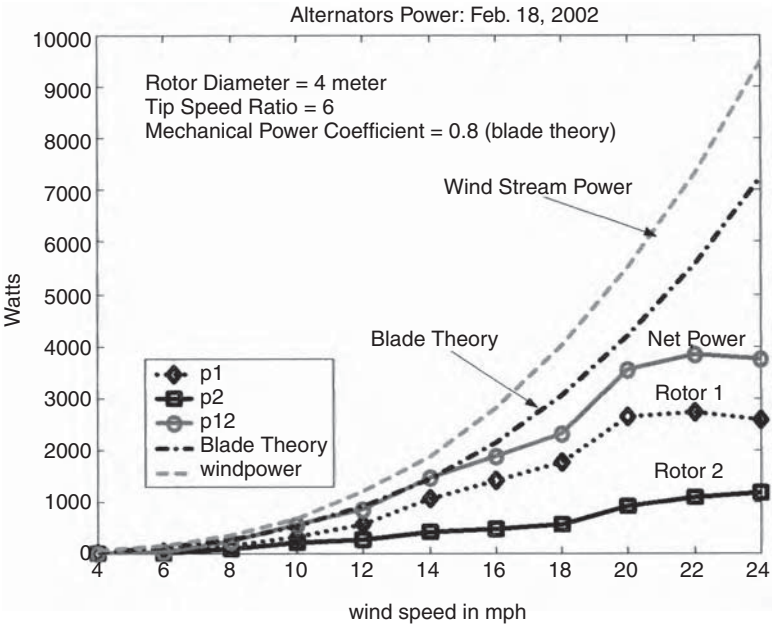

FIGURE 19.31 Net power generation with wind speed in units of mph.

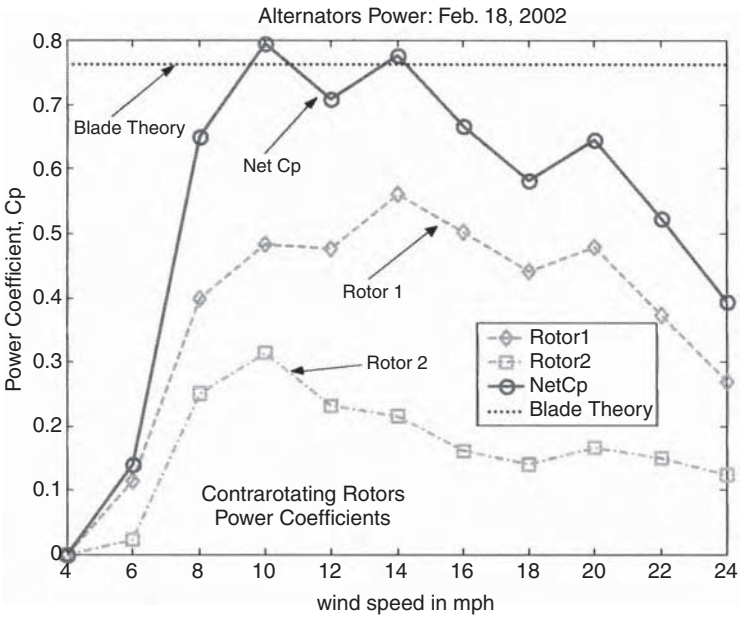

FIGURE 19.32 Power coefficients of contrarotating rotors.

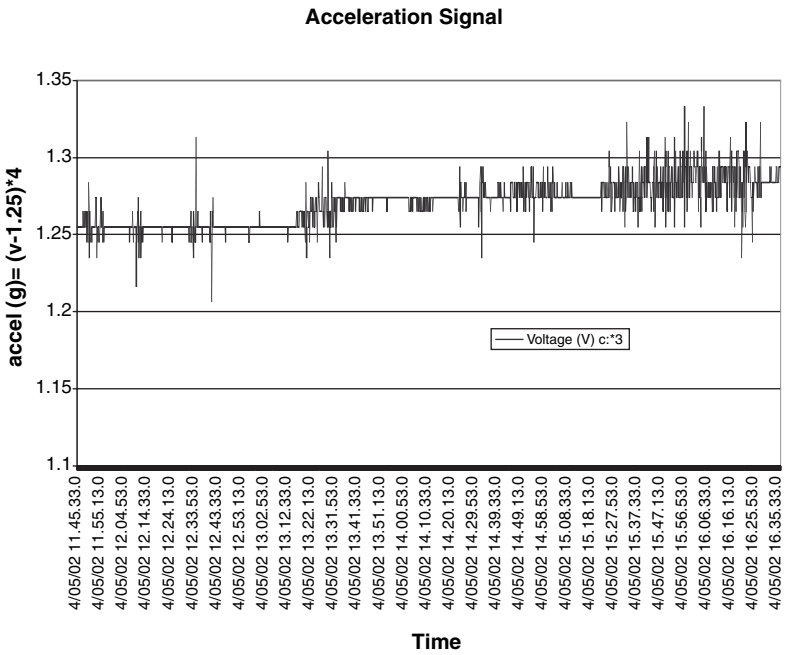

FIGURE 19.33 Acceleration of dual-rotor assembly (raw data).

concern. An acceleration sensor was installed near the leeward generator shaft. This sensor was made by Crossbow and was rated at ±4 g per volt of signal. From the raw data presented in Figure 19.33, we note that the peak acceleration does not exceed ½ g even at peak-load condition. One possible reason for such low acceleration levels could be that the passage frequency of a contrarotating system due to relative angular velocity is higher than that of a single-rotor system. Another reason could be that the vortex is straightened out by the contrarotating leeward rotor. Consequently, the low-frequency excitations are seen to be washed away. Thus, the contrarotating system seems to be beneficial in minimizing the buffeting effect of wind turbine blades.

19.6 WIND FARM POWER DENSITY

The present study focuses on enhancing wind farm energy production with the use of contrarotating wind turbines. We define the farm power density (*FPD*), a measure of economic merit of a wind farm, as the electric power capacity per unit area of the farm, expressed in MW/km^2 or MW/acre. To maximize the *FPD*, each turbine's power conversion must be efficient and also occupy the minimal land area in the wind farm.

Consider a wind farm in an area of 1 km^2, with a turbine spacing in the lateral direction of mD and a spacing in the wind direction of nD, in which D is the diameter

of the rotor in meters, and m and n are spacing constants depending on the aerodynamic characteristics of the rotor.

The number of wind turbines (N) in the 1-km^2 farm is given by:

$$N = \frac{10^6}{mnD^2} \tag{19.14}$$

If p is the rotor power density in W/m^2, then the wind farm power density is given by the following:

$$FPD = \left(\frac{N\pi D^2 p}{4}\right) \text{W/m}^2 \text{ or } FPD = \frac{\pi p}{4mn} \text{ MW/km}^2 \tag{19.15}$$

Thus, the wind farm power density given by Equation 19.15 is independent of the rotor diameter but is directly related to the rotor power density and inversely proportional to the spacing (m and n). The rotor spacing is fixed using aerodynamic efficiency considerations. Then, the only parameter that could improve wind farm energy production is the rotor power density p. For a given wind farm location, the rotor power density is the same whether the rotor diameter is small or large. However, a dual-contrarotating-rotor system can improve the rotor power density. Field tests have shown that the power density of the dual-rotor system is about 30 to 40% better than the single-rotor system. Thus, the wind farm power production and revenue can increase by 30 to 40% by implementing the contrarotating system.

19.7 RETROFIT IMPLEMENTATION AND PAYBACK

Suggested means of implementing the contrarotating rotor system are described in the following subsections.

19.7.1 Dual Wind Turbines Back-to-Back in Tandem

This approach, shown in Figure 19.34, uses two wind turbines assembled back-to-back in tandem with dedicated generators such that their rotors spin in opposite directions. This concept can readily be used to retrofit existing wind farms with an additional rotor on each tower.

Many utility-scale generators are provided with a dual-winding system that can operate efficiently at two ranges of wind speeds: (1) the smaller unit for wind speeds less than 15 mph and (2) the larger unit for wind speeds greater than 15 mph. Such a twin-generator unit can be programmed to operate at a combined power rating in an upgraded version of the contrarotating system and could produce as much as 40% more power.

If the existing generator is not provided with a dual-winding (twin-generator) system, then it is economical to add a generator and a rotor in back-to-back configuration. Torque hubs identical to those used in the existing system can be adopted.

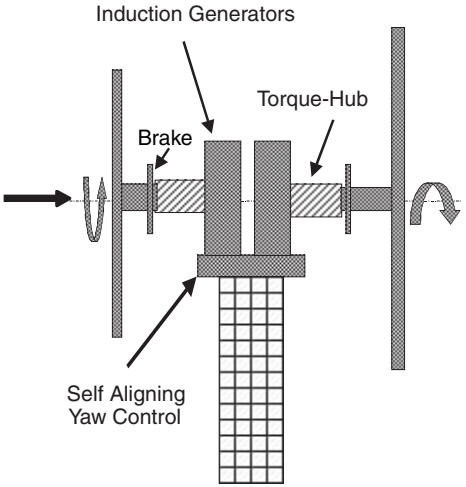

FIGURE 19.34 Contrarotating rotors in back-to-back configuration with dedicated generators.

19.7.2 Contrarotating Rotors on a Single Generator

If the existing generator is provided with a twin-wound armature system, it can be used for higher power ratings. Here, the torque hub will change the direction of output so that both rotors drive the same generator shaft. Hence, a certain amount of engineering effort and tooling is built into the unit cost. Figure 19.35 depicts a contrarotating dual-rotor system that drives a single direct-drive generator. However, there is a need for a torque-hub adapter that couples the generator shaft.

In a new generator specially designed for the contrarotating turbine system, a single generator with one armature and one rotor spinning in opposite directions could be more economical.

19.7.3 Retrofit Cost and Payback Period

To estimate the payback time of an upgrade, we must first itemize the cost of the elements of the upgrade. The revenue a wind turbine can generate for an installed unit depends on the site's power capacity. Based on that, the additional energy the contrarotating rotor can generate every year is then estimated. The simple payback period is the additional initial capital cost of the upgrade divided by the additional annual revenue of the contrarotating rotor system. This is estimated to be 4 to 5 yr with 30% efficiency improvement.

19.8 CONCLUSIONS

The test data presented in this chapter suggest the following conclusions for contrarotating wind turbines:

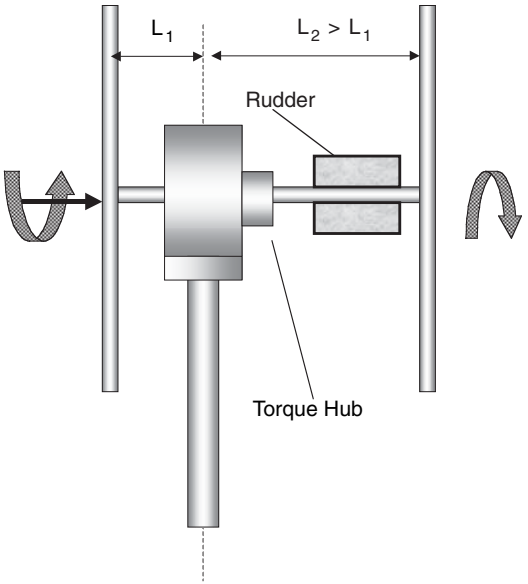

FIGURE 19.35 Contrarotating rotors driving a single generator.

- Larger-diameter rotors can generate the same amount of additional energy without using a dual-rotor system, but fewer turbines can be accommodated on the wind farm. Thus, the wind farm in a given area may not produce more power by increasing the rotor diameter. This is because a large percentage of the wind energy is dissipated in the exit wind without being harnessed. Additionally, larger blades will be subjected to severe dynamic loads, frequent maintenance, and shorter fatigue life.
- Leeward rotors of contrarotating turbines can produce 25 to 40% additional power from the same wind stream.
- Slowly moving rotors are found to be more efficient, suggesting that the large utility-scale wind turbines that operate at 15 to 20 rpm benefit more from contrarotating rotors.
- The occurrence of the buffeting phenomenon of dual rotors is found to be less likely.
- A simple bevel gear system could be used to transmit the net torque generated by the two tandem rotors to an existing electric-power-generating unit.
- The weight and torque of two rotors counterbalance each other, leading to a reduced moment and bending stress on the tower.
- Based on these findings, retrofitting existing wind turbines with dual rotors or manufacturing counter-rotating armature and rotors with single generators could economically benefit the wind farm. The additional cost invested may be recovered in 4 to 5 yr, which may attract additional investors.
- More prototype tests are needed on large utility-scale contrarotating wind turbines.

ACKNOWLEDGMENT

This chapter is based on the research conducted by Dr. Kari Appa, principal investigator, Appa Technology Initiatives, Lake Forest, CA, and Bangalore, India. This research was funded by the California Energy Commission. With permission.

REFERENCES

1. Appa, K., Counter Rotating Wind Turbine Systems, Final Report Submitted to California Energy Commission, April 2002.
2. Betz, A., *Wind-Energie und Ihre Ausnutzung durch Windmuehlen*, Vandenhoeck and Ruprecht, Goettingen, Germany, 1926.
3. ASME, The First 500 Kilowatt Curtis Vertical Steam Turbine, Newport, RI, February 1903, An International Historic Mechanical Engineering Landmark, ASME, July 23, 1990.
4. Tangler, J.L., The Nebulous Art of Using Wind-Tunnel Airfoil Data for Predicting Rotor Performance, Proceedings of the 21st ASME Wind Energy Conference, Reno, Nevada, January 2002.
5. Gasch, R. 1996. *Windkraftanlagen, Grundlagen und Entwurf*, B.G. Teubner, Stuttgart, Germany, 1996.

Appendices

Appendix 1: National Electrical Code® (Article 705)

Portions applicable to renewable power sources are reprinted here from NFPA 70, the *National Electrical Code® Handbook,* Seventh Edition, Copyright © 1996, with permission from the National Fire Protection Association, Quincy, MA 02269. This reprinted material is not the complete and official position of the National Fire Protection Association on the referenced subject, which is represented only by the cited standard in its entirety.

Article 705 Interconnected Electric Power Production Sources

Contents

705-1. Scope. This article covers installation of one or more electric power production sources operating in parallel with a primary source(s) of electricity.

(FPN): Examples of the types of primary sources are a utility supply, on-site electric power source(s), or other sources.

This article sets forth basic safety requirements for the installation of generators and other types of power production sources that are interconnected and operate in parallel. Power sources include any system that produces electric power. They include not only electric utility sources, but also on-premises sources, ranging from rotating generators (see Article 445) to solar photovoltaic systems (see Article 690) to fuel cells.

The purpose of this article is to address the basic safety requirements, specifically related to parallel operation, for the generators and other power sources, the power system that interconnects the power sources, and equipment that is connected to these systems. Proper application of these systems requires a thorough review of the entire power system.

705-2. Definition. For purposes of this article, the following definition applies:

Interactive System: An electric power production system that is operating in parallel with and capable of delivering energy to an electric primary source supply system.

705-3. Other Articles. Interconnected electric power production sources shall comply with this article and also the applicable requirements of the following articles:

	Article
Generators	445
Solar Photovoltaic Systems	690
Emergency Systems	700
Legally Required Standby Systems	701
Optional Standby Systems	702

705-10. Directory. A permanent plaque or directory, denoting all electrical power sources on or in the premises, shall be installed at each service equipment location and at locations of all electric power production sources capable of being interconnected.

Exception: Installations with large numbers of power production sources shall be permitted to be designated by groups.

705-12. Point of Connection. The outputs of electric power production systems shall be interconnected at the premises service disconnecting means. See Section 230-82, Exception No. 6.

Exception No. 1: The outputs shall be permitted to be interconnected at a point or points elsewhere on the premises where the system qualifies as an integrated electric system and incorporates protective equipment in accordance with all applicable sections of Article 685.

Exception No. 2: The outputs shall be permitted to be interconnected at a point or points elsewhere on the premises where all of the following conditions are met:

a. The aggregate of nonutility sources of electricity has a capacity in excess of 100 kW, or the service is above 1000 volts;

b. The conditions of maintenance and supervision ensure that qualified persons will service and operate the system; and

c. Safeguards and protective equipment are established and maintained.

The point of interconnection is required to be at the premises service disconnecting means. This requirement may be difficult to meet for systems 100 kW or smaller. It is intended to prevent the indiscriminate interconnection of small generators or other sources of power without proper protection against fire and electric shock. See Figure 705-1. It is important to utilize disconnect devices (switches, etc.) suitable for the purpose.

The requirement specifying "at the premises service disconnecting means" permits connection ahead of the disconnect or on the load side. This is to accommodate the safe work practices of many utilities that provide a readily accessible disconnect for dispersed generation. It is a contract matter between the utility and the customer and does not adversely affect the safety of the premises wiring; therefore, it is not within the scope of the *Code*.

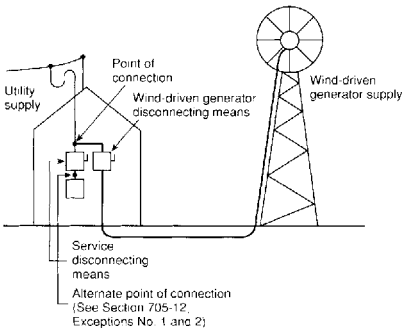

Figure 705-1. The point of interconnection is required to be at the premises service disconnecting means.

The two exceptions recognize that generators and other power sources can be safely connected elsewhere on the premises system. These locations include where the premises has an integrated electrical system as set forth in Article 685, where the total generator capacity on premises is greater than 100 kW, or where the service is greater than 1000 volts.

Experience has proved that a higher level of design input and more responsible installation are used for larger systems than are commonly used for small systems (100-kW or less, 600-volt or less services).

705-14. Output Characteristics. The output of a generator or other electric power production source operating in parallel with an electric supply system shall be compatible with the voltage, wave shape, and frequency of the system to which it is connected.

(FPN): The term compatible does not necessarily mean matching the primary source wave shape.

The level of output voltage and frequency must be controlled to permit real power and reactive power to flow in the intended amount and proper direction. Control of the driver speed causes real power (kW) to flow from a rotating generator. Control of voltage causes reactive power (kVAr) to flow to or from a synchronous generator. The parallel operation of generators is a complex balance of several variables. These are design parameters and are beyond the scope of the *Code*. A considerable amount of data is available for equipment application and design.

The output characteristics of a rotating generator are significantly different from those of a solid-state power source. Their compatibility with other sources and with different types of loads will be limited in different ways.

Where either the power source or the loads have solid-state equipment, such as inverters, uninterruptible power supplies (UPS), or solid-state variable speed drives, harmonic currents will flow in the system. See Figures 705-2, 705-3, and 705-4. These multiples of the basic supply frequency (usually 60 Hz) cause additional heating, which may require derating of generators, transformers, cables, and motors. Special generator voltage control systems are required to avoid erratic operation or destruction of control devices. Circuit breakers may require derating where the higher harmonics become significant.

Significant magnitudes of harmonics may be inadvertently matched to system resonance and result in opening of capacitor fuses, overheating of circuits, and erratic operation of controls. The usual solution is to detune the system by rearrangement or installation of reactors, or both.

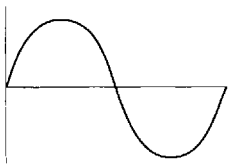

Figure 705-2. Typical output wave shape of rotating generator and system wave shape normally encountered with motor, lighting, and heating loads.

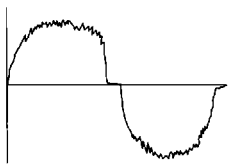

Figure 705-3. Typical output wave shape with inverter source. Motors and transformers will be driven by harmonic-rich voltage and may require derating.

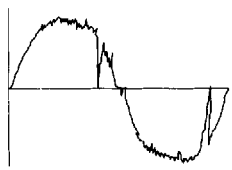

Figure 705-4. Wave shape typical of system with variable speed drive, rectifier, elevator, and uninterruptible power supply loads. Source generator may require derating, and special voltage control may be needed.

705-16. Interrupting and Withstand Rating. Consideration shall be given to the contribution of fault currents from all interconnected power sources for the interrupting and withstand ratings of equipment on interactive systems.

705-20. Disconnecting Means, Sources. Means shall be provided to disconnect all ungrounded conductors of an electric power production source(s) from all other conductors. See Article 230.

705-21. Disconnecting Means, Equipment. Means shall be provided to disconnect equipment, such as inverters or transformers, associated with a power production source, from all ungrounded conductors of all sources of supply.

Exception: Equipment intended to be operated and maintained as an integral part of a power production source exceeding 1000 volts.

An example of equipment covered under the exception is a generator designed for 4160 volts and connected to a 13,800-volt system through a transformer. The transformer and generator are to be operated as a unit. A disconnecting means is not required between the generator and transformer. However, a disconnecting means is required between the transformer and the point of connection to the power system.

705-22. Disconnect Device. The disconnecting means for ungrounded conductors shall consist of a manually or power operable switch(es) or circuit breaker(s):

(1) Located where accessible;

(2) Externally operable without exposing the operator to contact with live parts and, if power operable, of a type that can be opened by hand in the event of a power supply failure;

(3) Plainly indicating whether in the open or closed position; and

(4) Having ratings not less than the load to be carried and the fault current to be interrupted.

For disconnect equipment energized from both sides, a marking shall be provided to indicate that all contacts of the disconnect equipment may be energized.

(FPN No. 1): In parallel generation systems, some equipment, including knife blade switches and fuses, are likely to be energized from both directions. See Section 240-40.

(FPN No. 2): Interconnection to an off-premises primary source could require a visibly verifiable disconnecting device.

The requirements for disconnects in Section 705-22 are probably the most significant and important requirements in Article 705. A disconnecting means is to serve each generating source. This device or another will be the service-entrance disconnect. Still another may be applied to separate the generating systems.

The basic requirement in Section 705-22 recognizes the success of applying switches as well as molded-case circuit breakers in this service. Most safe work practices on the premises utilize these disconnect devices.

The disconnect at the service entrance is required for disconnecting the premises wiring system from the utility. The utility safe work practices may also utilize this disconnect device. Utility work practices may require a visibly verifiable disconnect device. For this reason, some utility contracts require that a visible break be provided. The second Fine Print Note is intended to bring attention to this common utility requirement.

705-30. Overcurrent Protection. Conductors shall be protected in accordance with Article 240. Equipment overcurrent protection shall be in accordance with the articles referenced in Article 240. Equipment and conductors connected to more than one electrical source shall have a sufficient number of overcurrent devices so located as to provide protection from all sources.

(1) Generators shall be protected in accordance with Section 445-4.

(2) Solar photovoltaic systems shall be protected in accordance with Article 690.

(3) Overcurrent protection for a transformer with a source(s) on each side shall be provided in accordance with Section 450-3 by considering first one side of the transformer, then the other side of the transformer, as the primary.

705-32. Ground-Fault Protection. Where ground-fault protection is used, the output of an interactive system shall be connected to the supply side of the ground-fault protection.

Exception: Connection shall be permitted to be made to the load side of ground-fault protection provided that there is ground-fault protection for equipment from all ground-fault current sources.

The larger systems have become very sophisticated and involve many special relays. The more common relays are under- and over-voltage, under- and over-frequency, voltage-restrained overcurrent, anti-motoring, loss-of-field, over-temperature, and shutdown for derangement of the mechanical driver. Small-generator installations cannot justify the cost of these switchgear-type relays. Small-generator protection is comprised of more common devices with fewer features. Application guides are available in technical literature and manufacturers' data.

It is important to note that the requirements in Article 705 are only for protection against conditions that may occur because generating sources are being operated in parallel. It is essential that the installation also meet the requirements of the referenced articles to provide the basic protection and safeguards for all equipment, whether or not it is involved with more than one source.

705-40. Loss of Primary Source. Upon loss of primary source, an electric power production source shall be automatically disconnected from all ungrounded conductors of the primary source and shall not be reconnected until the primary source is restored.

(FPN No. 1): Risks to personnel and equipment associated with the primary source could occur if an interactive electric power production source can operate as an island. Special detection methods can be required to determine that a primary source supply system outage has occurred, and whether there should be automatic disconnection. When the primary source supply system is restored, special detection methods can be required to limit exposure of power production sources to out-of-phase reconnection.

(FPN No. 2): Induction-generating equipment on systems with significant capacitance can become self-excited upon loss of primary source and experience severe over-voltage as a result.

When two interconnected power systems separate, they will drift out of synchronism. When the utility separates, there is a risk of damage to the system if restoration of the utility occurs out of phase. If the timing of the reconnection is random, there will be violent electromechanical stresses. These can destroy mechanical components such as gears, couplings, and shafts, and can displace coils. It is essential to disconnect the premises or generator from the primary source. Many technical guides are available from which to select appropriate protective systems and equipment for large systems. A limited choice of low-cost devices is still available for application to small systems.

Induction generators are commonly used today. They have characteristics quite different from synchronous machines. They are more rugged because of the construction of the rotor. They are less expensive because of their basic design, availability, and type of starting and control equipment. Theoretically, an induction machine can continue to run on an isolated system if a large capacitor bank provides excitation. In reality, an induction machine will lose stability and be shut down quickly by one of the protective devices.

705-42. Unbalanced Interconnections. A 3-phase electric power production source shall be automatically disconnected from all ungrounded conductors of the interconnected systems when one of the phases of that source opens.

Exception: An electric power production source providing power for an emergency or legally required standby system.

705-43. Synchronous Generators. Synchronous generators in a parallel system shall be provided with the necessary equipment to establish and maintain a synchronous condition.

705-50. Grounding. Interconnected electric power production sources shall be grounded in accordance with Article 250.

Exception: For direct-current systems connected through an inverter directly to a grounded service, other methods that accomplish equivalent system protection and that utilize equipment listed and identified for the use shall be permitted.

Appendix 2: Sources of Further Information on Renewable Energy

U.S. National Renewable Energy Laboratory (NREL)
Technical Inquiry Service
1617 Cole Boulevard
Golden, CO 80401
Phone: (303) 275-4099
Fax: (303) 275-4091

NREL offers a number of outreach services, ranging from consumer information clearinghouses to electronic bulletin boards, to its various audiences. The following is a list of these informative resources for wind, solar, and all other types of renewable energy:

Electronic Information Server
This service provides general and technical information about NREL and may be accessed through Gopher at gopher.nrel.gov or through the Web at http://www.nrel.gov or via modem at (303) 275-INFO.

Document Distribution Service (DDS)
DDS is the central repository for technical documents published by NREL.
Phone: (303) 275-4363
Fax: (303) 275-4053
E-mail: evanss@tcplink.nrel.gov

United Nations Division of Sustainable Development
Department of Economic and Social Development
United Nations Headquarters
New York, NY 10017
Web: www.un.org/esa/sustdev

Energy Efficiency and Renewable Energy Clearinghouse (EREC)
EREC provides information and technical assistance on subjects related to energy efficiency and renewable energy technologies.
P.O. Box 3048
Merrifield, VA 22116
Phone: (800) 363-3732
TDD: (900) 273-2957
BBS: (800) 273-2955
E-mail: doe.erec@nciinc.com

Energy Efficiency and Renewable Energy Network
This electronic service on the Internet serves as a gateway and repository of multimedia information on energy efficiency and renewable energy technologies.
Phone: (900) 363-3732
Web: http://www.eren.doe.gov

Renewable Electric Plant Information System (REPIS)
REPIS, which is supported by DOE's Office of Utility Technologies, is an electronic database of core information on grid-connected renewable electric plants in the U.S. REPIS contains information on renewable power of more than 103,000 MW installed capacity, approximately 89% of which is hydroelectric.
Phone: (303) 275-4643
Fax: (303) 275-4611
E-mail: sinclair@tcplink.nrel.gov

Renewable Resource Data Center (RReDC)
RReDC is the online information distribution service for the Resource Assessment Program at NREL. Sponsored by DOE, RReDC provides information about a variety of renewable resources in the U.S. The information includes publications, data, maps, algorithms, and links to other sources of renewable energy.
Phone: (303) 275-4638
Web: http://rredc.nrel.gov

Technical Inquiry Service (TIS)
TIS informs the scientific, industrial, and business communities about NREL's R&D activities and those of NREL subcontractors.
Phone: (303) 275-4065
Fax: (303) 275-4091
E-mail: rubin@tcplink.nrel.gov

Technology and Business Ventures Office
Access to collaborative and sponsored research, cost-shared subcontracts, NREL facilities, visiting researcher programs, and cooperative research and development agreements is available to individuals and businesses through this office.
Phone: (303) 275-3008
Fax: (303) 275-3040
E-mail: technology_transfer@nrel.gov
Web: http://www.nrel.gov

Visitors Center
The NREL visitors center provides an interactive environment in which you can explore how solar, wind, and other types of renewable resources can provide energy to your industry, farm, community, and home.
Phone: (303) 384-6566
E-mail: griegog@tcplink.nrel.gov

SOLAR ENERGY INFORMATION SOURCES

International Solar Energy Society
P.O. Box 116300
University of Florida/D. Goswami
Gainesville, FL 32611-6300
Phone: (352) 392-0812
Fax: (302) 392-1071
E-mail: solarjrl@mae.ufl.edu
Web: www.ises.org

American Solar Energy Society
2400 Central Avenue
Boulder, CO 80301
Phone: (303) 443-3130
Fax: (303) 443-3212

British Photovoltaic Association
The Warren, Bramshill Road
Eversley, Hamshire RG27 OPR
United Kingdom
Phone: +44 (0) 118 932 4418
Fax: +44 (0) 118 973 0820

Solar Trade Association Ltd.
Pengillan, Lerryn, Lostwithiel
Cornwall, United Kingdom

MANUFACTURERS OF SOLAR CELLS AND MODULES IN THE U.S.

Advanced Photovoltaic Systems, Inc.
P.O. Box 7093
Princeton, NJ 08543

Applied Solar Energy Corporation
15751 East Don Julian Road
City of Industry, CA 91746

ASE Americas, Inc.
4 Suburban Park Drive
Billerica, MA 01821

GE/AstroPower, Inc.
Solar Park
Newark, DE 19716-2000

ENTECH
P.O. Box 612
DFW Airport, TX 75261

EPV Energy Photovoltaics
P.O. Box 7456
Princeton, NJ 08543

Evergreen Solar
49 Jones Road
Waltham, MA 02154

Iowa Thin Film Technologies
ISU Research Park #607
Ames, IA 50010

SunPower Corporation
430 India Way
Sunnyvale, CA 94086

SunWatt Corporation
RFD Box 751
Addison, ME 04606

Kyocera America, Inc.
8611 Balboa Avenue
San Diego, CA 92123

A.Y. McDonald Mfg. Co.
4800 Chavenelle Road-Box 508
Dubuque, IA 52004-0508

Midway Labs, Inc.
2255 East 75th Street
Chicago, IL 60649

Sanyo Energy Corporation
2001 Sanyo Avenue
San Diego, CA 92073

Siemens Solar Industries
4650 Adohr Lane
Camarillo, CA 93011

BP Solar/Solarex Corporation
630 Solarex Court
Frederick, MD 21701

Solec International, Inc.
12533 Chadron Avenue
Hawthorne, CA 90250

Spire Corporation
One Patriots Park
Bedford, MA 01730

Tideland Signal Co.
P.O. Box 52430
Houston, TX 77052

United Solar Systems Corporation
9235 Brown Deer Road
San Diego, CA 92121-2268

Utility Power Group
9410 DeSoto Avenue, Unit G
Chatsworth, CA 91311

WIND ENERGY INFORMATION SOURCES

As wind energy technology gains more widespread acceptance as an economically and technically viable resource, an increasing number of people representing electric utilities, the news media, the research community, political and regulatory leaders, and local communities are searching for up-to-date, accurate information on this clean, renewable energy resource. The following sources compiled by the American Wind Energy Association can provide a range of general and technical information about wind.

American Wind Energy Association (AWEA)
122 C Street, NW, Fourth Floor
Washington, DC 20001
Phone: (202) 383-2500
Publications: (202) 383-2520
Fax: (202) 383-2505

Energy Efficiency & Renewable Energy Network
This electronic service on the Internet serves as a gateway and repository of multimedia information on energy efficiency and renewable energy technologies.
Phone: (800) 363-3732

National Climatic Data Center
151 Patton Avenue, Room 120
Asheville, NC 28801-2733
Phone: (704) 271-4800
Fax: (704) 271-4876

National Wind Technology Center
1617 Cole Boulevard
Golden, CO 80401
Phone: (303) 384-6900
Fax: (303) 384-6901

National Technical Information Service
U.S. Department of Commerce
5285 Port Royal Road
Springfield, VA 22161
Phone: (703) 487-4650

Sandia National Laboratories
P.O. Box 5800-MS 0899
Albuquerque, NM 87185
General Phone: (505) 845-0111
Technical Info: (505) 845-8287

National Institute of Science & Technology
Energy Inventions & Innovations
U.S. Department of Commerce
Room Al15, Building 411
Gaithersburg, MD 20899-0001
Phone: (301) 975-5500

UNIVERSITY WIND ENERGY PROGRAMS IN THE U.S.

A number of universities offer courses in renewable energy technology through environmental science or engineering departments. In addition to classes, they work with industry partners to conduct valuable research. Institutions offering specific wind energy curricula and research programs include the following:

Alternative Energy Institute
West Texas A&M University
P.O. Box 248
Canyon, TX 79016
Phone: (806) 656-2295

University of Colorado
Electrical & Computer Engineering Department
Campus Box 425
Boulder, CO 80309
Phone: (303) 492-7010

Montana State University
Chemical Engineering Department
302 Cableigh Hall
Bozeman, MT 59717
Phone: (406) 994-4543

New Mexico State University
Southwest Technology Development Institute
Dept. 3 SOLAR
P.O. Box 30001
Las Cruces, NM 88003-9001
Phone: (505) 646-1846

Ohio State University
Aero and Astronautical Research
2300 West Case Road
Columbus, OH 43220
Phone: (614) 292-5491

Oregon State University
Mechanical Engineering Department
Corvallis, OR 97331
Phone: (503) 737-2218

Southwestern Technical College
401 West Street
Jackson, MN 56143
Phone: (507) 847-3320 xi7i

Tennessee State University
3500 John A. Merritt Boulevard
Nashville, TN 37209-1561
Phone: (615) 320-3268

Tennessee Technological University
Department of Mechanical Engineering
Cookeville, TN 38505-5014
Phone: (615) 372-3273

U.S. Merchant Marine Academy
Alternative Energy Research Program
Kings Point, NY 11024
Phone: 516-773-5743
E-mail: brownd@usmma.edu

University of Arizona
AME Department
Tucson, AZ 85721
Phone: (602) 621-2235

University of Massachusetts
Renewable Energy Research Laboratory
College of Engineering
E Lab Building
Amherst, MA 01003
Phone: (413) 545-4359

University of Northern Iowa
Industrial Technology Center
Cedar Falls, IA 50614-0178
Phone: (319) 273-2756

University of Texas, El Paso
Mechanical Engineering Department
500 W. University Avenue
El Paso, TX 79968-0521
Phone: (915) 747-5450

University of Utah
Mechanical Engineering Department
Salt Lake City, UT 84112
Phone: (801) 581-4145

International Solar Energy Society
P.O. Box 116300
University of Florida/D. Goswami
Gainesville, FL 32611-6300
Phone: (352) 392-0812
Fax: (302) 392-1071
E-mail: solarjrl@mae.ufl.edu
Web: www.ises.org

PERIODICALS ON WIND ENERGY

Wind Energy Weekly
Published 50 times a year, the *Wind Energy Weekly* provides up-to-date information on utility requests for proposals, federal and state regulatory activity, project development, international business opportunities, and energy and environmental policy.
American Wind Energy Association
122 C Street. NW, Fourth Floor
Washington, DC 20001
Phone: (202) 383-2500

Home Power Magazine
This bimonthly magazine provides information about residential wind systems, as well as information on other renewable technologies and residential products.
P.O. Box 520
Ashland, OR 97520
Phone: (916) 475-3179

Independent Energy
Published 10 times a year, this magazine provides information for the independent power industry and includes periodic updates on the wind industry.
620 Central Avenue, North
Milaca, MN 56353
Phone: (612) 983-6892

Wind Energy Technology: Generating Power from the Wind
This bimonthly publication provides current worldwide information on wind turbine design, performance, wind resource identification, legal/institutional implications, and environmental aspects.
National Technical Information Service
U.S. Department of Commerce
5285 Port Royal Road
Springfield, VA 22161

Windpower Monthly
This Danish magazine provides up-to-date information on all aspects of the international wind industry.
P.O. Box 496007, Suite 217
Redding, CA 96099
Phone: (415) 775-1985

Wind Directions
Wind Directions contains current technical and commercial information on wind power plants and technologies worldwide.
European Wind Energy Association
26 Spring street
London W2 1JA
United Kingdom
Phone: +44 (0) 171 402 7122
Fax: +44 (0) 171 402 7125
E-mail: ewea@ewea.org
Web: http://www.ewea.org

Solar Energy Journal
P.O. Box 116300
University of Florida/D. Goswami
Gainesville, FL 32611-6300

Phone: (352) 392-0812
Fax: (302) 392-1071
E-mail: solarjrl@mae.ufl.edu
Web: www.ises.org

Renewable Energy World
James & James Ltd.
8-12 Camden High Steeet, London, U.K.
Phone: +44-20-7387-8558
E-mail: rew@jxj.com

INTERNATIONAL WIND ENERGY ASSOCIATIONS

British Wind Energy Association
Lincoln's Inn House
42 Kingsway
London WC2B 6EX
United Kingdom
Phone: +44 171 404 3433
Fax: +44 171 404 3432

Canadian Wind Energy Association
2415 Holly Lane, Suite 250
Ottawa, Ontario KIV 7P2
Canada
Phone: (613) 736-9077

Danish Wind Power Association
(Wind Turbine Owners' Organization)
Phone: +45 53 83 13 22
Fax: +45 53 83 12 02

European Wind Energy Association
26 Spring Street
London W2 1JA
United Kingdom
Phone: +44 (0) 171 402 7122
Fax: +44 (0) 171 402 7125
E-mail: ewea@ewea.org
Web: http://www.ewea.org

Finnish Wind Power Association
Phone: +358 0 456 6560
Fax: +358 0 456 6538

FME Groep Windenergic
(Dutch Wind Energy Trade Association)
Phone: +31 79 353 1100
Fax: +31 79 353 1365

French Wind Energy Association
63 Collet de Darbousson
Valbonne 06560
France
Phone: +33 93 65 0970

German Wind Energy Association
Dorfangerweg 15
Unterfoehring 85774
Germany
Phone: +49 899506411

Gujarat Energy Development Agency
Suraj Plaza II, 2nd Floor, Sayaji Gunj
Vadodara — 390 005, India
Fax: +91-265-363120

Hellenic Wind Energy Association (Greece)
Phone: +30 1 603 9900
Fax: +30 1 603 9905

Indian Renewable Energy Development Agency
Core-4 A, East Court, Ist Floor
Habitat Center Complex, Lodi Road
New Delhi — 110 003, India
Fax: +91-11-460-2855

Indian Ministry of Non-Conventional Energy Sources
Block 14, CGO Complex
Lodi Road
New Delhi — 110 003, India
Fax: +91-11-436-1298

Institute Catalia d'Energia
Avenue Diagonal, 453 Bis. Atic
08036 Barcelona, Spain
Fax: +343-439-2800

Norwegian Wind Energy Association
Phone: +47 66 84 63 69
Fax: +47 66 98 11 80

Romanian Wind Energy Association
Phone: +40 1 620 67 30/260
Fax: +40 1 312 93 15

RISO National Laboratory
P.O. Box 49
4000 Roskilde, Denmark
Tel: +45 46 77 50 35
Fax: +45 46 77 50 83
Web: www.risoe.dk/amv/index.html

Tata Energy Research Institute
Darbari Seth Block, Habitat Place
New Delhi — 110 003, India
Phone: +91-11-460-1550
Fax: +91-11-462-1770
E-mail: mailbox@teri.res.in
Web: http://www.teriin.org

Vindmolleindustrien
(Association of Danish Wind Turbine Manufacturers)
Norre Voldegadc 48, OPGB.
Kobenhaven K DK-1358
Denmark
Phone: +45 33–779988

WIND POWER SYSTEM SUPPLIERS IN THE U.S.

The following is a partial list of wind turbine manufacturers and developers in the U.S. A complete, current list and company profile can be obtained from AWEA at the following address:

American Wind Energy Association
122 C St., NW, Fourth Floor
Washington, DC 20001
Phone: (202) 383-2520
Fax: (202) 383-2505 fax
E-mail: windmail@awea.org

Atlantic Orient Corporation
P.O. Box 1097
Norwich, VT 05055
Phone: (802) 649-5446
Fax: (801) 649-5404

Bay Winds
1533 Kimball Street
Green Bay, WI 54302
Phone: (920) 468-5500

Bergey Windpower Company
2001 Priestley Avenue
Norman, OK 73069
Phone: (405) 364-4212
Fax: (405) 364-2078
E-mail: mbergey@bergey.com

GE Wind Energy
13000 James Road
Tehachapi, CA
Web: www.gewindenergy.com

Lake Michigan Wind & Sun Ltd.
East 3971 Bluebird Road
Forestville, WI 54213-9505
Phone: (414) 837-2267
Fax: (414) 837-7523
E-mail: lmwands@itol.com

Southwest Windpower
2131 North First Street
Flagstaff, AZ 86001
Phone: (520) 779-WIND
Fax: (520) 779-1485
Web: http://www.windenergy.com

Wind Turbine Industries Corporation
16801 Industrial Circle, SE
Prior Lake, MN 55372
Phone: (612) 447-6064
Fax: (612) 447-6050

WindTech International, L.L.C.
P.O. Box 27
Bedford, NY 10506
Phone: (914) 232-2354
Fax: (914) 232-2356
E-mail: info@windmillpower.com
Web: http://www.windmillpower.com

World Power Technologies, Inc.
19 N. Lake Avenue
Duluth, MN 55802
Phone: (218) 722-1492
Fax: (218) 722-0791
E-mail: wpt@cp.duluth.mn.us
Web: http://www.webpage.com/wpt/

EUROPEAN WIND ENERGY MANUFACTURERS AND DEVELOPERS

The following is a partial list of wind turbine manufacturers and developers in Europe. A complete, current list and company profile can be obtained from the EWEA at the following address:

European Wind Energy Association
26 Spring Street
London, W2 1JA, United Kingdom
Tel: +44 171 402 7122
Fax: +44 171 402 7125
E-mail: ewea@ewea.org
Web: www.ewea.org

ABB Motors OY
PL 633
65101 Vaasa
Finland
Tel: +358 10 22 4000
Fax: +358 10 22 47372

Aerpac B.V.
P.O. Box 167
Bedrijvenpark Twente 96
Almelo 7600 A
The Netherlands
Tel: +31 546 549 549
Fax: +31 546 549 599
E-mail: aerpac@worldaccess.nl

ATV Enterprise
Actipole St. Charles
13710 Fuveau
France
Tel: +33 4 42 29 14 62
Fax: +33 4 42 29 14 61

A/S Wincon West Wind
Hedemoelle Erhvervsvej 4
DK-8850 Bjerringbro
Denmark
Tel: + 45 86 68 1700
Fax: +45 86 68 1734

Bonus Energy A/S
Fabriksvej 4
7330 Brande
Denmark
Tel: +45 97 18 11 22
Fax: +45 97 18 30 86
E-mail: bonus@bonus.dk

Desarrollos Eolicos SA
Avenida de la Buhaira, 2
41018 Sevilla
Spain
Tel: +34 95 493 7000
Fax: +34 95 493 7017

Ecotecnia SCCL
Amistat 23 1st
08005 Barcelona
Spain
Tel: +34 93 225 7600
Fax: +34 93 221 0939
E-mail: ecotecnia@ecotecnia.com
Web: www.ecotecnia.com

Enercon GmbH
Dreekamp 5
26605 Aurich
Germany
Tel: +49 421 24 9920
Fax: +49 421 24 9960
E-mail: export@enercon.de
Web: www.enercon.de

KK Electronic A/S
Cypresvej 6
7400 Herning
Denmark
Tel: +45 97 22 1033
Fax: +45 97 21 1431

E-mail: main@kk-electronic.dk
Web: www.kk-electronic.dk

Italian Vento Power Corporation (IVPC)
Via Circumvallazione 54/H
83100 Avellino, Italy
Tel: +39 825 781 473
Fax: +39 825 781 472
E-mail: 104124.2261@compuserve.com

L M Glasfiber A/S
Rolles Mollevej 1
6640 Lunderskov
Denmark
Tel: +45 75 58 51 22
Fax: +45 75 58 62 02
E-mail: info@lm.dk
Web: www.lm.dk

Windpower Ltd.
Riverside House, Meadowbank
Furlong Road
Bourne End, SL8 5AJ, United Kingdom
Tel: +44 1628 532300
Fax: +44 1628 531993
Web: www.enterprise.net

NedWind BV
Postbus 118
3910 AC Rhenen
The Netherlands
Tel: 31 317 619 004
Fax: 31 317 612 129
E-mail: wind.turbines@nedwind.nl
Web: www.nedwind.nl

NEG Micon A/S
Alsvej 21
DK-8900 Randers
Denmark
Tel: +45 87 10 5000
Fax: +45 87 10 5001
E-mail: mail@neg-micon.dk

NEG Micon (UK) Ltd.
Taywood House, 345 Ruislip Road
Southall, Middlesex, UB1 2QX, United Kingdom
Tel: +44 181 575 9428
Fax: +44 181 575 8318

Nordex Balke-Durr GmbH
Svindbaek
7323 Give
Denmark
Tel: +45 75 73 44 00
Fax: +45 75 73 41 47
E-mail: nordex@nordex.dk
Web: www.nordex.dk

Renewable Energy Systems Ltd.
Pilgrims Lodge, Holywell Hill
St. Albans, Herts, AL1 1ER, United Kingdom
Tel: + 44 1727 797900
Fax: + 44 1727 797929
Web: www.res-ltd.com

RISO National Laboratory
P.O. Box 49
4000 Roskilde
Denmark
Tel: +45 46 77 50 35
Fax: +45 46 77 50 83
Web: www.risoe.dk/amv/index.html

Riva Wind Turbines
Via Emilia Ponente 72
40133 Bologna, Italy
Tel: +39 51 413 0511
Fax: +39 51 413 0650

SeaWest Energy Corporation
1455 Frazee Road, Suite 900
CA 9210, San Diego
Tel: +1 619 293 3340
Fax: +1 619 293 3347
E-mail: seawestsd@aol.com

Stork Product Engineering
P.O. Box 379
1000 AJ Amsterdam
The Netherlands
Tel: +31 205 563 444
Fax: +31 205 563 556

Valmet Power Transmission, Inc.
P.O. Box 158
40101 Jyvaskyla
Finland
Tel: +358 14 296 611
Fax: +358 14 296 868

Vergnet SA
6 Rue Henri Dunant
45410 Ingre
France
Tel: +33 2 38 227 500
Fax: +33 2 38 227 522
E-mail: vergnet@wanadoo.fr

Vestas Wind Systems A/S
Smed Hanseen Vej 27
6940 Lem
Denmark
Tel: +45 97 34 11 88
Fax: +45 97 34 14 84
E-mail: vestas@vestas.dk
Web: www.vestas.dk

West S.P.A.
Alenia/West
Viele Maresciallo Pilsudsky 92
I-00131 Roma, Italy
Tel: +39 6 80 77 88 33
Fax: +39 6 80 77 88 48

Western Windpower Ltd.
Stroud House, Russell Street
Stroud, Gloucestershire
GL5 3AN, United Kingdom
Tel: +44 1453 579408
Fax: +44 1453 766770

Zond International Ltd.
Prince Consort House
27-29 Albert Embankment
London, SE1 7TJ, United Kingdom
Tel: + 44 171 793 2800
Fax: + 44 171 820 3401
E-mail: zond@compuserve.com

RESEARCH AND CONSULTANCY

Bond Pearce
Ballard House
West Hoe Road
Plymouth, PL1 3AE, United Kingdom
Tel: +44 1752 266633
Fax: +44 1752 225350

ECN Renewable Energy
Postbus 1
1755 ZG Petten
The Netherlands
Tel: +31 224 56 41 84
Fax: +31 224 56 32 14
Web: www.ecn.nl

Elsamprojekt A/S
Kraftvaerksvej 53
7000 Fredericia
Denmark
Tel: +45 79 23 3333
Fax: +45 75 56 4477
Web: www.elsamprojekt.dk

Garrad Hassan & Partners Ltd.
The Coach House
Folleigh Lane, Long Ashton
Bristol, BS18 9JB, United Kingdom
Tel: +44 1275 394360
Fax: + 44 1275 394361

Banque Paribas
37 Place du Marche, St Honore
75001 Paris
France
Tel: +33 1 42 98 77 38
Fax: +33 1 42 98 19 89

BTM Consult A/S
I C Christensens Alle 1
6950 Ringkobing
Denmark
Tel: +45 97 32 5299
Fax: +45 97 32 5593
E-mail: btmcwind@post4.tele.dk
Web: www.home4.inet.tele.dk

China Fulin Windpower Development
No 1, Dongbinhe Road
Youanmenwai, Fengtai District
100054 Beijing
P.R. China
Tel: +86 10 635 304 17
Fax: +86 10 635 304 15

Eole
BP 72
13702 La Ciotat Cedex
France
Tel: +33 4 42 08 14 66
Fax: +33 4 42 08 16 56
E-mail: eole@topnet.fr

ESD Ltd.
Overmoor Farm
Neston
Wiltshire, SN13 9TZ, United Kingdom
Tel: +44 1225 816804
Fax: +44 1225 812103
Web: www.esd.co.uk

Espace Eolien Developpement
16 Rue Faidherbe
59000 Lille
France
Tel: +33 3 20 74 04 00
Fax: +33 3 20 74 04 07
Web: www.espace-eolien.fr

Grant Rush & Co. Ltd.
Preston Park Station
Clermont Road
Brighton, BN1 6SG, United Kingdom
Tel: +44 1273 540410

Fax: +44 1273 504028
E-mail: grant_rush@gb3.global.ibmail

Institutt for Energiteknikk
P.O. Box 40
2007 Kjeller
Norway
Tel: +47 63 80 6180
Fax: +47 63 81 2905
Web: www.ife.no

La Compagnie du Vent
Horizon 21, 650 rue Louis Lepine
Le Millenaire, 34000 Montpellier
France
Tel: +33 4 99 52 64 70
Fax: +33 4 99 52 64 71
E-mail: cabinet.germa@wanadoo.fe
Web: perso.wanadoo.fr/cabinet.germa

LMW Renewables BV
P.O. Box 279
3770 AG Barneveld
The Netherlands
Tel: +31 342 421 986
Fax: +31 342 421 759

Mees Pierson N.V.
Camomile Court
23 Camomile Street
London, EC3A 7PP, United Kingdom
Tel: +44 171 444 8712
Fax: +44 171 444 8810

NRG Systems, Inc.
110 Commerce Street
05461 Hinesburg, VT
Tel: +1 802 482 2255
Fax: +1 802 482 2272

Shell International Renewables
Head Biomass & Wind
Shell Centre
London, SE1 7NA, United Kingdom
Tel: +44 171 934 3386
Fax: +44 171 934 7470

Synergy Power Corporation
20/F Wilson House
19-27 Wyndham Street, Central
Hong Kong
Tel: +852 2846 3168
Fax: +852 2810 0478
E-mail: SynergyPowerCorp@compuserve.com

Teknikgruppen AB
P.O. Box 21
19121 Sollentuna
Sweden
Tel: +46 8 444 5121
Fax: +46 8 444 5129

Tractebel Energy Engineering
Avenue Ariane 7
B-1200 Brussels
Belgium
Tel: +32 2 773 8345
Fax: +32 2 773 9700

Trillium Pakistan (Pvt) Ltd.
10th Floor, AWT Plaza
5 The Mall
Rawapindi-Cantt.
Pakistan
Tel: +92 51 56 21 07
Fax: +92 51 56 80 44
E-mail: Trillium@PakNet1.ptc.pk

Tripod Consult APS
Gladsaxe Mollevej 21
2860 Soborg
Denmark
Tel: +45 39 66 66 22
Fax: +45 39 66 66 99
E-mail: tripod@tripod.dk

NATIONAL ASSOCIATIONS

Austrian Wind Energy Association
IG Windkraft-Österreich
Mariahilferstrasse 89/22
1060 Vienna
Austria

Tel: +43 1 581 70 60
Fax: +43 1 581 70 61
E-mail: IGW@atmedia.net

British Wind Energy Association
26 Spring Street
London W2 1JA, United Kingdom
Tel: +44 171 402 7102
Fax: +44 171 402 7107
E-mail: bwea@gn.apc.org
Web: www.bwea.com

Bundesverband Windenergie
Am Michelshof 8-10
53177 Bonn
Germany
Tel: +49 228 35 22 76
Fax: +49 228 35 23 60
E-mail: bwe_bonn@t-online.de
Web: www.wind-energie.de

Danish Wind Turbine Manufacturers Association
Vester Voldgade 106
DK-1552 Copenhagen
Denmark
Tel: +45 33 73 0330
Fax: +45 33 73 0333
E-mail: danish@windpower.dk
Web: www.windpower.dk

Danmarks Vindmolleforening
Egensevej 24
Postboks 45
4840 Nr Alstev
Denmark
Tel: +45 54 43 13 22
Fax: +45 54 43 12 02
Web: www.danmarks-vindmoelleforening.dk

Dutch Wind Energy Bureau
Postbus 10
6800AA Arnhem
The Netherlands
Tel: +31 26 355 7400
Fax: +31 26 355 7404

Finnish Wind Power Association
P.O. Box 846
FIN-00101 Helsinki
Finland
Tel: +358 9 1929 4160
Fax: +358 9 1929 4129
Web: www.fmi.fi

Fordergesellschaft Windenergie E.V.
Elbehafen
25541 Brunsbuttel
Germany
Tel: +49 48 52 83 84 16
Fax: +49 48 52 83 84 30
E-mail: info@egeb.de

France Energie Eolienne
Institut Aerotechnique
15 rue Marat
78210 Saint-Cyr-l'Ecole
France
Tel: +33 1 30 45 86 01
Fax: +33 1 30 58 02 77

Hellenic Wind Energy Association
PPC, DEME
10 Navarinou Str
10680 Athens, Greece
Tel: +30 1 36 21 465
Fax: +30 1 36 14 709

Irish Wind Energy Association
Kellystown
Slane, County Meath
Ireland
Tel/fax: +353 41 267 87

ISES — France/ADEME
500 Route des Lucioles
05560 Valbonne
France
Tel: +33 4 93 95 79 18
Fax: +33 4 93 95 79 87

ISES – Italia
Piazza Bologna, 22 A/9 3
00162 Roma, Italy
Tel: +39 6 44 24 9241
Fax: +39 6 44 24 924
E-mail: info@isesitalia.it
Web: www.isesitalia.it

Japanese Wind Energy Association
Mechanical Engineering Lab.
1-2 Namiki, Tsukuba
305 Ibaraki-Ken
Japan
Tel: +81 298 58 7014
Fax: +81 298 58 7275

Netherlands Wind Energy Association
TU Delft, Institute for Wind
Stevinweg 1
2628 CN, Delft
The Netherlands
Tel: +31 15 27 85 178
Fax: +31 15 27 85 347

Romanian Wind Energy Association
Power Research Institute Bd
Energeticienilor 8
76619 Bucharest
Romania
Tel: +40 1 32 14 465
Fax: +40 1 32 22 790

Turkish Wind Energy Association
EiE Idaresi Genel Mudurlugu
Eskisehir Yolu 7km No. 166
06520 Ankara
Turkey
Tel: +90 312 287 8440
Fax: +90 312 287 8431

Acronyms

AC	Alternating Current
ASES	American Solar Energy Society
AWEA	American Wind Energy Association
Ah	Ampere-hour of the battery capacity
BIPV	Building-integrated photovoltaics
BWEA	British Wind Energy Association
C_p	Rotor energy conversion efficiency
C/D	Charge/discharge of the battery
DC	Direct current
DOD	Depth of discharge of the battery
DOE	Department of Energy
DWIA	Danish Wind Industry Association
ECU	European currency unit
EDF	Energy delivery factor
EPRI	Electric Power Research Institute
EWEA	European Wind Energy Association
GW	Gigawatts (10^9 watts)
GWh	Gigawatthours
HV	High voltage
HVDC	High-voltage direct current (transmission)
IEA	International Energy Agency
IEC	International Electrotechnical Commission
ISES	International Solar Energy Society
kW	Kilowatts
kWh	Kilowatthours
LV	Low voltage
LVRT	Low voltage ride-through
MW	Megawatts
MW_a	Megawatts accumulated
MW_e	Megawatts electric
MWh	Megawatthours
NEC	National Electrical Code®
NOAA	National Oceanic and Atmospheric Administration
NREL	National Renewable Energy Laboratory
NWTC	National Wind Technology Center
PV	Photovoltaic
QF	Qualifying facility
SOC	State of charge of the battery
SRC	Specific rated capacity (kW/m^2)

THD	Total harmonic distortion in quality of power
THM	Top head mass (nacelle + rotor)
TPV	Thermophotovoltaic
TSR	Tip speed ratio (of rotor)
TWh	Trillion (10^{12}) watthours
UCE	Unit cost of energy
W_p	Watt peak

PREFIXES:

k	kilo (10^3)
M	Mega (10^6)
G	Giga (10^9)
T	Trillion (10^{12})

Conversion of Units

The information contained in the book comes from many sources and many countries using different units in their reports. The data are kept in the form they were received by the author and were not converted to a common system of units. The following is the conversion table for the most commonly used units in the book:

To Change From	Into	Multiply By
mph	m/sec	0.447
kn	m/sec	0.514
mi	km	1.609
ft	m	0.3048
in.	cm	2.540
lb	kg	0.4535
Btu	W·sec	1054.4
Btu	kW·h	2.93×10^{-4}
Btu/ft^2	W·sec/m^2	11357
Btu/h	W	0.293
Btu/ft^2/h	kW/m^2	3.15×10^{-7}
Btu/h/ft^2/°F	W/m^2/°C	5.678
hp	W	746
gallon of oil (U.S.)	kWh	42
gal (U.S.)	l	3.785
barrel of oil	Btu	6×10^6
barrel	gal (U.S.)	42

Further Reading

1. Masters, G.M., *Renewable and Efficient Electric Power Systems*, John Wiley & Sons, 2004.
2. Markvart, T., *Solar Electricity*, 2nd ed., John Wiley & Sons, 2004.
3. Burton, T., Sharpe, D., Jenkins, N., and Bossanyi, E., *Wind Energy Handbook*, Garrad Hassan and Partners, Bristol, U.K., 2003.
4. Thresher, R.W., Chief Editor, *Wind Energy*, International Journal for Progress and Applications in Wind Power Conversion Technology, Wiley Inter Science Publication, Chichester, U.K.
5. Goswami, Y.D., Chief Editor, *Solar Energy*, Journal of the International Solar Energy Society, Elsevier Science Publishers, U.K.
6. Manwell, J.F., McGowan, J.F., and Rogers, A.L., *Wind Energy Explained, Theory, Design and Applications*, John Wiley & Sons, 2002.
7. Archer, M.D. and Hill, R., *Clean Energy from Photovoltaics*, Imperial College Press, World Scientific Publishing Co, London, 2001.
8. Dorf, R.C., *Technology, Humans, and Society: Towards a Sustainable World*, Academic Press, San Diego, 2001.
9. Hinson, P., *Wind Power Comes of Age,* British Wind Energy Association, London, 1999.
10. Boer, K.W., *Advances in Solar Energy, Annual Review of R & D*, American Solar Energy Society, Boulder, CO, 1996.
11. Komp, R.J., *Practical Photovoltaics*, Aatec Publications, Ann Arbor, Michigan, 1995.
12. Gipe, P., *Wind Energy Comes of Age*, John Wiley & Sons, New York, 1995.
13. Spera, D.A., *Wind Turbine Technology*, American Society of Mechanical Engineers, New York, 1994.
14. Lof, G., *Active Solar Systems*, MIT Press, Cambridge, MA, 1993.
15. Freris, L.L., *Wind Energy Conversion Systems*, Prentice Hall, London, 1990.
16. Eggleston, D.M. and Stoddard, F.S., *Wind Turbine Engineering Designs*, Van Nostrand Reinhold Company, 1987.
17. Johnson, G.L., *Wind Energy Systems*, Prentice Hall, London, 1985.
18. Park, J., *The Wind Power*, Cheshire Books, Palo Alto, CA, 1981.
19. Frost, W., Long, B.H., Turner, R.E. *Engineering Handbook on the Atmospheric Environmental Guidelines for Use in Wind Turbine Generator Development.* NASA-TP-1359. Huntsville, AL: National Aeronautics and Space Administration, Marshall Space Flight Center, 1978.
20. Danish Wind Energy Association, Asynchronous (Induction) Generators, 23 April 2003.
21. Danish Wind Energy Association, Size of Wind Turbines, 23 April 2003.
22. Yogi Goswami, D., Kreith, F., and Kreider, J.F., *Principles of Solar Engineering*, Taylor & Francis, 2000.

Index

C

D

E

F

G

H

I

J

K

L

M

Q

R

S

T

U

V

W

Y

Z